

Management of Ground Movement Hazards for Pipelines

CRES Project No. CRES-2012-M03-01

Final Report

Principal Investigator: Yong-Yi Wang

ywang@cres-americas.com

Center for Reliable Energy Systems (CRES)



5858 Innovation Drive
Dublin, OH 43016
www.cres-americas.com
614-376-0834

February 28, 2017

CRES QUALITY CONTROL SHEET

REPORT TITLE: Management of Ground Movement Hazards for Pipelines

DATE: February 28, 2017

PREPARED BY:

(Signature)



(Print)

Yong-Yi Wang, Ph.D.

REVIEWED BY:

(Signature)

(Print)

Immediate Supervisor or Reviewer, and Title

APPROVED BY:

(Signature)

(Print)

Immediate Supervisor or Approver, and Title

REPORT

PRODUCTION BY:

Document Editor

PROJECT TEAM

MEMBERS:

Acknowledgment

The work covered in this report is a product of collaborative effort. Many sponsors shared their field experiences. Many of the recommendations came from practical experience. In addition to providing financial support to the project, many of the sponsors actively participated in the drafting, reviewing, and revising this report. The broad expertise within this JIP group permitted the coverage of a wide range of subjects; all of which can contribute to the effective management of ground movement hazards.

A group of geotechnical experts from operating companies provided the most relevant and practical advice on the identification, assessment, mitigation, and monitoring of ground movement hazards. I could not have asked for a better group of experts to share ideas.

Individuals from inspection service providers contributed to the discussion and documentation of latest inspection technology. I am grateful for their contribution to the section in ILI technology, including the detection and sizing of girth weld imperfections, new and developing inspection techniques, and various monitoring techniques.

For various reasons, the names of many contributors can't be mentioned here. This JIP benefited greatly from the expertise of Mr. Don West, Mr. Doug Dewar, Mr. Alex Mckenzie-Johnson, Mr. Will Webster, Steve Rapp, and Mr. Jim Hart. Dr. Dan Jia of CRES performed multiple rounds of reviews and editing of the draft report and coordinated meetings and presentations. A number of other staff members at CRES contributed and reviewed various sections of this report. This report would not be possible without their diligence and dedication.

Yong-Yi Wang

JIP

Management of Ground Movement Hazards

Disclaimer

This report represents the collective efforts of many experts in the area of managing ground movement hazards. Although every effort is made to ensure the highest quality of the data, information, methodology, et al, presented in the report, the information may not be complete. Methods of evaluating and responding to ground movements vary according to the characteristics of the ground movements, locations, regulations, company policies, and other factors that affect the approach(es) selected. The processes and approaches reviewed, proposed, or recommended represent the experience and knowledge of the contributors and are not intended to be all encompassing. They should not be interpreted as prescriptive and/or mandatory requirements, nor standard practice. Certain emerging technologies are covered to illustrate possible tools and methodologies potentially available in the future. Their effectiveness should be proven before application.

In publishing this report, the PI and other contributors, their employers, and the sponsors, make no warranty or representation, expressed or implied, with respect to the accuracy, completeness, usefulness, or fitness for purpose of the information contained herein, or that the use of any information, method, process, or apparatus disclosed in this report may not infringe on privately owned rights. The PI and other contributors, their employers, and the sponsors, assume no liability with respect to the use of, or for damages resulting from the use of, any information, method, process, or apparatus disclosed in this report. By accepting the report and utilizing it, you agree to waive any and all claims you may have, resulting from your voluntary use of the report, against the PI and other contributors, their employers, and the sponsors.

JIP Sponsors

Alliance

Boardwalk

ConocoPhillips

Enbridge

Enterprise Products

Kinder Morgan

NiSource

PG&E

ROSEN

Shell

Southern California Gas

Southern Star

Spectra Energy

TD Williams

TransCanada

Williams

Management of Ground Movement Hazards for Pipelines

Executive Summary

Introduction

Ground movements, such as landslides and subsidence/settlement, can pose serious threats to the integrity of pipelines. The consequence of a ground movement event can vary greatly. Certain types of ground movements are slow moving and can be monitored and mitigated before a catastrophic failure. Other forms of ground movements can be difficult to predict. The most effective approach could be hazards avoidance, proactive means to reduce strain demand on pipelines, and/or building sufficiently robust pipeline segments that have high tolerance to the strain demand.

The overall objective of this project is the development of a best-practice document on managing ground movement hazards. The hazards of focus in this project are landslides and ground settlement, including mine subsidence. It is the intention of the JIP group that this document addresses nearly all major elements necessary for the management of such hazards.

Differences in Managing Internal Pressure and Loads Imposed by Ground Movement

There are important differences in the ways the pipeline industry managing internal pressure and loads imposed by ground movement. The loads of primary concern, caused by ground movement, act in the length direction of the pipelines (customarily termed longitudinal direction). Traditional pipeline designs primarily focus on pressure containment through limiting the hoop stress to a certain percentage of the specified minimum yield stress (SMYS). Although pipeline design standards, such as ASME B31.4 and B31.8, nominally limit the longitudinal stress to 90% of SMYS, this limit is typically considered only in the design phase (for lines after the applicable standards came in place). Longitudinal stresses on pipelines are typically not monitored or actively managed except in segments which are expected to have high stresses or heightened risk of failures from historical experience. The “design limit” on longitudinal stresses is treated very differently from limits on internal pressure.

A Few Key Concepts

The possible failure modes in an event of ground movements are

- Tensile rupture,
- Compressive buckling/wrinkling, including possible obstruction to the passage of ILI pigs,
- Leaks due to high local tensile strains at wrinkles/buckles, and
- Time-delayed failures (e.g., fatigue) at location of wrinkles/buckles.

The principal drivers to potential failures can be different among different pipelines, depending on the vintage, inspection practice, and site-specific ground conditions. For vintage pipelines built without 100% inspection of girth welds, the leading causes can be large flaws occasionally left from initial construction and additional stress (sometimes a small increment) imposed on the pipelines from historical norms. Modern pipelines could fail even with 100%

inspection of girth welds due to unintentional girth weld strength undermatching and heat-affected zone (HAZ) softening.

Pipelines built using linepipes procured by current industry standards, such as API 5L, and with girth welds qualified, inspected, and constructed by current industry standards, such as API 1104, can have varying degrees of strain tolerance. These pipelines are not guaranteed to have high resistance to longitudinal stresses or strains. The strain capacity of pipe segments with API 5L compliant linepipe and API 1104 compliant girth welds can vary from as low as 0.2% to well over 2%.

ASME B31.4 and B31.8 permit pipelines to be designed to have allowable longitudinal strain up to 2%, provided conditions stated in the standards are met. This allowable design strain limit is often misquoted and misused as strain capacity (the strain level a pipeline can sustain without negative consequence). The language in the standards provides a good overview of various factors that must be considered when pipelines are expected to experience high longitudinal strain. On the other hand, the standards do not provide specific conditions by which the strain limit of 2% can be achieved.

Hydrostatic test pressure alone is not an effective way to “weed-out” poor quality girth welds unless the girth welds already have a leak path or are very close to failure under normal operational conditions. The incremental increase in longitudinal stress due to the internal pressure increase from operating pressure to hydrotest pressure is quite small.

Identification and Assessment of Ground Movement Hazards

The methods and processes for the identification, characterization, assessment, and evaluation of landslide and settlement/subsidence hazards are extensively covered. A framework is provided to identify and assess the potential effects of landslide and settlement/subsidence hazards on pipelines. This is accomplished by first providing definitions of geologic processes, geologic hazards, and potential pipeline hazards and vulnerability. The significant potential geologic hazards that may impact pipelines in North America are briefly addressed and described. Detailed descriptions of landslide and settlement/subsidence processes and hazards, including the potential effects on pipelines, are provided. General methods and processes used to identify, classify, and evaluate landslide and settlement/subsidence hazards in a phased approach are described.

Determination of the Longitudinal Stresses/Strains Acting on Pipelines

Girth weld integrity is a major focus in managing ground movement hazards. All girth welds experience some nominal level of stresses that arise from field welding and operational conditions such as internal/external pressure and temperature differentials. Tie-in welds may experience higher stresses than mainline welds due to misalignment of pipe ends, change in stiffness between two sides of the welds, and uneven support conditions. In the absence of large flaws, these stresses typically would not cause integrity concerns.

Stresses and strains from ground movement can have a large range of variation. High stresses generated by ground movement have been one of the key contributing factors to girth weld failures.

Various methods to determine stresses and strains are extensively covered in this report, including working principles, limitations, accuracy, reliability, field experience, and cost. The methods include (1) established methods with mature technology, such as strain gauges and Inertial Measurement Units (IMU), (2) maturing technology with limited successful applications, such as fiber optic cables, and (3) new technology being developed with underlining working principles either proven or being validated.

The use of IMU is extensively covered in this report, including

- working principles, including various instrumentations in an IMU,
- typical sensitivity and accuracy of IMU ILI tools,
- basic processing of the inertial survey data,
- limitations and possible ways to overcome the limitations,
- processes and procedures to identify strain of interest,
- recommended protocol to characterize and report strains of interest by ILI service providers,
- possible ways to validate/verify IMU data,
- example strain features, and
- field experience in using IMU and correlations of horizontal and vertical strains from IMU with data/information from other sources.

Fitness-for-Service (FFS) Assessment and Supporting Information/Data/Tools

In broad terms, FFS assessment involves the comparison of strain demand and strain capacity. A pipe segment or a weld is deemed safe when the strain capacity is higher than the strain demand by a sufficient margin. FFS assessment procedures are divided into three categories, depending on the loading mode and the level of strain demand:

- FFS procedures under small tensile strain,
- FFS procedures under moderate to large tensile strain, and
- FFS procedures under compressive strain.

Within each category, the procedures are covered with the following elements:

- Applicability and limits,
- Fundamental basis,
- Key considerations and key input parameters to the procedures, and
- Example applications.

A few notable examples are (1) alternative X-Ray criteria using FFS principles, (2) tensile strain capacity of vintage linepipe with manual girth welds, and (3) tensile strain capacity of modern pipelines.

To support the FFS assessment, mechanical properties of pipeline girth welds of various vintage are collected, analyzed, and reported. Typical flaw types and dimensions found in girth welds are also reported.

To further support FFS assessment, the capability and limitations of various inspection tools relevant to the detection and sizing of girth weld anomalies are reviewed.

Mitigation and Monitoring

Mitigation can be viewed as the management of the geologic hazard or threat and its potential effects on a pipeline. Once mitigation is implemented, its performance will need to be monitored to assure that the mitigation measures continue to work, and the integrity of the pipeline is protected, or to identify developing adverse effects that may need response and additional mitigation.

Hazard mitigation can take many forms, including avoiding the hazard, stabilizing and controlling the hazard, reducing the effects of the hazard on the pipeline, and/or increase pipe strain capacity. Mitigation can also include just monitoring the hazard and/or its effects on the pipeline with the intent to address the hazard/threat issues when (and if) they reach a critical stage.

Monitoring of the hazard and/or its effects on the pipeline is commonly done after a mitigation approach/strategy/methodology has been implemented and as an interim step prior to mitigation if the mitigation cannot be performed immediately. The monitoring may be focused on: (1) verifying there is no/minimal slope movement once landslide stabilization has been implemented to assure that the stabilization efforts are working, (2) tracking the movement of the hazard (i.e., hazard monitoring) to monitor when the hazard has diminished or minimized, or (3) tracking the response of the pipeline to landslide and settlement/subsidence movements (i.e., pipe monitoring).

Typically, monitoring incorporates a combination of strategies and methods. Additionally, the nature of the mitigation in combination with the nature of the hazard, drive the development of the monitoring plan/program.

Both mitigation and monitoring are dependent on the development of a site-specific geologic (hazard) model resulting from Phases II/III efforts of hazard identification, characterization and evaluation. The site-specific geologic model provides the physical understanding of the hazard, including the location, dimensions, geometry, nature, and level of activity. These data are critical to identifying and developing mitigation and monitoring strategies. The development of a site-specific geologic model often requires the engagement of qualified geologic and geotechnical professionals.

Brief summaries of the various common potential mitigation alternatives are provided, including descriptions of the benefits and limitations of each alternative, also addressing

combinations of the alternatives. Common monitoring strategies, and techniques and methodologies are also provided.

Overall Management Process

Beyond the integrity management process from the viewpoint of geotechnical engineers, more refined quantitative assessment using FFS principles can be applied to prioritize mitigation activities and assist the decision on proper mitigation methods.

The assessment can be broadly divided into two categories: (1) screening or ranking the locations of interest and (2) site-specific assessment to determine the risk of failure and mitigation measures. The process of determining strain demand limits, which involves strain capacity and a safety factor on strain capacity, is provided. The output of the FFS assessment can be used in both screening/ranking and site-specific assessment.

For screening and ranking, the following critical issues are covered:

- (a) Default reporting threshold for IMU tools, and
- (b) Classification of locations of high strains.

For site-specific assessment, the application of the FFS assessment procedures is linked to the potential level of impact if an event were to occur. The recommended default values of input parameter for FFS assessment are set to produce different levels of conservatism. The higher the level of impact, the more conservative the assessment outcome becomes. These default values can be replaced when site-specific values are known.

Table of Contents

Executive Summary	iv
Table of Contents	ix
1 Introduction.....	1
1.1 Ground Movement Hazards Relative to Industry Practice	1
1.2 Possible Failure Modes in an Event of Ground Movement.....	2
1.2.1 Tensile Rupture.....	2
1.2.2 Compressive Buckling.....	2
1.2.3 Leaks due to High Local Tensile Strain at Wrinkles/Buckles	2
1.2.4 Time-Delayed Failures at Location of Wrinkles/Buckles	2
1.3 Drivers to Failures in an Event of Ground Movement	8
1.4 Project Objective.....	9
1.5 Work Scope and Report Structure	9
2 Methods and Processes for the Identification and Assessment of Hazards	10
2.1 Overview.....	10
2.1.1 General.....	10
2.1.2 Organization of this Section	12
2.2 Definitions of Geologic Processes, Hazards, Pipeline Vulnerability	12
2.3 Potential Geologic Hazards that May Affect Pipelines in North America	13
2.3.1 Landslide Hazard	14
2.3.2 Ground Subsidence/Settlement Hazard	14
2.3.3 Water Erosion Hazards	17
2.3.4 Wind (Aeolian) Erosion Hazard	20
2.3.5 Seismic Hazard	22
2.3.6 Volcanic Hazard	23
2.3.7 Expansive/Collapsible Soil Hazard	24
2.3.8 Shallow Groundwater Hazard.....	25
2.3.9 Glacier and Permafrost Hazard.....	25
2.4 Description of Potential Landslide and Settlement/Subsidence Geologic Hazards	25
2.4.1 Nature and Effects of Ground Movement (Landslide) Hazards	26
2.4.1.1 Landslide Types, Processes, Triggering Mechanisms and Features	26
2.4.1.2 Potential Effects of Landslide Movement on Pipelines	45
2.4.2 Nature and Effects of Settlement/Subsidence Hazards.....	53
2.4.2.1 Settlement/Subsidence Types, Processes and Triggering Mechanisms	53
2.4.2.2 Potential Effects of Settlement/Subsidence on Pipelines	73
2.5 Methods for Hazard Identification, Characterization, Assessment and Evaluation	75
2.5.1 General.....	75
2.5.2 Primary Tools to Complete a Phased Approach to Hazards Assessment.....	77
2.5.3 Description of Phase I Geologic Hazards Screening	83
2.5.4 Description of Phase II Geologic Hazards Reconnaissance	92

2.5.5	Description of Phase III Geologic Hazards Investigation	99
3	Characterization of Stresses and Strains Affecting Girth Weld Performance	101
3.1	Stresses in a Joint of Linepipe	101
3.2	Stresses Affecting Girth Weld Performance.....	101
3.2.1	Stresses in the Construction Phase.....	101
3.2.1.1	Residual Stress from Welding.....	101
3.2.1.2	Stresses from Pipe Lifting and Lowering-in during Construction	102
3.2.1.3	Tie-in Stress.....	102
3.2.1.4	Backfill and Overburden Stresses	102
3.2.1.5	Stresses in Special Construction Methods	102
3.2.1.6	Stresses during Hydrostatic Pressure Testing	102
3.2.2	Stresses during Pipeline Service	103
3.2.3	Baseline Stresses and Strains	104
3.2.4	Cyclic Stress on Girth Welds.....	105
3.2.5	Stresses of Pipes on Slopes	105
3.3	Overview of Methods of Measuring of Stresses and Strains in Pipelines	105
3.4	Pipe-Soil Interaction Models	106
3.4.1	Structural Pipe-Soil Interaction Models	106
3.4.2	Continuum Pipe-Soil Interaction Models	107
3.4.3	Pros and Cons of Various Pipe-Soil Interaction Models	108
3.5	Comparison of Various Stress/Strain Measurement Techniques	108
4	Utilization of IMU Data for Identifying Strain Locations of Interest.....	109
4.1	Principles of IMU	109
4.2	Typical Sensitivity and Accuracy	112
4.3	Basic Processing of Inertial Survey Data	113
4.3.1	Numerical Integration	113
4.3.2	Numerical Differentiation.....	114
4.4	Limitations of Inertial Survey Data	117
4.5	Identification of Strain Locations of Interest from IMU Data.....	119
4.6	Protocol for Characterization/Reporting at Strain Locations of Interest	122
4.6.1	Items Tabulated for Features of Interest	122
4.6.2	Items Plotted for Features of Interest.....	123
4.6.3	Notes for Bend Strain Reporting	125
4.6.4	Specialized Processing.....	126
4.6.5	Additional Information in an IMU Report.....	127
4.7	Verification of IMU Survey Data	128
4.8	Example Pipeline Strain Features	131
5	Mechanical Properties of Pipe and Girth Welds.....	132
5.1	Introduction.....	133
5.2	Evolution of Pipe Manufacturing	133

5.2.1	Type of Pipe.....	133
5.2.2	Steel Chemical Composition and Rolling Practice.....	134
5.2.3	Stress-Strain Response.....	134
5.3	Evolution of Construction Practice.....	135
5.4	Pipeline Mileage by Construction time	136
5.5	Pipe and Girth Weld Properties from Group A	137
5.5.1	Characteristics of the Pipelines of Group A	137
5.5.2	Matrix of Mechanical Tests	138
5.5.3	Pipe Tensile Properties	139
5.5.3.1	Features and Dimensions of Tensile Specimens	139
5.5.3.2	Stress-Strain Curves	139
5.5.3.3	Actual Strength vs. Specified Minimum Strength	144
5.5.4	Girth Weld Tensile Properties and Strength Mismatch	146
5.5.4.1	Dimensions and Features of Tensile Specimens	146
5.5.4.2	Stress-Strain Curves	146
5.5.4.3	Girth Weld Strength Mismatch	148
5.5.5	Girth Weld Hardness Profile.....	149
5.5.6	Charpy Impact Energy	152
5.5.7	Cross-Weld Tensile Test.....	155
5.5.7.1	Overview of the Test	155
5.5.7.2	Performance of Girth Welds with Natural Flaws	159
5.5.7.3	Performance of Girth Welds with Artificial Flaws	163
5.5.7.4	Estimation of Apparent Toughness by Residual CTOD	164
5.5.8	General Observations from Group A Data	166
5.6	Pipe and Girth Weld Properties from Group B.....	166
5.6.1	Overview of the Group B Materials and Tests	166
5.6.2	Non-Destructive Testing Techniques	167
5.6.2.1	Magnetic Particle Inspection (MPI)	167
5.6.2.2	Phased Array Ultrasonic Testing (PAUT)	167
5.6.3	Summary of NDT Results and Distribution of Flaws.....	167
5.6.3.1	Planar Flaws Detected by NDT.....	168
5.6.3.2	Volumetric Flaws Detected by NDT.....	171
5.6.4	Matrix of Mechanical Tests	174
5.6.5	Base Pipe Tensile Properties.....	174
5.6.6	Girth Weld Tensile Properties	177
5.6.7	Comparison of Base Metal and Girth Weld Strength	178
5.6.8	Macrohardness Traverse	180
5.6.9	Charpy Impact Energy	181
5.6.10	Cross-Weld Tensile Tests	185
5.6.10.1	Test Results of Natural Flaw CWT Specimens.....	187

5.6.10.2	Test Results of Artificial Flaw CWT Specimens	192
5.6.10.3	Exposed Flaws after CWT Testing	193
5.6.11	Measure of Fracture Toughness with Residual CTOD.....	195
5.6.12	General Observations from Group B Data	201
5.7	Pipe and Girth Weld Properties from Group C.....	201
5.7.1	Characteristics of the Welds of Group C	201
5.7.2	Pipe Tensile Properties	201
5.7.3	Cross-Weld Tensile Strength.....	202
5.7.4	Type and Dimensional Distribution of the Flaws from Group C	203
5.7.4.1	Flaw Types	203
5.7.4.2	Flaw Dimensions.....	204
5.7.5	Results of the Full-Scale Tests.....	206
5.7.6	General Observations from Group C Data	208
5.8	Pipe and Girth Weld Properties from Group D	208
5.8.1	Overview of the Welds	208
5.8.2	Matrix of Mechanical Tests	208
5.8.3	Pipe Tensile Properties	209
5.8.3.1	Features and Dimensions of Tensile Specimens	209
5.8.3.2	Test Results	209
5.8.4	All-Weld Metal Tensile Properties and Strength Mismatch.....	211
5.8.4.1	Features and Dimensions of Tensile Specimens	211
5.8.4.2	Test Results	211
5.8.5	Girth Weld Hardness Profile.....	212
5.8.6	Charpy Impact Energy	215
5.8.7	CTOD Fracture Toughness Testing.....	216
5.8.8	Wide Plate Tests	216
5.8.8.1	Overview of the Test	216
5.8.8.2	Defects in Wide Plate Test Specimens.....	218
5.8.8.3	Summary of Test Results	218
5.8.9	General Observations from Group D Data	219
5.9	Data in Other Sources	220
5.10	Summary of Material Characteristics and Recommendations.....	220
5.10.1	Key Features of Material Characteristics.....	220
6	Detection and Sizing of Girth Weld Anomalies	222
6.1	Overview of ILI	222
6.2	Typology of Girth Weld Anomalies	223
6.2.1	Geometrical Weld Inhomogeneities	225
6.2.2	Volumetric Anomalies at/in Girth Weld.....	225
6.2.3	Planar Anomalies at/in Girth Weld.....	226
6.3	Main Categories of ILI Tools	226

6.3.1	Ultrasonic Wall Thickness Measurement Tools	227
6.3.2	Ultrasonic Crack Detection Tools.....	228
6.3.3	Axial Magnetic Flux Leakage.....	230
6.3.4	EMAT Crack Detection	231
7	Fitness-for-Service Assessment	233
7.1	Framework of FFS Assessment	233
7.2	FFS Assessment at Small Tensile Strains.....	234
7.2.1	Applicability of Traditional Stress-Based FFS Assessment Procedures	234
7.2.2	Fundamentals of Stress-Based FFS Assessment Procedures.....	235
7.2.3	Key Considerations in Applying Stress-Based FFS Assessment Procedures...237	
7.2.3.1	Characterization of Girth Weld Flaws	238
7.2.3.2	Flaw Types	238
7.2.3.3	Flaw Height	239
7.2.3.4	Fracture Toughness	239
7.2.3.5	Applied Stress Level	240
7.2.4	Alternative X-Ray Criteria.....	240
7.3	FFS Assessment at Large Tensile Strains.....	242
7.3.1	Factors Affecting Tensile Strain Capacity.....	242
7.3.2	Physical Process of Tensile Rupture.....	243
7.3.3	Applicability of Tensile Strain Models.....	244
7.3.3.1	Tensile Strain Models for New Pipeline Construction	244
7.3.3.2	Tensile Strain Models for In-Service Pipelines with Manual Girth Welds 245	
7.3.3.3	Use of Tensile Strain Equations in CSA Z662 Annex C	245
7.3.4	Building Blocks of PRCI-CRES Models.....	245
7.3.4.1	Limit States	246
7.3.4.2	Crack-Driving Force	247
7.3.4.2.1	Development of Crack-Driving Force Relations.....	247
7.3.4.2.2	Parametric Form of Crack-Driving Force Relations	247
7.3.4.3	Toughness.....	248
7.3.4.3.1	Form of Toughness and Test Specimens	248
7.3.4.3.2	Obtaining Apparent Toughness from Traditional Test Specimens	249
7.3.4.3.3	Obtaining Apparent Toughness from Resistance Curves.....	250
7.3.4.4	Selection of Test Specimens	250
7.3.4.5	Predicted TSC vs. Toughness Options.....	250
7.3.5	Structure of PRCI-CRES Models	251
7.3.6	Correlating Parameters in PRCI-CRES Models	252
7.3.7	Application of CRES Tensile Strain Models.....	252
7.3.7.1	Role of Tensile Strain Models.....	252
7.3.7.2	Applications at Levels 2 and 3	253
7.3.7.3	Applications at Level 4	255

7.3.7.3.1	Example 1 – Use of Weld Cap Overbuild to Enhance TSC	255
7.3.7.3.2	Example 2 - Application of Level 4 to Modern Girth Welds	260
7.3.8	Tensile Strain Models for Manual-Welded Pipelines	260
7.3.8.1	Model Setup	260
7.3.8.2	Example Results	263
7.3.9	Means to Enhance TSC	264
7.4	FFS Assessment of Compressive Buckling	265
7.4.1	Different Test Setup and its Significance	265
7.4.2	Compressive Strain Capacity (CSC) and its Significance	265
7.4.3	Models for Compressive Strain Capacity	270
7.4.3.1	CSA Z662 Models	270
7.4.3.2	DNV OS F101 Models	271
7.4.3.3	API RP 1111 Models	272
7.4.3.4	University of Alberta (UOA) Models	272
7.4.3.5	CRES Models	274
7.4.3.5.1	Equations for Compressive Strain Capacity	274
7.4.3.5.2	Recommended Geometry Imperfections	275
7.4.3.5.3	Applicable Ranges	276
7.4.4	Comparison of Models with Test Data	277
7.4.4.1	Experimental Database	277
7.4.4.2	Evaluation with Testing Data Having All Input Parameters	277
7.4.4.3	Evaluation with All Testing Data	277
8	Mitigation and Monitoring	283
8.1	Overview	283
8.2	Hazard Mitigation Techniques and Methodologies	285
8.2.1	Hazard and Consequence Avoidance	285
8.2.2	Hazard Stabilization	292
8.2.2.1	Landslide Stabilization	293
8.2.2.2	Karst Inverted Soil/Rock Filter for Sinkholes and Karst Chimneys	305
8.2.2.3	Permafrost Maintenance of Thermal Regime	306
8.2.3	Reduce Strain Demand and Increase Pipe Strain Capacity	306
8.3	Hazard Monitoring	316
8.3.1	General	316
8.3.1.1	Types of Monitoring	316
8.3.1.2	General Approach and Guidelines	317
8.3.2	Ground Monitoring	317
8.3.2.1	Visual Monitoring/Site Inspections	317
8.3.2.2	Subsurface Monitoring	327
8.3.2.2.1	Slope Inclinometers	327
8.3.2.2.2	Shape Accel Arrays (SAAs)	335

8.3.2.2.3	Extensometers.....	336
8.3.2.2.4	Downhole Time Domain Reflectometry (TDR).....	338
8.3.2.2.5	Piezometers.....	342
8.3.2.2.6	Ball Markers	350
8.3.2.3	Land Based Surface Monitoring	357
8.3.2.3.1	Conventional and Global Positioning System (GPS) Surveys	357
8.3.2.3.2	Monuments Directly Attached to Pipelines.....	364
8.3.2.3.3	Ground Based LiDAR (a.k.a. Terrestrial LiDAR Scanning)	365
8.3.2.4	Aerial/Satellite Based Surface Monitoring	371
8.3.2.4.1	InSAR	371
8.3.2.4.2	Airborne LiDAR.....	378
8.3.3	Pipe Monitoring.....	385
8.3.3.1	Use of IMU in Conjunction with Other ILI Tools	385
8.3.3.2	Overview of Strain Gauges	391
8.3.3.3	Traditional Strain Gauges.....	395
8.3.3.3.1	Resistance Type Gauges.....	395
8.3.3.3.2	Vibrating Wire (VW) Strain Gauge.....	397
8.3.3.4	Fiber Optic Strain Gauges and Cables	403
8.3.3.4.1	FO Strain Gauges.....	404
8.3.3.4.2	FO Cables	406
8.3.4	Selection of Methods	412
8.3.5	Frequency of Data Collection and Analysis	416
9	Overall Management Process	420
9.1	Longitudinal Stress and Strain Limits in Standards.....	421
9.1.1	Limits on Longitudinal Stress.....	421
9.1.1.1	ASME B31.4-2012.....	421
9.1.1.2	ASME B31.8-2010.....	422
9.1.1.3	Summary on the Longitudinal Stress Limits.....	422
9.1.2	Limits on Longitudinal Strain.....	426
9.1.2.1	Requirements in Current Standards.....	426
9.1.2.2	Significance of the Terms in Currents Standards.....	427
9.2	Acceptance of FFS Assessment for In-Service Pipelines.....	427
9.3	Effectiveness of Hydrostatic Testing in Exposing Poor-Quality Girth Weld.....	428
9.4	Potential Drivers to Failure in Vintage versus Modern Girth Welds	428
9.5	Overall Integrity Management Process.....	429
9.5.1	Screening and Ranking of High Strain Locations	429
9.5.1.1	Screening for High Strain Locations.....	429
9.5.1.1.1	Default Strain Capacity of Girth Welds	429
9.5.1.1.2	Default Baseline Strain Not Included in IMU Strain Measurement.....	430
9.5.1.1.3	Default Threshold for IMU Report.....	430

9.5.1.2 Ranking of High Strain Locations..... 430

9.5.2 Determination of Strain Capacity430

9.5.2.1 Tensile Strain Capacity 430

9.5.2.1.1 Low Strain Demand..... 430

9.5.2.1.2 Moderate to High Strain Demand..... 431

9.5.2.2 Compressive Strain Capacity 431

9.5.2.2.1 Load-Controlled Loading 431

9.5.2.2.2 Displacement-Controlled Loading 432

9.5.3 Safety Factor and Strain Demand Limit432

9.5.3.1 Safety Factor on Tensile Rupture..... 432

9.5.3.2 Safety Factor on Compressive Buckling..... 432

9.5.3.3 Alternative Approach to Setting Strain Demand Limit..... 432

9.5.4 Site-Specific Assessment.....433

9.5.4.1 Level of Impact 433

9.5.4.2 Recommended Default Values..... 433

9.5.5 Situations Necessitating Specialized Analysis434

9.5.6 Monitoring after Assessment.....434

10 Issues Not-Addressed in This Project.....435

10.1 Hazards Other Than Landslides and Subsidence.....435

10.2 Consistency in Strain Measures.....435

10.3 Post-Buckling Behavior.....435

10.4 Behavior of Anomalies in the Presence of High Longitudinal Strains.....436

10.5 Mitigation Measures when Strain Capacity is Potentially Inadequate436

Appendix A Field Measurements for Stress Estimation438

Appendix B Example Plot Packages of Inertial Survey Data443

Appendix C Sample Specification Language for Inertial Survey RFP.....459

C.1 Identification of Strain Locations of Interest from IMU Data.....459

C.2 Items to be Tabulated for Features of Interest459

C.3 Items to be Plotted for Features of Interest.....460

C.4 Additional Guidance for Bend Strain Reporting460

C.5 Additional Deliverables462

Appendix D Considerations in Pipe Replacement463

D.1 Scope of this Document.....463

D.2 Loading on Girth Welds and Design Assumptions464

D.3 Why Are Additional Considerations beyond Codes Necessary?.....465

D.4 Evolution of Materials and Their Response to Welding.....465

D.5 Features of Modern Linepipes that are Detrimental to Pipeline Performance466

D.5.1 Design, Construction, and Maintenance Practice470

D.6 Consequence of HAZ Softening.....470

D.7 Major Gaps in Current Codes and Standards.....473



D.8	Considerations in Pipe Specifications.....	474
D.9	Recommendations.....	475
D.9.1	Pipe Segments already in Service.....	475
D.9.2	Near-Term Planned Pipe Replacement.....	475
D.10	Long-Term Actions to Ensure Adequate Strain Capacity	475
Appendix E	Newer and/or Developing Pipe Monitoring Techniques	477
E.1	Residual Stress Measurement by IIT.....	477
E.1.1	Field Application of the IIT to Measure Residual Stress.....	479
E.2	Alternating Current Stress Measurement.....	480
E.2.1	Introduction.....	480
E.2.2	Theoretical Background.....	480
E.2.3	Sensor Technology	482
E.2.4	Sensor Validation.....	482
E.2.5	Current Inspection Capabilities and Limitations	483
E.2.6	Case Studies.....	484
E.3	eStress System	487
E.3.1	Working Principle and Description of Technology.....	487
E.3.2	Current Status of this Technique	488
E.4	Acoustic Birefringence	490
E.4.1	Working Principle and Description of Technology.....	490
E.4.2	Field Applications of Prototype Systems.....	491
E.4.3	Current Status of this Technique	492
E.5	MWM-Meandering Winding Magnetometer.....	492
E.5.1	Working Principle and Description of Technology.....	492
E.5.2	Current Status of this Technique	493
Appendix F	Apparent Toughness and Constraint Effects on Toughness	495
F.1	Concept of Apparent Toughness.....	495
F.2	Fundamental Basis of Fracture Mechanics	495
F.3	Experimental Evidence of the Effects of Constraint	496
F.4	Validity Limit of Fracture Toughness	499
F.5	Toughness at the Point of Tensile Failure	499
F.6	Appropriate Values of Apparent Toughness	500
	Nomenclature	501
	References.....	504

1 Introduction

Abstract

This section starts with an introduction to the ground movement hazards and their consequences. The broad industry approaches as related to requirements in codes and standards are briefly described. Various failure modes related to ground movement hazards are shown. The principal drivers to girth weld failures are highlighted.

The broad project objectives and work scope are listed. The overall structure of the report and responsible parties for each individual section are given.

1.1 Ground Movement Hazards Relative to Industry Practice

Ground movements, such as landslides and subsidence/settlement, can pose serious threats to the integrity of pipelines. The consequences of a ground movement event can vary greatly. Certain types of ground movements are slow moving and can be monitored and mitigated before a catastrophic failure. Other forms of ground movements can be difficult to predict. Occasionally catastrophic failures occur. Such incident can lead to significant damage to properties and cause injuries or even death.

Traditional pipeline designs primarily focus on pressure containment through limiting the hoop stress to a certain percentage of the specified minimum yield stress (SMYS). Although pipeline design standards, such as ASME B31.4 and B31.8, nominally limit the longitudinal stress to 90% of SMYS, this limit is typically considered only in the design phase (for lines installed after the applicable standards came in place). Longitudinal stresses on pipelines are typically not monitored or actively managed except in segments which are expected to have high stresses or heightened risk of failures from historical experience. The “design limit” on longitudinal stresses is treated very differently from limits on internal pressure. Historically, failures due to longitudinal stresses/strains are relatively rare. Therefore, the historical approach seems reasonable.

Girth welds tend to be the weakest link in the integrity of a pipeline subjected to ground movement hazards. There is a prevailing misunderstanding about the longitudinal stresses or strains a girth weld can take if the girth welds are qualified and inspected by industry standards such as API 1104. In reality, girth welds made to comply with API 1104 are not guaranteed to have high resistance to longitudinal stresses or strains. The analysis of the basic requirements in girth weld procedure qualification and experimental tests of completed welds can show that the strain capacity of API 1104 compliant girth welds can vary from as low as 0.2% (equivalent to approximately 60,000 psi stress) to more than 2%. More on the implications of API 1104 compliant welds is given in Appendix D. For welds made before the qualification and inspection criteria came in force, one of the major contributors to girth welds’ low tolerance to longitudinal stresses or strains is the potential for relatively large flaws remaining after construction because inspection of all welds was not required.

Managing ground movements is a complex undertaking. In formulating the most appropriate approach, one must take into account the local geotechnical conditions, historical

experiences, pipe and weld tolerance level to stresses and strains, likelihood of failure, and consequences. The tolerance to stresses and strains is related to the evolution of pipe steel manufacturing, welding practice, and inspection techniques. In addition, the availability of data on geotechnical conditions and pipe characteristics can vary significantly from one pipeline to another.

1.2 Possible Failure Modes in an Event of Ground Movement

1.2.1 Tensile Rupture

Pipelines subjected to ground movement hazards may experience high longitudinal stress/strain, in tension or in compression. When the longitudinal stress/strain is in tension, the primary integrity concern is the ability of the girth weld to sustain such stress/strain. If the tensile strain demand is higher than the strain capacity of a girth weld, a leak or rupture may occur at the girth weld. An example of such rupture is shown in Figure 1-1.

A few other examples of tensile failure of girth welds in vintage pipelines are shown in Figure 1-2, taken from a PHMSA presentation at the 2012 API-AGA Joint Committee meeting on Oil & Gas pipeline welding practices [1]. In some of the girth weld failure incidents of vintage pipelines, pre-existing hydrogen assisted cracking of the weld metal or HAZ (heat-affected zone), as shown in Figure 1-3, is thought to be a major contributing factor [1].

1.2.2 Compressive Buckling

When the longitudinal stress/strain is in compression a wrinkle may be formed if the stress/strain is sufficiently high, as shown in Figure 1-4 and Figure 1-5. Large wrinkles/buckles are possible (see Figure 1-6 and Figure 1-7).

When a segment of a pipeline is subjected to a large compressive strain, the pipe may push the cover open at a pre-existing overbend as shown in Figure 1-7 and Figure 1-8. The pipe segment may buckle if the compressive strain is sufficiently high.

1.2.3 Leaks due to High Local Tensile Strain at Wrinkles/Buckles

The formation of a wrinkle or buckle may or may not be an immediate structural integrity concern. Cracks may form in the vicinity of a severe wrinkle or buckle (see Figure 1-9 and Figure 1-10). Large hoop strain is generated in the vicinity of severe wrinkles and buckles. Such hoop strain may be sufficiently large to cause integrity concerns if the wrinkle/buckle affects a seam weld of compromised properties (e.g., anomalies in certain ERW pipes).

1.2.4 Time-Delayed Failures at Location of Wrinkles/Buckles

Severe wrinkles can cause damage to pipe coating, which may initiate corrosion-related concerns: either regular corrosion or stress-corrosion cracking. The other long-term structural integrity concern of wrinkle/buckles is the possible flaw initiation and growth through fatigue mechanism. Liquid pipelines may experience cyclic longitudinal stress due to large pressure fluctuation and temperature change. The longitudinal stress fluctuation of gas pipelines is generally believed to be low. However, gas pipelines can experience fluctuating longitudinal stress due to the changes in the pipe's temperature.



Figure 1-1 Girth weld tensile rupture and the resulting fire from a TV news report



Figure 1-2 Examples of tensile failure of girth welds [1]

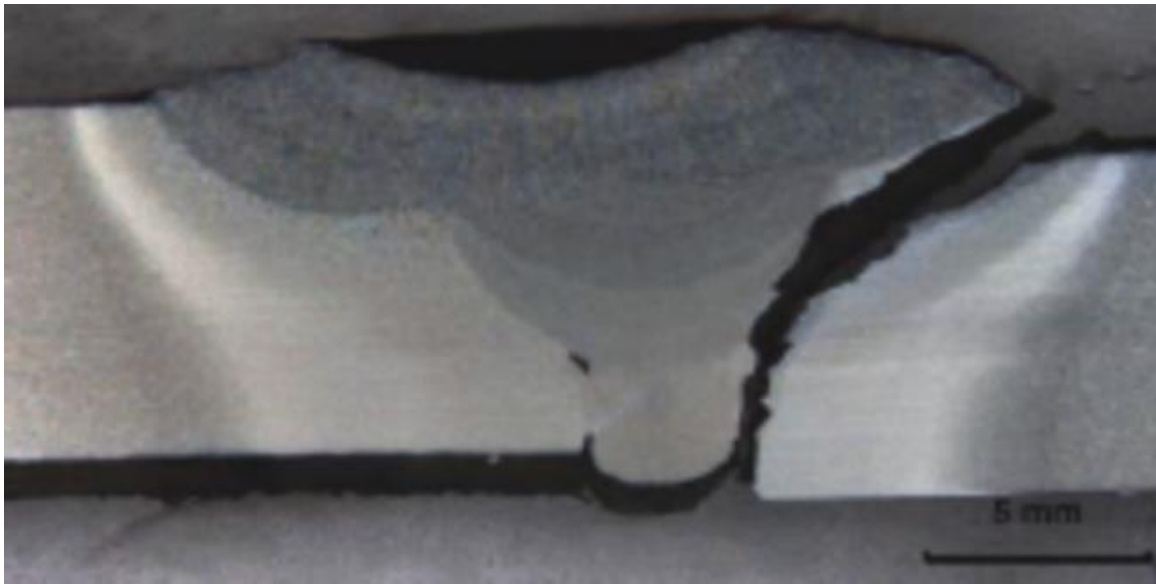


Figure 1-3 Hydrogen assisted HAZ cracking in a vintage girth weld [1].



Figure 1-4 Wrinkle formation at zero internal pressure



Figure 1-5 Example of pipe bulging and wrinkle formation (in-service pipeline) from axial compression due to valley closure resulting from longwall mining



Figure 1-6 A severe wrinkle formed at zero internal pressure.



Figure 1-7 A severe buckle formed at zero internal pressure.



Figure 1-8 A segment of a pipeline that heaved out of the ground



Figure 1-9 Wrinkle formation near a girth weld and the resulting cracking of pipe wall at the apex of the wrinkle

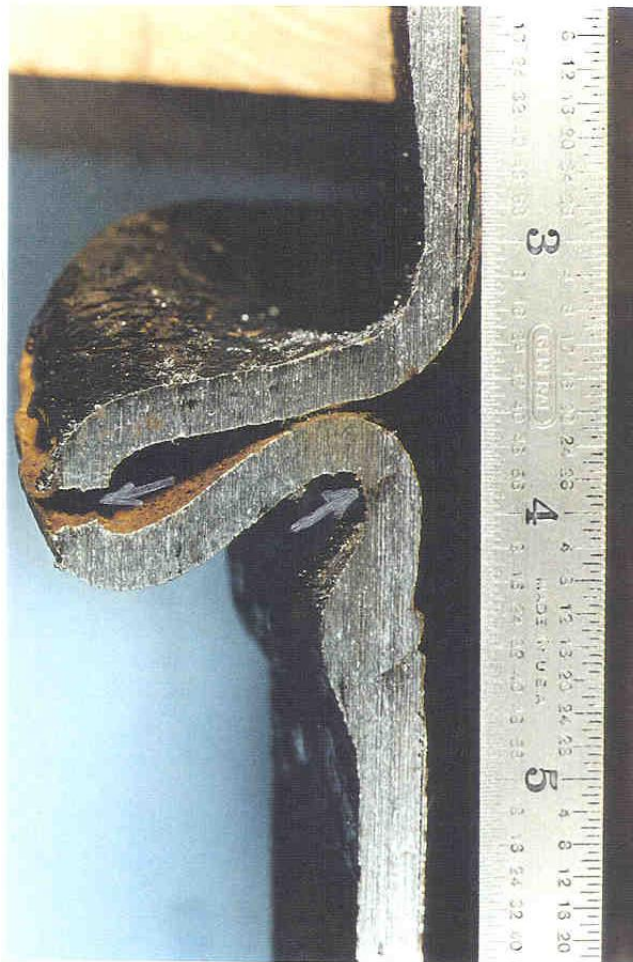


Figure 1-10 Cross-sectional view of the wrinkle and the pipe wall cracking of the wrinkle shown in Figure 1-9

1.3 Drivers to Failures in an Event of Ground Movement

Traditional pipeline designs primarily focus on pressure containment through limiting the hoop stress to a certain percentage of the specified minimum yield stress (SMYS). Historically, failures due to longitudinal stresses/strains are relatively rare. Designing against longitudinal stresses/strains is typically not a primary concern.

Failures of girth welds are usually associated with additional stresses imposed on the welds beyond the historical level of stresses. The disturbance of the support conditions would subject the welds to longitudinal load or bending moment which results in additional longitudinal tensile stresses. The disturbance of the support conditions may come from ground settlement, landslide, soil creep, or nearby construction activities. Another source of additional stresses is the thermal stress when the pipeline experiences colder than usual temperature such as from compressor station bypass or unusually cold temperature.

For many vintage pipelines, girth welds were not subjected to 100% inspection at the time of construction. Occasionally large flaws remained after the pipelines were put in service. These flaws can compromise the strain capacity of the girth welds, thus contributing to failures when additional longitudinal stresses are imposed.

When the girth welds of a pipeline are subjected to 100% inspection per construction standards, such as API 1104, large weld flaws typically don't exist after the pipeline is put in service. However, high strain capacity is not necessarily guaranteed even if the pipes are procured per modern standards, such as API 5L, and the girth welds are fabricated, inspected, and accepted by modern construction standards, such as API 1104. Girth welds qualified to API Standard 1104 are only required to have a cross-weld tensile strength equal to or greater than the specified minimum ultimate tensile strength (UTS) of the pipe. Since pipe strength is almost always greater than the specified UTS, the standard 1104 effectively allows for weld strength under matching, i.e., weld strength being lower than the strength of the pipe. In an event that ground movement results in overall longitudinal stress exceeding the specified UTS, strain can concentrate at the girth welds, leading to premature failure. More on this subject is given in Appendix D.

Hydrostatic testing is performed to verify the integrity of pipelines. These do not effectively test the ability of a pipeline to withstand longitudinal stress/strain; the longitudinal stress due to internal pressure in a buried (fully restrained) pipeline is only 30% of the hoop stress.

Failures due to longitudinal loads are relatively rare. This is, in a major part, attributable to the low longitudinal stresses experienced by typical buried pipelines. In the absence of ground movement hazards or other uncommon conditions, such as compressor station bypass or unusual weather conditions, the highest stresses on the girth welds of onshore pipelines typically occur during the pipeline construction stage, e.g., lifting and lowering-in, HDD, etc. After surviving the construction phase, undetected flaws can remain dormant for decades without any negative consequences.

1.4 Project Objective

The overall objective of this project is the development of a best-practice document on managing ground movement hazards. The hazards of focus in this project are landslides and ground settlement, including mine subsidence. It is the intention of this JIP ground that this document should address nearly all major elements necessary for the management of such hazards.

1.5 Work Scope and Report Structure

This project covers all key elements related to the integrity management of pipelines subjected to ground movement hazards. The major elements of the work scope are as follows.

- (1) Possible failure modes and drivers to failures (Section 1),
- (2) Identification and assessment of landslides and settlement/subsidence hazards (Section 2),
- (3) Stresses potentially affecting pipeline performance in an event of ground movement (Section 3)
- (4) Utilization of IMU in the identification of strain locations of interest (Section 4),
- (5) Mechanical property and flaw characteristics of vintage girth welds (Section 5),
- (6) Detection and sizing of girth weld anomalies (Section 6),
- (7) Fitness-for-service assessment (Section 7),
- (8) Mitigation and monitoring (Section 8),
- (9) Overall strategy and procedures of managing ground movement hazards (Section 9), and
- (10) Issues not addressed in this project, gaps, and ideas for future research and development (Section 10).

2 Methods and Processes for the Identification and Assessment of Hazards

Abstract

This section describes methods and processes for the identification, characterization, assessment, and evaluation of landslide and settlement/subsidence hazards. The processes described in this section are intended to assist pipeline owners/operators in identifying, locating, characterizing, understanding, and then managing landslide and settlement/subsidence hazards that may affect their pipeline systems.

A framework is provided to identify and assess the potential effects of landslide and settlement/subsidence hazards on pipelines. This is accomplished by first providing definitions of geologic processes, geologic hazards, and potential pipeline hazards and vulnerability. The significant potential geologic hazards that may impact pipelines in North America are briefly addressed and described. Detailed descriptions of landslide and settlement/subsidence processes and hazards, including the potential effects on pipelines, are provided. General methods and processes used to identify, classify and evaluate landslide and settlement/subsidence hazards in a phased approach are described and presented herein.

2.1 Overview

2.1.1 General

This section provides and describes recommended methods and processes for the identification, characterization, assessment and evaluation of landslide and settlement/subsidence hazards. The methods and processes described can assist pipeline owners/operators to identify, locate, characterize, understand, and then manage landslide and settlement/subsidence hazards that may be affecting their pipeline systems. The implementation of these processes is typically undertaken by trained professionals (primarily geoscientists and engineers) experienced in the identification, assessment and mitigation of geologic hazards; working with pipeline owners and operators to guide their geologic hazards programs. This section also provides the background information necessary for the discussion of landslide and settlement/subsidence hazard mitigation alternatives and hazard monitoring that are addressed in Section 8.

The focus of this section is on naturally-occurring or human-triggered geologic processes that may result in geologic hazards to pipelines; specifically landslide and settlement/subsidence hazards. Geologic hazards in general, and landslides and subsidence/settlement hazards in particular, can significantly affect the integrity of pipelines depending on the exposure to the hazard.

Because of the long, linear nature of pipeline systems, they often cross varied terrain and geologic conditions that may be susceptible to landslides and settlement/subsidence [2, 3, 4, 5, 6]. The early, timely and systematic identification, mapping, characterization and threat classification of potential landslide and settlement/subsidence hazards along pipeline alignments is important. This information allows owners/operators to understand the nature, spatial distribution, magnitude, extent and level of activity of the hazards, and thus, their potential impacts on the pipelines. Additionally, with this information, pipeline owners/operators can

implement informed hazard mitigation measures and informed risk management and operational decisions. The timely and systematic identification of the hazards and appropriate mitigation actions can reduce the hazards to pipeline integrity and maintain public and environmental health and safety.

The overall process of addressing geologic hazards and their effects on pipelines can be described as involving four basic steps or elements. These are: 1) hazard identification, 2) hazard characterization, assessment and threat classification, 3) hazard mitigation, and 4) hazard monitoring. The process begins with the systematic identification of the hazards and carries on through successive steps to both understand the nature of the hazards and their potential impacts (threats) on the pipeline, and to focus on those hazards where mitigation needs to be considered and implemented. The final step involves monitoring the performance of the mitigation measures. Although the steps are essentially sequential and successive, they are closely connected, inter-related and iterative, as illustrated below in Figure 2-1.



Figure 2-1 Basic steps in addressing geologic hazards

In this section, we primarily address the elements of the first two steps in the process of managing landslide and settlement/subsidence hazards: the methods and processes to identify the hazards and assess and classify the potential threats the hazards may have on a pipeline. Hazard mitigation and monitoring are explicitly addressed in Section 8.

The development of the processes makes use of previous texts, technical papers and journal articles regarding geologic hazards and pipelines. Examples of previously proposed guidelines and frameworks for geologic hazard management for pipelines or other linear facilities include those of [5, 6, 7, 8, 9, 10, 11, 12, 13].

Lier [14] provides an example of a commercially available geologic hazard management system for existing pipelines. Zaleski [15] provides the owner/operator's perspective on the implementation of geologic hazard management systems. Davidson, et al., [16] provide an example of a state of the art quantitative geologic hazard assessment for a proposed liquids pipeline routed through geologic hazard-prone plateaus and mountain ranges of central and

northern British Columbia that follows the susceptibility assessment approach of [5]. Davidson et al [16] noted that although the program is quantitative it still requires expert judgments to be made for key susceptibility model parameters.

This section is directed toward pipeline owners/operators that have yet to develop a formal geologic/geotechnical hazard identification and assessment program to address landslide and settlement hazards, or that currently address individual issues as they arise. The information in this section may also be used to update or revise existing owner/operator geologic hazard management programs.

The information in this section, although primarily developed for existing pipelines, can also be applicable for new or proposed pipelines. For proposed pipelines the information can be used for initial route/alignment selection, validation of the route/alignment with respect to geologic hazards, and development of an inventory of hazards that can be used for permitting and future risk management of the pipeline.

We stress that any geologic hazard management program requires the input of a geoscientist or geotechnical engineer with local/regional knowledge of the geologic processes and potential geologic hazards within a specific study area or region. Often this expertise will come from outside the pipeline company. While these outside experts will have specific geologic hazard experience, they may not have pipeline related experiences. As a result, there should be owner/operator input during the scoping, implementation and operation of a geologic hazards management program, particularly during the determination of threat/susceptibility levels. As noted by Davidson, et al., expert judgments will be required even for the most rigorous quantitative approach to geologic hazard management [16].

2.1.2 Organization of this Section

This section provides a framework to identify and assess the potential effects of landslide and settlement/subsidence hazards on pipelines. This is accomplished by first providing definitions of geologic processes, geologic hazards, and potential pipeline hazards and vulnerability in Section 2.2. Although the focus of this JIP is on landslide and settlement/subsidence hazards, other significant potential geologic hazards that may impact pipelines in North America are briefly addressed and described in Section 2.3. Detailed descriptions of landslide and settlement/subsidence processes and hazards, including the potential effects on pipelines, are provided in section 2.4. Section 2.5 provides the general methods and processes used to identify, classify and evaluate landslide and settlement/subsidence hazards in a phased approach.

2.2 Definitions of Geologic Processes, Hazards, Pipeline Vulnerability

Geologic hazards that could affect a pipeline system are the result of naturally-occurring, active geologic processes. These geologic processes occur in the absence of a pipeline system, and only become hazards or potential hazards if they affect, or potentially affect the integrity of an existing pipeline, or the routing, design and construction of a proposed pipeline. That is, the processes become potential hazards or potential threats if they lead to, or result in adverse consequences to the pipeline, or pipeline system.

Although geologic processes (i.e., hazards) are naturally-occurring, they can also be triggered or exacerbated by human activity or intervention. For example, the construction and operation of a pipeline can trigger a landslide on ground that would have otherwise been stable. Another example is underground resource extraction, which can lead to surface settlement/subsidence and localized differential surface displacement, on ground that would have been otherwise hazard free.

Whether a particular pipeline is vulnerable, or is exposed to the effects of the potential geologic processes (hazards) depends on many factors. These factors may include:

- The location, type, nature, age, activity, rate and extent of the geologic process (hazard) relative to the pipeline and its orientation.
- The pipeline's exposure to the geologic hazard, and the likelihood of the consequences of pipeline damage or rupture if the hazard or threat is active.
- The type, age, material, design parameters, and construction methods and practices of the pipeline.
- The operational and maintenance environment, processes and procedures of the pipeline.

2.3 Potential Geologic Hazards that May Affect Pipelines in North America

Although the focus of the JIP is on landslide and settlement/subsidence hazards, there are numerous other potential geologic hazards that could also affect pipelines (or other facilities) in North America [e.g., 6, 17, 18, 19, 20, 21]. The nature and potential effects on pipelines of these hazards are briefly discussed below to illustrate the comprehensive breadth and variety of natural hazards that could adversely affect the integrity of pipelines. The common geologic processes/hazards that could potentially affect pipeline systems in North America, at a minimum, include:

- Landslides
- Ground subsidence/settlement (collapse of underground mine workings, subsurface bedrock dissolution [karst], subsurface fluid withdrawal)
- Water erosion (river and stream [watercourse], coastal, ground surface, subsurface)
- Wind (aeolian) erosion
- Seismic (ground shaking, surface fault rupture, liquefaction, induced landslide, tsunami, seiche, ground deformation)
- Volcanic (lava flow, lahar, tephra, pyroclastic flow, volcanic earthquakes, ground deformation)
- Expansive/collapsible soils
- Shallow groundwater
- Glacier and permafrost (outburst flooding, cracking, heave, subsidence, thawing causing/triggering landsliding)
- Snow avalanches and ice falls (not discussed in detail in this document)

2.3.1 Landslide Hazard

The nature and potential effects of landslide movement on pipelines are discussed in detail in Section 2.4. In general, however, a landslide is defined as the “movement of a mass of rock, debris, or earth down a slope,” and encompasses landslide processes such as debris flows, rotational landslides, translational landslides, soil creep, topples, earth flows, rock falls, or debris slides [22, 23, 24, 25]. Figure 2-2 shows a complex landslide in the Northwest Territories that has elements of translational and flow landslides. Landslide movement and displacement can damage or rupture pipelines by [2, 26]:

- Shearing the pipe with differential displacement along the vertical and/or lateral landslide limits, along the subsurface rupture surface, or along internal failure surfaces of the landslide,
- Putting the pipe into compression, tension and bending during downslope movement of the soil and rock mass,
- Undercutting and exposing the pipe (in the event that material flows out from underneath the pipeline), or
- Physically impacting shallowly-buried or exposed pipe in the event of a rapid debris flow or rock fall impact.

2.3.2 Ground Subsidence/Settlement Hazard

The nature and potential effects of ground subsidence on pipelines is discussed in detail in Section 2.4.2. In general, ground subsidence is a gradual or sudden sinking/settlement of the ground surface resulting from the removal or movement of subsurface materials [9, 3, 27]. The principal causes of ground subsidence are subsurface fluid withdrawal with associated aquifer system compaction, the collapse of underground mine workings, subsurface dissolution of bedrock, drainage of organic soils, thawing of permafrost, and natural soil consolidation [3, 28, 27, 29]. Ground subsidence/settlement may result in:

- Broad compressive and tensile stresses/deformation across wide areas,
- Local tilting, and
- Differential displacement across distinct linear discontinuities such as faults and fissures along the edges of the subsidence (Figure 2-3 and Figure 2-4).

Ground subsidence and settlement can adversely affect pipelines and surface structures [e.g., 30, 31, 41, 32, 33, 34, 35, 36, 37, 38, 39]. The subsidence may impart broad tensile or compressive stresses on the pipeline at the center and limits of the area of subsidence and at significant distances from the limits as with longwall coal mining, or concentrated shearing stresses at specific linear discontinuities or lateral limits of the subsidence [40]. In addition, subsidence deformation may change the surface and groundwater hydrologic conditions [37].



Figure 2-2 Complex landslide with translational sliding and flow landslide movement types along the Mackenzie River, Northwest Territories (Photo by: D. West, Year: 2006)

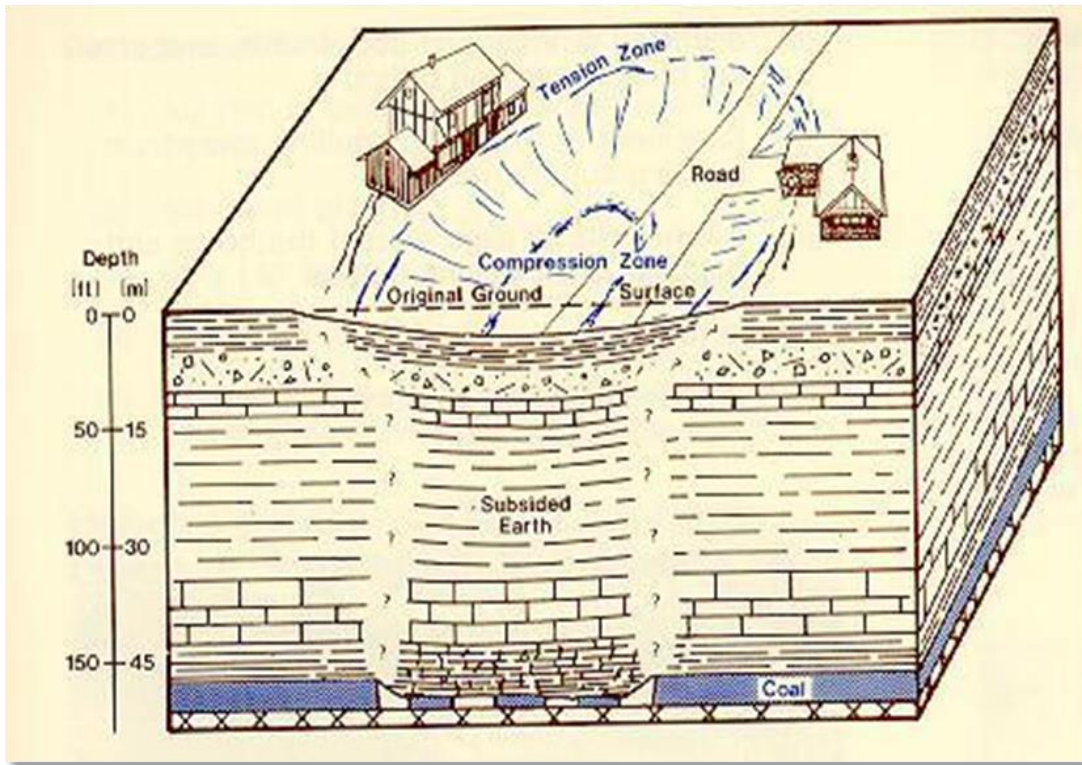


Figure 2-3 Illustration of location and types of surface subsidence deformation above a collapsed underground room-and-pillar coal mine (modified from [41]).



Figure 2-4 Surface subsidence from subsurface block caving above the Ridgeway Mine in New South Wales, Australia [42]

2.3.3 Water Erosion Hazards

Water erosion hazards that have the potential to affect pipelines may be divided into those related to moving water in rivers and streams (watercourse hazards), those related to shoreline or coastal erosion along the margins of water bodies (lakes, reservoirs, oceans), erosion of the ground surface from precipitation and local runoff, and subsurface erosion by groundwater in the pipe trench. Descriptions of each of these potential water erosion hazards and their potential effects on pipelines are summarized in the following bullets:

- River and stream (watercourse) pipeline exposures due to:
 - Vertical channel movement
 - Local scour: Lowering of the streambed in an isolated area due to secondary currents generated by obstructions in the channel (e.g., bridge piers, riprap banks, logjams, or channel confluences).
 - General Scour: lowering of the bed elevation in a reach due to channel constriction (e.g., armored pipeline crossing).
 - Degradation: lowering of the streambed throughout a reach of the river, due to an increase in flow in the channel, decrease in sediment supply, lowering of the bed level downstream (e.g., meander cutoffs or head-cutting).
 - Aggradation: raising of the bed level throughout a reach, due to increase in sediment supply or reduction in flow in the channel.
 - Horizontal (lateral) channel migration
 - Bank erosion: the gradual loss of bank material (often from an outside bend) typically with a corresponding deposition of sediment on the inside of the bend (point bar).
 - Channel avulsion: the sudden relocation of the channel, typically on an alluvial fan. Alluvial fan avulsions are often a complete change of channel location resulting from the natural process of channel infilling with sediment (as channel slope reduces on fan) and the stream overflowing banks onto a new, lower portion of the fan. Sometimes old channels are reoccupied. Logjams or narrowing of channel width often exacerbates sediment deposition and triggers avulsions.
 - Meander loop cutoffs: is a special case of bank erosion, where a long meander bend exists and flow “shortcuts” across a narrow neck of land. Can be sudden (during a large flood) or gradual. This results in the creation of oxbow lake, shortening of the main channel, increases in bank erosion (to lengthen channel to stable slope), degradation upstream and aggradation downstream,
- Shoreline and coastal (waterbody) pipeline exposures resulting from shoreline wave erosion.

- General right-of-way (ROW) surface erosion from incident rainfall that may take the form of sheetwash, rilling and gullyng:
 - The surface erosion may be caused and/or exacerbated by pipeline construction and operation activities.
 - In areas of where drainage is concentrated due to natural processes and/or as a result of construction on or uphill from the right of way, including access roads, there may be a hazard of exposing pipelines due to surface erosion.
- Subsurface erosion/piping due to groundwater flow in the pipeline backfill:
 - Pipeline backfills, even when compacted, act as preferential flow paths in sloping areas. If erodible backfill is present, piping may occur.
 - The piping forms voids in the subsurface within the backfilled pipe trench, which may collapse and form sinkholes or depressions at the surface.

Pipelines exposed by water erosion processes or hazards may be subjected to increased corrosion hazards from water and air, to physical damage from impacts by debris, and to increased vertical and lateral loading for which they were not designed [43]. Bryndum [44] discussed the potential modes of damage and/or failure for exposed and unburied pipelines in watercourses or waterbodies (including areas of surface and subsurface erosion) which are generally summarized as follows:

- Hydrodynamic loading from the force of water flowing against a partially exposed and/or free-spanned pipeline. Included within hydrodynamic loading is the potential for strikes from either the bedload material and/or large woody debris (LWD) in the system. In some instances during lateral encroachment and/or piping, additional vertical loading is caused by the pipeline cover that has not been eroded.
- Vibration loads due to vortex shedding in a free-spanned pipeline.

Additionally, exposed pipelines subjected to any water flow will likely have their coating systems removed by the water and/or bedload flows potentially making them more susceptible to corrosion. The issue may not be field-identified because exposures typically occur during flooding events that may expose and then re-bury a pipeline segment without the operator's knowledge.

An example of significant pipeline exposure from lateral stream channel migration and vertical scour (erosion) is illustrated in Figure 2-5. The exposed pipelines in Figure 2-5 were originally buried below the floodplain surface. A thick (approximately 70 ft; 21 m) artificial fill was placed in the floodplain and over the pipelines. The pipelines became exposed when concentrated flood flows, constricted by the artificial filling of the floodplain, reduced the available flood dissipation area, and resulted in lateral channel migration and vertical erosion. When exposed, these pipes then became subjected to hydrodynamic loads (from both flood flows and low flows) and loads from the impact of LWD.

Figure 2-6 illustrates pipeline exposure from drainage avulsion on an alluvial fan. The lateral erosion and pipe exposure also created significant vertical loading on the pipe where cover material remained after exposure.



Figure 2-5 Pipeline exposure resulting from lateral channel migration and vertical erosion in western Washington. (Photo by: A. Kammereck, Year: 2007)



Figure 2-6 Channel avulsion on an alluvial fan triggered by an upstream log jam diverting flow down a pipeline ROW. A 36-inch mainline was partially exposed and undermined by the avulsion channel. (Photo by: D. Dewar, Year: 2011)

2.3.4 Wind (Aeolian) Erosion Hazard

Wind (aeolian) erosion is typically a hazard to pipelines where surface deflation occurs in agricultural, semi-arid and arid regions and loose, exposed surficial material (e.g., silt and fine sand) is moved along the surface, bounced across the surface (saltation) and/or lifted into the air (suspension) [45]. Potential hazards to pipelines from wind erosion include the loss of cover, exposure of the pipeline, formation of unintended spans, and erosion of the pipe coating (e.g., sand blasting). Figure 2-7 shows the effects of long-term wind erosion and the resulting erosional deflation of the ground surface as the area of erosion encroaches on a pipeline ROW.

Commonly, the main hazard to a pipeline in an area of thinned cover resulting from wind erosion is third-party mechanical damage (e.g., where modern mechanical agricultural ground disturbances can be as deep as 4 ft (1.2 m) rather than the historical depths not exceeding 2 ft (0.6 m)). Figure 2-8 shows an area in Saskatchewan where wind erosion has significantly

reduced the soil cover over a pipeline in an agricultural field such that continued agricultural activities in the field could result in pipe damage.



Figure 2-7 Wind erosion and deflation (lowering) of the ground surface is encroaching on a pipeline ROW (arrows) in eastern Washington. (Photo by: D. West, Year: 1996)



Figure 2-8 Wind erosion in Saskatchewan which has reduced the cover over a 6-inch pipeline from the installed 3 ft (1.2 m) to 1 foot (0.3 m). (Photo by: B. Moore, Year: 2007)

2.3.5 Seismic Hazard

Common earthquake processes that result in potential seismic hazards to pipelines and pipeline facilities include: active fault displacement (with surface rupture), strong earthquake shaking, soil liquefaction, earthquake-induced landslides, tsunami, seiche (standing wave in a closed water body) and ground deformation (broad uplift and subsidence) [19, 46, 47, 21]. O'Rourke and Liu [26] have further defined the more common specific potential seismic hazards to buried pipelines as falling into permanent ground deformation (PGD) hazards and earthquake wave propagation hazards. The PGD hazards include:

- Fault rupture (differential ground displacement),
- Earthquake-induced landslide displacement,
- Soil lateral spreading resulting from soil liquefaction,
- Ground settlement due to strong ground shaking of loose soil or from soil liquefaction, and
- Pipe buoyancy resulting from soil liquefaction.

The PGD hazards may result in localized compression, tension or shearing stresses on pipelines where they are subject to the concentrated effects of the PGD such as at the margins of a landslide or at a fault crossing, or the PGD hazard may be distributed such as in ground deformation associated with liquefaction-induced lateral spreading [26].

Figure 2-9 shows the surface fault scarp along the Lost River Range frontal fault in Idaho that occurred during the 1983 magnitude 7.3 Borah Peak Idaho earthquake. The maximum vertical surface fault displacement (e.g., PGD) measured along the approximately 23 miles (36 km) of fault rupture ranged from 8 to 9 ft (2.4 to 2.7 m) [48].

Wave propagation hazards to buried pipelines are characterized by the transient strain and curvature in the ground associated with the strength/intensity of the passage of the earthquake waves during an earthquake [26]. Strong earthquake shaking with significant duration may also severely damage or destroy pipeline surface facilities (e.g., compressor or pump stations) if they are under-designed for seismic effects.



Figure 2-9 Eight- to nine-foot-high surface fault scarp on the Lost River Range frontal fault that formed during the 1983 magnitude 7.3 Borah Peak, Idaho earthquake. (Photo by: D. West, Year: 2010)

2.3.6 Volcanic Hazard

The predominant processes that may result in volcanic hazards to pipelines include [49, 50]:

- Tephra (ash) fallout,
- Lava flow,
- Pyroclastic flow,
- Lahar run-out (earth or debris flow of volcanic origin),
- Other landslide activity triggered by eruptions,
- Ground deformation, and
- Volcanic earthquakes.

Figure 2-10 illustrates the types of potential volcanic processes and their geographic distribution around a volcano. Most of the volcanic processes, and therefore the potential hazards, are geographically constrained to the close proximity of the volcanic edifice, however, lahars (earth or debris-flows) and tephra (ash) can be deposited at some distance from the

volcano, with lahars generally spatially confined to drainages and associated proximal alluvial fans [49, 50]. In addition, landslides, including lahars, can occur at a volcano in the absence of an eruption.

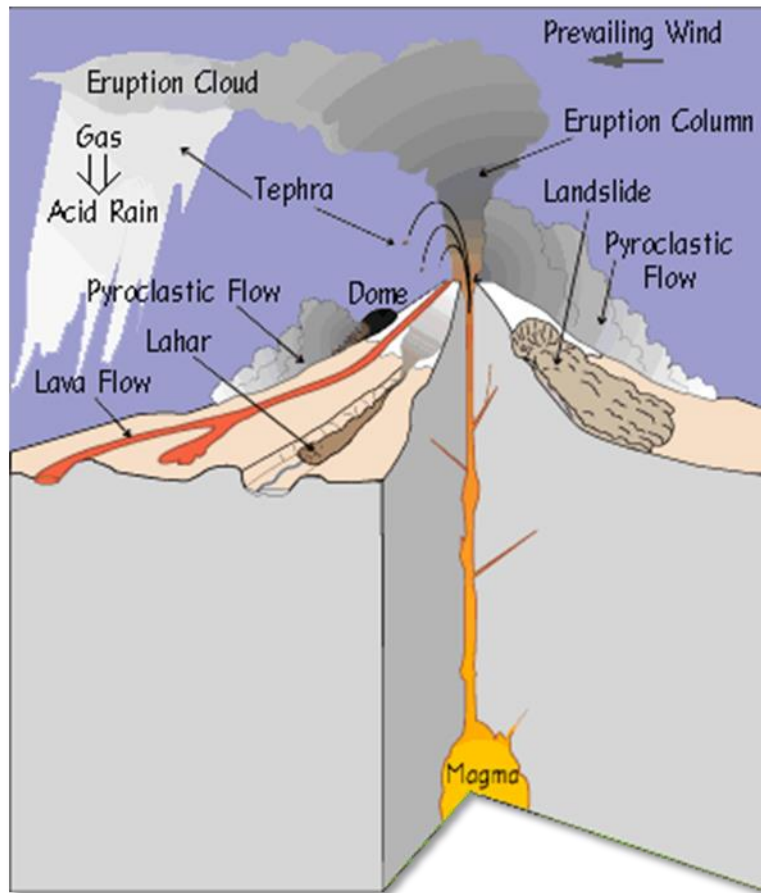


Figure 2-10 Illustration of typical volcanic processes [49]

2.3.7 Expansive/Collapsible Soil Hazard

Expansive surface and near-surface soils or soft rock may experience considerable volume change, usually related to a seasonal increase or decrease in soil water content [51]. Such soils are also known as expansive or swelling clays and may have documented swelling/expansion of 8 to 46 percent and measured swelling pressures of nearly 40 psi (2.8 kg/cm²) [52]. Structures/facilities located or buried in expansive clay (e.g., pipelines, tunnels, culverts, etc.) may be subjected to large magnitudes of lateral swelling pressures. The lateral swelling pressures may result in damage even with little evidence of vertical swelling [53]. Each year in the United States, expansive soils cause about \$2.3 billion in damage to houses, other buildings, roads, pipelines and other structures [54, 55]. Expansive soils are often associated with clay minerals (e.g., smectite-montmorillonite or bentonite) derived or chemically weathered from clay-rich sedimentary rock (shale), or igneous rock such as volcanic ash [54].

Collapsible soils are those that are susceptible to large volumetric changes/strains when they become saturated [56, 57]. The collapsing soils can result in large differential settlements that

can reduce the serviceability of structures and infrastructure [56]. Loose soils, such as wind-blown (aeolian) loess are most susceptible to collapse, and the amount of collapse is dependent on the relative density and thickness of the deposit [57].

2.3.8 Shallow Groundwater Hazard

Shallow groundwater can result in pipe buoyancy if not identified and mitigated [40, 58]. Fluctuating shallow groundwater may also adversely affect pipelines that are not designed to address this hazard by putting the pipe into cyclic stress conditions associated with the continued rise and fall of groundwater elevation. Pipe buoyancy, including fluctuating shallow groundwater, may lead to adverse pipe buckling and bending. Such shallow groundwater fluctuations may occur where agricultural land is seasonally irrigated. Shallow groundwater could also contribute to soil liquefaction under strong earthquake shaking depending on the type and nature of the soil. Rizkalla [5] provides a detailed discussion of the causes of, and mitigation for pipeline buoyancy. Seasonally saturated soil can also be a risk factor for stress corrosion cracking.

2.3.9 Glacier and Permafrost Hazard

Permafrost hazards in North America are generally geographically constrained to northern arctic latitudes and higher elevation alpine/mountainous regions. Potential permafrost hazards may be triggered or exacerbated by warming related to climate change or man-caused ground disturbance [59]. Potential permafrost hazards to pipelines, whether in arctic or alpine regions include [60, 61, 59]:

- Permafrost and glacier-related floods which may lead to pipeline exposure (breaching of moraine lake dams, failure of temporary dams, growth and breaching of thermokarst lakes, enhanced runoff from melting permafrost, glacier outburst, seasonal changes in glacier runoff)
- Glacier advance, surge and retreat which may cover or uncover pipelines
- Permafrost-related landslides (periglacial debris flows, rockfall along a rock glacier front, rapid or very slow movement of frozen debris-lobes, deep-seated landslides triggered by permafrost thawing; landslides are discussed in Sections 2.3.1 and 2.4.1)
- Permafrost thaw settlement, subsidence and heave (subsidence/settlement discussed in Sections 2.3.2 and 2.4.2)

2.4 Description of Potential Landslide and Settlement/Subsidence Geologic Hazards

The detailed focus and discussion in this section is on landslide and subsidence/settlement hazards with descriptions of the types, nature, location, extent, magnitude, and potential amounts and rates of movement of the hazards. The potential primary physical effects on a pipeline by each hazard are also described as part of each hazard's physical description.

2.4.1 Nature and Effects of Ground Movement (Landslide) Hazards

2.4.1.1 Landslide Types, Processes, Triggering Mechanisms and Features

As defined previously, a landslide involves the downward, or downslope movement of a mass of soil or rock due to gravity. A landslide occurs when the downslope component of forces (driving forces) acting on the slope exceeds the resistance of the materials underlying the slope (resisting forces). Driving forces can be increased by changes to slope geometry (e.g., erosion or grading), or by increased loading on the slope (e.g., placing fill on the slope or earthquake shaking). Resisting forces can be reduced by mechanical and chemical weathering of the material underlying the slope (which weaken the material), and by increased/raised groundwater/pore water pressure levels in the slope.

Landslides may be shallow (at or near the ground surface; i.e., only a few feet thick) or they may be deep-seated (several tens to hundreds of feet thick), and may occur extremely rapidly, in seconds, minutes or hours, or as extremely slow, on-going processes occurring over months, years and centuries. Temporal physical changes to the environment such as storms, earthquakes, undercutting and erosion by streams, and/or activities of humans can initiate or trigger landslides. The stability of a slope is directly related to the:

- Material properties of the soil and rock in the slope,
- Surface and groundwater/pore water conditions,
- Slope geometry, and
- State of stress and stress history of the slope

Landslide Types and Processes

Landslides can be organized into different types based on the form or type of movement and on the soil and/or rock material that makes up the landslide [22]. In general, and as defined by Cruden and Varnes [25] and Highland and Bobrowsky [22], there are five basic landslide movement types which include: fall, topple, slide, spread and flow. These basic movement types are illustrated on Figure 2-11.

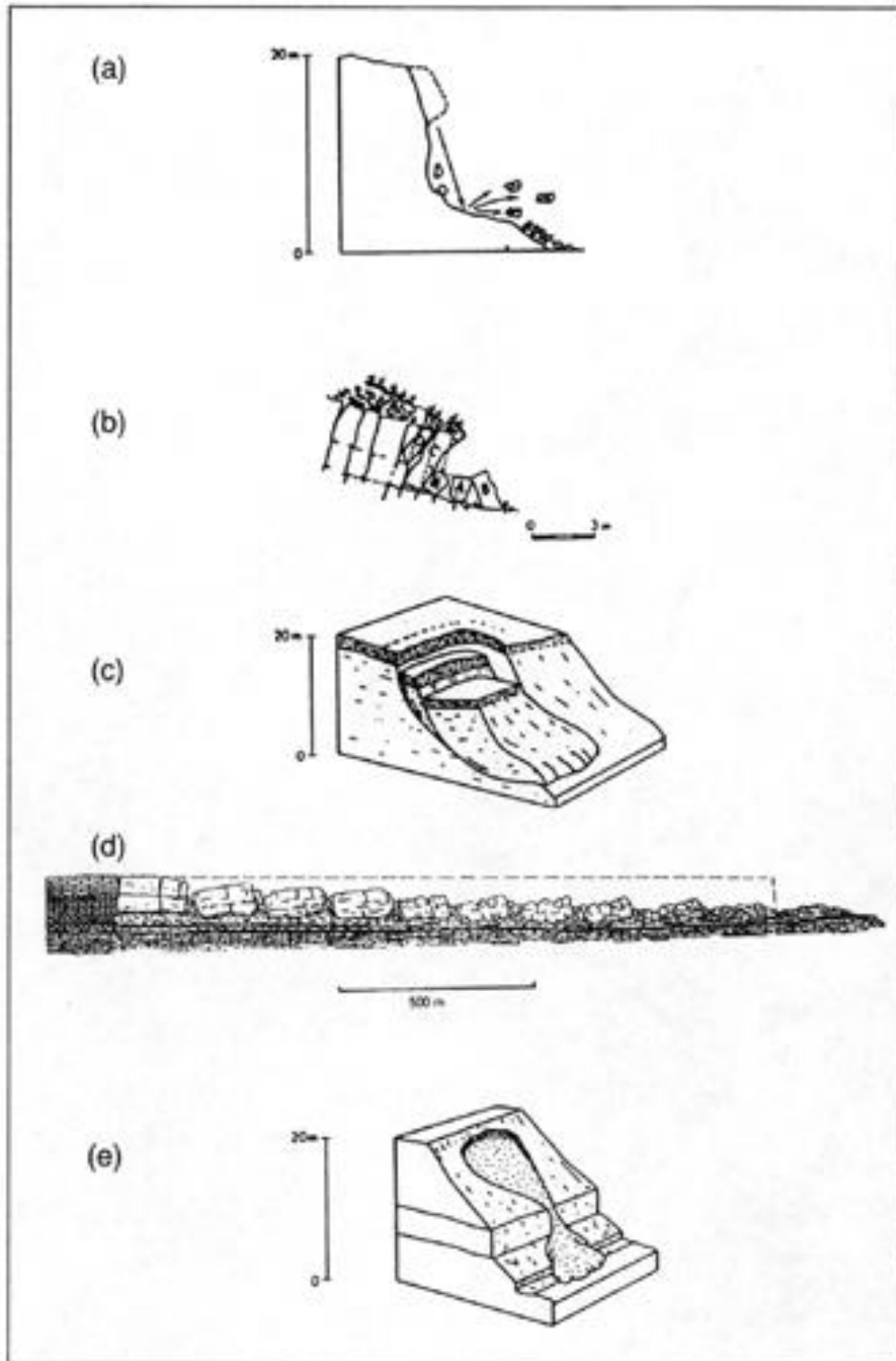


Figure 2-11 Basic landslide movement types from [25] (a) fall; (b) topple; (c) slide (rotational slide shown); (d) spread; (e) flow.

Falls occur as a detachment of soil or rock from a steep slope on a surface from which little or no shear displacement takes place. After detachment, the material descends by free falling, bouncing or rolling. Except where the displaced landslide mass is undercut (e.g., streams or waves), a fall will be preceded by small sliding or toppling, and the movement of falls is typically very rapid to extremely rapid [25]. Extremely rapid flows of dry debris caused by large falls and slides are commonly referred to as rock-fall avalanches or rock avalanches by many landslide practitioners [25].

Topples are the forward rotation out of the slope of a mass of soil or rock about a point or axis. Topples commonly occur in basalt columns or metamorphic and sedimentary rocks with steeply dipping joints, metamorphic foliation or bedding [25].

Slides are the downslope movement of a soil or rock material which occurs primarily on surfaces of rupture, or on thin zones of intense shear strain [25]. Slides typically occur either as translational slides, where the zone of rupture is planar or undulating and sliding is out over the original ground surface, or as rotational slides, where the surface of rupture is curved. Slides may also occur with a combination of translational and rotational movements known as a compound slide [25]. Rotational slides are often referred to as slumps by some practitioners but it is recommended that the term “slump” not be used when describing landslides because there is no widely accepted definition for this ambiguous term. In some geographic areas slides are colloquially referred to as “slips.”

Spreads are defined by Cruden and Varnes [25] “as an extension of a cohesive soil or rock mass combined with a general subsidence of the fractured mass of cohesive material into softer underlying material.” Spreads usually occur on very gentle, low-angle slopes, or almost flat terrain where a stronger upper layer of rock or soil undergoes lateral extension and moves along an underlying softer, weaker layer [22]. Spreads can result from liquefaction or from softer material squeezing out from underneath a harder more cohesive material. Liquefaction resulting from shaking due to seismic events commonly triggers spreads [25].

Flows are a spatially continuous movement in which there is significant internal deformation, and the material behaves like a viscous fluid. There is a gradational transition from slides to flows, depending on such variables as water content, mobility, and evolution of the movement. Slides can evolve into extremely rapid flows as a displaced material loses cohesion, gains water or encounters steeper slopes [25]. The term “flow” can encompass landslide events such as debris avalanches, debris flows, debris torrents, lahars and earth flows.

Cruden and Varnes [25] classify the type of material in a landslide as:

- *Bedrock (Rock)*, a hard or firm mass that was intact and in its natural place prior to being displaced,
- *Debris*, a coarse soil material in which between 20 and 80 percent of the particles are gravel-sized or larger, and the remainder are sand-size or smaller; or
- *Earth*, a fine soil material in which 80 percent of the particles are sand-sized or smaller.

Table 2-1 lists the typical landslide types, and their names based on whether they are primarily made up of bedrock, coarse soil (debris) or fine soil (earth).

Table 2-1 Landslide movement types and landslide classifications/names based on material (modified from [25] and [23])

Type of Movement	Type of Material		
	Bedrock	Predominantly Coarse Soil (Debris)	Predominantly Fine Soil (Earth)
Fall	Rock fall	Debris fall	Earth fall
Topple	Rock topple	Debris topple	Earth topple
Slide (rotational, translational)	Rock slide	Debris slide	Earth slide
Spread	Rock spread	Debris spread	Earth spread
Flow	Rock flow	Debris flow	Earth flow
Complex (combination of two or more principal types of movement)			

Landslide movement and landslide material types form the basic nomenclature for classifying landslides. Landslides are also classified by the use of the following descriptors [25]:

- Activity state (e.g., active, suspended, reactivated, dormant, inactive),
- Spatial distribution and how they are moving (e.g., advancing, enlarging, etc.),
- Style (e.g. single and multiple landslides, complex, composite and successive),
- Rate of movement (e.g., slow to extremely rapid, see below), and
- Water content.

As an example, a landslide may involve more than one type of movement such that it could be described as a “complex, extremely rapid, dry, rock fall-debris flow” [25].

With the exception of falls (which can have instantaneous, short-term velocities of hundreds of miles/hour), the velocity of landslide events can vary from fractions of an inch per year to feet per second, depending on the landslide movement type, the properties of the soil and rock slope, the water content, the slope angle and the triggering event [25]. Extremely slow movement (fractions of an inch per year) is often referred to as “creep” or soil creep. Table 2-2 lists typical landslide velocities, and the common landslide movement types that are associated with the typical velocities for a landslide velocity classification proposed by Cruden and Varnes [25]. The ability to mitigate the adverse effects of landslide movement becomes more viable the slower the landslide velocity. Velocity classes 1, 2 and 3 have low enough rates of movement that, depending upon the type and nature of the facility or structure at risk, landslide mitigation may be possible (Table 2-2). In addition, initiation of fast moving landslides would not likely be detected in time to attempt stabilization or mitigation.

Table 2-2 Proposed landslide velocity scale (modified from [25] and [22])

Velocity Class	Typical Velocity	Description	Common Landslide Types
7	>5 m/sec	Extremely Rapid	Falls, Topples, Debris Flows
6	3 m/min to 5 m/sec	Very Rapid	Falls, Debris Flows
5	1.8 m/hr to 3 m/min	Rapid	Falls, Debris Flows, Earth Flows, Slides, Spreads
4	13 m/month to 1.8 m/hr	Moderate	Slides, Earth Flows, Spreads
3	1.6 m/yr to 13 m/month	Slow	Slides, Earth Flows, Spreads
2	16 mm/yr to 1.6 m/yr	Very Slow	Slides, Earth Flows, Spreads
1	<16 mm/yr	Extremely Slow	Topples, Slides, Flows

The most common landslides, as classified by movement type and material type that appear to affect pipeline systems in North America include: rock fall, translational rock slide, rotational and translational debris/earth slides, debris flow, earth flow, and debris/earth spreads. Soil creep (considered a slow earth flow) is also often a recognized slope movement hazard on slopes traversed by pipelines. Examples of these more common landslides are described and illustrated in the following paragraphs.

Rock falls may result in large blocks of rock impacting the ground surface as illustrated in Figure 2-12 and Figure 2-13. A rock fall which occurs on a steep, or vertical rock slope can result in large rock blocks which may fall uncontrolled directly to the ground surface, or bounce and impact the ground surface damaging surface structures and imparting significant loads and stress to the near subsurface.

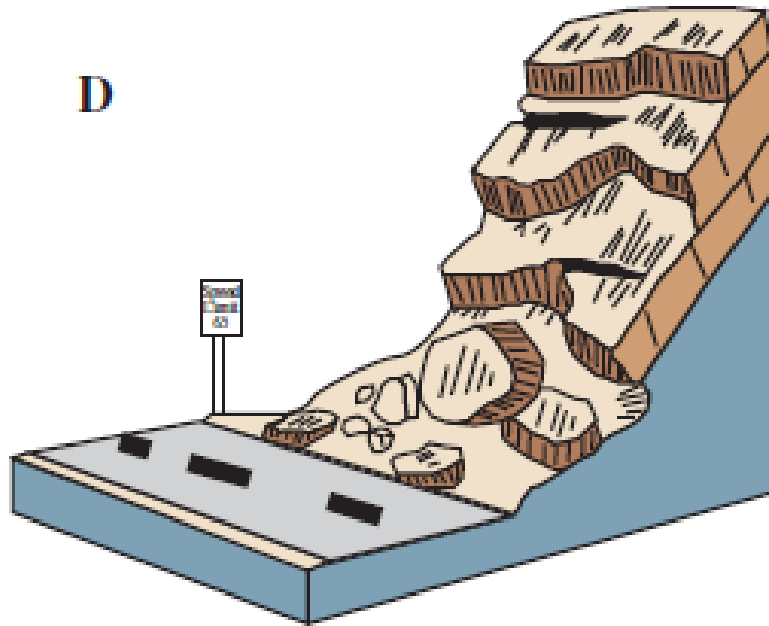


Figure 2-12 Schematic of a rock fall [23]



Figure 2-13 Rock fall blocks on highway SR 20 in Washington (Source: WSDOT, Year: 2011)

Translational rock, debris and earth slides are some of the most common landslide types world-wide [22]. They move downslope along a relatively planar failure surface (e.g., faults, joints, bedding surfaces, contact between rock and soil, permafrost layer), with little backward rotational movement, and they may extend over long distances [22] (Figure 2-14 and Figure 2-15). Translational slides are generally shallower than rotational slides, with a depth to length ratio less than 0.1 [22]. The movement of translational slides ranges from extremely slow to rapid (Table 2-2). In many circumstances the translational movement's displaced mass can break up and transition into a flow type movement. The material in a translational slide may vary from earth to slabs of bedrock.

Very slow to extremely slow translational rock/earth slides are common in river valleys inclined into clay shales and other deposits containing flat or shallowly-dipping weak layers of rock or earth. The rupture surface is typically flat or shallowly dipping into a river valley (refer to Figure 2-16). These translational slides are deep-seated and typically quite large (up to several miles in length and width). Pipelines typically cross these features when they were not delineated or recognized during the initial planning and construction of the pipeline. Miller and Cruden [62] provide an example of a large translational landslide and associated river dam.

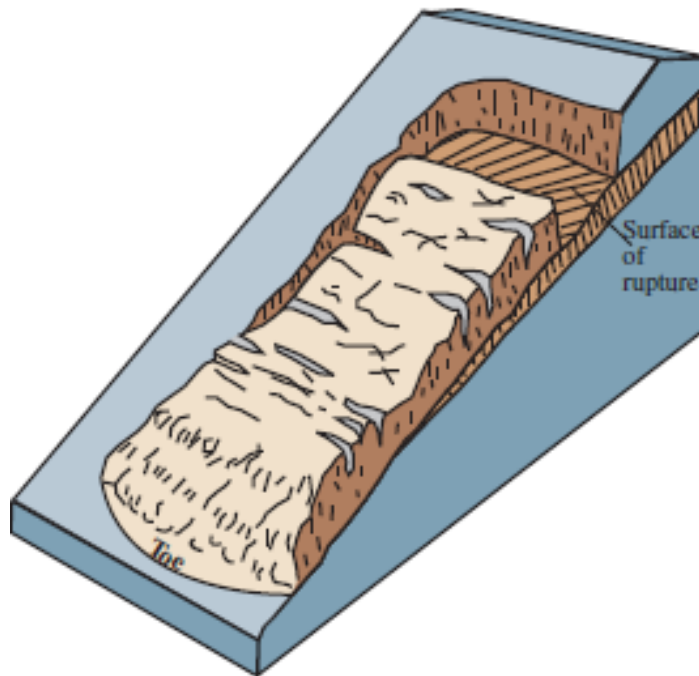


Figure 2-14 Schematic of a surficial translational earth slide [23]



Figure 2-15 Example of an ancient translational rock slide on a steep slope in dipping, bedded basalt bedrock in eastern Washington and which transitioned into a rock/debris avalanche/flow (Photo by: D. West, Year: 1977).

Rotational rock, debris and earth slides exhibit upward-curved rupture surfaces, and the movement of the landslides is generally rotational about an axis that is parallel to the contour of the slope [22] (Figure 2-17 and Figure 2-18). Rotational slides form concave topography in the head area and convex topography in the zone of accumulation in the lower portions of the slide. The slide mass may move as a coherent body with little internal deformation, with the upper, head portions of the mass moving vertically downward, and exhibiting backward tilting. Rotational slides are typically associated with moderate to steep slopes (e.g., 20° to 40°) but can occur on shallower slopes, they involve relatively homogenous material, and the surface of rupture has a depth-to-length ratio ranging from 0.3 to 0.1 [22]. The complex La Conchita rotational earth/debris slide-earth flow in California (Figure 2-18) exhibited backward tilting of the landslide mass and also maintained relatively coherent material in the mass. The velocity of rotational slides may be extremely slow to rapid (Table 2-2).

Debris flows are a form of very rapid to extremely rapid landslide movement (Table 2-2) that are saturated and flow downslope essentially as a slurry on steep slopes and in steep gullies or canyons [22] (Figure 2-19 and Figure 2-20). They may be prevalent on steep slopes denuded by fire, drought or logging and which are also subject to intense rainfall events. The movement of debris flows is generally shallow with thin dimensions relative to the long axis of the flow run-out, and the debris usually terminates beyond the toe of the slope in fan-like lobes (Figure 2-19 and Figure 2-20).



Figure 2-16 Deep seated very slow translational earth slide in Cretaceous clay shale bedrock in the McKay River Valley, northeastern Alberta. The inset is a schematic cross-section through the slide (Photo by: D. Dewar, Year: 1996).

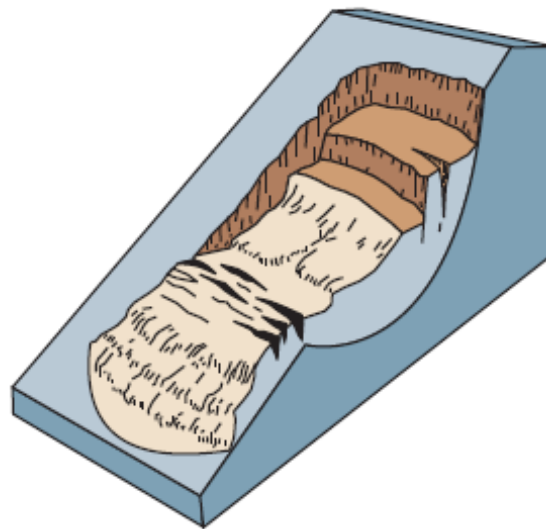


Figure 2-17 Schematic of a rotational earth slide with an earth flow at the toe [23]



Figure 2-18 The 1995 La Conchita complex rotational earth/debris slide-earth flow in (Photo by: R.L. Schuster, USGS, Location: California, Year: 1995)

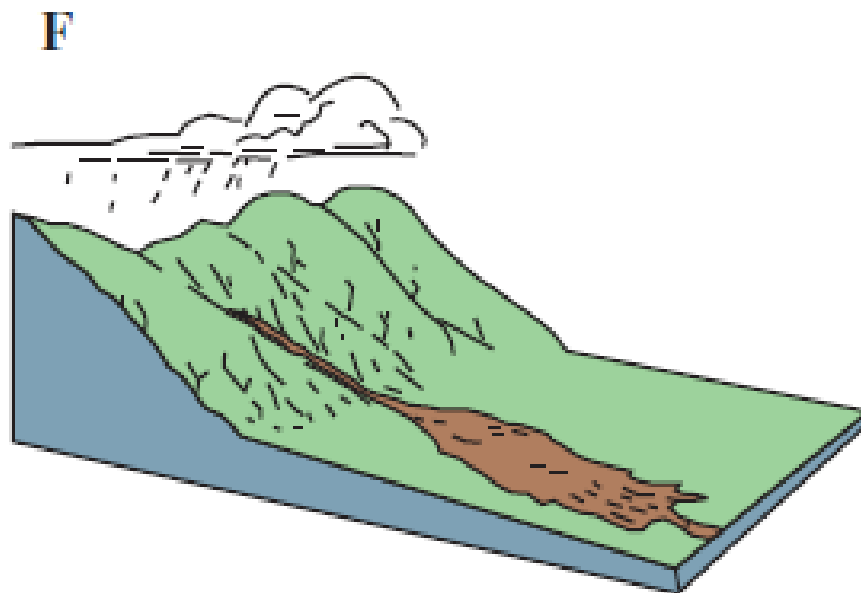


Figure 2-19 Schematic of a debris flow [23]



Figure 2-20 Debris flow in steep, forested terrain (Photo by: D. West, Location: Western Washington, Year: 2006)

Earth flows commonly have a characteristic hourglass shape [23] (Figure 2-21 and Figure 2-22). The material in the zone of depletion/source area becomes liquefied and runs out downslope forming a bowl-like depression in the zone of depletion/source area, and a fan-shaped run-out in the zone of accumulation/deposition area. As the term implies, earth flows by definition involve fine grained material. However, the term is commonly applied to landslides with larger-sized material including rock debris. For example, the earth flow of Figure 2-22 involved bedrock debris broken by landslide movement. Earth flows may be very slow to rapid (Table 2-2).

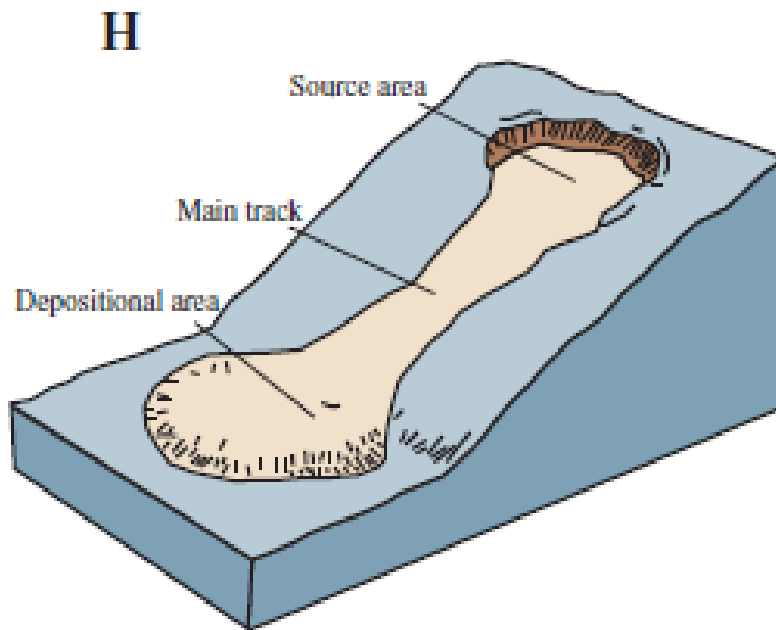


Figure 2-21 Schematic of an earth flow [23]



Figure 2-22 Earth flow along the Columbia River in Washington; the landslide occurred along a weak sedimentary interbed in the nearly horizontal Columbia River basalt and flowed through a drainage channel to spread out downslope. (Photo by: D. West, Year: 1995)

Soil creep (slow earth flow) consists of the imperceptibly slow, steady downslope movement of generally shallow, slope-forming soil or rock [22] (Figure 2-23 and Figure 2-24). The occurrence of creep may be seasonal (associated with seasonal saturation of the soil layer on slopes), continuous, or progressive where it may lead to landslide displacement [22]. Creep may be regional in extent or localized. The velocity of creep (a slow earth flow) is extremely slow to very slow. Creep generally occurs shallower than typical pipeline burial depths, and thus rarely affects buried pipelines. In forested areas, creep is commonly expressed in the formation of “pistol-butted” tree trunks as illustrated in Figure 2-25.

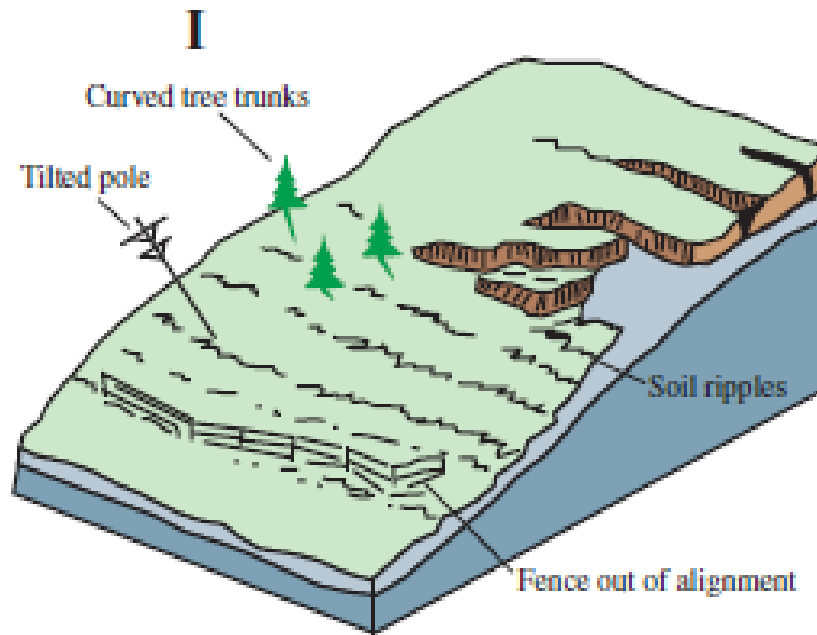


Figure 2-23 Schematic of the surface effects of soil creep [23]



Figure 2-24 Shallow soil creep (extremely slow earth flow) evident in vegetation on clayey silt till slope (Photo by: D. Dewar, Location: North central British Columbia, Year: 1998)



Figure 2-25 Pistol-butted tree trunks on a slope in northern California. The curved bases of the tree trunks are evidence of the very slow to extremely slow downslope flow movement (soil creep) of the shallow, near-surface soil. In alpine environments, the curved trunk may also be influenced by snow loads. (Photo by: D. West, Year: 2013)

Lateral spreads are distinctive because they typically occur on very gentle slopes or nearly flat terrain where a more competent upper layer undergoes extension and moves above a weaker/softer underlying layer [22, 23] (Figure 2-26 and Figure 2-27). Lateral spreads commonly occur where soil liquefies during seismic shaking or where underlying layers flow. The softer material may subside, translate, rotate, disintegrate, liquefy and/or flow. Lateral spreads resulting from liquefaction commonly require shallow groundwater in combination with granular soil (sand, silt and gravel) and strong earthquake shaking. Evans and Brooks [63] discuss quick clay, i.e., lateral spread landslides in sensitive glaciomarine clays which are common in previously glaciated areas adjacent to oceans. An example of a quick clay landslide is shown in Figure 2-28. The velocity of spreads may be very slow to extremely rapid (Table 2-2).

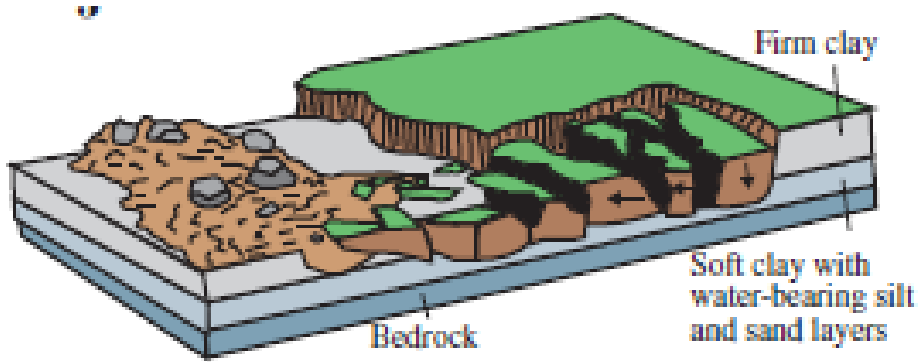


Figure 2-26 Schematic of a lateral spread [23]



Figure 2-27 Lateral spread landslide triggered by the 1983 Borah Peak, Idaho earthquake fault rupture and strong earthquake shaking (Photo by: D. West, Year: 1986)



Figure 2-28 The 1993 Lemieux Slide near Ottawa, Ontario. A rapid retrogressive lateral spread triggered by liquefaction of sensitive marine clays. [63]

Landslide Triggering Mechanisms

The common causes or triggers of landslides are listed in Table 2-3. The basic origins of these triggers can be geological, morphological, physical, or human-caused. Many times, the cause or trigger of a landslide is not a single thing, but is the result of several triggering mechanisms. Experience along a number of pipeline systems in North America indicates that there is a fairly common subset of triggering mechanisms which have caused landslides that have affected the pipelines. For reference, these common triggering mechanisms are in italics in Table 2-3.

Table 2-3 Common cause/triggers of landslide movement (modified from [25] and [23])

Cause/Trigger Category	Cause/Trigger (<i>Italics indicate common triggers</i>)
Geological	<ul style="list-style-type: none"> • <i>Weak rock or soil</i> • <i>Sensitive rock or soil</i> • <i>Weathered rock or soil</i> • Sheared, broken rock or soil • Jointed/fissured rock or soil • Adversely oriented rock structure • <i>Contrast in groundwater permeability</i> • <i>Contrast in soil stiffness</i>
Morphological	<ul style="list-style-type: none"> • Tectonic or volcanic uplift • Glacial rebound • <i>Fluvial (stream) erosion of slope toe</i> • Wave erosion of slope toe • Glacial erosion of slope toe • Erosion of lateral margins of landslide • Subsurface erosion (piping, dissolution) • Deposition loading of slope or slope crest • <i>Vegetation removal (fire, drought)</i>
Physical	<ul style="list-style-type: none"> • <i>Intense rainfall</i> • <i>Rapid snowmelt</i> • <i>Prolonged, exceptional precipitation</i> • <i>Elevated groundwater</i> • Rapid drawdown (floods and tides) • <i>Earthquake shaking</i> • <i>Volcanic eruption (1980 eruption of Mt. St. Helens)</i> • <i>Thawing of permafrost</i> • Freeze-thaw weathering • Shrink-swell weathering
Human-caused	<ul style="list-style-type: none"> • <i>Excavation of slope or slope toe</i> • <i>Loading of slope or slope crest</i> • <i>Drawdown (reservoirs)</i> • <i>Deforestation (clear-cutting, development)</i> • <i>Irrigation (domestic, agricultural)</i> • <i>Drainage modifications</i> • Mining • Artificial vibration (including blasting) • <i>Water leakage from utilities</i>

Landslide Features

Landslides have recognizable physical/geomorphic features that are used to identify the type of landslide and to document the dimensional, physical and geometric characteristics of a particular landslide [25]. The individual features help to describe and understand the location, nature, extent (laterally and vertically), and magnitude of potential landslide effects on a pipeline. The typical features of a landslide (complex earth slide-earth flow) are illustrated in the block diagram of Figure 2-29, and the La Conchita landslide in California provides a natural example of a landslide with these features (Figure 2-18).

Almost all landslides have a zone of depletion where the movement initiates, and from which the landslide mass/material moves downslope, and a zone of accumulation downslope to which the landslide mass moves (Figure 2-29). Thus, there is erosion (loss) of slope material in the zone of depletion and deposition of material in the zone of accumulation. There are lateral limits to a landslide that are termed the flanks, and looking downslope, there is a right flank and left flank, which typically form lateral scarps oriented down the fall line of the slope in the zone of depletion (Figure 2-29). There is a main scarp at the upper limit of the landslide, alternatively and more commonly termed the head scarp, which is oriented across the slope (Figure 2-29). The main body of the landslide is in the zone of depletion, while the foot or toe is in the zone of accumulation. There is often back tilting and internal deformation of the main body of the landslide which may produce transverse scarps and closed depressions that could form sag ponds in larger landslides, and the main body, as well as the toe may exhibit hummocky (rumpled and disturbed) terrain. Transverse cracks may form at the transition from the main body to the toe, and radial cracks may form in the toe area. Crown cracks (tension cracks) may also be present behind or upslope of the main scarp indicating possible enlargement of the landslide through retrogression of the main scarp.

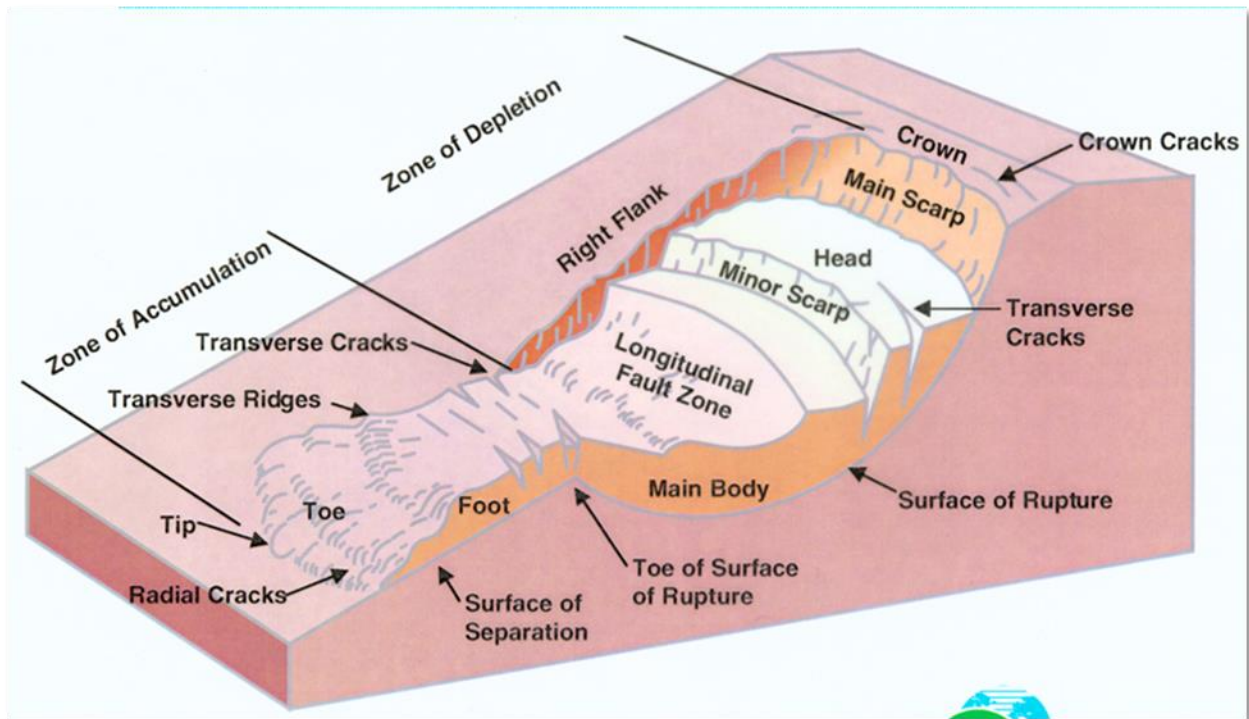


Figure 2-29 Typical physical and geometric features of a landslide (modified from [64] and [23])

2.4.1.2 Potential Effects of Landslide Movement on Pipelines

The potential effects of landslide movement on a pipeline will depend on a number of factors including:

- Pipe burial depth (including any above-ground pipe)
- Pipe diameter, wall thickness, grade of steel, specification/quality of welds, and coating type
- Presence of interacting anomalies
- Dimensions and geometry of the pipe trench, and the material properties (e.g., grain size, grain/particle shape, consistency/density, moisture content and strength) of pipe trench backfill
- Landslide type, dimensions, material properties, moisture content, and velocity
- Landslide depth relative to pipe burial depth
- Pipeline crossing location on or adjacent to landslide, and
- Pipeline orientation relative to the direction of landslide movement and landslide mass deformation (axial, transverse, oblique)

Experience with landslides and pipelines in North America indicates that there are eight common scenarios for a landslide to potentially damage or rupture a pipeline. These eight common pipeline/landslide interaction scenarios are summarized below, and the first seven are illustrated on Figure 2-30.

1. Sliding or slow flow movement parallel (axial) to the pipe orientation (refer to Figure 2-30[1] and Figure 2-31). The pipe would likely be in tension in the main scarp and main body areas and in compression in the toe area of the landslide. Where the landslide occurs at the depth of burial of the pipeline, landslide and backfill material may be dragged across and along the pipe likely damaging the coating.
2. Discrete sliding or slow flow movement oblique to the pipe axis (refer to Figure 2-30[2]). Landslide-induced loading on the pipe generally depends on the skew angle of the oblique movement relative to the pipeline.
3. Discrete sliding or slow flow movement perpendicular (transverse) to the pipe axis (refer to Figure 2-30[3] and Figure 2-32). Transverse movement typically puts the pipe in bending or shear at the slide flanks, and, depending on the nature of the movement, may put the pipe in tension in the body of the landslide as the landslide mass extends downslope.
4. Discrete sliding or flow movements exposing or free-spanning a pipeline by sliding/flowing around or from under the pipe and removing support. Exposure can be either perpendicular to movement (refer to Figure 2-30[4] and Figure 2-33) or parallel (refer to Figure 2-30[1]).
5. Sliding or flow movements depositing material on top of a pipeline (refer to Figure 2-30[5]). The effect on the pipe could be negligible, because the increase in effective stress and associated loading on the pipeline may be insignificant when compared to the actual strength of the pipeline. Operational access issues may occur depending on the depth of burial.
6. Rock fall, rock topple or debris flow impact-loading on an exposed, or above a buried pipeline (Figure 2-30[6]). Rock fall and rock topple onto an above-ground pipeline may result in damage to, or rupture of the pipeline, but have little or no effect on a buried pipeline depending on the depth of burial. However, if large rock fall blocks, similar to those illustrated in Figure 2-13 were to directly impact a ROW surface above a shallowly-buried pipeline, the pipe could be dented or ruptured.
7. Debris flow or earth flow movements exposing then hydro-dynamically failing a pipeline or failing the pipeline by having severe deformations in the zone below the landslide accumulation (refer to Figure 2-30[7] and Figure 2-34)
8. Secondary hydrotechnical effects of landsliding including:
 - a. Outburst flooding associated with the failure of landslide-dammed lakes or impoundment of water by landslide accumulation/deposits (e.g. translational slides or debris flows) as shown on Figure 2-35). Costa and Schuster, Miller and Cruden, DTec Consulting, and Guthrie et al [65, 62, 66, 67] describe formation, failure and potential hazards associated with valley damming as a result of landsliding.

- b. Channel avulsion associated with landslide accumulation/deposits, or due to debris floods or higher bed loads resulting from upstream landsliding (refer to Figure 2-6 for avulsion example).

Typically, as the complexity of the landsliding increases, the complexity of the loading on the pipeline will also increase. Every pipeline/landslide situation is unique given the number of variables that are considered and each landslide scenario should be assessed individually.

Landslide/Pipeline Interaction Scenario*	Schematic Plan View	Schematic Profile
1. Movement parallel to pipe axis		
2. Movement oblique to pipe axis		
3. Movement perpendicular to pipe axis		
4. Exposure or free span of pipe due to movements		
5. Deposition over pipeline		
6. Impact on pipe from rock fall/topple		
7. Flows hydro-dynamically loading pipeline		

Figure 2-30 Common landslide/pipeline interaction scenarios

Note: * Scenario number 8, secondary hydrotechnical landslide effects are not represented on Figure 2-30.

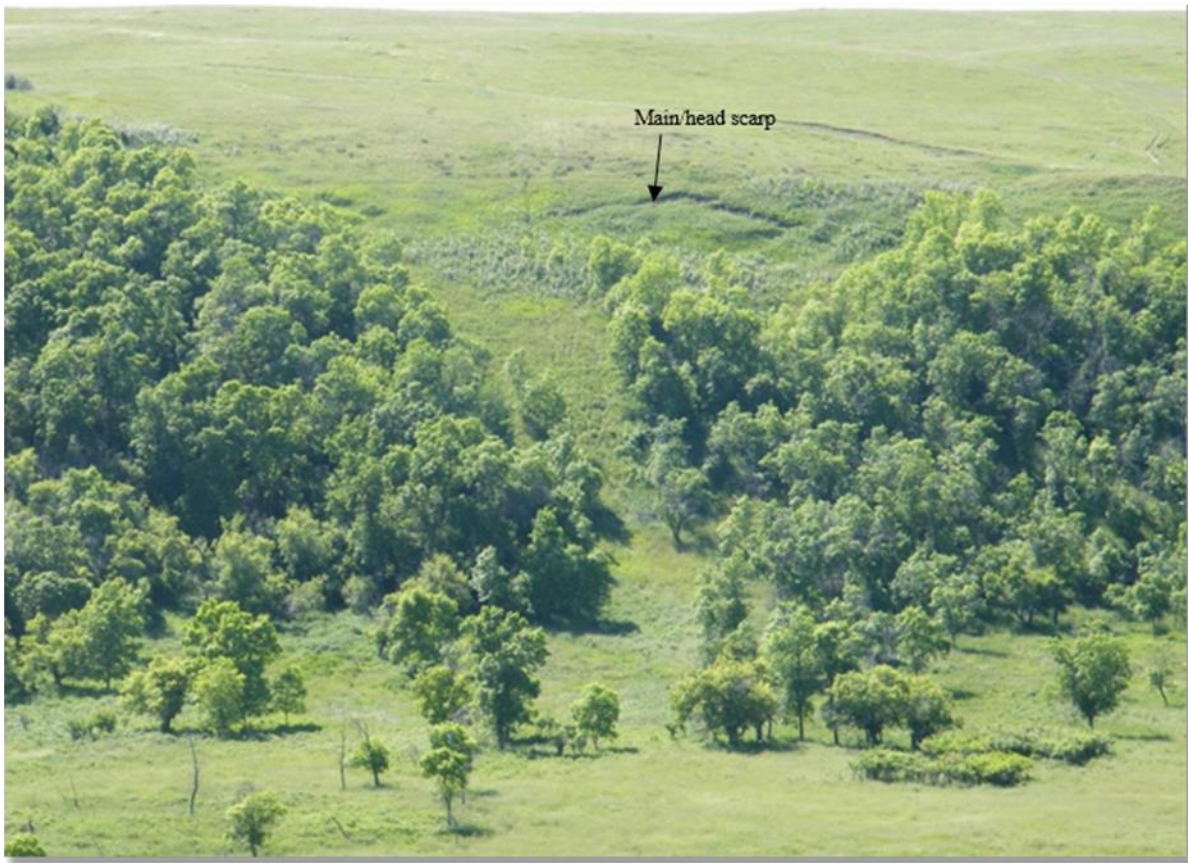


Figure 2-31 Shallow, very slow translational earth slide. Slide is moving parallel to pipeline axis. (Photo by: D. Dewar, Location: Saskatchewan, Year: 2011)



Figure 2-32 Pipeline bending associated with transverse downslope movement of large deep-seated, very slow moving translational earth slide. Both a 12-inch and 30-inch pipeline are bent by approximately 6.5 ft of landslide movement over the past 50 years. The fixed (stable) end is near the top of the photograph with movement from left to right. (Photo by: D. Dewar, Location: Central British Columbia, Year: 1998)



Figure 2-33 Exposed oil pipeline in the main/head scarp of a debris slide (Photo by: R. Wartlik, Location: Central British Columbia, Year: 1990)



Figure 2-34 Pipeline rupture on a 16-inch natural gas mainline, which is routed along the toe of a mountain slope at the Zymoetz River, as a result of a debris flow. Rupture occurred during the initial scouring of the existing alluvial fan, during the initial stages of the event and prior to deposition of debris. Note the extent of the burned area as a result of the rupture and ignition [68].



Figure 2-35 Stream diversion during high flow event that failed highway embankment exposing and free spanning 24-inch mainline. A debris flood clogged an undersized highway culvert directing water down the highway and across the pipeline ROW. A significant amount of the upstream sediment in the debris flood was derived from landslides higher in the watershed. (Photo by: D. Dewar, Year: 2011)

2.4.2 Nature and Effects of Settlement/Subsidence Hazards

2.4.2.1 Settlement/Subsidence Types, Processes and Triggering Mechanisms

Land subsidence is a gradual settling or sudden sinking of the Earth's surface resulting from the subsurface movement of earth materials (rock and soil) [9, 3]. More than 17,000 mi² (44,000 km²) in 45 states of the United States have been affected by surface subsidence [9, 3]. Ground subsidence contributes to permanent inundation of coastal lands because sea level encroaches into the settled areas; it aggravates watercourse flooding, alters topographic gradients, and ruptures the ground surface [3]. These changes to the ground surface can adversely affect buried pipeline systems.

The primary settlement/subsidence hazards that could affect a pipeline system include both naturally-occurring subsidence processes, and subsidence processes that are caused or triggered by human activity. The primary types of settlement/subsidence of the ground surface that could be hazards to, and affect pipeline systems include:

- Naturally-occurring processes
 - Subsurface dissolution of bedrock (limestone and dolomite [karst], evaporite [gypsum, halite or salt])
 - Thawing of permafrost (thaw settlement)
 - Soil piping
- Human-caused/triggered processes
 - Fluid withdrawal and aquifer system compaction (groundwater, oil and gas)
 - Collapse of underground mine openings (abandoned mines, solution mining, active coal mines [longwall, room and pillar])
 - Drainage of organic soil
 - Hydrocompaction of soil
 - Localized settlement/subsidence of pipe trench and pipe construction backfill

Naturally-Occurring Processes

The subsurface dissolution of bedrock is a naturally-occurring process that can be influenced by human activity. The dissolution typically occurs in soluble carbonate (e.g., limestone, dolomite) sedimentary bedrock, or in soluble evaporite (e.g., gypsum, salt) sedimentary bedrock. Carbonate dissolution occurs in slightly acidic water (either as rainfall on the ground surface or subsurface flow of groundwater) [69, 9, 27, 29, 70, 71, 72]. The dissolution of bedrock in the subsurface forms small to large voids or caverns that settle or collapse, producing subsidence/settlement features at the ground surface which are termed karst topography/terrain [70, 72]. The prominent surface subsidence features in karst terrain are sinkholes, which are closed depressions in the ground that have no natural external surface drainage [70, 71]. According to [70], about 20 percent of the United States is underlain by karst terrain. There are essentially three type of sinkholes produced from the dissolution of bedrock [71]. These sinkhole types are generally characterized on the basis of the presence and thickness of soil cover over the soluble bedrock, their relative size, the rate at which the sinkholes develop, and the severity of the subsidence effects of the sinkhole at the ground surface [70, 71]. The three types of sinkholes are listed below and briefly discussed in the following paragraphs.

- Dissolution sinkholes
- Cover-subsidence sinkholes
- Cover-collapse sinkholes

Dissolution sinkholes form where there is no, or only a thin soil cover (overburden) over carbonate or evaporite bedrock. Rainfall and surface water infiltrate through fractures and joints in the bedrock, which gradually dissolve the rock and carry it away in solution. This results in small, shallow surface depressions which may fill with water forming ponds (often called sag ponds) and wetlands. The voids underlying dissolution sinkholes are generally small, and may be filled with soil.

Cover-subsidence sinkholes involve thicker amounts of overburden over the soluble bedrock, and the soil is typically granular and permeable (e.g., sand) [71]. Dissolution of the underlying soluble bedrock results in voids below the soil cover, and the sandy, permeable soil spalls (moves) into the underlying voids forming a soil-filled depression (sinkhole) at the ground surface. Cover-subsidence sinkholes tend to form gradually over time [70]. Figure 2-36 shows a cover-subsidence sinkhole formed in gypsum, evaporite bedrock in the Andes of Argentina.



Figure 2-36 A cover-subsidence sinkhole formed from dissolution of evaporite bedrock (gypsum) in the Andes of Argentina. The sinkhole is about 80 ft diameter and 30 ft deep. (Photo by: D. West, Year: 2011)

Cover-collapse sinkholes can form abruptly, over a period of hours to a few days, and result in significant damage to surface and near surface infrastructure [71, 70, 27]. Cover-collapse sinkholes commonly occur where the overlying soil is clay-rich which allows for soil-bridging over a dissolution cavity/void in the subsurface bedrock. Eventually, the void suddenly breaches to the surface creating the sinkhole. Cover-collapse sinkholes may vary in size from as little as 3 ft diameter to several hundred feet diameter [70] (Figure 2-37 and Figure 2-38).



Figure 2-37 A cover-collapse sinkhole formed from collapse of a limestone dissolution cavern. (Source: AP photograph, Location: Winter Park, Florida, Year: May 1981)



Figure 2-38 A cover-collapse sinkhole formed in carbonate karst terrain. (Source: Reuters/Springer photograph, Location: China, Year: February 2013)

Human activities, such as groundwater extraction (which changes the groundwater flow regime), the re-direction of surface runoff associated with surface development, including pipeline construction (which changes the location and intensity of surface flows), the loading of the ground surface associated with surface development (building structures, pipeline construction), and mining, singly or in combination may accelerate or exacerbate the bedrock dissolution process and contribute to the formation of dissolution, cover-subsidence and cover-collapse sinkholes [9, 73, 74, 75, 76, 71, 27].

Karst terrains typically have surface subsidence features that are oriented or located depending on the underlying local bedrock structure in combination with the surface and groundwater regimes. The surface distribution of the features may appear to be relatively random or linear.

The thawing of permafrost is generally a natural, widespread process commonly confined to the arctic and subarctic regions of North America where continuous, discontinuous and sporadic permafrost are located [77]. Based on the mapping of [77], sporadic permafrost also exists in lower latitude alpine regions of the United States and Canada. Although a natural process, the thawing is being accelerated and exacerbated by climate change, which is resulting in warming

at the higher latitudes [77]. In addition, local permafrost thawing can be triggered, or accelerated by human activities such as pipeline construction and operation.

The thawing of permafrost results in thaw settlement, which does not occur uniformly, and creates a chaotic ground surface with small hills and wet depressions called thermokarst [77]. When thermokarst occurs beneath roads, houses, pipelines or airfields, their structural integrity is threatened [77]. Large-scale field research by [77] indicates that as much as 22 ft of subsidence, over a 26-year period, has resulted from thaw settlement. Thaw settlement can be attributed to [78]:

- Melting of ice-rich upper soil layers which reduce ice volume, causing the soil formation to compact.
- Soil consolidation with fluid expulsion, where melt water flows from the thawed zone and the soil contracts.
- Reduction of inter-granular pore water pressure when the phase change (ice to water) results in an increase of inter-granular stress and soil compaction.
- Reduction in soil formation stiffness as the permafrost thaws, where there is a loss of support provided by the pore ice.

Piping is defined as “subterranean erosion of surficial materials by flowing groundwater that results in the formation of tubular conduits due to the removal of particulate matter” [79]. When the soil material above the conduit collapses, sinkholes, and/or gullies can be formed at the ground surface.

Human-Caused/Triggered Processes

Of the human-caused or triggered subsidence/settlement processes, subsurface fluid withdrawal with aquifer system compaction, and collapse of underground mine workings appear to be the most common and geographically they affect extensive areas of North America. These two subsidence processes are described in detail below, while the remaining human-caused processes are only briefly addressed.

Subsurface fluid withdrawal and the resulting aquifer system compaction account for more than 80 percent of the identified surface subsidence in the United States and most of that subsidence is attributed to the exploitation of groundwater resources, while the remaining sources include the extraction of oil and gas [3, 9, 27]. According to [3], the withdrawal of the subsurface fluids from clastic sediments (coarse grained soil or rock) in the United States has permanently lowered the elevation of about 10,000 mi² (~26,000 km²) of land.

Permanent ground subsidence from subsurface fluid withdrawal occurs when there is a reduction in the fluid pressure in the pore spaces and fractures in the soil or rock, and the soil or rock compacts inelastically to fill the empty granular void space [9, 3]. From a geotechnical point of view, the lowering of the water table increases the effective stress in a soil which increases the overburden or vertical pressure which results in settlement. The aquifer system includes both aquifers (subsurface stratum capable of flowing and producing water) and aquitards (a water-saturated sediment or rock whose permeability is so low it cannot transmit any

useful amount of water). Both aquifers and aquitards undergo differing degrees of permanent compaction and deformation, but almost all of the permanent subsidence from aquifer system compaction is from the compaction of the aquitards [3].

The types of subsidence features at the surface associated with aquifer system compaction include broad regional elevation decreases and localized ground failures associated with fissures and surface faults [3, 9, 80, 81, 82, 34]. Regional subsidence is generally broadly distributed with small lateral (sub-horizontal) strains and low angles of slope tilt, even when associated with several meters of maximum vertical displacement in the center of the basin [3]. The broad subsidence generally does not affect pressurized or pumped pipelines (e.g., gas and oil) but can affect pipelines that depend upon gravity such as water supply pipelines and sewer lines [3].

Local concentrated extension and differential vertical displacement associated with fissures and faults, respectively, can affect pipeline infrastructure. In addition, fissures without discernible extension can expose pipelines and result in unsupported spans. Figure 2-39 and Figure 2-40 illustrate extensional and differential displacement earth fissures in Arizona and Nevada created by groundwater withdrawal and aquifer system compaction.



Figure 2-39 Earth fissure in Nevada at a mine facility with an above-ground mine process pipeline (Source: AMEC presented in 2004 ADOT workshop [83])



Figure 2-40 Horizontal separation and differential vertical displacement of about 1.5 ft (0.5 m) across an earth fissure in Arizona [83]

Earth fissures tend to occur along the margins of subsiding alluvial basins near exposed, or shallowly-buried bedrock, or over zones of laterally-changing sedimentary characteristics (facies changes), where land subsidence from groundwater withdrawal, water level lowering and aquifer system compaction have occurred differentially [83]. Sheng et al [34] note that the location, type, and magnitude of earth fissuring is influenced by several factors including the in-situ stress, pre-existing geologic structure and the depth/thickness of the aquifer from which withdrawal is occurring.

Using the results of 1976 to 1989 geodetic monitoring, Holzer [82] studied earth fissures in subsiding basins at three areas in Arizona, Nevada and California, and noted that they exhibited both horizontal extension and differential subsidence (displacement) across the fissures. The locations of the fissures are spatially associated with either subsurface bedrock highs within the aquifer system or with pre-existing tectonic faults [82]. Holzer [82] concluded that for the 13-year monitoring period, the differential subsidence across the fissures in Arizona ranged from about 1.6 to 2.8 in (41 to 71 mm), with total horizontal displacements ranging from about 0.2 to 2.2 in (5 to 56 mm), while the annual rate of opening of the fissures ranged from 30 to 120

microstrain/year. For another 9.8-mile-long (16-kilometer-long) earth fissure in Arizona, originally identified in 1949 and formally named the Picacho fault, the total differential displacement across the feature has been about 2 ft (0.6 m) [82].

Surface subsidence due to the collapse of underground mine openings is related to active mines and abandoned mines. The focus here is on active and abandoned underground coal mines because of their prevalence and geographic extent in North America. Active coal mining in North America, and elsewhere, employs two basic extraction methods which are room-and-pillar and longwall [37, 35, 41, 31]. Longwall mining is termed a high-extraction process where all of the coal is removed along a working face, and surface subsidence is planned, while room-and-pillar mining is a low-extraction process where only about 40 to 50 percent of the coal is removed (in modern mines), and subsidence is not expected or planned [41, 31]. Bauer [31] also notes that retreat mining is sometimes employed where most of the pillar supports of a room-and-pillar mine are removed, increasing extraction to about 80 to 90 percent of the coal.

In room-and-pillar mining (whether an active mine or abandoned), surface subsidence can occur above the mine (even though unplanned) due to failure of the mine roof, the pillars, or the mine floor [31]. Mine roof failures in room-and-pillar mines are not generally considered to be a cause of surface subsidence unless the mine is at a very shallow depth (e.g., less than 200 to 300 ft (61 to 91 m) depth), and the bedrock is thin and weak; then the surface manifestation of roof failure is small holes or pits [41, 31] (Figure 2-41 and Figure 2-42).

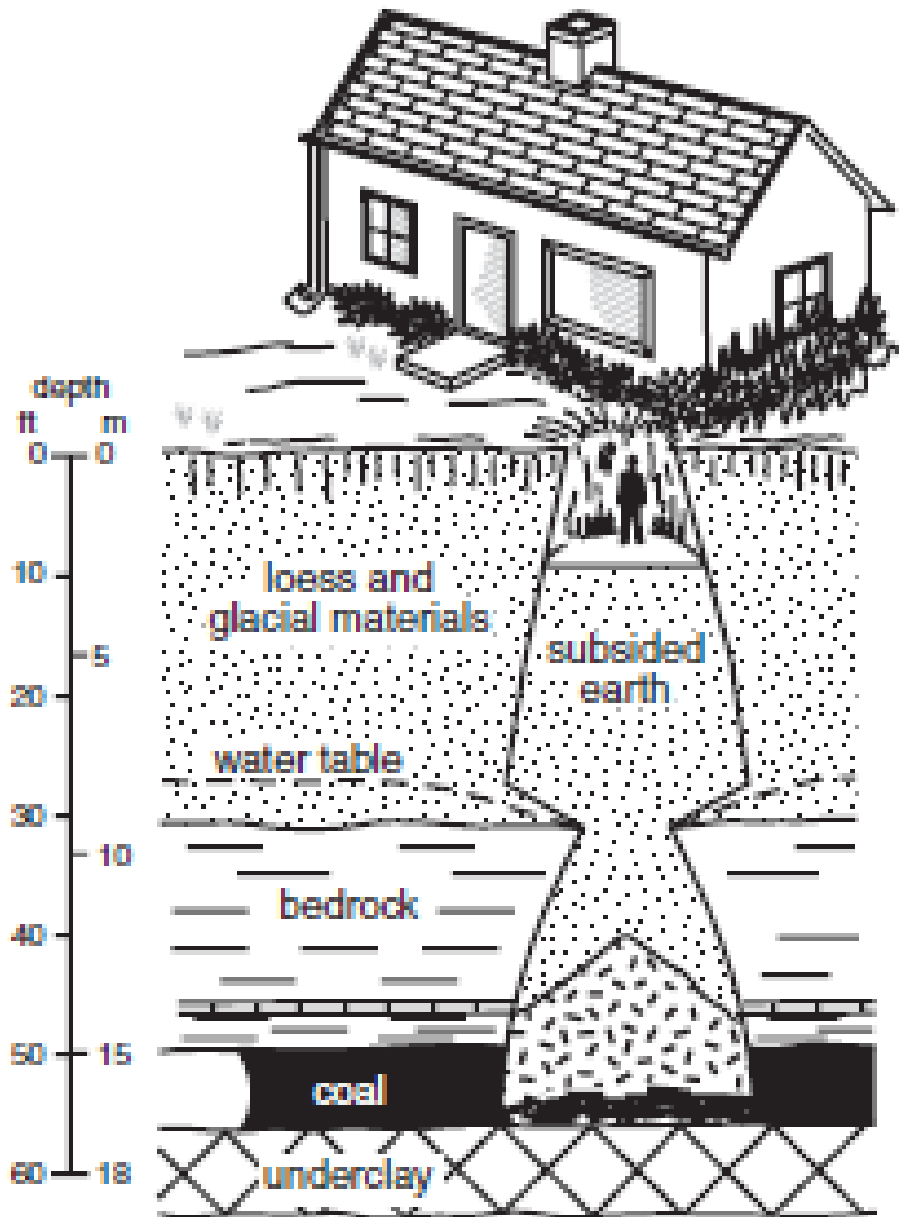


Figure 2-41 Diagram of coal mine pit subsidence [41]



Figure 2-42 Surface subsidence pit above a coal mine (Source: S. English, Location: Harrison County, West Virginia, Year: 1970)

While pillar failures are rare in modern room-and-pillar coal mining, floor failure is the most common cause leading to surface subsidence in Illinois [31]. Coal mines in Illinois commonly have weak claystone in the mine floors, and the vertical load of the overlying rock imparted on the bases of the pillars causes the claystone to squeeze into the rooms from under the pillars resulting in surface subsidence [31]. Figure 2-3 illustrates an example of surface subsidence above a room-and-pillar coal mine, and indicates that tensional stresses and cracks occur along the distal edges of the zone of subsidence and compressive stresses occur in the middle of the subsidence associated with the maximum vertical depression which may be several feet. The timing of subsidence associated with room-and-pillar coal mining may be a few years to decades or centuries [31].

In longwall mining, planned surface subsidence takes place essentially concurrently as the mining occurring at depth advances along the coal seam [31, 32, 35, 37]. In longwall mining, the roof of the mine collapses in a planned manner behind the working face as the face advances along the coal bed or seam. This zone of collapse progresses vertically upward toward the ground surface and its effective width increases laterally from the width of the mined area. The angle at which the subsidence extends away from the limit of mining is termed the angle of draw, and may be between about 10° and 45° from vertical depending on local geology, coal seam depth and longwall panel width [31, 35, 32, 37].

The surface movements associated with longwall mining are both vertical and horizontal; that is the ground drops vertically and moves horizontally toward the center of the trough of subsidence [31]. Gray and Bruhn, Dunrud, MSEC, and Bauer [37, 38, 32, 31] divide the primary types of surface subsidence movement and deformation associated with longwall mining into:

- Vertical displacement; which achieves its maximum amount above the central portion of the coal extraction area, and the amount of subsidence can be about 45 to 90 percent of the seam thickness
- Tilting; which is the difference in the amount of vertical movement within the subsidence trough; if tilt is uniform, it produces little surface damage; differential tilt, however, produces a curved surface with a higher potential for surface damage
- Horizontal displacement and strain; which produce tensile strains near the edges of the subsidence trough and compressive strains near the center of the subsidence trough; differential horizontal displacement produces damage to surface structures and can impose high longitudinal strains on pipelines and other linear structures.

Figure 2-43 schematically illustrates, in cross-section, the types and locations of these primary longwall subsidence deformation features. In Figure 2-43, the longwall mine is advancing from right to left at the working face.

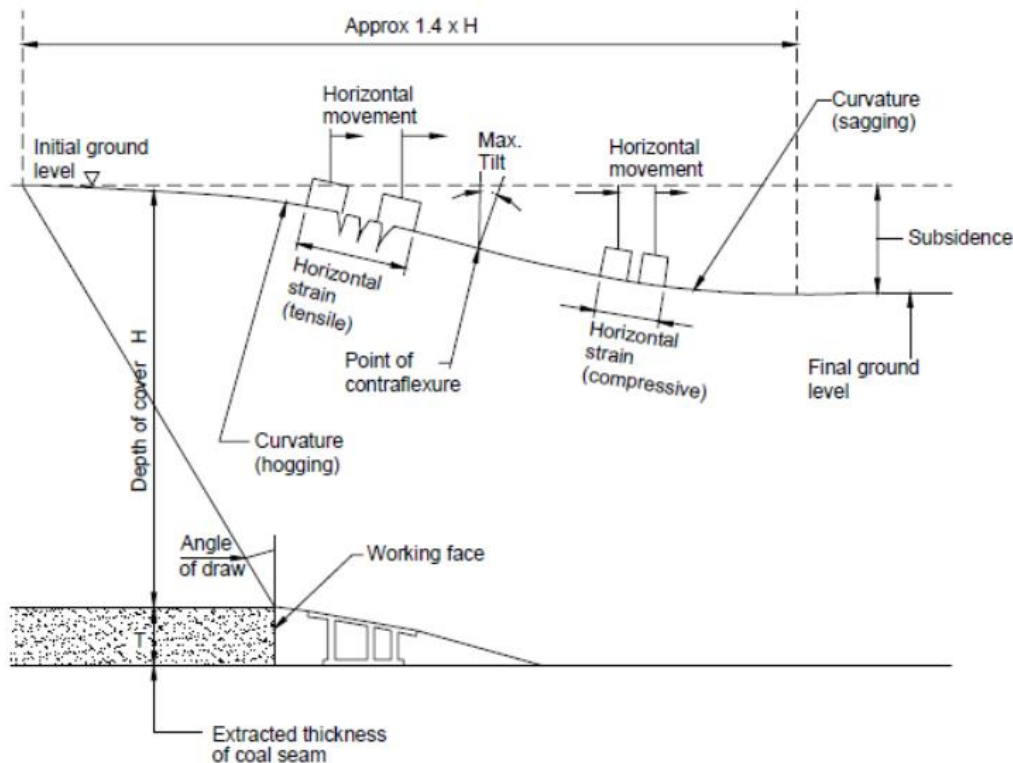


Figure 2-43 Subsidence deformation features associated with longwall mining [32]

The surface subsidence deformation features associated with active longwall mining are successive and wave-like (dynamic) as the working face of the mine advances laterally at depth. For example, and referring to Figure 2-43, as the working face approaches any given point, the surface will at first undergo tensile strain, then tilting as the working face passes underneath, followed by compressive strain after the face has passed, and finally maximum vertical subsidence of the ground surface. Figure 2-44 illustrates the effects of surface trough subsidence on Interstate 79 (I-79) that was above a longwall mine in Pennsylvania. The depth to the mine was about 600 ft (183 m).



Figure 2-44 Surface subsidence trough across I-79 in Pennsylvania located above a longwall mine. (Photo by: R. Turgeon, Year: 1982)



Figure 2-45 Graben at 30-inch pipeline over longwall mine in Pennsylvania

Typically, the surface subsidence deformation above a longwall mine occurs within the limits of the angle of draw (Figure 2-43), [37, 32]. Typical predicted amounts of total subsidence over a longwall mine (within the angle of draw) may approach 1.5 m (5 ft) [84], however, this may not be applicable for coal seam greater than 10 ft (3 m) thick. MSEC [84] also notes that predicted incremental and total tilt deformation may approach +6 mm/m and -7 mm/m, while incremental and total strain may exceed +1 mm/m and -1.6 mm/m (+0.1%/-0.16%). The width of cracking from tensile strain at the edges of the subsidence is dependent on the thickness of cover over the mine, but appears to vary from as much as 200 mm (8 in) with 50 to 100 m (165 to 330 ft) of cover to as little as 5 to 20 mm (0.2 to 0.8 in) with 200 to 600 m (660 to 2,000 ft) of cover. TEC [33], however, has reported tension cracks up to 50 cm (20 in) wide above a longwall mine in Australia.

Surface surveys at pipelines crossing longwall mines in Pennsylvania have recorded up to around 5 ft (1.5 m) vertical drop, and 3 ft (1 m) horizontal movement. Ground strains in the direction longitudinal to the pipelines, as calculated from changes in the surveyed locations of hubs installed at ~100 ft (30 m) intervals, have been as high as around +/-2%. Maximum

compressive strain occurred at the bottoms of valleys, suggesting significant down-slope soil movement coincident with mine subsidence.

Although the predicted and almost all of the measured surface deformation associated with longwall mining occur above the mined area and to a lesser extent outward within the angle of draw, there is also far-field surface deformation related to longwall mining such as horizontal valley closure and vertical “upsidence” (uplift) of valley bottoms, which may occur 1 to 2+ km (0.6 to 1.2+ miles) from the longwall mine panel and well outside the angle of draw [85, 32, 84, 86, 87, 88, 89]. Several examples of the far-field deformation effects from longwall mining in Australia and the United States (Pennsylvania) are discussed below. These examples come from the available literature, and are also anecdotal from the work conducted for pipelines in Pennsylvania.

The far-field movements associated with longwall mining were first noted in Australia about 20 years ago where horizontal movements of hundreds of millimeters have been recorded [89]. Although the mechanism of these movements is uncertain, possible explanations include one, or a combination of factors such as pre-mining stress relaxation, valley bulging, regional joint patterns, shearing of valley walls, and bedding plane shear failure [89].

Valley stress relief, as described by Ferguson [90], has become widely recognized and accepted in the United States. Valley closures and deformations of the valley floor reported in conjunction with Australian longwall coal mining are similar to observations of valley stress relief. The movements are small and have only been recorded by careful topographic surveying, and surveys of structural damage or ground deformations. It appears the most likely features to be damaged are structures, such as concrete dams and pipelines, which extend across valleys in areas of significant relief.

In Australia, the areas of longwall mining where significant horizontal movements have been observed all exhibit pronounced local topographic relief and a high ratio of horizontal to vertical pre-mining ground stress. Most if not all United States coal fields also have a high ratio of horizontal to vertical pre-mining ground stress. Observed surface movements in Australia have included horizontal valley closure, valley base (bottom) uplift and regional mining-induced horizontal displacement. Lateral valley bulging is a natural phenomenon, resulting from the formation and ongoing development (i.e., erosion) of the valley, but the process is accelerated by longwall mining, to varying degrees, whenever the mining occurs beneath, or adjacent to valleys [32, 84, 86]. Geodetic survey results show that horizontal movements of up to 25 mm (1 in) can occur even where underground longwall coal mining is about 1.5 km (1 mile) from the survey monuments. Movements are generally directed toward the mined longwall panel. However, in some cases, the movements are in the direction of the nearby valley, or of the major principal stress.

Factors which influence valley bulging and closure movements as a result of longwall mining include [32, 84, 86]:

- Mine geometry and the nature of mining

- Valley location relative to the mined panel
- Valley depth
- Geology
- Horizontal in-situ stress

An example of significant adverse effects of valley closure from longwall mining in the United States includes the experience at Ryerson Station Dam in Greene County, Pennsylvania. Ryerson Station Dam is a 515-foot-long (157-meter-long) concrete gravity dam which was completed in 1960. Annual structural and leak inspection reports indicated no major problem until July 2005. In July 2005, leakage from the east side of the dam reached 80 gallons per minute (300 liters per minute), and the dam exhibited significant structural deformations. The leakage and the structural damage resulted in a determination by the Pennsylvania Department of Dam Safety that it was necessary to drain the reservoir. Subsequently, it was determined that breaching of the dam to prevent impounding water was also necessary.

The Ryerson Station Dam axis is oriented east-west across the valley of the North Fork of the Dunkard Fork of Wheeling Creek (Figure 2-46). The top of the dam is at about elevation 979 ft (298 m) above mean sea level (AMSL). The hillside at the east end of the dam rises steeply to above elevation 1,300 ft (396 m) AMSL. The ground surface at the west end of the dam does not rise above elevation 1,100 ft (335 m) AMSL for a considerable distance from the dam. The hillsides and valley of the North Fork are underlain by sedimentary rock strata consisting of interbedded shale and sandstone with lesser amounts of limestone, claystone and coal (including the Pittsburgh Coal seam). The Pittsburgh Coal seam is at approximate elevation 600 ft (183 m) AMSL, about 350 ft (107 m) below the dam elevation. This coal seam was mined by longwall methods in a panel located northeast of the dam (Figure 2-46). Figure 2-47 is a schematic cross-section of the topographic and subsurface coal and longwall coal mine features at the Ryerson Station Dam.

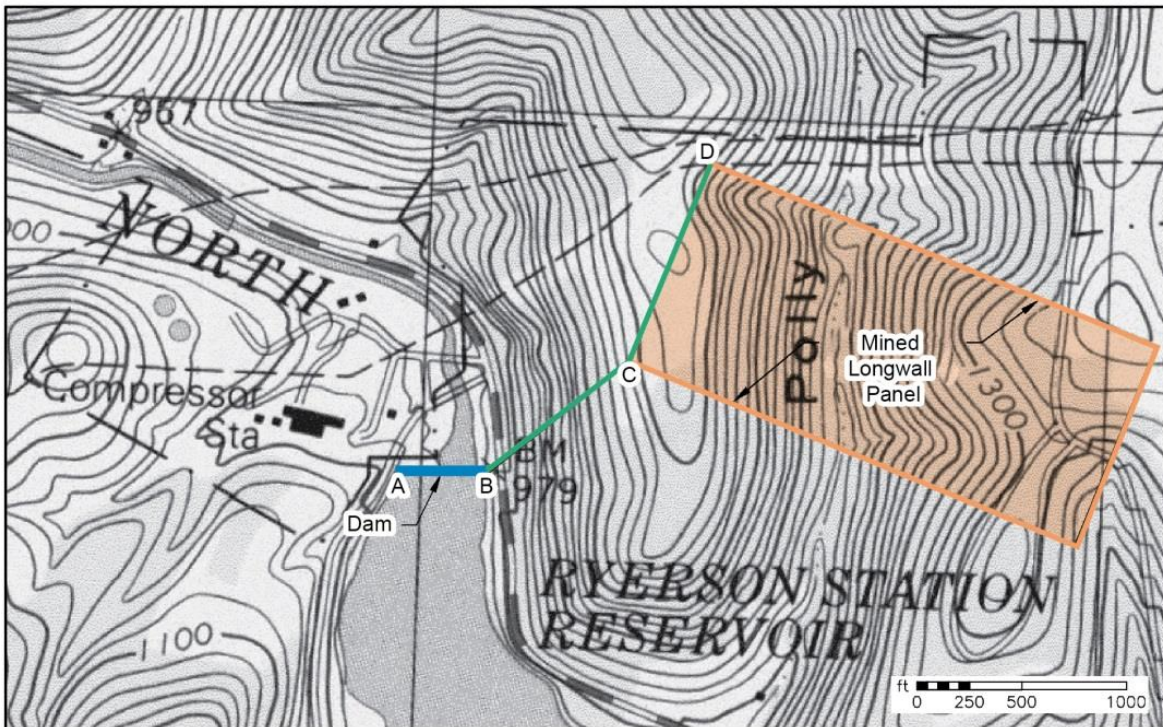


Figure 2-46 Plan map of Ryerson Station Dam and longwall mine panel

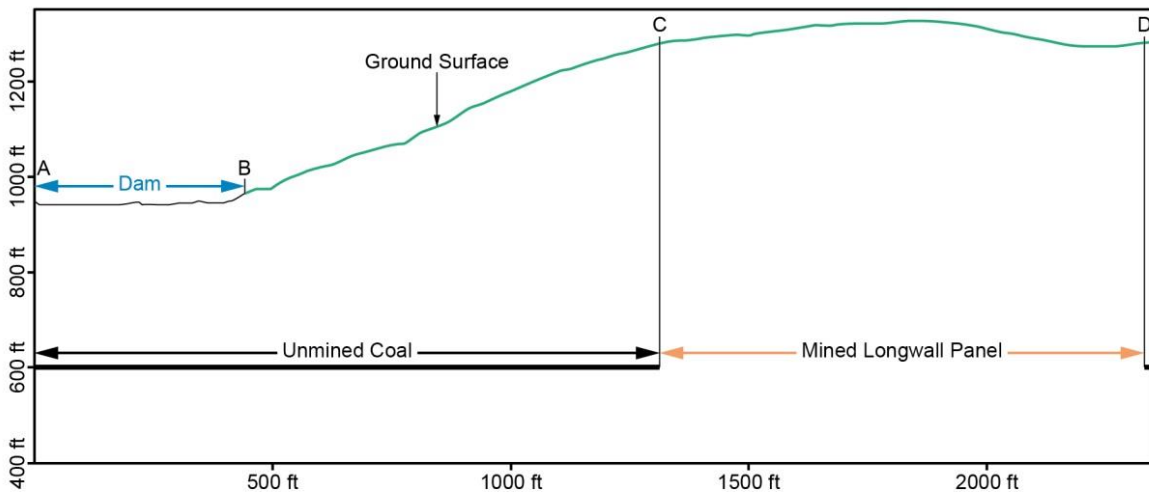


Figure 2-47 Schematic cross-section at Ryerson Station Dam (see Figure 2-46 for section location)

Significant structural movement of the Ryerson Station Dam, evident just following observation of the July 2005 leakage, included 2 in (5 cm) of westward movement of the east side of the dam, and uplift of the east side by several inches. A longwall mine panel was being excavated just northeast of the dam, where the western portion of the panel extended under the

high hill, elevation 1,340 ft (409 m) AMSL, that forms the steep slope above the east end of the dam (Figure 2-46 and Figure 2-47). The closest edge of the mined panel to the east end of the dam was approximately 900 ft (274 m). The mined Pittsburgh Coal seam was at a level approximately 350 ft (107 m) below the dam and over 700 ft (213 m) below the high hill to the east.

Because of the temporal similarities of the longwall mining and the observation of the excessive leakage, mining was considered a possible cause. However, it was anticipated that movements above and near the mined panel would be downward into and toward the panel. Lateral forces on the dam due to readjustment of the rock strata in the hillside as a result of mining had not been previously recognized in southwestern Pennsylvania.

Mining of a longwall panel, located approximately 4,000 ft (1,220 m) west of the Ryerson Station Dam under high hills north of the North Fork, was started on November 23, 2005, and was completed in late March 2006. This panel lies below high hills (approximate elevation 1,300 ft [396 m] AMSL) with the valley of the North Fork (approximate elevation 940 ft [287 m] AMSL) located to the south. Although this panel is well west of the dam, it was of interest due to its location under high hills adjacent to the North Fork of the Dunkard Fork of Wheeling Creek, a topographic and longwall mining relationship similar to Ryerson Station Dam.

The panel was mined from east to west under high hills with State Route 21 located in the North Fork Valley at the toe of the high hills. Geodetic survey monitoring points were established along Route 21. Survey points at and near the southeast corner of the mine panel, as expected, moved toward the undermined area. A private bridge located approximately 200 ft (61 m) south of the southeast corner of the panel also moved north toward the mine panel. A residence located approximately 300 ft (91 m) southeast of the southeast corner of the panel moved about 1 in (2.5 cm) south, away from the mine panel, between January 20 and February 13, 2006. Survey points further west along State Route 21 also moved away from the mine panel.

Examination of the results of the survey data indicated that the greatest heave occurred where State Route 21 was closest to the toe of the steep hillside. This heave or rotational uplift being greatest where the road is closest to the toe of the high hills is similar to the observations at the east end of Ryerson Station Dam.

Mining of another longwall panel began on April 26, 2006, and moved westward toward the South Fork of Dunkard Creek. This panel was generally under high hills rising slightly above elevation 1,400 ft (427 m) AMSL. Northward, the ground surface slopes down to the former lake created by Ryerson Station Dam at about elevation 970 ft (296 m) AMSL.

During a subsurface investigation in early 2006, five inclinometers were installed in the rock strata below the Ryerson Station Dam and along its center line. No movements were recorded by these inclinometers until mining occurred 2,500 ft (762 m) south of the dam in the summer and fall of 2006.

In September 2005, while movements were still being recorded at Ryerson Station Dam, an out-of-service pipeline was observed to have heaved out of a stream bed approximately 1,500 ft

(457 m) downstream of the dam. Two pipelines located in a compressor station on the bank left just downstream of the dam (Figure 2-46) also moved. These pipes were located approximately 1,200 ft (366 m) from the longwall panel.

Another example of far-field surface deformation associated with longwall mining in Pennsylvania involves Interstate 70 in Washington County. In 1999 and 2000, during longwall mining beneath the highway, ground deformations were monitored using Time Domain Reflectometry to interrogate coaxial cable installed in seven deep holes [91]. Deformations occurred within the overburden over 1,000 ft (305 m) in front of the mine panel face, well beyond the limits of anticipated movement around the mine panel [91].

In Greene County, Pennsylvania, in late November 2008, cracks were noticed in the ground above an in-service natural gas pipeline that crossed the valley formed by the South Fork of Dunkard Creek. A week later, the ground at the location of the cracks had heaved about one foot (0.3 m). Excavation of the pipeline showed it to be wrinkled on the inside of an overbend at the high stream bank. The steep slopes of the valley walls at this location had a history of landslides and evidence of sliding was present on both slopes. However, slope inclinometers installed in the steep slopes did not detect landslide movements. The only new activity in the vicinity was coal mining. The longwall mine panel advanced under a hill west of the South Fork to within 200 ft (61 m) of the wrinkled pipe. In the absence of landsliding, longwall mining-triggered valley closure is the only possible cause of the observed damage.

Another form of mining that can lead to surface subsidence is *solution mining*. Potash solution mining occurs in Saskatchewan, and solution mining for salt deposits occurs in northern plains states of the United States. The removal of salt and potash deposits at depth has led to surface subsidence. For example, solution mining of salt deposits in Kansas resulted in the formation of a 300-meter-diameter (1,000-foot-diameter) sinkhole, because a large solution cavity was created at depth in the mining process, and the overlying material collapsed to the surface [73].

Retreat room and pillar mining was initiated in the latter part of the 19th century to achieve greater production of coal. The distinction from partial extraction mines was that pillars left in first-stage partial mining were now extracted in a second stage of mining. In some mines this second stage took place immediately after first-stage mining, in other mines pillars were removed long after initial room and pillar development.

This pillar removal, sometimes termed total or high extraction room and pillar mining, systematically removes coal pillars from one end of a mine panel to the other, allowing the mine roof to collapse to the floor.

Ideally, subsidence of the ground surface in a properly executed pillar extraction operation takes place contemporaneously with pillar extraction [37]. However, surface subsidence may not occur for an extended amount of time and when it does appear may do so in an unpredictable pattern.

Human-caused drainage of organic soils, which are typically located in floodplains, results in the microbial decomposition of the organic-rich soil material, converting organic carbon to

CO₂ and water [9]. This process results in desiccation of the soil, and a reduction in soil volume which translates into a loss in ground surface elevation, hence surface subsidence. Along a pipeline, the desiccation of the organic soil can result in the ground settling down around the pipeline exposing the pipeline to the surface elements (Figure 2-48).



Figure 2-48 Pipeline exposure in western Washington due to drainage of organic soil which has allowed soil desiccation, subsequent loss of organic soil volume, and ground settlement (loss of ground surface elevation) around the pipeline. (Photo by: D. West, Year: 2005)

Hydrocompaction of soil generally involves loose, dry, low-density deposits that compact when they are wetted [92]. Such deposits mantle extensive areas in North America. Hydrocompaction, has produced widespread subsidence of the land surface, and may occur under natural overburden load or may occur only with the addition of a surcharge load [92].

Deposits that subside because of hydrocompaction are generally one of two types: 1) loose, moisture-deficient silty to sandy alluvial deposits; and 2) moisture-deficient loess and related aeolian deposits. Such deposits occur in regions where seasonal rainfall seldom, if ever is sufficient to penetrate below the root zone; thus, they have remained moisture deficient throughout their post-depositional history and are readily susceptible to hydrocompaction when they are artificially wetted [92]. Subsidence due to hydrocompaction is a concern in the design

and maintenance of aqueducts, buildings, pipelines, highways, and other major engineering structures.

Localized settlement/subsidence of pipe trench backfill material and pipeline construction fill material may also occur, and adversely affect the pipeline. This settlement/subsidence may result from:

- Consolidation of loose and/or poorly placed granular pipe bedding material
- Consolidation of very soft or soft fine-grained bedding material
- Soil piping, from groundwater flow along the pipe trench bottom resulting in the development and collapse of voids around the pipe, or
- Thawing of frozen/snow rich backfill material when it melts

The consolidation and collapse of the backfill soil around the pipe may cause buckling or bending stresses on the pipe.

2.4.2.2 Potential Effects of Settlement/Subsidence on Pipelines

Surface settlement/subsidence, whether from aquifer system compaction, dissolution of the underlying bedrock, collapse of underground mine workings, or of from a number of other natural and human-triggered processes, results in vertical ground displacement, ground tilting and horizontal ground displacement. These ground displacements result in horizontal compressive and tensile stresses at the surface, bending of the ground surface and localized cracking and differential displacement. Tensile strains, ground cracking and potential differential displacement from subsidence tend to develop at the distal limits of the area of subsidence, whether from collapse of underground coal mine workings, from aquifer system compaction, or from subsurface bedrock dissolution [32, 93, 37]. Compressive strains tend to develop toward the area of maximum subsidence [32, 93, 37]. Note that in the case of longwall mining, the subsided area advances along the length of the mined panel and the tension and compression zones move with it.

Figure 2-3 and Figure 2-43 schematically illustrate the surface location and distribution of tensile and compressive strains above a collapsed room-and-pillar coal mine, and a longwall coal mine panel, respectively. Figure 2-4, Figure 2-42, Figure 2-44, and Figure 2-45 show how surface subsidence deformation may be manifested and distributed above actual collapsed underground mines whether abandoned or active. Potential pipe bending may occur where the pipeline spans a sinkhole or collapse pit above an underground mine [93] or karst subsidence feature. Pipe breakout may occur where compressive stresses are concentrated along the pipe axis forcing the pipe to rise out of the ground through the trench backfill material.

As mentioned in this section, far-field surface deformation may occur associated with longwall mining. This includes valley closure and valley bulging (upsidence) which may be located as much as one to two or more kilometers (0.6 to 1.2+ miles) from the mine workings.

There are several potential modes of failure for pipelines exposed to the surface effects of settlement/subsidence. Marino [93] has examined the effects of coal mine subsidence on

pipelines, and these appear to also be generally applicable to other forms of large-scale settlement/subsidence that have been described previously. For pipelines exposed to the effects of coal mine subsidence, the primary potential failure modes appear to be [93]:

- Axial tension
- Axial compression, with buckling (Figure 1-5 and Figure 2-49)
- Lateral bending
- Ground breakout from pipe uplift (Figure 2-50)



Figure 2-49 Example of pipe buckling from high axial compression resulting from longwall mining



Figure 2-50 Uplifted pipe and ground breakout due to longwall mining.

These potential failure modes may operate individually or in combination and how the pipeline behaves in these potential failure modes is dependent on several factors related to the type, nature and magnitude of the particular subsidence process, the nature and characteristics of the pipe, and the nature of the pipe backfill material. Marino [93] has identified many of these factors which include:

- Pipe orientation relative to the size, pattern and distribution of the surface subsidence features
- Pipe properties (wall thickness, diameter, coating, steel strength, and pipe condition)
- Operating pipe stress
- Trench pipe bedding and backfill conditions (strength, stiffness, compaction)
- Subsidence feature/conditions (nature, geometry, magnitude of subsidence and differential displacement, pipe exposure length)

2.5 Methods for Hazard Identification, Characterization, Assessment and Evaluation

2.5.1 General

In this section, a qualitative method to systematically identify and characterize geologic hazards is presented to provide the necessary technical background and data input for the

development of hazard mitigation and hazard monitoring. The processes and methods are directed toward landslide and settlement/subsidence hazards, but can also be applicable to other geologic hazards. Geologic hazard mitigation and monitoring, as applied to landslide and settlement/subsidence hazards, are addressed in Section 8.

The phased approach hazard assessment is directed toward the development of a GIS-based database of hazards so the pipeline owner/operator can develop an inventory of landslide and subsidence hazards and manage the risks from the identified hazards. The focus is on locating or developing GIS databases regarding the topography, geology, existing landslides, economic coal-rich geologic units, and on landslide hazards and subsidence hazards (karst, abandoned and planned underground mines, areas of subsurface fluid withdrawal). Being in GIS format, these data can be readily entered into the growing database of hazards along the pipeline, and the hazard data can be manipulated and evaluated in GIS.

A general three-phased approach is commonly employed to identify, assess, classify and evaluate potential geologic hazards that may be a threat to pipeline integrity. The phases allow for successively more detailed assessments/investigations to be employed. The implementation of the assessment phases typically requires qualified and experienced geoscientists and geotechnical engineers. The geologic hazard identification, characterization and evaluation work should be performed by professionals that have local and regional knowledge of the specific geological hazards in the proposed study area/region. The three hazard identification, assessment and evaluation phases are:

- Phase I is primarily an office-based, regional-scale screening assessment using publically available topographic, geologic and remote sensing data along with any available background information the owner/operator can supply to identify potential geologic hazards that may affect a pipeline or pipeline system. An initial inventory of potential hazards is developed and classified by their potential threats to pipeline integrity. The Phase I screening is typically augmented with an aerial reconnaissance (e.g., helicopter) along the pipeline to confirm/verify the office-based assessment and to identify any potential hazards that may have recently occurred, or were not contained in, or visible from the available regional-scale data. Based on the threat classification, the hazards of concern are prioritized for study in the next phase of assessment. The results of Phase I screening are typically entered into a GIS database management system.
- Phase II typically involves site-specific, non-intrusive field geomorphic and geologic reconnaissance mapping to confirm the existence and threat levels of previously identified hazard features and identify those features that may require Phase III investigations. The information and data collected during the Phase II reconnaissance provide a better, more detailed and site-specific understanding of the location, nature and extent of a hazard, and its potential threat to the pipeline. The data compiled in Phase II are entered into a GIS database, and may update the data from the Phase I assessment.
- Phase III includes both office- and field-based site-specific investigations, and focuses on the hazard(s) of concern confirmed in the Phase II reconnaissance. The Phase III

investigations commonly include detailed surface and subsurface geologic and geotechnical site/hazard characterization to support the development of alternative hazard mitigation designs, and ultimately the development of appropriate hazard monitoring programs.

The third phase of the three-phased approach can, and often does include the identification of hazard mitigation alternatives, development of a preferred mitigation design, implementation of the preferred mitigation design alternative, and development and installation of site-specific hazard monitoring. The development of hazard mitigation and monitoring, as it applies to landslide and subsidence hazards, is detailed in Section 8.

2.5.2 Primary Tools to Complete a Phased Approach to Hazards Assessment

The phased approach to identifying, characterizing and evaluating potential landslide and settlement/subsidence hazards involves the use of many and varied investigative tools, techniques and resources. The information and data to implement these tools and techniques may be publicly-available or published, and come from Federal, state/provincial, and local agencies, institutions, and professional organizations; they may be operational and maintenance data from the pipeline owner/operator; and most importantly, they include remote sensing data that come from public and private sources or the pipeline owner/operators.

The tools and techniques have several purposes. They may be used for the detection or identification of a hazard, they are used in the characterization of the potential hazard, and many of the tools can also be used in short and long-term hazard monitoring. Table 2-4 provides a summary of the primary tools, techniques and resources commonly employed in the three phases of a geologic hazards assessment. They are also the primary tools and investigative techniques that would be used to identify, assess and evaluate landslide and settlement/subsidence hazards.

Table 2-4 Primary data, tools and techniques used in the phased approach geologic hazards assessment

Assessment Phase	Data Source or Type	Tool, Technique	Attributes/Comments
<i>Phase I</i>	Published, Publicly-Available Data	Detailed topographic maps and digital elevation model (DEM) data	Detailed topographic maps (1:20,000- to 1:25,000-scale) show large-scale geomorphic features and cultural features that may relate to geologic hazards, such as disrupted terrain (landslides) and closed depressions (subsidence features). DEM data (e.g., 10-meter, or larger) can be manipulated to create hillshades to accentuate geomorphic features and help identify geologic hazards.
		Regional- and large-scale geologic maps and geology reports	Geologic maps may delineate landslides as distinct geologic units, and subsidence features as distinct geomorphic features. Geology maps and reports may tie specific geologic units to landsliding or the presence of karst features and underground mineral or coal resources. The geologic map data may be in the form of print copies, .pdfs or as GIS databases.
		Regional- and large-scale geologic hazard mapping and hazard reports	Hazard mapping may delineate landslide and subsidence (karst, coal mine) areas and features. Hazard reports may describe the nature and distribution of landslide-susceptible geologic units or the distribution of karst-producing bedrock and underground coal mines. The geologic hazard map data may be in the form of .pdfs or as GIS databases.
		Abandoned and planned or permitted mine maps	Many authorities map abandoned underground mines, and where there is active underground mining, permits and approval to mine are required. The permit process allows for the new mine layout to be reviewed and addressed in hazard identification. Abandoned or planned surface mining (including rock or gravel quarries) map data are also used. The surface and underground mine maps may be .pdfs or GIS databases.
	Pipeline Owner/Operator Data	Pipeline centerline GIS shapefiles	An accurate, GIS-based pipeline centerline location is needed to be able to put the pipeline in spatial context with the identified and mapped landslide and subsidence hazards.
		O&M experience	Pipeline operations and maintenance records may identify locations where landslide or settlement/subsidence has been observed and documented, or repairs have been made. Geotechnical consulting reports may be present in owner/operator data files.

Table 2-4 Primary data, tools and techniques used in the phased approach geologic hazards assessment (Cont'd.)

Assessment Phase	Data Source or Type	Tool, Technique	Attributes/Comments
<i>Phase I</i>	Pipeline Owner/Operator Data	ILI IMU bending strain data, caliper tool and to a lesser extent Magnetic Flux Leakage Tool (MFL) dent/wrinkle indications	ILI IMU data can be used to detect geometry related anomalies, bending strains, and during successive runs could be used to determine pipeline areas of apparent strain or displacement related to landslides or subsidence. Additionally, in limited cases MFL data can be used detect landslide related dents or wrinkles.
	Remote Sensing Data	Published or pipeline owner/operator LiDAR DEM data	<p>Many states/provinces may have widespread LiDAR DEM data coverage in bare-Earth layers. Pipeline owner/operators may also have such data along the pipeline alignment or route. These DEM data are possibly the most important for use in identifying geologic hazards, particularly landslide and subsidence. The DEM data are used to develop hillshades and slope maps for the identification and characterization of geomorphic features that may be related to geologic hazards.</p> <p>LiDAR DEM data should be high resolution and high quality, with at least three (3) returns per pulse (including the first and last pulse), a minimum of four (4) pulses per square meter, a scan angle less than 20°, and with nominal swath sidelap of 50 percent and 100 percent double coverage. That is, they should be appropriate for detailed geomorphic analysis of the terrain, and should meet the minimum LiDAR data collection specifications as indicated by the examples in Appendix 3-A. These LiDAR specifications are minimum requirements for providing the quality and resolution needed for reliable DEM data in order to undertake appropriate and complete geologic hazard assessments and mapping.</p>
		Stereoscopic alignment aerial photographs	Aerial photographs, historically obtained for alignment sheets, may be in stereo-pairs and can be used to identify landslide and subsidence features. This method is used less frequently in favor of the LiDAR methods described above. The scales of aerial photographs typically range from 1:1000 to 1:40,000.

Table 2-4 Primary data, tools and techniques used in the phased approach geologic hazards assessment (Cont'd.)

Assessment Phase	Data Source or Type	Tool, Technique	Attributes/Comments
<i>Phase I</i>	Remote Sensing Data	Regional, high altitude and detailed, large-scale stereoscopic aerial photographs	Federal and state/provincial agencies often have wide coverage of stereoscopic black-and-white, and color aerial photographs which are used in the identification of geomorphic features indicative of landslide movement and ground subsidence.
		Google Earth™ and Bing™ historical aerial photograph imagery	Historical, low and high quality aerial photography of the same location may indicate changes that are the result of landslide, subsidence or development that may trigger hazards.
		Pictometry™ imagery	High quality vertical and oblique format aerial photographs (primarily color) that can be used to identify geologic hazards. Localized coverage.
		Satellite (e.g., LANDSAT, SPOT) imagery	Satellite, visual band imagery with low to high quality for the identification of landslides and subsidence features. Open access data are often lower quality, while the high-resolution data can be expensive.
	InSAR data	Satellite-based InSAR data can provide information on the location, magnitude and rate of ground movement for both landslides and subsidence. Typically requires multiple pass analysis which can be extremely expensive.	
Aerial Reconnaissance	Helicopter (preferred) or fixed-wing (only suitable for flat terrain but you cannot stop and review sites)	All of the tools and techniques for a Phase I assessment, described above, have limitations in quality and level of detail. In addition, they are only snapshots in time of when the mapping, data or remote sensing imagery were obtained or completed. The aerial reconnaissance provides a current close-up view of the terrain along the pipeline ROW so that the current geomorphology can be viewed for evidence of ground disturbance related to landslides or subsidence. Field checks could be conducted during a helicopter aerial reconnaissance.	
<i>Phase II</i>	Phase I Tools, Techniques (as appropriate)	See above	The Phase II assessment may have focused, site-specific use of tools and techniques from the Phase I assessment. For example, aerial reconnaissance may be targeted at specific locations, areas or sites

Table 2-4 Primary data, tools and techniques used in the phased approach geologic hazards assessment (Cont'd.)

Assessment Phase	Data Source or Type	Tool, Technique	Attributes/Comments
<i>Phase II</i>	Non-intrusive field assessments	Geomorphic and geologic reconnaissance	Selected potential hazard sites from the Phase I assessment receive detailed, non-intrusive geomorphic and geologic mapping to more completely identify the lateral limits of the hazard relative to the pipeline, and estimate the magnitude and rate of movement. For landslides, this may include pipeline locating (e.g., every 10 ft; 3 m), including pipe depth, to evaluate whether the pipeline may have been deflected/displaced by landslide movement, or whether the pipe may be deep and possibly below landslide movement. For potential longwall mining subsidence, it may include identification and mapping of steep slopes and valley walls away from the mine limits. The field mapping and data points are recorded and plotted on GIS-based GPS tablets and handheld units so that the field data can be easily entered into the hazards GIS database.
		Site geodetic topographic survey	The collection and use of detailed site-specific traditional geodetic survey topographic data. May include pipeline centerline survey with pipe depths, and specific points/features of the landslide or subsidence feature. The detailed topographic base could also be obtained from site-specific LiDAR DEM.
		Project- or site-specific LiDAR	Collection, processing and use of high resolution LiDAR DEM data for the production of detailed site topography.
<i>Phase III</i>	Phase I and II Tools, Techniques (as appropriate)	See above	Continued application, as appropriate, of selected investigative tools and techniques identified for Phase I and II assessments.
	Intrusive, and semi-intrusive, site-specific field investigations	Test pit/trench	Test pits or test trenches allow for the examination of the near subsurface (to depths of 15 to 20 ft; 4.5 to 6 m) geologic and geotechnical conditions, particularly for a shallow landslide. The depth/thickness of the landslide relative to the pipe can be investigated and these data used for the development of hazard mitigation options. Soil samples are often analyzed for geotechnical properties.
		Geotechnical borehole	The subsurface geologic and geotechnical conditions to depths of tens to hundreds of feet can be investigated to document and evaluate the subsurface material properties and geometry of landslides and to install instrumentation including slope inclinometers and piezometers.

Table 2-4 Primary data, tools and techniques used in the phased approach geologic hazards assessment (Cont'd.)

Assessment Phase	Data Source or Type	Tool, Technique	Attributes/Comments
<i>Phase III</i>	Intrusive, and semi-intrusive, site-specific field investigations	Geophysics	Various geophysical methods/techniques (e.g., GPR, EMI, seismic refraction, seismic reflection) can be used, with favorable conditions, to image the subsurface structure, stratigraphy and geometry of landslides, and the structure, size and nature of voids for subsidence features.
		Slope inclinometer and other borehole movement monitoring devices including ShapeAccelArrays™ and TDR Cables	Typically installed in a geotechnical borehole to identify the depth interval(s), amounts and rates of subsurface movement/displacement. Used for both characterization and monitoring, for landslide-specific investigations and subsidence investigations.
		Piezometer	There are numerous types of piezometers including standpipes, which record the water level in the standpipe, and vibrating wire, pneumatic and pressure transducers that are used to determine the pore water pressure at the depth or zone it is installed at. Used as input to determine the impact of groundwater conditions on landslide movement and effects on groundwater from the passage of longwall mine panel.
		Survey monitoring points	The installation of surface monitoring points around a landslide or subsidence feature which aids in understanding the lateral limits of deformation and the magnitude and rate of surface movement (x, y, z). A series of survey monitoring points is installed as a detection, characterization, and monitoring tool.
	Office-based analyses and evaluations	Slope stability and hydrotechnical analyses	For landslides, and to support the development of mitigation alternatives, geologic and geotechnical analyses, including slope stability modeling/analysis to understand critical/sensitive factors controlling slope stability. In addition, because surface and groundwater, and their control, also factor into slope stability, hydrotechnical analyses may need to be completed to support mitigation alternatives.
		Modeling of nature and extent of settlement/subsidence	For subsidence, modeling and analyses to understand the potential extent and magnitude of subsidence to support the development of mitigation alternatives and monitoring plans.

2.5.3 Description of Phase I Geologic Hazards Screening

As stated previously, a Phase I assessment is primarily an office-based, regional-scale screening study using publicly available topographic, geologic, remote sensing, and pipeline operations/maintenance data (e.g., GIS databases) to identify potential landslide and settlement/subsidence hazards that may affect a pipeline or pipeline system. In addition to identifying the hazards, a Phase I screening is the first attempt to characterize the nature of the hazard, and to classify the relative hazard/threat level for each landslide or settlement/subsidence hazard. With the location and the initial potential threat/hazard level characterized for each potential hazard, we can develop an initial inventory of hazards.

The identification and mapping of the landslide and settlement/subsidence hazards is usually confined to some distance from the pipeline centerline or the edge of the ROW. This is because the hazard of concern may be off the ROW, but the geologic process that results in the hazard extends to the ROW and pipeline, or future activity of the process may migrate to the ROW and pipeline. For these reasons, an envelope/swath of a few hundred feet to as much as a few thousand feet centered on the pipeline may be set for the Phase I screening depending on the hazard(s) to be addressed, and the nature of the project. The study area envelope should be determined by a geoscientist and/or geotechnical engineer to reflect regional hazards and topography. As an example, in mountainous terrain, the study area swath should extend to the height of land. Alternatively, in flat areas with few hazards, the study area could be restricted to as little as about 330 ft (100 m) from the centerline of the pipeline. Additionally, the study area should be extended upstream and downstream at stream crossings to determine if there is any landslide activity in the valleys, and to more fully understand the nature and potential extent of the hazards. Figure 2-51 shows alterations of study area boundaries to consider a stream valley crossing, as they relate to the collection of LiDAR data. In the example, significant potential stream valley landslide hazards would be missed if the swath was kept narrow. The LiDAR swath would be completely adequate for the surrounding flat to gently undulating terrain.

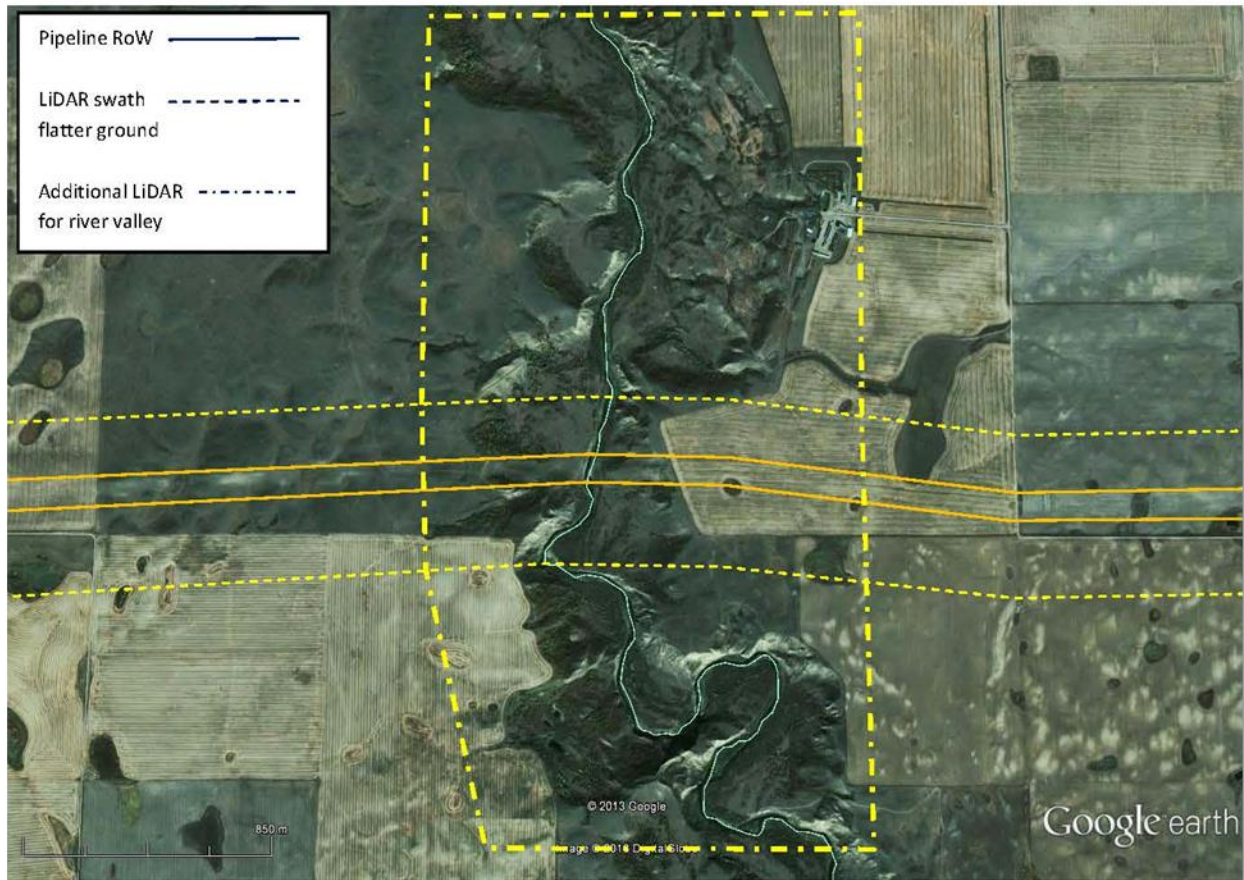


Figure 2-51 Sketch of typical pipeline LiDAR surveys for flat and gently sloping ground and recommended expansion of survey at major stream valley crossing location. (Source: Google Earth™ coverage, Location: Swift Current Creek Valley in Saskatchewan)

Prior to the identification and mapping of the hazards, qualitative threat/hazard classification criteria are typically developed. These criteria are specific to the nature, quality and detail of the available data, and are customized for use on the specific hazard assessment project, for the specific pipeline or pipeline system. The landslide and subsidence hazards could be assigned a qualitative and relative initial threat/hazard classification that ranges from “low” to “moderate” to “high”. These threat/hazard classifications are commonly based on:

- The proximity or location of the hazard relative to the pipeline,
- The nature and potential severity of the hazard relative to the pipeline, and
- The age of the most recent movement or level of activity of the hazard.

For example, the closer the particular hazard is to the pipeline, the higher its threat level may be, and if the hazard crosses the pipeline, it may have the highest classification. Similarly, the more active the hazard is, then the higher the threat level could be. Although the threat/hazard criteria are developed at the beginning of the Phase I screening, their use and continual

refinement continues through the remaining phases. Because most of the data used in the Phase I screening are regional-scale, the identified threat/hazard classifications are preliminary and need confirmation in later phases. Thus, with new, more detailed data obtained in subsequent phases (e.g., Phase II and Phase III), the threat level of a hazard may change.

Examples of possible preliminary landslide and subsidence threat/hazard classification criteria for existing pipelines are provided in Table 2-5 and Table 2-6, respectively. The actual classification criteria would be developed for the specific project, and would likely differ from these examples. As part of the continuing evaluation process (Figure 2-1), hazard/threat levels are revised as needed whenever new information is acquired.

Table 2-5 Example of possible landslide hazard/threat classification criteria for pipelines and for a specific study area

Potential Hazard/Threat Level¹		
Low	Moderate	High
-Dormant ² landslide crossed by a pipeline with low potential for renewed activity. -Landslide (of any age) between 20 and 100 ft (6 and 30 m) of the ROW. -Slopes steeper than 40 percent (22°) with no geomorphic evidence or historical record of landslide activity. -Geologic formations or units underlying a pipeline which are prone to landslides and with topographic conditions conducive to landslide activity, but with no mapped landslides.	-Active ² or recently active ² landslide within 20 ft (6 m) of a pipeline with no obvious observed geomorphic or instrumental evidence of disturbance across a pipeline centerline. -Debris flow run-out crossed by a pipeline. -Active ² or recently active ² shallow or small landslide across a pipeline centerline, but with failure surface that is above a pipeline. -Active ² or recently active ² landslide that has been mitigated or repaired.	-Active ² or recently active ² landslide with geomorphic or instrumental evidence ³ of disturbance across a pipeline centerline. -Debris flow source area or transport zone that crosses, or is within 20 ft (6 m) of a pipeline. -Rock fall hazard in close proximity to a pipeline.

Notes:

- 1) Landslide hazard/threat classifications are based on the apparent threat to a pipeline from a landslide, and are based on a combination of the landslide characteristics (such as size, type, and nature and level of activity) and the spatial relationship of the landslide to one or more pipelines; i.e., a landslide that crosses or intersects an individual pipeline is a higher hazard to that pipeline than a landslide located some distance away, or one that is upslope may be less hazardous than one located downslope or vice versa.

- 2) The age of most recent activity is an important consideration in evaluating a landslide hazard. In this table, landslide age is qualitative, and is expressed as “active,” “recently active,” or “dormant.” An active landslide is defined as one that has geomorphic or documented evidence of activity within the last 10 years, a recently active landslide is defined as one that has geomorphic or documented evidence of activity from 10 to 200 years ago, and a dormant landslide is defined as a landslide with geomorphic evidence that the most recent activity was more than about 200 years before present.
- 3) Instrumental evidence of ROW disturbance refers to quantitative data that indicate landslide movement on a ROW. Examples of sources of quantitative data could include pig data (e.g., IMU bending strain), repeat surveying of known points (i.e., monitoring points), slope inclinometer measurements, or indications of landslide induced strain from strain gauge measurements. Data sources could also include remote sensing data, such as repeated LiDAR or InSAR surveys.

Table 2-6 Example of possible -settlement/subsidence hazard/threat classification for pipelines

Subsidence Hazard	Potential Hazard/Threat Level		
	Low	Moderate	High
Subsurface Bedrock Dissolution (karst)	-Areas mapped as being underlain by potentially karstic or pseudokarstic formations (e.g., limestone, gypsum, lava tubes), and more than 160 m (525 ft) from apparent karst features (e.g., sinkholes).	-Sinkholes or areas with evidence of subsurface voids (e.g., disappearing streams) between 60 and 160 m (200 to 525 ft) of the ROW. -Areas mapped as karst terrain by state agencies, but with no mapped sinkholes, or evidence of sinkholes during aerial reconnaissance.	-Mapped sinkholes or evidence of subsurface voids (e.g., disappearing streams) within 60 m (200 ft) of ROW. -ROW areas historically impacted by sinkholes or other karst phenomena.
Underground Mine Collapse (abandoned and operational coal mines)	-Within region or area of abandoned underground coal mines, but ROW greater than 200 m (660 ft) from mapped abandoned underground mine, and there is no geomorphic evidence of surface subsidence.	-Evidence or maps of abandoned underground room-and-pillar coal mines between 140 and 200 m (460-660 ft) of ROW. -Planned underground coal mining (e.g., longwall) between 140 and 1,000 m (460-3,300 ft) of ROW, if topography is conducive to valley closure.	-Evidence or maps of abandoned or planned underground coal mines directly below ROW, or within 140 m (460 ft) of ROW, or within the expected area of subsidence of planned longwall mining. -ROW areas historically impacted by subsidence resulting from collapse of room-and-pillar coal mines.
Aquifer System Compaction (subsurface fluid withdrawal)	-Areas with known, extensively exploited groundwater aquifers, but with no reported subsidence that has resulted in damage to surface facilities, such as roads or structures. -Areas that contain oil and gas well fields (exploration and/or production), but there appears to be no reported subsidence that has resulted in damage to surface facilities such as road or structures.	-Areas that contain oil and gas, or groundwater well fields that have subsidence, but no reported damage resulting from this subsidence.	-Areas that contain oil and gas, or groundwater well fields that have documented evidence of fluid withdrawal-caused subsidence that has damaged roads and structures. -Areas that have documented evidence of fluid withdrawal subsidence that has resulted in the formation of fissures or faults.

For landslides, the focus of the hazard identification in the Phase I screening is on performing a geomorphic analysis of the remote sensing imagery to identify landslide features. Because landslides disturb the Earth's surface, a geomorphic analysis of the terrain visible in the remote sensing imagery is undertaken. High resolution LiDAR, using a bare Earth DEM, is a common and preferred tool for the geomorphic analysis because it strips the vegetation so that disturbed landslide features such as the sheared lateral limits, the main scarp in the head area, the toe, and the hummocky/disturbed main body of the landslide are typically visible. When using traditional stereoscopic aerial photography and or ortho-imagery, the vegetation may disguise landslide features making it a less preferred but also a viable option depending on the scale and quality of the photography, and whether an aerial reconnaissance is undertaken as part of the Phase I screening. The landslide limits are mapped, each landslide is given a distinctive identifier code, and the initial threat/hazard classification for each landslide is assigned.

Figure 2-52, a LiDAR hillshade image, shows the 18 mi² (47 km²) Cascade-Bonneville landslide complex in the Columbia River Gorge of Washington. The landslide initially formed during the late Pleistocene and early Holocene (~10,000 years ago), major translational and flow displacement into the Columbia River occurred about 200 to 600 years ago [94, 95], and locally active portions of the slide are moving very slowly (approximately 150 to 200 mm/year; 6 to 8 in/year).

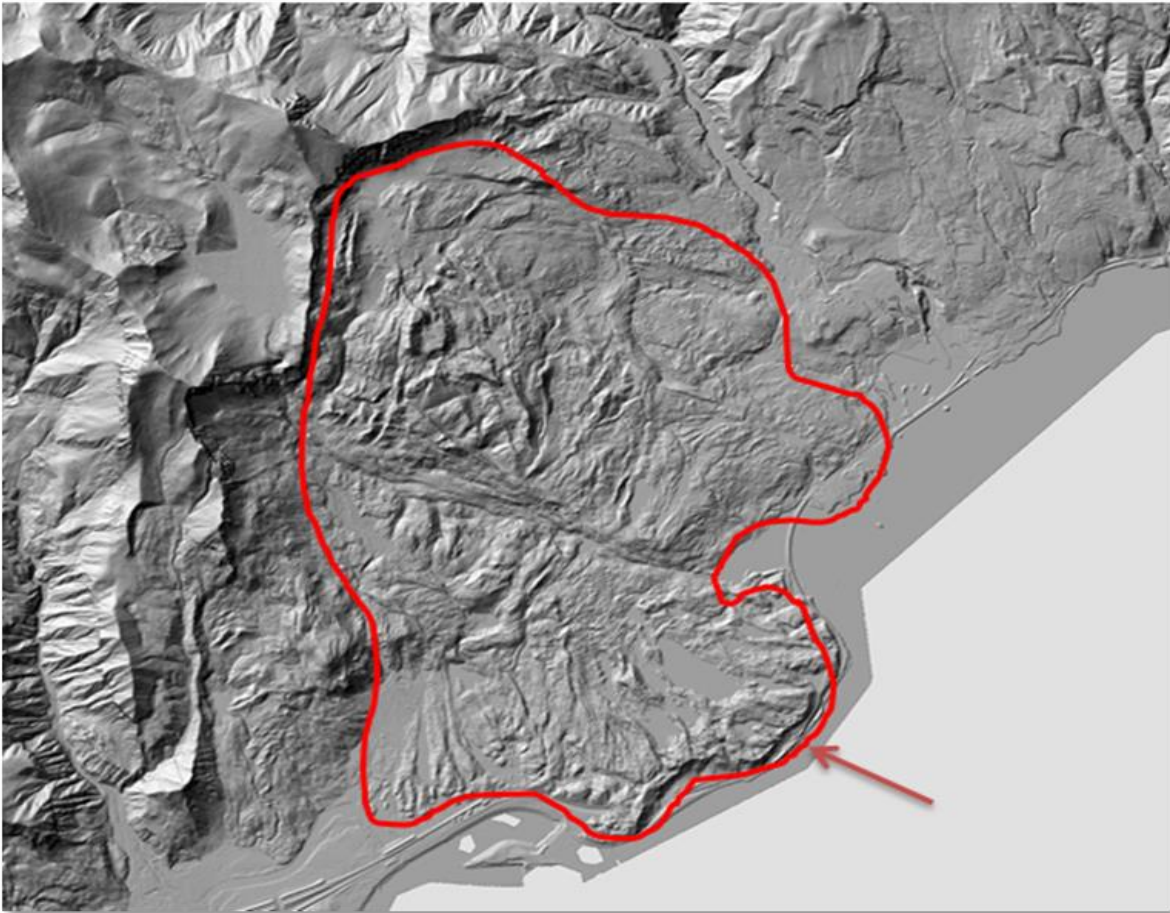


Figure 2-52 LiDAR hillshade image of the 18 mi² Cascade-Bonneville landslide complex (approximate outline in red) in the Columbia River Gorge of Washington. The toe of most recent major movement of the landslide into the Columbia River is shown by the arrow. (Puget Sound LiDAR Consortium)

For subsidence features, excepting new or planned underground mines, the focus is also on a geomorphic review of remote sensing imagery to look for disturbed ground (e.g., sinkholes, closed depressions, fissures) associated with collapse of subsurface karst caverns, underground mines or subsurface fluid withdrawal. Again, LiDAR hillshade imagery works well to highlight such subsidence features. Figure 2-53 illustrates karst sinkholes near Utica, Minnesota imaged on a LiDAR hillshade.

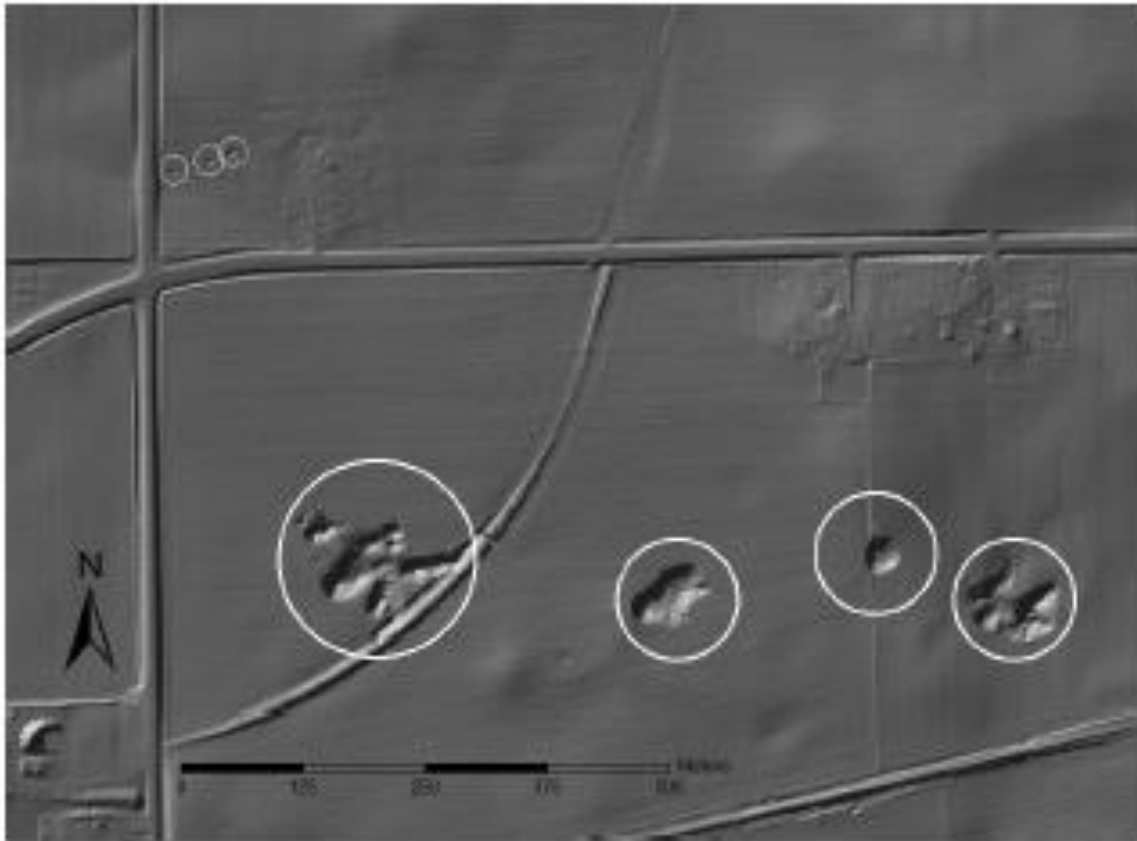


Figure 2-53 Karst sinkholes and closed depressions (circles) visible on a LiDAR hillshade image of an area near Utica, Minnesota [96]

The Phase I screening should include an aerial reconnaissance (e.g., helicopter preferred, or fixed-wing aircraft) to confirm/verify the office-based assessment, and to identify any potential hazards that may not have been mapped previously. Based on the threat/hazard classification, the hazards of concern (typically the moderate and high hazards) are prioritized for study in the next phase of assessment.

The results of the Phase I are typically entered into a GIS database management system. In addition, tables and maps of the identified hazards are developed in Phase I. Table 2-7 is an example listing of identified landslides from a Phase I screening for a pipeline system in the western United States. Figure 2-54 is a map excerpt of identified and mapped landslides from a Phase I screening for a pipeline in the eastern United States.

Table 2-7 Example of list of steeper slopes and landslides identified from a Phase I screening for a pipeline system in the western United States

Beginning MP	Ending MP	Threat/Hazard Classification	Comments
0.0	2.0	Low	Slopes > 40 percent
7.42	--	Moderate	Potential debris flows from canyon to west of ROW
10.0	27.0	Low	Slopes > 40 percent
16.42	--	Moderate	Potential debris flows from canyon to west of ROW
18.3	--	Moderate	Potential dormant landslide across ROW
30.45	--	Moderate	Potential dormant landslide across ROW
31.5	43.0	Low	Slopes > 40 percent
63.29	63.8	Moderate	Toe of potentially dormant landslide across ROW
206.3	--	High	Small active landslide about 30 m (100 ft) downslope of ROW; potential to retrogress upslope to ROW
206.43	--	Moderate	Small active landslide upslope of ROW
231.4	--	Moderate	Small active landslide undercut by stream to east of ROW.

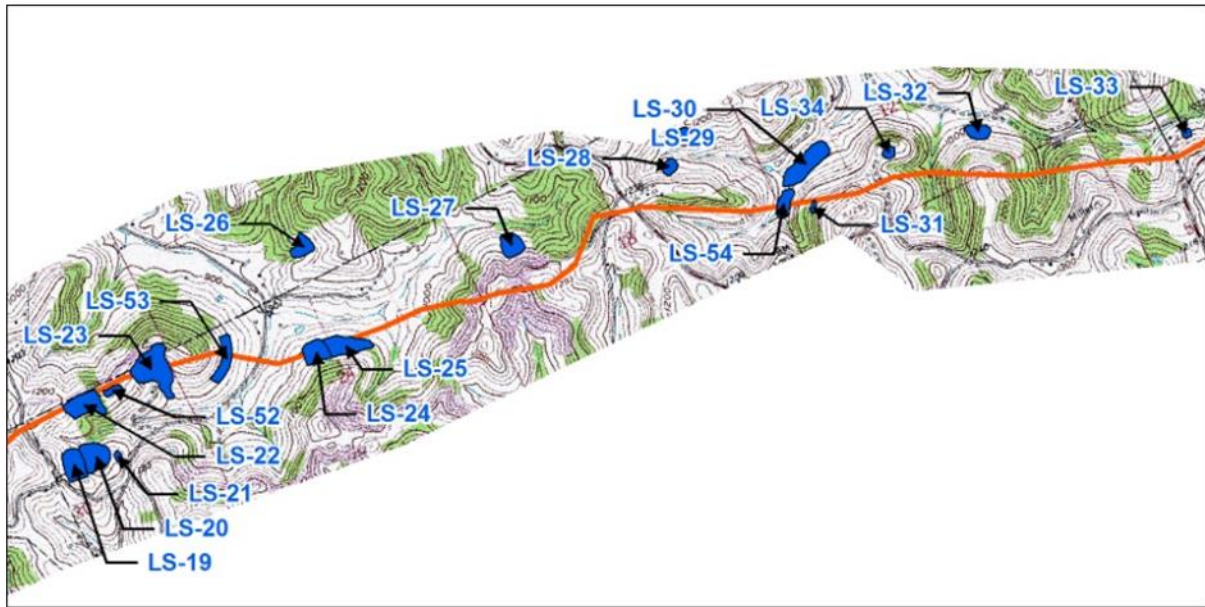


Figure 2-54 Map of landslides identified from a Phase I screening in the eastern United States with individual landslide identifier codes.

The results of the Phase I screening are reviewed and evaluated to identify and select those landslide and subsidence hazards recommended for further, site-specific assessment in Phase II. Commonly, the high threat hazards are automatically recommended for further assessment/investigation. The moderate threat level hazards may also be recommended for Phase II assessment depending on the nature and location of the hazard relative to the pipeline, and the completeness and quality of the data used to support the threat classifications.

2.5.4 Description of Phase II Geologic Hazards Reconnaissance

The Phase II hazards reconnaissance is the first site-specific field work undertaken for the hazards recommended from the Phase I screening. The Phase II reconnaissance emphasizes and employs non-intrusive, ground-based geomorphic and geologic assessments and mapping (Figure 2-55) of the high threat, and commonly, selected moderate threat landslides and subsidence hazards identified in the Phase I screening that may affect a pipeline. The field data are typically collected on GIS-based, precision GPS units/tablets on which the Phase I screening hazards are plotted along with topographic, geologic and LiDAR base maps. The GPS units/tablets allow for drawing features and taking detailed field notes that can be entered into the GIS hazard database. Alternatively, field notes can be entered directly into other mobile devices and automatically added to the GIS database.



Figure 2-55 Geomorphic and geologic field mapping of an active earth flow landslide adjacent to a ROW (Photo by: D. West, Location: Ohio, Year: 2012)

For landslides, the type, nature, age and lateral and vertical limits are described and documented in detail based on the site-specific surface geomorphic and geologic reconnaissance. Additionally, it is always recommended that the pipeline should be located and marked in the field; for example, on 10-foot (3-meter) centers, including the pipe depth. It may become evident following the location that the line has been displaced or deflected by landslide movement depending on the landslide interaction scenario. Additionally, a surface survey of the ground contours, pipeline surface locations and measured pipeline depths may allow for the preliminary detection of possible vertical deformation of the pipeline.

The threat/hazard level assigned from the Phase I screening is re-evaluated based on the Phase II work, and is verified, or revised based on the site-specific reconnaissance. The site-specific data collected for each hazard site are entered into the GIS database to update the database. Any new landslide hazard sites, identified during the Phase II reconnaissance are also described, assigned a unique identifier, documented, and added to the database.

Examples of high and moderate threat/hazard landslides investigated during a Phase II field geomorphic and geologic reconnaissance are illustrated in Figure 2-56, Figure 2-57, Figure 2-58,

and Figure 2-59, respectively. The examples are from a Phase II reconnaissance completed for a pipeline operator in the eastern United States.

In Figure 2-56, landslide G-417 illustrates a high threat/hazard level landslide that crosses a pipeline. (In Figure 2-56, there are other high threat landslides with red boundaries and low threat landslides with green boundaries.) The landslide was initially mapped on a LiDAR hillshade base in Phase I, and in the field the lateral limits of the landslide were confirmed or revised, and documented on a GIS-based, GPS tablet that allows for precisely locating polygons (shapes) and allows for the documentation of detailed notes of the nature of the landslide. The LiDAR hillshade clearly shows the fresh, hummocky nature of landslide G-417, that it has disrupted otherwise uniform slope topography, and that it crosses the pipeline. In the Phase I screening, G-417 was classified a high threat/hazard because it appeared to be active or recently active and it crossed the pipeline. However, from the LiDAR hillshade the nature of the ROW, that is whether it was disturbed or not, could not be determined. Thus, the nature and condition of the ROW across the landslide were examined during the Phase II reconnaissance. During the Phase II field geomorphic and geologic reconnaissance, it was observed that the toe and body of the landslide disturbed the ROW surface, and appeared to be less than 10 years old based on its geomorphic expression (Figure 2-57).

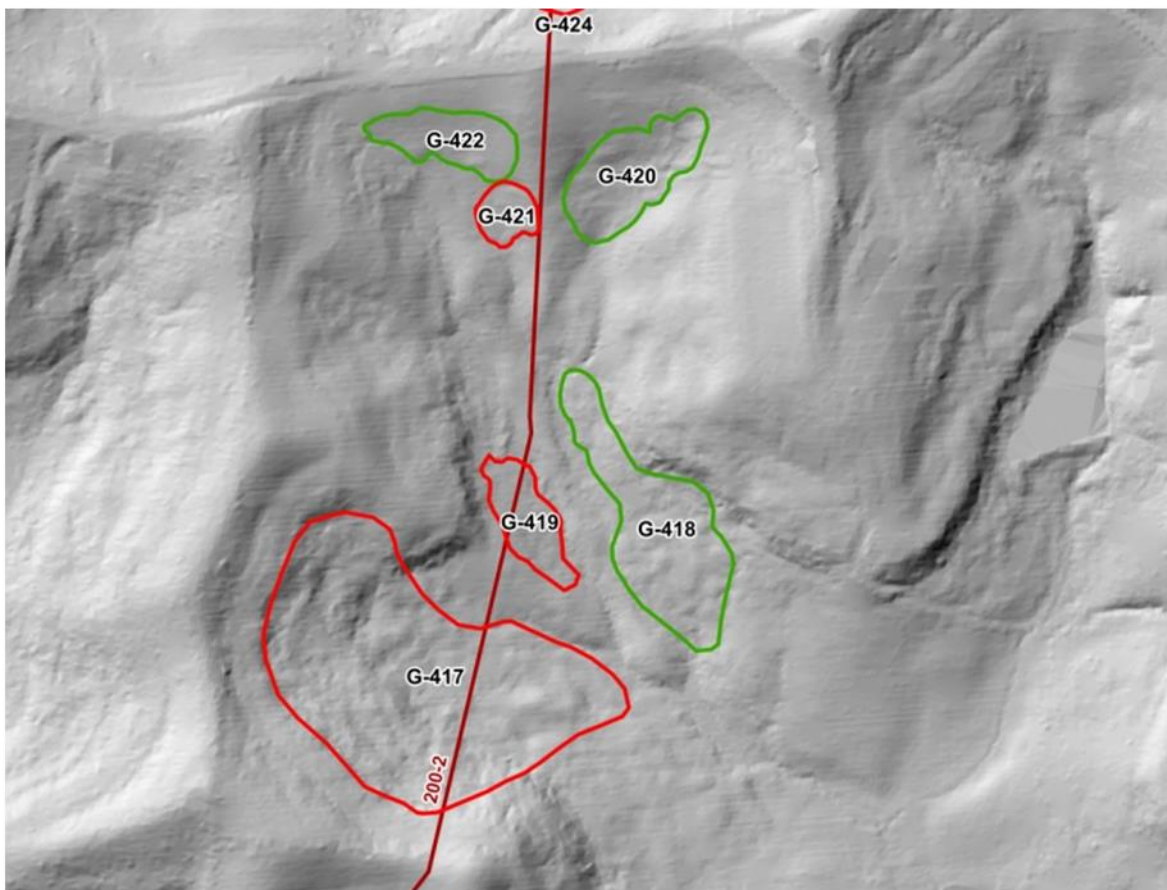


Figure 2-56 LiDAR hillshade example of a “high” threat level landslide, G-417, that crosses the pipeline.



Figure 2-57 “High” threat level landslide G-417 with pronounced toe (at arrow), that disturbs the ROW and has geomorphic evidence of movement less than 10 years old.

A moderate threat/hazard level landslide, G-130, is depicted on Figure 2-58. The landslide exhibits subdued hummocky topography and it crosses the ROW and pipeline. However, based on the Phase II field geomorphic and geologic reconnaissance, it was observed that the landslide did not disturb the ROW surface (Figure 2-59). Rather, the ROW surface was smooth, lacking the subdued hummocky topography of the landslide surface either side of the ROW, suggesting no landslide movement across the ROW after grading of the ROW. Because of these geomorphic conditions observed in the field, the landslide was classified with a moderate threat/hazard level.

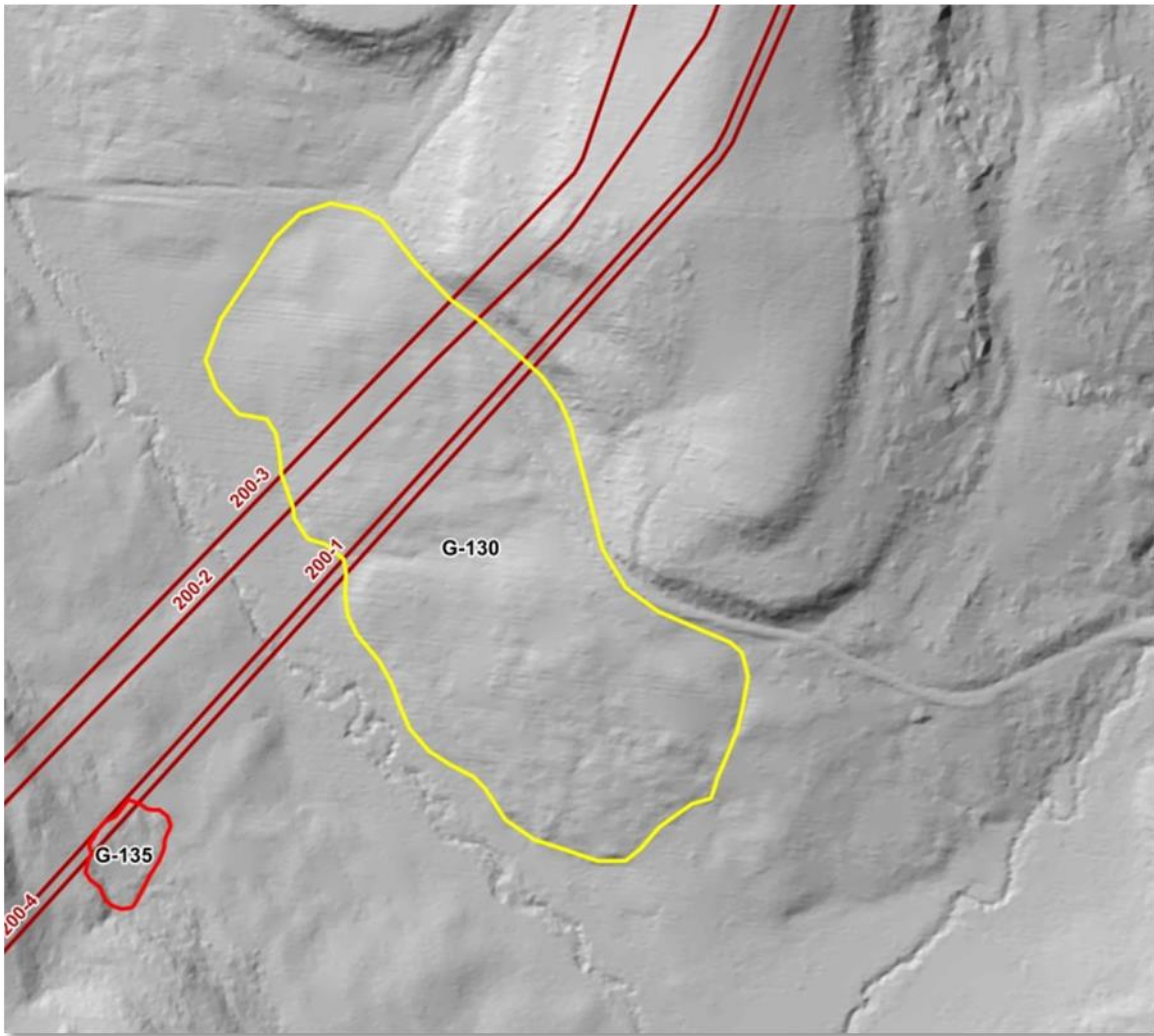


Figure 2-58 LiDAR hillshade example of a “moderate” threat level landslide G-130 that crosses the pipeline, but has no apparent geomorphic evidence of post-construction ROW movement.



Figure 2-59 “Moderate” threat level landslide G-130 with no geomorphic evidence of post-construction disturbance of the ROW surface; the arrow shows the apparently undisturbed ROW surface that crosses undisturbed through the older landslide.

For subsidence hazards, Phase II reconnaissance work may involve the following activities depending on the type of subsidence hazard being addressed from the Phase I screening:

- Aquifer system compaction from subsurface fluid withdrawal:
 - Field geomorphic and geologic reconnaissance of the high and selected moderate threat/hazard subsidence features from the Phase I screening such as fissures with horizontal separation and differential vertical offset
 - Mapping and documentation of the surface subsidence features including type, length, width, vertical separation, orientation, proximity relative to the pipeline (e.g., crossing, parallel, projecting toward, etc.), and age of most recent movement, on to GIS-based, precision GPS instruments
 - Re-evaluation and revision, as appropriate, of the Phase I threat/hazard level classifications
- Karst subsidence:

- Field geomorphic and geologic reconnaissance of the high and selected moderate threat/hazard features identified in the Phase I screening such as sinkholes and closed depressions
- Targeted geophysics to image potential subsurface voids (Figure 2-60)
- Mapping and documentation of the type, nature, shape, fractures, depth, age and location with respect to the pipeline
- Re-evaluation and revision, as appropriate, of the Phase I threat/hazard level classifications
- Underground mine subsidence:
 - Field geomorphic and geologic reconnaissance and mapping of high and selected moderate abandoned mine threat/hazard areas to examine whether there are surface features that may be associated with the underground mines that could affect the pipeline
 - For planned longwall mines, review of the mine plans and establishment of contacts with the mine. Review of topography (high relief and valley bottoms) along the pipeline within 1¼ miles (2 km) of the mine as it relates to potential valley closure.
 - For planned room and pillar or retreat mines, review of pillar plans and available stratigraphy to quantify risk of subsidence
 - Re-evaluation and revision, as appropriate, of the Phase I threat/hazard level classifications

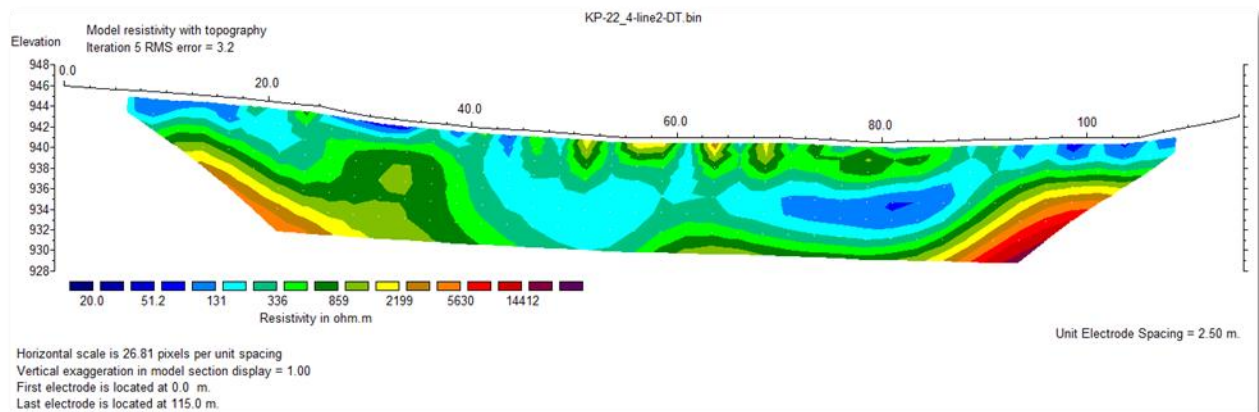


Figure 2-60 Example of ERI Dipole-Dipole geophysical results for investigation of karst terrain along a pipeline ROW

The high threat/hazard landslides and subsidence features that remain following the Phase II reconnaissance are typically recommended for Phase III investigation.

2.5.5 Description of Phase III Geologic Hazards Investigation

The Phase III assessment is undertaken for those landslide and subsidence high threat/hazard sites. The intent is typically to develop the detailed site-specific data that are necessary for the

development of threat/hazard mitigation alternatives, and for the development of threat/hazard monitoring programs/plans. A Phase III assessment may include site-specific subsurface investigations (Figure 2-61), and more detailed surface investigations to be able to collect the necessary detailed data. The common types/tools/techniques for the Phase III intrusive field investigations are summarized in Table 2-4.



Figure 2-61 Installation of a slope inclinometer in a geotechnical exploration borehole for a Phase III landslide investigation along a pipeline ROW (Photo by: A. McKenzie-Johnson, Location: Southern Indiana, Year: 2010)

The site-specific investigations and their data, which provide the physical characteristics of the particular hazard, combined with engineering analyses and modeling of the behavior of the hazard can be used to develop mitigation/monitoring concepts and designs (Section 8).

3 Characterization of Stresses and Strains Affecting Girth Weld Performance

Abstract

This section covers stresses that may exist in a joint of linepipe and stresses in a segment of pipelines. The stresses in a joint of a linepipe may include forming stress from pipe manufacturing and field cold bending. These stresses are self-balanced and typically don't affect the behavior of girth welds. Stresses that may affect girth weld behavior may come from field welding, operational conditions such as internal/external pressure and temperature differentials. Tie-in welds may experience higher stresses than mainline welds due to alignment, change in stiffness between two sides of the welds, and uneven support conditions. Stresses and strains from ground movement can have a large range of variations. High stresses generated by ground movement have been one of the key contributing factors to girth weld failures.

In the absence of changing pipe support conditions and increased stresses at bends, hydrostatic test does not impose high incremental longitudinal stress over stress levels existing under normal operational conditions. In contrast, lowering the temperature of linepipe can impose high levels of longitudinal tensile stress. From the viewpoint of girth weld integrity, the temperature effects, either during hydrostatic testing or in service, should be considered in girth weld integrity assessment.

Various methods for measuring and estimating stresses and strains in pipelines are introduced. Only the pipe-soil interaction models are covered in details in this section. Other methods are covered in Section 8 and Appendix E.

3.1 Stresses in a Joint of Linepipe

Stresses in a joint of linepipe may come from multiple sources. Some level of stress exists when pipes leave their manufacturers due to the pipe forming process and cold expansion. Linepipes may experience stresses during transportation. There could be residual stresses from field bending. The pipe forming and field bending stresses are self-balanced and should not affect girth welds. The stresses during transportation are typically within the elastic range. These stresses return to their original state at the completion of the transportation.

Stresses “locked-in” a joint of pipe can affect the performance of the pipe, especially if pipes experience plastic deformation. These locked-in stresses contribute to the total stresses experienced by the pipes when the pipes are subjected to additional loads during service. However, these locked-in stresses typically do not affect girth weld performance.

3.2 Stresses Affecting Girth Weld Performance

3.2.1 Stresses in the Construction Phase

3.2.1.1 Residual Stress from Welding

Stresses affecting girth welds start at the girth welding stage. Welding residual stresses occur in part due to the shrinkage of deposited weld metal during the cooling of the deposited weld metal. There is a local bending created by the welding residual stress. For large D/t pipes, the

longitudinal residual stress (transverse to the welding direction) is in tension on the ID side of the pipe and in compression on the OD side. The hoop residual stress is in tension [97, 98].

3.2.1.2 Stresses from Pipe Lifting and Lowering-in during Construction

After completing mainline welding, inspection, and field coating, the next phase of pipeline construction is lowering pipe into the trench. For most onshore pipelines, girth welds experience their highest longitudinal stress during this phase of their life. The lifting and lowering-in stress is typically in the range of 40% to 90% SMYS for an X70 pipe. The lowering-in stress is primarily driven by the contour of the pipe profile, i.e., lifting height, spacing between the sidebooms, and the horizontal offset between the pipe support (skids) and trench [99, 100]. The magnitude of the stress is not related to pipe grade as the material behavior is in the elastic range. However, the structural integrity significance of the stress is affected by pipe grade. For instance, a 40 ksi longitudinal stress is 77% of SMYS for an X52 pipe while the same magnitude of the stress is 50% of SMYS for an X80 pipe. Everything else being equal, the 40 ksi stress is likely to be more significant to an X52 pipe than an X80 pipe. The stresses from the lifting and lowering-in are relieved once the pipe is laid on the bottom of the trench, provided that the trench contour and pipe bends are properly matched.

3.2.1.3 Tie-in Stress

During tie-in welding, ends of pipes may have to be moved for alignment. Tie-in welds are often made near changes in pipe stiffness at crossings and bends. The varying pipe stiffness may cause the stresses to be concentrated at tie-in welds. In addition, there could be differential settlement near tie-in welds. The bedding/support at tie-in welds could be different from that of the mainline welds. In some cases pipe may be forced into position in order to make a tie-in weld. All these conditions can lead to high stresses at tie-in welds.

It is generally believed that the longitudinal stresses at tie-in welds are higher than those at mainline welds.

3.2.1.4 Backfill and Overburden Stresses

After backfill, stresses on the girth welds may come from spanning of the pipeline support or uneven bedding which can lead to bending moment along the pipeline. However, backfill (overburden) is thought to generate stresses primarily in the hoop direction (e.g., due to ovaling).

3.2.1.5 Stresses in Special Construction Methods

Girth welds can experience longitudinal stress during HDD from the pull-back force and curvature of the HDD profile. Occasionally, pneumatic hammers are used to assist pull-back operation. The action of the pneumatic hammer can generate cyclic longitudinal stress which may warrant fatigue assessment in some situations.

3.2.1.6 Stresses during Hydrostatic Pressure Testing

During the hydrostatic pressure test, longitudinal tensile stress is generated due to the Poisson's effect. In a restrained straight pipeline segment on flat terrain, the maximum pressure corresponding to a hoop stress of 100% SMYS can produce a longitudinal stress of 30% SMYS.

However, additional longitudinal stress may be generated from the weight of the water when there is uneven support or soil settlement. In addition, bending moments may be generated due to hydrostatic test pressure at bends and other fittings [101].

In the absence of significant settlement stress, the longitudinal stress during the hydrostatic pressure test is fairly low. This low stress level is based on the assumption that the pipe at the time of hydrostatic testing has the same temperature as that at the time of pipe lowering-in. Any temperature differential between hydrostatic test temperature and lowering-in temperature can introduce additional stresses.

3.2.2 Stresses during Pipeline Service

Stresses during normal pipeline service may come from a number of sources:

1. *Lock-in stresses from the pipeline construction.* Apart from welding residual stress and stresses from temperature differential, the “lock-in” longitudinal stress after construction is principally related to the “lateral bending” of the pipes. The lateral bending may come from uneven support and overburden, forced movement of pipe ends during tie-in welding, and forced alignment of pipes to trench or HDD profiles. The subject of welding residual stress is complex. For most pipeline girth welds experiencing longitudinal tensile stress, the effects of welding residual stress on the girth weld integrity under static loads are small. Welding residual stresses are a more important factor in fatigue life assessment of girth welds.

2. *Internal pressure.* A tensile longitudinal stress is generated from the Poisson’s effect when a pipe is pressurized. The magnitude of the longitudinal stress is 30% of the hoop stress for a restrained straight segment of a pipeline on flat terrain without bends.

3. *Thermal stress.* It is generally assumed that a pipe is in a near-stress-free state when the pipe is laid at the bottom of a trench (absent of tie-in stress and/or settlement stress). During service, pipes are generally at a temperature different from that during lowering-in operation. The temperature difference creates a longitudinal thermal stress. If the service temperature is lower than the construction temperature, the longitudinal stress is tensile.

4. *Ground movement.* Ground movement includes all forms of movements that tend to impose motion on a pipeline, including soil creep, landslide, settlement, earthquake, et al. The magnitude of the stresses and strains imposed by ground movements can vary greatly. In contrast, the magnitude of the stresses from the first three sources listed above has limited ranges. Consequently, ground movement is typically the major determining factor that can generate sufficiently high stress to rupture a girth weld.

5. *Unsupported pipe span or insufficient negative buoyancy.* An exposed pipe section or a pipe section in a body of water that is not sufficiently weighed down can move laterally or vertically. Such movement can produce both static and cyclic stresses on the girth welds. An exposed pipe segment can experience bending moment and “cable force” due to the weight of the pipe and its content [102].

3.2.3 Baseline Stresses and Strains

A typical scenario of longitudinal stresses from internal pressure, temperature differential, and other locked-in stresses is shown in Table 3-1. All pipelines are operated at a Class 1 location design factor, i.e., the hoop stress is at 72% SMYS. To highlight the possible tensile longitudinal stress, it is assumed that the pipeline is constructed at a relatively high ambient temperature of 80 °F and operated at 40 °F, thus having a temperature differential of -40 °F. This temperature differential would produce a tensile longitudinal stress of approximately 8.0 ksi¹.

The longitudinal stress from internal pressures is proportional to the magnitude of the internal pressure. At the same design factor, the magnitude of the longitudinal stress from internal pressure increases with pipe grade (SMYS), but remains at the same percentage of the SMYS. The longitudinal stress from temperature differential is only affected by the magnitude of the temperature differential, not by the pipe grade. With the increase of pipe grade, the total stress becomes a smaller percentage of SMYS at the same temperature differential and design factor.

Table 3-1 Stresses and strains from internal pressure, temperature differential, and other locked-in stresses

Pipe Grade	Pipe Yield Strength	lowest service Temperature	Construction Temperature	Design Factor	Longitudinal Stress from Pressure / SMYS	Longitudinal Stress from Pressure	Thermal Stress	Other Locked-In Stresses	Total Pressure, Thermal, and Other Stresses	Total Thermal, Pressure, and Other Stresses / SMYS	Baseline Strain
	(ksi)	(F)	(F)		(%)	(ksi)	(ksi)	(ksi)	(ksi)	(%)	(%)
X52	52	40	80	0.72	21.6	11.2	8.0	10.0	29.2	56.2	0.10
X60	60	40	80	0.72	21.6	13.0	8.0	10.0	31.0	51.6	0.10
X65	65	40	80	0.72	21.6	14.0	8.0	10.0	32.0	49.3	0.11
X70	70	40	80	0.72	21.6	15.1	8.0	10.0	33.1	47.3	0.11

In Table 3-1, a locked-in stress of 10 ksi is added to the stresses from internal pressure and temperature differential. The locked-in number is an educated guess for illustrative purpose. The actual locked-in stress can vary greatly among different construction conditions and

¹ The precise number depends on the coefficient of thermal expansion. Various references put the coefficient at 6.5×10^{-6} to nearly 8.0×10^{-6} in/in°F. This current calculation uses a coefficient of 6.67×10^{-6} in/in°F.

practice. When all the stresses are added together, the corresponding baseline strain is approximately 0.10%.

3.2.4 Cyclic Stress on Girth Welds

For buried pipelines, temperature and pressure fluctuations are typically the source of cyclic longitudinal stresses. For gas pipelines, the magnitude and the number of cycles of pressure fluctuation are low. The temperature fluctuation is also sufficiently low so fatigue flaw growth in girth welds is typically not a concern in gas pipelines. In contrast, liquid pipelines can experience high magnitude and large numbers of pressure cycles. In some cases, fatigue flaw growth in girth welds can be a concern.

3.2.5 Stresses of Pipes on Slopes

Pipelines on slopes may experience additional longitudinal stresses in comparison to pipelines in flat terrain. This is especially true at the locations near over-bends (peaks) and sag-bends (valleys). When the slope is sufficiently steep, the soils may not provide sufficient force to hold the pipeline in place, particularly when fine grained backfill soils become saturated during wetter times of the year or extreme precipitation events. Tensile and/or compressive stresses may be generated near over-bends and sag-bends.

3.3 Overview of Methods of Measuring of Stresses and Strains in Pipelines

The applied strain on the pipeline, alternatively termed strain demand, may be estimated from pipe operations and environmental conditions, such as geotechnical features and soil conditions. There are principally four types of methods available for estimating strain demand.

- (1) *IMU (Inertial Measurement Unit)*. IMU provides centerline position of pipelines. Successive IMU runs detect pipe movements which can be analyzed and converted to so-called “bending strain.” However, uniform tensile or compressive strains (sometimes termed *extensional strains*) can’t be detected by IMU as there is no curvature change of pipes. Extensional strains can come from thermal expansion or compression or internal pressure, or from soil movement parallel with the pipeline. In most cases, the bending strains are reported when the values are greater than a threshold value (typically greater than 0.125%). The utilization of IMU is detailed in Sections 4 and 8.
- (2) *Pipe-Soil Interaction Models*. These models start from the estimated amount of ground or soil movement which may come from historical data, ground or aerial surveys, or other methods; see Section 8. The impact on the pipe of such movements is estimated through pipe-soil interaction (PSI) models. PSI models of various complexities may be used to estimate strains imposed on the pipeline due to the ground movement [103,104,105].
- (3) *Direct Measurement*. Strain gauges have been widely used in locations of expected high strains. Fiber optic cables can provide strains over long segments of pipelines. The direct measurement techniques are covered in Section 8.3 and Appendix E.

(4) *In-Situ Stress Measurement*. A number of vendors claim that stresses in a pipeline may be measured by the change of steel's magnetic signature and other properties under stress. In general, the consistency and accuracy of these methods in field application are not well established at the time of this writing; however this appears to be a developing field. One of the major challenges for integrity assessment is differentiating the stresses from pipe forming (pipe manufacturing and cold field bending) and the stresses from actively applied external loads. Only the stresses from external loads are of concern in assessing the integrity of the pipelines. These techniques are covered in Appendix E.

3.4 Pipe-Soil Interaction Models

For a buried pipeline, loads (often represented in stresses or strains) are induced when there is a differential motion between the pipeline and surrounding soil. The application of the pipe-soil interaction models often starts from the characterization of the soil movement. Many factors affect the loads imparted on the pipeline by the soil. These factors are taken into account in the pipe-soil interaction models to various degrees. The most important factors related to the pipe-soil interaction modeling are [106]:

- Ability to simulate large relative displacement of pipeline,
- Correct modeling of the pipe-soil interface behavior,
- Selection of appropriate constitutive models,
- Accurate estimation of the soil constitutive parameters,
- Proper consideration of loading rate effects,
- Coupling effects from oblique pipe movement, and
- Recognizing the range of applicability of recommendations over a wide range of soil condition in practice.

3.4.1 Structural Pipe-Soil Interaction Models

The most widely used pipe-soil interaction models use structural beam elements to represent the pipe and spring elements to represent the resistance of soil to the pipe movement as shown in Figure 3-1 [107]. The spring elements are in three orthogonal directions: longitudinal (axial), transverse horizontal, and transverse vertical. The beam and spring elements are incorporated into a finite element package, such as ABAQUS®, to assess the pipe response for a given soil movement condition.

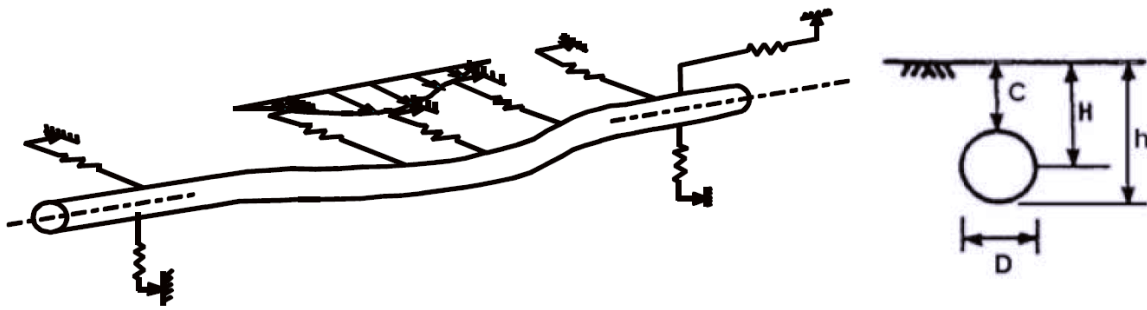


Figure 3-1 Structure model representing the pipe-soil interaction [107]

One of the key inputs in the structural pipe-soil interaction models is the representation of the stress-dependent load-deformation characteristics of the springs. The ASCE guidelines were formerly the standard reference for the representation [108]. These guidelines have been replaced by the American Lifelines Alliance (ALA) “Guidelines for the Design of Buried Steel Pipe” [109]. The representation of the spring characteristics in the guidelines was developed by Honegger and Nyman as given in a PRCI report [110].

3.4.2 Continuum Pipe-Soil Interaction Models

In a continuum pipe-soil interaction model, such as the one shown in Figure 3-2 [106], the pipe is represented by shell or solid elements. The complex pipe response, such as ovalization and wrinkling, can be properly modeled. In contrast, beam elements in the structural models are not capable of representing such behavior. The soil is modeled as a continuous medium, thus allowing proper representation of complex soil behavior such as shear load transfer. In addition, variable circumferential and longitudinal pressure distribution can be properly presented in such models. The continuum pipe-soil model implemented by C-CORE using commercial finite element package ABAQUS/Standard® was able to simulate large relative displacement and account for pipe and soil nonlinearity, relative slip and rotation and separation at the pipe-soil interface [111,112].

While C-CORE’s continuum model uses implicit finite element solver in ABAQUS/Standard, BMT Fleet has been developing a 3D continuum model that uses Smooth Particle Hydrodynamic (SPH) method in LS-DYNA® [113]. This model has been applied to simulate the pipeline response to a translational slide [114].

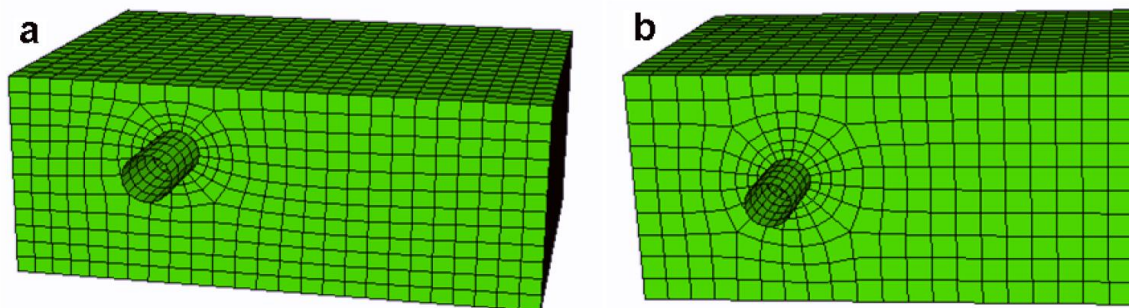


Figure 3-2 Continuum model representing pipe-soil interaction

3.4.3 Pros and Cons of Various Pipe-Soil Interaction Models

The principal advantage of the structural pipe-soil interaction models is its computational efficiency. However, the force-displacement relationship representing the resistance of the soil is a simplification that introduces modeling errors and prevents certain key features from being properly modeled. In contrast, the continuum pipe-soil interaction models provide more realistic representation of the physical mechanism at the expense of computational efficiency. In addition, there is limited availability of realistic soil constitutive models. The expertise required to apply the continuum models is higher than that required for the structural models.

3.5 Comparison of Various Stress/Strain Measurement Techniques

Each of the strain estimation/determination methods discussed in Sections 3.3 and 3.4 offers certain advantages and disadvantages. For instance, the strains measured by strain gauges are considered highly reliable. However, strain gauges can only monitor isolated locations. Pipe and soil interaction models can be used for long segments of pipelines. The strains computed from such models are highly dependent on the spring parameters which are related to soil properties. Site-specific soil properties are generally not available unless a geotechnical soil sampling program has been performed, and can change over time or even from season to season as the water content in the soil changes, which can affect soil properties.

The applicability and limitations of various methods are covered when such methods are introduced in details in Sections 4 and 8 and Appendix E.

4 Utilization of IMU Data for Identifying Strain Locations of Interest

Abstract

This section starts with the working principles of IMU, including various instrumentations in an IMU. The concept of pig length is introduced. The typical sensitivity and accuracy of IMU ILI tools are given along with the meaning of the parameters. The basic processing of the inertial survey data, including numerical differentiation and integration, is introduced. One significant part in the appropriate use of IMU tools is the recognition of their limitations. Here the limitations of the tools are introduced. The significance and possible ways to overcome the limitations are explained.

The processes and procedures to identify strain of interest are described in details. Another key part of this section is the recommended protocol to characterize and report strains of interest by ILI service providers. Possible ways to validate/verify IMU data are also given. This is an essential part of the appropriate use of IUM data, as explained throughout this report, that all monitoring techniques have their advantages and limitations.

4.1 Principles of IMU

As discussed by Hart, et al. [115], there are several in-line inspection (ILI) vendors who perform inertial surveys using high resolution inertial survey tools (smart pigs). These ILI tools travel downstream within the pipe bore carried forward by the flow. Because the axis of the tool body runs nominally coincident with and parallel to local orientation of pipe centerline, data from an inertial survey can be used to compute detailed three-dimensional geometry (position and curvature) profiles to represent the trajectory of the pipe centerline. The primary instruments on an inertial survey tool are gyroscopes and odometers.

- The Inertial Measurement Unit (IMU) includes an orthogonal triad of interferometer fiber optic angle rate gyroscopes and a corresponding orthogonal triad of uniaxial accelerometers. The IMU is housed within a cup or wheel supported canister of the pig. These instruments, which are typically sampled at 50 to 100 Hz, respond to the motion of the tool as it travels down a path which is nominally coincident with the pipeline centerline.
- Odometers measure the along-the-pipe “chainage” distance travelled by the pig. The odometer data can also be used to compute the instantaneous travel velocity of the pig.

Additional instruments are often deployed on an inertial survey tool including:

- Spring loaded radially oriented mechanical caliper arms which measure the geometry of the pipe bore to measure the inside diameter profile and to characterize features such as ovality, dents, ripples, wrinkles and buckles. The mechanical calipers are also used to locate the girth welds and wall thickness changes in the pipeline. Most tools deploy a single ring of at least 16 and up to hundreds of individual caliper arms around the pipe circumference. Some tools deploy two separated caliper rings with the arms offset to the midpoint between the arms on the adjacent ring in order to increase the circumferential resolution. Moreover, caliper tools equipped with eddy current based proximity sensors

at the caliper arms are able to compensate for lift-off effects caused by debris or girth weld penetration so that the contour of a deformation is more accurately captured when caliper arm liftoff occurs.

- Pressure and temperature gauges.
- Some vendors utilize “Combination Tools” which also include an axial or Circumferential Magnetic Flux Leakage (CMFL) or ultrasound (UT) instrumentation canister for measuring the pipe wall thickness/metal loss.

As discussed in Reference [115], the gyroscopes measure the rate of rotation of the tool with respect to an inertial reference frame. The accelerometers measure both the acceleration due to gravity and the acceleration of the inertial system with respect to the inertial reference frame. When the inertial system is stationary with respect to the earth, the accelerometers measure the gravity vector and the gyroscopes measure the earth rotation vector. This allows for determination of the pre-survey or post-survey orientation of the tool with respect to the local level reference frame, i.e., pitch, yaw, and roll. The orientation of the tool during the survey is obtained primarily by integration of the angle rate gyroscope readings after subtraction of the earth rotation. The inertial data processing develops the profile of the pitch and azimuth orientation of the path travelled by the pig during the survey. As shown in Figure 4-1, the pitch angle describes the inclination angle of the pig in the vertical plane (nose up is positive, nose down is negative) while as shown in Figure 4-2, the yaw (or azimuth) angle describes the angle between the pig travel direction/heading and north (yaw is clockwise negative, azimuth is clockwise positive).

For large diameter pipelines (typically \geq NPS24), the inertial survey tool consists of a single supported canister body while for small diameter pipelines (typically $<$ NPS24), the inertial survey tool is essentially a “train” of several supported canister bodies. Each canister is supported on a pair of flexible neoprene cups or support wheels which means that the orientation of the canister containing the IMU is always measured over a finite length – this length is typically in the range between 1 and 1.5 pipe diameters. The cup-to-cup or support-to-support length of the canister containing the IMU is referred to herein as L_{pig} to acknowledge that the gyroscope-established orientation of the tool is not instantaneous – it is always measured over this length.

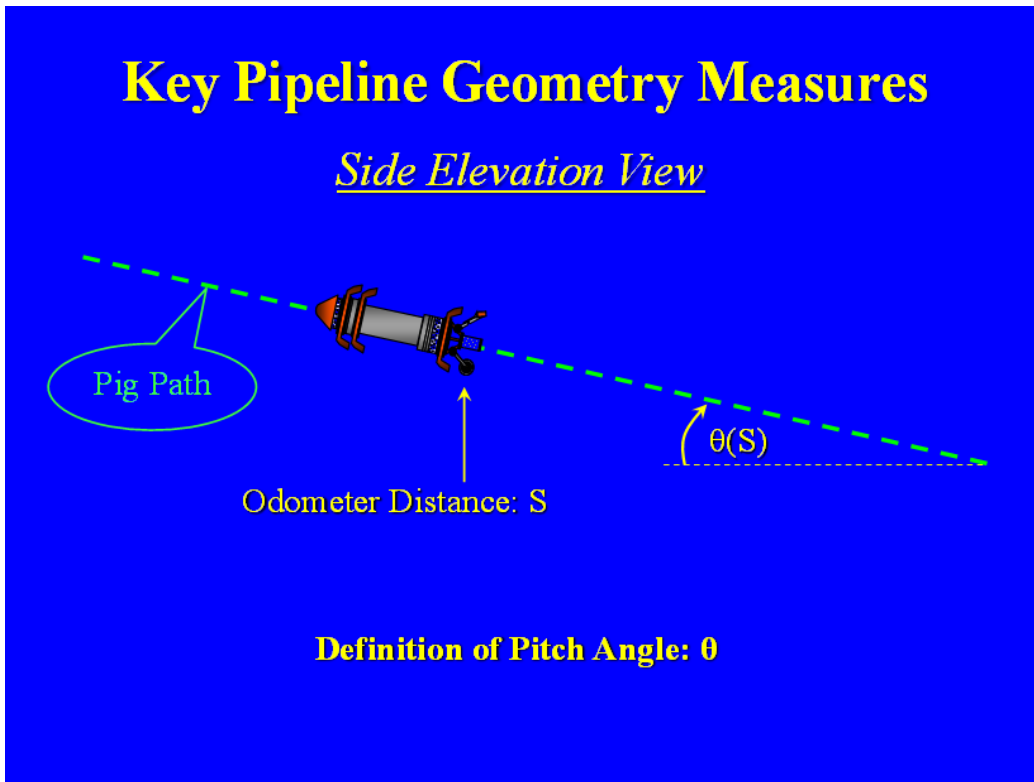


Figure 4-1 Definition of Pitch Angle θ

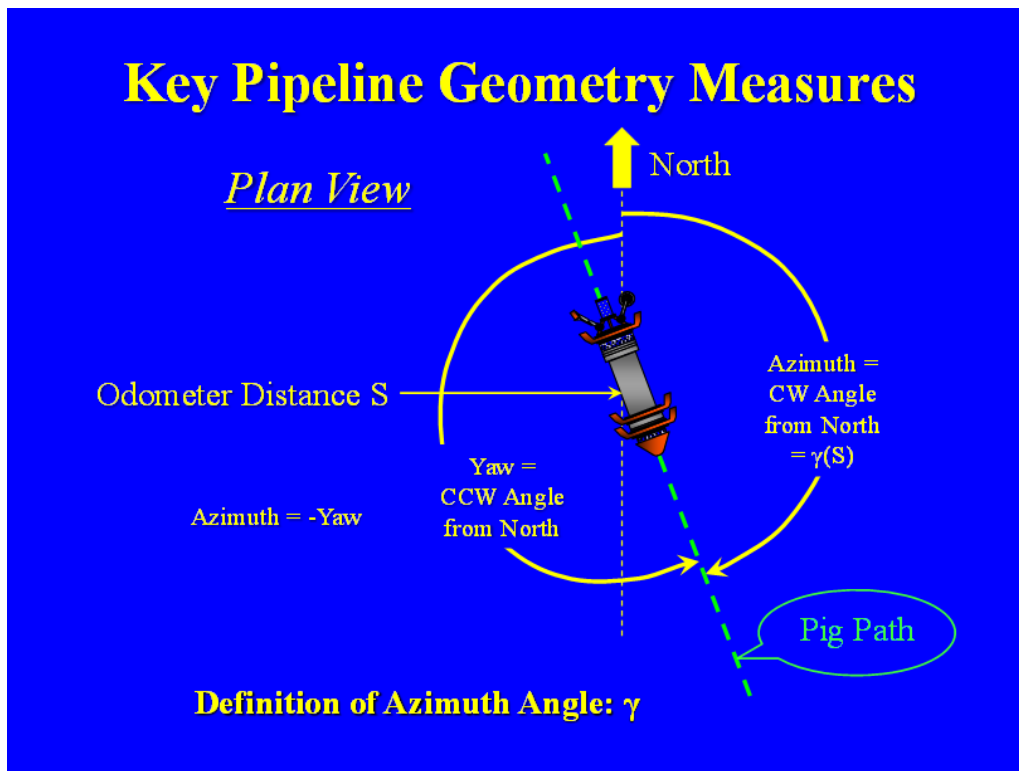


Figure 4-2 Definition of Azimuth/Yaw Angle γ

4.2 Typical Sensitivity and Accuracy

As previously noted, the inertial tool travels along with the pipe flow. Optimal tool velocities are in the range of 1 to 4 m/s (3 to 13 ft/s). As discussed in Reference [115], different IMU survey vendors provide different specifications related to the accuracy of the inertial survey data. For example, specified accuracies published for the Geopig® are as follows:

- Mapping Survey Accuracy 1:2000 (depending on the distance between tie-points)
- Dent/Feature Size: ± 2.5 mm
- Dent/Feature Orientation: $\pm 2^\circ$ arc
- Ovality: ± 2.5 mm
- Weld-to-Weld Distance: ± 12.5 mm
- Curvature Detection/Accuracy: $\pm 2500D$ Radius of Curvature, $\pm 0.02\%$ Strain
- Bend Angle Detection/Accuracy: $\pm 0.1^\circ$

As another example, the ROSEN RoGeo·Xt® tool for detection and sizing of deformations equipped with an IMU for XYZ mapping has the following specifications:

Feature	Accuracy	Detection Threshold
ID Changes	0.8 mm (0.03 in)	0.8 mm (0.03 in)
Ovality	1%	1%
Dent Depth	up to 0.8 mm (0.03 in)*	
Bend Strain Determination	$\pm 0.02\%$	$\pm 0.02\%$
Radius Determination	2500 D	

*depending on pipeline diameter

where the values are given for a confidence level of 80%.

Although some vendor reports/papers show results providing bending strain accuracies of $\pm 0.005\%$ to $\pm 0.01\%$ strain, the best available directly *specified* bending strain accuracy is $\pm 0.02\%$ strain (which is equivalent to a bend radius of $\pm 2500D$). Some vendors specify a larger detection threshold for an initial inertial survey (e.g., 0.125% bending strain or 400D).

The detection threshold describes the sensitivity of a measurement system, typically in terms of minimum detectable sizes, while the accuracy describes how accurately a defect can be sized once detected. For meaningful detection thresholds and sizing accuracies, a confidence level should always be provided. Typical specified confidence levels provided by ILI vendors are 80%, 85% or 90%. To achieve comparability between specified values with different confidence levels, the following conversion factors can be applied for normally distributed random errors:

80% and 85%: 1.123

85% and 90%: 1.143

80% and 90%: 1.283

4.3 Basic Processing of Inertial Survey Data

As presented in Reference [116], there are two main data processing procedures that are commonly applied to pipeline inertial survey data, namely: (1) numerical integration of the pitch and azimuth angle data with the odometer distance data to develop three-dimensional coordinates of the pipe centerline; and (2) numerical differentiation of the pitch and azimuth angle data with the odometer distance data to develop pipeline curvature profiles. This section provides an overview of these procedures.

4.3.1 Numerical Integration

The gyroscope and odometer data can be used to compute the path of the pig (which is taken to be the same as the pipe centerline) relative to known starting and ending points, using numerical integration. Euler integration is a straight-forward and reliable integration method wherein the relative three-dimensional position of a profile point “ $k+1$ ” is computed based on the pitch and azimuth (i.e., the slope of the profile) at a closely spaced adjacent point “ k ”. As described in Reference [116], in between the known coordinate tie-points, the incremental position changes of the pipe centerline path are computed using Euler integration of the pitch (θ) and azimuth (γ) angles with the odometer distance data (S) as follows:

$$\Delta N = \Delta S \cdot \cos \theta \cdot \cos \gamma \quad (4-1)$$

$$\Delta H = \Delta S \cdot \sin \theta \quad (4-2)$$

$$\Delta E = \Delta S \cdot \cos \theta \cdot \sin \gamma \quad (4-3)$$

where ΔN , ΔH , ΔE are the increments of Northing (N), elevation (H) and Easting (E) along the pipe profile, ΔS is the along-the-pipe distance increment between odometer data points “ k ” and “ $k+1$ ”, and θ and γ are the pitch and azimuth angles corresponding to odometer data point “ k ” (where the integration direction is from “ k ” to “ $k+1$ ”). The calculated centerline coordinate path is then translated and rotated such that the starting and ending coordinates pass exactly through the coordinates at the known tie-points. The integration can be performed over a selected length of the pipeline in both the forward direction and the backward directions and the average of the forward and backward profiles can be used for the final pipeline geometry. The tie-points are typically established by above ground GPS positioning at accessible crossings such as highways or access roads. Known physical locations including traps, crossovers, taps, and valves are aligned following the run. Moreover, AGMs are typically placed at the above ground tie-point locations so that they can be easily identified in the field. Typical tie-point intervals range from roughly 1000 m to 6000 m (0.6 – 3.7 miles).

The specified accuracy of the pipe position profile is typically 1/2000th of the distance from the nearest tie-point. For a distance between tie points of say 4,000 m (2.5 miles), the position error midway between the tie points for a single survey can reach ± 1 m (3 ft) (i.e., 4000/2/2000), which corresponds to up to 2 m (7 ft) difference between two surveys. This illustration neglects inaccuracies in the tie point coordinates. For tie point coordinates established using GPS, it should be noted that the elevation coordinate can be 2 to 3 times less accurate than the

corresponding horizontal coordinates – this effect should be considered when the depth of the pipeline is important (e.g., depth of cover determination, or depth of pipe below crossings, etc.).

Out-of-Straightness (OOS) plots are often used to display the relative horizontal and vertical position profiles as a function of chainage over a region of interest. OOS plots present the relative position profiles as deviations from a straight line with zero OOS at the beginning and end of the plot. OOS plots can be obtained by integrating locally between additional control points selected at the upstream and downstream ends of the feature of interest and performing a coordinate transformation from the Northing-Easting-Elevation coordinates into the horizontal and vertical OOS deviations from a straight line connecting the feature end points. Example plots are provided in Appendix B.

4.3.2 Numerical Differentiation

As discussed in Reference [116], the pitch (θ) and azimuth (γ) angle data can also be numerically differentiated with respect to the odometer distance data (S) to develop profiles of the pipe vertical and horizontal curvature. As illustrated schematically in Figure 4-3 and Figure 4-4, the vertical curvature (Ψ_V) and horizontal curvature (Ψ_H) are calculated as the change in pitch and azimuth angles ($\Delta\theta$ and $\Delta\gamma$), respectively, over a specified change in pipe distance (ΔS) along the path:

$$\Psi_V = \frac{\Delta\theta}{\Delta S} = \frac{\Delta\theta}{L_{gauge}} \quad (4-4)$$

$$\Psi_H = \frac{\Delta\gamma}{\Delta S} \cdot \cos \theta = -\frac{\Delta\gamma}{L_{gauge}} \cdot \cos \theta \quad (4-5)$$

The resultant curvature (Ψ_R) is:

$$\Psi_R = \sqrt{\Psi_V^2 + \Psi_H^2} \quad (4-6)$$

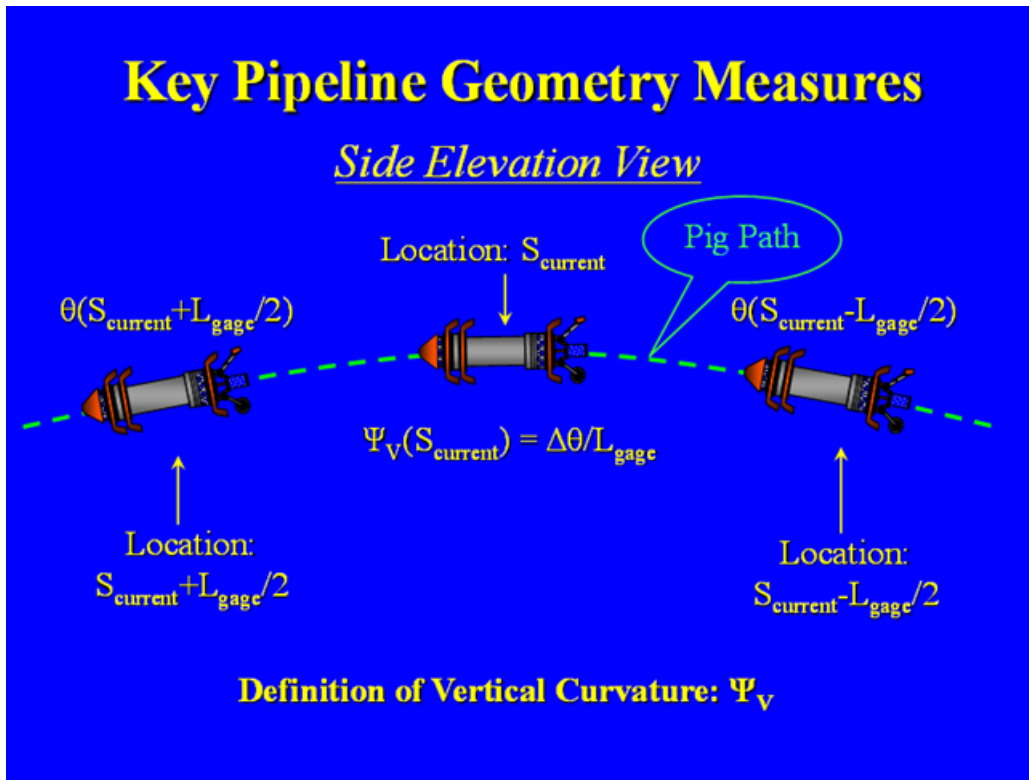


Figure 4-3 Illustration of Calculation of Vertical Curvature Ψ_V

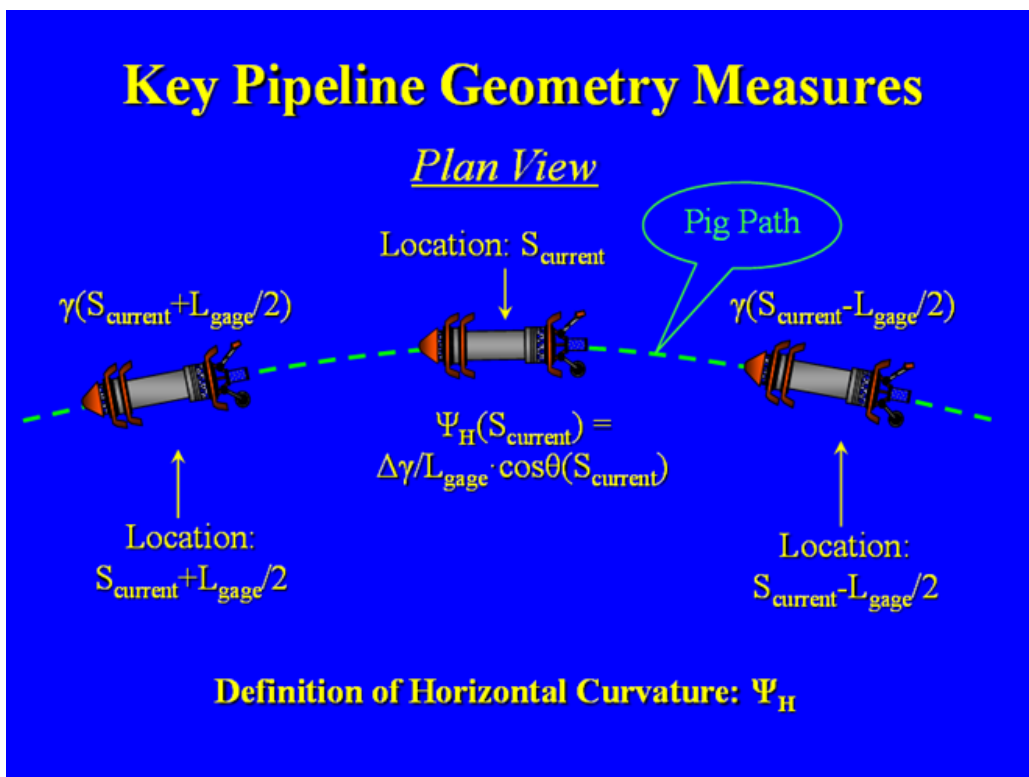


Figure 4-4 Illustration of Calculation of Horizontal Curvature Ψ_H

The vertical, horizontal and resultant bending strains are directly related to the corresponding curvature terms based on the assumption that plane sections remain plane as follows:

$$\varepsilon_V = \Psi_V \cdot \frac{D}{2} \quad (4-7)$$

$$\varepsilon_H = \Psi_H \cdot \frac{D}{2} \quad (4-8)$$

$$\varepsilon_R = \Psi_R \cdot \frac{D}{2} \quad (4-9)$$

where D is the outside diameter of the pipe. In order to reduce noise (e.g., due to tool dynamics and minor imperfections along the pipeline) in the curvature signal, it is typically computed over length of 3 to 6 pipe diameters. The distance over which the curvature is calculated is normally referred to as the gauge length L_{gage} . The sign convention used in equations (4-4) and (4-5) above is that sag bends and left turns correspond to positive vertical and horizontal curvatures, respectively. In other words, positive vertical bending strain corresponds to tension at the 6:00 orientation on the pipe cross section and positive horizontal bending strain corresponds to tension at the 3:00 orientation on the pipe cross section (looking downstream). The sign convention for curvature and bending strain is somewhat arbitrary and vendors may use different definitions.

The most efficient curvature calculation is based on a simple finite difference approach. The $\Delta\theta$ and $\Delta\gamma$ numerators in equations (4-4) and (4-5), respectively, are computed as the difference between the pitch or azimuth at a distance of $L_{gage}/2$ downstream and at a distance of $L_{gage}/2$ upstream of a given odometer distance coordinate. If the upstream or downstream location ($\pm L_{gage}/2$) falls between two discrete pitch or azimuth values, the pitch or azimuth value used in the difference calculation is obtained by linear interpolation between the adjacent values. The main advantage of the finite difference approach is that it is very efficient numerically. The main disadvantage of the finite difference approach is that it tends to amplify noise that is present in the underlying orientation data.

Somewhat smoother and more accurate curvature profiles can be computed using a “regression line” method where the curvature is computed as the slope of a least-squares line fit through the profiles of θ vs. S and γ vs. S over the gauge length L_{gage} . Figure 4-5 provides a schematic illustration of the regression line processing in θ vs. S space. At the current odometer distance coordinate, the least-squares fit lines on θ and γ as functions of S over the length L_{gage} centered on the current distance coordinate are expressed (in the general linear form $y=mx+b$ where m and b are the slope and intercept of the line) as follows:

$$\theta(S) = \Psi_V \cdot S + \theta_0 \quad (4-10)$$

$$\gamma(S) = \Psi_H \cdot S + \gamma_0 \quad (4-11)$$

The main advantages of the regression line approach are that it tends to smooth out noise that is present in the underlying orientation data and that for a given gauge length, it is more accurate

than the finite difference approach. The main disadvantage of the regression line approach is that developing the regression line fit involves additional numerical calculations than would be required using the finite difference approach.

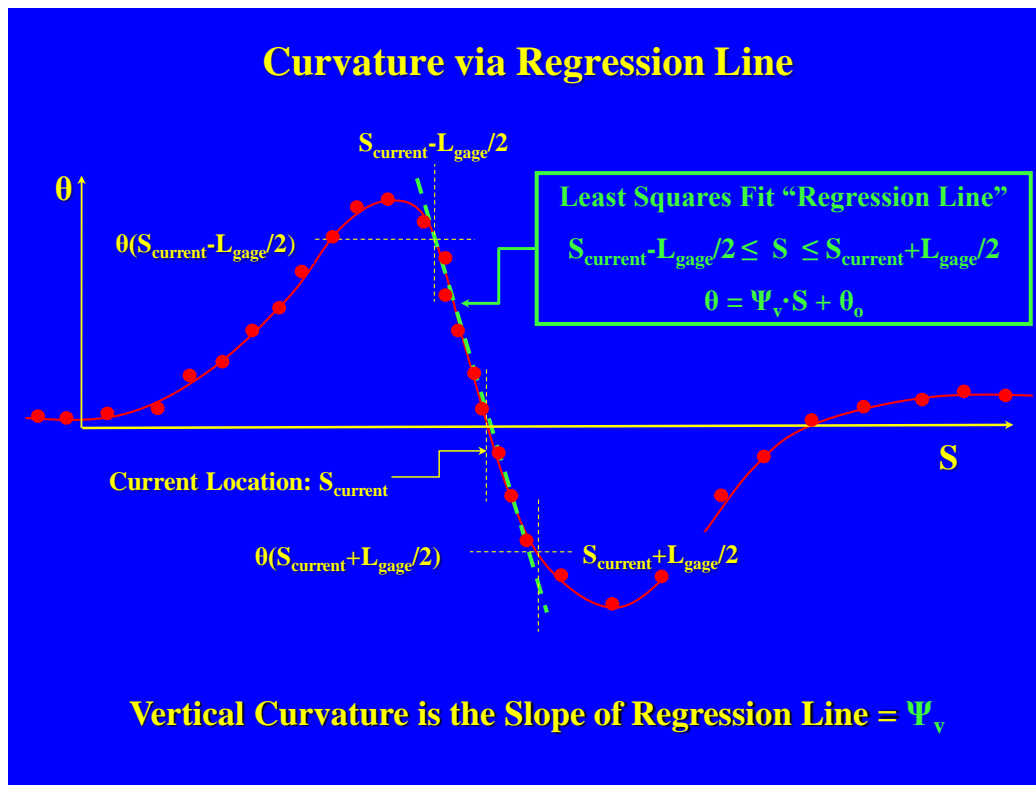


Figure 4-5 Illustration of Vertical Curvature Calculation Based on Regression Line

Based on our experience with inertial survey data, a high degree of repeatability with respect to the important features of the bending strain profiles (i.e., the parts of the signal associated with real pipeline movement) is typically observed in overlays of pipeline curvature/bending strain profiles obtained from different surveys. When running a subsequent survey with the same tool, subtle differences can be expected at girth welds and bends for example due to different tool velocities and slight differences in the pig-to-pipe attitude during the run. These differences can be more pronounced when the subsequent survey is run with a different tool or by a different vendor, particularly if the lengths of the pig (L_{pig}) are significantly different. Various vendors have published papers that document survey repeatability and comparisons with discrete strain gauge measurements (e.g., see References [117], [118] and [119]).

4.4 Limitations of Inertial Survey Data

While pipeline inertial surveys provide an extremely refined basis for characterizing pipeline geometry, there are several limitations to this technology that are worth noting:

- The specified accuracy of calculated pipeline coordinates between tie-points is limited to nominally $1/2000^{\text{th}}$ of the distance from the tie points (due to gyroscope bias and odometer error). This isn't necessarily viewed as a significant limitation since pipeline

curvature and orientation profiles (which are independent of tie-point coordinates) can be used directly to identify and characterize features of interest. This limitation can be overcome by reducing the distance between tie-points or using artificial tie-points to investigate local out-of-straightness (OOS) features.

- Inertial survey technology is only capable of capturing pipeline curvature/bending strain; it does not capture strains at the pipe centerline. This limitation is not normally a significant concern for situations which are dominated by bending action but centerline strain effects (e.g., cable action) can become significant for very long transverse ground movement features or ground movements which run parallel to the axis of the pipeline. For long transverse ground movement features, this limitation can be overcome by post-processing the survey results using specialized procedures developed to estimate pipe centerline strain effects (e.g., see Reference [115]) or by utilizing the pipeline profile data in a finite element model with realistic longitudinal pipe-soil resistance.
- Pipeline curvature developed from inertial survey data must always be associated with a curvature calculation gauge length (L_{gauge}). The effects of gauge length should be evaluated for every survey on a case-by-case basis to arrive at a value that is long enough to minimize the effects of noise in the data but not so long that it underestimates the true curvature. Overlay plots of curvature/bending strain calculated using multiple gauge lengths provide a useful basis for extracting more detailed information regarding certain pipeline features (e.g., delineation of cold bends, mitered welds, etc.). For girth welds located very close to cold bends, it may not be possible to determine how much of the calculated bending strain directly at the weld is real strain vs. how much is due to “leakage” of the curvature from the bend (i.e., a bend can influence curvature calculations over an influence length up to $(L_{gauge} + L_{pig})/2$ outside of the bend).
- Inertial survey data will always contain “noise” due to the dynamic response motion of the pig body as its support wheels/cups encounter features along the pipeline. These noise features are related to deviations of the pipe from a continuous, perfect cylinder. Within the pipe joints, these features include minor imperfections in the pipe wall such as expander marks and out of roundness. At girth welds, the pig body can experience “kicks” as the support wheels/cups encounter weld geometry features such as the weld bead, high-low misalignments, and subtle angular misalignments. While these girth weld features may be distinguishable in caliper and MFL data, it isn’t practicable to distinguish the details of these features in the inertial data with the exception of an angular misalignment which will manifest as a short length step change in the tool orientation (typically in the pitch signal with a step height in the range of say 0.5° to as much as 2°). The curvature calculations can show high curvatures at girth welds due to these “kick” features. Experienced analysts will understand that this is a spurious component of the curvature feature related to pipe noise - not real pipe strain. The effects of this noise can be managed by using longer curvature calculation gauge lengths and/or using regression line instead of divided difference differentiation. Typically, the dynamic

response of the pig to these features is characterized by a relatively short wavelength oscillation signature in the tool orientation signals. As described in References [116] and [123] these features can be removed from the calculated curvature/bending strain profiles using low-pass filtering techniques (i.e., removal of spurious short wave length/high frequency features while preserving long wave length/low frequency features).

- Inertial survey vendors typically specify optimal tool velocities in the range of 1 to 4 m/s (3 – 13 ft/s). In very steep terrain the extremes of the range should be avoided to allow for changes in speed due to gravity. For lines with faster flow velocities, gas bypass technology would be required as a workaround to keep the tool velocity within the acceptable range.
- Inertial survey tools always measure orientation (e.g., pitch and azimuth angles) over a finite length (L_{pig}). This may not be important unless you are undertaking a detailed analysis such as a finite element model. There is no “work-around” for this limitation – the analyst must simply be aware of it and understand where it might be important (e.g., for very short angle change features). An example of this limitation would be a pig stepping over a mitre bend where it would “soften” the feature.

4.5 Identification of Strain Locations of Interest from IMU Data

Inertial surveys are often applied for the purpose of “mapping” of the pipeline geometry which is computed based on numerical integration of the inertial measurement unit (IMU) and odometer data relative to specified tie point coordinates. The mapped geometry can be used for identification and locating key features and components along the pipeline alignment. While the mapping information is useful, the calculated pipe centerline position coordinates are unlikely to identify areas of anomalous pipeline movement or strain since the accuracy of the position profiles is limited by the distance between tie points. In order to identify such areas, it is necessary to review the pipe orientation and curvature profiles which are essentially the 1st and 2nd derivatives of the position profiles.

For pipelines which may be subjected to ground movement, there is a key interest in screening the bending strain and/or curvature profiles, which are computed based on numerical differentiation of the IMU and odometer data. In order to identify locations along the pipeline that may have been deformed due to differential ground movement, the analyst must be able to distinguish the pipeline geometry signatures associated with field bends (and fabricated elbows) from the pipeline geometry signatures associated with ground movement-induced transverse bending of the pipe. Key aspects that can be used to make this distinction are described as follows:

- (1) Curvature signals resulting from field cold bends and fabricated elbows (i.e., intentional bends) tend to be fairly short (e.g., the angle change or turn of an individual bend is *always* contained within a single joint length between two girth welds). Cold bends and elbows will normally stand out as significant, abrupt angle change ramps in the pitch and/or azimuth profiles with very large strain/curvature values. For example, ASME B31.8 [120] minimum cold bend radii (18D for NPS12 and smaller and 30D for NPS20

and larger) corresponds to bending strains in the range of roughly 1.7% to 2.7%. The curvature profile associated with an elbow or a cold bend typically exhibits a single curvature lobe of a given sign with no side-lobes of the opposite sign.

- (2) Ground movement-induced curvature signatures on the other hand, will tend to develop over relatively long lengths (e.g., spanning over one or more girth welds sometimes up to several hundred feet) and are often characterized by one or more sinusoidal shaped “lobes” along the pipeline. Sinusoidal curvature signatures are associated with sinusoidal ground movement shapes for example, within a long landslide where some sections of the slide will displace further downhill than adjacent sections. Ground movement-induced curvature signals associated with a fairly well-defined block or lobe of ground movement often exhibit a 3-lobe “W-shape” variant of sinusoid corresponding to one dominant curvature lobe (nominally centered on the ground movement) and two lesser side-lobes with curvature of the opposite sign. Another important distinction is that ground movement-induced strain features are usually much less pronounced than intentional bends with a bending strain amplitude “threshold of interest” in the range of roughly 0.2%.
- (3) The pitch and azimuth profiles often provide a useful way to identify possible ground/pipeline movement locations. In the absence of ground movement induced geometry changes, a pipeline will normally consist of a series of straight runs and intentional bends. Straight runs appear as flat regions in the pitch and/or azimuth profiles while intentional bends appear as steep ramps in the pitch and azimuth profiles. This means that a section of pipeline consisting of only straight runs and bends (i.e., not subjected to ground movement) will exhibit an essentially pure “stair-stepped” pitch and azimuth profiles. Locations where the pitch and/or azimuth profiles also exhibit underlying longer wavelength features consisting of gentle/gradual ramps or one to several sinusoidal “lobes” in addition to the typical stair-stepped signature are usually associated with ground movement.

Based on the observations outlined above, ground movement-induced pipeline geometry features can be distinguished from intentional pipeline bends based on:

- *Length*: Individual cold bends and elbows will always be contained between two girth welds while ground movement induced features will extend over one or more girth welds with lengths extending up to several hundred feet.
- *Bending Strain Amplitude*: Maximum bending strains for typical pipeline cold bend radii are in the range of roughly 1% to 2% while ground movement-induced strain features are much less pronounced with peak bending strain amplitude “thresholds of interest” in the range of roughly 0.2%.
- *Pitch and Azimuth Profiles*: Locations where the pitch or azimuth profiles show long wavelength features consisting of gentle/gradual ramps or one to several sinusoidal “lobes” along the pipeline *in addition* to the typical stair-stepped signature associated with straight runs and bends are usually associated with ground movement.

As part of a strain screening for a given inertial survey, it is expected that the profiles of vertical, horizontal and resultant bending strain will be computed for the entire length of the pipeline and that the resultant bending strain profiles be screened for locations of interest. The vendor should have leeway in identifying or “flagging” anomalous bending strain features based on experience and/or using their standard feature screening procedures. In the absence of a vendor-defined approach for flagging anomalous bending strain features, the following approach is recommended:

- For the first inertial survey of a pipeline, a screening criterion that “flags” all locations along the pipeline with a peak resultant bending strain of 0.2% or more based on a curvature calculation gauge length of 10 ft (3 m) which also have a feature signature length that is longer than one pipe joint (i.e., it extends over one or more girth welds) should be used. The screening threshold of 0.2% should be an adjustable parameter that can be specified for any given inertial survey. Operators may choose to tie the screening threshold to elastic stress-equivalent strain measure. For example, a threshold strain value of $0.9 \cdot \text{SMYS}/E$ can be used to reference the B31.8 longitudinal stress limit of 90% SMYS [120].
- Secondary confirmation of the feature can be obtained by reviewing the pitch and/or azimuth profiles for the existence of long-wavelength ramp or sinusoidal features.

For pipelines that have been subjected to more than one inertial survey, the screening concepts described above can be supplemented to also look for specified survey-to-survey changes in the geometry profiles. In order to compare the geometry data from different surveys at the same point along the pipeline, it is common practice to use the odometer distance at selected girth welds as a basis for connecting the two pipeline geometry profiles [121]. This is usually accomplished by scaling the odometer distance between selected girth welds from the new survey to match the odometer distance between the same selected girth welds from the old survey or visa-versa. Note that this “odometer matching” isn’t necessarily carried out for every girth weld but rather using a selected subset of girth welds that are separated by odometer distances on the order of 100 m or less. Once the odometer matching is carried out, profile plots of various geometric quantities (e.g., vertical and horizontal bending strain) can be developed directly overlaying the data from different surveys. As described in Reference [122], it is also possible to calculate and plot difference profiles of selected geometric quantities by interpolating the data to a common odometer distance grid (e.g., typically from the survey with the finest data spacing). As a preliminary basis for screening using survey-to-survey changes, profiles of bending strain *differences* (i.e., changes) with peak values in the range of $\pm 0.04\%$ is recommended.

As described above, the ILI service provider should have leeway in identifying or “flagging” anomalous bending strain features based on experience and/or using their own anomaly feature screening procedures. As part of the screening process, it is expected that the vendor will experiment with a range of different curvature calculation lengths in order to establish and justify the gauge length used to report strain features of interest on a case-by-case basis. The selected

gauge length should strike a balance between the tendency for short gauge lengths to amplify noise in the data and the tendency for long gauge lengths to underestimate curvature. Based on years of experience on pipelines ranging from NPS10 through NPS48, it has been found that a gauge length of 10 ft (or 3 m) will *normally* provide an acceptable balance and hence, this value is used as the “default” recommended curvature calculation gauge length in the “flagging” procedure described above. The shortest gauge length that would normally be considered is L_{pig} . For real (non-noise) strain features which develop over long lengths, large differences in the curvature profiles computed using gauge lengths of L_{pig} vs. 10 ft would not be expected. However, the differences become more pronounced for short features such as bends, mitered welds, etc.

4.6 Protocol for Characterization/Reporting at Strain Locations of Interest

Once a strain location of interest has been identified or flagged by the geometry screening process, it is expected that key information describing the feature(s) of interest will be extracted, tabulated and plotted. This section summarizes a recommended approach for characterizing and reporting the pertinent information as well as a set of notes and comments related to bending strain reporting.

4.6.1 Items Tabulated for Features of Interest

For all areas that are flagged by the screening process, the vendor should have leeway to tabulate all information considered pertinent to describing the feature of interest (subject to client requirements and/or feedback). As a minimum, it is recommended that the following information be tabulated:

- Unique feature name or identifier.
- Starting/ending odometer distance and estimated length of the feature.
- Coordinates of the mid-point of the feature e.g., Easting-Northing or Latitude-Longitude (WGS-84 decimal degrees) and elevation relative to a specified datum.
- Peak values of the vertical, horizontal and resultant/total bending strain anywhere within the feature calculated using a 10 ft (3 m) curvature calculation gauge length.
- ID number and/or odometer distance of all girth welds that are encompassed by the strain feature.
- Maximum values of vertical, horizontal and resultant/total bending strain calculated using a 10 ft (3 m) curvature calculation gauge length at any of the girth welds spanned over by the feature (or a tabulation of these strains at each girth weld within the feature).
- Average tool velocity across the feature.
- A brief narrative description of the feature.
- A listing of any supplemental notes or comments regarding the feature.

4.6.2 Items Plotted for Features of Interest

For all areas that are flagged by the screening process, the ILI service provider should have leeway to plot all information that is considered pertinent to describing the geometry of the feature of interest (subject to client requirements and/or feedback). As a minimum, it is recommended that the following information be plotted:

- Along-the-pipe profile view of the pipe centerline elevation vs. odometer distance. The pipe elevation profile may alternately be characterized using vertical out of straightness (OOS) plots showing the vertical deviation of the calculated pipe centerline path as a function of odometer distance between selected end points with zero OOS.
- Plan view “map” of Easting vs. Northing (or Longitude/Latitude). A plan view of the pipeline geometry may alternately be presented using horizontal out of straightness (OOS) plots showing the horizontal (plan) deviation of the calculated pipe centerline path as a function of odometer distance between selected end points with zero OOS.
- Pitch angle (degrees) vs. odometer distance.
- Azimuth or yaw angle (degrees) vs. odometer distance.
- Along-the-pipe profile view plots of vertical, horizontal and resultant bending strain calculated using a 10 ft (3 m) curvature calculation gauge length vs. odometer distance.
- Measured wall thickness and diameter (if available from the survey).

Figure 4-6 presents a sample package illustrating some of the geometry plots described above. The format of Figure 4-6 is attractive since it provides a compact overall view of the aligned pipeline geometry features including position, orientation and bending strain profiles on a single page. Alternate geometry presentation packages may also be acceptable.

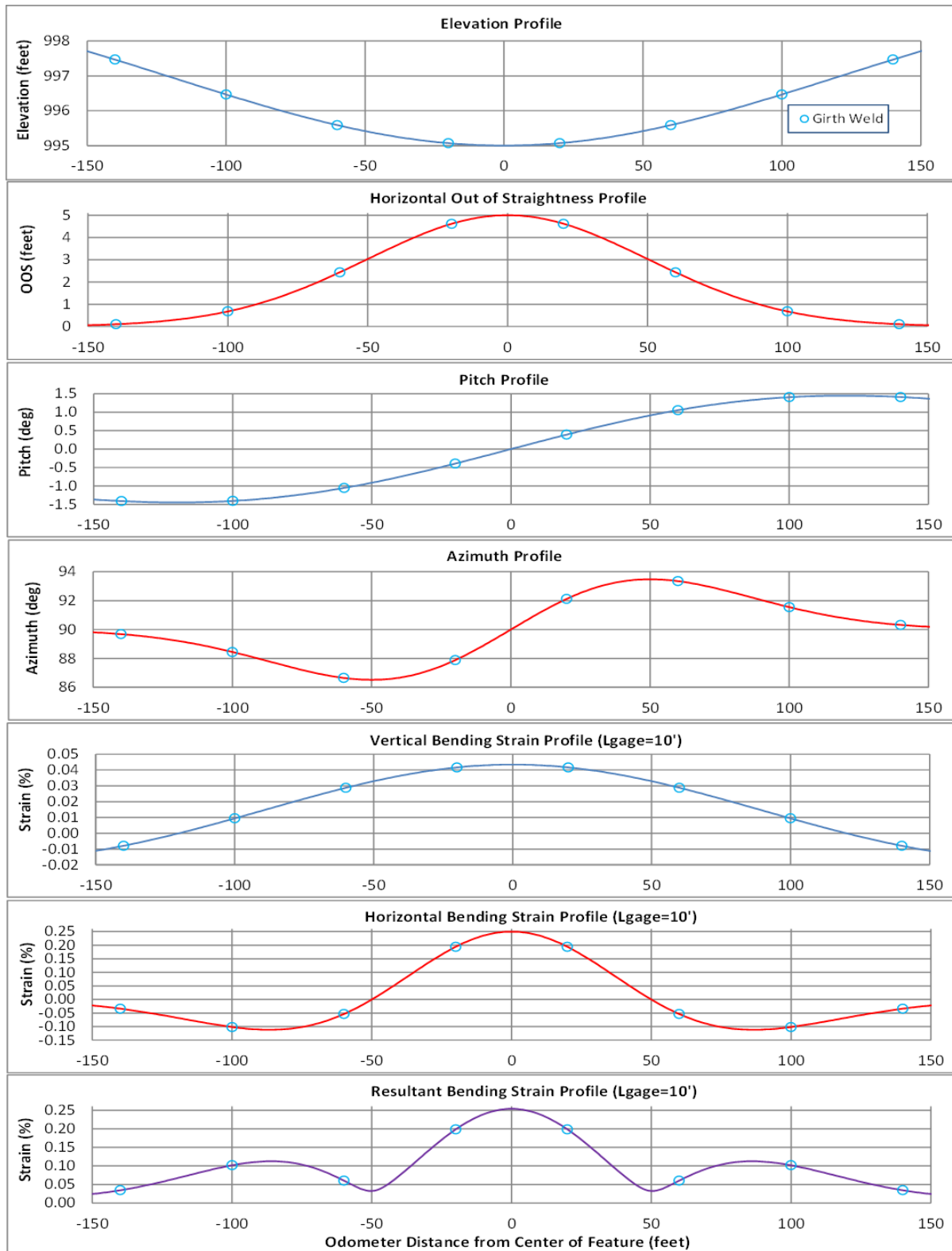


Figure 4-6 Illustration of acceptable plot package

4.6.3 Notes for Bend Strain Reporting

The following notes/comments are provided for additional information.

1. In all along-the-pipe profile view plots, the locations of pipeline girth welds should be clearly identified (e.g., using a symbol like “o” or “+” (see Figure 4-6), or using a distinct vertical line at the odometer distance of each girth weld, etc.).
2. All-along-the pipe profile view plots should be presented over an odometer distance long enough to fully encompass the length of the feature of interest with say an additional pipe joint of length on either end (e.g., say ± 40 to ± 50 ft). Plots of this sort typically span over 200 to 300 ft. The plots should be nominally centered on the high strain zone.
3. Plots vs. odometer distance should show the odometer distance on the X axis and the quantity of interest on the Y axis. The Y axis should be “*auto-scaled*” (i.e., maximum Y axis value slightly larger than Y_{\max} and minimum Y axis value slightly smaller than Y_{\min}) in order to provide an exaggerated/zoomed view of the quantity of interest wherein the details of the signal will be clearly visible.
4. The units of all plotted and tabulated quantities should be clearly denoted in all plots and tables.
5. All references to curvature and/or bending strain should identify the curvature calculation gauge length (e.g., a 10 ft (or 3 m) curvature calculation gauge length).
6. For each high strain zone, it should also be noted whether or not any pipe ovality or out-of-roundness was detected. If the inertial survey also includes high resolution caliper measurements, then the screening criteria may be extended to include a review of the caliper data. For the areas flagged by the bending strain criteria discussed above, detailed profile plots of pipe out of roundness (if present) should also be included. Also, any locations with dents or ovality features of 2% of the pipe diameter or more should be identified and plotted in the screening report. Any vendor-specific calculations for localized through-wall bending strains due to pipe wall deformations should also be provided together with any associated documentation.
7. Similarly, any high strain zone at/near a girth weld should note whether or not rotational or translational misalignment (or other defect) was detected at the weld. Angular misalignments at girth welds (i.e., accidental miters) are sometimes readily visible as very short, nearly vertical offsets (i.e., like a step function) in the pitch and azimuth profiles.
8. For each high strain zone, it should be noted whether or not any metal loss was detected at/near the high strain location if such information is available.
9. Additional plots that may be worth presenting to characterize pipeline features of interest include a profile plot of the circumferential angle or o'clock orientation corresponding to the orientation of the resultant bending strain. More compact spatial plot packages can be achieved by overlaying different signals on the same plot (e.g., pipe elevation on the left

vertical axis and vertical bending strain on the right vertical axis) – see Example 1 in Appendix B.

10. For pipelines subjected to multiple inertial surveys, it may be useful to develop versions of these plots which directly overlay the data and/or the *differences* in the data from two or more different surveys. In order to align the data from different surveys, it is common practice to scale the chainage distance between selected girth welds from the new survey to match the chainage distance between those welds from the old survey (this is sometimes referred to as “chainage matching”) [121].

4.6.4 Specialized Processing

The main thrust of the reporting requirements outlined herein is toward basic presentation of the pipeline geometry information needed to characterize strain location of interest. However, there are certain situations where more advanced/specialized inertial data processing methods and techniques may be required. Examples of detailed processing applications that are not discussed in detail herein include the following:

1. *Gauge Length*. For the plots of bending strain vs. odometer distance, it may be useful to overlay the bending strain profiles computed using two different calculation gauge lengths (e.g., a 10 ft (3 m) curvature calculation gauge length and a gauge length equal to the support to support length of the pig canister containing the IMU). Plots of this sort can be used to delineate the beginning and ending locations of pipeline bends which may be useful for estimating strains at girth welds located in close proximity to a bend or in between two bends.
2. *Curvature Calculation Method*. Evaluation of curvature calculation method e.g., comparison of divided difference method vs. regression line method (or other methods). Different methods can have somewhat different “influence lengths” for the same curvature calculation gauge length.
3. *Noise*. Minor oscillations and vibration of the inertial survey tool is inevitable during a survey as the support wheels or cups encounter imperfections in the pipe wall, kicks at girth welds, and other features. These motions, which are commonly referred to as noise, are exhibited in the pitch and azimuth profiles as short wave length features, much shorter than the wavelengths associated with real ground/pipe movement. The noise in the orientation signals tends to be amplified by numerical differentiation to obtain pipe curvature/bending strain. As discussed in References [116, 122, 123], it is possible to low-pass filter the pitch and azimuth data to rigorously remove this short wave length noise from the signal. The filter parameters must be carefully selected so that real features are not filtered out of the data.
4. *Digital Pigging*. As described in Reference [123], digital pigging is the process of operating on a postulated (or measured) pipeline position coordinate profile in order to obtain a corresponding profile of orientation over a specified pig length (e.g., pigged pitch and/or azimuth) and the corresponding curvature profile computed for a specified gauge length. In some situations, an improved understanding of a real pipeline geometry

feature can be obtained using digital pigging techniques wherein a purely analytical geometry is postulated and digitally pigged and the results are compared to the measured profile.

5. *Centerline Strain Estimation.* As previously noted, inertial survey technology only captures the pipeline curvature/axial bending strain – it does not capture pure axial strains that are uniform around the full pipe circumference. In certain situations, it may be desirable to estimate pure axial strain effects for example by post-processing the survey results using specialized approximate procedures (e.g., see Reference [115]). Another approach to estimate pure axial strain effects is by utilizing pipe geometry profile data in a finite element model with realistic longitudinal pipe-soil resistance.
6. *Dent Correction.* As the support wheels or cups of the inertial tool travel over an asymmetric ovality or a dent in the pipe wall, there will be a tendency for the path of the pig to deviate from the path of the pipe centerline. Using centerline correction methods, it is possible to adjust the effect of the dent/ovality out of the path. More details can be found in Reference [116].

4.6.5 Additional Information in an IMU Report

Reference API1163 [124] provides guidance for ILI report contents. The vendor strain report should also always include the following information:

- A summary of the tool detection threshold and accuracy specifications including the gyroscope type and sampling rate.
- A summary of the sensor accuracies.
- At least a basic description of the numerical algorithm used to compute curvature/bending strain and applied data analysis parameters
- Documentation of the accuracy realized during the survey (i.e., what was the realized position accuracy and curvature/bending strain accuracy and did they meet or exceed specifications?).
- A summary ILI data quality assessment for the survey (e.g., was the tool run within the range of essential variables, was there any sensor malfunction, etc.)
- A profile plot of the tool velocity during the entire survey.
- A detailed drawing of the tool that is used to perform the survey showing all pertinent dimensions (including the distances between all canister supports) and the locations of all sensors.

The vendor may also provide specialized software that can be used by operator representatives to view and/or export selected quantities of the inertial survey data along selected sections of the alignment.

Once the vendor strain report is reviewed, additional detailed digital data files may be requested by the operator for some or all the locations that were flagged by the data screening to perform more detailed analysis. The detailed data files should be provided in digital (CSV or

ASCII) format for a specified distance upstream and downstream of the location of interest. The following columns of data would be included at the raw (or shortest possible) data spacing:

1. UTM Northing coordinate (m or ft) and/or Latitude specified in WGS-84 decimal degrees
2. UTM Easting coordinate (m or ft) and/or Longitude specified in WGS-84 decimal degrees
3. Pipe centerline elevation referenced to Mean Sea Level (m or ft)
4. Tool velocity (m/s or ft/s)
5. Pipe chainage distance (m or ft)
6. Pitch angle (degrees)
7. Azimuth or yaw angle (degrees)
8. Vertical bending strain (%) for a 10 ft (3 m) gauge length (or a different gauge length justified by the vendor)
9. Horizontal bending strain (%) for a 10 ft (3 m) gauge length (or a different gauge length justified by the vendor)
10. Total/resultant bending strain (%) for a 10 ft (3 m) gauge length (or a different gauge length justified by the vendor)
11. Vertical bending strain (%) for a gauge length equal to the cup-to-cup (or wheel-to-wheel) length of the pig canister containing the IMU
12. Horizontal bending strain (%) for a gauge length equal to the cup-to-cup (or wheel-to-wheel) length of the pig canister containing the IMU
13. Total/resultant bending strain (%) for a gauge length equal to the cup-to-cup (or wheel-to-wheel) length of the pig canister containing the IMU

A summary tabulation of the girth weld detection data should also be provided over the length of the exported data set containing a tally of the chainage distance associated with each girth weld as well as a summary of diameter changes to identify whether any ovality or wrinkles are associated with strain anomalies.

4.7 Verification of IMU Survey Data

A pipeline owner or operator may have an interest in validating data from an inertial survey at a location or at a subset of locations along a pipeline which have been flagged by the inertial data screening process. This section provides an overview of profile measurement procedures that may be used for verifying pipeline inertial survey data based on comparison with discrete pipeline profiles measured in the field by either GPS or conventional survey techniques.

When an inertial survey validation effort is undertaken, it is envisioned that a location of interest (i.e., study area) on the pipeline will be selected for the verification study and that a field survey will be performed at this location via pothole excavation to expose the top of the pipe at a grid of selected points extending at least one pipe joint beyond each end of the extent of the apparent area of pipeline movement (the end points are considered to be stationary). As a minimum, the field survey will obtain Northing-Easting-Elevation coordinate triples at a

marked/punched pipe top-dead-center (TDC) spot at each girth weld across the study area and possibly at additional TDC grid points between some or all of these girth welds. The accuracy of the geometry profile established from the pothole survey will tend to increase with reduced pothole spacing so prior to conducting the pothole survey, it is expected that coordination with the surveyors and careful planning and pre-analysis will be undertaken to plan the pothole spacing. The idea behind limiting the excavation to relatively small potholes that expose only a relatively small swath of the top of pipe is to capture the discrete “as-found” trajectory of the pipe without allowing the pipe to spring back elastically toward the un-deflected geometry in response to more excessive excavation. If the pipe will be fully excavated after the pothole survey is completed for stress relief purposes, it may also be useful to accurately survey the “as-relieved” (or “as-left”) pipeline geometry at the same grid of TDC points for comparison with subsequent inertial surveys.

The field survey measurements can be made using any acceptable field survey method (e.g., conventional survey methods, triangulation, differential GPS system, or a combination of these methods). In any case, the surveyors should clearly specify the type of the system(s) used together with the accuracy of the surveyed coordinates. Multiple, repeated survey “shots” can allow for a statistical characterization of the error at each survey point. Modern differential GPS systems can yield a horizontal accuracy of about ± 0.02 m or ± 0.07 ft for individual measurements. Recent experience with field pothole surveys indicates that very accurate (i.e., sub-centimeter) coordinates with high repeatability can be obtained based on conventional surveying techniques.

Once the field survey is complete, the field survey data must then be compared to the inertial survey data. The most appropriate approach to overlay the data sets is to utilize the field surveyed coordinates at the outermost potholes at each end of the study area (i.e., the stationary points) as “local” upstream and downstream tie points and to perform numerical integration of the pitch, azimuth and odometer data (see Section 4.3.1 for methodology) to establish the inertial profile between these tie points. This is because the Northing, Easting and Elevation coordinates of the field survey points are likely to be more accurate than the originally delivered coordinates as integrated from the inertial data between the nearest “global” upstream and downstream tie points (i.e., the nearest upstream and downstream points used to tie the overall inertial survey). Although the along-the-pipe distance between the individual pothole survey points can be estimated based on the straight-line distance, it is preferable to utilize the odometer distance data from the inertial survey to generate a local, along-the-pipe distance measure for each potholed survey point. This means that each point in the inertial data set and the pothole data set will have a relative odometer distance, Northing, Easting and Elevation coordinates. For the purposes of overlaying and comparing plots of the pipe position established from the inertial and pothole surveys, horizontal and vertical out-of-straightness (OOS) plots running between the local tie points at the outermost potholes are considered to be superior to conventional map plan view or elevation views since they allow amplification and improved visualization of the out-of-straightness features. OOS profiles are developed using a coordinate transformation from the Northing-Easting-Elevation coordinates into the horizontal and vertical OOS deviations from a

straight line connecting the outermost pothole tie-points. Note that the transformation to OOS is applied to both the inertial data and the pothole survey data.

A simple validation approach has been put forward by ROSEN. This approach is considered to be relatively straight forward and can likely be implemented by pipeline operator personnel. The approach is summarized as follows. For the validation of the IMU survey, the relative coordinates of the pipe at the pothole locations from the inertial data are directly compared to the corresponding field surveyed coordinates of the pipe at the pothole locations. If the relative coordinates match, the trajectory shape and thus the calculated strain can be considered to be verified. In other words, if the field surveyed and inertial survey position coordinates at the pothole locations are identically matched, then the inertial survey has been validated. While it is agreed that this is a reasonable and defensible premise, it is considered almost inevitable that the inertial survey coordinates at the pothole locations *will not* exactly match the corresponding field surveyed coordinates. In this case, more detailed calculations may be undertaken in an effort to better characterize and quantify the differences between the inertial and field surveyed pipeline geometry. It may be acceptable to judge the “match” between inertial and pothole profiles by comparing the difference profiles to the 1:2000 position accuracy specification. In some cases, it may be possible to explain the differences between the profiles as additional movement that the pipeline experienced during the time interval between when the inertial and pothole surveys were performed. In some cases, it may be reasonable to selectively discard a subset of the field survey points for example if it is believed that the field surveyed point did not correspond exactly to the pipe TDC point of the pipe (e.g., the survey was performed under high water table conditions and the point punched/marked for the survey was underwater and located off of the true TDC spot).

A more rigorous validation approach involves developing more detailed comparisons of the inertial and field surveyed profiles and their numerical derivatives. This approach is significantly more complicated than the simple approach described above, and because it falls into the category of “specialized processing” (see Section 4.6.4), it may be outside of the expertise of the pipeline operator personnel. Cubic spline interpolation or curve fitting to a finer grid of points between the field surveyed pothole coordinates provides a more continuous profile for comparison of the overall shape/OOS of the pipeline. The more continuous interpolated profile allows for numerical differentiation (e.g., using divided difference or digital pigging calculation to establish pipeline slope/orientation (i.e., relative pitch and azimuth) profiles which can also be differentiated numerically to establish horizontal and vertical curvature profiles for the pothole survey. As always, the numerical curvature/bending strain profiles will likely be sensitive to the curvature calculation method, gauge length, etc. As previously noted, in some cases it may be reasonable and defensible to selectively discard a subset of the field survey points for example if it is believed that the field surveyed point did not correspond exactly to the true TDC point of the pipe. It may also be justifiable to smooth out the 1st and 2nd derivative profiles using low-pass filtering procedures.

In the final analysis, the field verification report should document the accuracy of the field survey coordinates (including notes/comments for example if the surveyed point may have been off of TDC) as well as the expected accuracy of the inertial survey profile between the local tie points (i.e., based on the $\pm 1:2000$ accuracy specification). In cases where the inertial and field surveyed pipe position profiles do not match identically, the additional analysis undertaken to develop more detailed comparisons of the inertial and field surveyed profiles should be documented in detail. If possible, the apparent error between the inertial survey profile and the field surveyed profile should be characterized.

To the extent possible, the field work, pipe locating/marketing and the documentation of the validation study should follow recommendations given in References [125, 126].

4.8 Example Pipeline Strain Features

Appendix B provides several example strain feature geometry plot packages and data tabulations.

5 Mechanical Properties of Pipe and Girth Welds

Abstract

One of the major inputs in quantitative assessment of girth welds' tolerance to longitudinal stresses or strains is material property, such as strength, strain hardening capacity, and toughness. In most cases, such information is not available for in-service pipelines.

This section covers two main parts: (1) history of linepipe manufacturing and the resulting characteristics of material properties and (2) a large collection of test data of linepipes and girth welds. The information is presented so the material properties of pipe and girth welds can be estimated with reasonable accuracy when case-specific data are not available.

The general observations from the available data are as follows.

- There is a considerable variation in the actual pipe strength relative to the pipe grade. In all cases, the yield strength in hoop direction meets or exceeds the SMYS of that particular grade. In some cases, the yield strength in the longitudinal direction can be lower than the SMYS. In some extreme cases, the yield strength in hoop direction is 30+ ksi above SMYS.*
- There can be considerable anisotropy in linepipes. The stress-strain curves in the longitudinal direction can be quite different from those in the hoop direction.*
- The UTS in the longitudinal and hoop direction is usually similar.*
- Pipe strength on either side of a girth weld can be quite different. In most cases, though, the strength is similar.*
- There has been a large decrease in pipe's strain hardening capacity from hot rolled and normalized pipes with high carbon (0.2%) to microalloyed steels with low carbon.*
- The strength of the deposited weld metal is often less than the actual strength of the pipe. In most cases, this strength undermatching does not lead to strain concentration in the girth weld due to the weld cap reinforcement.*
- Weld cap reinforcement can play a significant role in compensating the possible weld strength undermatching when such undermatching is not overly excessive. Some vintage girth welds are found to have a wide and smooth cap reinforcement which is beneficial to weld's tolerance to longitudinal stresses and strains.*
- The SMAW welds made in 1940s onwards are expected to behave in ductile manner under normal service conditions for buried pipelines, i.e., temperature warmer than -10 °C.*
- Charpy values taken from testing of multiple specimens indicate that, on the average, the Charpy toughness at -10 °C is greater than 20-30 ft-lb.*
- There can be large variations, sometime by a factor of up to 5-6, in individual Charpy impact energy for specimens with notches in HAZ. Consequently, Charpy transition curves with multiple specimens tested at the same temperature give better indications of material's behavior than the customary tests of three specimens at a single temperature.*

- *A lower bound apparent toughness for vintage welds is around 0.3 mm. In most cases, a reasonable lower-bound toughness is around 0.40-0.60 mm for vintage welds. Some welds can have apparent toughness in excess of 1.0 mm.*
- *The measured tensile strain capacity of SMAW welds fabricated in 1940-1960s from specimens with natural construction flaws give a strain capacity as low as 0.2-0.3% and as high as >2.0%*

5.1 Introduction

One of the major obstacles in assessing a pipeline's tolerance to longitudinal stresses and strains is the lack of relevant material properties. This is especially true for vintage pipelines and pipelines with a history of multiple owners and operators. The original design, construction, and inspection records may have never existed in a useful form or may be missing.

Even under the best circumstances that the original design, construction, and inspection records are available, the records may not be sufficient for a quantitative assessment of the pipeline's tolerance to longitudinal stresses and strains. For instance, pipe grade only represents the minimum yield strength in the pipe's hoop direction. The actual strength of the pipe can be significantly higher. Girth welds are qualified to meet the specified minimum strength. Consequently, a girth weld can have weld strength significantly lower than the actual strength of the pipe, which leads to low tolerance to longitudinal stresses and strains due to the strain concentration in the welds. On the other hand, if the pipe strength is close to the specified minimum values, a weld may have strength close to or even higher than the strength of the pipe. In this case, the weld's tolerance to longitudinal stresses or strains can be much higher.

In addition to the weld strength mismatch, other factors that can have significant impact on girth welds' tolerance to longitudinal stresses and strains are (1) weld profile, (2) pipe's stress-strain behavior in the longitudinal direction, (3) existence of weld flaws, and (4) toughness of the material where the flaws are located. For most in-service pipelines, such information does not exist.

This section covers two main parts: (1) history of linepipe manufacturing and the resulting characteristics of material properties and (2) a large collection of test data of linepipes and girth welds. The coverage of the linepipe manufacturing is far from comprehensive. The focus is on the characteristics that are relevant to managing ground movement hazards. The test data are meant to illustrate the "typical" characteristics of the pipes and girth welds. "Outliers" can exist for a specific pipeline of interest. The possible variations of material properties are duly considered in Section 9.

5.2 Evolution of Pipe Manufacturing

5.2.1 Type of Pipe

The method of linepipe manufacturing over time in North America is schematically shown in Figure 5-1. The transition between historical practices versus modern practice occurred approximately in 1950-1970s.

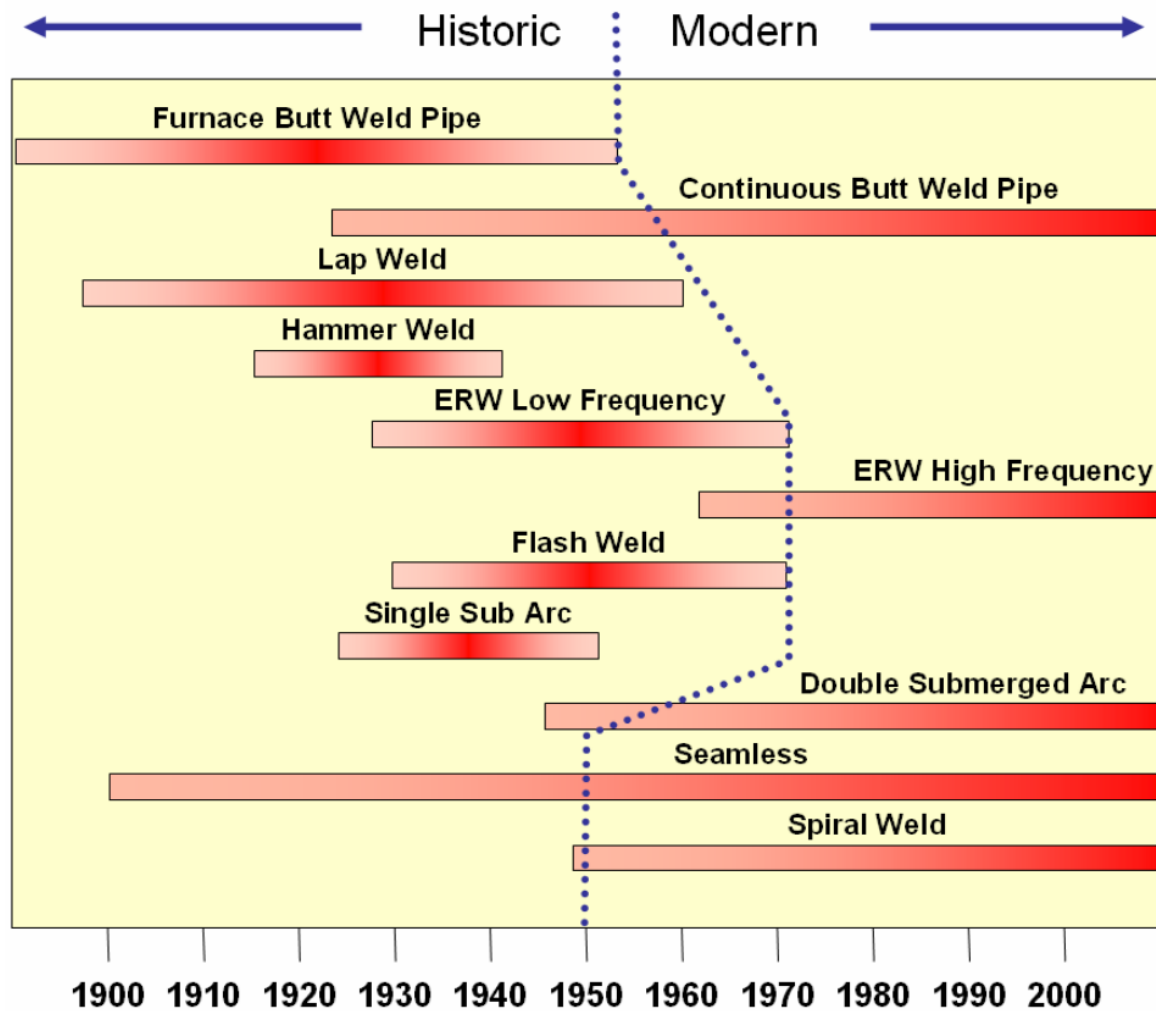


Figure 5-1 Evolution of pipe manufacturing practice [127]

5.2.2 Steel Chemical Composition and Rolling Practice

The evolution of the pipe's chemical composition, rolling practice, and grade as viewed in late 1990s is shown in Figure 5-2 [128]. There has been a steady reduction in carbon content since the introduction of TMCP and accelerated cooling process as the pipe grade moved up. In the case of X70 pipes, the carbon content has reduced to as low as <0.02% as shown in Figure 5-3 [129].

5.2.3 Stress-Strain Response

As it will be shown in Sections 5.5 to 5.9, there has been accompanying changes in the stress-strain response of the linepipe steels. When pipe steels were manufactured with high carbon (0.2%) by hot rolling and normalization, the steels exhibit very high strain hardening capacity with a typical Y/T ratio around 0.62. After the introduction of TMCP and microalloying (with the reduction in carbon content), there has been an appreciable reduction in linepipe's strain hardening capacity with a typical Y/T ratio of 0.85-0.90 or even higher. In some extreme cases, the Y/T ratio has reached 0.95 or even higher.

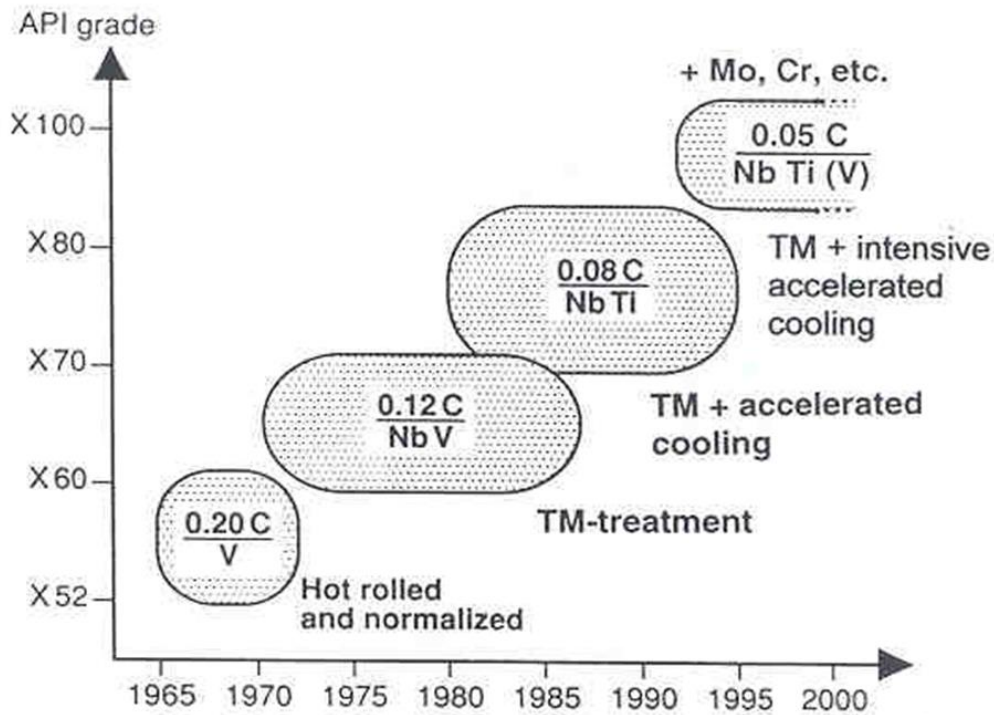


Figure 5-2 Evolution of chemical composition, rolling practice, and grade over time [128]

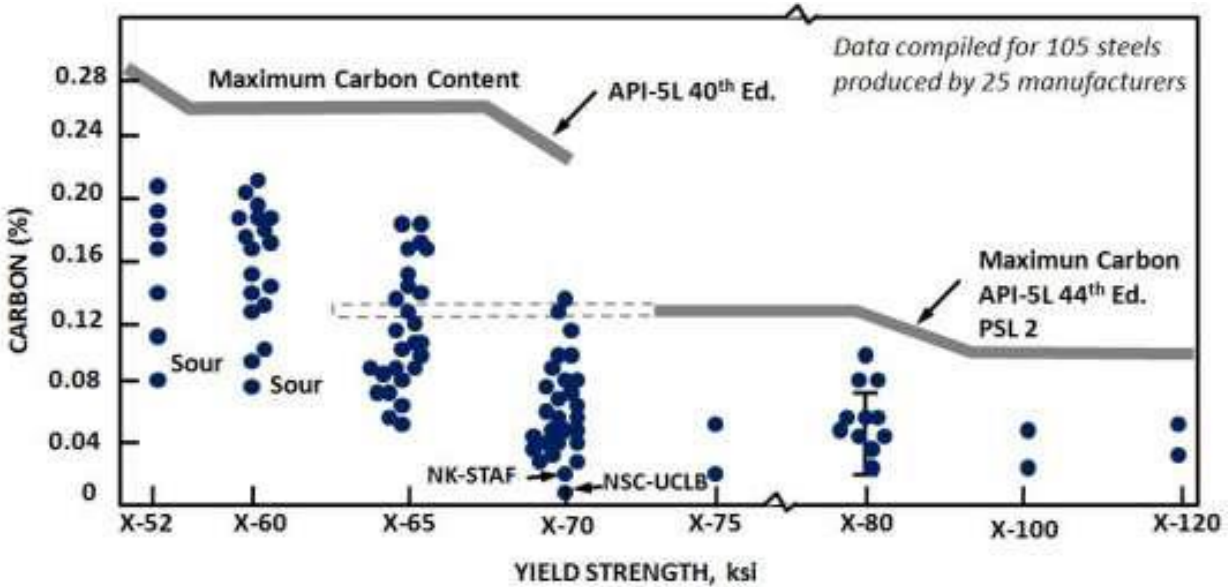


Figure 5-3 Carbon content versus pipe grade [129]

5.3 Evolution of Construction Practice

The evolution of pipeline construction practice is shown in Figure 5-4 [127]. “Stick welding” has been in use since the mid-1910s. One of the key factors influencing the integrity of vintage girth welds is the existence of flaws after construction. This is principally related to inspection practice, not necessarily welding procedures. Before the introduction of federal

regulations in 1970, the percentage of girth welds inspection was uneven. After 1970, virtually 100% girth welds were inspected, even though the federal regulations do not require such high percentage of inspection.

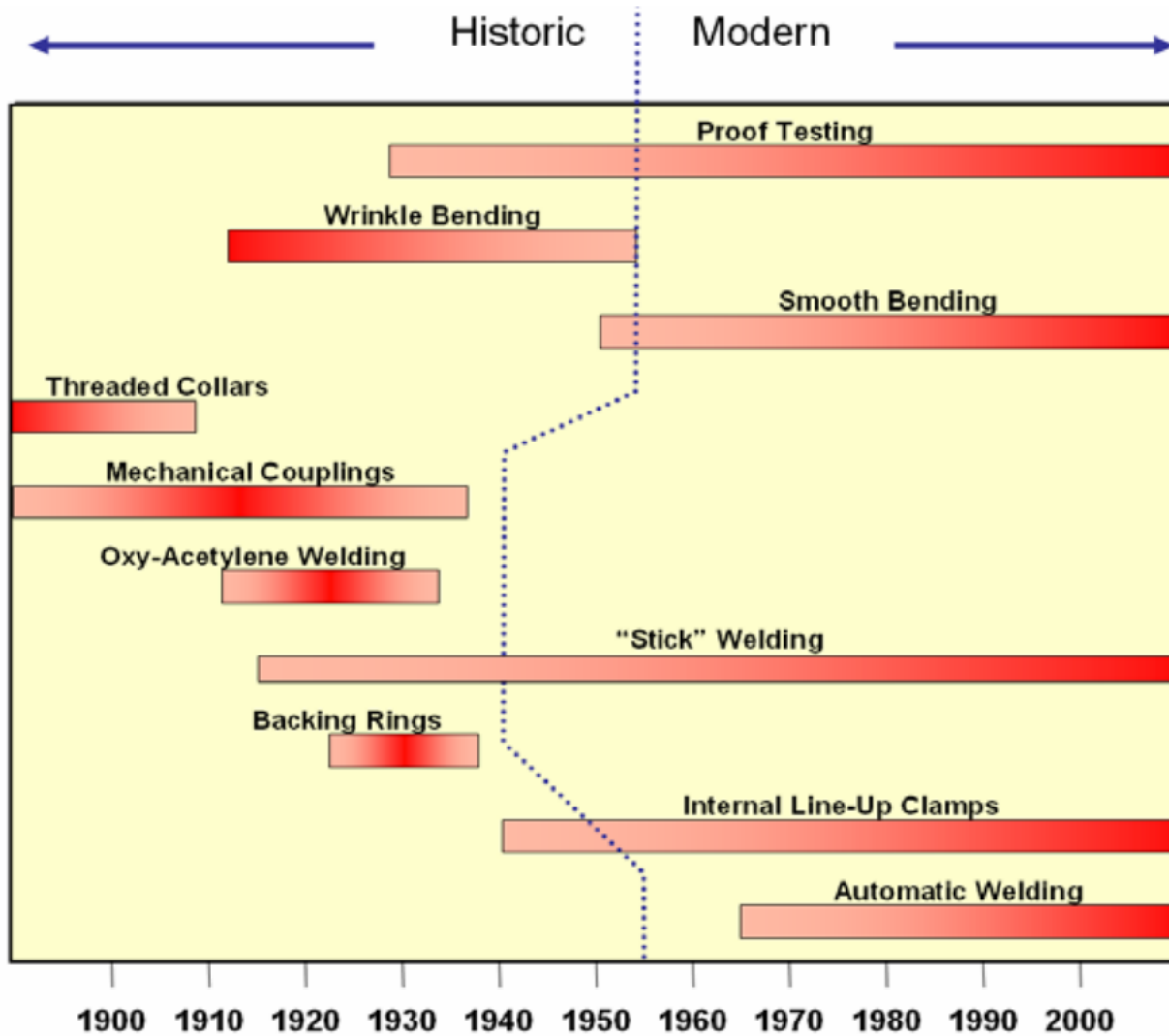


Figure 5-4 Evolution of pipeline construction practice [127]

5.4 Pipeline Mileage by Construction time

The mileage of pipelines and the construction time by decades is shown in Figure 5-5, Figure 5-6, and Figure 5-7 [130]. Approximately 55% of the hazardous liquid pipelines, 59% of the natural gas transmission pipeline, and 31% of the natural gas distribution pipelines were built before the 1970s. The peak construction time for natural gas and liquid pipelines was in the 1950s and 1960s.

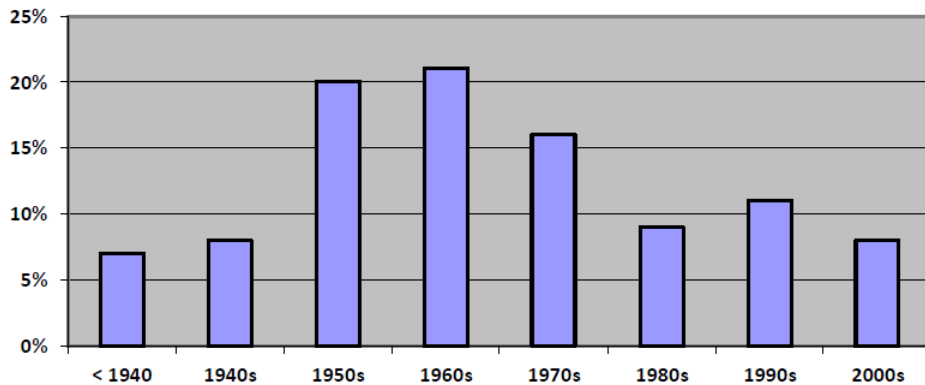


Figure 5-5 Hazardous liquid pipelines mileage by decade of construction

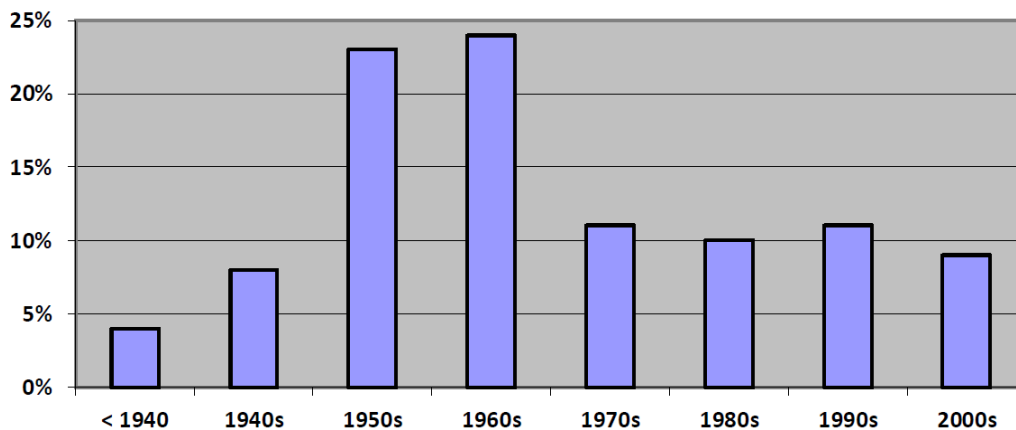


Figure 5-6 Gas transmission pipelines mileage by decade of construction

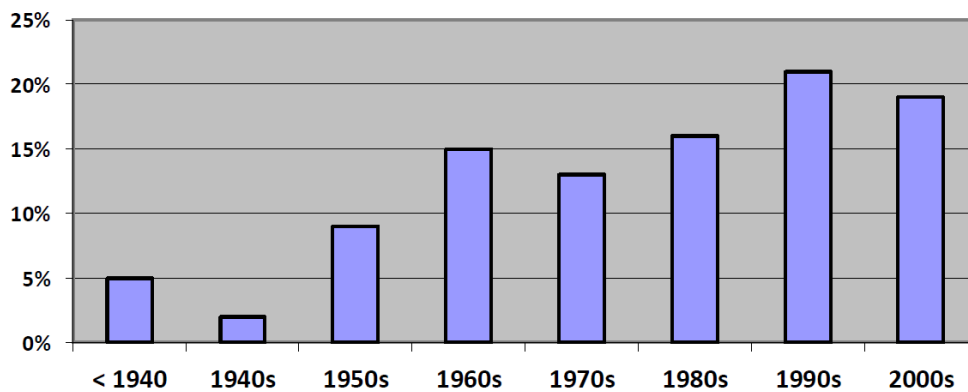


Figure 5-7 Gas distribution pipelines mileage by decade of construction

5.5 Pipe and Girth Weld Properties from Group A

5.5.1 Characteristics of the Pipelines of Group A

The mechanical properties of four pipelines, Lines 1, 2, 3, and 4, were investigated through an extensive mechanical test program. Lines 1 and 2 were constructed in 1952 and 1957, respectively. Both lines were constructed with API grade X52 and had a diameter of 30 inch and

a nominal wall thickness of 0.375 inch. Line 3 was constructed around 1968 of API grade X60, 36-inch OD and 0.375-inch WT. Line 4 was constructed in 1990 of API grade X65, 36-inch OD and wall thickness of 0.385 inch and 0.572 inch. The characteristics of those four pipelines were summarized in Table 5-1. Lines 1, 2, and 3 are pre-regulation pipelines. Line 4 is a post-regulation pipeline².

Table 5-1 Characteristics of four pipelines from Group A

Line No.	Pipe Grade	OD	WT	Year of Construction
		inch	inch	
1	X52	30	0.375	1952
2	X52	30	0.375	1957
3	X60	36	0.375	1968
4	X65	36	0.385, 0.572	1990

5.5.2 Matrix of Mechanical Tests

Four girth welds from each of Lines 1 and 2 and two girth welds from each of Lines 3 and 4 were selected for mechanical testing. The mechanical test program includes

- base pipe tensile,
- all-weld metal tensile,
- hardness traverse,
- Charpy transition curves in impact energy,
- cross-weld tensile with natural flaws, and
- cross-weld tensile test with artificially introduced planar flaws.

Table 5-2 shows the complete mechanical test matrix.

²Line 3 is a pre-regulation pipeline by construction time. As shown in the sections that follow, the characteristics of mechanical properties of Line 3 is close to modern low-carbon steels. Pre-regulation pipelines are often referred to as “vintage pipelines” and post-regulation pipelines are often referred to as “modern pipelines”. Such designation is accurate in terms of inspection practice, but not entirely accurate in differentiating mechanical properties.

Table 5-2 Mechanical test matrix of Group A

Type of Test	No. of Material	Notch Location		Replicate Specimens		Specimen Circumferential Location	Temperature		Total Number of Specimens
Macro	6		N/A	1	3	12, 6 weld o'clock and positions with large misalignment	1	Room Temp	22
Microhardness Traverse	6		N/A	1	2	two weld o'clock positions with least amount of misalignment	1	Room Temp	12
Charpy	6	2	Weld and HAZ	3	3	12, 3, and 6 o'clock	1	-5C	108
Charpy Transition	6	2	Weld and HAZ	3	1	Choose one location that gives the lowest Charpy at -5C	5	varies from low to upper shelf	180
All Weld Metal Tensile	6		N/A	1	2	6 and 3 o'clock	1	Room Temp	12
Base Metal Tensile, Longitudinal	6		N/A	1	4	12, 3, 6, 9 o'clock positions w.r.t the long-seam weld	2	Room and -20C	48
Base Metal Tensile, Hoop	6		N/A	1	4	12, 3, 6, 9 o'clock positions w.r.t the long-seam weld	2	Room and -20C	48
Instrumented Cross-weld Tensile with Natural Flaws	2		N/A	1	4	Use the location that has the largest natural flaws	1	Room Temp	8
Instrumented Cross-weld Tensile with Manufactured Flaws	5	2	Weld and HAZ	2	1	Choose one location that gives the lowest Charpy at -5C	2	Room and -20C	40

5.5.3 Pipe Tensile Properties

5.5.3.1 Features and Dimensions of Tensile Specimens

Standard tensile tests were conducted on the base pipe materials. Round-bar specimens had nominal 6.35 mm (1/4 in) diameter and 25.4 mm (1.0 in) gauge length. The tensile tests were conducted in both longitudinal and hoop directions at the room temperature and -20 °C. For the base metal tensile tests, four specimens were cut from 12, 3, 6 and 9 o'clock positions with respect to the long-seam weld for each pipeline. The 12 o'clock specimens were cut about 4 inches away from the long-seam weld.

5.5.3.2 Stress-Strain Curves

The stress-strain curves of the base pipe material of all four lines are given in Figure 5-8 to Figure 5-15. The overall characteristics of the pipes may be summarized as follows.

- The behavior of Lines 1 and 2 (both X52) vs. Lines 3 (X60) and 4 (X65) is very different. Lines 1 and 2 have much higher strain hardening rate than Lines 3 and 4. The grade X52 pipes made in the 1950s have excellent strain hardening capacity.

- Although the grade increased from X52 for Lines 1 and 2 to X60 and X65 for Lines 3 and 4, the UTS of all pipes is quite close, all in the range of 550-600 MPa.
- The yield strength, and in some cases UTS, in hoop direction is higher than that in the longitudinal direction.
- The strength at -20 °C is higher than the strength at the room temperature.
- There is a good consistency in pipe tensile properties at different o'clock positions.

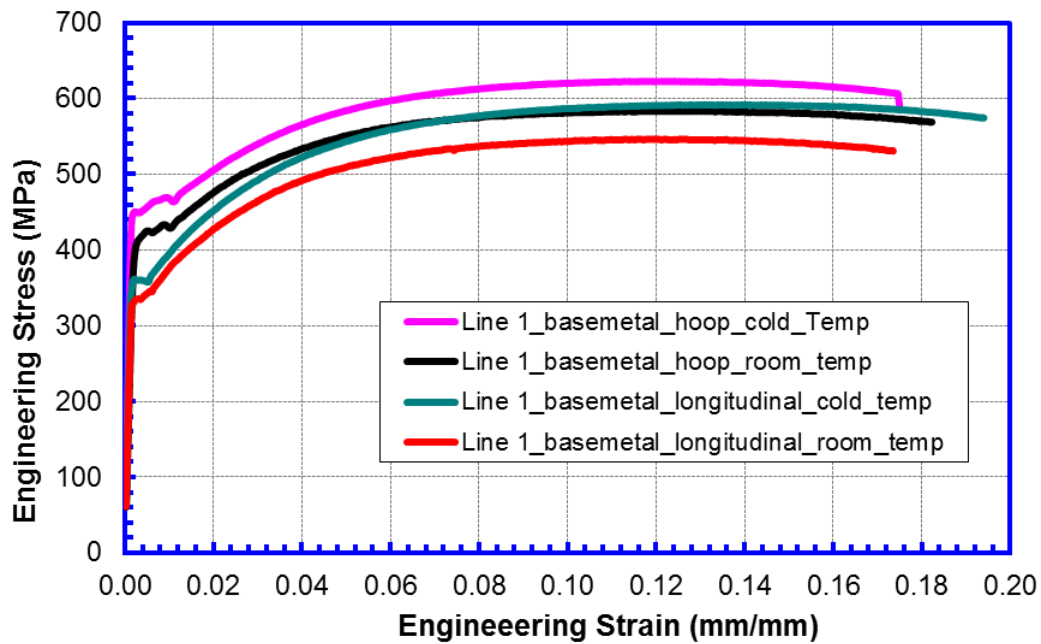


Figure 5-8 Hoop and longitudinal tensile stress-strain curves at room temperature and -20 °C of Line 1

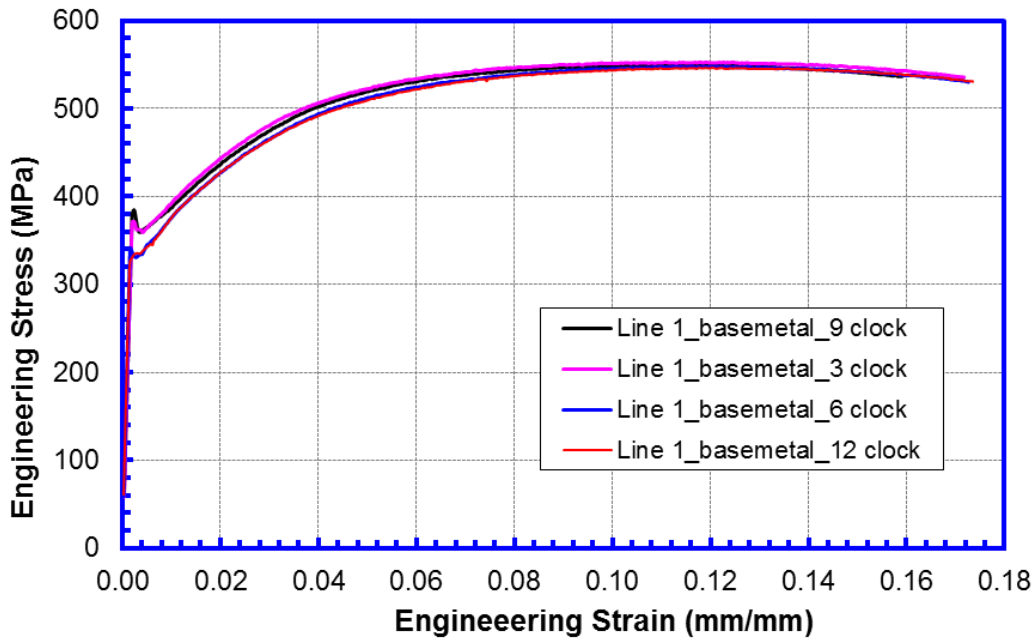


Figure 5-9 Longitudinal tensile stress-strain curves from four o'clock positions at room temperature of Line 1

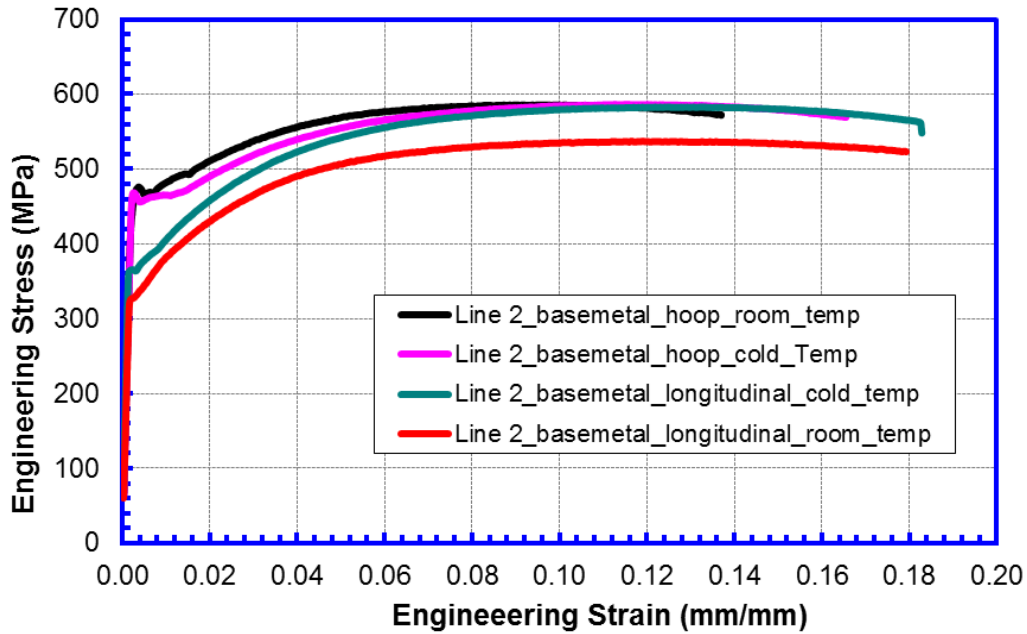


Figure 5-10 Hoop and longitudinal tensile stress-strain curves at room temperature and -20 °C of Line 2

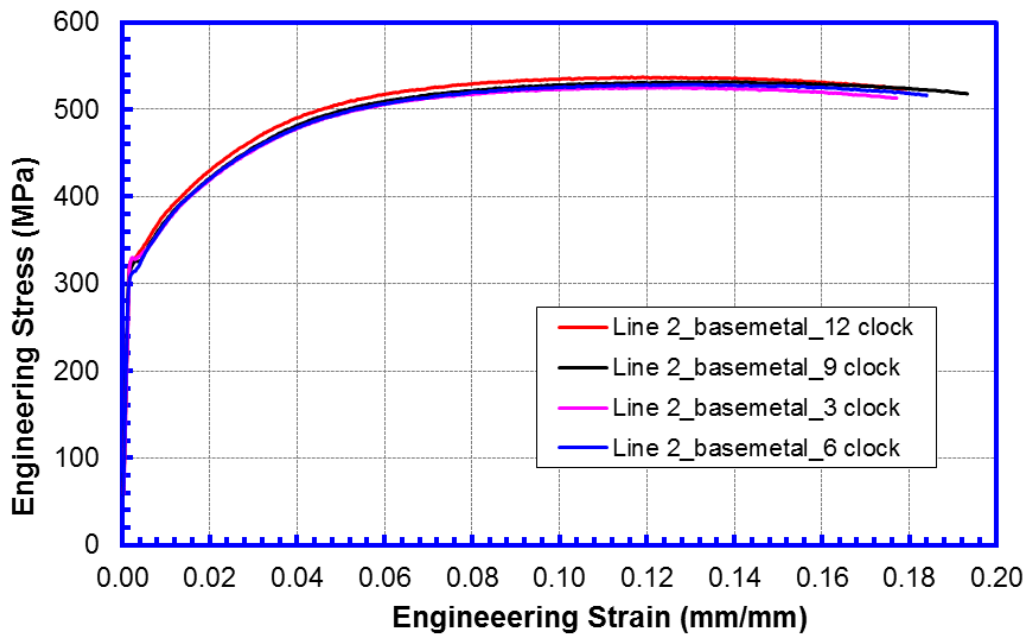


Figure 5-11 Longitudinal tensile stress-strain curves from four o'clock positions at room temperature of Line 2

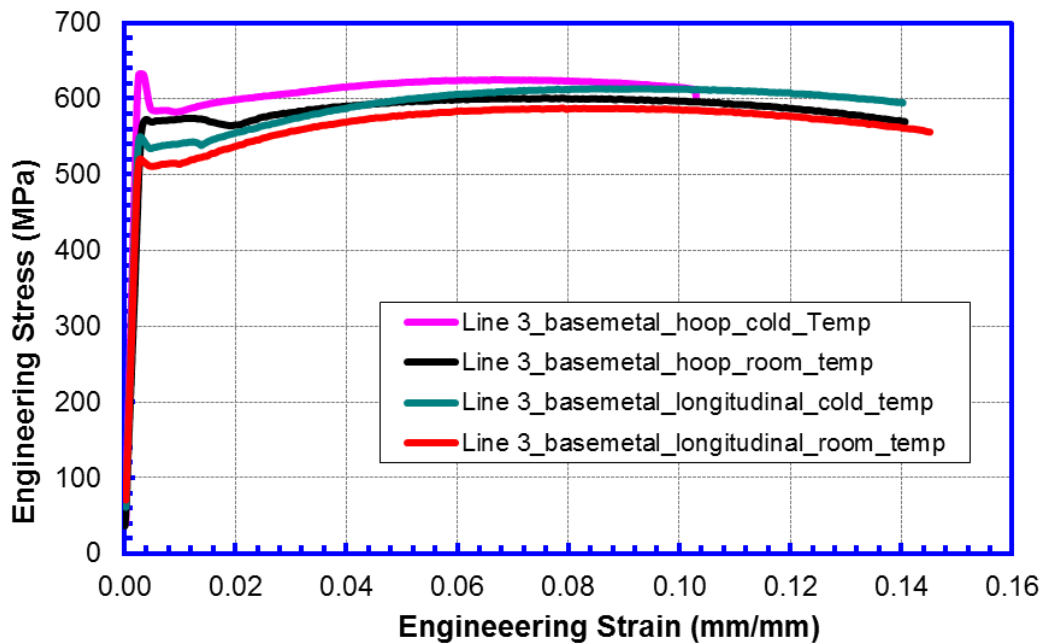


Figure 5-12 Hoop and longitudinal tensile stress-strain curves at room temperature and -20 °C of Line 3

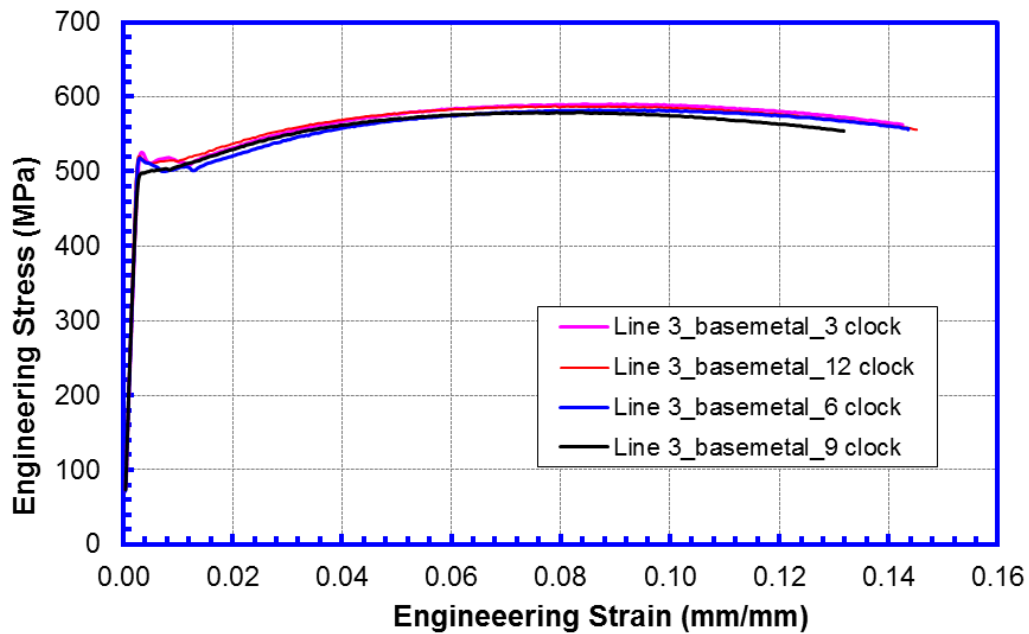


Figure 5-13 Longitudinal tensile stress-strain curves from four o'clock positions at room temperature of Line 3

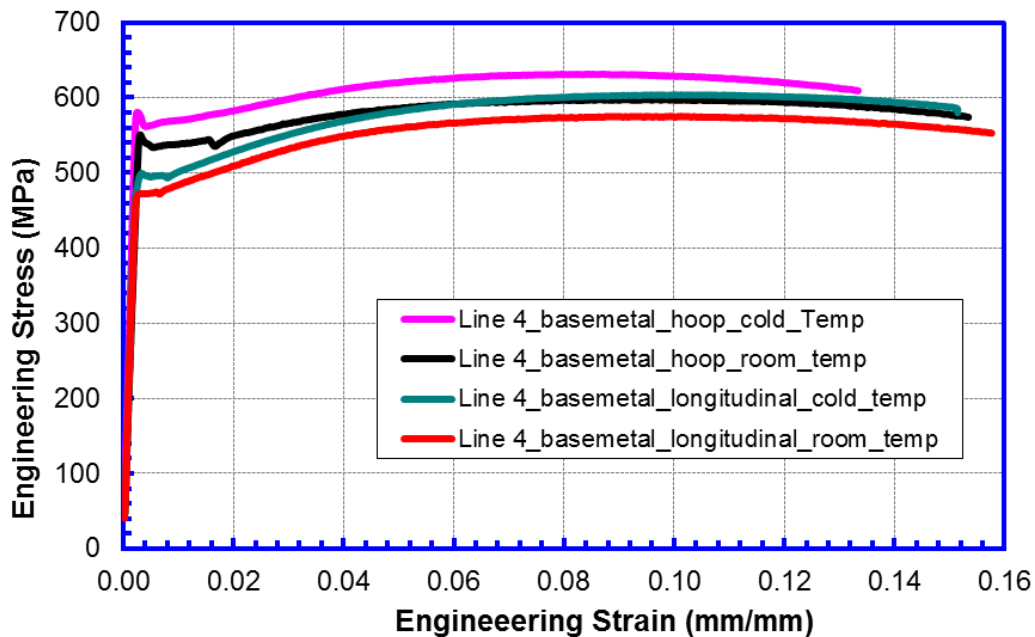


Figure 5-14 Hoop and longitudinal tensile stress-strain curves at room temperature and -20 °C of Line 4

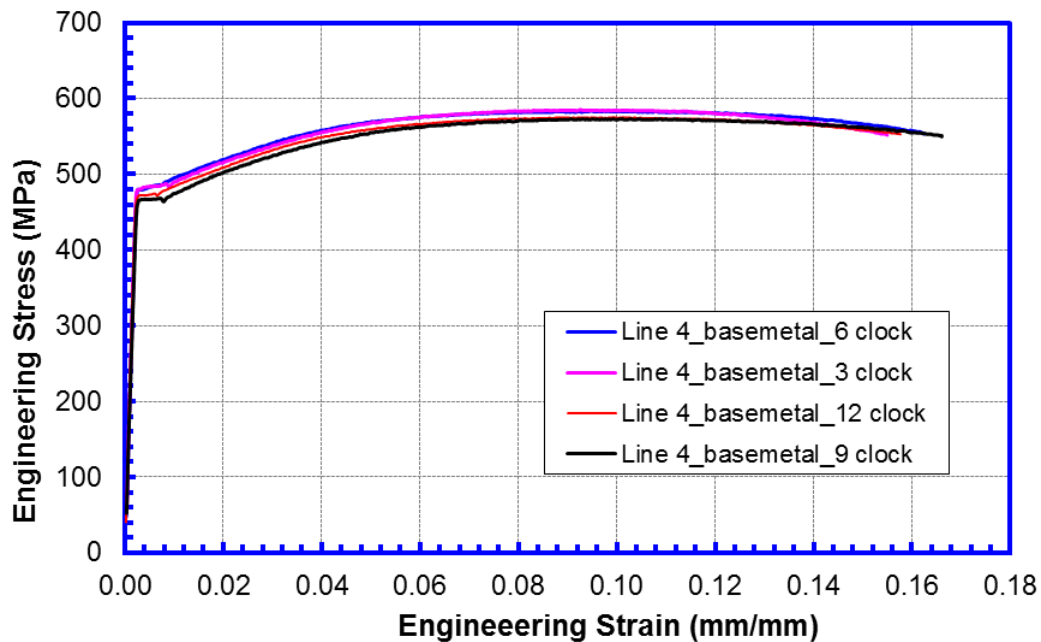


Figure 5-15 Longitudinal tensile stress-strain curves from four o'clock positions at room temperature of Line 4

5.5.3.3 Actual Strength vs. Specified Minimum Strength

The comparison of the measured strength, both yield and UTS, and the specified minimum values is shown in Figure 5-16 and Figure 5-17. The following trend may be observed.

- With the exception of the yield strength of the X52 pipes in the longitudinal direction, the average yield strength and UTS are approximately 10 ksi above the specified minimum values.
- The yield strength of the X52 pipes in the longitudinal direction is slightly lower than specified minimum yield strength.
- Linepipe standards specify that the yield strength in the loop direction must meet the specified minimum values. All pipes meet the specifications in terms of strength.

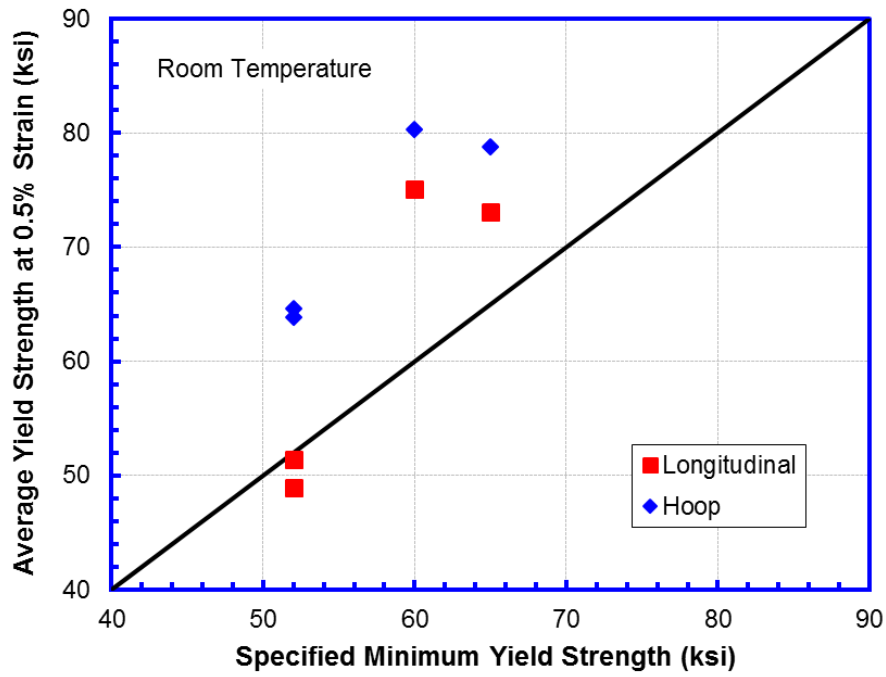


Figure 5-16 Measured yield strength vs. SMYS

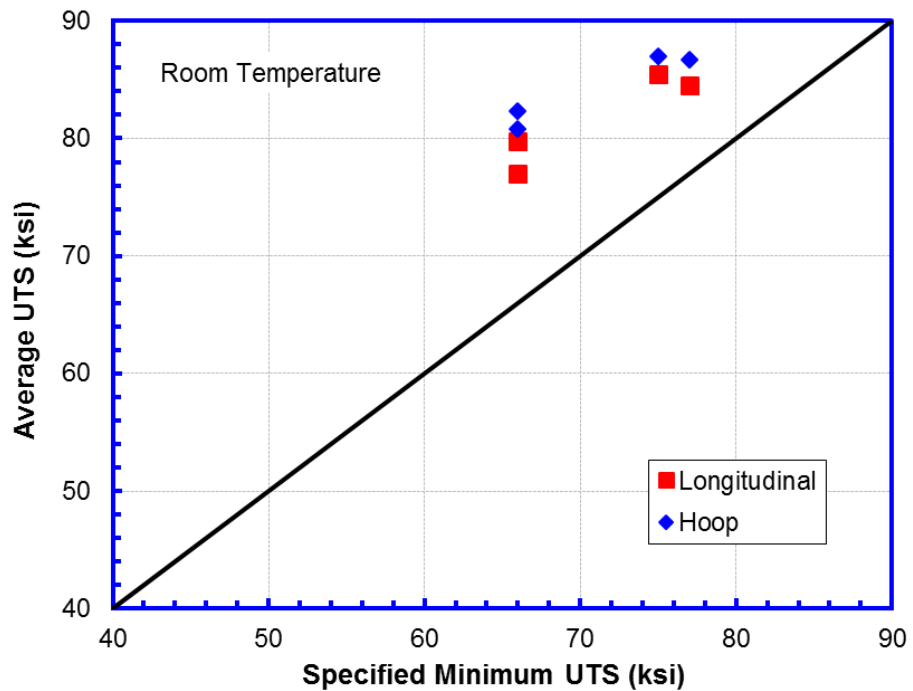


Figure 5-17 Measured UTS vs. specified minimum UTS

5.5.4 Girth Weld Tensile Properties and Strength Mismatch

5.5.4.1 Dimensions and Features of Tensile Specimens

All-weld metal tensile tests were conducted on the girth welds at room temperature. The round-bar tensile specimens of the largest possible gauge length were cut along the welding direction at 3 and 6 o'clock positions with respect to the seam weld.

5.5.4.2 Stress-Strain Curves

The stress-strain curves of the weld metals are given in Figure 5-18 to Figure 5-21 for all four lines. The UTS in the two o'clock positions are generally close. The yield strength in the 3 or 9 o'clock position is slightly higher than that in the 6 o'clock position. The yield strength and UTS of the girth welds in Lines 1 and 2 are approximately 450 MPa and 550 MPa, respectively. The yield strength and UTS of the girth welds in Lines 3 and 4 are approximately 500 MPa and 600 MPa, respectively. The girth welds in Lines 3 and 4 are stronger than those in Lines 1 and 2 by approximately 50 MPa.

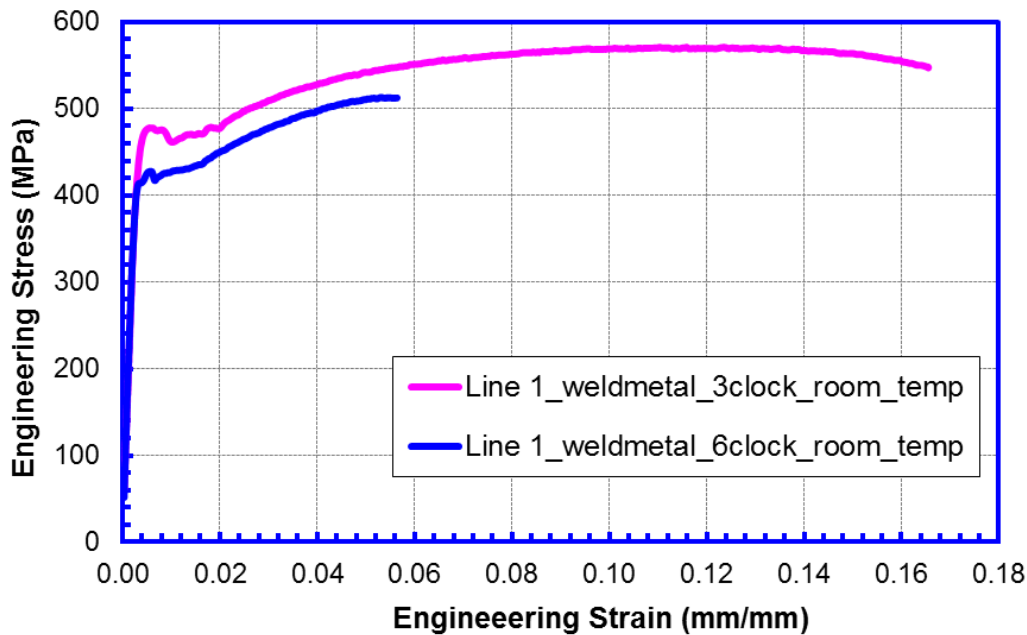


Figure 5-18 All-weld-metal stress-strain curves at room temperature and two o'clock positions of Line 1

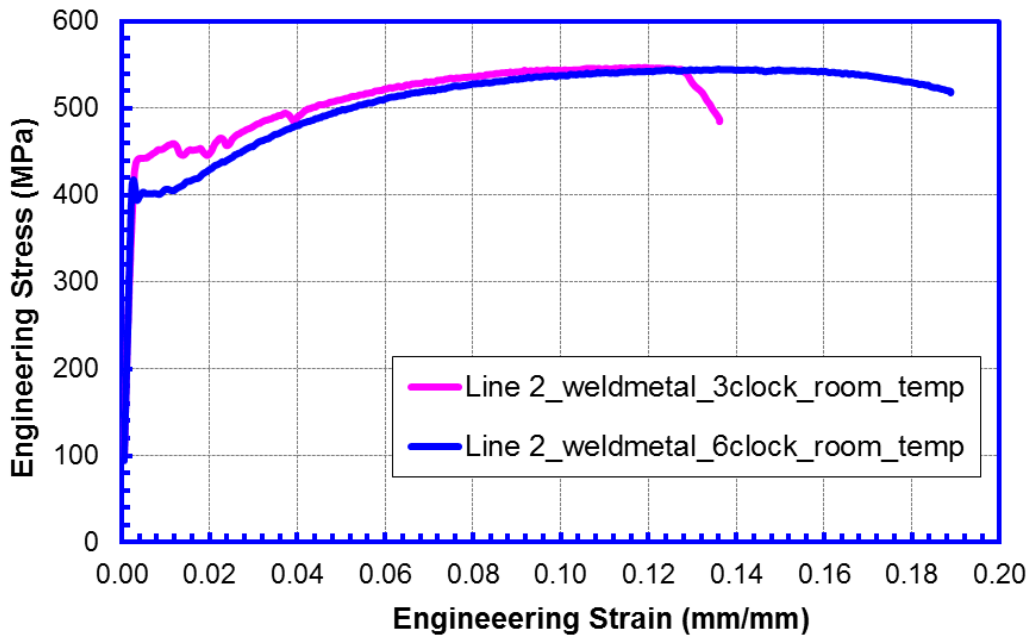


Figure 5-19 All-weld-metal stress-strain curves at room temperature and two o'clock positions of Line 2

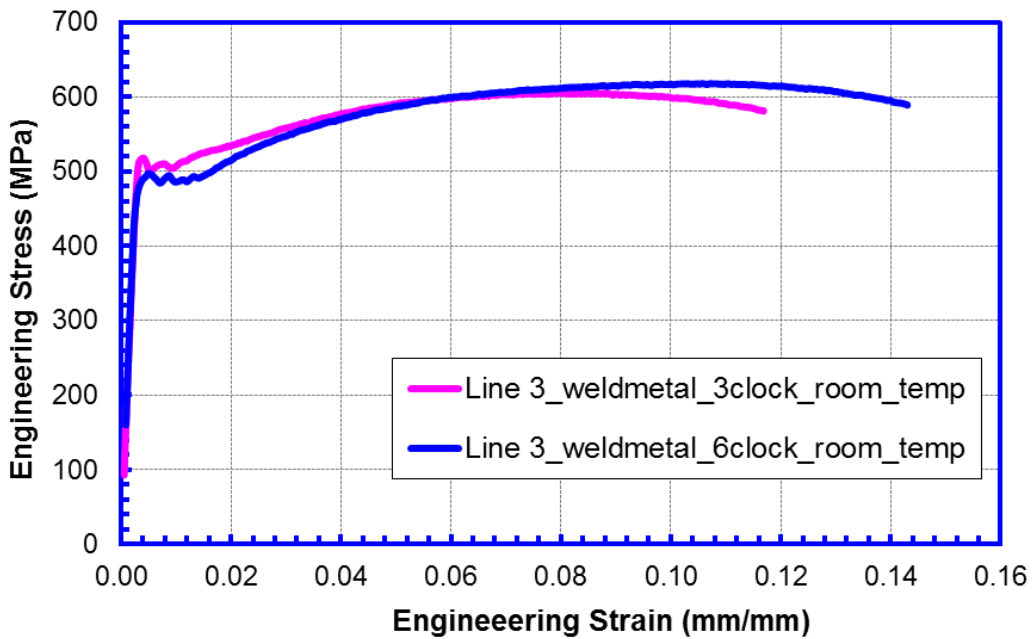


Figure 5-20 All-weld-metal stress-strain curves at room temperature and two o'clock positions of Line 3

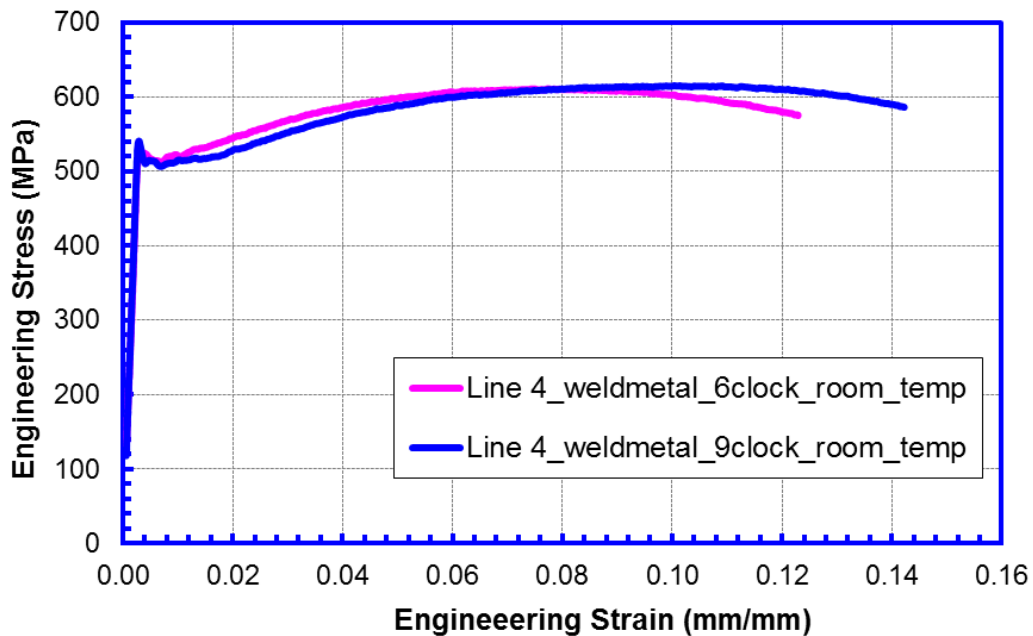


Figure 5-21 All-weld-metal stress-strain curves at room temperature and two o'clock positions of Line 4

5.5.4.3 Girth Weld Strength Mismatch

The weld strength mismatch as measured by the ratio of UTS is shown in Figure 5-22. Approximately evenmatching is achieved when the measured weld strength is compared with the measured pipe strength. Overmatching of 15-20% is achieved when the measured weld strength is measured against the specified minimum UTS of the pipes.

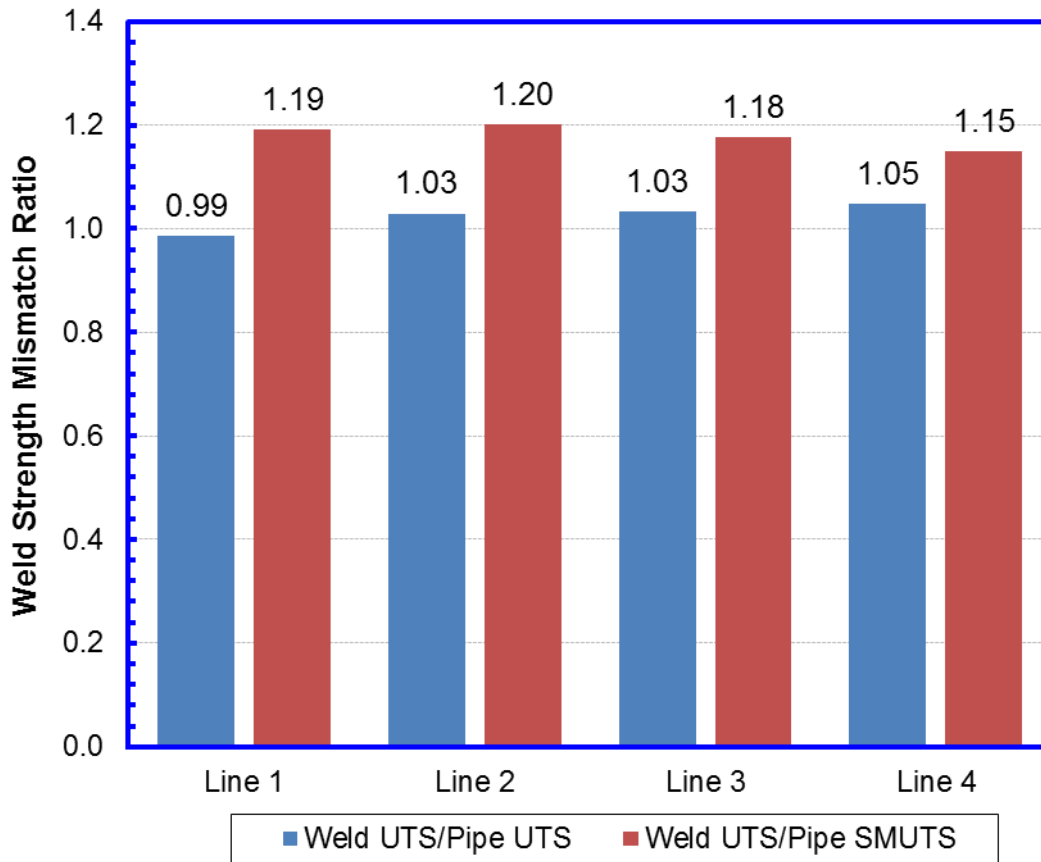
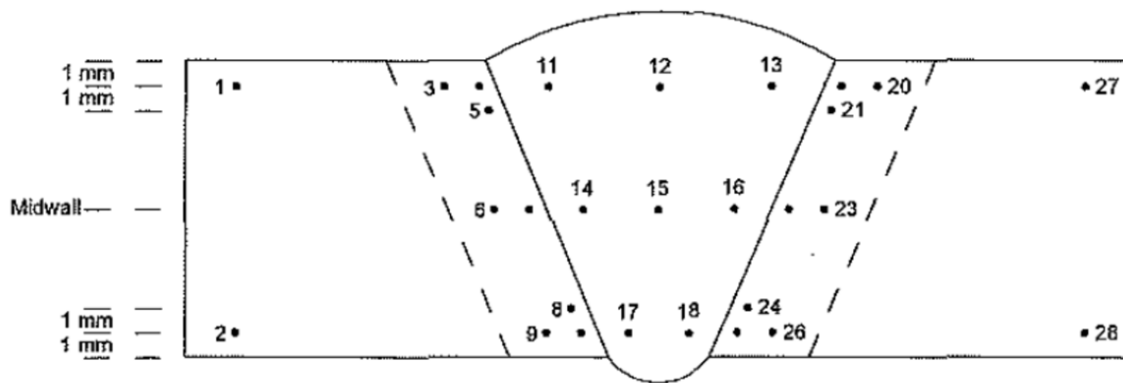


Figure 5-22 Weld strength mismatch from Group A

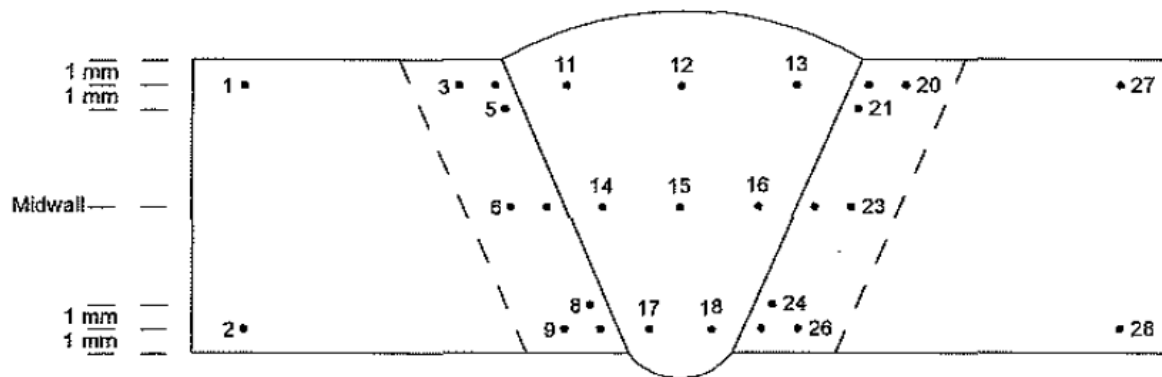
5.5.5 Girth Weld Hardness Profile

Hardness traverse tests were conducted on two specimens selected from the macro specimens with the least amount of high-low misalignment for each line. The locations and values of the hardness measurement are shown in Figure 5-23 to Figure 5-26. In most cases, the hardness in the HAZ is higher than that in the pipes or deposited weld metals.



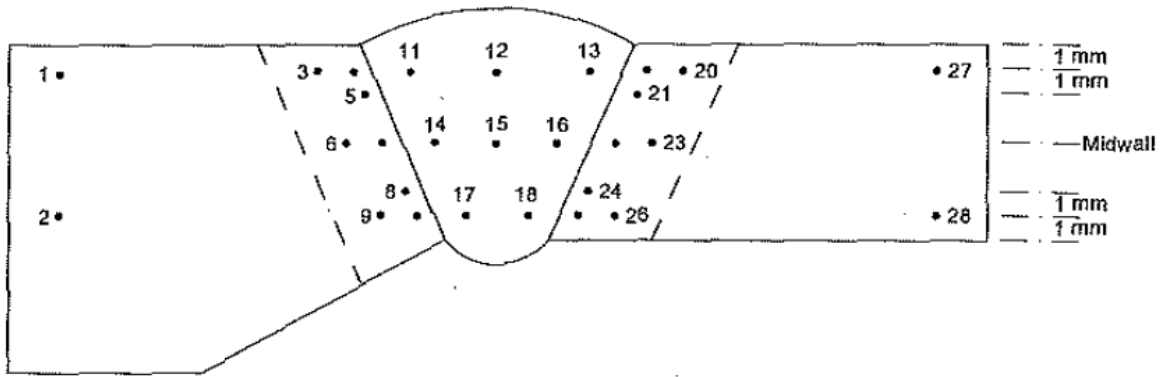
Parent Metal		HAZ		Weld Metal		HAZ		Parent Metal	
1	187	3	187	11	180	19	224	27	184
2	182	4	195	12	173	20	217	28	183
		5	189	13	171	21	214		
		6	186	14	168	22	183		
		7	183	15	164	23	185		
		8	182	16	163	24	184		
		9	190	17	169	25	183		
		10	185	18	168	26	181		
Average	185	Average	187	Average	170	Average	196	Average	184

Figure 5-23 Hardness profile of a girth weld of Line 1



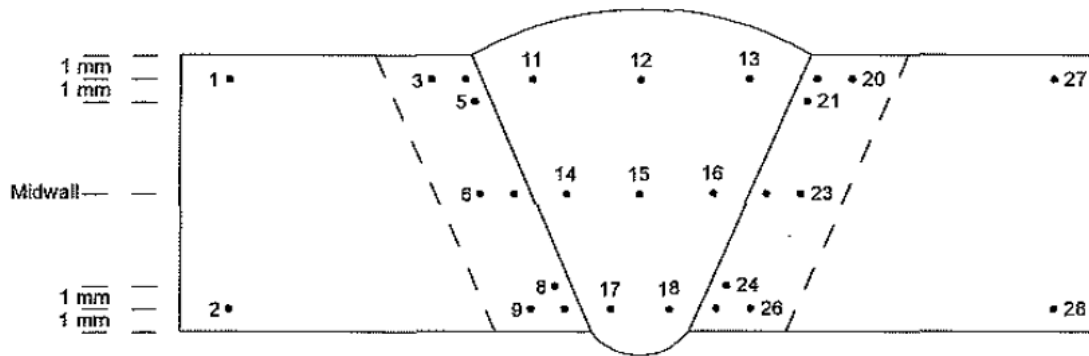
Parent Metal		HAZ		Weld Metal		HAZ		Parent Metal	
1	195	3	180	11	142	19	185	27	184
2	189	4	193	12	153	20	179	28	175
		5	182	13	144	21	208		
		6	167	14	160	22	198		
		7	168	15	154	23	196		
		8	179	16	158	24	182		
		9	186	17	156	25	179		
		10	187	18	154	26	178		
Average	192	Average	180	Average	153	Average	188	Average	180

Figure 5-24 Hardness profile of a girth weld of Line 2



Parent Metal		HAZ		Weld Metal		HAZ		Parent Metal	
1	170	3	181	11	209	19	195	27	196
2	180	4	209	12	200	20	185	28	197
		5	217	13	199	21	194		
		6	208	14	204	22	209		
		7	234	15	191	23	196		
		8	211	16	197	24	202		
		9	183	17	184	25	194		
		10	205	18	182	26	181		
Average	175	Average	206	Average	196	Average	195	Average	197

Figure 5-25 Hardness profile of a girth weld of Line 3



Parent Metal		HAZ		Weld Metal		HAZ		Parent Metal	
1	196	3	178	11	246	19	239	27	204
2	189	4	227	12	232	20	190	28	197
		5	233	13	224	21	236		
		6	179	14	193	22	219		
		7	203	15	204	23	210		
		8	218	16	201	24	221		
		9	214	17	177	25	213		
		10	209	18	176	26	201		
Average	193	Average	208	Average	207	Average	216	Average	201

Figure 5-26 Hardness profile of a girth weld of Line 4

5.5.6 Charpy Impact Energy

The objective of the Charpy impact tests was to determine the ductile-to-brittle transition temperature and the upper-shelf impact energy of the girth welds. The Charpy impact tests were conducted on the girth welds with notches into both the weld metal centerline and HAZ. The notch of the weld centerline specimens and the HAZ specimens was oriented in the through-thickness direction. The HAZ notch was introduced with the notch line intercepting the fusion boundary at the 1/3 pipe wall location from the pipe OD. The Charpy impact tests were conducted first on the specimens taken from 12, 3 and 6 o'clock positions with respect to the girth welds at -5 °C. The weld o'clock position with the lowest Charpy energy at -5 °C was then selected for the tests of the Charpy transition curves. Based on the results of Charpy impact tests at -5 °C, the 12 o'clock position had the lowest Charpy energy for all the girth welds tested. The pipe wall thickness and necessary machining limited the Charpy specimens to sub-size of either 10×8.0 mm or 10×7.5 mm. The transition curves of the converted full-size Charpy energy are shown in Figure 5-27 to Figure 5-30. The welds with notch at the weld metal centerline have the higher transition temperature than those with notch at the HAZ. The welds with notch at the HAZ have the larger upper-shelf impact energy than those with notch at the weld metal centerline.

The transition temperatures and upper shelf energy overall have not changed for welds made in early 1950s to 1990s. The impact energy at -10 °C is 35 ft·lb and higher. The transition temperature, measured at the temperature at the mid-transition point by Charpy energy, is -20 °C or lower. There tend to be more scatter in the Charpy energy in HAZ-notched specimens than weld centerline notched specimens.

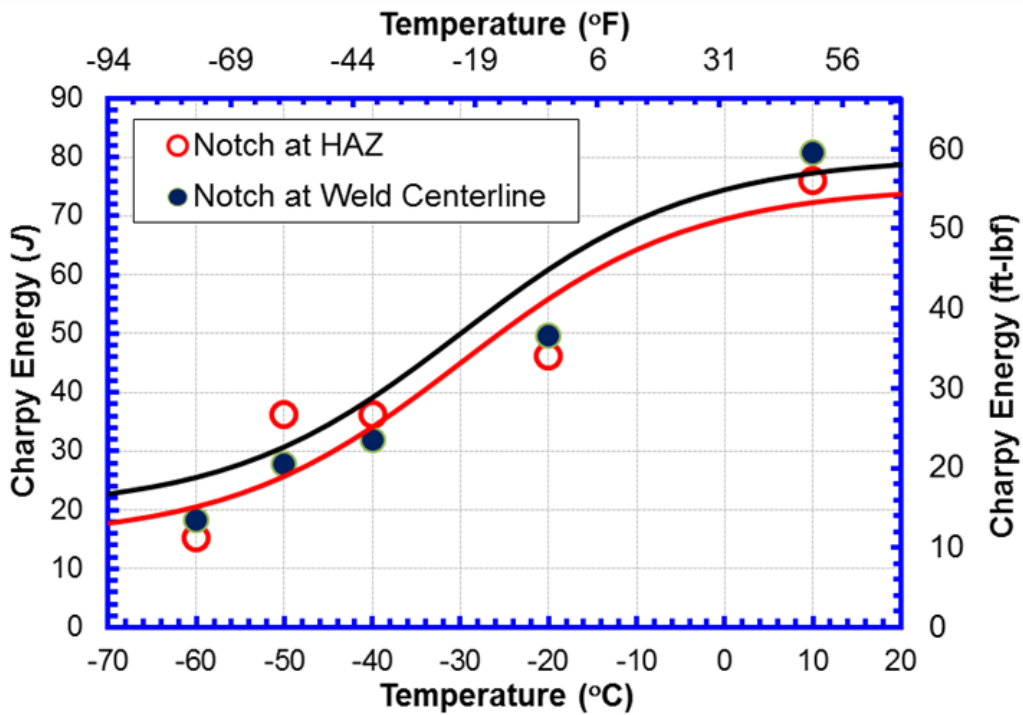


Figure 5-27 Charpy transition curves of a girth weld of Line 1

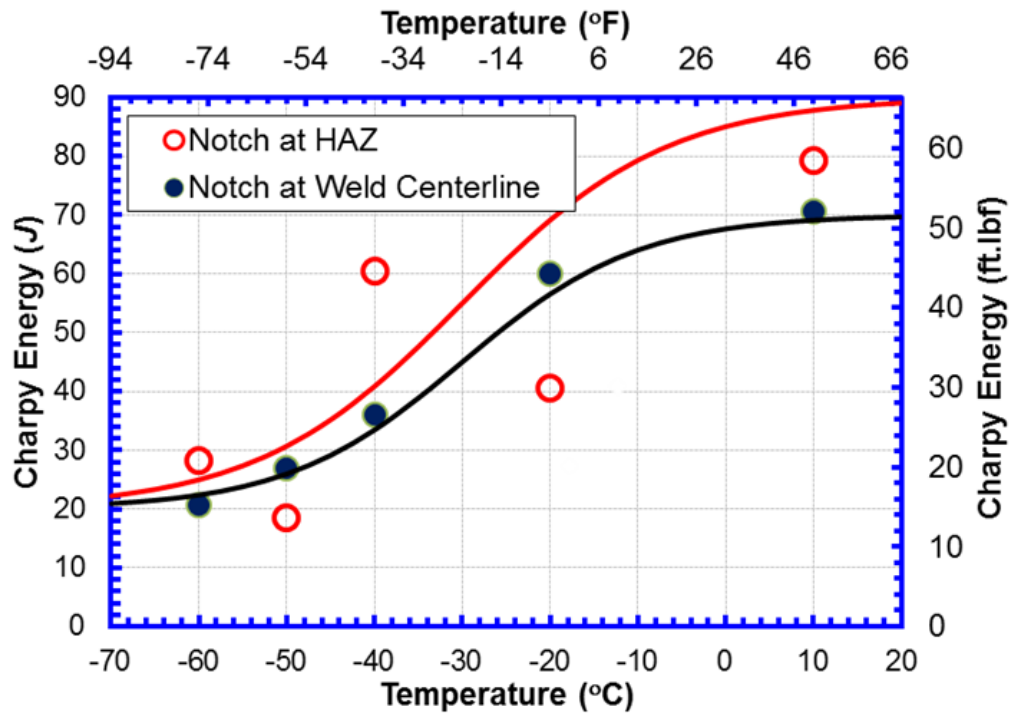


Figure 5-28 Charpy transition curves of a girth weld of Line 2

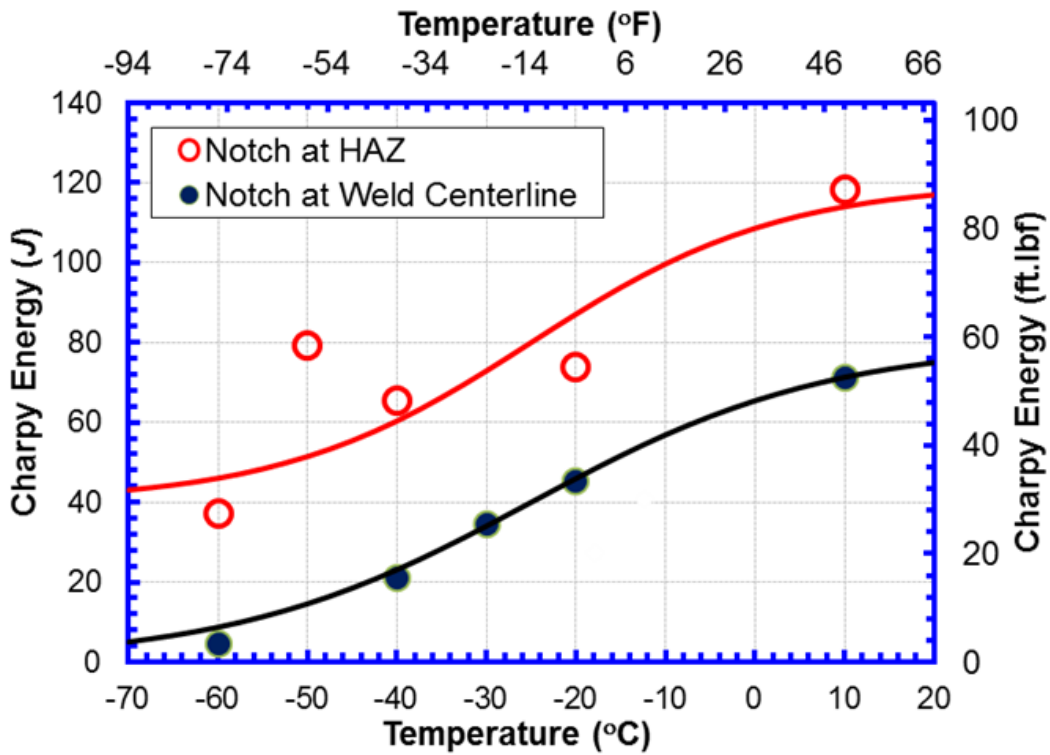


Figure 5-29 Charpy transition curves of a girth weld of Line 3

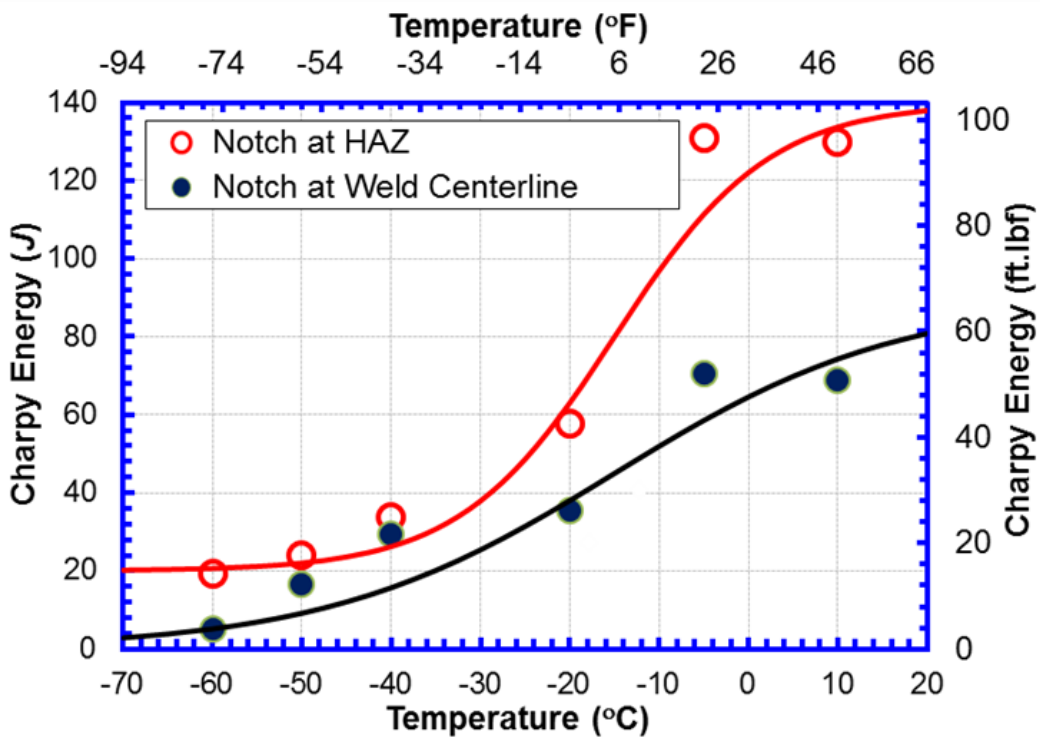


Figure 5-30 Charpy transition curves of a girth weld of Line 4

5.5.7 Cross-Weld Tensile Test

5.5.7.1 Overview of the Test

The instrumented cross-weld tensile tests were conducted on the girth welds of all four lines. Figure 5-31 shows the nominal dimensions of the specimens and the locations of the three clip gauges. The dimensions in this figure are not to scale. These gauges are used to measure the deformation across the weld and in the base pipe on either side of the weld. A few selected test samples are shown in Figure 5-32.

Two types of the specimens were tested: specimens with natural flaws and specimens with artificially introduced planar flaws. The natural flaw samples were selected by the appearance of the weld profiles, principally the appearance on the root side. Two specimens were selected from Line 1 and four specimens were selected from Line 2. No specimens were selected from Lines 3 and 4 as no obvious flaws could be found in those welds from the appearance.

For the specimens with artificially introduced flaws, the specimens were selected at circumferential locations with the lowest Charpy energy at -5 °C. EDM notches were machined into the weld centerline or HAZ from the ID side as shown in Figure 5-33. The nominal depth of the flaws was 3 mm, simulating one weld bead height. The flaws cover the entire specimen width of nominally 1.5 in.

The test results are summarized in Table 5-3.

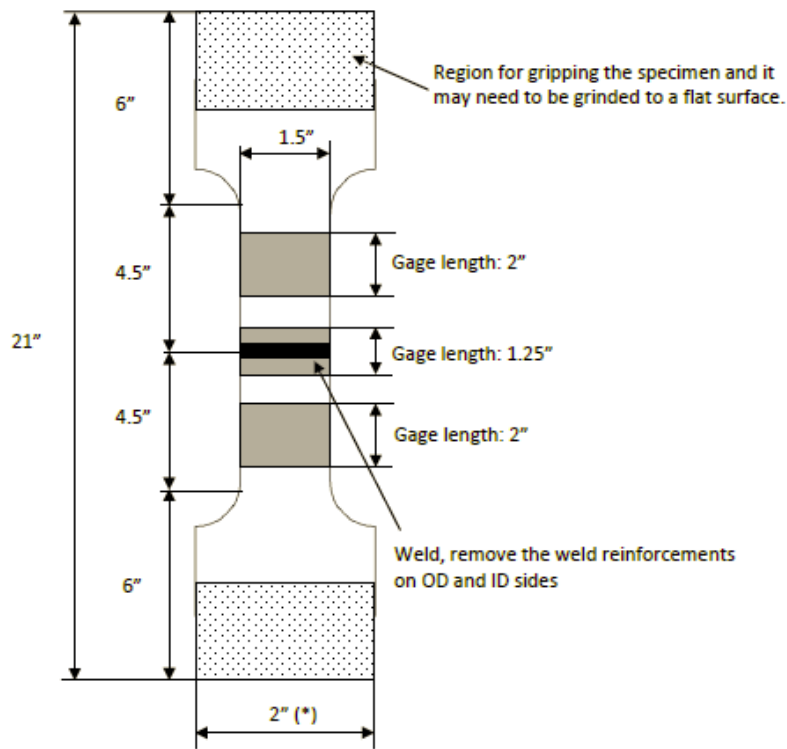


Figure 5-31 Schematic of the cross-weld tensile specimens (dimensions are not to scale)

* This is the nominal dimension



Figure 5-32 Cross-weld tensile specimens

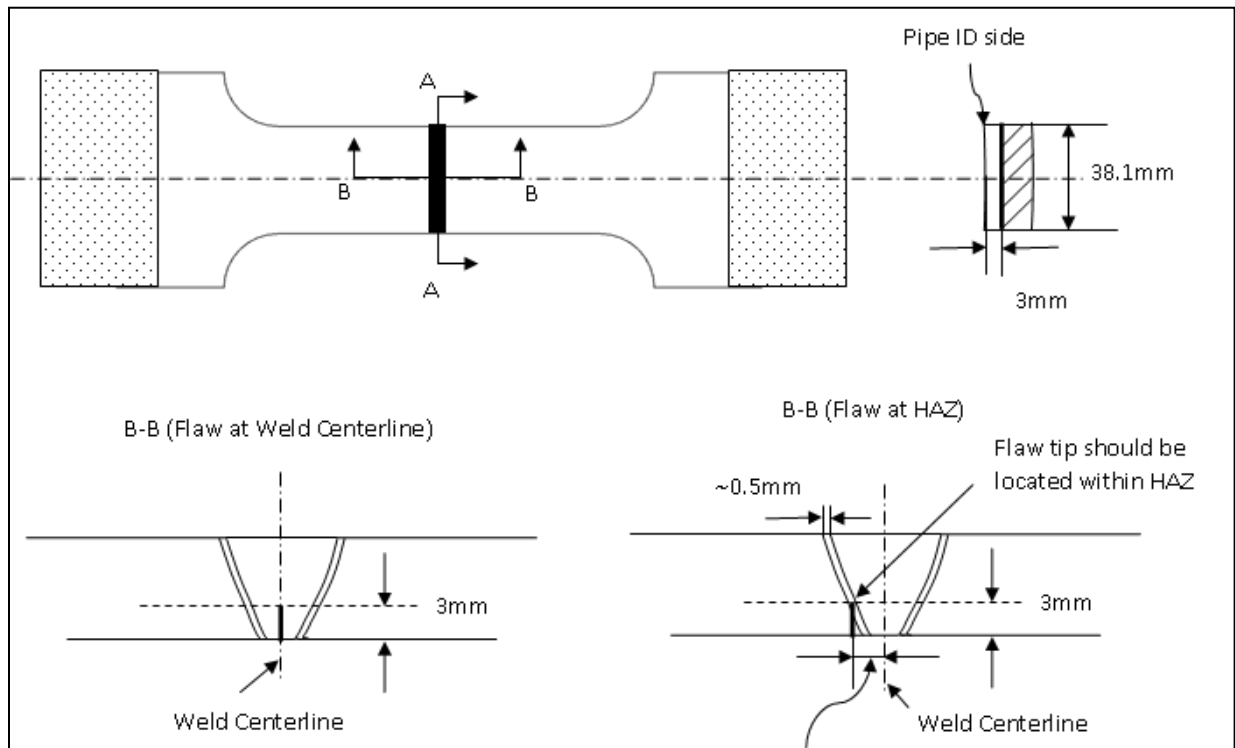


Figure 5-33 Schematic of manufactured flaw of the cross-weld tensile specimens

Table 5-3 Summary of cross-weld tensile test results of Group A

Pipe	Natural Flaw?	Flaw Depth (mm)	Flaw Depth /Wall Thickness	Temp (°C)	Notch Location	Clock Position	Strain at Peak Load (%)				Peak Load (KN)	Gross Section Stress at Peak Load		Residual CTOD (mm)		
							Top Gage	Cross-weld Gage	Bottom Gage	Ave. Strain		(MPa)	(ksi)			
Line 1	No	3	0.32		Room	HAZ	5-6	0.28	0.76	0.40	0.34	114	370	53.7		
							11-12	0.26	0.67	0.24	0.25	113	347	50.4		
						Weld Center Line	7	0.36	0.96	0.28	0.32	115	351	51.0		
							10	0.28	0.82	0.28	0.28	98	312	45.3		
						-20	HAZ	4-5	0.67	1.45	0.68	0.68	132	394	57.2	
								10-11	0.36	0.98	0.29	0.32	110	365	52.9	
	Yes				Room	Weld Center Line	5	0.32	0.93	0.35	0.34	125	374	54.3		
							10-11	0.25	0.73	0.29	0.27	99	344	49.9		
						HAZ	11-12	1.02	1.18	1.07	1.05	124	417	60.4		
							12-1	1.60	2.55	1.82	1.71	128	452	65.5		
Line 2	No	3	0.32		Room	HAZ	12-1	0.40	0.78	0.37	0.39	108	343	49.7	1.97	
							6-7	0.86	1.07	0.33	0.60	113	360	52.1	1.37	
						Weld Center Line	12-1	0.92	1.02	0.57	0.75	122	397	57.6		
							8-9	0.35	0.94	0.73	0.54	111	354	51.3		
						-20	HAZ	11-12	0.37	1.17	0.80	0.59	127	383	55.5	
								5-6	1.15	1.36	0.53	0.84	119	399	57.9	
	Yes				Room	Weld Center Line	11-12	0.72	1.47	0.82	0.77	129	411	59.6		
							5-6	0.33	1.21	0.50	0.42	108	355	51.5		
						HAZ	1-2	5.97	5.74	2.18	4.08	146	494	71.7		
							11-12	1.42	1.87	0.69	1.06	132	428	62.1		
Line 3	No	3	0.32		Room	HAZ	8-9	0.46	2.47	0.48	0.47	152	433	62.8	1.97	
							11-12	0.36	1.84	0.35	0.36	134	446	64.7	1.37	
						Weld Center Line	11-12	0.28	1.09	0.32	0.30	127	411	59.6	1.21	
							8-9	0.36	1.15	0.33	0.35	143	422	61.2	1.17	
						-20	HAZ	12-1	0.59	3.21	0.50	0.55	161	544	78.9	
								9-10	0.31	1.37	0.51	0.41	147	434	63.0	
	Yes				Room	Weld Center Line	2-3	0.32	1.31	0.40	0.36	143	458	66.5	1.10	
							10-11	0.29	2.16	0.44	0.37	164	542	78.6	1.18	
						HAZ	12-1	0.27	4.11	0.48	0.38	170	522	75.8	1.88	
							8-9	0.26	2.38	0.41	0.34	159	513	74.4	1.18	
Line 4	No	3	0.32		Room	HAZ	7-8	0.26	1.65	0.32	0.29	158	484	70.3	1.30	
							9	0.31	1.44	0.32	0.32	144	447	64.9	1.58	
						Weld Center Line	12-1-2	0.48	3.14	0.43	0.46	148	486	70.4	1.44	
							8-9	0.46	2.78	0.39	0.43	147	459	66.6	1.57	
						-20	Weld Center Line	12-1	0.24	1.27	0.33	0.29	161	495	71.8	
								8-9	0.34	1.80	0.37	0.36	158	493	71.4	1.02
	No	3	0.21		Room	HAZ	10-11-12	2.70	4.37	3.18	2.94	262	529	76.7	2.24	
							10-11	2.86	5.71	2.68	2.77	257	544	78.9	2.55	
						Weld Center Line	4-5-6	1.41	2.62	2.17	1.79	249	515	74.6	1.88	
							4-5	1.42	2.21	1.71	1.57	254	525	76.1	1.20	
-20						HAZ	3-4-5	3.28	4.53	1.71	2.50	259	557	80.8	2.15	
							9-10	0.76	1.94	1.89	1.33	252	547	79.3	0.91	
Weld Center Line						4-5	1.75	1.68	0.95	1.35	255	527	76.4			
						10-11	2.46	2.72	0.74	1.60	264	554	80.4	0.86		

5.5.7.2 Performance of Girth Welds with Natural Flaws

For the 6 specimens having natural flaws, the averaged strains in the base pipe material (from the measurement at the either side of the weld) at either fracture or the maximum load are as follows.

- Two welds from Line 1: 1.05%, 1.71%, and
- Four welds from Line 2: 1.06%, 1.19%, 2.03%, and 4.08%.

The specimen from Line 2 with the averaged base pipe strain of 2.03% was tested to fracture at a cross weld strain of 3.53%. The fracture surface of this specimen is shown in Figure 5-34. The tests of other five specimens were terminated at a strain level beyond the maximum load, but prior to specimen fracture.

Cross-weld testing of the girth welds with natural flaws from all four lines was also conducted prior to the work described above [131]. One interesting feature noted from those tests is that some welds cracked in the weld region, but the eventual failure did not occur in this region. For two of the Line 1 cross-weld specimens, the girth welds were not broken when the tests were stopped due to load drop. Significant cracking was observed in the weld region, see Figure 5-35 and Figure 5-37. These specimens were broken in liquid nitrogen along the cracked planes. The failure surfaces of the broken specimens are shown in Figure 5-36 and Figure 5-38. The weld cracking and fracture surface of Line 3 and Line 4 girth welds are shown in Figure 5-39 to Figure 5-42. The cracking was initiated in the weld region first. As the load increases, the strain hardening in the weld region increased the weld strength sufficiently that the deformation was transferred to the base pipe material. Load drop occurred due to the necking of base pipe material without fracture the specimen in the cracked weld region.



Figure 5-34 Fracture surface of a girth weld with natural flaws

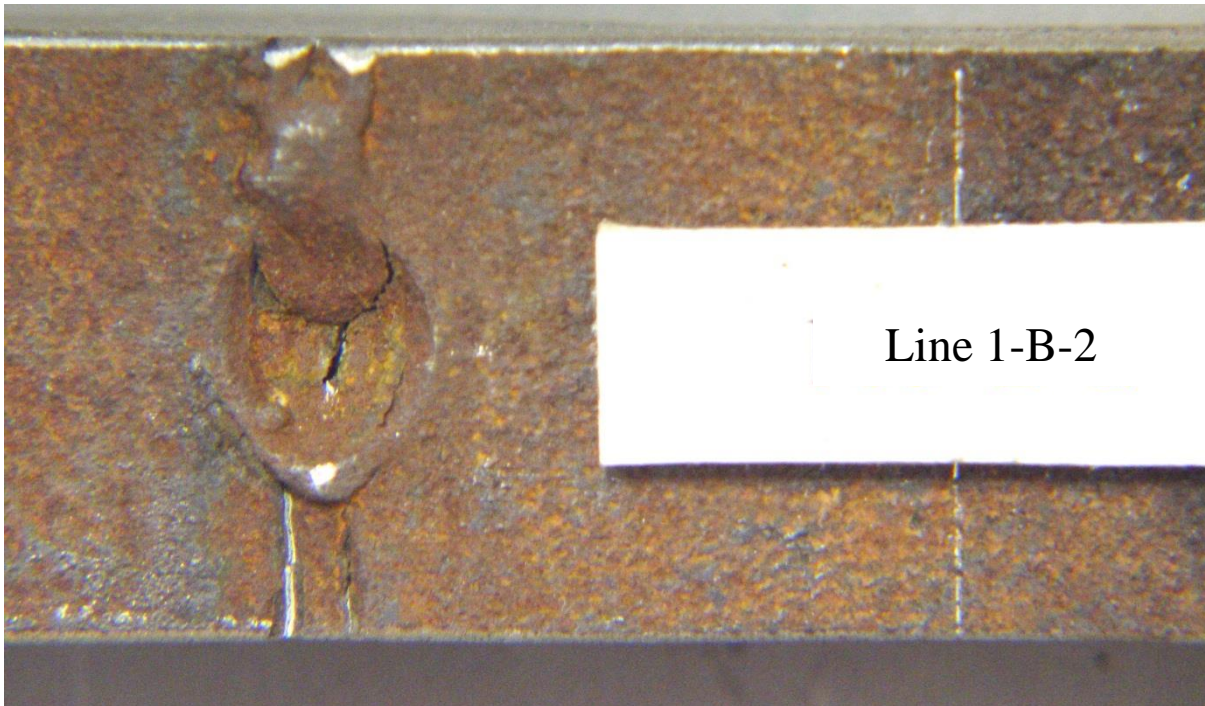


Figure 5-35 Cracking in the weld of Specimen Line 1-B-2 after the test was stopped due to load drop

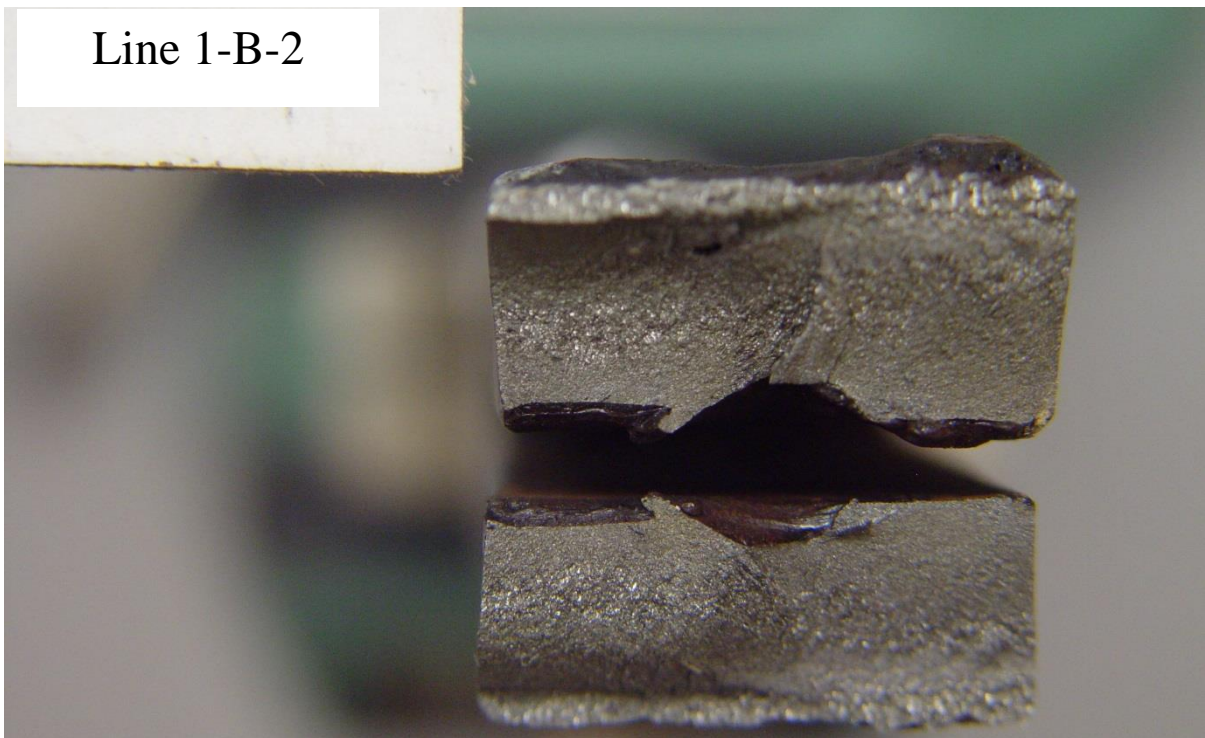


Figure 5-36 Weld failure surface of Specimen Line 1-B-2 after the cracked weld was broken in liquid nitrogen

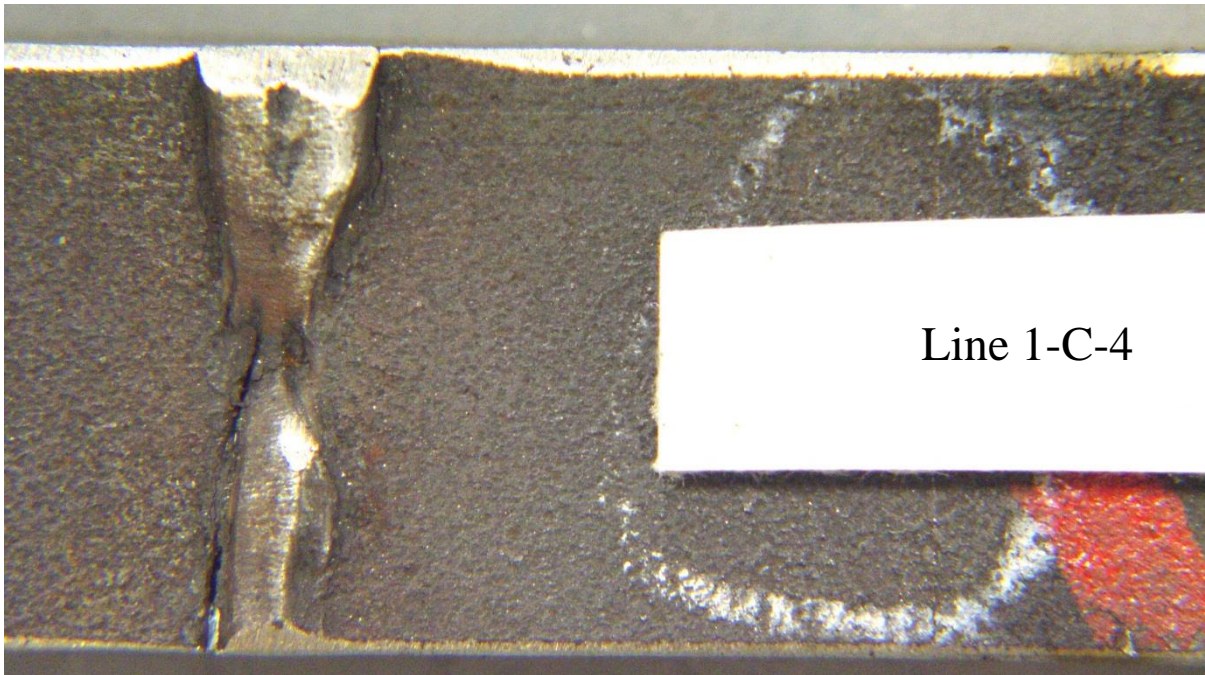


Figure 5-37 Cracking in the weld of Specimen Line 1-C-4 after the test was stopped due to load drop

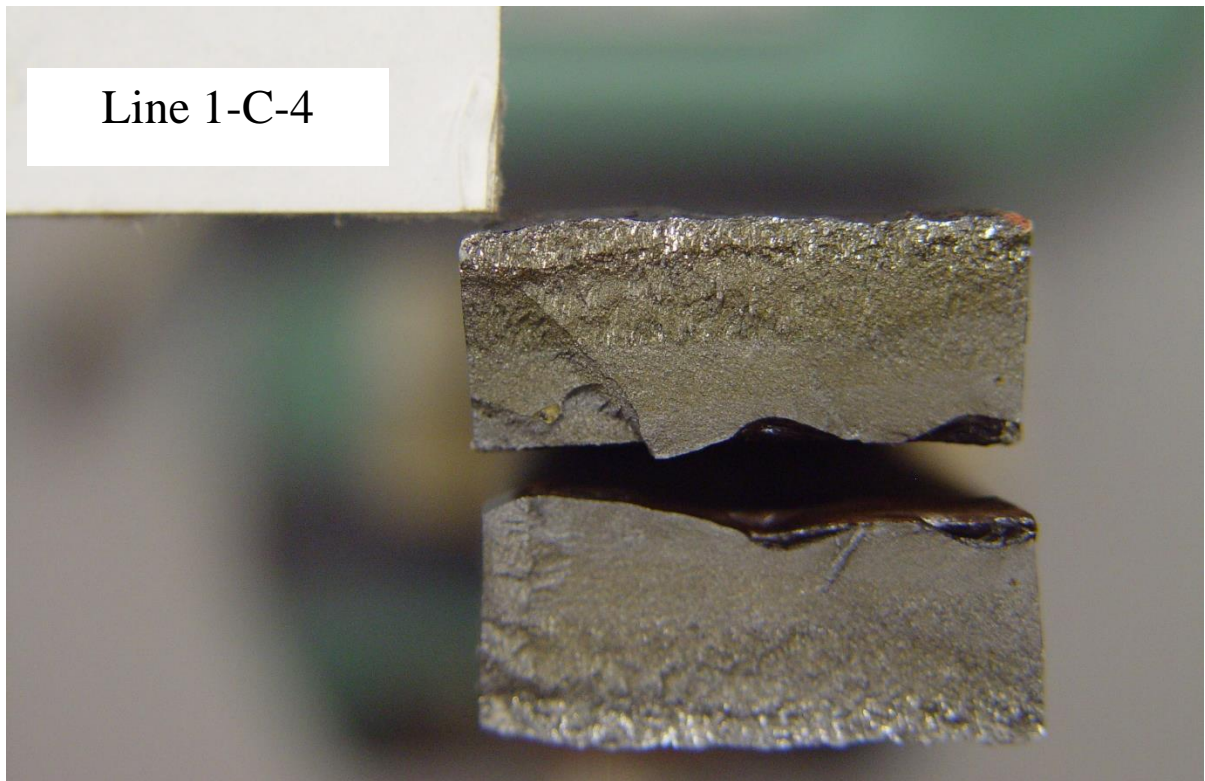


Figure 5-38 Weld failure surface of Specimen Line 1-C-4 after the cracked weld was broken in liquid nitrogen



Figure 5-39 Weld cracking observed after the test of Specimen from Line 3

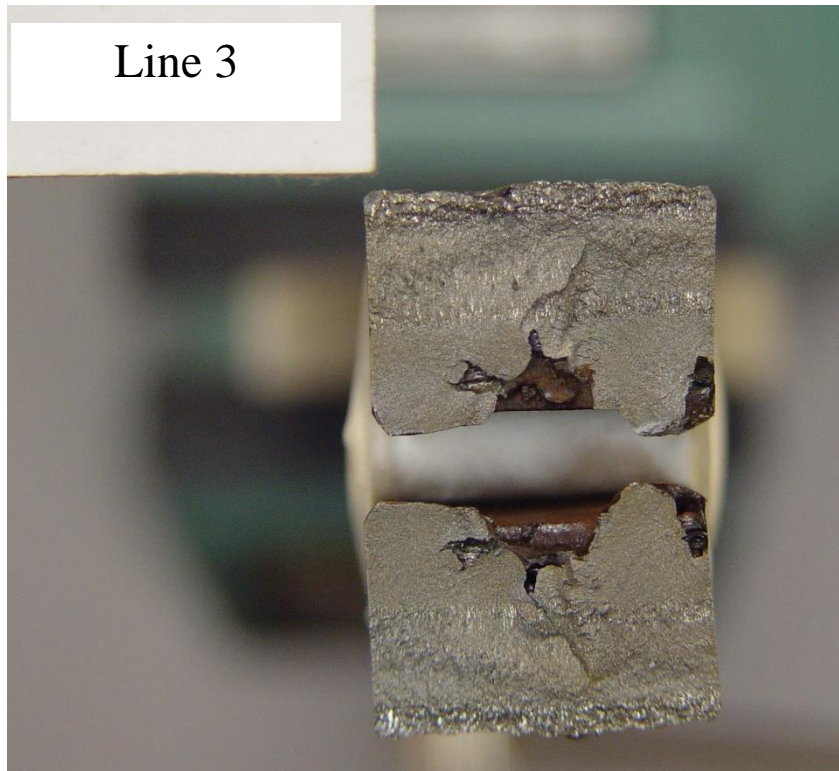


Figure 5-40 Weld defect revealed after the cracked weld of Line 3 was broken in liquid nitrogen

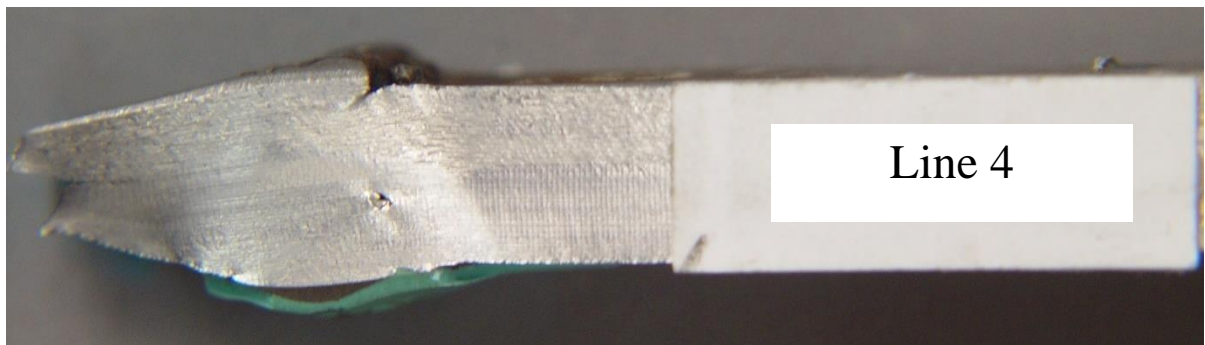


Figure 5-41 Weld cracking observed after testing of Line 4 cross-weld tensile specimen



Figure 5-42 Girth weld from Line 4 was fractured in liquid nitrogen after cross-weld tensile test, showing the fracture path along the fusion line/HAZ

5.5.7.3 Performance of Girth Welds with Artificial Flaws

Out of the 40 CWT specimens with artificial flaws, 4 specimens tested at $-20\text{ }^{\circ}\text{C}$ from Lines 3 and 4 fractured. No specimens tested at room temperature fractured. The specimen shown in Figure 5-43 with weld centerline flaw fractured at cross-weld strain of 1.27% and remote strain of 0.29%. The specimen shown in Figure 5-44 with HAZ flaw fractured at cross-weld strain of 1.37% and remote strain of 0.41%.

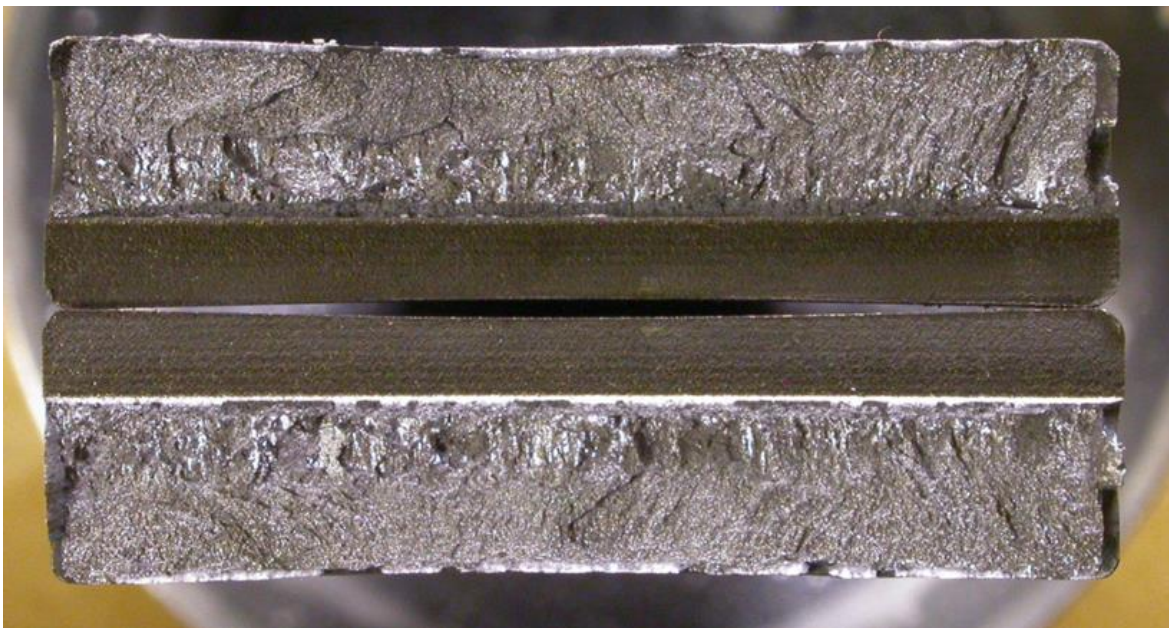


Figure 5-43 Fracture surface of a girth weld with an artificial flaw

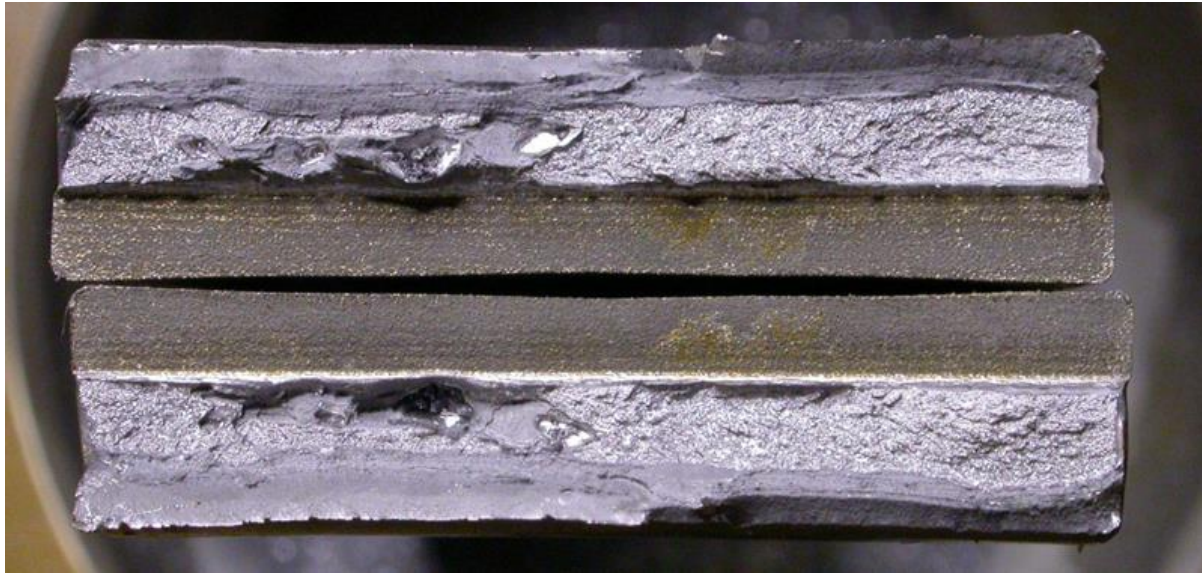


Figure 5-44 Fracture surface of a girth weld with an artificial flaw

5.5.7.4 Estimation of Apparent Toughness by Residual CTOD

As will be described in Section 7.3.4, one of the most critical parameters in predicting girth weld tensile strain capacity is its apparent CTOD toughness. This toughness is maximum blunting a planar flaw can sustain at the incipient flaw growth (i.e., initiation). The cross-weld tensile tests described here were not instrumented to detect initiation during test. It is, however, possible to determine the extent of residual blunting (after unloading) from the flaw tip profile after the completion of test. For specimens that did not fracture along the flawed plane, the residual blunting represents the minimum level of blunting the flaw can sustain without the initiation of flaw growth. For specimens that fractured along the flawed plane, the contribution from flaw growth can be subtracted to obtain the maximum residual blunting.

The residual CTOD toughness was measured from the photograph of the notch using 90-degree rule as shown in Figure 5-45. The side view of the specimen notch from Lines 3 and 4 after the test is shown in Figure 5-45 to Figure 5-47. The residual CTOD values before subtracting the initial notch width (about 0.2 mm) are summarized in Figure 5-48.

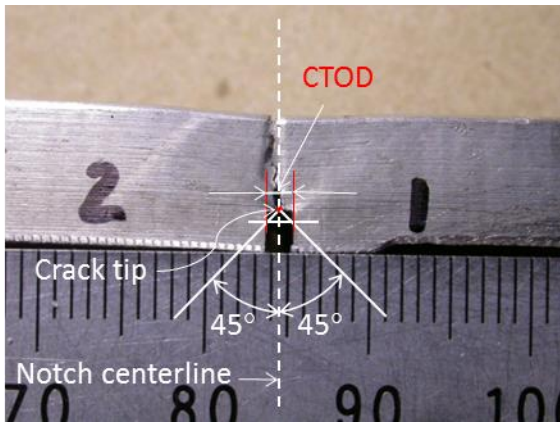


Figure 5-45 Side view of specimen from Line 3-1-1 at the termination of the test

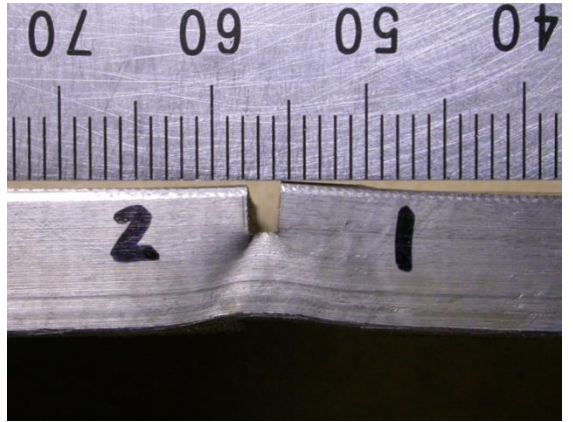
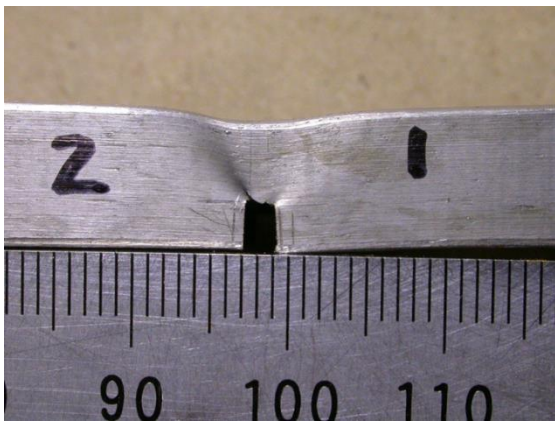


Figure 5-46 Side view of specimen Line 3-1-3 at the termination of the test



Figure 5-47 Side view of specimen Line 4-1-4a at the termination of the test

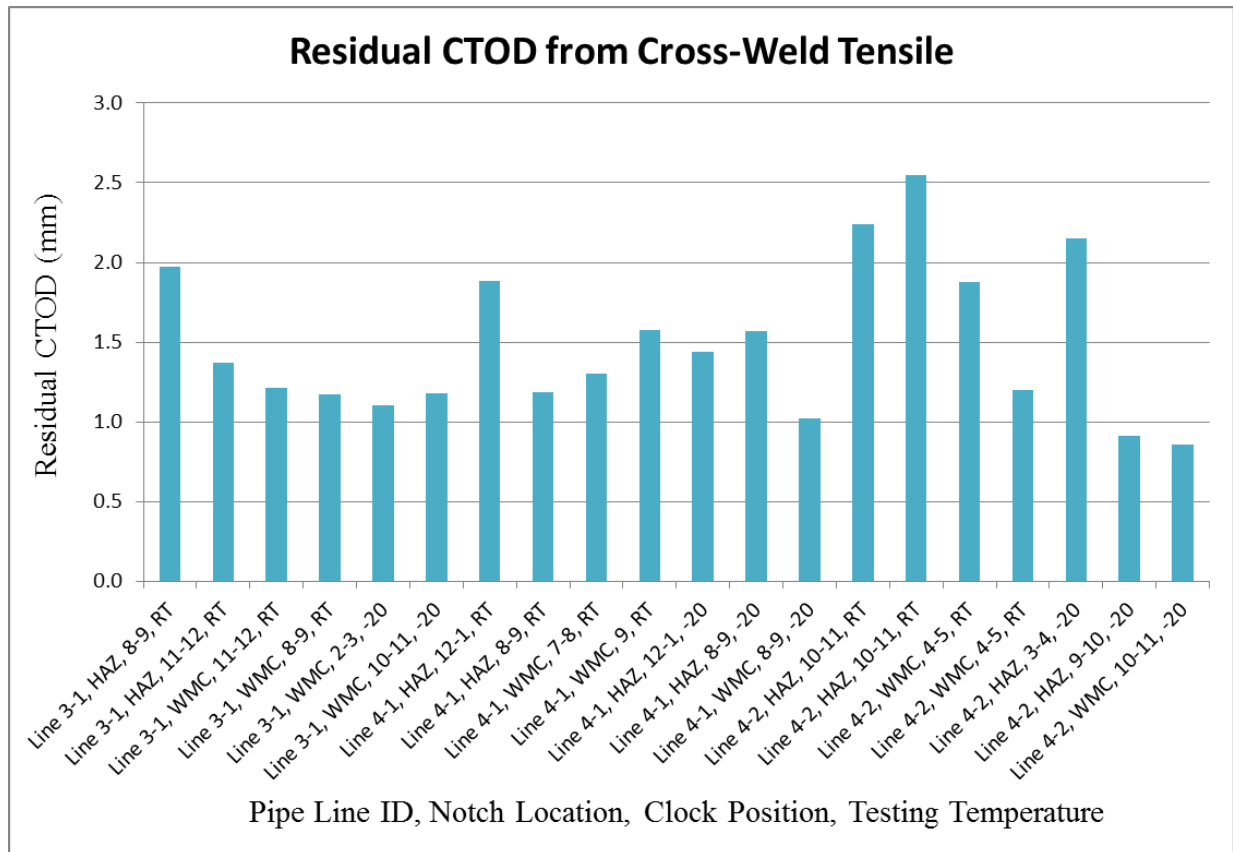


Figure 5-48 Residual CTOD vs. specimen characteristics

5.5.8 General Observations from Group A Data

- The welds are expected to behave in a ductile manner at normal service temperature as low as -10 °C. Only a few cross-weld tensile specimens fracture at test temperature of -20 °C, while none fractured at room temperature.
- The cross-weld tensile specimens with the worst natural flaws were able to sustain a strain 1.0% and above.
- The cross weld tensile tests for specimens with artificial flaws indicate that the flaw can sustain a large amount of blunting without growth. The residual CTOD measured directly from the specimen deformation profiles of Lines 3 and 4 welds has a minimum value of ~0.8 mm. In most case, the residual CTOD is 1.0 mm and above.

5.6 Pipe and Girth Weld Properties from Group B

5.6.1 Overview of the Group B Materials and Tests

Group B consists of 23 X52 vintage girth welds with 26-inch diameter and 0.281-inch wall thickness. Non-destructive tests (NDT) were first conducted on 10 randomly selected welds out of the 23 welds. These 10 girth welds were constructed in 1950 – 1956. The results of the NDT inspection were used to select the locations of material property test specimens and cross-weld

tensile test specimens along the circumference of the welds. After extracting these specimens, material property tests and cross-weld tensile tests were conducted.

5.6.2 Non-Destructive Testing Techniques

The 10 selected vintage girth welds were inspected using two non-destructive testing (NDT) techniques: Magnetic Particle Inspection (MPI) and Phased Array Ultrasonic Testing (PAUT).

5.6.2.1 Magnetic Particle Inspection (MPI)

In this technique, a magnetic field is applied to the girth weld using a hand-held electro-magnetic yoke, and magnetic particles (dry powders or wet ferrous suspensions) are applied to the tested weld area. The presence of a flaw in the tested weld area causes a leakage in the magnetic flux. This flux leakage leads to a build-up of the ferrous particles at the flaw and forms a visible flaw indication.

5.6.2.2 Phased Array Ultrasonic Testing (PAUT)

PAUT is an ultrasonic testing technique that uses an array consisting of multiple ultrasonic transducers which can be individually controlled and excited. PAUT can be used to detect weld anomalies and can be used to determine the depth, height, and length of flaws. Unlike MPI which can only detect surface anomalies, PAUT can detect both surface flaws as well as embedded flaws.

5.6.3 Summary of NDT Results and Distribution of Flaws

Out of the total of 110 flaws detected, 75 were planar flaws and 35 were volumetric flaws. The types of planar flaws detected were inadequate penetration (IP), lack of fusion (LOF), and root crack (RC). The types of volumetric flaws detected were slag/porosity and burn-through. The types of flaws detected are shown in Figure 5-49. The number of flaws detected in each weld is shown in Figure 5-50.

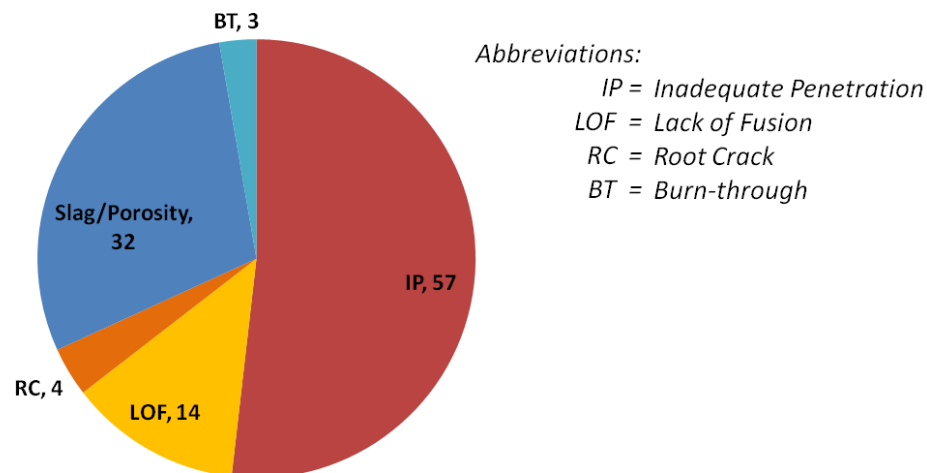


Figure 5-49 Types of flaws detected by NDT

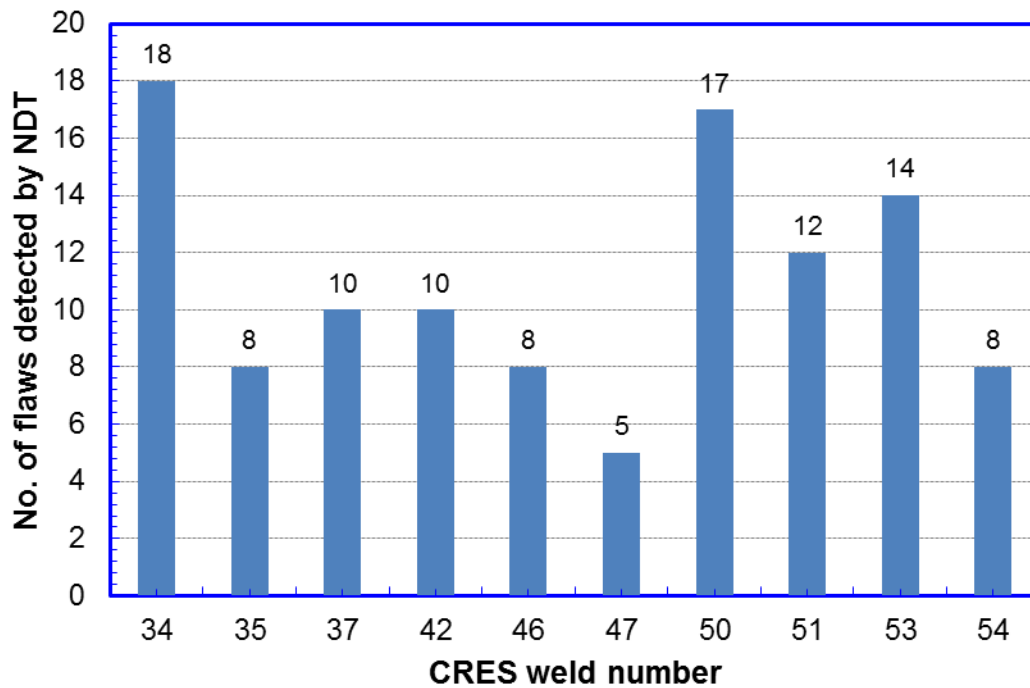


Figure 5-50 Number of flaws detected by NDT in each of the 10 vintage girth welds

5.6.3.1 Planar Flaws Detected by NDT

Figure 5-51 to Figure 5-53 provide the characteristics of the planar flaws detected by NDT. Note that the ‘flaw area’ values shown in Figure 5-53 do not necessary reflect to the actual area of the flaws. The flaw area value plotted here was obtained by determining the product of each detected flaw’s height and length (thus, assuming that it has a rectangular geometry – which may not be the case always). Figure 5-54 and Figure 5-55 show the distribution of the 75 planar flaws, divided into groups based on the flaw height and flaw length, respectively.

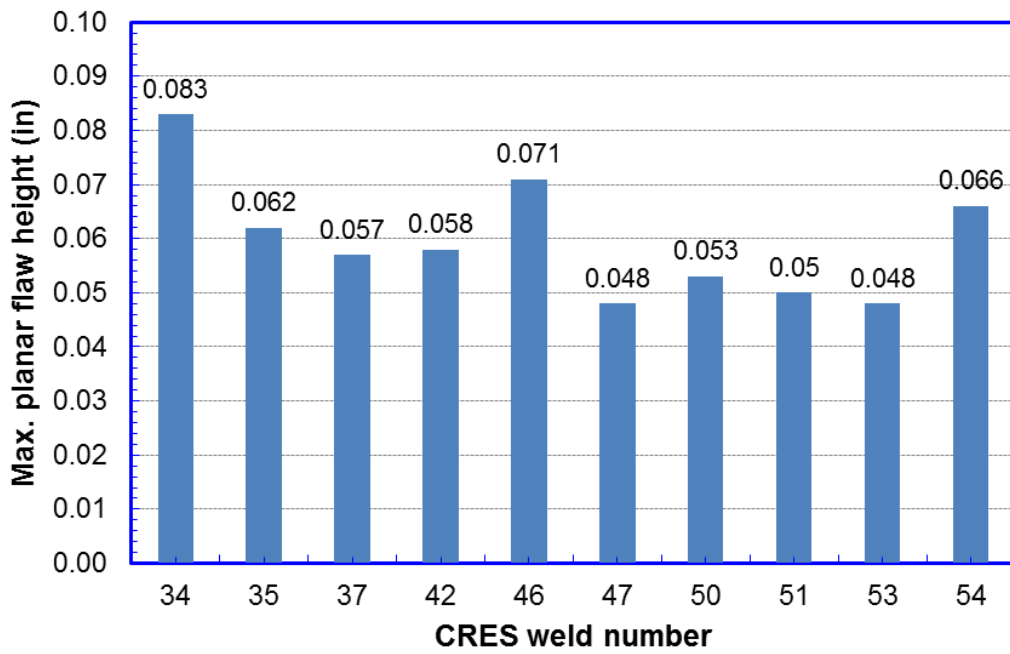


Figure 5-51 Maximum planar flaw height reported in each weld by NDT

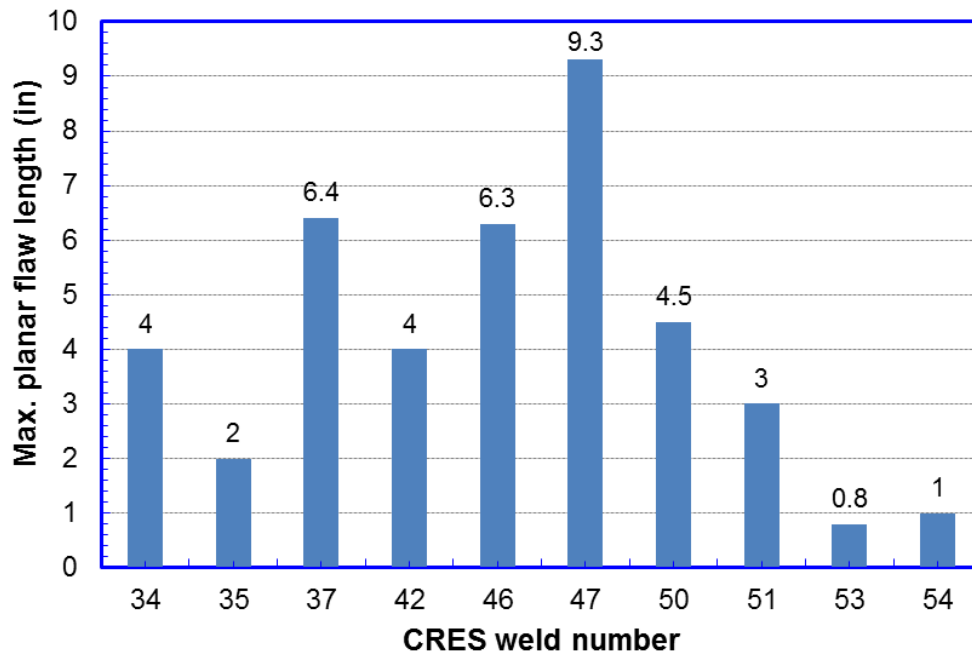


Figure 5-52 Maximum planar flaw length reported in each weld by NDT

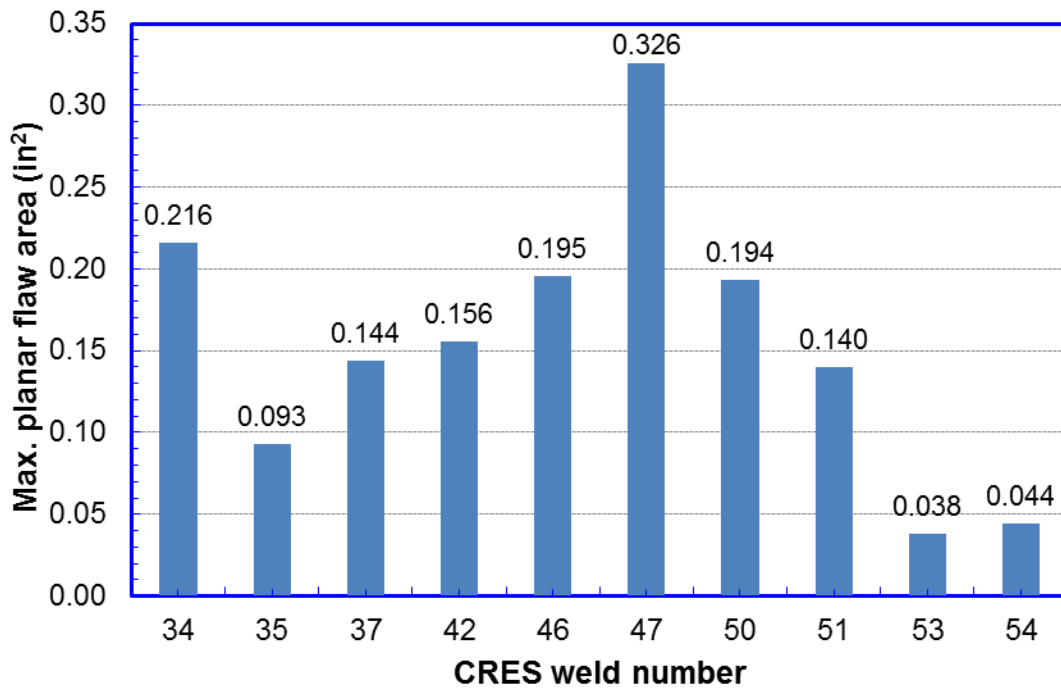


Figure 5-53 Maximum computed area of planar flaws in each weld

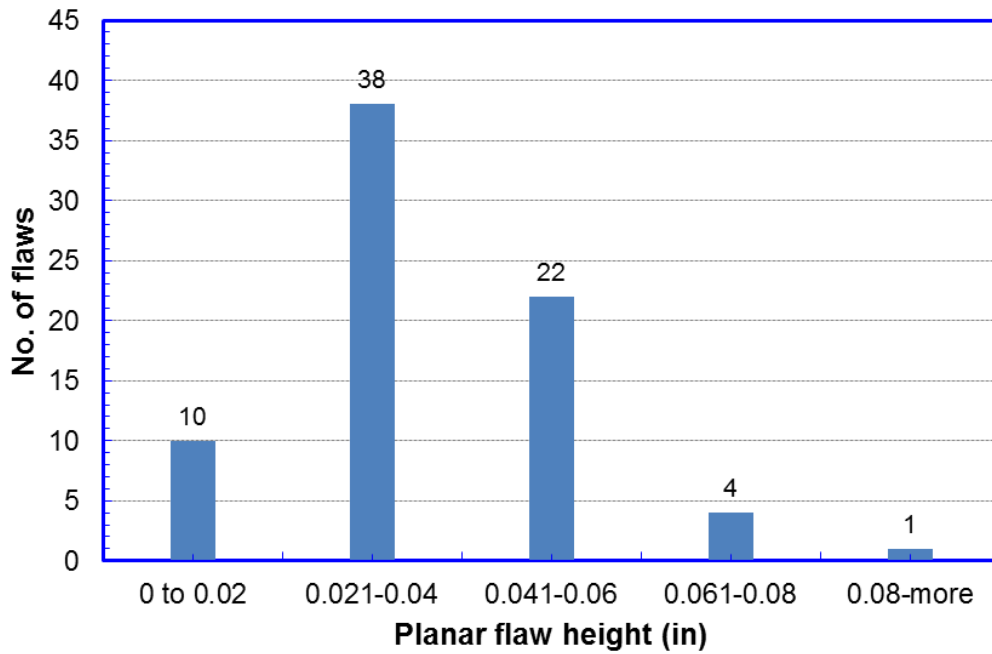


Figure 5-54 Distribution of reported planar flaw height by NDT

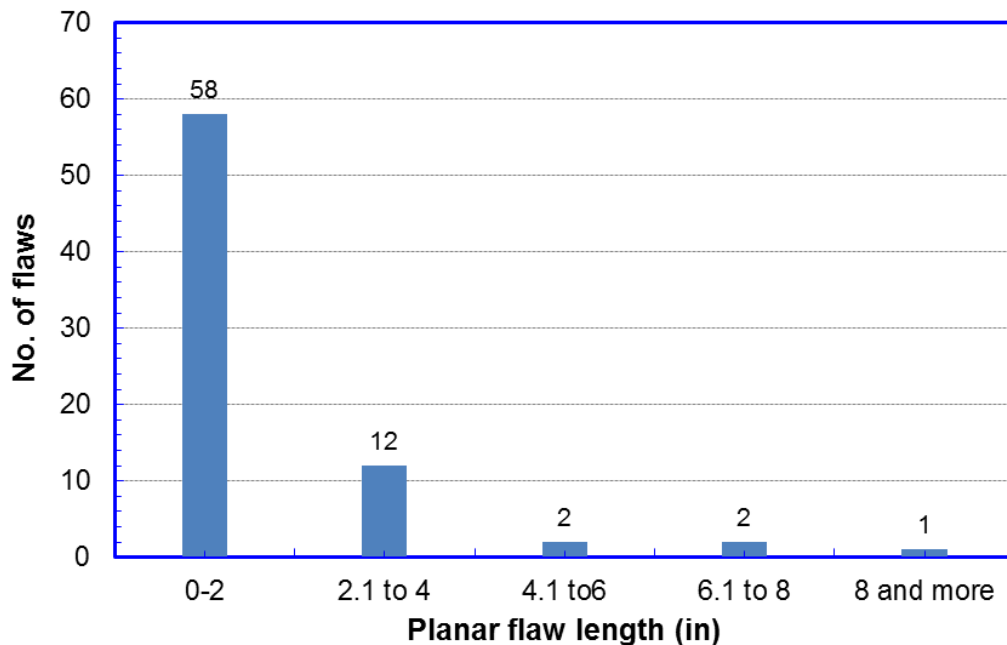


Figure 5-55 Distribution of reported planar flaw length by NDT

Looking at each weld individually:

- The maximum flaw height ranges from 0.048 in to 0.083 in.
- The maximum flaw length ranges from 0.8 in to 9.3 in.
- The maximum flawed area ranges from 0.038 in² to 0.326 in².

Most of planar flaws detected have a recorded height less than 0.08 in (2 mm) and recorded length less than 4 in.

5.6.3.2 Volumetric Flaws Detected by NDT

Figure 5-56 to Figure 5-60 provide the characteristics of the volumetric flaws detected by NDT.

Looking at each weld individually:

- The maximum flaw height ranges from 0.05 in to 0.145 in.
- The maximum flaw length ranges from 0.5 in to 7.3 in.
- The maximum flawed area ranges from 0.03 in² to 0.409 in².

Most of volumetric flaws detected have a recorded height less than 0.08 in (2 mm) and recorded length less than 6 in.

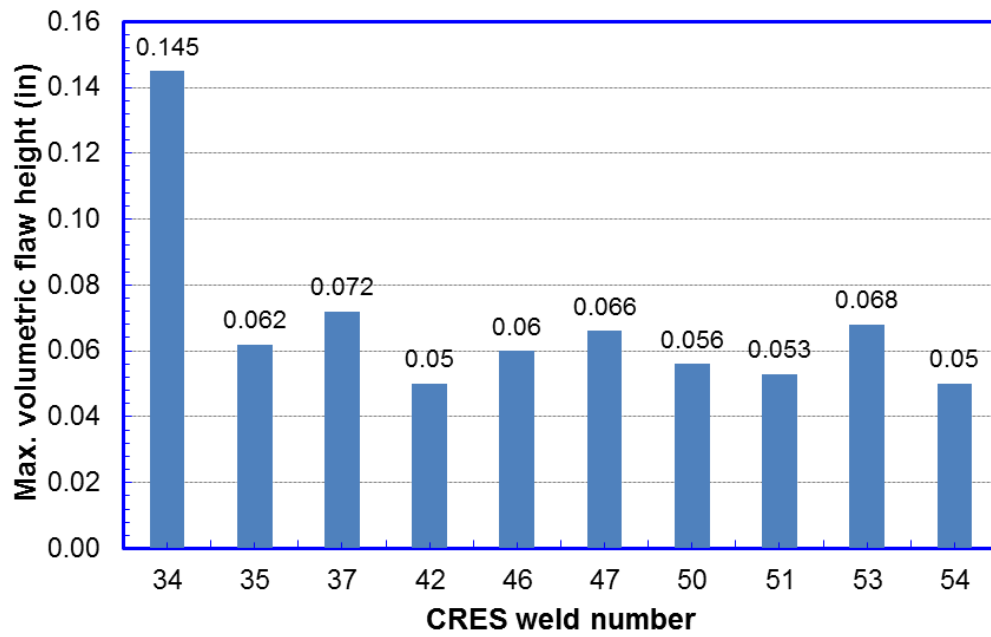


Figure 5-56 Maximum reported volumetric flaw height in each weld

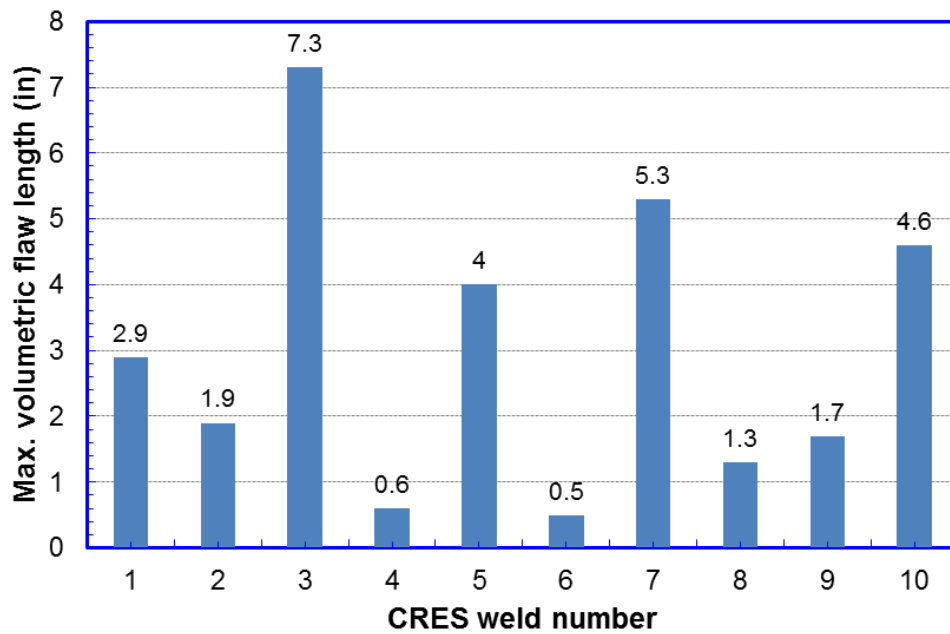


Figure 5-57 Maximum reported volumetric flaw length in each weld

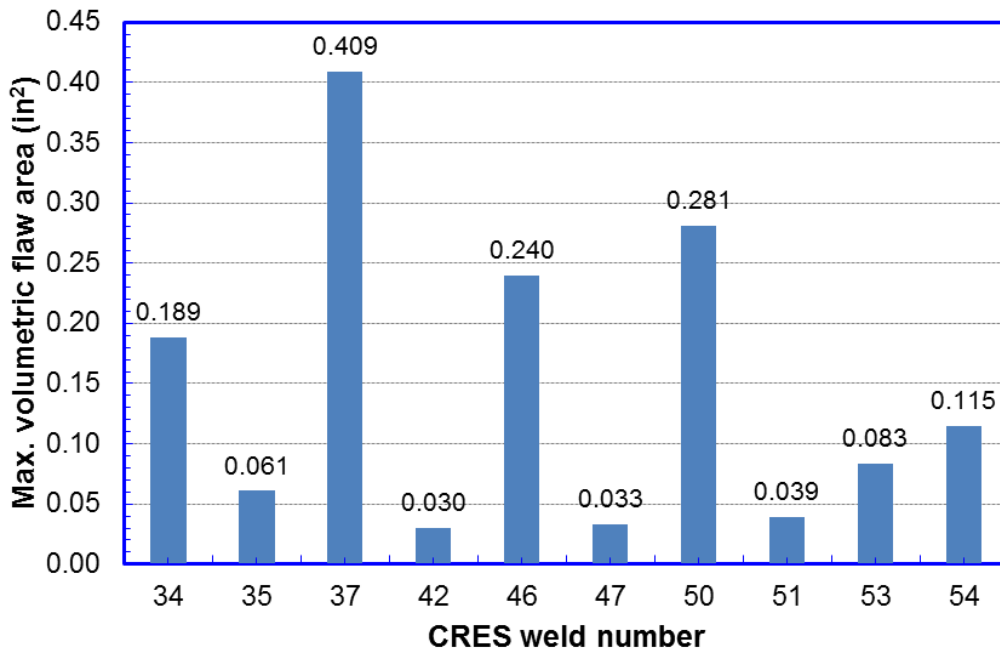


Figure 5-58 Maximum computed area of volumetric flaws in each weld

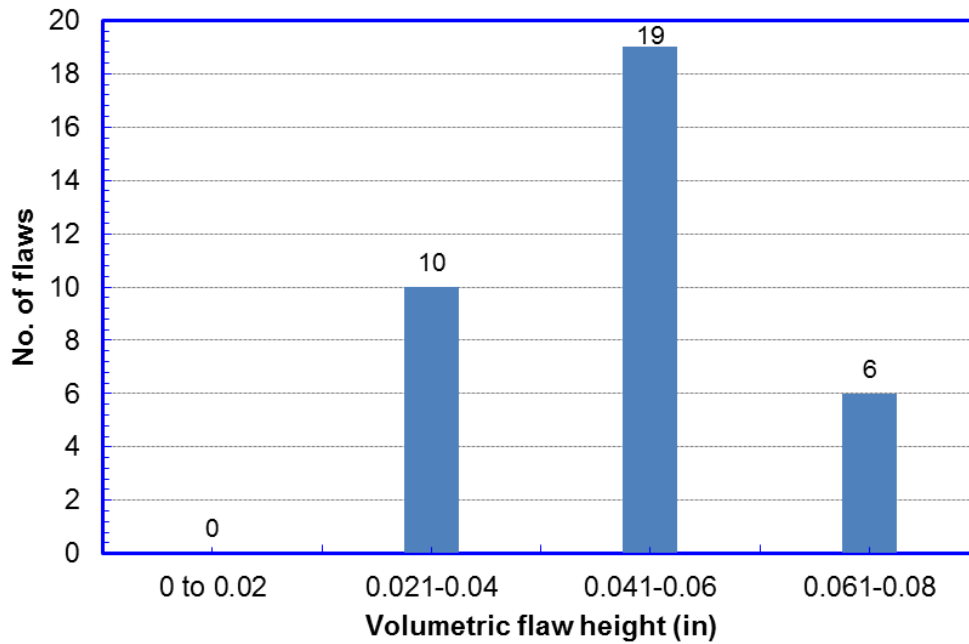


Figure 5-59 Distribution of reported volumetric flaw height by NDT

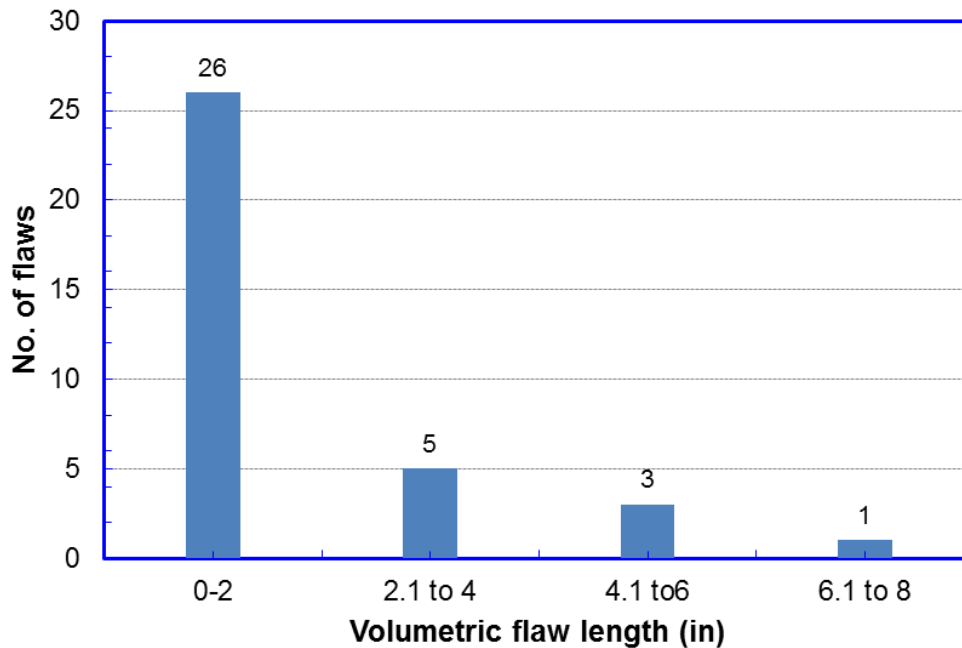


Figure 5-60 Distribution of reported volumetric flaw length by NDT

5.6.4 Matrix of Mechanical Tests

The mechanical test program includes

- Base pipe tensile,
- All weld metal tensile,
- Macrohardness traverse,
- Charpy transition curves in impact energy,
- Cross-weld tensile with natural flaws, and
- Cross-weld tensile test with artificially introduced planar flaws.

5.6.5 Base Pipe Tensile Properties

In order to determine the tensile properties of the base metal in the longitudinal (along the length of the pipe) direction and hoop (circumferential) direction, 14 longitudinal direction round bars, 13 hoop direction round bars specimens were extracted from base metal pipe. The specimens were selected from weld areas close to the locations from which cross-weld tensile (CWT) specimens were extracted. This allows the tensile properties determined from the round bar tensile specimens to be close to the tensile properties of the CWTs tested. Weld regions close to seam welds were avoided. Also, for selection of all-weld round bar specimens, weld locations with flaws (found using NDT) were avoided.

Figure 5-61 shows the dimensions of the base metal longitudinal round bar specimen. The diameter of the reduced section of the specimen is 0.118 in (3 mm). The dimensions of the specimen were chosen so as to maximize the diameter of the reduced section, at the same time

ensuring that the grip section's diameter and length would be large enough to enable holding the specimen in a stable manner during the test.

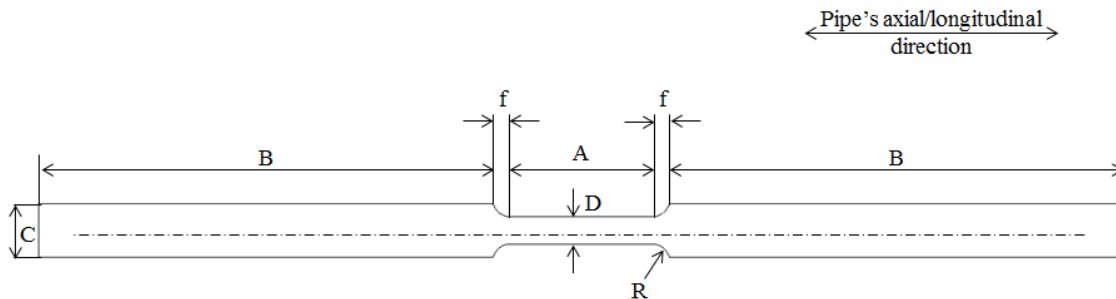
Figure 5-62 shows the dimensions of the base metal hoop round bar specimen. Note that the all weld metal round bar specimens have the same dimensions as the base metal hoop direction specimens. The diameter of the reduced section of these specimens is 0.118 in (3 mm). The length of the grip sections (dimension 'B' in Figure 5-62) is short because of the curvature of the pipe. Hence, to ensure a stable grip during the tests, these round bar specimens were threaded and threaded grip adaptors were used to hold the specimens in positions during the tests.

Figure 5-63 shows the ultimate tensile strength (UTS) and 0.2% yield strength (0.2% YS) of the base metal longitudinal round bar specimens. Figure 5-64 shows the UTS and 0.2% YS of base metal round bar hoop direction specimens.

The yield strength in the hoop direction is around 52 ksi or slight higher, meeting the minimum strength requirements of X52. The yield strength in the longitudinal direction is slightly lower by a few ksi.

Figure 5-66 compares the UTS of the base metal round bar in longitudinal direction and base metal round bar in hoop direction. This comparison is a measurement of anisotropy in the base metal. In most cases, the UTS in both directions are close. However, for pipe no. 37, 42, and 53, the UTS in longitudinal direction is higher than the UTS in hoop direction by as much as 10 ksi. The averaged UTS in both direction is around 80 ksi. The averaged Y/T ratio in the longitudinal direction is around 0.62.

Base Metal Round Bar Tensile - Longitudinal Direction



Pipe WT (nominal) = 0.281"

D = Diameter of reduced section = 3 ± 0.25 mm = 0.118 ± 0.010 "

A = Length of reduced section = 15.7 ± 0.1 mm = 0.618 ± 0.004 "

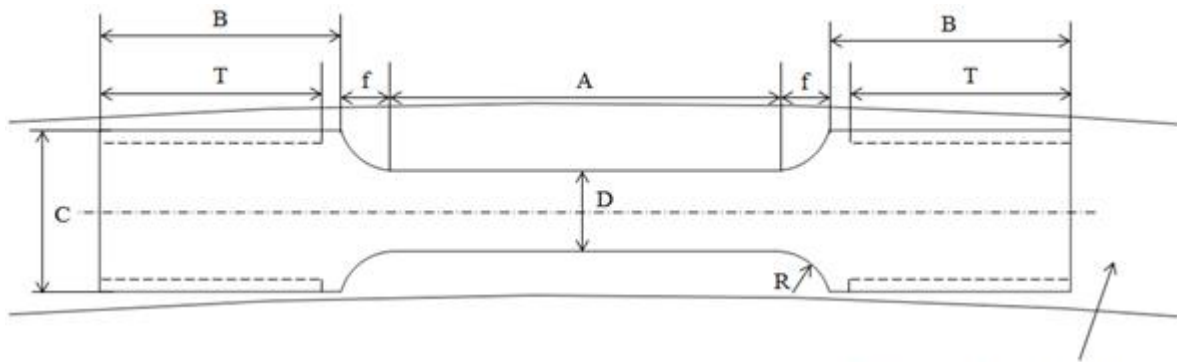
B = Grip section length = 50.8 mm = 2"

C = Diameter of grip section = 6 ± 0.25 mm = 0.236 ± 0.010 "

f = length of filleted section = 2 mm = 0.787"

R = Radius of fillet = 2 mm = 0.787"

Figure 5-61 Dimensions of the base metal longitudinal round bar tensile specimen



- D = Diameter of reduced section = $3 \pm 0.25 \text{ mm} = 0.118 \pm 0.010''$
- A = Length of reduced section = $14.2 \pm 0.1 \text{ mm} = 0.559 \pm 0.004''$
- B = Grip section length = $9 \pm 0.25 \text{ mm} = 0.354 \pm 0.010''$
- C = Diameter of grip section = $6 \pm 0.25 \text{ mm} = 0.236 \pm 0.010''$
- f = length of filleted section = $2 \text{ mm} = 0.787''$
- R = Radius of fillet = $2 \text{ mm} = 0.787''$
- T = Threaded length = $7.5 \text{ mm} = 0.3''$
- Threading (metric) \rightarrow M 6 x 1 mm

Figure 5-62 Dimensions of the base metal and all weld metal hoop direction round bar tensile specimen

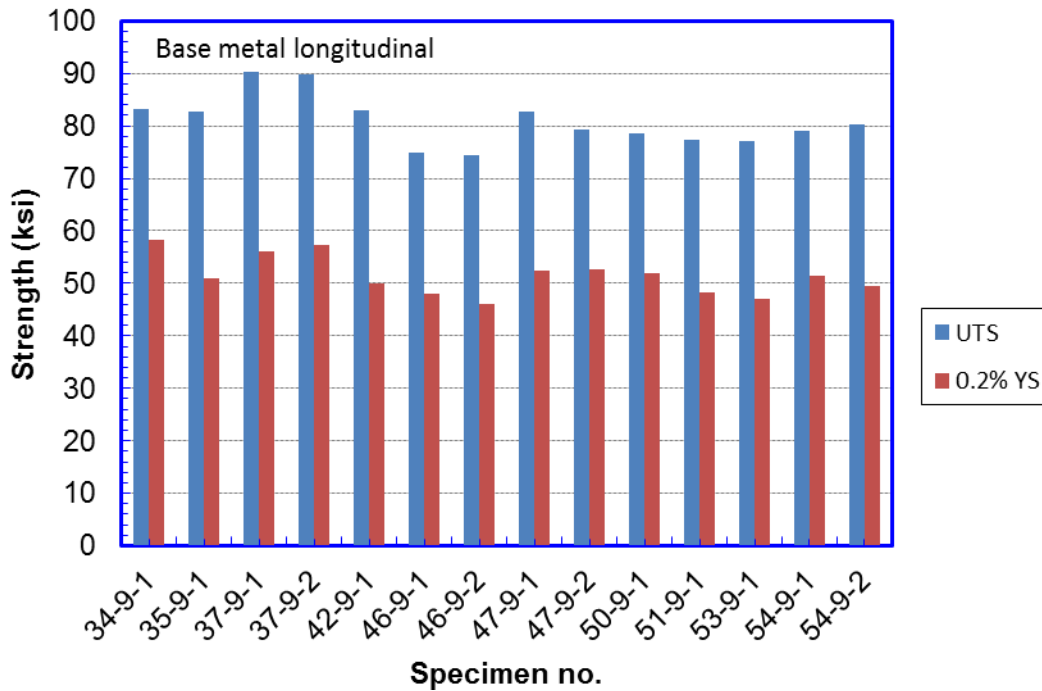


Figure 5-63 Mechanical properties of base metal round bar longitudinal direction specimens

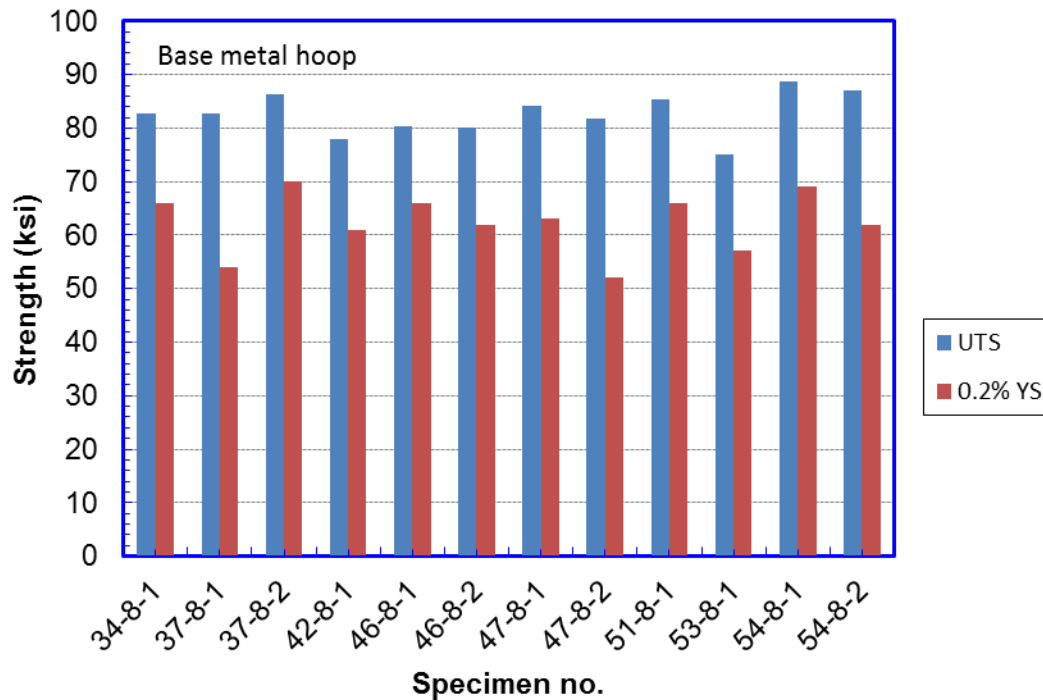


Figure 5-64 Mechanical properties of base metal round bar hoop direction specimens

5.6.6 Girth Weld Tensile Properties

In order to determine the tensile properties of weld metal in hoop (circumferential) direction, 14 hoop direction round bar specimens were extracted. Similar to the base metal specimens, the weld metal specimens were selected from weld areas close to the locations from which cross-weld tensile (CWT) specimens were extracted. Weld regions close to seam welds were avoided. Also, for selection of all weld round bar specimens, weld locations with flaws (found using NDT) were avoided.

As mentioned in sub-section 5.6.5 and shown in Figure 5-62, the dimensions of the all weld metal round bar specimens are same as those of the base metal hoop direction round bar specimens.

Figure 5-65 shows the ultimate tensile strength (UTS) and 0.2% yield strength (0.2% YS) of the weld metal round bar hoop direction specimens. The average yield strength is around 60 ksi and the averaged UTS is around 75 ksi, giving an averaged Y/T ratio of 0.80.

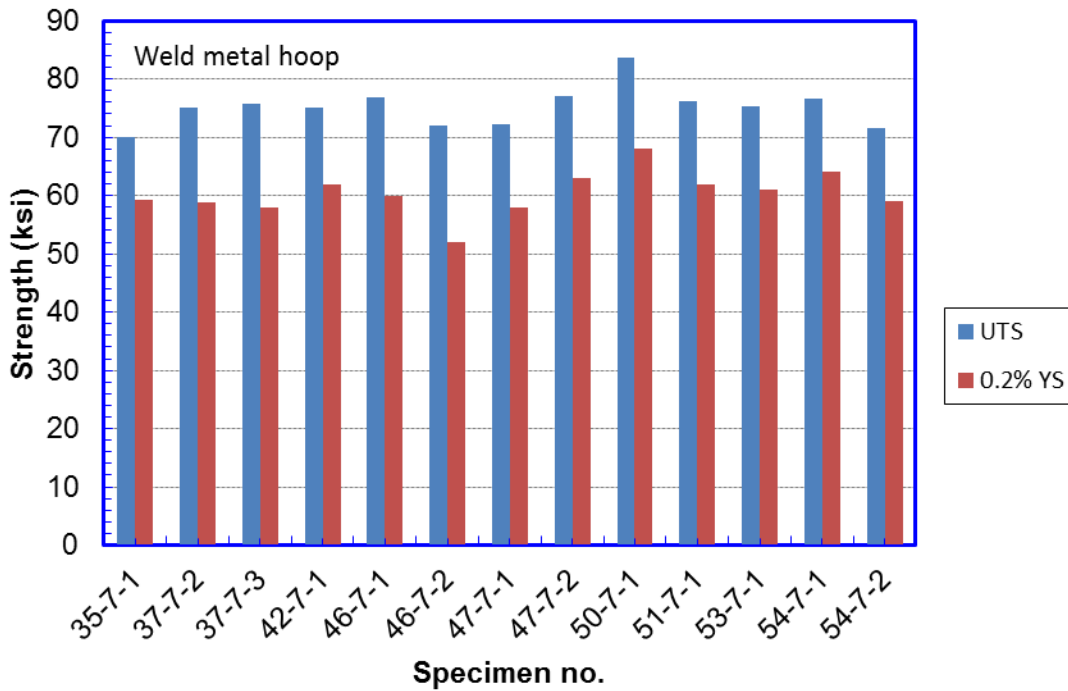


Figure 5-65 Mechanical properties of weld metal round bar hoop direction specimens

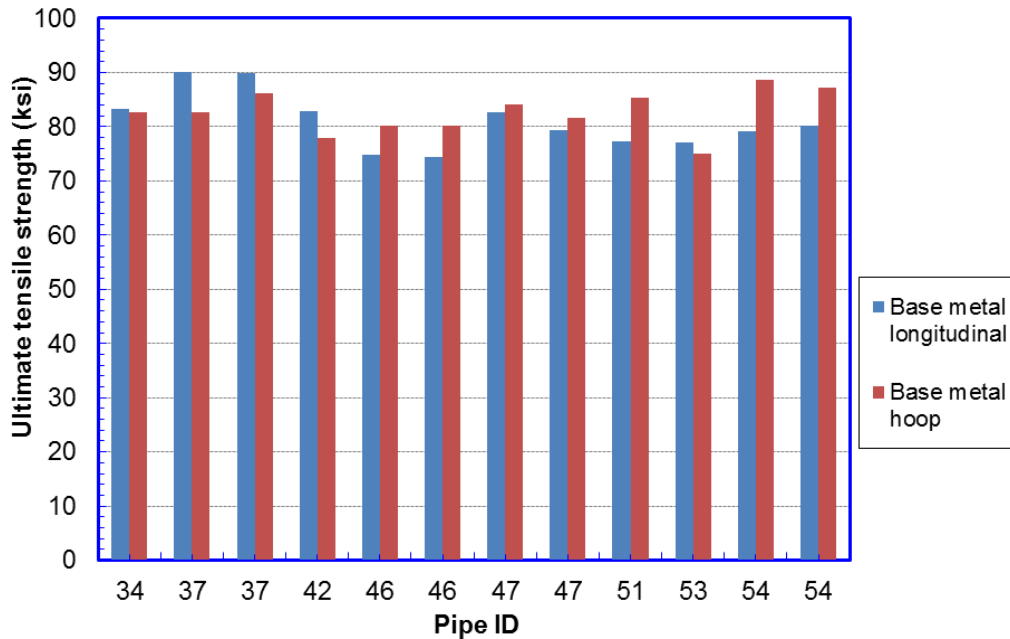


Figure 5-66 Comparison of UTS of base metal round bar longitudinal direction and base metal round bar hoop direction

5.6.7 Comparison of Base Metal and Girth Weld Strength

Figure 5-67 compares the UTS of base metal round bar in longitudinal direction and weld metal round bar in hoop direction. Except pipe no. 46 and 51, the UTS of the weld metal is lower than that of the base pipe materials. Figure 5-68 compares the 0.2% yield strength of base

metal round bar in longitudinal direction and weld metal round bar in hoop direction. For all the specimens, the 0.2% yield strength of weld metal is higher than base metal.

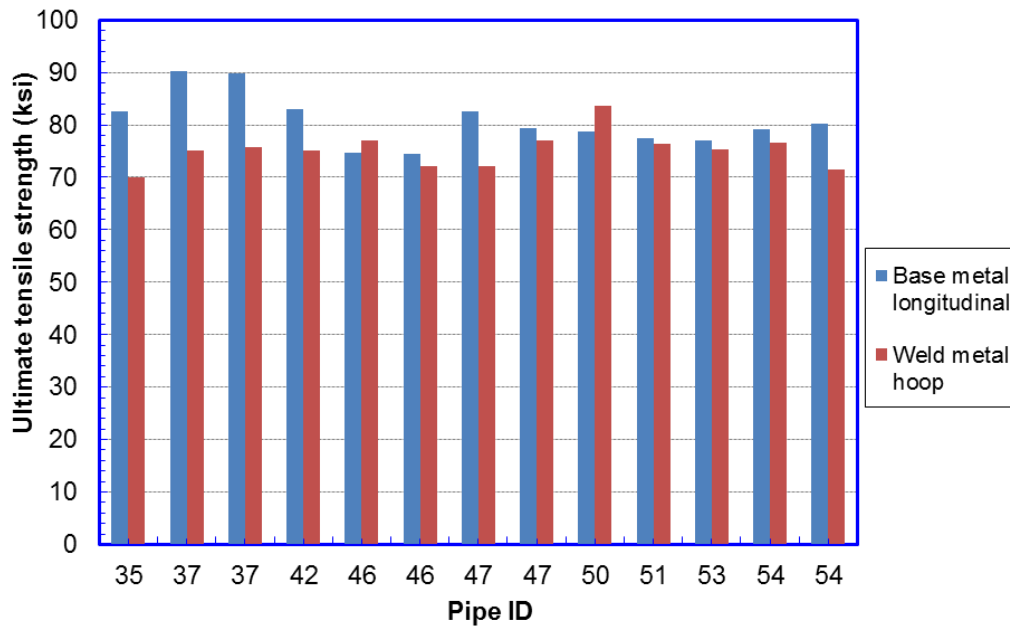


Figure 5-67 Comparison of UTS of base metal round bar longitudinal direction and weld metal round bar hoop direction

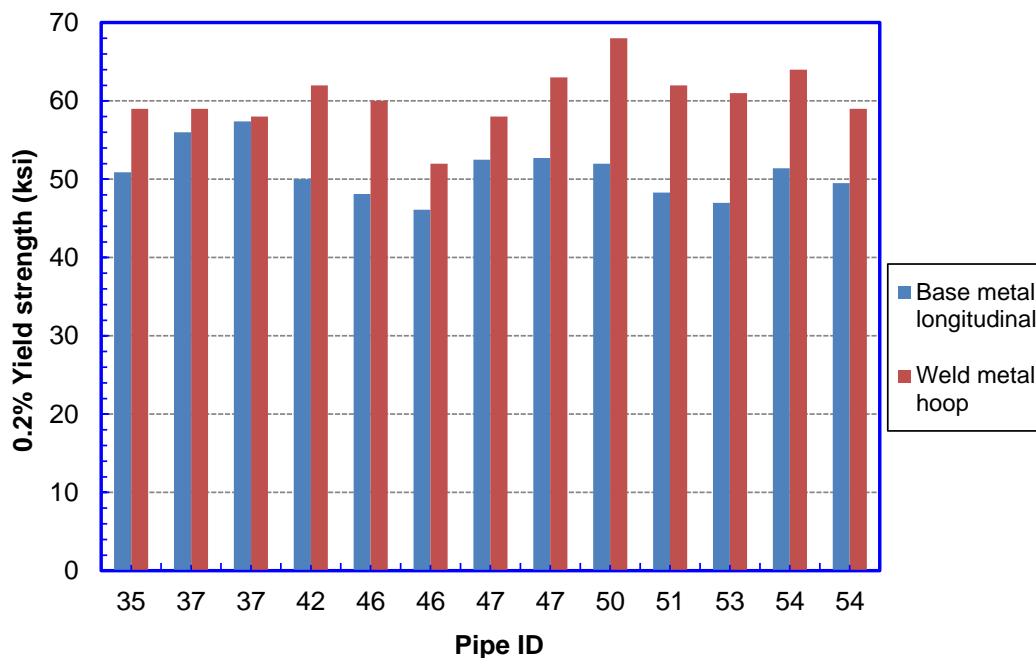


Figure 5-68 Comparison of 0.2% yield strength of base metal round bar longitudinal direction and weld metal round bar hoop direction

5.6.8 Macrohardness Traverse

A total of 12 macrohardness specimens were chosen from 10 welds so that the flaw locations detected by NDT were avoided. Figure 5-69 shows the dimensions of the specimen used for macrohardness traverse and Figure 5-70 shows the locations of 28 hardness indentations (10 kg Vickers).

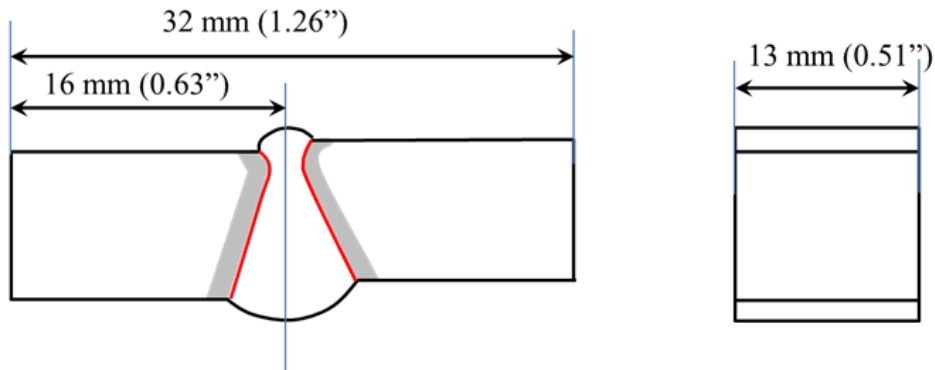


Figure 5-69 Dimensions of the macro specimens

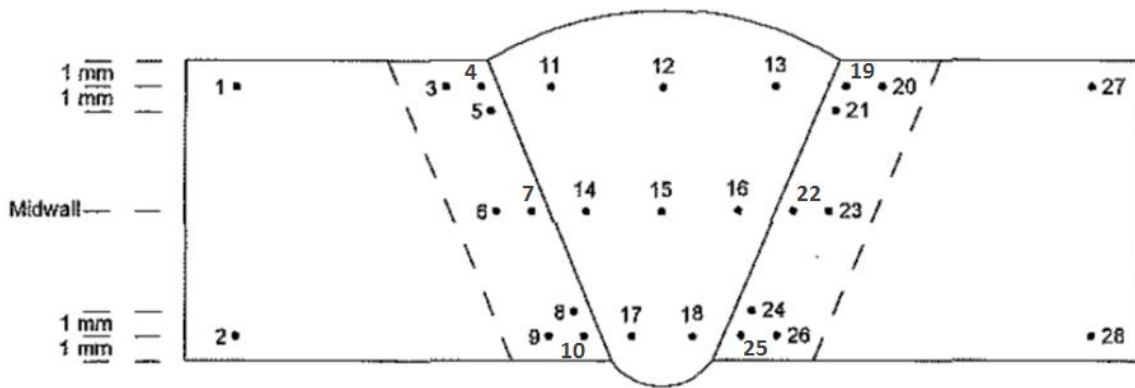


Figure 5-70 Locations of hardness indentations

The macrohardness results are shown in Table 5-4. The macrohardness data shows that all test welds had an average WM/BM hardness ratio slightly less than unity; this indicates that the UTS of the weld metal is lower than that of the base pipe material. The hardness of the weld metal is in the range of ~ 83% to 91% of the hardness of base pipe materials. This trend is consistent with the directly measured UTS as shown in Figure 5-67. With the exception of two welds, the hardness of the HAZ is the same as that of the base pipe material. For the other two welds, the hardness of the HAZ is ~ 91% of the base pipe material's hardness.

Table 5-4 Summary of macrohardness traverse of 12 samples of Group B

CRES Weld #	Macro Sample ID #	Average Vickers Hardness Number			Hardness Mismatch Ratio	
		BM	WM	HAZ	WM/BM	HAZ/BM
34	34-6-1	180	169	178	0.91	1.00
35	35-6-1	176	163	184	0.91	1.00
37	37-6-1	185	166	184	0.91	1.00
42	42-6-1	180	168	176	0.91	1.00
46	46-6-1	183	168	175	0.91	1.00
46	46-6-2	180	154	172	0.83	1.00
47	47-6-1	182	160	182	0.91	1.00
47	47-6-2	181	158	186	0.83	1.00
50	50-6-1	179	163	170	0.91	0.91
51	51-6-1	181	160	176	0.91	1.00
53	53-6-1	179	159	168	0.91	0.91
54	54-6-2	191	176	187	0.91	1.00

5.6.9 Charpy Impact Energy

The specimens were selected from weld areas with no NDT detected flaws as well as no seam welds nearby. A total of 108 Charpy V-notch (CVN) specimens were machined; 18 Charpy specimens each were machined out of 6 test welds (these 6 welds were randomly chosen out of the 10 test welds which were subjected to NDT).

The Charpy specimens were sub-sized with a 5-mm width because the pipe WT (7.14 mm/ 0.281 in) is less than the standard 10 mm Charpy specimen width. Figure 5-71 shows the dimensions of the CVN specimens along with their locations in the weld region. Half of the 108 CVN specimens had the notch in HAZ and the rest had a weld center line (WCL) located notch.

Since the specimens were sub-sized, the Charpy impact energies reported were converted to full-size equivalent values, by scaling the reported energies by the ratio of the cross-sectional area of the sub-sized specimens to that of the standard specimens.

Figure 5-72 and Figure 5-73 show the transitions curves obtained using Charpy HAZ notched specimens and Charpy WCL notched specimens, respectively. Figure 5-74 and Figure 5-75 show the curves plotted after adjusting the impact energies and temperatures to reflect full scale values. The full scale Charpy upper shelf energy of the HAZ notched specimens and the WCL notched specimens is ~36 ft·lb and ~44 ft·lb respectively. The full scale Charpy transition temperatures of the HAZ notched and the WCL notched specimens are ~31.5 °F and ~4.5 °F respectively. Table 5-5 and Table 5-6 summarize the Charpy test data for the HAZ notched and WCL notched specimens, respectively.

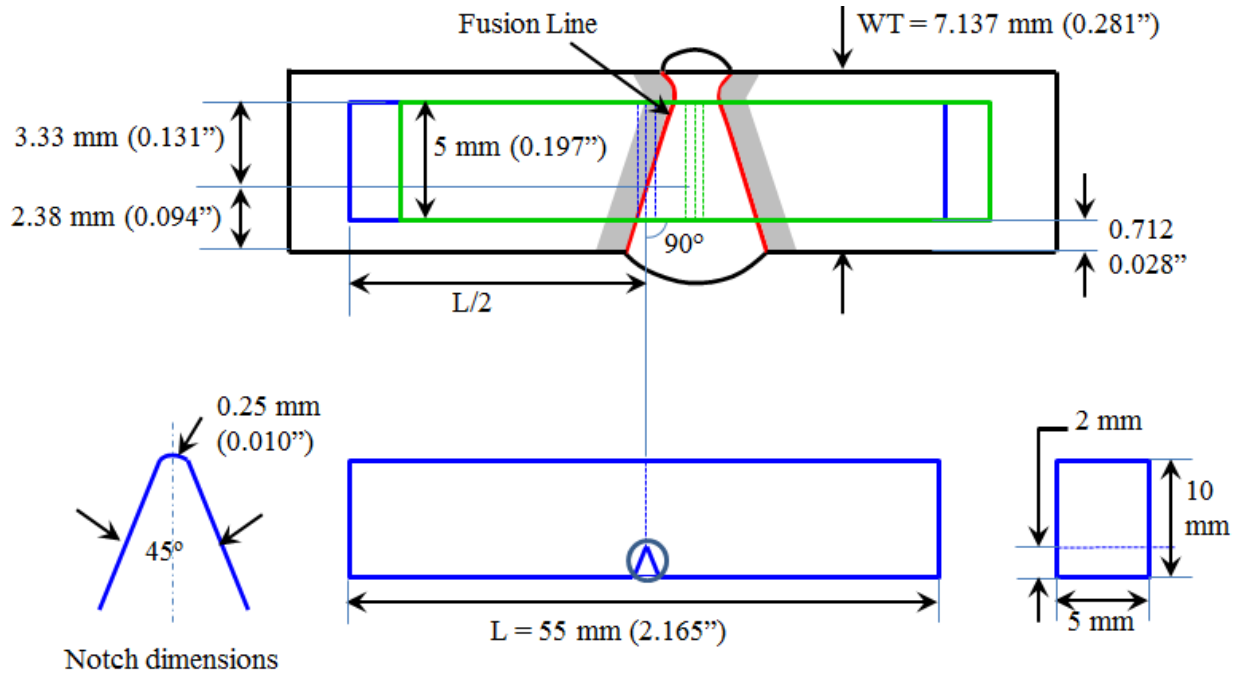


Figure 5-71 Dimensions of Charpy specimens; the locations of the HAZ notch CVN and WCL notch CVN specimens are shown in blue and green respectively (not to scale).

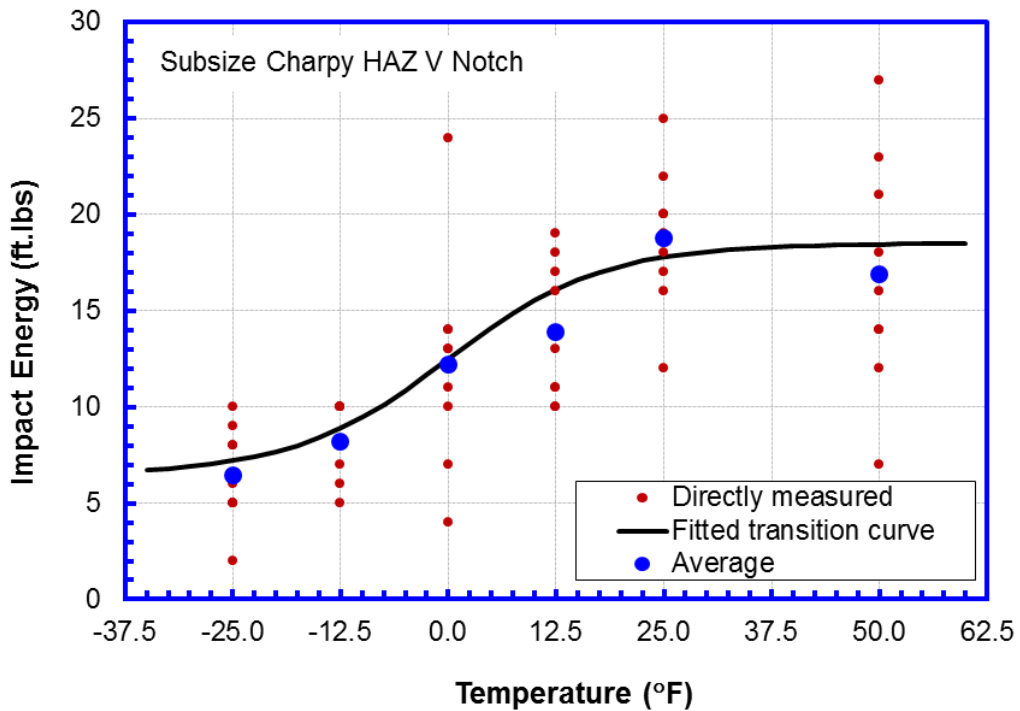


Figure 5-72 Transition curve of Charpy HAZ notch specimens of Group B

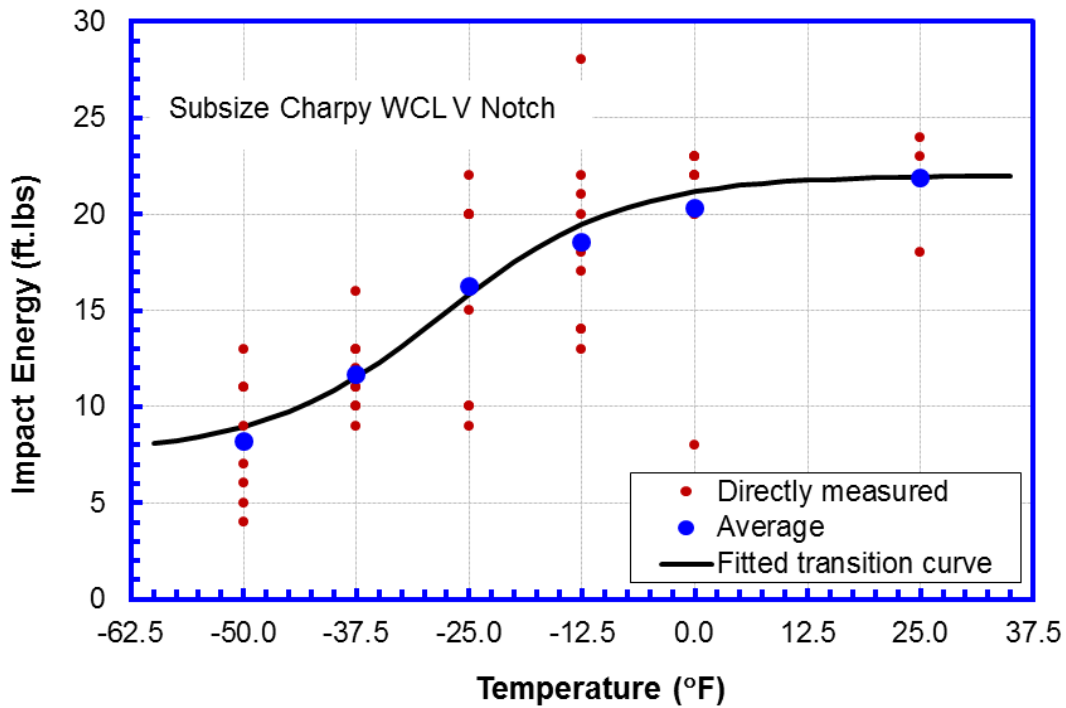


Figure 5-73 Transition curve of Charpy WCL notch specimens of Group B

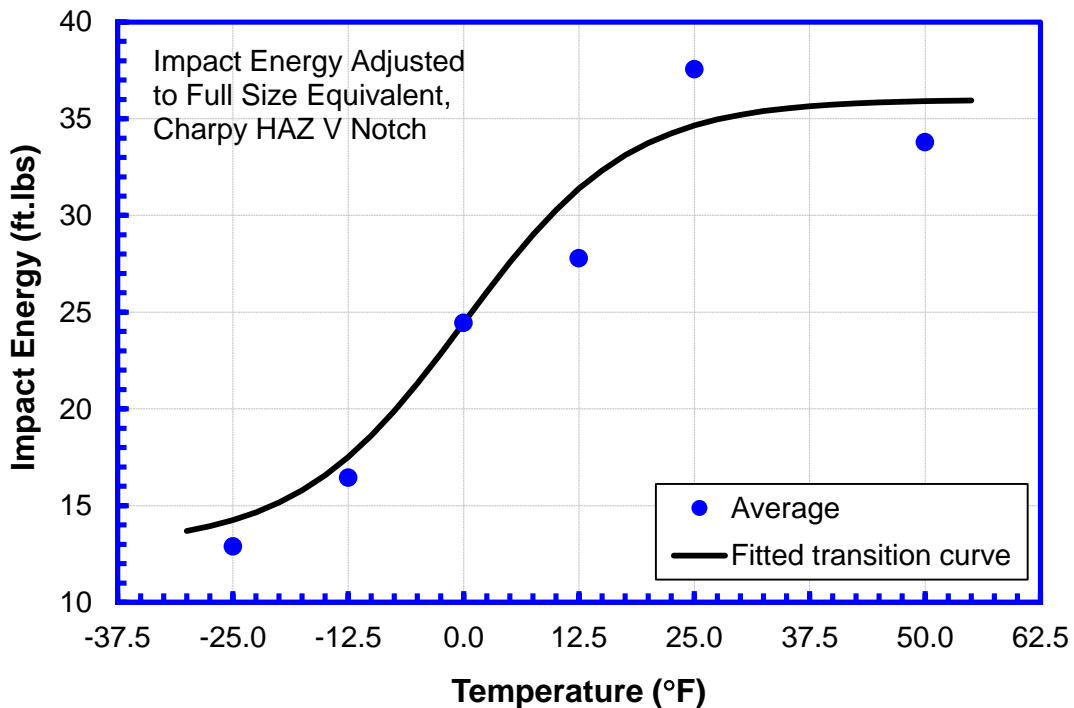


Figure 5-74 Adjusted transition curve of Charpy HAZ notch specimens of Group B

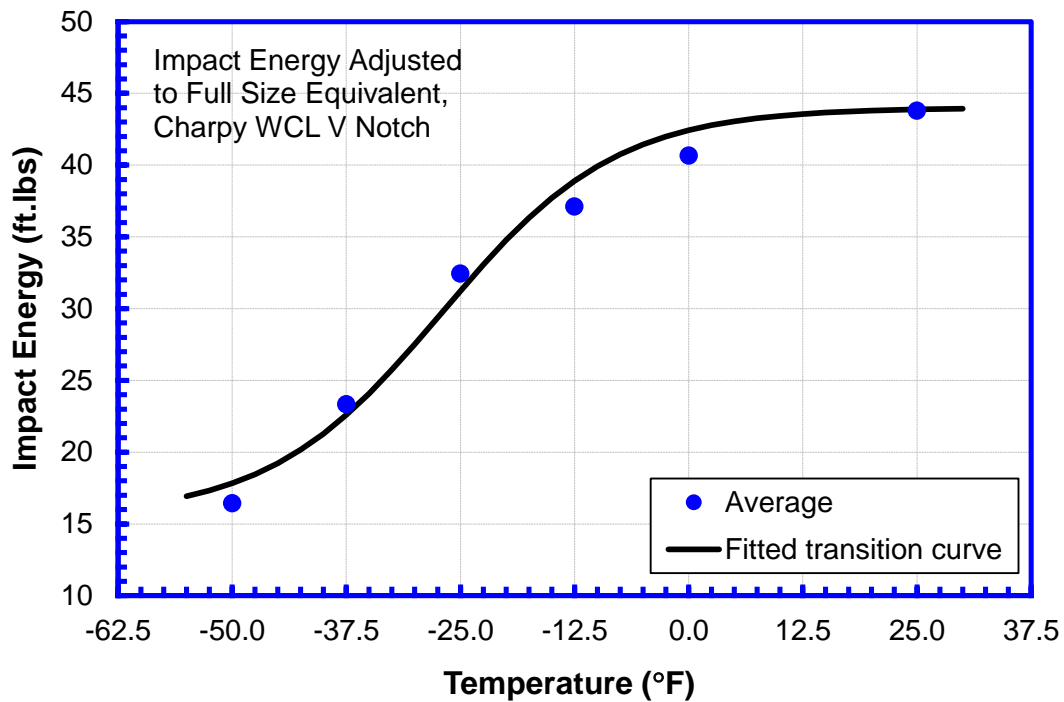


Figure 5-75 Adjusted transition curve of Charpy WCL notch specimens of Group B

Table 5-5 Average Charpy energy for HAZ notch specimens of Group B

Temperature (°F)	Charpy Impact Energy-HAZ (ft·lb)	
	Measured	Full-Size Equivalent
-25.0	6.4	12.9
-12.5	8.2	16.4
0.0	12.2	24.4
12.5	13.9	27.8
25.0	18.8	37.6
50.0	16.9	33.8

Table 5-6 Average Charpy energy for WCL notch specimens of Group B

Temperature (°F)	Charpy Impact Energy WCL (ft·lb)	
	Measured	Full-Size Equivalent
-50.0	8.2	16.4
-37.5	11.7	23.3
-25.0	16.2	32.4
-12.5	18.6	37.1
0.0	20.3	40.7
25.0	21.9	43.8

5.6.10 Cross-Weld Tensile Tests

Two types of cross-weld tensile (CWT) specimens, with natural flaws and artificial flaws, were tested to measure the tensile strength in presence of flaws in weld. The specimens were extracted along the circumference of all the ten pipes based on locations and dimensions of flaws measured by NDT. The natural flaw specimens were chosen so as to include the flaws in the specimen. Artificial flaw specimens were chosen from the areas along the circumference with no flaws.

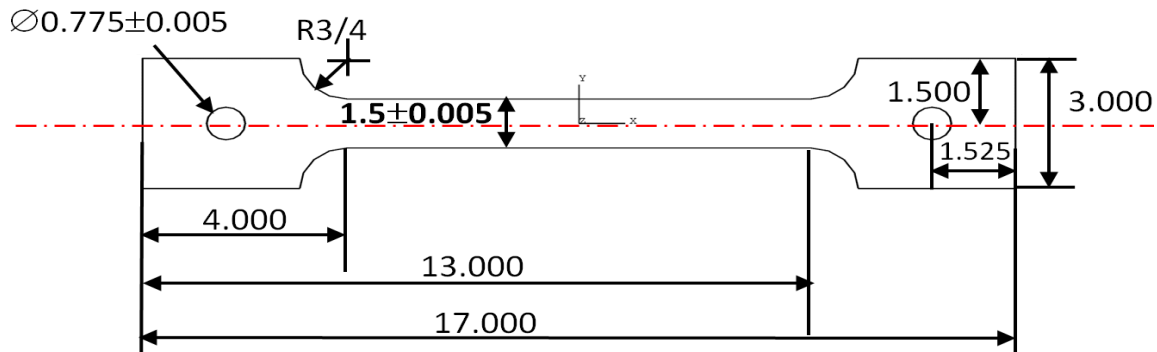


Figure 5-76 Dimensions of natural flaw cross-weld specimen

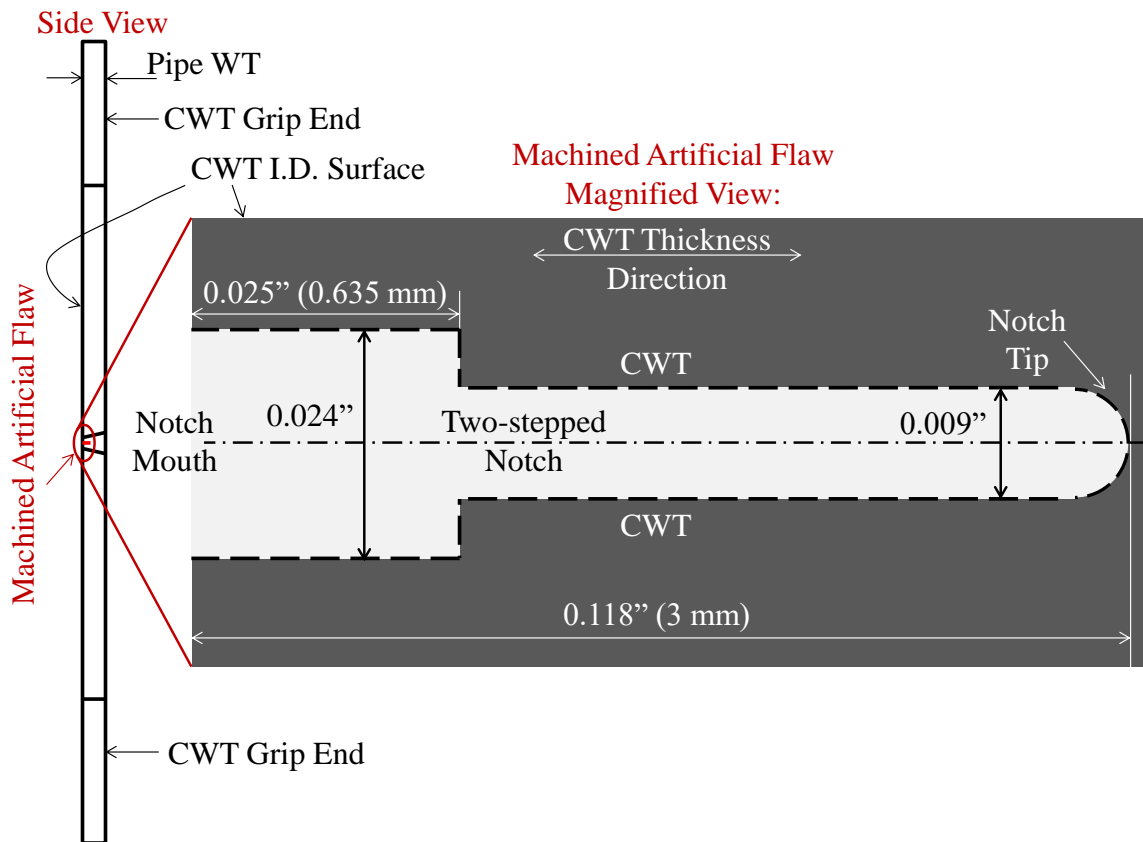


Figure 5-77 Dimensions of an artificial flaw

Figure 5-76 shows the dimensions of dog-bone shaped natural flaw and artificial flaw cross-weld tensile specimen. The dimensions of artificial flaw specimens are same as the natural flaw except the artificial notch (flaw) cut in weld metal or HAZ. Figure 5-77 shows the dimensions of artificial flaw. Figure 5-78 shows the artificial notch in weld metal and HAZ. A total of 37 natural flaw specimens and 28 artificial flaw specimens were extracted from 10 welds.

In order to measure the deformation of weld (cross-weld strain, blue bracket) and deformation of base pipe (remote strain, red bracket), a laser extensometer and clip gauges were used as shown in Figure 5-79. The test set up is shown in Figure 5-80.

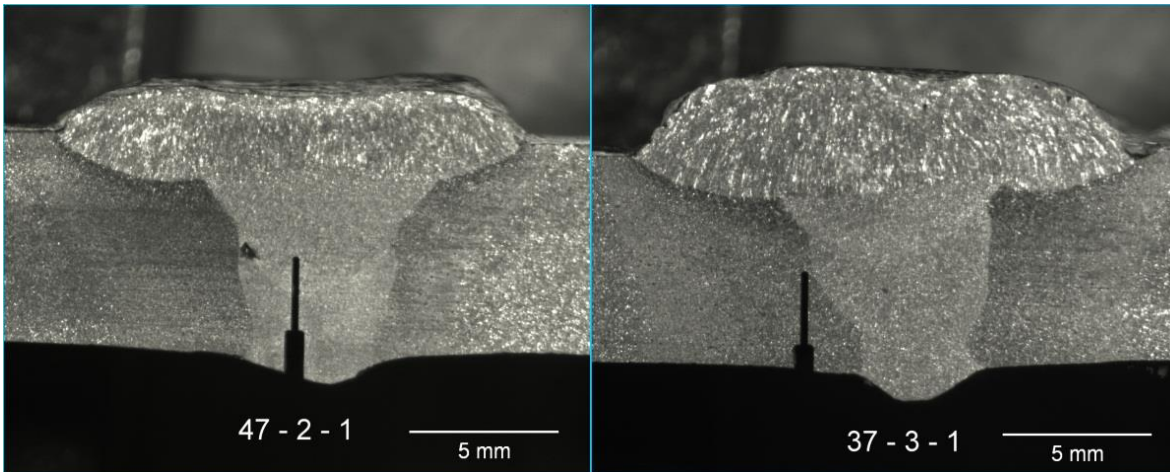


Figure 5-78 Machined flaws in Weld metal (WM) and heat-affected zone (HAZ)

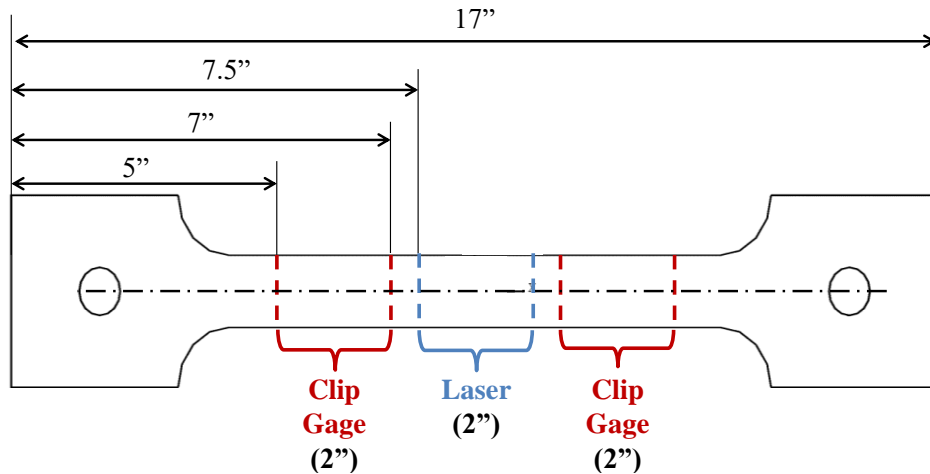


Figure 5-79 Location of clip gauges and laser extensometer

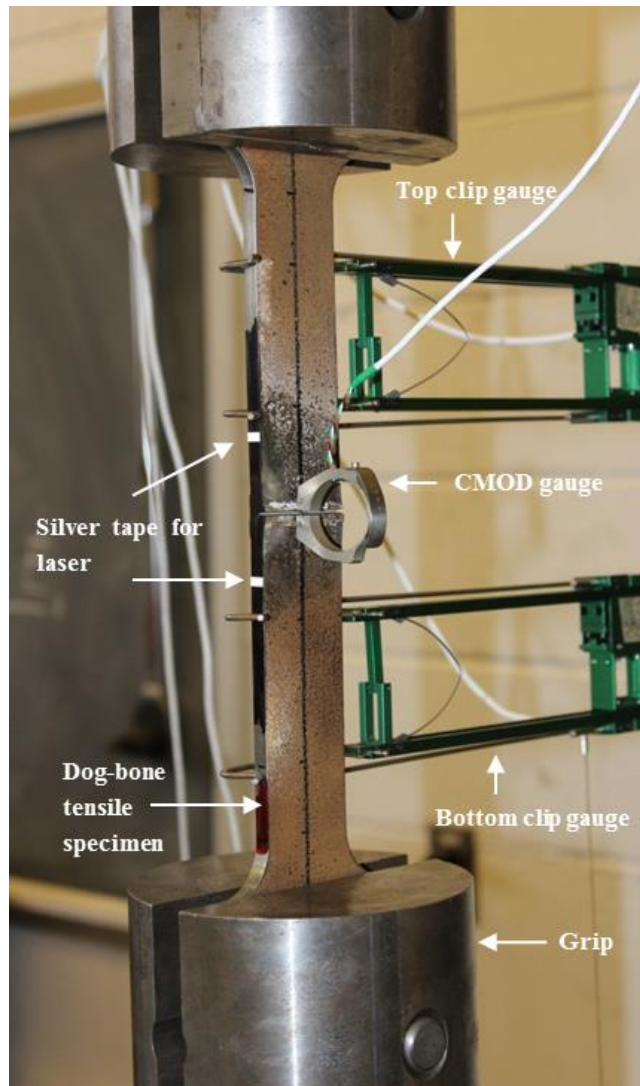


Figure 5-80 Setup for cross-weld tensile tests

5.6.10.1 Test Results of Natural Flaw CWT Specimens

Seven out of 37 natural flaw CWTs failed in weld and remaining specimens failed in base metal. Figure 5-81 shows the natural flaw CWT specimen failed in weld and Figure 5-82 shows its stress-strain curves. Table 5-7 is the summary of the tensile test results of natural flaw CWT specimens failed in weld. Figure 5-83 shows a natural flaw specimen failed in base metal and Figure 5-84 shows its stress-strain curves.

Table 5-8 is the summary of test results of CWT specimens with natural flaws that failed in the base metal. The term ‘N/A*’ in the table refers that the flaw was detected by NDT but was not visible as the specimen did not break into the plane of flaw. The specimen 47-10-1 did not contain any flaw but was tested only for the comparison purpose.



Figure 5-81 A CWT specimen with natural flaw failed in the weld region.

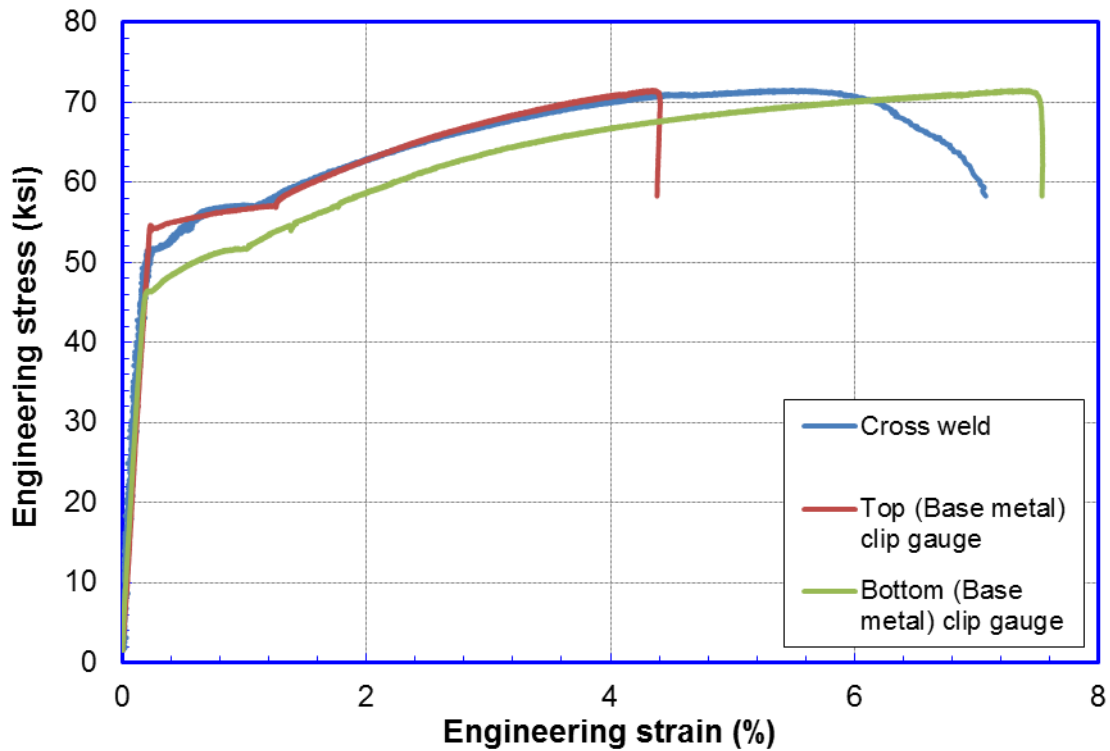


Figure 5-82 Stress-strain curves of a specimen with natural flaw failed in the weld region

Table 5-7 Summary of CWT specimens with natural flaws failed in the weld region

Specimen ID	O' clock Position	Flaw Dimension (in)		Maximum Stress		Base Metal 0.2% YS	Strain at Maximum Stress (%)		
		NDT	Physical Measurement				Base Metal (Bottom)	Base Metal (Top)	Cross-Weld
				MPa	ksi	ksi			
34-1-2	3 to 4	0.25	0.64	455	66	48	2.7	3.4	2.5
34-1-3	4 to 5	1.37	1.98	492	71	48	7.4	4.3	5.5
		2.64	2.58						
37-1-5	6 to 7	0.76	1.11	546	79	53	5.0	9.7	5.7
37-1-6	10 to 11	0.23	0.64	514	75	50	3.1	4.6	3.2
47-1-3	5 to 6	0.89	1.59	503	73	51	5.3	5.1	5.3
47-1-4	5 to 6	0.89	0.95	524	76	52	12.4	8.2	6.3
51-1-4	11 to 12	0.66	0.96	457	66	51	3.0	2.0	2.3



Figure 5-83 CWT specimen 34-1-1 with natural flaw failed in the base metal

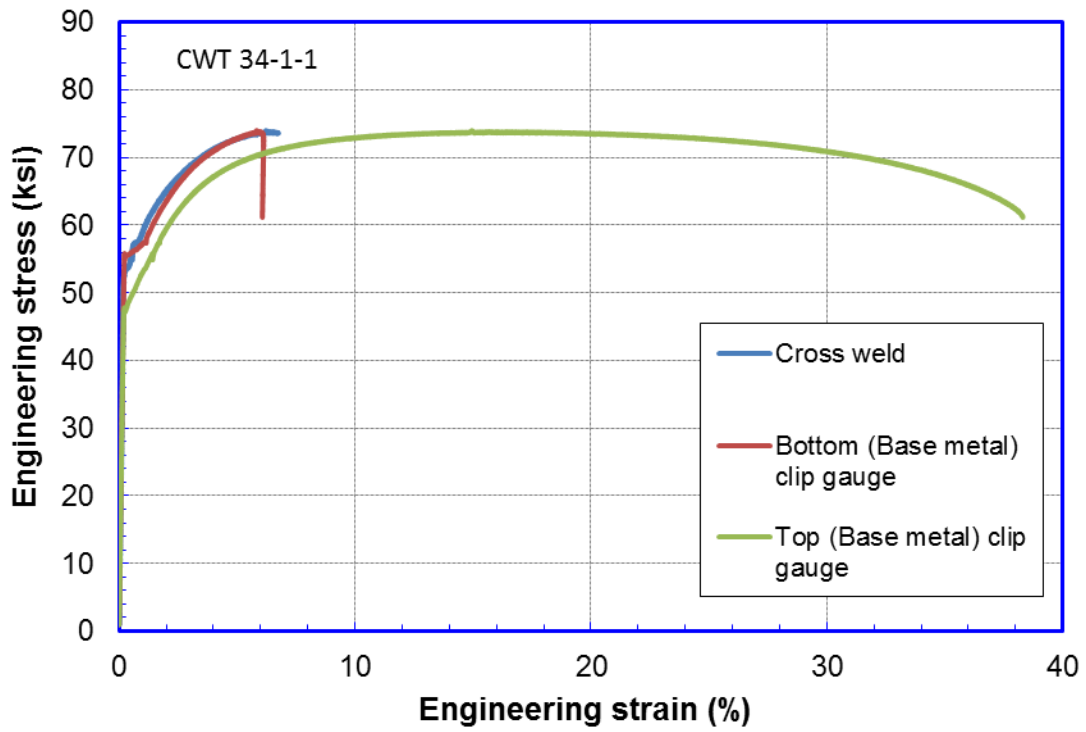


Figure 5-84 Stress-strain curves of a CWT specimen with natural flaw failed in base metal

Table 5-8 Summary of test results of specimens with natural flaws failed in the base metal

Specimen ID	Specimen O' clock Position	Flaw Dimension (in)		Maximum Stress		Base Metal 0.2% YS	Strain at Maximum Stress (%)			Failure Location
		NDT	Physical Measurement				Base Metal (Bottom)	Base Metal (Top)	Cross-Weld	
				MPa	ksi	ksi				
34-1-1	2 to 3	0.66	0.64	508	74	49	5.7	14.1	6.1	Top
34-1-4	1 to 2	1.09	0.79	503	73	49	6.1	14.2	6.3	Top
35-1-1	3 to 4	0.81	0.32	518	75	50	11.0	6.3	5.6	Bottom
35-1-3	6 to 7	0.84	0.79	503	73	49	14.4	4.3	6.5	Bottom
35-1-4	0 to 1	1.45	1.27	508	74	51	6.1	13.6	5.2	Top
		1.55	1.59							
37-1-1	2 to 3	1.07	0.64	549	80	56	6.1	12.1	6.2	Top
37-1-2	3 to 4	1.22	2.06	554	80	52	6.2	12.1	6.4	Top
37-1-4	5 to 6	0.46	0.64	544	79	52	5.2	11.8	6.3	Top
37-1-7	11 to 12	--	0.635	550	80	50	10.3	4.8	5.2	Bottom
37-1-9	0 to 1	1.04	N/A*	551	80	54	11.8	6.2	5.4	Bottom
42-1-1	1 to 2	1.30	N/A*	524	76	50	6.2	13.2	5.6	Top
42-1-2	6 to 7	0.99	1.11	519	75	71	3.0	8.6	3.4	Top
46-1-1	2 to 3	1.17	0.79	508	74	49	13.5	8.2	6.3	Bottom
46-1-2	2 to 3	1.52	0.35	501	73	49	13.3	7.4	6.3	Bottom
46-1-3	4 to 5	0.79	0.64	506	73	49	6.7	15.3	6.1	Top
46-1-4	4 to 5	0.79	0.64	511	74	50	6.2	12.5	6.2	Top
47-1-1	2 to 3	0.66	0.64	530	77	52	12.5	9.6	6.5	Bottom
47-1-2	2 to 4	0.66	0.79	527	76	50	13.6	7.7	5.8	Bottom
47-1-5	6 to 7	0.89	0.95	524	76	50	13.1	9.0	6.4	Bottom
47-10-1	3 to 5	--	--	526	76	52	12.9	8.5	6.3	Bottom
50-1-1	0 to 1	1.35	N/A*	500	72	52	11.5	5.3	6.6	Bottom
50-1-2	1 to 2	1.35	0.64	502	73	52	5.9	10.9	6.5	Top
50-1-3	1 to 2	0.66	1.11	505	73	51	10.1	5.8	6.3	Bottom
50-1-4	2 to 4	0.66	0.96	505	73	50	6.0	10.7	5.1	Top
51-1-1	2 to 3	0.56	0.48	519	75	52	10.5	3.6	4.3	Bottom
51-1-3	11 to 12	0.86	1.27	528	77	52	4.1	11.8	5.2	Top
53-1-1	1 to 2	1.24	1.25	516	75	48	12.9	5.8	6.5	Bottom
53-1-2	5 to 6	1.19	N/A*	506	73	49	10.1	6.8	6.4	Bottom
54-1-1	2 to 3	0.64	N/A*	525	76	51	5.1	12.0	5.1	Top
54-1-2	3 to 4	1.27	0.32	528	77	48	12.6	5.0	4.8	Top
54-1-3	5 to 7	1.68	0.79	539	78	52	5.7	11.1	N/A	Top

5.6.10.2 Test Results of Artificial Flaw CWT Specimens

All the 28 artificial flaw CWT specimens failed in the weld. The specimens either broke completely or partially when the test was stopped at 90% of the maximum tensile load. Figure 5-85 shows the stress-strain curves of one the artificial flaw specimen. Figure 5-86 and Figure 5-87 show the completely broken and partially broken artificial flaw CWT specimens.

Table 5-9 provides the summary of tensile testing of artificial flaw CWT specimens.

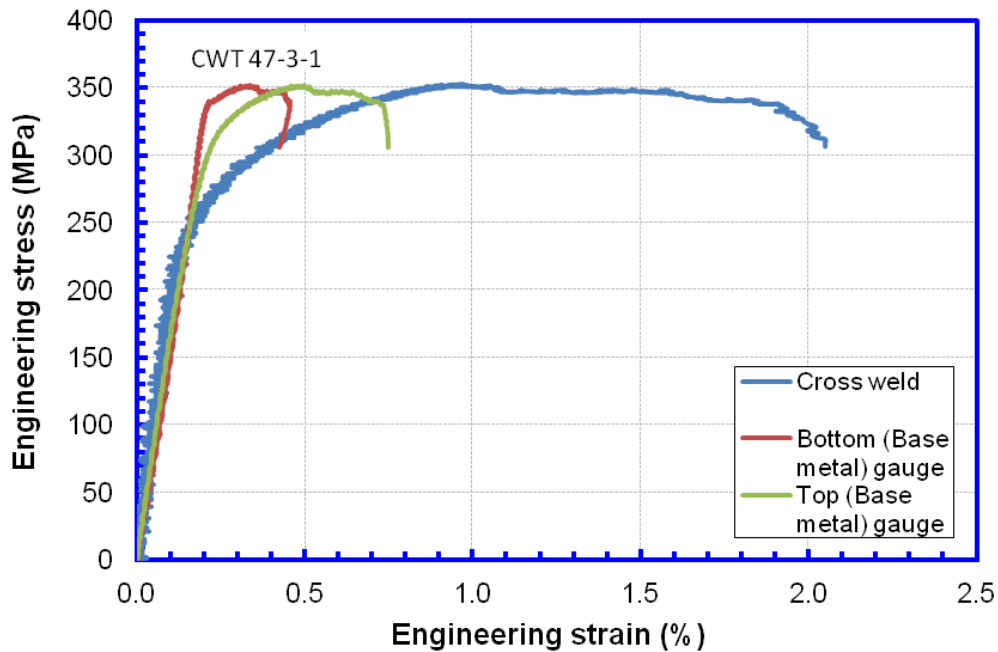


Figure 5-85 Stress-strain curves of artificial flaw CWT



Figure 5-86 Artificial flaw CWT specimen completely broken in weld

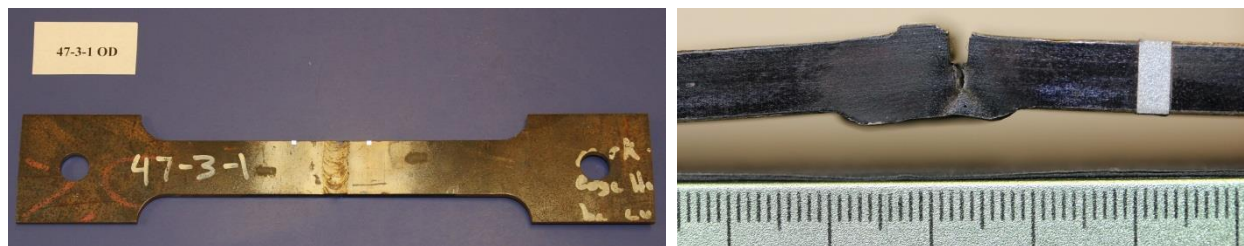


Figure 5-87 Top view and side view of artificial flaw CWT specimen partially broken in weld

Table 5-9 Summary of test results cross-weld tensile specimens with artificial flaws

Specimen ID	Notch Location	Specimen O'clock Position	Maximum Stress		Strain at Maximum Stress (%)		
			MPa	ksi	Base Metal (Bottom)	Base Metal (Top)	Cross Weld
34-2-1	Weld	7 to 8	336	49	0.4	0.3	1.2
34-3-1	HAZ	7 to 8	365	53	1.1	0.4	1.6
35-2-1	Weld	7 to 8	403	58	2.3	1.2	1.6
35-2-2	Weld	10 to 11	343	50	0.8	0.2	1.2
35-3-1	HAZ	7 to 8	342	50	0.1	1.0	0.9
35-3-2	HAZ	11 to 12	340	49	0.2	0.2	1.0
37-2-1	Weld	7 to 8	377	55	0.3	0.6	0.9
37-3-1	HAZ	7 to 8	353	51	0.2	0.6	0.8
42-2-1	Weld	3 to 4	344	50	0.2	0.5	0.9
42-3-1	HAZ	4 to 5	369	54	0.9	0.8	1.1
46-2-1	Weld	6 to 8	347	50	0.7	0.3	1.0
46-2-2	Weld	10 to 11	352	51	0.4	0.5	1.2
46-3-1	HAZ	7 to 8	352	51	0.5	0.9	1.2
46-3-2	HAZ	11 to 12	330	48	0.2	0.2	0.7
47-2-1	Weld	0 to 2	350	51	0.4	0.4	1.2
47-2-2	Weld	7 to 9	342	50	0.2	0.5	1.2
47-3-1	HAZ	1 to 2	352	51	0.3	0.5	1.0
47-3-2	HAZ	8 to 9	368	53	0.7	0.8	1.7
50-2-1	Weld	10 to 12	354	51	0.2	0.2	1.1
50-3-1	HAZ	11 to 12	386	56	0.8	1.4	2.0
51-2-1	Weld	7 to 8	371	54	0.2	0.8	1.3
51-3-1	HAZ	7 to 9	389	56	1.8	1.0	1.6
53-2-1	Weld	7 to 8	379	55	0.6	1.4	1.7
53-3-1	HAZ	7 to 8	369	54	0.2	1.1	1.6
54-2-1	Weld	7 to 8	345	50	0.2	0.2	1.0
54-2-2	Weld	9 to 10	352	51	0.2	0.5	0.6
54-3-1	HAZ	7 to 9	379	55	0.8	0.2	1.3
54-3-2	HAZ	10 to 11	360	52	0.4	0.2	0.7

5.6.10.3 Exposed Flaws after CWT Testing

Figure 5-88 to Figure 5-91 show the exposed flaws after CWT testing. Few CWTs did not break in the plane of flaws at the end of test. Those were further broke opened in liquid nitrogen to expose the flaws.

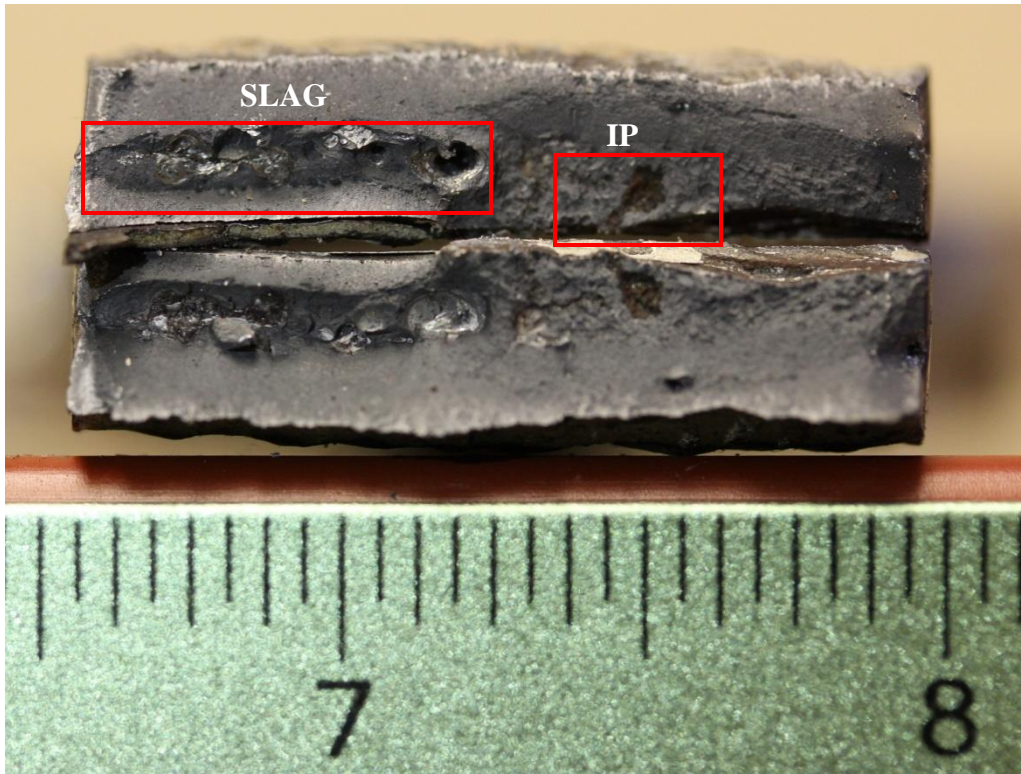


Figure 5-88 Broken CWT surface showing Slag and Inadequate penetration (IP) flaws

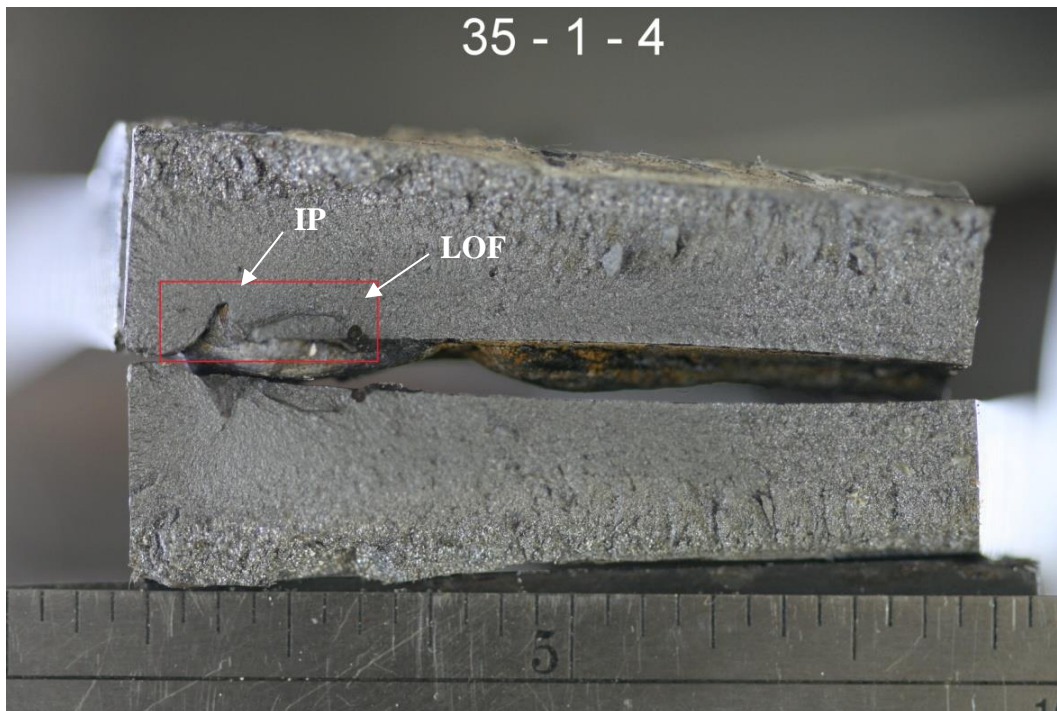


Figure 5-89 Broken CWT surface showing lack of fusion (LOF) and inadequate penetration (IP) flaws

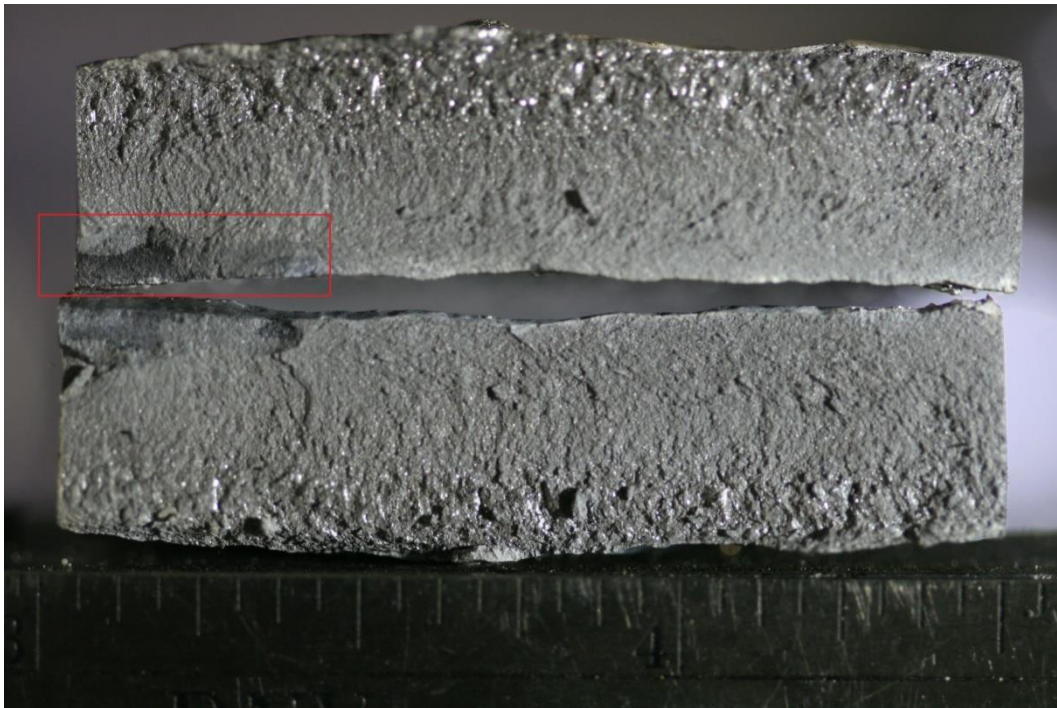


Figure 5-90 Broken CWT surface showing root crack (RC) flaw

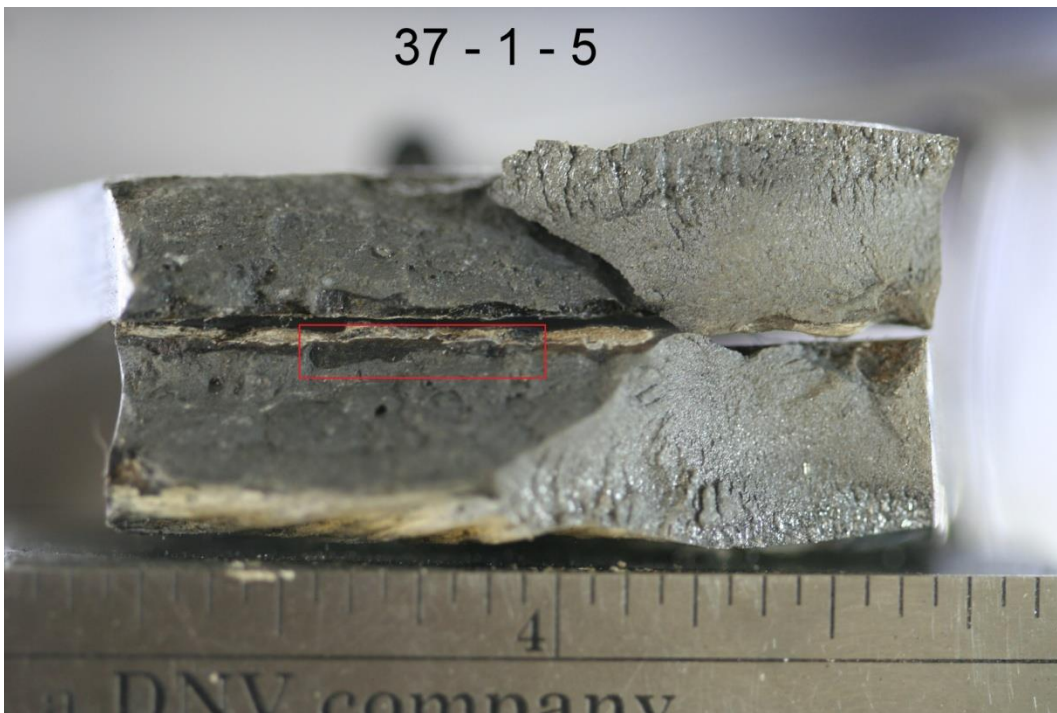


Figure 5-91 Broken CWT surface showing inadequate penetration (IP) flaw

5.6.11 Measure of Fracture Toughness with Residual CTOD

Figure 5-92 shows the load-displacement relation of an artificial flaw specimen 34-2-1 as recorded by CMOD gauge.

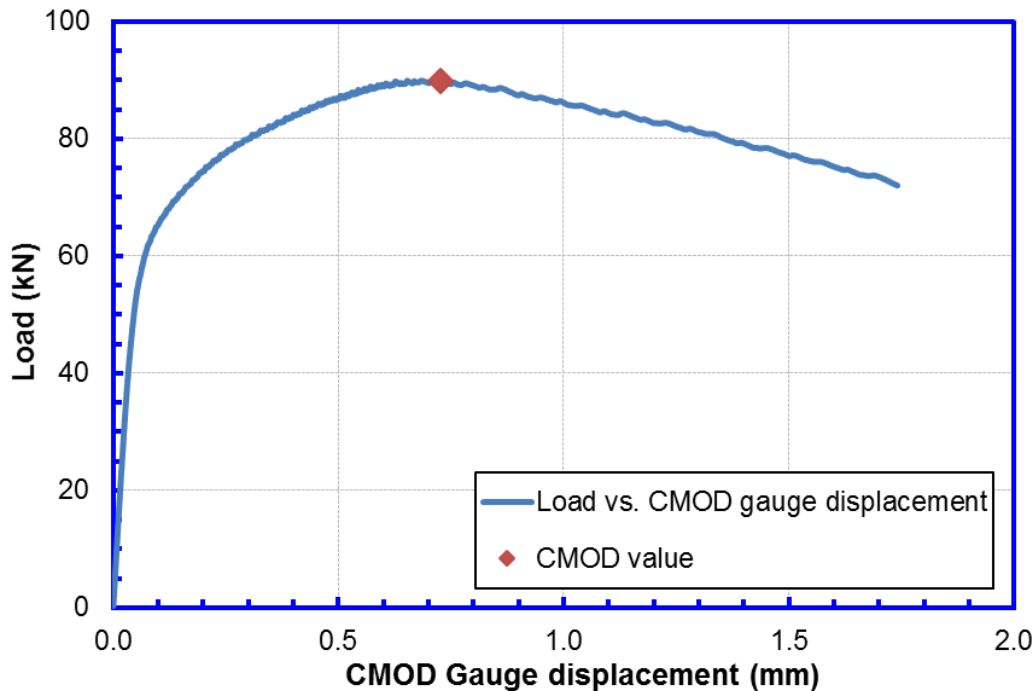


Figure 5-92 Load-CMOD relation for an artificial flaw specimen 34-2-1

The CMOD results could not be recorded for all the artificial flaw CWT specimens as either the clip gauge fell off during testing or the geometry of the sample was not suitable for the mounting of clip gauge. The I.D. protrusion in case of HAZ notch artificial flaws made it impossible to mount the CMOD gauge on the sample except specimens 35-3-2 and 54-3-2.

At the end of tensile testing, at 90% of the maximum load, 7 specimens completely broke and the remaining 21 specimens remained partially broken. Figure 5-93 shows the artificial flaw CWT specimen completely broken in weld. Figure 5-94 shows the artificial flaw CWT specimen and its side view, partially broken in weld.



Figure 5-93 Artificial flaw CWT specimen completely broken in weld



Figure 5-94 Top view and side view of artificial flaw CWT specimen partially broken in weld

The Crack tip opening displacement (CTOD) value for partially broken specimens was measured from the photograph of the notch. The method followed for the measurement of CTOD value from photograph is explained in Figure 5-95. The residual CTOD value was obtained by subtracting the initial notch width (0.2 mm) from the measured CTOD value. The ratio $\left(\frac{CTOD}{CMOD}\right)$ was obtained, for 10 specimens, for which the CMOD gauge data was available. The values used for calculating this ratio are included in Table 5-10. This ratio was further used to estimate the CTOD value of completely broken specimens. The flow chart in Figure 5-96 explains the procedure followed for measuring the CTOD value. The CTOD value for 2 specimens could not be estimated as the CMOD gauge data was not available.

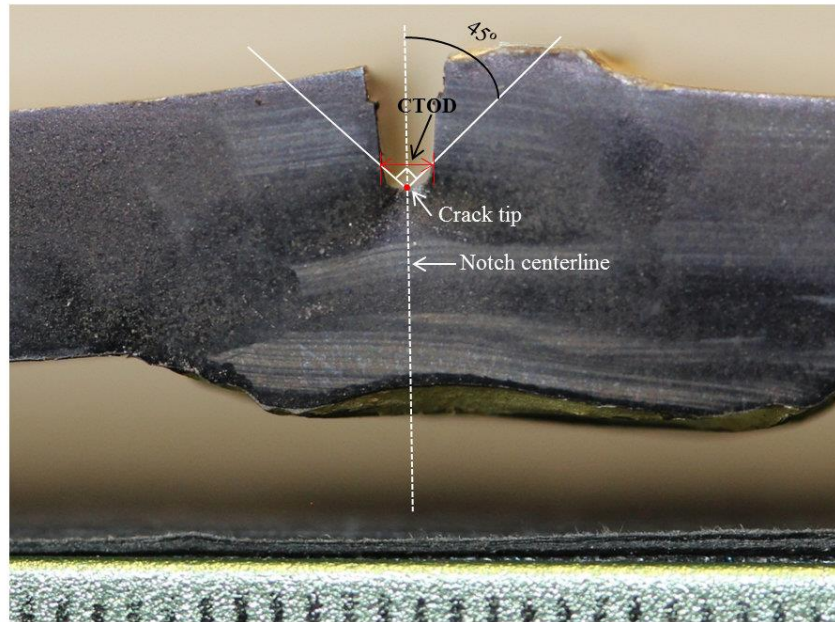


Figure 5-95 CTOD measurement procedure from CWT specimen photograph

Table 5-10 CTOD-CMOD relation

Specimen ID	CMOD at End of Test (mm)	Residual CTOD - Initial Notch Width (mm)	CTOD/CMOD
35-2-1	1.30	1.02	0.78
35-2-2	2.03	1.32	0.65
37-2-1	1.22	0.92	0.75
42-2-1	1.58	1.12	0.71
47-2-1	1.82	1.42	0.78
47-2-2	1.91	1.12	0.59
50-2-1	1.90	1.42	0.75
51-2-1	1.72	1.22	0.71
53-2-1	1.71	1.14	0.67
54-2-1	1.70	1.12	0.66
Median		1.13	0.71
Standard Deviation		0.16	0.06

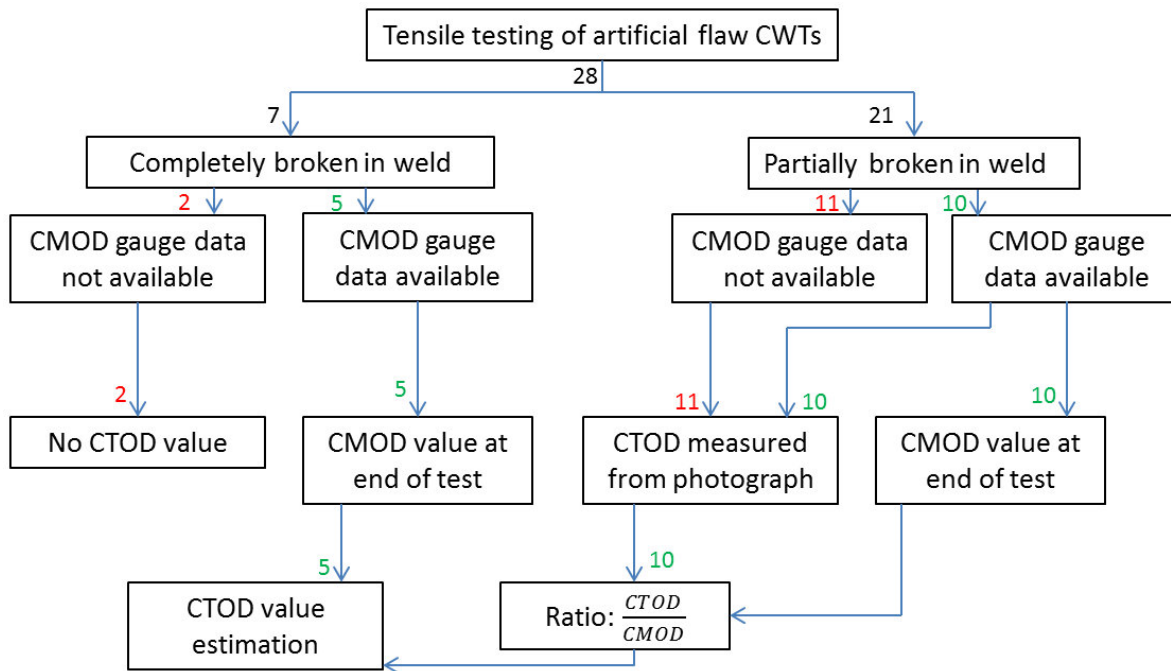


Figure 5-96 Flow chart of the procedure followed for measuring the CTOD value for artificial flaw specimens

Table 5-11 and Table 5-12 summarize the CTOD values for weld metal notch and HAZ notch artificial flaw specimens, respectively. CTOD value for completely broken specimens 34-3-1 and 37-3-1 could not be estimated because of the unavailability of CMOD gauge data.

Table 5-11 CTOD of artificial flaw specimens with weld metal notch

Specimen ID	Status of Sample	CMOD at End of Test (mm)	Residual CTOD - Initial Notch Width (mm)
34-2-1	Completely broken in weld	1.74	1.24
35-2-1	Partially broken in weld	1.30	1.02
35-2-2	Partially broken in weld	2.03	1.32
37-2-1	Partially broken in weld	1.22	0.92
42-2-1	Partially broken in weld	1.58	1.12
46-2-1	Completely broken in weld	0.98	0.69
46-2-2	Partially broken in weld	N/A	0.55
47-2-1	Partially broken in weld	1.82	1.42
47-2-2	Partially broken in weld	1.91	1.12
50-2-1	Partially broken in weld	1.90	1.42
51-2-1	Partially broken in weld	1.72	1.22
53-2-1	Partially broken in weld	1.71	1.14
54-2-1	Partially broken in weld	1.70	1.12
54-2-2	Completely broken in weld	1.50	1.07
Median			1.12
Standard Deviation			0.24

Table 5-12 CTOD of artificial flaw specimens with HAZ notch

Specimen ID	Status of Sample	CMOD at End of Test (mm)	Residual CTOD - Initial Notch Width (mm)
34-3-1	Completely broken in HAZ	N/A	N/A
35-3-1	Partially broken in HAZ	N/A	0.92
35-3-2	Completely broken in HAZ	1.46	1.04
37-3-1	Completely broken in HAZ	N/A	N/A
42-3-1	Partially broken in HAZ	N/A	0.89
46-3-1	Partially broken in HAZ	N/A	1.22
46-3-2	Partially broken in HAZ	N/A	0.72
47-3-1	Partially broken in HAZ	N/A	0.92
47-3-2	Partially broken in HAZ	N/A	0.72
50-3-1	Partially broken in HAZ	N/A	1.92
51-3-1	Partially broken in HAZ	N/A	1.32
53-3-1	Partially broken in HAZ	N/A	1.12
54-3-1	Partially broken in HAZ	N/A	1.62
54-3-2	Completely broken in HAZ	1.05	0.75
Median			0.98
Standard Deviation			0.37

5.6.12 General Observations from Group B Data

- From round bar tensile tests, it is apparent that, there is anisotropy in UTS along longitudinal and hoop direction of base metal (pipe).
- There is a weld metal strength undermatch as compared to base metal strength in all but 2 out of the 10 tested vintage girth welds.
- The macrohardness data also shows a case of weld strength undermatch, with the weld metal strength.
- The full scale Charpy transition curves indicate that the weld and base metals of the test welds are on the upper shelf of the ductile-to-brittle transition curve at room temperature.
- The CWT specimens with artificial flaw consistently showed the maximum stress capacity reduction when compared with base metal UTS.

5.7 Pipe and Girth Weld Properties from Group C

5.7.1 Characteristics of the Welds of Group C

After a girth weld failure in 1981, a full-scale test program was launched to evaluate the girth weld performance of in-service vintage pipelines [132]. A total of 68 full-scale tests were conducted on grossly defective girth welds in late 1980s and early 1990s. The defective girth welds were cut out from pipelines of 18-inch OD and nominally Grade B pipes. The wall thickness ranges from 7.8 mm to 10.4 mm, with the majority of the wall thickness around 8.0-8.5 mm.

The time of girth weld fabrication are not known. From the grade of the material, it is almost certain that the welds would be qualified as vintage girth welds. The majority of the welds are listed as of “MMA” type, a few are listed as of “CO₂” type.

5.7.2 Pipe Tensile Properties

The tensile samples of the pipe metal were tested and the results are shown in Figure 5-97. The average values of yield strength and UTS are 49.2 ksi (339 MPa) and 70.2 ksi (484 MPa), respectively. The averaged Y/T ratio is therefore 0.70. The lowest yield strength obtained from the pipe samples is 45.7 ksi which is close to the SMYS of X46. Although the pipe was nominally Grade B which was equivalent to X35, its actual yield strength was better described by X46.

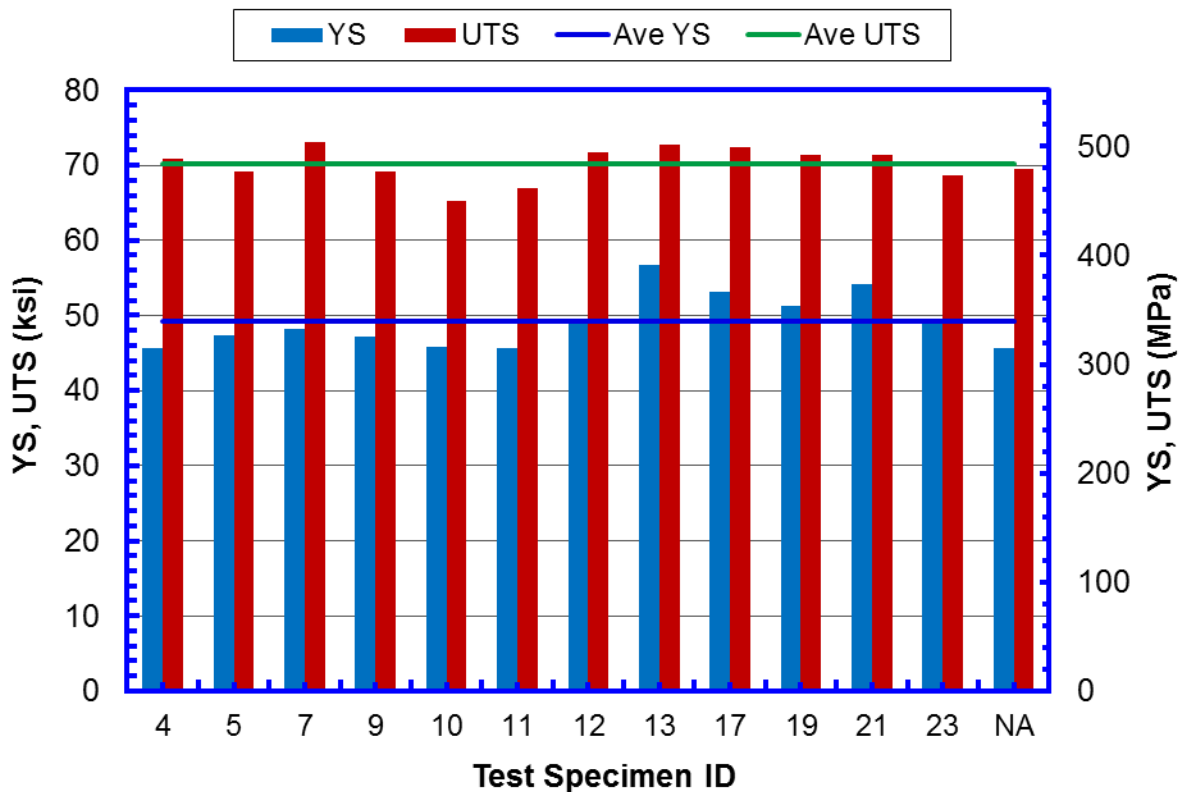


Figure 5-97 Pipe tensile material properties from Group C

5.7.3 Cross-Weld Tensile Strength

Cross-weld specimens with a width ranging from 14.23 mm to 22.6 mm were tested at 5 °C by applying across-weld tensile load. The specimens had various defect depth. The lower bound failure stress is approximately in a linear relationship with the defect depth as shown in Figure 5-98. The approximate lower bound failure stress for welds without defect is 60.9 ksi (420 MPa). This failure stress is between the average yield strength and UTS of the pipe. In the absence of brittle fracture, the failure stress is expected to be close to the UTS of the material. These test results indicate that the UTS of the weld is likely below that of the base pipe material.

Seven out of the 17 test samples failed by cleavage, indicating that the welds would have brittle fracture risk if the load is sufficiently high.

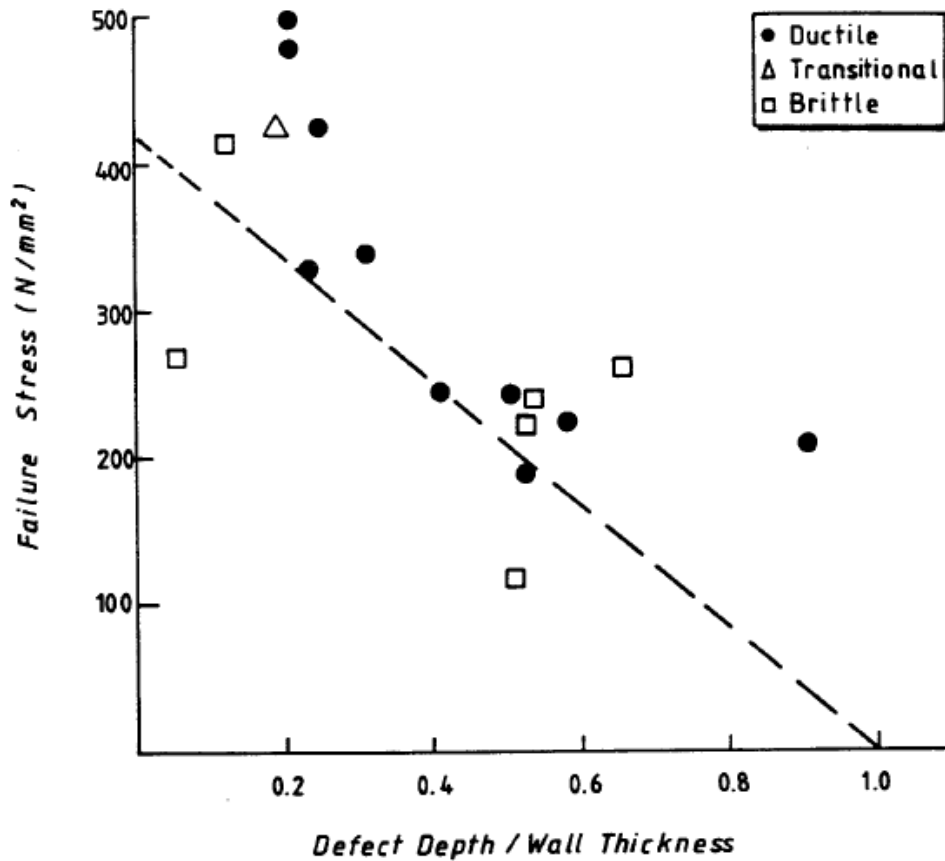


Figure 5-98 Cross-weld failure stress as a function of defect depth

5.7.4 Type and Dimensional Distribution of the Flaws from Group C

5.7.4.1 Flaw Types

A total of 1743 flaws were found in the full-scale tests. The most common flaws were root concavity (245), slag inclusions (199), porosity and void (195), incomplete root (177), arc burns (160), bad pick-up (113), lack of root fusion (107), and burn-through (79). Figure 5-99 shows the flaw types and the corresponding percentage of each type of flaws.

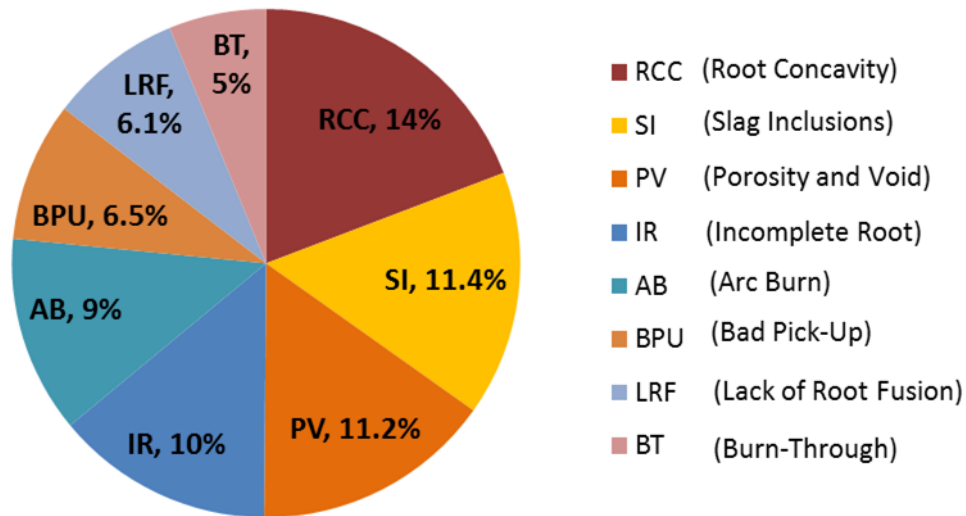


Figure 5-99 Types of flaws in Group C

5.7.4.2 Flaw Dimensions

The amount of weld length (% circumference) containing flaws is shown in Figure 5-100. It shows that almost half of the tested welds (30 out of 68 welds) have 75% to 100% pipe circumference containing flaws. Figure 5-101 shows the distribution of the total flaw length in each individual weld among all the welds. Around one half of the 68 tested welds have the total flaw length ranging from 200 mm to 399 mm.

The 54 of the 68 full-scale specimens contained a total of 261 flaws of burn-through (79), arc burns (160), and crater cracks (22). The longest individual flaw length of those flaws is shown in Figure 5-102. A length of 15 mm can be roughly selected as the longest individual flaw length of all three flaws.

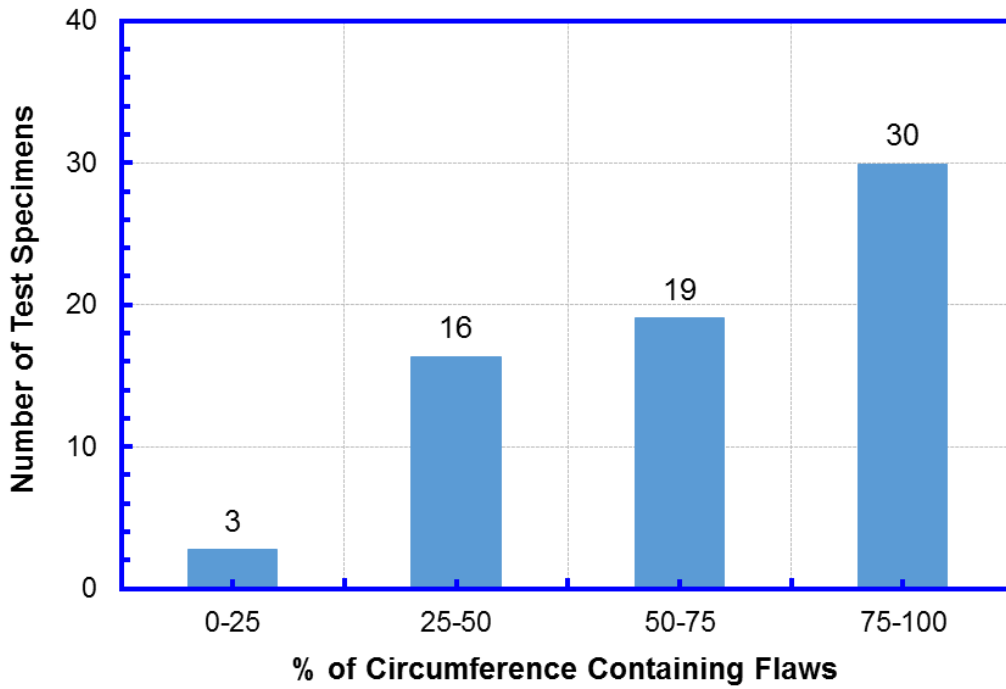


Figure 5-100 Number of welds containing flaws with the circumferential length fall within certain range

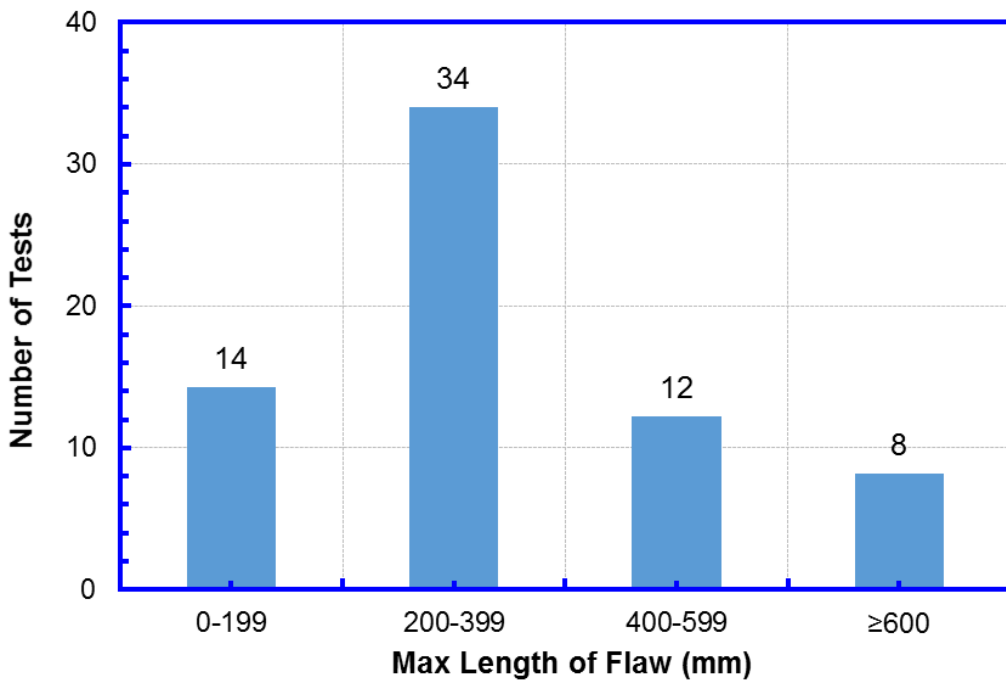


Figure 5-101 Distribution of total girth weld flaw length from Group C

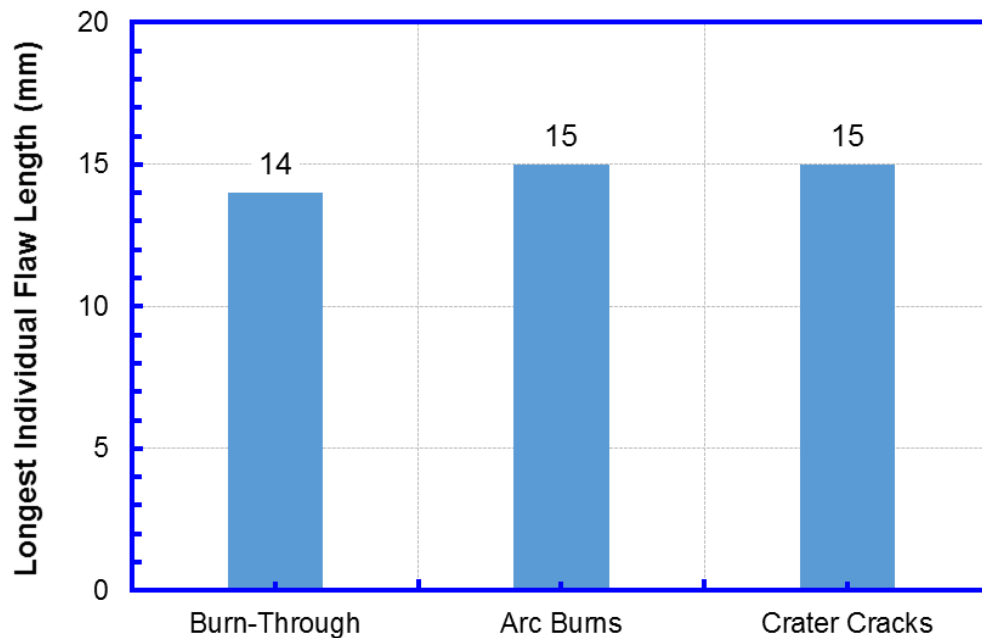


Figure 5-102 Longest individual flaw length of burn-through, arc burns and crater cracks flaws from Group C

5.7.5 Results of the Full-Scale Tests

The full-scale test specimens were loaded in tension. The tests were stopped when either (1) rupture occurred or (2) the strain reaches 1% or the stress reaches 100% SMYS (46 ksi), whichever occurred first. Among the 68 specimens tested, 36 failed during tests (i.e., rupture occurred before the tests were stopped). The remaining 32 did not fail during the test and all 32 survived a strain of 1%. Twenty-seven of the 32 specimens also survived 100% SMYS. The 36 tests that failed by through-wall fractures recorded failure stresses in the range of 64 to 116% yield strength. Only two tests failed below 91% yield strength and 13 tests failed below 100% yield strength. The results of all full-scale tests are shown in Figure 5-103.

If surface-breaking (root and cap) flaws are combined into one single length, the relationship between test failure and combined surface flaw length can be shown in Figure 5-104. There is a clear trend that the probability of failure increases with the increase of surface flaw length.

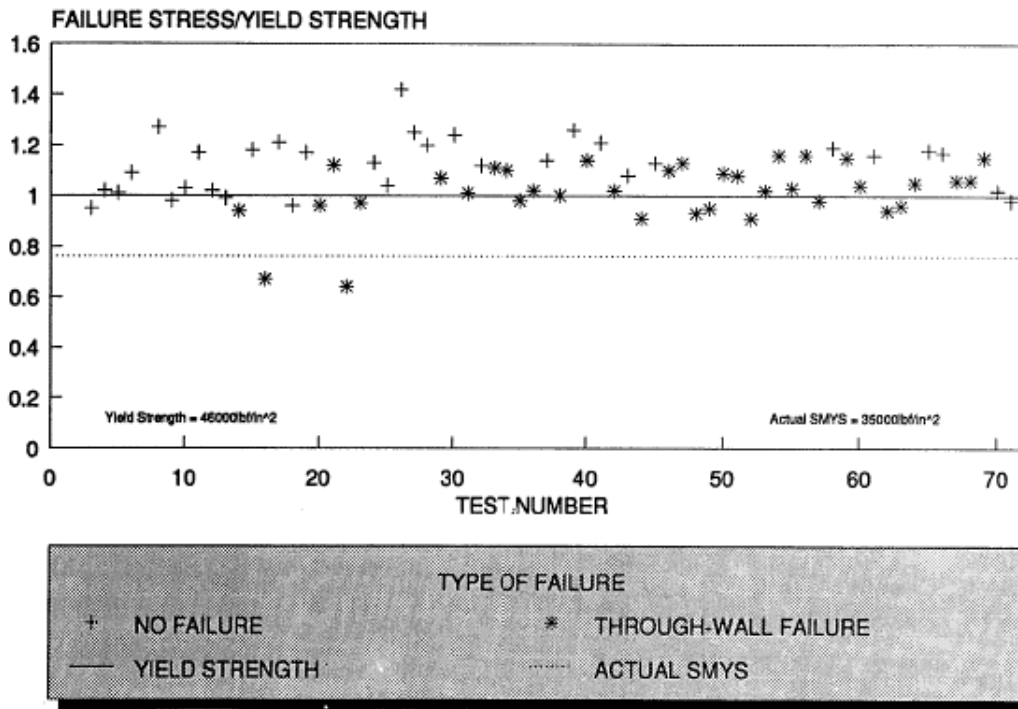


Figure 5-103 Failure stresses of full-scale tests from Group C

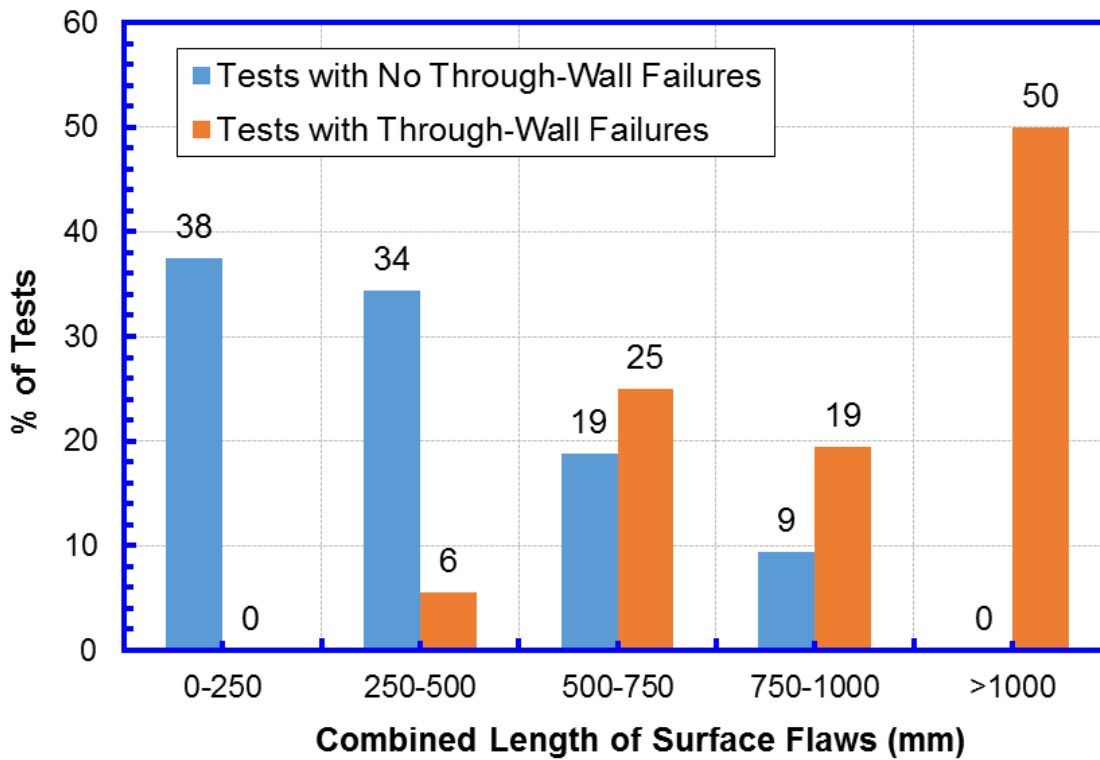


Figure 5-104 Percentage of tests as a function of surface flaw length from Group C

5.7.6 General Observations from Group C Data

A few general conclusions may be drawn from the Group C data.

- The nominally Grade B pipes (SMYS =35 ksi) can be better described as X46 (SMYS = 46 ksi). The averaged value of yield strength and UTS are 49.2 ksi (339 MPa) and 70.2 ksi (484 MPa), respectively. The corresponding Y/T ratio is 0.70.
- The lower bound UTS of the weld is estimated at 60.9 ksi (420 MPa). This value is about 10 ksi below the averaged UTS of the pipe.
- Most of the welds have many flaws. The total length of the flaws in any individual weld is quite long.
- The failure stress of the finite-width cross-weld tensile test specimens is approximately linear to the depth of the defect. This indicates that the failure event is mostly strength-dominated event, not brittle fracture-dominated event. However, the tests also showed that the welds would have brittle fracture risk when the load is sufficiently high.
- Despite having massive amount of flaws, approximately one-half of the welds survived to a strain of 1.0%. Only two of the 68 tests failed at a stress level less than 91% SMYS.
- There is a clear increase of failure probability with the increase of the surface-breaking flaw length.

5.8 Pipe and Girth Weld Properties from Group D

5.8.1 Overview of the Welds

Three girth welds (termed as weld X, weld Y and weld Z) were made to an API 5L X70 linepipe of 30 in OD and 0.441 in (11.2 mm) wall thickness [133]. The welds were fabricated in early 1990s using a SMAW process and 80 ksi (E8010-G or E55010-G) tensile strength cellulosic electrodes. These electrodes were chosen to obtain overmatching deposited weld metal. During welding, the typical workmanship weld defects were introduced to the welds. After welding, the complete circumference of each weld was radiographed to determine the defect length actually achieved.

5.8.2 Matrix of Mechanical Tests

The three girth welds were subjected to a large variety of mechanical tests as detailed in Table 5-13. The detailed test setup and results are discussed in the following subsections.

Table 5-13 Testing matrix of Group D

Type of Test	# of Specimens			Total # of Specimens
	Weld X	Weld Y	Weld Z	
Hardness Traverses	10	10	4	24
Pipe Metal Tensile	1	1	1	3
All-weld Metal Tensile	1	1	1	3
Charpy V Impact	9	9	9	27
CTOD B×2B Tests	4	4	4	12
Curved Wide Plate	5	5	2	12

5.8.3 Pipe Tensile Properties

5.8.3.1 Features and Dimensions of Tensile Specimens

The tensile properties were determined by the round bar 6 mm (0.236 in) diameter specimens at the ambient temperature. The pipe metal tensile tests were conducted on longitudinal specimens, i.e. orientation of the specimen axis was perpendicular to the direction of the girth weld. The specimens were machined from unflattened blanks. All specimens were tensile loaded at 21 °C and the elongation was measured by an extensometer on a gauge length of 25 mm (1 in). For each test, the 0.2% and 0.5% offset proof stress, the ultimate tensile strength, and the yield to tensile ratio were determined.

5.8.3.2 Test Results

The results of the pipe metal tensile tests are show in Table 5-14.

Table 5-14 Pipe material tensile test results of Group D

Specimen #	0.2% YS		0.5% YS		UTS		Y/T (0.5% YS)
	MPa	ksi	MPa	ksi	MPa	ksi	
Pipe 011	517	75.0	539	78.1	644	93.4	0.84
Pipe 019	550	79.6	551	79.9	639	92.6	0.87
Pipe 016	585	84.8	592	85.8	691	100.2	0.86

The comparison of pipe metal yield strength and ultimate tensile strength obtained from tensile tests to those from mill certificates is shown in Figure 5-105 and Figure 5-106. The measured yield strengths at 0.5% strain of all pipes are higher than either the SMYS of X70 or the yield strength from the mill certificates. For example, for pipe 016, the measured yield strength at 0.5% strain is 592 MPa which is about 10% higher than the value from the mill certificates and 23% higher than the SMYS of X70 (483 MPa). For the ultimate tensile strength, the pipe 011 has the measured value which is very close to the one from mill certificates. The

UTS of pipe 019 and 016 is about 3% lower and 7% higher than the mill certificates, respectively. The Y/T ratio obtained from the tensile tests by using yield strength at 0.5% strain is in the range of 0.84 to 0.87

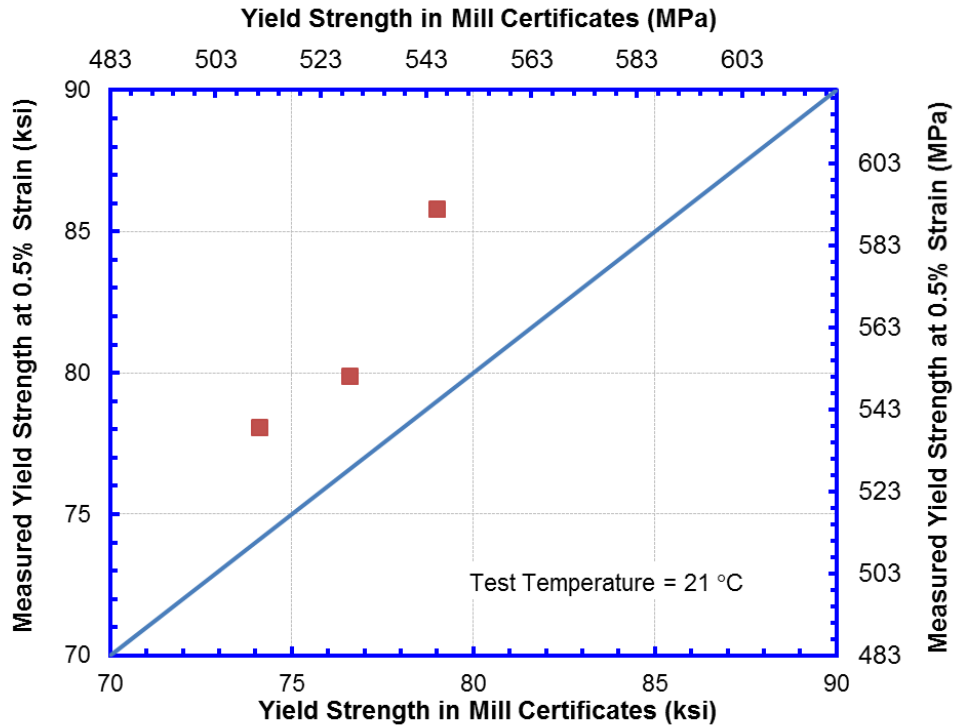


Figure 5-105 Measured yield strength vs. mill certificates

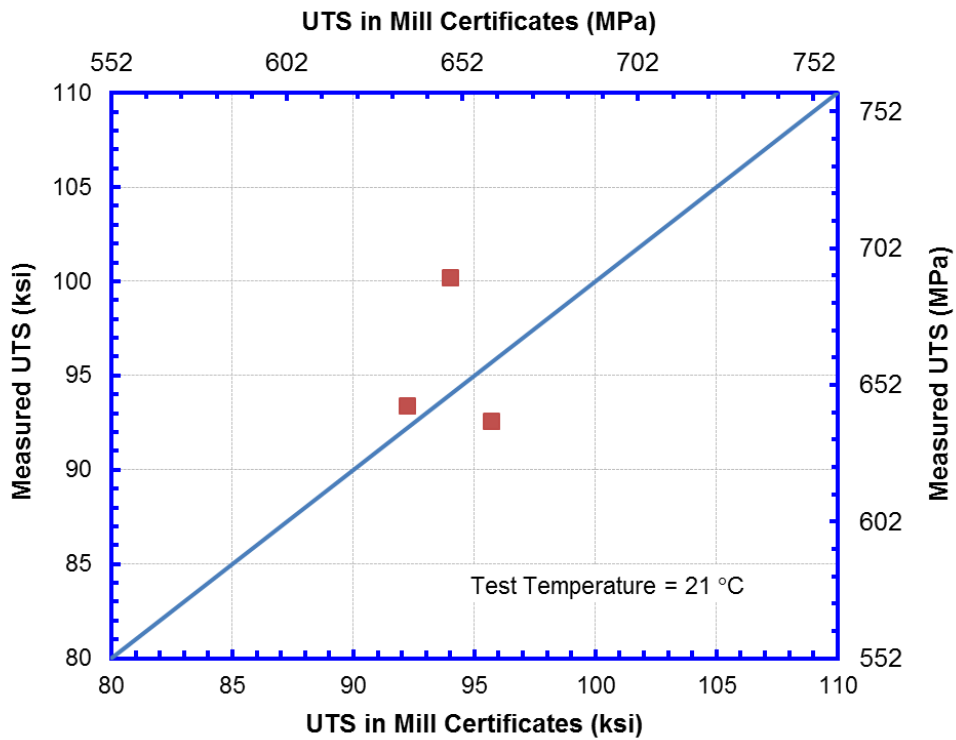


Figure 5-106 Measured UTS vs. mill certificates

5.8.4 All-Weld Metal Tensile Properties and Strength Mismatch

5.8.4.1 Features and Dimensions of Tensile Specimens

The test specimen had the same geometry and dimensions as the pipe tensile specimen, i.e. round bar of 6 mm in diameter and a gauge length of 25 mm. The test temperature was 21 °C.

5.8.4.2 Test Results

The all-weld metal yield and ultimate tensile strength are shown in Table 5-15. The measured yield strengths varied between 570 MPa (82.6 ksi) and 584 MPa (84.7 ksi).

Table 5-15 All-weld metal tensile test results of Group D

Specimen #	Sampling Location	0.2% YS		0.5% YS		UTS		Y/T (0.5% YS)
		MPa	ksi	MPa	ksi	MPa	ksi	
Weld X	8 o'clock	560	81.2	570	82.6	677	98.2	0.84
Weld Y	10 o'clock	580	84.1	584	84.7	687	99.6	0.85
Weld Z	4 o'clock	583	84.5	584	84.7	701	101.6	0.83

The weld strength mismatch ratio, defined as the ratio of the averaged weld UTS over the averaged pipe UTS, are show in Figure 5-107. The UTS of the pipe is taken either from the current tests or from the mill certs. The weld strength is generally a few percentage points higher

than the pipe strength. Pipe 106 has the highest strength, resulting in approximately evenly matched girth weld.

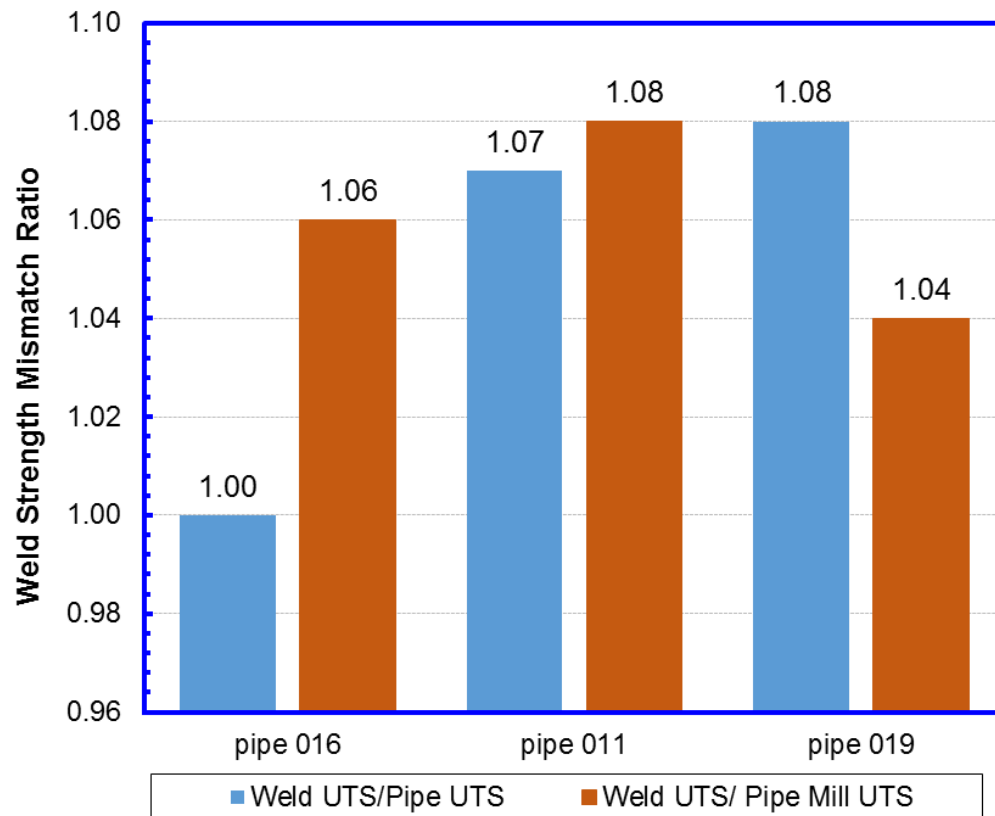


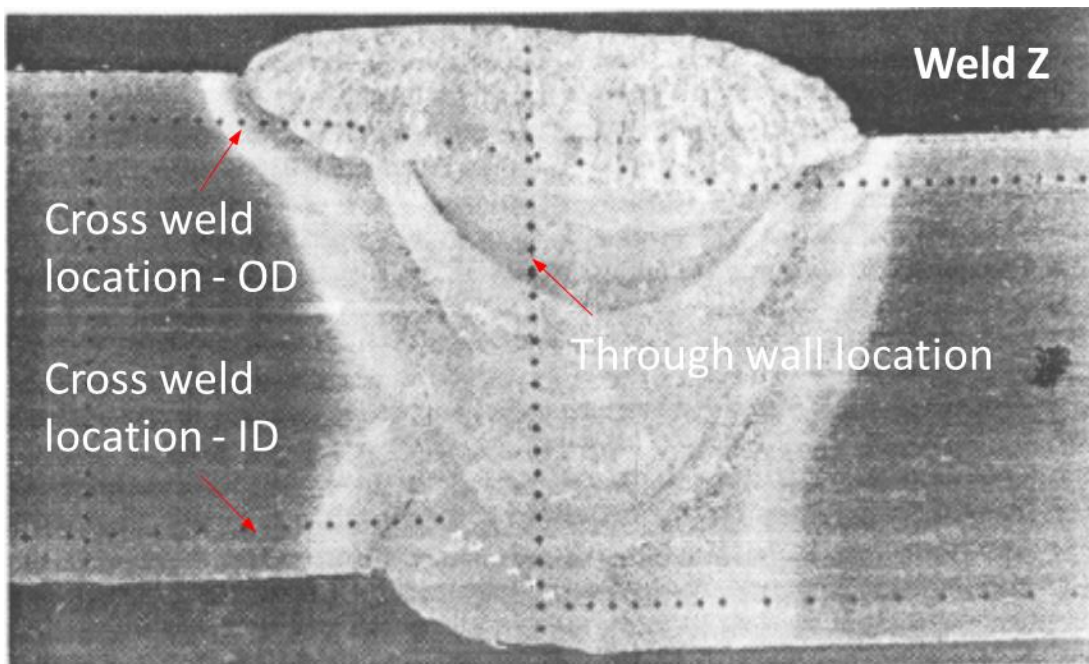
Figure 5-107 Weld strength mismatch from Group D

5.8.5 Girth Weld Hardness Profile

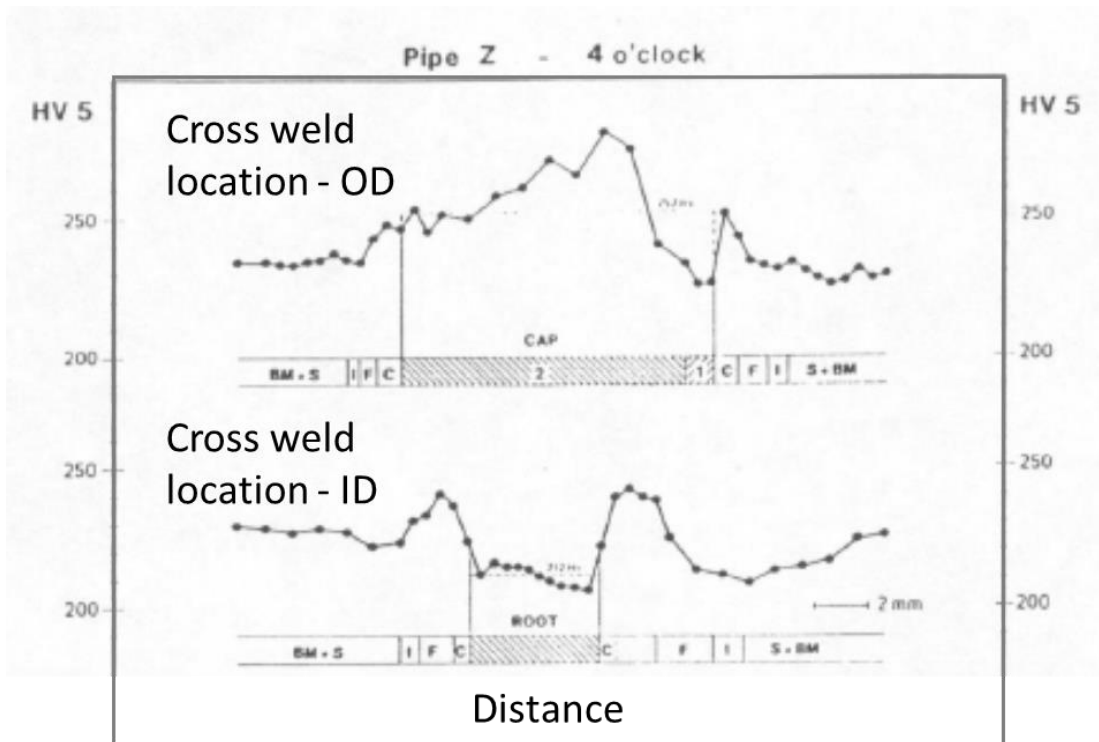
Hardness traverses in three macros (2, 6, and 8 o'clock), taken from Welds X and Y, were obtained. For Weld Z, the examination was limited to one macro taken from the 4 o'clock position. The hardness measurements were done either across the weld or through the thickness with a 50 N (HV5) proof load at a spacing of 0.5 mm (0.02 in). The average hardness levels of weld deposits and pipe materials are summarized in Table 5-16. The photomicrographs of girth weld cross section and hardness profiles are shown in Figure 5-108 for Weld Z as an example. The photomicrographs of Welds X and Y can be seen in Appendix A1 of [133].

Table 5-16 Hardness of the weld deposits and pipe material of Group D

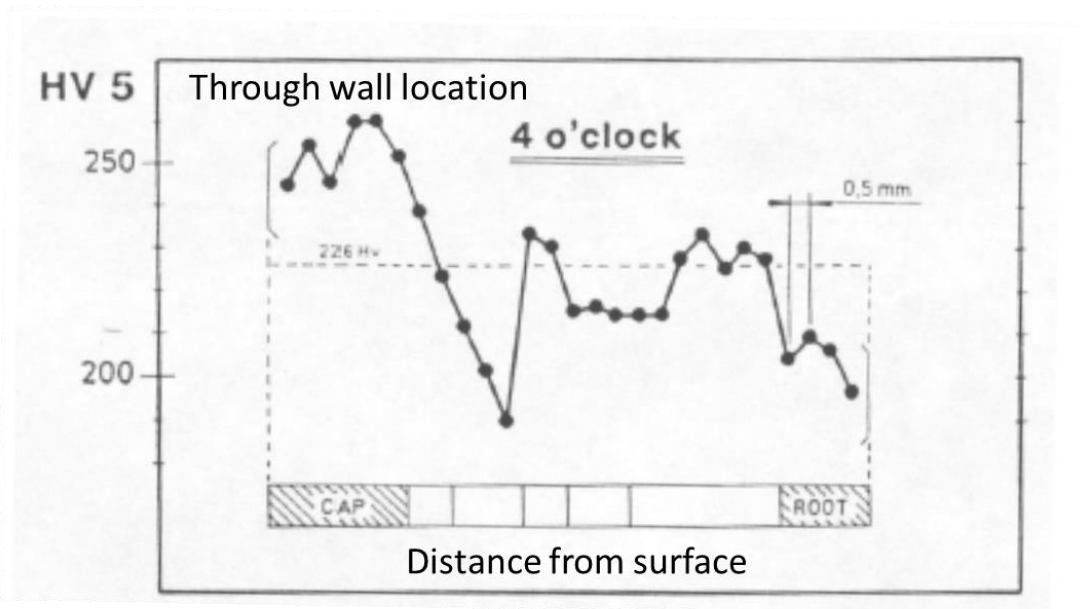
Weld	Sampling Location	Hardness Values (HV5)			Pipe
		Average Weld Deposit		Pipe Metal	
	o'clock	Root	Cap	Average	
X	2	221	234	227	pipe 016
	6	225	235		
	8	221	240		
Y	2	223	248	219 and 232	pipe 011 and pipe 019
	6	203	230		
	8	208	223		
Z	4	212	252	232	pipe 019



(a)



(b)



(c)

Figure 5-108 Hardness profiles of Weld Z from Group D: (a) girth weld cross section and hardness measurement locations; (2) hardness profiles at cross weld locations; (3) hardness profile at through wall location

5.8.6 Charpy Impact Energy

The Charpy V-notch impact tests were carried out to establish the E8010 weld deposit notch properties over a range of testing temperatures and to enable the energy absorption transition temperature to be derived. Full-size standard Charpy V-notch impact specimens of 55 mm (2.165 in) long and 10 mm (0.394 in) square section were extracted transversely to the weld (specimen longitudinal axis perpendicular to the weld) with the 2 mm deep “through thickness” notch in the weld metal center and perpendicular to the pipe surface. The notch bottom sampled the root, hot and filling passes. The Charpy impact tests were performed in accordance with ASTM E23, using specimens in triplicate at each of the test temperatures of -10 °C (+14 °F), -20 °C (-4 °F) and -30 °C (-22 °F). There are 9 specimens for each weld and 27 specimens for all welds. Figure 5-109 shows the results of all Charpy V-notch impact tests. Each data point of one weld was obtained by averaging the results of three individual test specimens. The average value in Figure 5-109 (shown as triangular markers) was obtained by averaging the impact energies of three welds. The Minimum/Maximum values (shown as dashed lines) were taken among all the specimens. At -10 °C (+14 °F), the minimum and averaged Charpy impact energy is approximately 20 and 30 ft·lb, respectively.

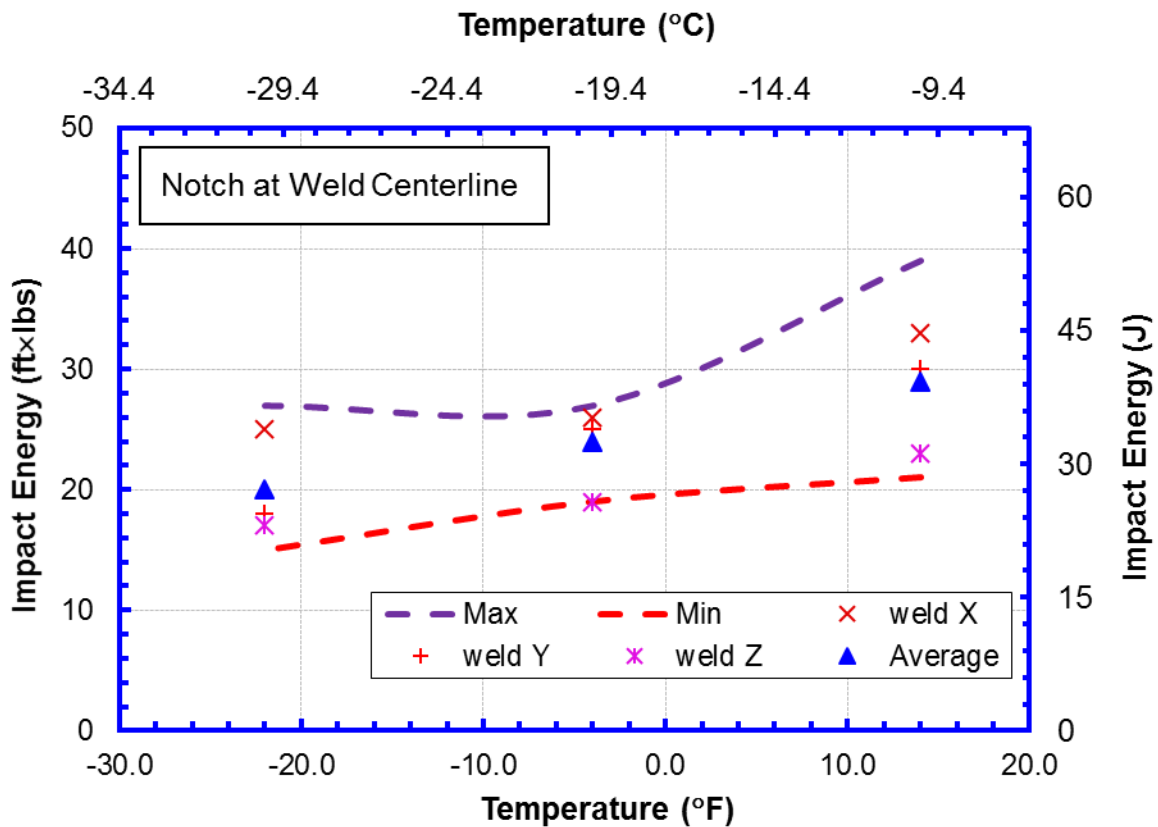


Figure 5-109 Charpy V-notch impact energy from Group D

5.8.7 CTOD Fracture Toughness Testing

Full wall thickness rectangular B×2B (B=11.2 mm) specimens were machined from the pipe samples with their longitudinal axis perpendicular to the axis of the girth weld. The test specimens were taken from the 2, 4, 6, 8 and 10 o'clock positions. All notches were generated at the weld deposit centerline and finished by applying fatigue loading under low stress intensity conditions at room temperature. The testing temperature is -30 °C (-22 °F). The CTOD test results are shown in Table 5-17. The minimum CTOD value of the tested weld deposits is 0.07 mm (Weld Z).

Table 5-17 CTOD test results of Group D

Specimen #	O'clock	CTOD	
		mm	inch
Pipe X			
A1	2	0.11	0.004
A2	2	0.20	0.008
B	6	0.19	0.007
C	8	0.18	0.007
Pipe Y			
D	2	0.17	0.007
E	4	0.19	0.007
F1	10	0.18	0.007
F2	10	0.22	0.009
Pipe Z			
G1	4	0.07	0.003
G2	4	0.17	0.007
G3	4	0.17	0.007
Average		0.17	0.007
Min		0.07	0.003
Max		0.22	0.009

5.8.8 Wide Plate Tests

5.8.8.1 Overview of the Test

The wide plate tests were conducted to determine the failure characteristics of tensile loaded wide plate test specimens containing workmanship type defects. The wide plate test specimens were extracted from one meter long pipe sections. The geometry and dimensions of the specimen are shown in Figure 5-110. The cap and root weld reinforcements were not removed.

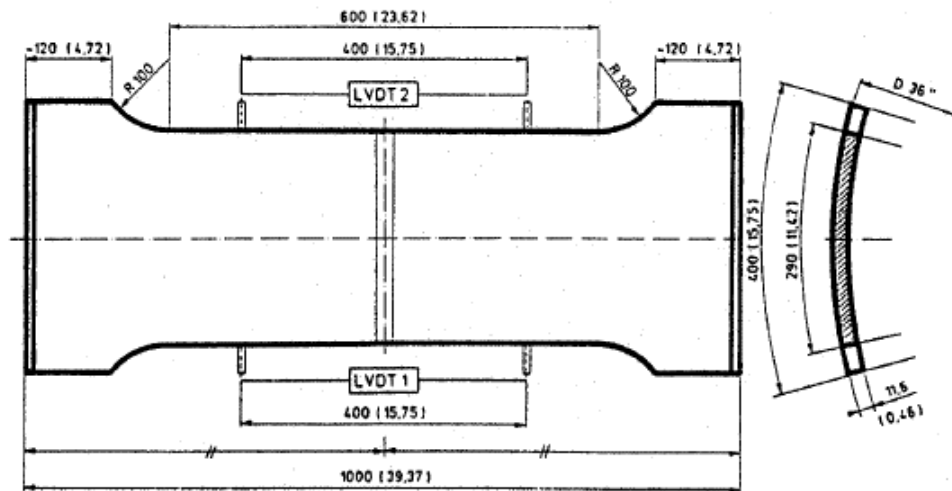


Figure 5-110 Geometry and dimensions of wide plate test specimens of Group D

The wide plate test specimens were tensile loaded in a closed loop servo-hydraulic control system. The tests were conducted at $-30\text{ }^{\circ}\text{C}$ ($-22\text{ }^{\circ}\text{F}$). During the test, the applied load and deformation occurring in a 20 mm gauge length straddling the weld were monitored and each was plotted autographically against the average overall extension of the test specimens. The deformations were measured by means of two spring loaded LVDTs. The applied load vs. overall extension and the weld metal elongation vs. overall extension records were used to determine the yield load and the maximum or failure load. The stresses were calculated regarding the gross section of the test plate. The strain values were obtained based on the deformation and gauge length. Upon completion of testing, each fracture surface was examined to determine the nature and the actual dimensions of the defect. Photographs of the broken specimens and fracture surfaces were taken. Figure 5-111 is a typical picture of a broken wide plate specimen. Finally, the position of the defect was identified and photographed.

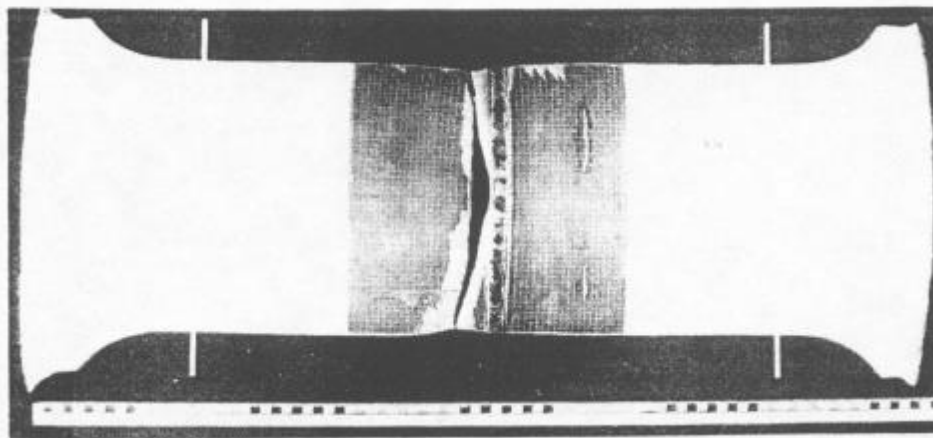


Figure 5-111 A fractured curved wide plate specimen from Group D

5.8.8.2 Defects in Wide Plate Test Specimens

The types and dimensions of the defects in the wide plate test specimens are summarized in Table 5-18. The dimensions in the column of “Measured Length” were determined after the wide plate testing.

Table 5-18 Types and dimensions of the defects in wide plate tests of Group D

Specimen #	Defect Type	Defect					
		Target Length		Length from NDT		Measured Length	
		mm	inch	mm	inch	mm	inch
Y3	Root bead - Incomplete Fusion	25	0.984	15	0.591	17.3	0.631
Z2		25	0.984	27	1.063	40.5	1.606
X1		12	0.472	11	0.433	29.5	1.161
X2	Cap - Incomplete Fusion	12	0.472	12	0.472	11.6	0.457
Y6		25	0.984	27	1.063	26.3	1.035
Y1	Fill - Lack of Side Wall Fusion	100	3.937	113	4.449	110.0	4.370
X3		50	1.969	40	1.575	43.0	1.693
X4	Elongated Slag (Wagon Tracks)	50	1.969	45	1.772	42.2	1.661
Y2		100	3.937	110	1.772	107.7	4.232
Y5	Root bead - Incomplete Penetration	12+16	0.600	22	0.866	19.2	0.783
X5		25	0.984	32	1.260	31.0	1.220
Z5		12+16	0.600	22	0.866	20.3	0.799

5.8.8.3 Summary of Test Results

A general summary of the test results is shown in Table 5-19. The test results are grouped by the defect types: (1) incomplete root bead fusion; (2) incomplete cap fusion; (3) lack of side wall fusion; (4) elongated slag (wagon tracks); and (5) incomplete root bead penetration. The length and depth of the defect were measured from the fracture surface after testing. The stresses and strains corresponding to 0.5% strain offset (may be viewed as a yield point) and final failure or maximum load are shown in Table 5-14. The stresses corresponding to the 0.5% strain offset are higher than the SMYS and the measured yield strength of the pipe. At the 0.5% offset strain, the cross-weld strains are highest for the welds with root bead incomplete fusion. This indicates that flaws of this type are likely to be more detrimental to the weld performance than other types of flaws investigated. The overall strains at the maximum load or failure are all greater than 2.0%, indicating those welds offers good resistance to longitudinal strains.

The fracture surfaces and the shapes and dimensions of the test specimens are available from reference [133].

Table 5-19 General summary of wide plate test results from Group D

Specimen #	Defect		Wide Plate Test Results (at -30 °C)				
	Type	Dim	Yield (0.5%)		Max. Load/Failure		
		L × D	Strength	Cross-Weld Strain	Stress	Cross-Weld Strain	Strain
		mm × mm	MPa	%	MPa	%	%
Y3	Root bead - Incomplete Fusion	17.3 × > 2	617	0.98	697	11.25	5.76
Z2		40.5 × 2.7	610	1.40	661	8.30	2.42
X1		29.5 × 3.0	604	1.00	702	18.15	5.38
X2	Cap - Incomplete Fusion	11.6 × 2.0	587	0.40	666	9.50	3.81
Y6		26.3 × 3.0	610	NA	706	NA	5.15
Y1	Fill - Lack of Side Wall Fusion	111.0 × 2.6	609	0.32	658	3.20	2.40
X3		43.0 × 3.3	596	0.70	639	6.10	2.17
X4	Elongated Slag (Wagon Tracks)	42.2 × 1.5	585	0.50	686	10.25	5.15
Y2		107.7 × 2.6	613	0.10	693	7.63	5.36
Y5	Root bead - Incomplete Penetration	19.9 × 2.2	612	0.40	698	15.50	6.14
X5		31.0 × 3.1	597	0.77	653	6.70	2.63
Z5		20.3 × 3.7	615	1.30	694	15.30	3.88

5.8.9 General Observations from Group D Data

- The measured yield strengths at 0.5% strain of all pipes are higher than either SMYS of X70 (+10 ksi) or the yield strength from the mill certificates (+5 ksi). The Y/T ratio obtained from the tensile tests by using yield strength at 0.5% strain is in the range of 0.84 to 0.87
- All the weld metals have either even- or over-matching strength in comparison with the strength of the pipes.
- The average and minimum Charpy V-notch impact toughness at -10 °C (+14 °F) is approximately 30 and 20 ft·lb.
- The minimum CTOD value of the tested weld deposits is 0.07 mm (Weld Z). For Weld X, the lowest CTOD value is 0.11 mm. For Weld Y, all CTOD values were greater than 0.17 mm.
- For the curved wide plate tests, the overall strains at the maximum load or failure are all greater than 2.0%, indicating that the welds have good resistance to longitudinal strains at -30 °C.

Wang et al. have shown that there can be marked increased in the tensile strength and strain hardening rates of both pipe materials and girth weld metals at temperatures lower than room

temperature at which most material characterization tests are conducted [134]. Since the wide plate tests were done at $-30\text{ }^{\circ}\text{C}$ and the tensile tests of the pipe materials and weld metals were done at room temperature, the wide plate specimens may have “gained advantage” in performance from the low temperature. The conventional wisdom is that a low temperature test is a more severe test condition than a room temperature test. This is only true if the failure event is fracture dominated, as the low temperature can lead to reduction in toughness. The performance of the wide plate indicates that the failure events were not fracture dominated. Therefore the $-30\text{ }^{\circ}\text{C}$ tests may have shown welds having better performance than they might have at higher temperature.

5.9 Data in Other Sources

In a PRCI-funded effort started in 2014, i.e., PRCI project SIA-1-4 [135], material properties and flaw characteristics of vintage girth welds are generated and analyzed. The basic material property data generated are similar to those shown above, include (i) pipe tensile properties in both hoop and longitudinal directions, (ii) all weld-metal tensile, (iii) macrohardness traverse, and (iv) Charpy impact transition curves with notches in the heat-affected zone (HAZ) and deposited weld metal. In addition, tensile tests were conducted on cross-weld specimens with natural flaws and artificially machined planar flaws. All tested girth welds were inspected using radiography and phased array UT. Thus, this work provides a coherent picture of the material properties, flaw characteristics, and stress and strain capacities of the tested vintage girth welds.

Some limited girth weld data are also available in PRCI project MATV-1-3 [136].

5.10 Summary of Material Characteristics and Recommendations

5.10.1 Key Features of Material Characteristics

The basic material property tests provide essential information for quantitative assessment of the stress and strain capacity of pipeline girth welds. The key information used in assessment include: pipe tensile strength, pipe strain hardening rate, weld strength mismatch, and toughness. The general observations from the data described above and test data available to CRES, but not shown above, are given below.

- There is a considerable variation in the actual pipe strength relative to the pipe grade. In all cases, the yield strength in hoop direction meets or exceeds the SMYS of that particular grade. In some cases, the yield strength in the longitudinal direction can be lower than the SMYS. In some extreme cases, the yield strength in hoop direction can be 30+ ksi above SMYS.
- There can be considerable anisotropy in linepipes. The stress-strain curves in the longitudinal direction can be quite different from those in the hoop direction.
- The UTS in the longitudinal and hoop direction is usually similar.
- In most cases, the pipe strength on either side of a girth weld is similar. In some minority cases, the strength difference can be quite large; much more than typical strength variation within a joint of pipe. This large difference is most likely caused by linepipes on either side of a girth weld coming from different heats of steels, different plate/coil

manufacturers, or even different pipe manufacturers. In cases where such large differences were found in vintage pipelines, records were not available to determine which of those scenarios might be at play.

- There has been a large decrease in pipe's strain hardening capacity from hot rolled and normalized pipes with high carbon (0.2%) to microalloyed steels with low carbon.
- The strength of the deposited weld metal is often less than the actual strength of the pipe. In most cases, this strength undermatching does not lead to strain concentration in the girth weld due to the weld cap reinforcement.
- Weld cap reinforcement can play a significant role in compensating the possible weld strength undermatching when such undermatching is not overly excessive. Some vintage girth welds are found to have a wide and smooth cap reinforcement which is beneficial to weld's tolerance to longitudinal stresses and strains.
- The SMAW welds made in 1940s onwards are expected to behavior in ductile manner under normal service conditions for buried pipelines, i.e., temperature warmer than -10 °C.
- Charpy values taken from testing of multiple specimens indicate that, on the average, the Charpy toughness at -10 °C is above 20-30 ft·lb.
- There can be large variations, sometime by a factor of up to 5-6, in individual Charpy impact energy for specimens with notches in HAZ. Consequently, Charpy transition curves with multiple specimens tested at the same temperature give better indications of material's behavior than the customary tests of three specimens at a single temperature.
- A lower bound apparent toughness for vintage welds is around 0.3 mm. In most cases, a reasonable lower-bound toughness is around 0.40-0.60 mm for vintage welds. Some welds can have apparent toughness more than 1.0 mm.
- The measured tensile strain capacity of SMAW welds fabricated in 1940-1960s from specimens with natural construction flaws give a strain capacity as low as 0.2-0.3% and as high as >2.0%.

6 Detection and Sizing of Girth Weld Anomalies

Abstract

This section consists of three main parts. In Section 6.1, available standards for ILI and general guidance on the use of ILI are given. In Section 6.2, various girth weld anomalies are tabulated with short descriptions. These anomalies are further divided into three categories: (1) geometrical weld inhomogeneities, (2) volumetric anomalies (metal loss and metal gain), and (3) planar anomalies (crack, notch, etc.). The characteristics of each category and its impact on ILI performance are described. In Section 6.3, the main categories of ILI tools and their working principles are explained.

One of the most detrimental girth weld anomalies is tightly-closed planar flaws, such as hydrogen cracks. Although a few free-flowing and tethered ILI tools are available for detecting such flaws, reliable information on the performance of these tools has been difficult to obtain. These tools are not covered in this section presently.

6.1 Overview of ILI

In-line inspection (ILI) tools are widely used to detect and size pipeline anomalies of different types. No single ILI tool is capable to identify all different types of girth weld and HAZ anomalies. ILI tools are usually specialized to detect a certain type of anomaly. For example there are metal loss tools, crack detection tools, caliper tools, etc. Diverse ILI tools based on different detection technologies (ultrasound, magnetic field, etc.) are developed to detect the same type of pipeline anomaly.

Several standards deal with the application of ILI tools, data analysis and reporting, including

- API Standard 1163, In-line Inspection Systems Qualification, serving as an umbrella document to be used with and complement standards,
- NACE SP01 02, In-line Inspection of Pipelines,
- POF 2009, Specifications and Requirements for Intelligent Pig Inspection of Pipelines, and
- ASNT ILI-PQ, In-line Inspection Personnel Qualification and Certification.

These documents are general guidelines for application of ILI technology and enable pipeline operators and ILI vendors to provide processes that consistently qualify the tools, personnel, procedures, and software utilized in the ILI industry.

A pipeline operator should first understand the exposure of the pipeline to specific anomalies types and then select appropriate ILI tools to detect the anomaly and size its dimensions. Even if the capabilities of the selected ILI tool are well proven, the pipeline operator should be aware of the limitations of ILI technology. Despite the general performance specifications, the actual inspection performance could be influenced by the specific pipeline properties, ILI tool configuration and inspection conditions (cleaning, product type, flow regime, tool speed, etc.). In addition, reporting requirements and data analysis procedures have a significant impact on the performance of ILI results.

6.2 Typology of Girth Weld Anomalies

ILI tools are specialized to specific anomaly types independently of their location (base material or girth weld). Therefore, it is important to understand different types of girth weld anomalies and then to differentiate them in categories associated to specific ILI tools and technologies.

Girth weld anomalies can be categorized by the ways they are created. MACAW's Pipeline Defects describes and shows pictures of more than 30 different examples of manufacturing related girth weld anomalies [137]. Table 6-1 shows an overview of these anomalies and associates them with morphology-related ILI categories (metal loss, crack-like, lamination, etc.)

Table 6-1 Overview of manufacturing related girth weld anomalies

Anomaly Type	Category	Description
Arc Strikes	may cause cracking	Caused by a misplaced electrode and creates a localized heat-affected zone that may produce hardening which is susceptible for cracking.
Burn Through	metal loss	Root bead is partially missing but is often covered by the next pass - also known as 'window'.
Cap Undercut	metal loss	Cap undercut is a smooth groove between the capping run of the weld and the parent plate.
Concave Root	metal loss	The root run has a concave profile and occur most commonly at the 6 o'clock position on the pipe.
Copper Cracking	crack	Fine cracking in the weld metal, often with associated copper inclusions, and concentrated at the grain boundaries.
Excess Cap Height	metal gain	Excess weld reinforcement on the cap, usually greater than 3 mm. It is more common at the 6 o'clock position.
Excess Penetration	metal gain	Excess weld metal in the root of the weld, usually more than 3 mm. It is most common at the 12 o'clock position.
Hydrogen Cracking of Cap HAZ	planar (crack)	This cracking originates at the edge of the weld cap and follows the heat-affected zone.
Hydrogen Cracking of Root HAZ	planar (crack)	'Cold cracks' initiate in the heat-affected zone of the root bead and propagate up the heat-affected zone or into the weld metal.
Hydrogen Cracking of Weld Metal	planar (crack)	Cracking in the weld metal which is often transverse to the weld axis and lying at an angle of 45° to the weld surface.

Table 6-1 Overview of manufacturing related girth weld anomalies (Cont'd.)

Anomaly Type	Category	Description
Repair Weld Crack	planar (crack)	Poor repair welding practice such as, lack of preheat or use of single back weld run instead of two can result in hydrogen cracks associated with the repair weld.
Lack of Side Wall Fusion	planar (lack of fusion)	Lack of side wall fusion occurs as planar discontinuities between successive weld passes or between the weld bead and the pipe.
Lack of Root Fusion	planar (lack of fusion)	Lack of fusion between the edge of a fully penetrated root bead and the root face on one side - also known as 'missed edge'.
Lack of Penetration	planar (lack of fusion)	This refers to an incomplete penetration of the weld through the full thickness of the joint to leave an un-fused crevice in the root run.
Lack of Inter Run Fusion	lamination	Horizontal lack of fusion between adjacent weld beads ('cold laps').
Misalignment	geometrical inhomogeneity	Misalignment of the pipe ends across the weld bead produces an asymmetric weld, which is also known as 'Hi-Lo'.
Misplaced Cap	geometrical inhomogeneity	The weld capping run is misplaced to one side so that it does not fully cover the underlying filler pass.
Parallel Slag Lines	lamination	Linear voids or slag inclusions are most commonly found between the first and second pass welds in manual 'stovepipe' welds.
Porosity Cluster	inclusion	Porosity cluster refers to a group of pores within the weld metal.
Porosity Isolated	inclusion	Isolated gas pores in the weld metal.
Porosity Piping	inclusion	Also known as wormholes or herring bone porosity this appears as elongated porosity in the weld bead.
Root Porosity	inclusion	Root porosity is comprised of a continuous pore in the center of the root bead. It is also known as 'hollow bead'.
Porosity Scattered	inclusion	Scattered gas pores in the weld metal are caused by the weld pool solidifying too rapidly whilst supersaturated with dissolved gas.
Root Bead Slag Intrusion	surf-break lam	Trapped slag at the inside edge of the root weld bead is often associated with a crack-like lack of fusion defect.
Root Undercut	planar	A groove or channel melted into the pipe metal adjacent to the root or cap run which has not been filled with weld metal.
Solidification Cracks	planar (crack)	This occurs as a crack in the center of the weld bead, especially within hot pass. It is also known as 'hot tear'.
Stop Start Defect	planar or metal loss	This appears as a lack of fusion, a lack of fill or a lack of penetration at the stop / start position, often in the root bead.

Table 6-1 Overview of manufacturing related girth weld anomalies (Cont'd.)

Anomaly Type	Category	Description
Trapped Slag	inclusion	Slag trapped between individual weaves of the weld run ('slag holes').
Tungsten Inclusions	inclusion	Isolated inclusions of un-dissolved tungsten in the weld bead only appear as white spots on the weld radiograph.

Girth welds are also affected by anomalies occurring during the operational life, such as corrosion, SCC, and mechanical damage. Manufacture-related planar anomalies (e.g. lack-of-fusion, lack-of-penetration) can grow during the pipeline operation and become a threat for the pipeline integrity. Other anomalies may also foster the development of corrosion and cracking defects. Hardened spots from arc strikes can, for example, develop cracking in high strength hardenable steels. High hardness might encourage preferential corrosion in HAZ (heat-affected zone).

Regardless of an anomaly's origin, its morphology is the main detection and identification criteria for ILI. Apart from mechanical damage, three main anomaly categories are:

- Geometrical weld inhomogeneities,
- Volumetric anomalies (metal loss and metal gain), and
- Planar anomalies (crack, notch, etc.).

Specific ILI tools are specialized in the detection and sizing of each of the above categories.

6.2.1 Geometrical Weld Inhomogeneities

Geometrical inhomogeneities of girth welds are frequently detected by ILI tools.

- Misalignment of the pipe ends (out of roundness) produce asymmetric girth weld (Hi-Lo).
- Concave root, misplaced caps, stop-start-defects, irregular trimming and weld repairs are further examples of weld inhomogeneities.

Apart from their impact on the pipeline integrity, weld inhomogeneities and internal volumetric anomalies (e.g., excess root penetration) could influence the alignment of the ILI tool to the pipe surface (e.g., lift-off of sensor carrier) and so impair the detection and sizing performance in the affected section.

6.2.2 Volumetric Anomalies at/in Girth Weld

Metal loss is the main category of volumetric anomalies.

- Preferential Weld Corrosion (PWC) occurs both in the girth weld metal and heat-affected zone. PWC could affect large areas of the girth weld circumference.
- Axially extended general corrosion crossing the girth weld (e.g., int. channeling) can affect and reduce weld thickness.

- Internal corrosion pits in the girth weld and HAZ of crude lines have often higher depths than the pits in the neighboring pipe materials.
- Cap undercut, burn-through (window), lack of fill (stop-start-defects) are examples of manufacturing related metal loss anomalies that affect girth welds.

Girth welds have extra material in the form of weld cap (typically 1 mm and more) and root penetration. Excess cap height (typically at 12 o'clock) and excess root penetration (typically at 6 o'clock) are typical examples of metal gain in the girth weld.

Because of the weld bead curvature and the irregular pattern of the weld cap reinforcement, it is difficult to define accurately a depth threshold as reporting criteria for metal loss anomalies in girth welds. Since the sound pipe wall or nominal WT is the typical reference for the depth sizing and reporting, metal loss anomalies in the girth weld are usually reported if the remaining weld thickness of the anomaly is significantly smaller than the neighboring sound pipe wall.

6.2.3 Planar Anomalies at/in Girth Weld

Several types of manufacturing related planar anomalies occur at/in the girth weld and heat-affected zone (HAZ).

- Hydrogen cracking initiates at the weld cap or root region. Although modern girth welding standards require the removal of hydrogen cracks, hydrogen cracks have been found in vintage pipelines due to lack of inspection at the time of construction and in modern pipelines due to delayed hydrogen cracking.
- Lack of fusion (LOF) could affect root bead, side wall and weld metal.
- Lack of penetration of the weld through the full thickness leaves an unfused crevice in the root.

Cracking anomalies in the girth weld and HAZ could also develop and grow during pipeline operation.

Complicated girth weld geometry (misalignment, lack or excess penetration, sharp trimming edges, etc.) may negatively affect the detection performance of ILI tools for planar anomalies.

6.3 Main Categories of ILI Tools

The most common ILI tools for volumetric and planar anomaly are based either on ultrasonic (UT) or on magnetic-flux-leakage technologies (MFL). Caliper tools for detection of pipe ID changes and geometrical deformations are not covered in this section.

- UT wall thickness measurement tools (UT WM) and circumferential MFL are used to detect and size the dimensions of volumetric anomalies.
- UT crack detection tools (UT CD) and axial MFL are used to detect and size the dimensions of planar and semi-planar anomalies.
- EMAT crack detection tools (Electro Magnetic Acoustic Transducer) are becoming increasingly popular to inspect planar anomalies in gas pipelines. Although the EMAT technology can be basically applied to both axial and circumferential anomalies, the available EMAT ILI tools are specialized to axial cracking.

The following figure shows the main categories of ILI tools.

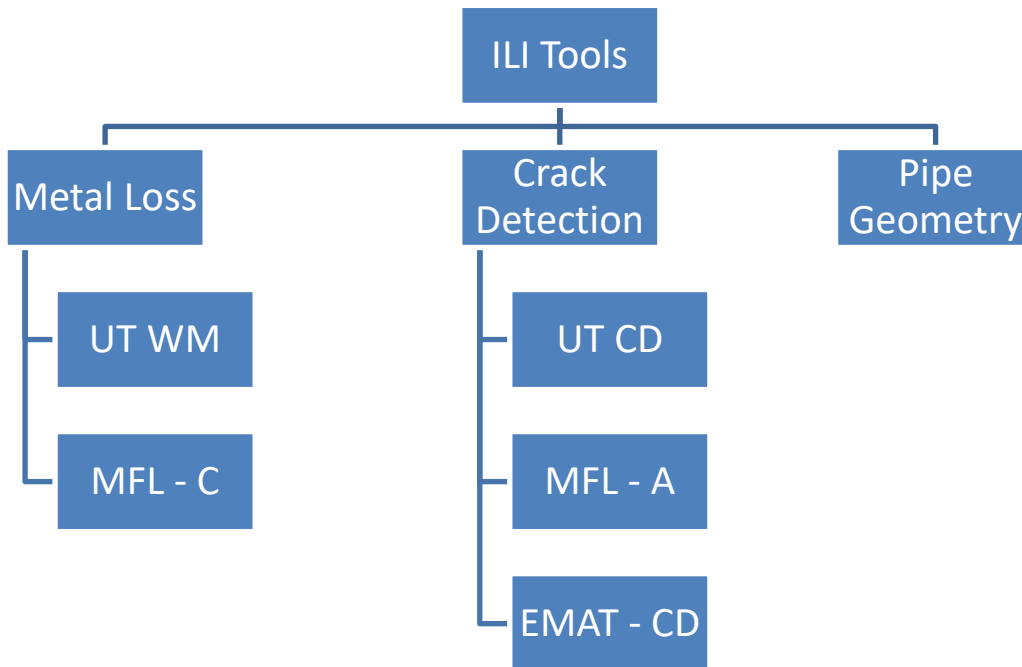


Figure 6-1 Overview of ILI tools and technologies

6.3.1 Ultrasonic Wall Thickness Measurement Tools

UT inspection is based on beam pulse echo technique. Figure 6-2 demonstrates its basic principle. In this technique, piezoelectric sensors are used as transmitter and receiver. The electrical excitation in the sensor is converted to an ultrasonic wave propagating in the liquid coupling medium and into the pipe wall or weld material. This wave is then reflected at interfaces, the multiple echoes reflected at front wall (internal surface of the pipeline) and back wall of the test material (pipeline) are received by the ultrasonic sensor and recorded.

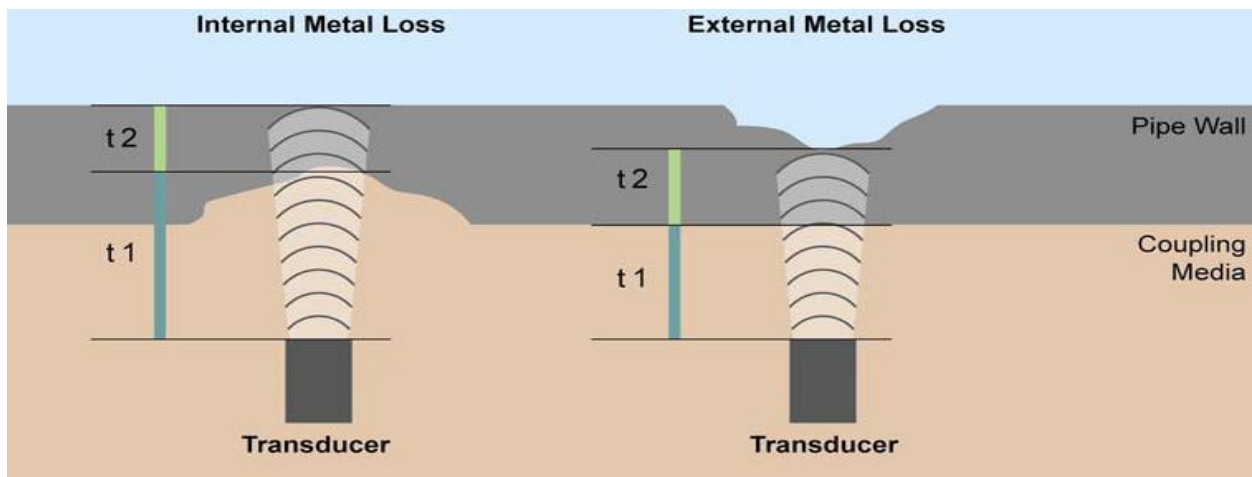


Figure 6-2 Schematic view of the ILI ultrasonic WT measurement (compression waves)

The UT wall thickness (WT) measurement is based on the so-called compression waves (straight beam) which propagate perpendicularly to the pipe surface (90°).

Measurement of the time-of-flight of reflected ultrasonic signal permits determination of the material thickness and the distance between the sensor and the front surface of the material (standoff distance).

- The measurement of WT and depth values is based on the sound velocity of steel which is constant (ca. 5920 m/s).
- The depth of internal anomalies can be additionally measured from the stand-off profile (redundant information). The sound velocity of the coupling medium influences calculation of the “Stand-off” (spacing between sensor and internal pipe surface).

The standard UT WM tools have a circumferential resolution (sensor spacing) of about 8 mm and axial resolution (data sampling rate) of about 1 mm to 3 mm. The circumferential resolution is defined for the tool class but the data sampling rate can be usually configured for the individual inspection run in consideration of the maximum tool speed during the run.

Since the volumetric anomalies in the girth welds are usually very short, it is useful to use tools with high resolution.

A typical performance specification of standard UT WM tools for metal loss anomaly is:

- Detection (POD of 90%) min. anomaly diameter of 10 mm and min. depth of 1.0 mm
- Depth sizing min. anomaly diameter of 20 mm and min. depth of 1.0 mm
- Depth sizing accuracy ±0.5 mm at 90% Confidence level

6.3.2 Ultrasonic Crack Detection Tools

The detection of planar anomalies is based on the UT shear waves (angle beam) which propagate transversally to the pipe wall. Figure 6-3 demonstrates its basic principle.

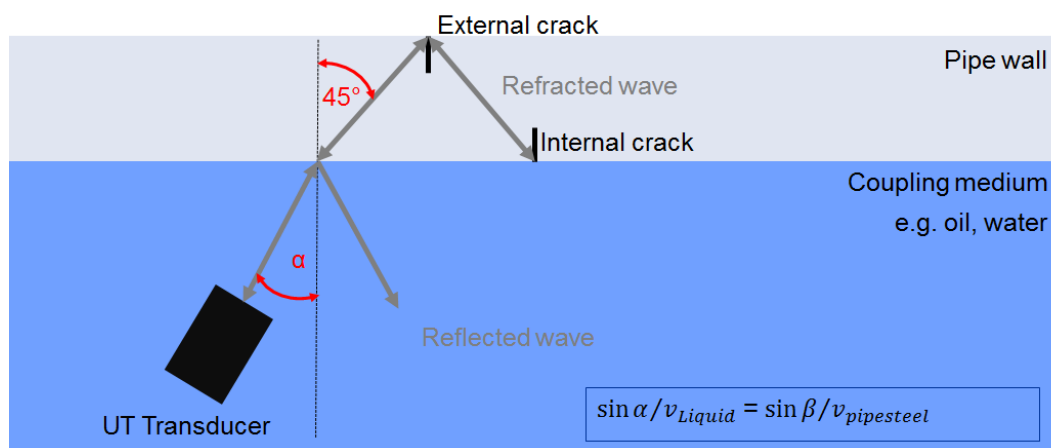


Figure 6-3 Schematic view of the ILLI ultrasonic crack detection (shear waves)

The shear waves should ideally propagate in 45° angle into the pipe wall. In order to achieve the optimum refracted angle of 45° in the pipe wall, the UT beam should propagate in the

coupling medium with an incidence angle of 16° to 19° , depending on the sound velocity in the propellant medium. Therefore, it is important to know the expected range of the sound velocity prior to the inspection in order to adopt mechanically the sensor-carrier to an inclination angle that creates the optimum propagation angle of the shear waves.

The attenuation of the coupling medium weakens the signal strength of UT shear waves. Highly damping liquids (e.g. heavy crude oil) can thus significantly reduce the signal strength and the quality of the UT data. Since the depth sizing is based on signal strength (amplitude), it is indispensable to know reliably the damping properties (attenuation) of the coupling medium (crude, diesel, water, etc.).

UT crack detection (CD) tools of different sensor carrier configuration are used for the detection of axially oriented and circumferential oriented planar anomalies. In both configurations, double number of angled sensors measure each position from two opposite sides. The sound beams of neighboring sensors overlap, enabling 100% coverage from each side.

In the UT CD tools for *axial cracks*, the UT sensors are circumferentially oriented and angled in both the clockwise (CW) and counter-clockwise (CCW) direction. The sensor spacing around the circumference for each direction (CW or CCW) is typically between of 7 mm to 10 mm. The UT CD tools for axial anomalies (UT CD-C) are the most commonly used crack detection tools, mainly for crude and liquid product pipelines.

In the UT CD tools for *circumferential cracks*, the UT sensors are axially oriented and angled in both the upstream (US) and downstream (DS) direction. The axial sensor spacing for each direction (US or DS) is typically in the range of 8 mm to 10 mm. The axial resolution (data sampling rate) is typically 2 mm to 3 mm.

The UT CD tools for circumferential anomalies (UT CD-A) are designated to detect circumferential planar anomalies of the girth weld and also in the pipe base material. UT CD-A tools are generally much less used in comparison to the tools for axial cracks detection. Figure 6-4 shows a schematic view of UT CD detection of circumferential crack at the girth weld.

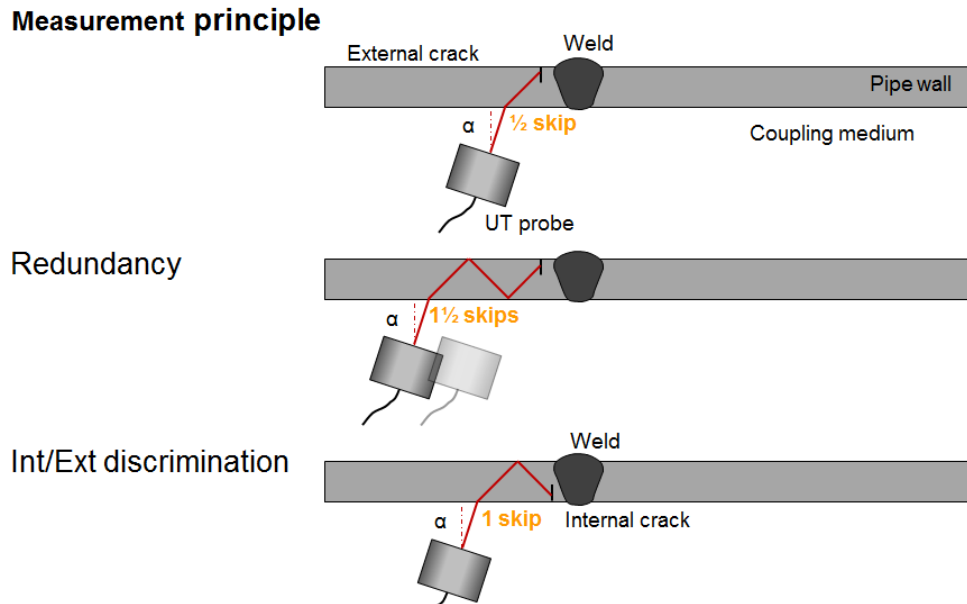


Figure 6-4 Schematic view of the UT detection of circumferential crack at girth weld

The depth sizing of the crack detection tools is historically provided in four depth classes (buckets):

- depth class of < 1 mm
- depth class of 1 mm – 2 mm,
- depth class of 2 mm to 4 mm
- depth class of > 4 mm

Up to crack depth of 4 mm, the crack depth is nowadays reported as a discrete depth with an accuracy interval (e.g. 2.7 mm \pm 1.0 mm). Crack depths above 4 mm cannot be further differentiated because of signal saturation.

6.3.3 Axial Magnetic Flux Leakage

Magnetic flux leakage (MFL) represents robust technology to detect and size structural changes and volumetric flaws at girth welds. By inducing a strong saturating magnetic field in the pipe wall high coverage of response signals is achieved. Between two yoke shoes a closed magnetic circuit is built easily penetrating a girth weld. Even smallest changes in the structure or thickness of the wall generate magnetic field disturbance signals. These are recorded with highly sensitive hall sensors or coils optionally in all three principal directions, axial, circumferential and radial.

The axial conventional MFL technology has the following major advantages making it suitable for girth welds anomalies:

- MFL is not only sensitive to volumetric flaws but also to the tiniest changes in the wall thickness.

- In addition to metal loss anomalies, the axial MFL tool can detect semi-planar anomalies with a very small volumetric component like lack of penetration, lack of fusion and cracks with an opening >0.1 mm. The axial MFL tools can contribute to distinguish semi-planar anomalies (e.g. lack of root penetration) from purely planar anomalies with negligible crack opening.

Semi-planar anomalies and open cracks have produce shorter magnetic flux leakage signal in comparison to volumetric anomalies. Therefore, it is useful to increase the resolution of the axial MFL tool for crack detection (higher data sampling rate).

The continuous data recording of an MFL tool at a girth weld creates a signal which is superimposing three principal sources:

- The normal structure of the weld causing a signal comparable to an inverted metal loss signal, because of the extra metal of the weld bead reinforcement. This normal girth weld signal has the major advantage to be principally homogenous for the entire circumference and very similar for all the welds of the same manufacturing. The detection of a flaw therefore mainly is defined as difference to the circumferential background or generally expected signal.
- The lift-off of the sensor pad caused by the weld root penetration, dynamically susceptible also to the passage velocity, i.e. impulses caused by the interaction.
- Abnormal structural elements in the girth weld or its vicinity.

The detection of a volumetric flaw at girth welds depends on the special individual combination of the three factors mentioned above. For instance, a 5% deep internal pinhole may cause a clearer signal in the center of the root than in straight pipe, but becomes invisible if the sensor starts to jump at a certain speed. The detection performance at girth welds is a complex individual consequence of all interacting factors, not only the geometry of the flaw itself. The differences in signal between the normal weld signal and the abnormal signal will also contain components which are affected by the individual mechanical and geometrical situation of the measurement at the girth weld.

6.3.4 EMAT Crack Detection

EMAT (Electro Magnetic Acoustic Transducer) is ultrasonic based NDE technology that does not require liquid coupling medium. Therefore, the EMAT based ILI tools are mainly used for the inspection of gas pipelines.

The ultrasonic waves are generated directly in the pipe wall. A coil induces eddy currents in the presence of a magnetic field and creates forces that excite ultrasound beam in the pipe wall.

EMAT technology can be basically applied both to volumetric anomalies (like UT WM) and to planar anomalies (like UT CD). EMAT technology is so far mainly used for crack detection. It has some significant differences in comparison to liquid coupled UT CD and axial MFL tools.

- EMAT does not require liquid coupling.

- The crack opening has no impact on the detection capability of the EMAT tools. Like the UT CD tools, EMAT tools can also detect purely planar anomalies without any volumetric component (crack without visible opening).
- The crack depth sizing of EMAT is discrete (no depth classes) and has no upper limit of the depth differentiation like UT CD tools with the signal saturation effect.
- EMAT tools for circumferential cracks and thus for girth weld anomalies are not commercially available presently.

7 Fitness-for-Service Assessment

Abstract

In this section, the framework of FFS assessment is first introduced. In broad terms, FFS assessment involves the comparison of strain demand and strain capacity. A pipe segment or a weld is deemed safe when the strain capacity is higher than the strain demand by a sufficient margin.

FFS assessment procedures are divided into three categories, depending on the loading mode and the level of strain demand:

- *FFS procedures under small tensile strain,*
- *FFS procedures under moderate to large tensile strain, and*
- *FFS procedures under compressive strain.*

Within each category, the procedures are covered with the following elements:

- *Applicability and limits,*
- *Fundamental basis,*
- *Key considerations and key input parameters to the procedures, and*
- *Example applications.*

The application of FFS assessment procedures under various field scenarios is described in Section 9 in which the overall hazards management process is outlined.

The sample applications, such as alternative X-Ray criteria and tensile strain capacity of manual welds, are meant to demonstrate the capabilities and possible use of FFS assessment for conditions outside general industry knowledge. The outputs/numbers in those sample application cases should not be taken literally as conditions for proper FFS assessment are site-specific.

7.1 Framework of FFS Assessment

Two predominant limit states associated with high longitudinal stresses and strains are tensile leak/rupture and compressive buckling (see Figure 7-1). The fitness of the pipeline may be assessed by comparing the strain demand and strain capacity, as shown Figure 7-2. If the capacity is determined to be greater than the demand by a sufficient margin of safety, the pipeline is deemed safe.

As described in Section 1.2, other limit states can involve (1) tensile failure in the hoop direction due to the local high hoop strains from wrinkles and buckles, (2) tear of materials in the longitudinal direction, e.g., along seam weld, due to very high location strains from severe wrinkles and buckles, and (3) fatigue flaw growth in areas of local high strains. Although procedures/tools are available to assess those limit states, such assessment requires specialized analysis on a case-by-case. The focus of this section is the assessment of tensile rupture, particularly that of girth weld, and compressive buckling.

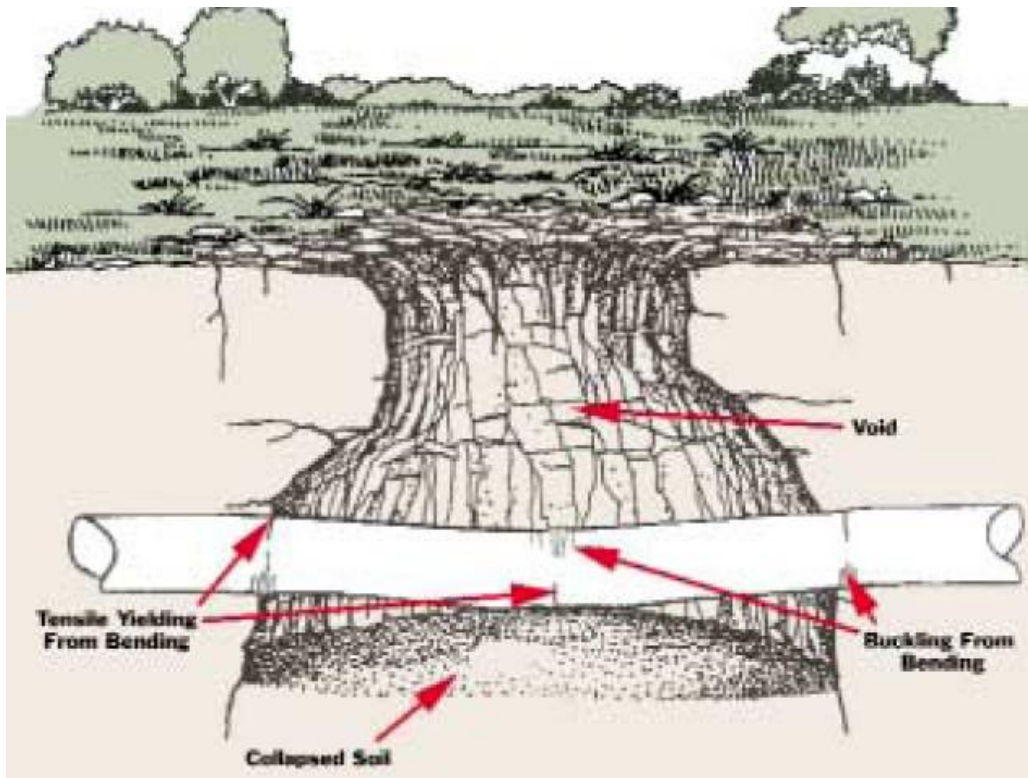


Figure 7-1 Possible failure models of a pipeline due to mine subsidence

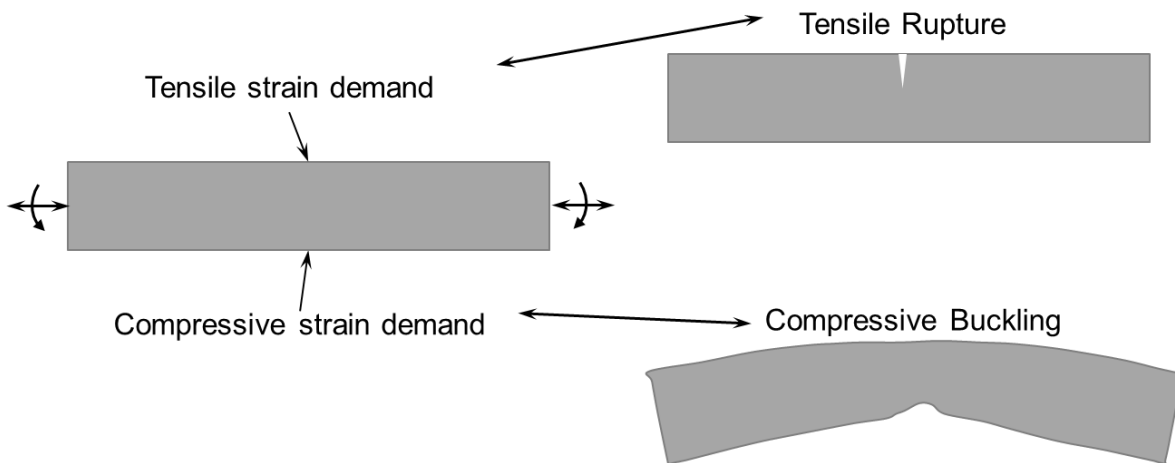


Figure 7-2 Schematic illustration of the relationship between strain demand and strain capacity in FFS assessment

7.2 FFS Assessment at Small Tensile Strains

7.2.1 Applicability of Traditional Stress-Based FFS Assessment Procedures

Traditional stress-based FFS assessment procedures are formulated to provide accurate assessment when the applied stress is slightly below the yield strength. The customary definition of linepipe’s yield strength is at 0.5% total strain. The 0.5% strain is beyond the elastic proportional limit for linepipe steels. For instance, if the material response is completely linear

elastic up to the yield strength, the proportional limit of the strain for a steel of yield strength of 60 ksi is 0.2% ($0.2\% = 60/30,000$, where 30,000 ksi is the elastic modulus of the steel). Figure 7-3 shows a sub-set of the stress-strain curves of Figure 5-9 at small strain and the definition of yield strength at 0.5% total strain. The strain at linear elastic limit is lower than 0.5% strain.

When strains are greater than elastic limit, the accuracy of stress-based assessment procedures in resolving strains becomes poor. These procedures are designed to resolve stresses. When the strains are greater than elastic limit, a small change in stress is associated with large change in strain. In order to resolve small changes in strains, the procedures need to be extremely precise in resolving stresses.

The upper bound strain level at which the stress-based FFS procedures may be applied can be determined by setting the upper limit of stress at 90% SMYS. The strain level corresponding to this stress level varies, depending on the yield strength of the material. For instance, for X52, X60, X65, and X70 pipes, the corresponding strain levels are 0.17%, 0.18%, 0.20%, and 0.21%, respectively. Therefore, the stress-based FFS procedures are good to strains levels up to approximately 0.2%.

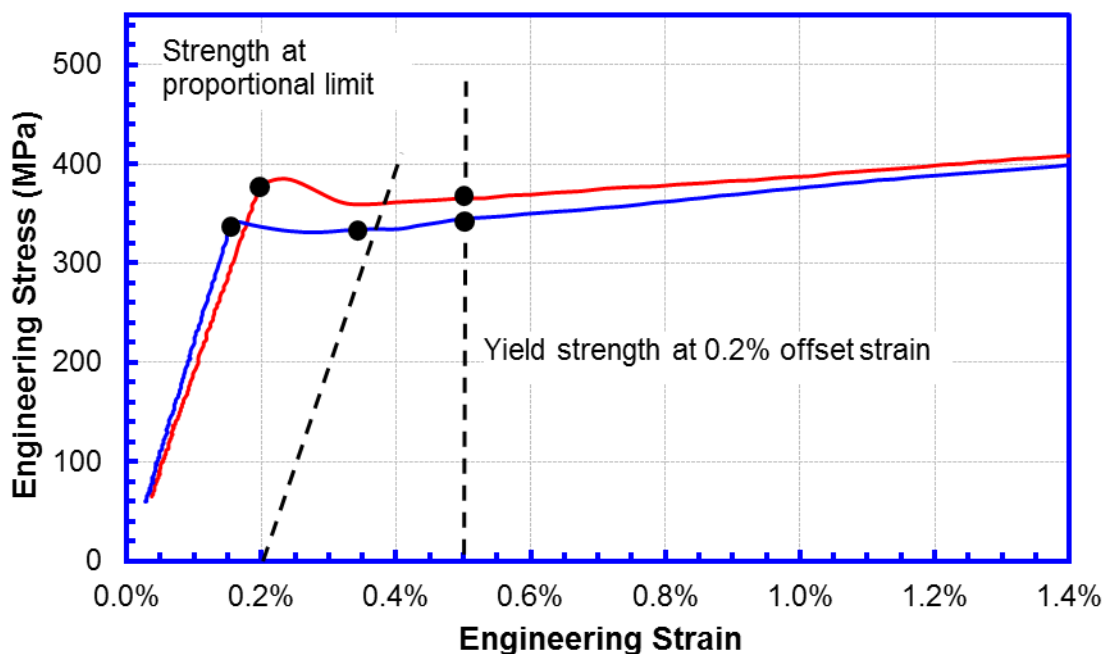


Figure 7-3 Definition of yield strength relative to stress-strain response

7.2.2 Fundamentals of Stress-Based FFS Assessment Procedures

Some of the most frequently used stress-based FFS procedures are API 1104 Annex A [138], CSA Z662 Annex K [139], BS7910:1999 [140], API 579 [141], and DNV OS F101 [142].

Most of the recent stress-based FFS assessment procedures use the concept of failure assessment diagram (FAD). The FAD approach was first proposed by the Central Electricity Generating Board (CEGB) in the United Kingdom in 1976. The procedure was termed R-6

procedure after the report number issued that year [143]. The original R-6 procedure used Dugdale strip yield model which was only applicable to elastic perfectly plastic materials. The procedure has since been extended to materials with strain hardening by replacing yield stress with flow stress (the average of the yield stress and tensile stress). The FAD-based ECA allows the simultaneous consideration of brittle fracture, plastic collapse, and the interaction between those two failure modes (elastic-plastic fracture). The three key components that constitute the FAD-based ECA are:

1. Failure assessment curve (FAC),
2. Stress ratio, S_r or L_r , and
3. Toughness ratio, K_r .

These three key components are shown graphically in Figure 7-4 [144]. The FAC is a locus that defines the critical states in terms of the stress and toughness ratios. The stress ratio is the ratio of the applied stress over the plastic collapse stress. It defines the likelihood of plastic collapse. The toughness ratio is the ratio of applied crack driving force over the material's fracture toughness. It defines the likelihood of fracture. For a structure with a known defect, the stress and toughness ratios define an assessment point in the FAC plane. If the point falls inside the FAC locus, the structure is deemed safe.

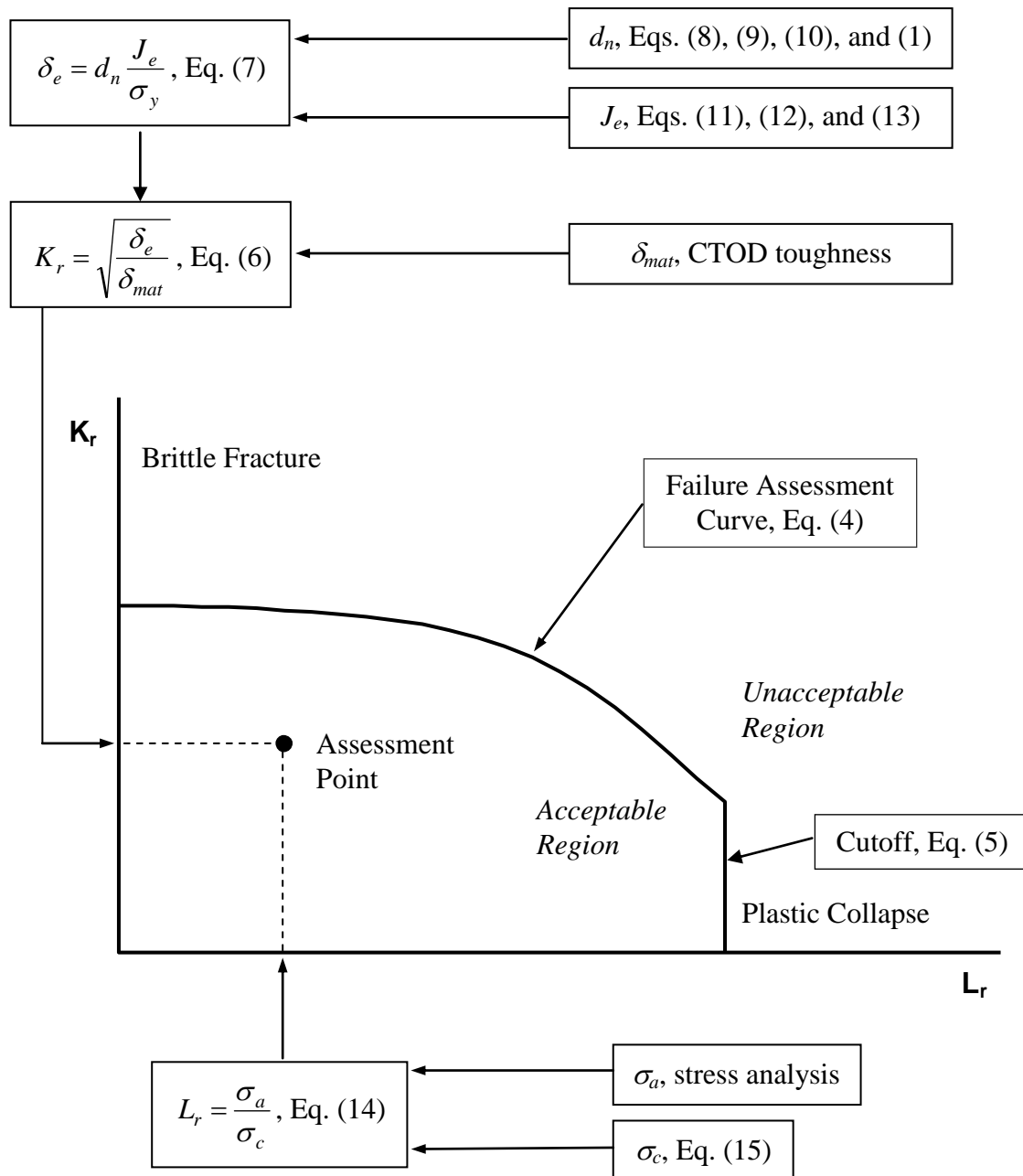


Figure 7-4 FAD structure and associated equations for the application of API 1104 Appendix A Option 2 approach. The equation numbers in the text boxed refer to the equations in the API 1104 Appendix A document.

7.2.3 Key Considerations in Applying Stress-Based FFS Assessment Procedures

For pipeline girth welds, the stress-based FFS assessment procedures, such as API 1104 Annex A and CSA Z662 Annex K, have been successfully applied to new pipeline construction. The fundamental basis of those procedures is applicable to in-service pipelines, when appropriate values of input parameters can be determined or estimated. For in-service pipelines, the FFS

procedures may be applied in one of two ways. The first one is comparing the critical flaw size (the maximum flaw size at the point of incipient failure) with the estimated flaw dimensions (that can come from ILI indications or other inspection methods). If the estimated flaw size is smaller than the critical size, the girth weld is deemed safe. The second approach is comparing the maximum permissible stress/strain at the point of incipient failure with the anticipated applied stress/strain on the weld. If the anticipated stress/strain is lower than the maximum permissible stress/strain, the weld is deemed safe for continued operation.

There are practical differences in applying FFS assessment procedures to in-service pipelines, particularly vintage pipelines, vs. new pipeline construction. The principle difficulties for in-service pipelines is the lacking of appropriate material properties, uncertainties with flaw dimensions and stresses experienced by the segment of interest, particularly girth welds. The estimation of those parameters is discussed below.

7.2.3.1 Characterization of Girth Weld Flaws

Girth weld flaws can be characterized by ILI tools or in-ditch inspection. ILI tools are further divided into free-flowing tools and tethered tools. ILI tools are preferred when inspecting long segments of pipelines. These tools are capable of locating and characterizing anomalies such as mechanical damage (dent and gouges), corrosion, wrinkles, and cracks. The possibility to find a particular anomaly depends on a number of factors, including the anomaly size and orientation, pipeline condition such as material variation, proximity to other features, construction practices, and debris and deposits, etc. [145, 146]. There are no universal intelligent pigs able to detect and size all laws. A given type of inspection tool is designed to look for a specific type of anomalies [147, 148, 149].

When performing FFS assessment, it is critical to recognize the capabilities and limitation of inspection tools. For instance, current MFL tools are capable of providing the length of indications of certain features in girth welds, but they are not capable of discerning the nature of the indications and the height or depth of anomalies. More on the capabilities and limitations of various tools are given in Section 6.

7.2.3.2 Flaw Types

Flaws in a girth weld can be either surface-breaking or buried in terms of their position in the pipe wall thickness direction. Flaws can be either volumetric, such as slag or porosity, or planar, such as cold cracking or IPD.

As shown in Section 5, a large proportion of the flaws in vintage girth welds are volumetric, such as porosities and slags. Extensive experimental tests have shown that that buried volumetric flaws are not a structural integrity concern in pipeline girth welds. Planar surface-breaking defects are the most detrimental to the integrity of girth welds. In API 1104 Annex A, buried flaws are conservatively treated as surface-breaking flaws of the same dimensions.

When the nature of the flaws is not precisely known, they are conservatively treated as planar surface-breaking flaws in FFS assessment.

7.2.3.3 Flaw Height

As shown in Section 5, most of the planar and volumetric flaws in vintage girth welds have a height of 2 mm. The length of those flaws can vary significantly, but most have a length of less than 4-6 in. The flaw height in some cases can be as high as 4-5 mm.

It's a generally sound practice to correlate flaw height with weld bead height. Most flaws are one weld bead height, typically 2-3 mm. In less common cases, the flaw height can be of two weld bead height, typically 4-6 mm.

In rare cases when hydrogen cracking was found to be a major contribution to field failures, the height of these cracks can be as large as nearly full nominal wall thickness; only weld cap provides the pressure boundary. It may be argued that, in some extreme cases, the flaw height can be such that only one weld bead is left as the remaining ligament (as the pressure boundary). This extreme assumption about flaw height is not reasonable for assessing long segments of pipelines as such instances are rare. Furthermore such assumption can lead to "predicting" failures of many welds. Such an outcome is not helpful in developing practical maintenance actions.

7.2.3.4 Fracture Toughness

One key difference between the new pipeline construction and the in-service pipeline is the availability of material's toughness. In new pipeline construction, the toughness is determined in the welding procedure qualification before field welding. For in-service pipelines, destructive testing of a particular weld of interest is not possible. Therefore, the toughness is often estimated from welds of similar vintage for which test data are available.

The material toughness in API 1104 Appendix A is expressed in CTOD. For in-service girth welds, the most widely available toughness is Charpy impact energy. A generally accepted conversion process from Charpy impact energy to CTOD toughness is used to derive the CTOD toughness. The Charpy energy may be converted to material's toughness in stress intensity factor (K_{mat}) [150],

$$\left(\frac{K_{mat}}{\sigma_y} \right)^2 = 0.52 \left(\frac{C_v}{\sigma_y} - 0.02 \right) \quad (7-1)$$

where K_{mat} is in the unit of $\text{MPa}\sqrt{\text{m}}$, the Charpy energy in the unit of Joule, and the yield strength in the unit of MPa.

The K_{mat} may be converted to J_{mat} (in the unit of MN/m) using the following relation,

$$J_{mat} = \frac{(K_{mat})^2}{E/(1-\nu^2)} \quad (7-2)$$

where E is elastic modulus in the unit of MPa and ν is the Poisson's ratio. The J_{mat} may be converted to CTOD toughness (δ_{mat}) through the following relation [151],

$$\delta_{mat} = d_n \frac{J_{mat}}{\sigma_y} \quad (7-3)$$

where d_n is a dimensionless conversion constant that is related to material's strain hardening exponent n . For most pipeline steels, the value of d_n is in the range of 0.5-0.8. The value of d_n can be obtained from Y/T ratio using a relationship in API 1104 Appendix A.

Equations (7-1) to (7-3) establish the relationship between Charpy impact energy and the CTOD toughness. For a given Charpy impact energy, the CTOD toughness is estimated from the relationship for the development of tolerable flaw size.

Test data from Section 5 show that a reasonable lower bound full-size Charpy energy is 20-30 ft-lb is converted to a CTOD toughness of 0.031-0.046 mm. This CTOD toughness is relevant to a test specimen under bending load. Girth welds with anomalies are under tension load. As shown in Appendix F, materials under tension behave tougher than under bending. The apparent increase in toughness is attributable to the so-called constraint effects [152]. The increase of toughness is generally accepted in the range of a factor of 2-3 as given in CSA Z662 Annex C [139].

Based on the evidence presented above, reasonable lower bound CTOD toughness for applying stress-based FFS assessment is 0.1 mm.

7.2.3.5 Applied Stress Level

Except in rare occasions, longitudinal stresses in pipelines are generally unknown. As shown in Table 3-1, a stress level of 50-60% SYMS is a reasonable baseline value. For lower grades, the stress level relative to SYMS is on the higher range, because the stress from temperature differential is independent of pipe grade. The design limit for longitudinal stress in ASME B31.4 and B31.8 is 90% SYMS for most pipelines.

For case-specific assessment, a stress level of 75%-90% SMYS is proposed. For screening purposes, a stress level of 60%-75% is proposed. These proposed stress levels are applicable for pipe segments with nominal settlement after construction, but without evidence of ground movement, unsupported spans, or insufficient negative buoyancy.

7.2.4 **Alternative X-Ray Criteria**

One of the key contributors to the occasional girth weld failures of vintage pipelines is the existence of large flaws left from construction. Given the difficulties associated with the detection and sizing of those flaws by in-line tools, an operator may choose in-ditch NDT – typically X-ray or ultrasonic testing (UT) – and decide if the welds should be repaired, cut out, or a segment of the pipeline should be replaced. The seemingly logical criteria for making such decisions are the workmanship flaw acceptance criteria in API 1104 or equivalent standard. In fact, bringing welds to current code requirements can be mandated by regulators.

The workmanship criteria in API 1104 are intended as a construction quality control measure with no built-in or assumed performance target. Flaw height, which plays a critical role in weld performance, is a not part of the criteria. All welds, regardless of their mechanical properties and wall thickness, have the same allowable length.

FFS procedures in Appendix A of API 1104 are applied to develop allowable flaw length a few sample cases, including a range of pipe diameter, wall thickness, and grades, as shown in Table 7-1. Two levels of longitudinal stress are assumed for the basis given above. Similarly two levels of CTOD toughness are assumed. The flaw heights are given as one weld bead height (2.5 mm), two weld head height (5.0 mm), or three weld bead height (7.5 mm). The maximum flaw height is capped to a limit so the remaining ligament would be approximately one weld bead height (2.5 mm), representing nearly worst case scenario. All flaws are planar surface-breaking.

The maximum allowable flaw length in Table 7-1 is capped at 25% of the pipe circumference even when the FFS assessment procedure produces greater allowable length. It is evident that the minimum allowable flaw length is slightly greater than 1.0 in, which is the allowable flaw length in the workmanship criteria for planar flaws. The allowable flaw length in most cases is much greater than 1.0 in. These sample cases demonstrate that FFS assessment procedures can be applied to achieve consistent level of integrity and safety while reducing the number of unnecessary repairs and cutouts. These sample cases also shown that the workmanship criteria in API 1104 are poorly suited for assessing the girth weld performance of in-service vintage pipelines.

Table 7-1 Allowable flaw length per API 1104 Appendix A FFS procedure with the listed pipe dimensions, material properties, and applied longitudinal stress level

Diameter and WT	Pipe Grade	Flaw Height	CTOD = 0.1 mm				CTOD = 0.2 mm			
			Longitudinal Stress / SMYS				Longitudinal Stress / SMYS			
inch, inch		mm	0.75		0.90		0.75		0.90	
			mm	inch	mm	inch	mm	inch	mm	inch
26, 0.281	X52	2.5	519	20.4	122	4.8	519	20.4	145	5.7
		4.5	108	4.3	44	1.7	185	7.3	68	2.7
	X60	2.5	514	20.2	110	4.3	519	20.4	137	5.4
		4.5	97	3.8	39	1.5	164	6.5	62	2.4
36, 0.375	X65	2.5	718	28.3	189	7.4	718	28.3	210	8.3
		5.0	135	5.3	49	1.9	231	9.1	87	3.4
		7.0	71	2.8	31	1.2	119	4.7	51	2.0
	X70	2.5	718	28.3	177	7.0	718	28.3	201	7.9
		5.0	126	5.0	45	1.8	217	8.5	82	3.2
		7.0	66	2.6	29	1.1	112	4.4	48	1.9
42, 0.500	X70	2.5	838	33.0	314	12.4	838	33.0	314	12.4
		5.0	223	8.8	72	2.8	420	16.5	138	5.4
		7.5	97	3.8	37	1.5	173	6.8	67	2.6
	X80	2.5	838	33.0	269	10.6	838	33.0	269	10.6
		5.0	190	7.5	58	2.3	347	13.7	120	4.7
		7.5	82	3.2	32	1.3	151	5.9	59	2.3

7.3 FFS Assessment at Large Tensile Strains

7.3.1 Factors Affecting Tensile Strain Capacity

The tensile strain capacity of a pipeline is dominated by the tensile strain capacity of its girth welds. The girth welds here refer to the entire weld region, including the weld metal, the fusion boundary, and the heat-affected zone (HAZ). Girth welds tend to be the weakest link due to the possible existence of weld defects and often deteriorative metallurgical and/or mechanical property changes from welding thermal cycles. Consequently, tensile strain capacity (TSC) is intrinsically related to the metallurgical and mechanical properties of linepipes and girth welding procedure.

The dominant factors that affect tensile strain capacity are:

- *Weld profile*, broadly referring to the cross-sectional profile of girth weld, including the height and width of weld cap reinforcement, high-low misalignment, etc.

- *Weld strength mismatch*, referencing to the relative strength different between the deposited weld metal and base pipe
- *Heat-affected zone softening, or lack of it*. Both the width of the softened zone and the magnitude of the softening are important.
- *Weld bevel geometry*. The bevel angle and the width of the weld metal relative to the thickness of the pipe are influencing factors.
- *Flaw type and dimensions*. Planar surface-breaking flaws are more detrimental than buried volumetric flaws. For most flaws with aspect ratios found in realistic welds, flaw height is more critical than flaw length.
- *Fracture toughness*. For pipes with light to moderate wall thickness (up to about 0.5 in or 12.7 mm), initiation toughness is much more important than stable ductile growth resistance.

7.3.2 Physical Process of Tensile Rupture

The physical process of a tensile strain failure starting from a planar girth weld flaw may be described as follows. Under increasing stress or strain, the flaw first blunts from the initial sharp flaw. The blunted flaw initiates ductile tearing upon further loading. The small ductile tear then grows in size, and eventually forms a growing flaw with a sharp tip. The initial blunted profile remains behind the sharp flaw. The evolution of the flaw profiles is shown in Figure 7-5.

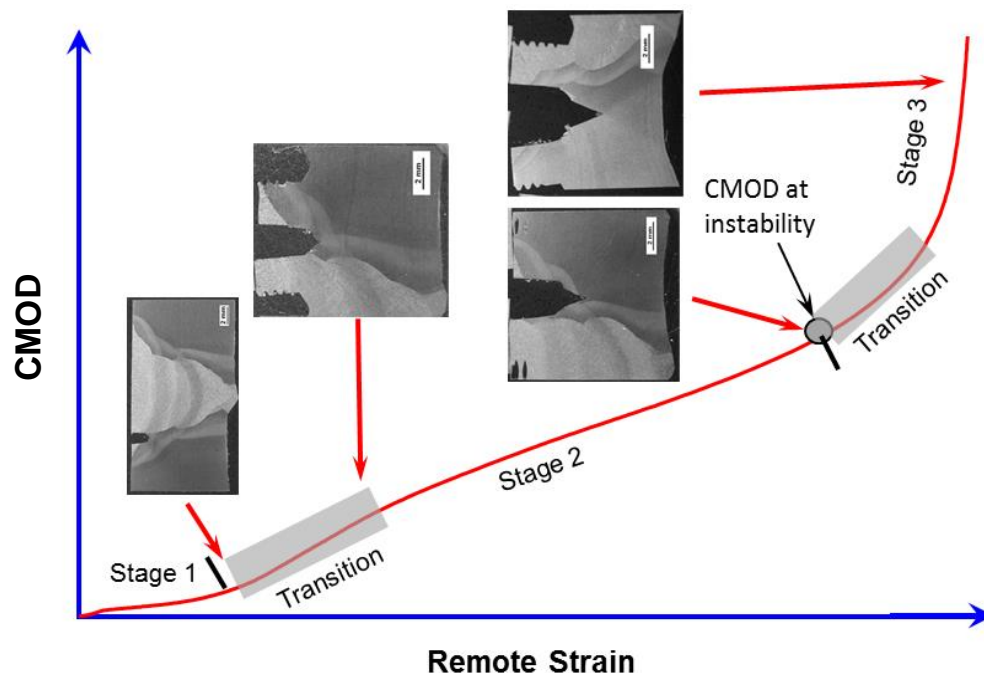


Figure 7-5 Behaviour of a girth weld flaw under increasing longitudinal tensile strain

The significance of flaw growth is shown by the sequence of the growth relative to the remote tensile strain. The strain vs. flaw growth history of the full-scale tests conducted by JFE

is shown in Figure 7-6 [153]. At 0.5 mm flaw growth, the strain is at approximately 2.4%. At the point of leakage, the strain is approximately 2.6% and the flaw growth is 2.0 mm. Much of the flaw growth occurs near the final leakage point accompanied by a small increase of remote strain. This and other similar tests have shown that once the flaw growth rate starts to accelerate, the remaining additional strain capacity is limited. Much of the strain capacity comes from the straining process prior to a small amount of flaw growth. Therefore, setting the limit state for tensile strain capacity at the ductile flaw initiation is a physically sound and accurate representation of material's strain capacity.

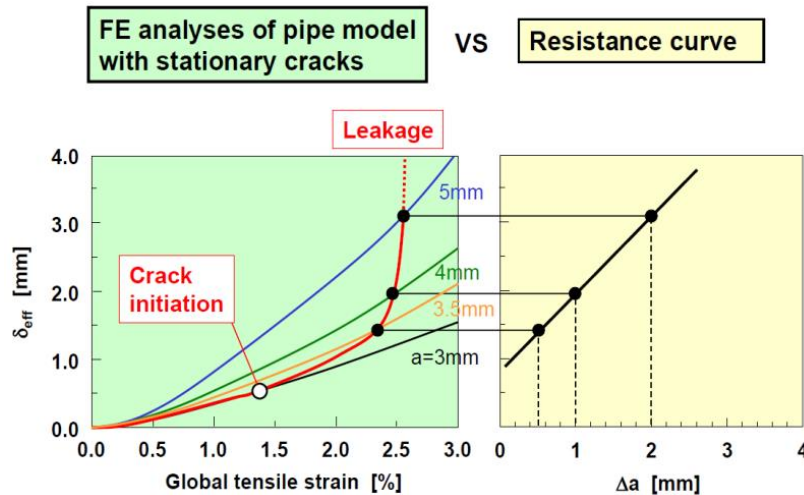


Figure 7-6 Flaw growth vs. strain history from a full-scale pipe test [153]

7.3.3 Applicability of Tensile Strain Models

7.3.3.1 Tensile Strain Models for New Pipeline Construction

Tensile strain models developed in the last decade principally targeted for new pipeline construction in areas expected to have ground movement hazards [154, 155, 156]. The two predominant models are the PRCI-CRES models developed with the support of US DOT PHMSA [157, 158, 159, 160] and the ExxonMobil models [161, 162, 163, 164, 165]. Early work supported by PRCI [166, 167, 168, 169, 170, 171, 172, 173] has been largely superseded by the more recent models. SINTEF was also earlier developer of tensile strain models [174, 175, 176]. Other less used or newer tensile strain models in various stages of development are those by JFE [177, 178, 179], the University of Gent [180] and TWI [181].

The intended principal applications of those modes are:

- New pipeline construction,
- Modern line steels,
- Mechanized welding processes, and
- Moderate to high level of applied strains. For instance, the PRCI-CRES models have a lower bound applicable strain of approximately 0.75%. The upper bound of

applicable strain is about one third of the pipe material's uniform strain. Many modern microalloyed linepipe steels have a uniform strain of 6-10%. Therefore, the models are good for strains up to a range of 2-3%³.

In Section 7.3.4, the PRCI-CRES models are further described as an example of the recent tensile strain models.

7.3.3.2 Tensile Strain Models for In-Service Pipelines with Manual Girth Welds

A PRCI funded effort is under way to develop tensile strain models for in-service pipelines with manual girth welds [182]. The initial focus is on pipelines constructed without the use of modern microalloyed steels, approximately before mid- to late 1960s in North America. The models are suitable for strains greater than approximately 0.2%. This work is scheduled to be completed by the first half of 2017.

7.3.3.3 Use of Tensile Strain Equations in CSA Z662 Annex C

In the 2007 Edition of CSA Z662 [183], a set of equations for computing tensile strain capacity was included as a Tier 2 approach based on work funded by PRCI [169, 170]. The equations gained popularity in some operators because its simplicity and ease of use. In the most recent publication of CSA Z662 (2015 Edition), these equations were removed from the Annex C without replacement. Although not officially confirmed, one of often-cited reasons is the equations *did not consider* the effects of internal pressure. This is a mischaracterization of the historical events and the outcome can be misleading.

By the time those equations were being incorporated in Annex C of CSA Z662, the potential impact of internal pressure on tensile strain capacity was starting to emerge, but there was no sufficient work to determine the magnitude of the impact. As a precautionary measure, the apparent toughness, which is used to compute tensile strain capacity, was set to have an upper bound limit of 0.3 mm. This effectively eliminated the possibility of over-predicting tensile strain capacity even in the presence of internal pressure. Recent comparisons of tensile strain capacity prediction among different models and with experimental data show that the equations in CSA Annex C were almost always conservative [184]. In some cases, these equations tend to be overly conservative. In summary, the equations in CSA Z662 Annex C are conservative, even when the internal pressure is not an input parameter in those equations.

7.3.4 Building Blocks of PRCI-CRES Models

The PRCI-CRES models are fully documented in two comprehensive reports to PHMSA [185, 186] and in conference publications [157, 158, 159, 187, 188]. These models are used as an example to demonstrate the concept of tensile strain models.

³ As described in Section 9.1.2, ASME B31.4 and B31.8 have a design strain limit of 2.0%. With uncertainties associated with factors affecting tensile strain capacity, it is recommended that upper bound strain demand limit be limited to 2.0% unless case-specific justifications can be made to allow for higher strain limit.

7.3.4.1 Limit States

Two limit states are recognized in the PRCI-CRES models.

The initiation-control tensile limit state is achieved when the crack driving force δ_F or δ_F reaches material's apparent toughness δ_A or δ_A . The apparent toughness is the toughness corresponding to the onset of stable tearing. Both δ_F and δ_A are represented by the crack tip opening displacement, i.e., CTOD. The strain corresponding to the apparent toughness is the tensile strain capacity (TSC), i.e., ϵ_t^{crit} . This limit state is schematically shown in Figure 7-7. The ductile instability limit state is achieved when the crack-driving force, δ_F , is about to exceed the resistance, δ_R , when the flaw grows. This limit state is schematically shown in Figure 7-8.

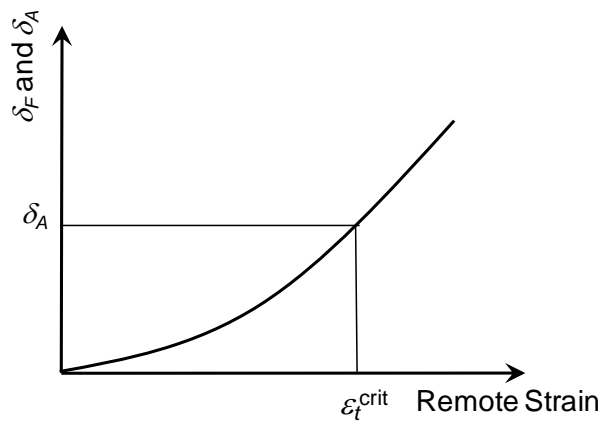


Figure 7-7 Schematic illustration of initiation-control limit state

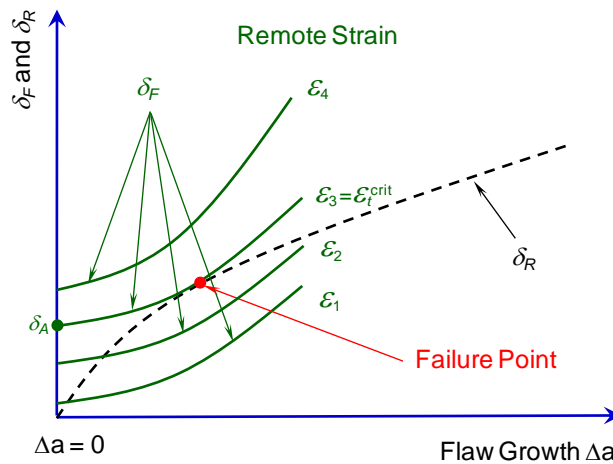


Figure 7-8 Schematic illustration of ductile instability limit state

7.3.4.2 Crack-Driving Force

7.3.4.2.1 Development of Crack-Driving Force Relations

The crack driving force, $CTOD_F$ or δ_F , is given as a function of remotely applied nominal strain, ε_F , as shown in Figure 7-7 and Figure 7-8. The relationship between δ_F and ε_F is obtained through extensive finite element analysis (FEA). The FEA incorporated the following parameters:

(1) Geometric parameters:

t	pipe wall thickness, mm,
a	flaw height, mm,
$2c$	flaw length, mm, and
h	girth weld high-low misalignment, mm.

(2) Material parameters:

σ_y	pipe yield strength, MPa,
σ_U	pipe ultimate tensile strength, MPa,
σ_U^W	weld metal tensile strength, MPa, and

(3) Loading parameter:

f_p	pressure factor, ratio of applied hoop stress to pipe yield strength.
-------	---

Weld profiles representing narrow-groove mechanized GMAW and standard groove SMAW and FCAW processes were incorporated into finite element models. A database of crack-driving force was generated from the FEA. Two sets of parametric equations, one for GMAW and one for FCAW/SMAW, were developed from the database. These equations use the following normalized parameters:

$\eta = a/t$	normalized flaw depth,
$\beta = 2c/t$	normalized flaw length,
$\psi = h/t$	normalized weld high-low misalignment,
$\xi = \sigma_y/\sigma_U$	base metal Y/T ratio,
$\Phi = \sigma_U^W/\sigma_U$	weld metal strength mismatch ratio
f_p	pressure factor, ratio of applied hoop stress to pipe yield strength.

7.3.4.2.2 Parametric Form of Crack-Driving Force Relations

The crack driving force relationship takes the following generic form,

$$\varepsilon_F = \min(\varepsilon_u, P(f_p)G(t)\varepsilon_p) \quad (7-4)$$

where ε_u is pipe uniform strain (uEL) and the functions $G(t)$ and $P(f_p)$ characterize the effect of wall thickness and internal pressure, respectively.

The function $G(t)$ is given as,

$$G(t) = \left(\frac{15.9}{t}\right)^{0.8096(1+1.503\psi^{1.229})} \quad (7-5)$$

and the function $P(f_p)$ is in the form of,

$$P(f_p) = \begin{cases} P_{max} - \frac{5}{3}f_p(P_{max} - 1) & \text{if } 0 \leq f_p < 0.6 \\ 1 & \text{if } 0.6 \leq f_p \leq 0.8 \end{cases} \quad (7-6)$$

A conservative and fixed value of 1.5 was initially given to P_{max} in [186]. A more refined relation was developed later as,

$$P_{max} = 2.25 - 2\frac{a}{t} \quad (7-7)$$

The function ε_p in Eq. (7-4) is given as,

$$\varepsilon_p = A \frac{F(\delta_F)}{1 + F(\delta_F)} \quad (7-8)$$

where the function $F(\delta_F)$ is

$$F(\delta_F) = (C\delta_F)^B \delta_F^D \quad (7-9)$$

A , B , C , and D in Eqs. (7-8) and (7-9) are fitted functions of normalized geometry and material properties [158].

7.3.4.3 Toughness

7.3.4.3.1 Form of Toughness and Test Specimens

Two forms of toughness, (1) initiation toughness as represented by apparent toughness and (2) resistance curves, may be used in the PRCI-CRES tensile strain models as shown in Figure 7-7 and Figure 7-8. Such toughness may be obtained from multiple types of test specimens, including traditional Charpy impact and standards three-point bend CTOD test specimens and low-constraint test specimens of shallow-notched three-point bend CTOD, SENT (single edge notched tension), and CWP (curved wide plate). The images of some toughness test options are given in Figure 7-9.



Figure 7-9 Images of various toughness test options that may provide input to the PRCI-CRES tensile strain models. Left: standard three-point bend CTOD; Middle: SENT; and Right: CWP

7.3.4.3.2 *Obtaining Apparent Toughness from Traditional Test Specimens*

As the apparent toughness represents the initiation toughness of girth welds under predominantly tensile loading, the relevant toughness is that from low-constraint specimens. A conversion process is provided for toughness obtained from traditional specimens.

The apparent toughness $CTOD_A$ may be estimated from Charpy upper shelf impact energy, U_{CVN} ⁴.

For welds of X52 to X65 linepipes, the conversion relation is given as,

$$\delta_A = \left(0.00590 \frac{\sigma_Y}{\sigma_T} - 0.00103 \right) U_{CVN}$$

For welds of X70 and X80 linepipes, the conversion relation is given as,

$$\delta_A = \left(0.00634 \frac{\sigma_Y}{\sigma_T} - 0.00155 \right) U_{CVN}$$

In the above equations, σ_Y is the yield stress at 0.5% total strain and σ_T is the ultimate tensile strength in the pipe longitudinal direction. The units of the Charpy energy U_{CVN} and $CTOD_A$ are Joule and mm, respectively. The maximum $CTOD_A$ that may be used from the conversion is 1.2 mm.

When upper-shelf CTOD toughness is available from standard CTOD test specimen, a multiplication factor of 1.5 - 2.0 may be applied to obtain $CTOD_A$. The recommended default conversion factor is 1.75. The conversion factor is applicable to standard SENB specimens without side grooves. It should be emphasized that the relevant CTOD toughness for conversion

⁴ These relations are valid for mechanized GMAW welds made onto modern microalloyed TMCP steels. Different relations are necessary for SMAW welds made onto vintage or modern steels.

must be from upper-shelf CTOD. A single CTOD toughness value from maximum load, i.e., δ_m , is not sufficient to indicate upper shelf behaviour [189].

7.3.4.3.3 *Obtaining Apparent Toughness from Resistance Curves*

The $CTOD_A$ may be obtained from resistance curves of low-constraint specimens, such as SENT, at a flaw growth $\Delta a = 0.5 - 1.0$ mm as illustrated in Figure 7-10. The selection of the amount of flaw growth depends on pipe wall thickness and possibly other parameters. Generally, the recommended Δa is 0.5 mm for pipe wall thickness of 12.7 mm or 1/2 in and 1.0 mm for pipe wall thickness of 25.4 mm or 1.0 in. When the pipe wall thickness is between above two extreme values, a linear interpolation may be used to determine the appropriate Δa value.

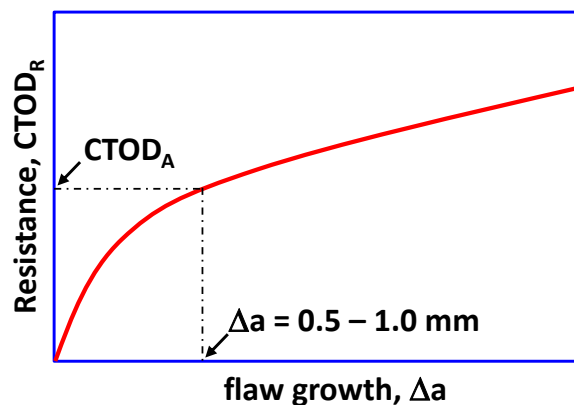


Figure 7-10 Schematic illustration of obtaining $CTOD_A$ from a resistance curve

7.3.4.4 Selection of Test Specimens

As described previously, the PRCI-CRES models accept toughness from multiple types of test specimens. If there is a choice, low-constraint tests are preferred to high-constraint tests. Similarly tests from large-scale specimens are preferred to small-scale specimens as the toughness used here is no-longer a material parameter. When a limited number of tests are done, resistance curves tend to have smaller variations than tests that generate single toughness values, such as traditional CTOD tests.

The selection of test specimens should be considered in conjunction with the recognition of difficulties of the tests and possible inconsistency in implementing test procedures by different labs. In some cases, uniformly acceptable test procedure may not exist, e.g., that for curved wide plate test.

7.3.4.5 Predicted TSC vs. Toughness Options

The allowance for multiple test specimen types inevitably introduces the possibility of non-uniqueness of the predicted TSC. This issue has always existed when assessments are done with multiple options of toughness. In stress-based assessment, such as that using BS 7910, results are generally different when toughness converted from Charpy, toughness from CTOD, or toughness from J -integral are used. Similarly, different results are obtained from different levels

of assessment, either in accepted assessment procedures like BS 7910 or in the PRCI-CRES models. The toughness conversion for the PRCI-CRES models is biased towards conservatism. As indicated previously, the toughness from traditional tests must be from upper-shelf behavior before the conversion.

7.3.5 Structure of PRCI-CRES Models

The PRCI-CRES models are organized in four levels as shown in Figure 7-11.

The Level 1 models are intended for quick estimations of the likely tensile strain capacity. The TSC is tabulated for selected pipe dimensions, material properties, and flaw size [186]. The apparent toughness is estimated from the upper shelf Charpy impact energy.

The Level 2 models are given in a library of parametric equations. The apparent toughness can be estimated from either the upper shelf Charpy impact energy or the upper shelf standard CTOD toughness.

The Level 3 models have two options. Level 3a uses an initiation-control limit state. Level 3b uses a ductile instability limit state. In Level 3a, the TSC is obtained by the use of the same library of parametric equations as in Level 2. The apparent toughness is obtained by a number of low constraint test options, including shallow-notched SE(B), SENT, or CWP.

The Level 4 models are structured in the same format as Level 3 models, except that the crack-driving force relations are directly obtained from FEA as opposed to from parametric equations. The toughness options are the same as in Level 3. This level allows for special cases when the specific weld geometry and material properties do not allow the use of the first three options. The Level 4 models should only be exercised by seasoned experts.

Level	Limit State	Target Application	Format of Models	Toughness Option
1	Initiation	Initial screening, feasibility study	Tabular	Upper shelf Charpy energy
2	Initiation	Nominal analysis	Equations	Upper shelf Charpy energy, CTOD or J from SENB
3a	Initiation	Advanced analysis	Equations	Single value CTOD or J from shallow-notched SENB, SENT, or CWP
				CTOD or J resistance curves from shallow-notched SENB, SENT, or CWP
3b	Ductile instability	Advanced analysis	Equations	CTOD or J resistance curves from shallow-notched SENB, SENT, or CWP
4a	Initiation	Case specific-analysis	Expert finite element analysis	Single value CTOD or J from shallow-notched SENB, SENT, or CWP
				CTOD or J resistance curves from shallow-notched SENB, SENT, or CWP
4b	Ductile instability	Advanced analysis	Expert finite element analysis	CTOD or J resistance curves from shallow-notched SENB, SENT, or CWP

Figure 7-11 Overall structure of the PRCI-CRES tensile strain models

7.3.6 Correlating Parameters in PRCI-CRES Models

The PRCI-CRES models correlate the following parameters.

(1) Pipe dimensions:

t pipe wall thickness, mm,

(2) Girth weld geometry feature

h girth weld high-low misalignment, mm.

(3) Flaw dimensions

a flaw height, mm,

$2c$ flaw length, mm, and

(4) Material tensile properties:

σ_y pipe yield strength, MPa,

σ_U pipe ultimate tensile strength, MPa,

σ_U^W weld metal tensile strength, MPa, and

(5) Material toughness:

Either initiation toughness (apparent toughness) or resistance curve

(6) Loading parameter:

f_p pressure factor, ratio of applied hoop stress to pipe yield strength.

(7) Tensile strain capacity

Tensile strain capacity may be obtained when other input parameters in Nos. (1)-(6) are known. Alternatively, necessary conditions of parameters in Nos. (1)-(6) can be determined for a target tensile strain capacity.

7.3.7 Application of CRES Tensile Strain Models

7.3.7.1 Role of Tensile Strain Models

Tensile strain models may be used in the design phase of a pipeline or in the integrity management of an existing pipeline. In the design phase, tensile strain models may be used for

- Setting linepipe specifications,
- Setting requirements for girth weld qualification,
- Determining flaw acceptance criteria, and
- Helping to develop field inspection procedures, such as treatment of high-low misalignment.

For the integrity management of existing pipelines, tensile strain models may be used for

- Assessing the risk of tensile rupture,
- Facilitating the decision-making on mitigation options, and
- Determining the intervention threshold in allowable strain demand.

7.3.7.2 Applications at Levels 2 and 3

The PRCI-CRES tensile strain models are very versatile. They may be used to estimate the tensile strain capacity (TSC) for a given set of conditions as shown in Figure 7-12. One of the major applications is the development of flaw acceptance criteria for field girth welding as shown in Figure 7-13. The models may also be used to play “what-if” scenarios to meet the same target level of TSC as shown in Figure 7-14. For instance, a balanced approach between weld toughness and strength mismatch may be developed against practical limits of welding processes and realistically-achievable material properties.

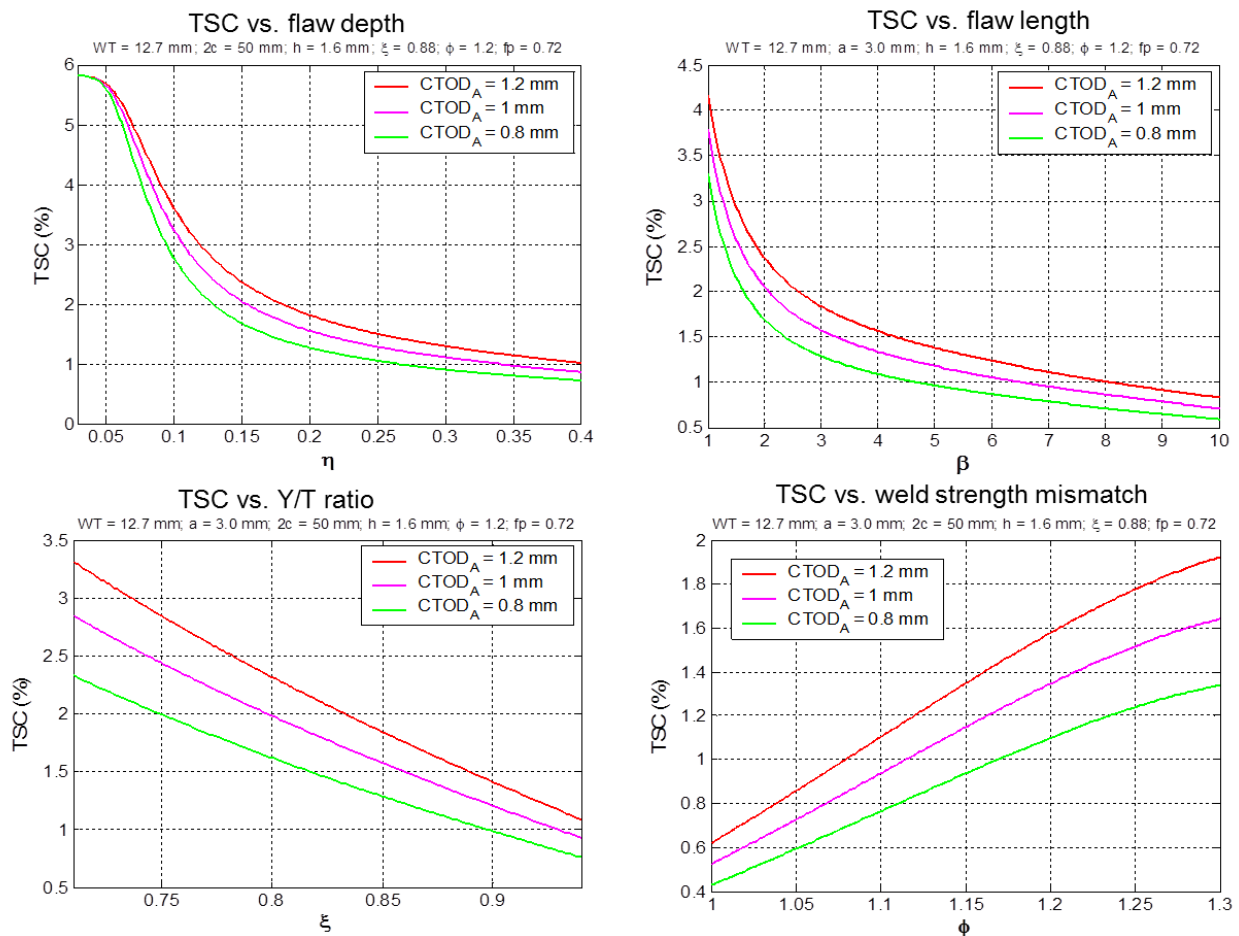


Figure 7-12 Sample applications of the PRCI-CRES tensile strain models in the form of tensile strain capacity (TSC) vs. various physical parameters

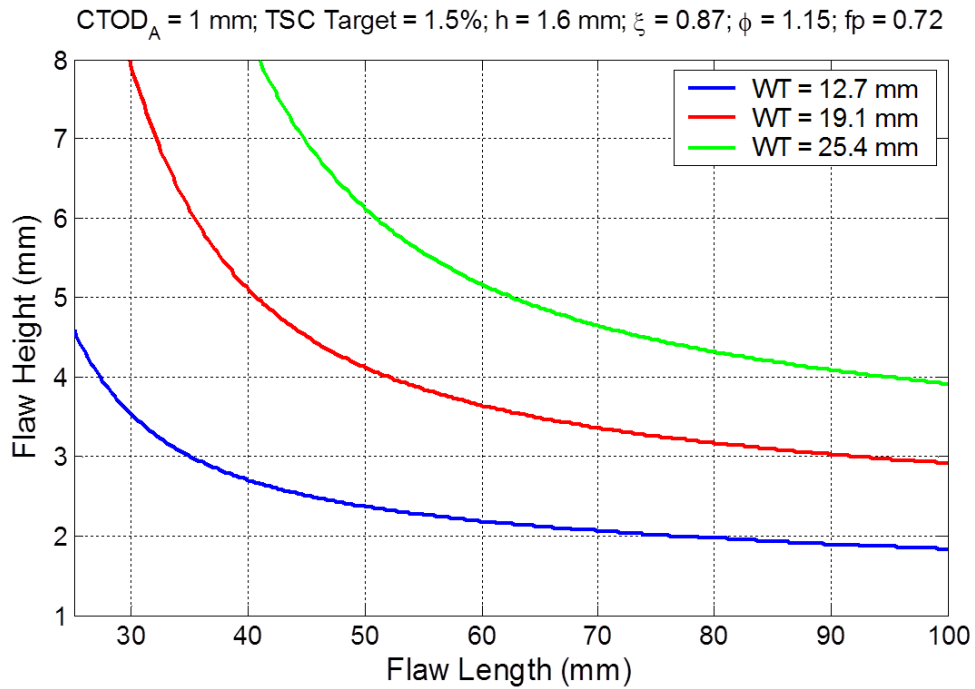


Figure 7-13 Sample applications of the PRCI-CRES tensile strain models in the form of flaw acceptance criteria with a target tensile strain capacity (TSC) of 1.5%

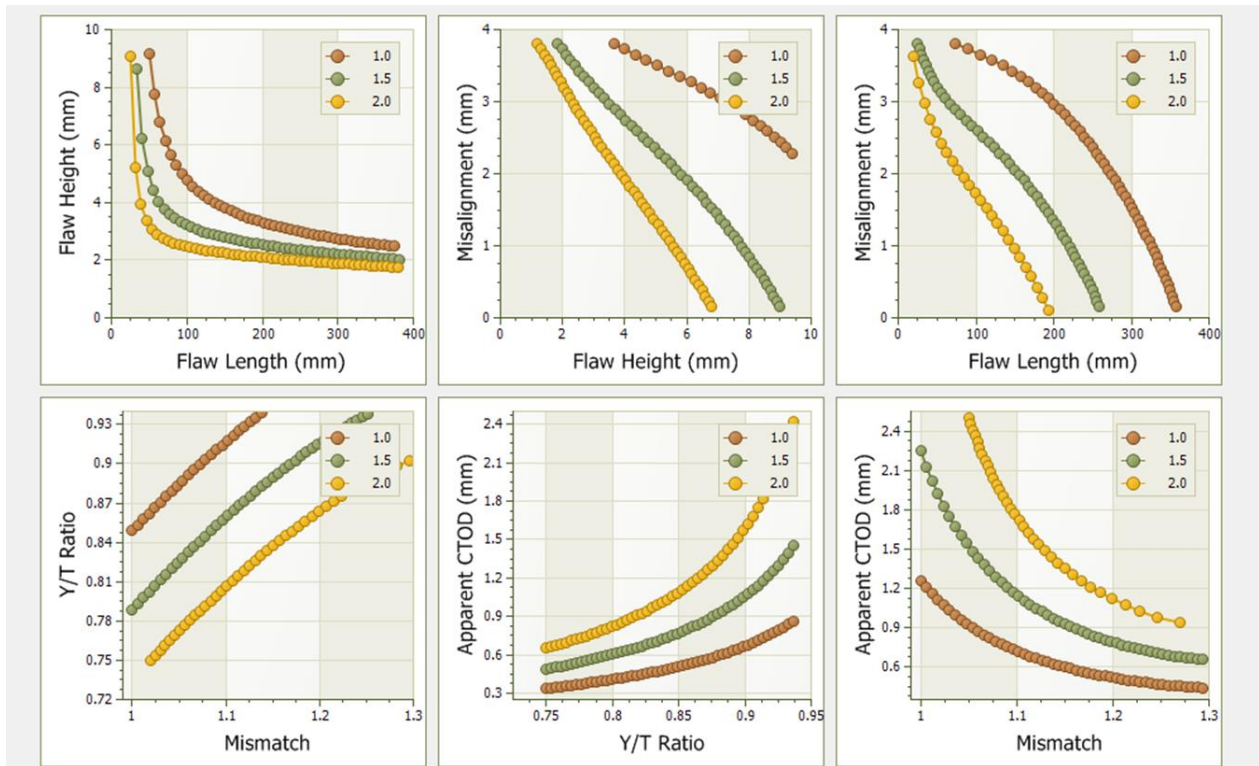


Figure 7-14 Sample applications of the PRCI-CRES tensile strain models at various levels of target tensile strain capacity (TSC)

7.3.7.3 Applications at Level 4

7.3.7.3.1 Example 1 – Use of Weld Cap Overbuild to Enhance TSC

One of the effective means of overcoming the potential strain concentration caused by weld strength undermatching and HAZ softening is building additional weld deposit at the girth weld, i.e., weld overbuild. As depicted in Figure 7-15, an overbuild can be achieved by depositing more weld metal at the cap than in a “normal” girth weld. The weld overbuild must have adequate thickness and width to ensure no excessive strain concentration occurs at the girth weld. On the other hand, too much weld overbuild would increase the cost of pipeline welding as the production rate of girth welding may be negatively affected. It is therefore important to have sufficient, but not excessive amount of weld overbuild.

The effectiveness and proper level of weld overbuild are assessed using Level 4a of the PRCI-CRES tensile strain models. The principal focus is the effects of weld profile on the crack driving force ($CTOD_F$). Level 4a of the PRCI-CRES models allows for the development of weld-specific crack-driving force relation.

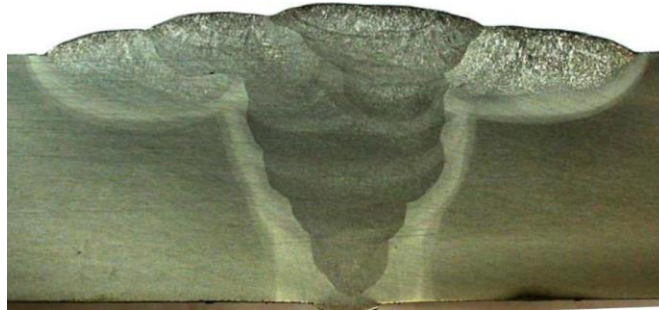


Figure 7-15 Cross section of a pipe girth weld with weld overbuild

The schematic of the finite element model is shown in Figure 7-16. The key parameters for the overbuild is its thickness and width. Figure 7-17 shows the overall model geometry and the detailed profile of the girth weld and the overbuild. The total length of the pipe used in the model is 10 times of the pipe OD. Only one half of the pipe was modeled due to symmetry conditions. Two flaw locations are analyzed: one in the weld central line, the other at the fusion boundary between the weld metal and HAZ, as shown in Figure 7-18. All flaws are introduced on the ID surface of the pipe. The sample case has a pipe outer diameter of 12.75 in (324 mm) and thickness of 0.5 in (12.7 mm).

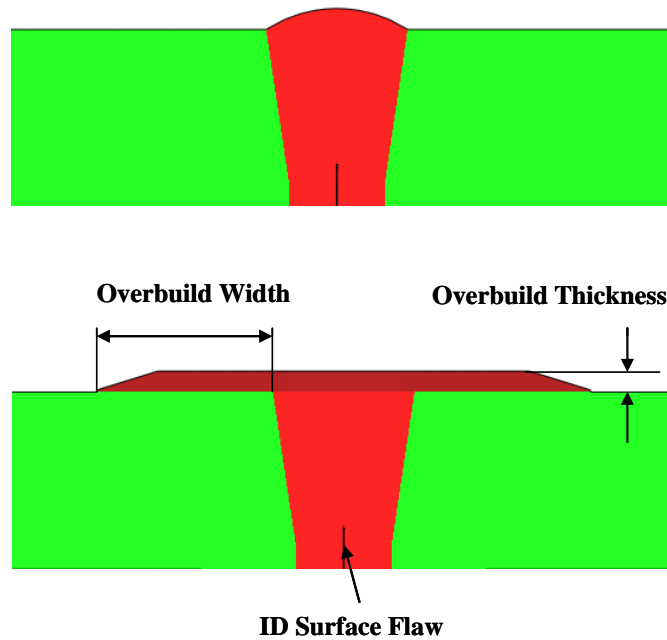


Figure 7-16 Schematic illustration of cross sections of a girth weld without overbuild (top) and a girth weld with overbuild (bottom)

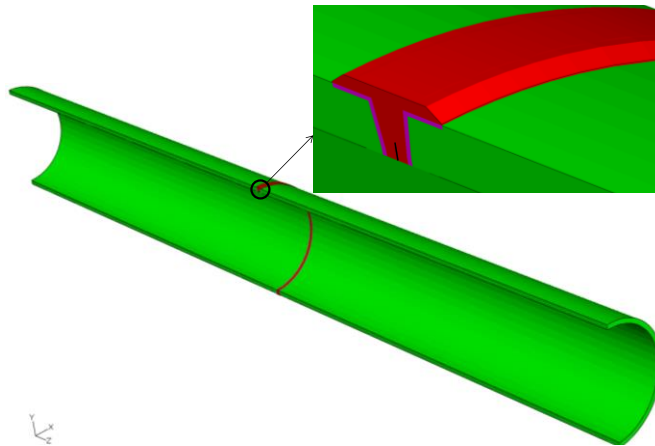


Figure 7-17 Geometry of the pipe and the girth weld with overbuild. The green region represents the base pipe; the red region represents the weld metal; the pink region represents the HAZ of both girth weld and overbuild. The black line in the middle of the weld represents the flaw.

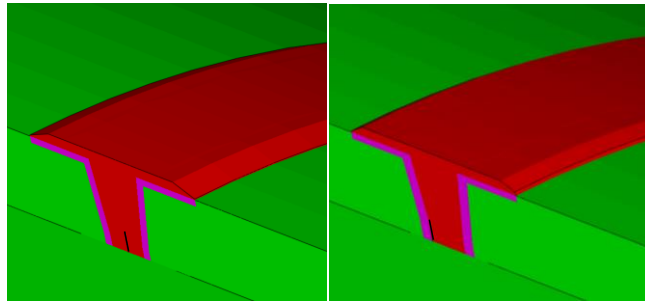


Figure 7-18 Flaw locations: at weld centerline (left) and at HAZ (right)

Figure 7-19 shows the crack driving force as a function of the remote strain for the flaw at the weld centerline with a size of 5.0×75.0 mm. The weld without the overbuild is estimated to have a TSC of ~0.6%. While all the weld overbuilds improve the strain capacity of the girth welds, those with 5.0-mm width show the least amount improvement. At this small width, increasing the thickness of the overbuild by 100% (from 1.5 mm to 3.0 mm) only improve the strain capacity slightly.

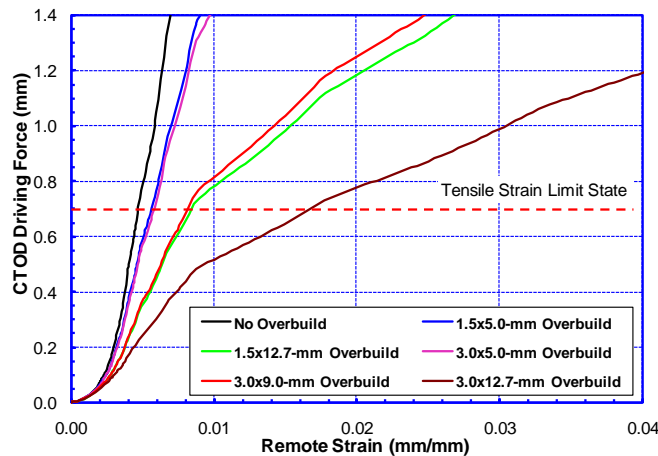


Figure 7-19 Crack driving force vs. remote strain relationship for 5.0×75.0 mm flaws at the weld centerline with various overbuild sizes

To understand the importance of overbuild width, the longitudinal strain distributions on the symmetry plane (where the deepest point of the flaw is located) are plotted for the flaw of 5.0×75.0 mm, all with the remote strain at 0.375% in Figure 7-20. The contours clearly show that the bands of high longitudinal strain emit from the crack tip and expand in the directions of 45° with respect to the flaw plane. For the no-overbuild case, the bands of high longitudinal strain expand and reach the OD surface of the pipe. The 1.5×5.0-mm overbuild provides some reinforcement, but its width is not enough to cover the bands of high longitudinal strain at the OD surface. When overbuild width is increased to 12.7 mm, the overbuild covers the bands of high longitudinal strain. The size of the high strain bands is a direct indication of the crack-tip deformation. Wide overbuild width leads to small amount of crack-tip deformation, therefore low crack driving force.

As shown in Figure 7-20, there are two small regions having black contours that indicate negative (compressive) strains. One of the regions is near the very crack tip. The other one is the two long strips on the ID surface at the either side of the crack (bottom of the contour plots). These negative strains are the result of numerical extrapolation of the strain values calculated in the elements' integration points. The steep strain gradient cause negative strains when the strain values at the integration points are extrapolated. The zones of negative strains could be reduced progressively with increasingly refined finite element mesh.

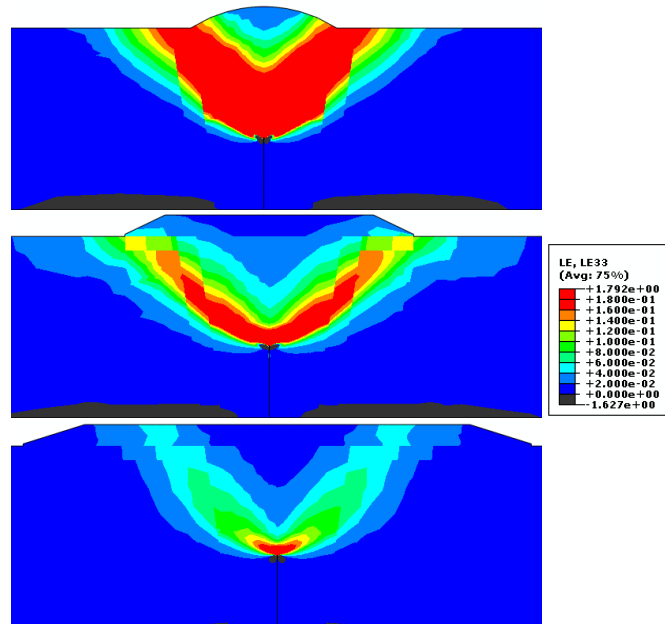


Figure 7-20 Longitudinal strain contours on symmetry plane with remote strain = 0.375% for flaw of 5.0x75.0 mm at the weld centerline. Top: no overbuild; middle: 1.5x5.0-mm overbuild; Bottom: 1.5x12.7-mm overbuild

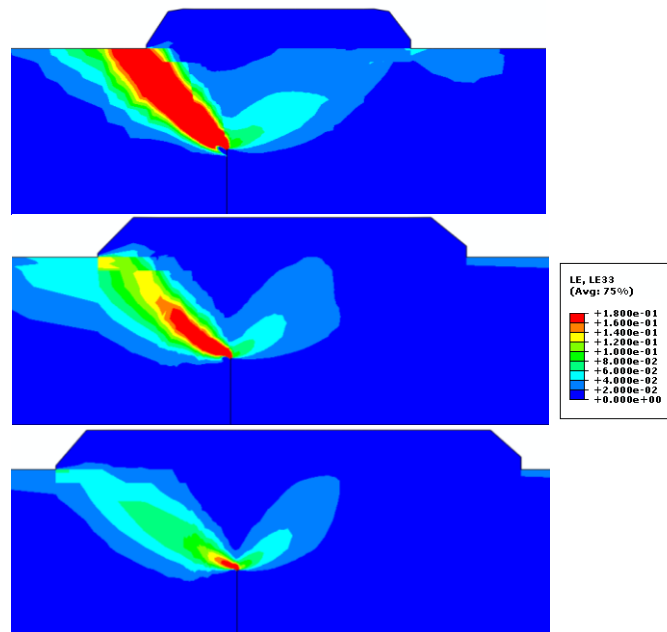


Figure 7-21 Longitudinal strain contours on symmetry plane with remote strain = 0.375% for flaw of 5.0x75.0 mm in HAZ. Top: 3.0x5.0 mm overbuild; middle: 3.0x9.0-mm overbuild; Bottom: 3.0x12.7-mm overbuild

The TSC of girth welds with planar weld and HAZ flaws was estimated using the Level 4a approach of the PRCI-CRES tensile strain models. The TSC and the associated flaw size and overbuild dimensions is shown in Table 7-2. It is evident that weld overbuild can be an effective method to enhance the TSC of girth welds. The flexibility of the Level 4a approach is demonstrated through the application of the same fundamental principles of Levels 1-3 to weld profiles not covered in the parametric crack-driving force relationships.

Table 7-2 Estimated TSC with weld overbuild of various size

Case #	Flaw Location*	Flaw Depth (mm)	Flaw Length (mm)	Overbuild Thickness (mm)	Overbuild Width (mm)	Estimated Tensile Strain Capacity (%)
1	WM	3.0	100.0	0.0	0.0	0.64
2	WM	3.0	100.0	1.5	5.0	0.81
3	WM	3.0	100.0	1.5	12.7	2.80
4	WM	3.0	100.0	3.0	5.0	0.80
5	WM	3.0	100.0	3.0	9.0	1.70
6	WM	3.0	100.0	3.0	12.7	>5.00
7	WM	5.0	75.0	0.0	0.0	0.47
8	WM	5.0	75.0	1.5	5.0	0.56
9	WM	5.0	75.0	1.5	12.7	0.84
10	WM	5.0	75.0	3.0	5.0	0.58
11	WM	5.0	75.0	3.0	9.0	0.82
12	WM	5.0	75.0	3.0	12.7	1.67
13	HAZ	3.0	100.0	0.0	0.0	0.64
14	HAZ	3.0	100.0	1.5	5.0	0.79
15	HAZ	3.0	100.0	1.5	12.7	2.24
16	HAZ	3.0	100.0	3.0	5.0	0.83
17	HAZ	3.0	100.0	3.0	9.0	1.57
18	HAZ	3.0	100.0	3.0	12.7	3.04
19	HAZ	5.0	75.0	0.0	0.0	0.47
20	HAZ	5.0	75.0	1.5	5.0	0.55
21	HAZ	5.0	75.0	1.5	12.7	0.81
22	HAZ	5.0	75.0	3.0	5.0	0.57
23	HAZ	5.0	75.0	3.0	9.0	0.75
24	HAZ	5.0	75.0	3.0	12.7	1.26

* WM: Weld Metal; HAZ: Heat-Affected Zone

7.3.7.3.2 Example 2 - Application of Level 4 to Modern Girth Welds

The Level 4a methodology can be applied to assess the impact of weld strength mismatch, HAZ softening, and weld bevel geometry. One of such applications is given in Appendix D.

7.3.8 Tensile Strain Models for Manual-Welded Pipelines

7.3.8.1 Model Setup

The Level 4a methodology has been applied manual girth welds. Extensive review of the cross-sectional profiles of girth welds fabricated in the 1940s to 1960s revealed that the weld profiles were quite different from those modelled in developing the Levels 1-3 procedures in the PRCI-CRES models. A typical weld macro is shown in Figure 7-22. In the FE models, the weld

profile is simplified into three material zones: (1) weld metal (WM), (2) heat-affected zone (HAZ), and (3) base metal (BM). To better characterize those three material zones, some key dimensions were selected and shown in Figure 7-22.

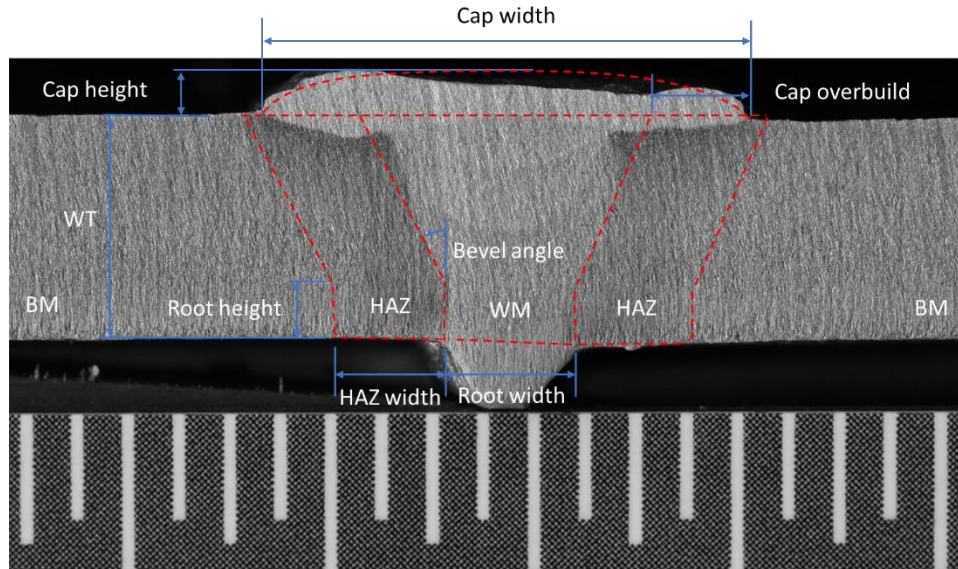


Figure 7-22 Weld macro of vintage girth welds

Compared to the modern mechanized girth welds, these girth welds often have a wide weld cap. Analysis of nearly 100 weld macros showed the weld cap overbuild had the mean value of 2.2 mm and a standard deviation of 0.8 mm. Since the pipe wall thickness of those girth welds is often less than 10 mm, the weld cap overbuild has a strong influence on TSC of those girth welds. The key dimensions of the representative girth weld profiles used in the analyses are shown in Table 7-3.

Table 7-3 Key dimensions of representative vintage girth weld profiles

WT		Root Width	Root Height	HAZ Width	Cap Height	Cap Width	Cap Overbuild	Bevel Angle
in	mm	mm	mm	mm	mm	mm	mm	degree
0.203	5.2	4.0	2.4	4.2	1.6	13.6	3.2	30
0.344	8.7	4.0	2.4	4.2	1.6	16.5	2.6	30
0.500	12.7	4.0	2.4	4.2	1.6	19.1	1.6	30

To develop the tensile strain capacity models, the FEA was conducted to calculate the crack-driving force relations. One example FEA model is shown in Figure 7-23. Due to the symmetry boundary conditions in the pipe circumference direction, only half of the pipe was modeled. The total length of the model is set at 6 times the pipe OD to eliminate the end effects on crack opening and to obtain a finite uniform strain zone. Eight-node brick (3-D solid linear) elements with reduced integration and hybrid interpolation functions were used where the non-linear geometric (large deformation) effect was enabled. The flaw was modeled in a semi-elliptical

shape and located on the ID surface of the pipe along the fusion line (i.e., HAZ flaws). The flaw size was kept constant during simulation and no flaw growth was modeled. The flaw dimensions are set from typically observed flaw dimensions and workmanship flaw acceptance criteria in the main body of API Standard 1104. The flaw depth is set at 2.5 mm, which is closed to one root bead height. The flaw depth is also set at 1.5 mm due to the thin pipe wall thickness of the vintage girth welds. The flaw length is set to three values of 12.7 mm (1/2 inch), 25.4 mm (1 inch) and 50.8 mm (2 inch) which would be a good representative of flaw length in the field.

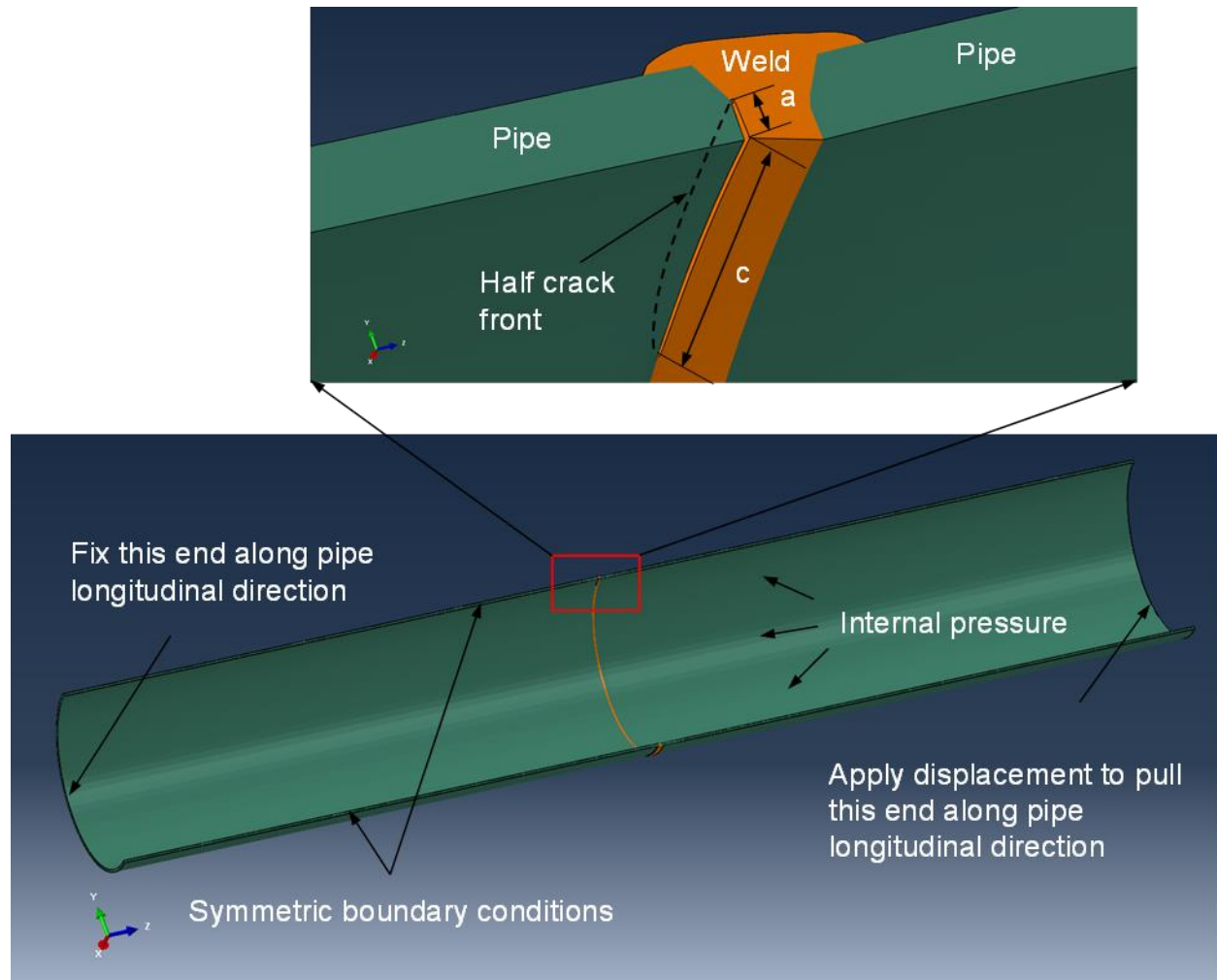


Figure 7-23 Example FEA model of a pipe with the vintage girth weld

The stress-strain curves of the pipe and weld metal were constructed and used in the FEA. The weld metal strength was assumed to be 20% below the strength of the pipe based on tests of vintage girth welds fabricated in 1940s to 1960s. These girth welds typically show little to no HAZ softening. For all cases analyzed, the HAZ was assumed to have the same material property as the pipe base metal. The FEA was conducted in two loading steps. In the first step, a prescribed internal pressure was applied to the ID surface of the pipe where the two pipe ends were free of constraints and loads. In the second step, the FE model was subjected to uniaxial

tension on one end and fixed on the other end along the pipe longitudinal direction while holding the internal pressure. The crack driving force curves, i.e., the relationship between the crack tip opening displacement ($CTOD_F$) and the remote strain, were determined from FEA.

7.3.8.2 Example Results

The crack driving force curves of all the analyzed cases were extracted from the FEA results. One example crack driving force curve is shown in Figure 7-24.

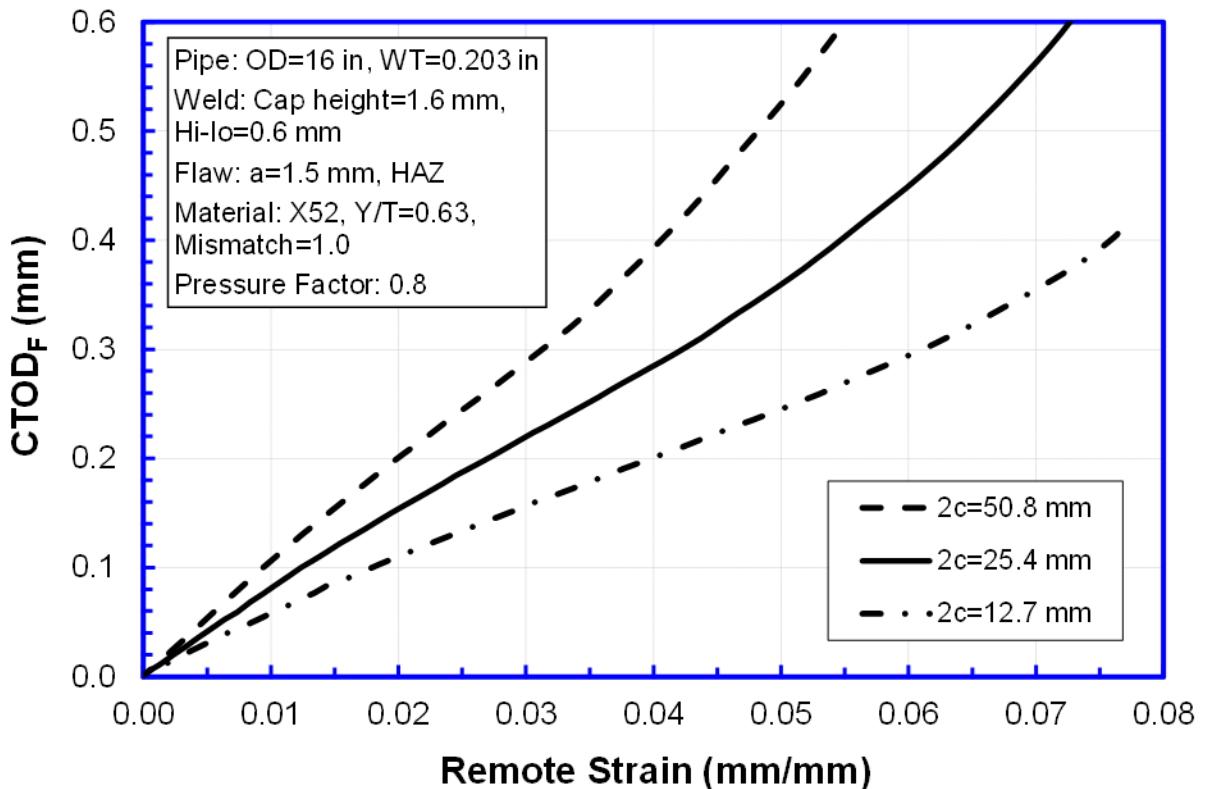


Figure 7-24 Example crack-driving force relations from FEA

Using the Level 4a methodology of the PRCI-CRES models, the TSC of the girth welds with various flaw dimensions, pipe wall thickness, and pipe Y/T ratios can be estimated for a range of apparent $CTOD$ toughness. The TSC of a sample case with a vintage X52 pipe of 0.344 in wall thickness is shown in Table 7-4.

Table 7-4 Sample TSC for a X52 vintage pipe with 0.344 in WT and Y/T ratio of 0.63

Flaw Height (mm)	Flaw Length (mm)	CTOD _A (mm)					
		0.3	0.4	0.5	0.6	0.7	0.8
1.5	12.7	1.20	1.57	1.92	2.24	2.50	2.73
	25.4	0.95	1.23	1.51	1.79	2.03	2.27
	50.8	0.76	0.98	1.20	1.41	1.61	1.80
2.5	12.7	1.12	1.45	1.77	2.06	2.32	2.56
	25.4	0.77	1.00	1.22	1.45	1.66	1.86
	50.8	0.56	0.71	0.87	1.02	1.17	1.31
5.0	12.7	1.29	1.64	1.95	2.24	2.49	2.72
	25.4	0.68	0.87	1.07	1.24	1.42	1.59
	50.8	0.41	0.52	0.63	0.74	0.84	0.95

7.3.9 Means to Enhance TSC

The beneficial effects of weld overbuild are straightforward to understand as described in the previous section. Historically weld cap reinforcement with smooth and wide profiles have played an important role in girth weld integrity. An example of such weld is shown in Figure 7-25. Although the wide weld cap was probably produced without the explicit intent of taking advantage of the weld reinforcement, the cap does serve to ensure that the weld region has sufficient overall strength to match the strength of the pipe. Experimental tests have shown that welds with such caps can effectively shield root cracks of small-to-moderate size from causing failure in the weld.

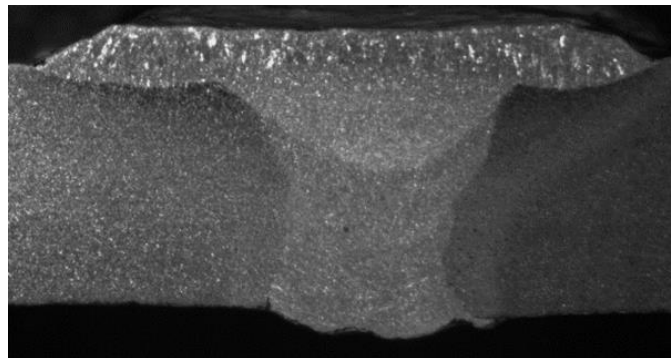


Figure 7-25 Cross section of a SMAW girth weld produced in the early 1950s

Having appropriate weld profiles can offset the negative impact of girth weld high-low misalignment on the weld integrity as described by Wang et al. [190]. Two girth welds were made purposely with a high degree of weld high-low misalignment. The mechanized GMAW

weld had a maximum misalignment of 21% of pipe wall thickness and a weld strength that is 5% higher than the weld strength. Yet all cross-weld tensile specimens necked outside the region in the base pipe material, including the specimens with the highest degree of misalignment. The manual SMAW weld has a maximum misalignment of 39% of the pipe wall thickness and a weld strength that is 5% below the strength of the pipe. With near-zero misalignment, the cross-weld tensile specimens necked outside the weld region. Even at the highest degree of misalignment, the joint strength was only reduced by a few percentage points. Similar to the analyzed welds with weld overbuild, the width of the welds needs to be sufficiently wide to offset the effects of the high degree of misalignment.

Having sufficient overbuild is necessary to reduce the crack driving force thus increasing TSC. Given the plastic strain emitting in a 45° pattern from the crack tip, the overbuild needs to extend approximately one wall thickness beyond the flaw plane if the ID flaw is shallow. Considering that HAZ flaws can be on either side of the deposited weld metal, the total width of the overbuild needs to be the weld metal width plus two wall thickness (one wall thickness on each side of the weld) to achieve the most effective reinforcement.

7.4 FFS Assessment of Compressive Buckling

7.4.1 Different Test Setup and its Significance

A pipe's resistance to compressive buckling is often experimentally measured using various forms of full-scale test setup. Figure 7-26 shows one possible test setup. A test section is attached between two loading arms. Lateral bending is applied to the test section through the rotation of the loading arms. The rotation is achieved through the hydraulic actuator at the other end of the loading arms. When the test section is pressurized, the end cap effects would exert a longitudinal tensile force on the test section. The actuator that generates the rotation also exerts a longitudinal force on the test section. To counter-act those longitudinal forces or generate a desired level of longitudinal force, a separate set of hydraulic actuator located right above or below the test section provide an independent loading mechanism.

Figure 7-27 shows a different test setup where the primary loading mechanism is longitudinal compression which is intended to test pipe's resistance to longitudinal compression. A wrinkle would form during such tests as shown in Figure 7-28.

Figure 7-29 shows yet another test setup in which lateral bending moment is applied through a four-point bending mechanism. This test setup has no mechanism to counter-act the tensile longitudinal force generated by the cap effects of internal pressure.

Different values of compressive strain capacity are reported from different test setups even when the test specimens have essentially the same properties. This difference is often not recognized by the industry in general.

7.4.2 Compressive Strain Capacity (CSC) and its Significance

A pipe's resistance to compressive longitudinal strain may be measured in various forms, such as the load vs. displacement, moment vs. bending angle, or moment vs. bending strain relations. One such example is shown in Figure 7-30. A key measure of the pipe's resistance to

compressive strain is determined at the point of maximum load or bending moment. The bending strain at the attainment of such load or bending moment is often termed *compressive strain capacity*.

At the point of maximum load or bending moment, only a small wrinkle is formed. If the deformation is stopped, as it could be the case with displacement controlled loading, pipe usually does not sustain damage of structural integrity concern. Wrinkles of structural significance generally experience strains much greater than the so-called compressive strain capacity. Such wrinkles are formed when the deformation is unrestrained. Further discussions on the significance of CSC and post-buckling behavior are given in Section 10.3.

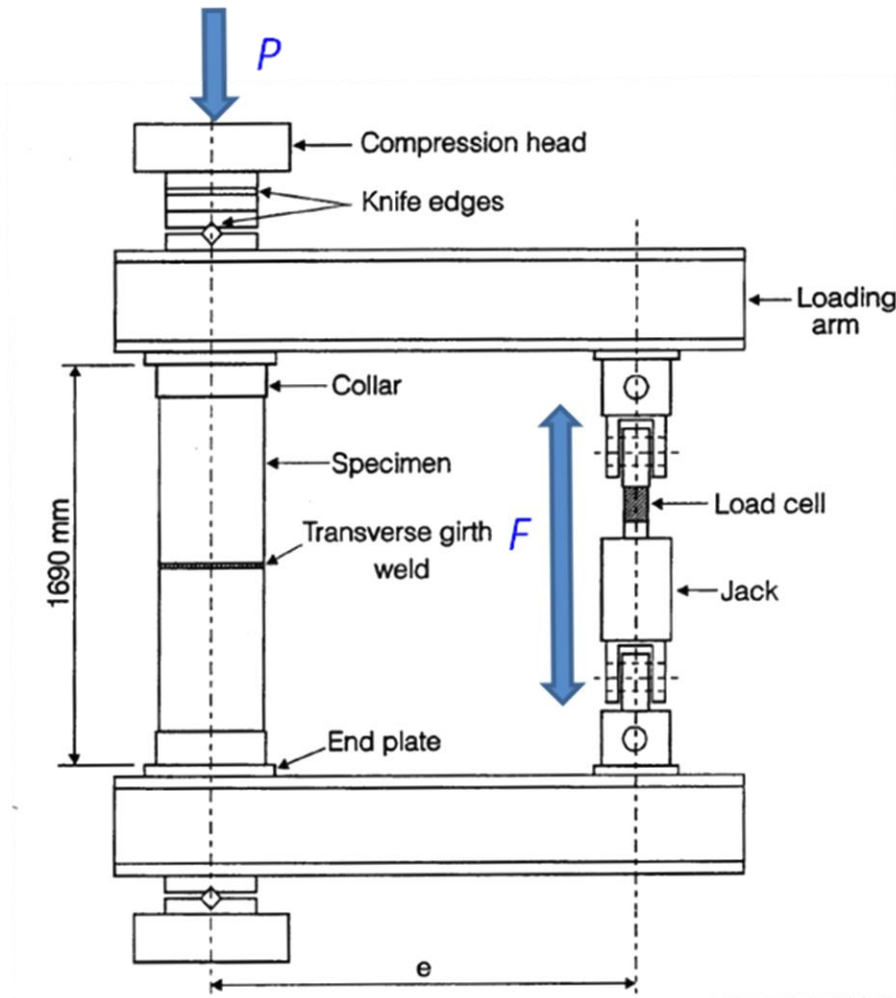


Figure 7-26 A test setup for testing a pipe's resistance to lateral bending



Figure 7-27 Full-scale compression tests for the Trans-Alaska pipeline [191]

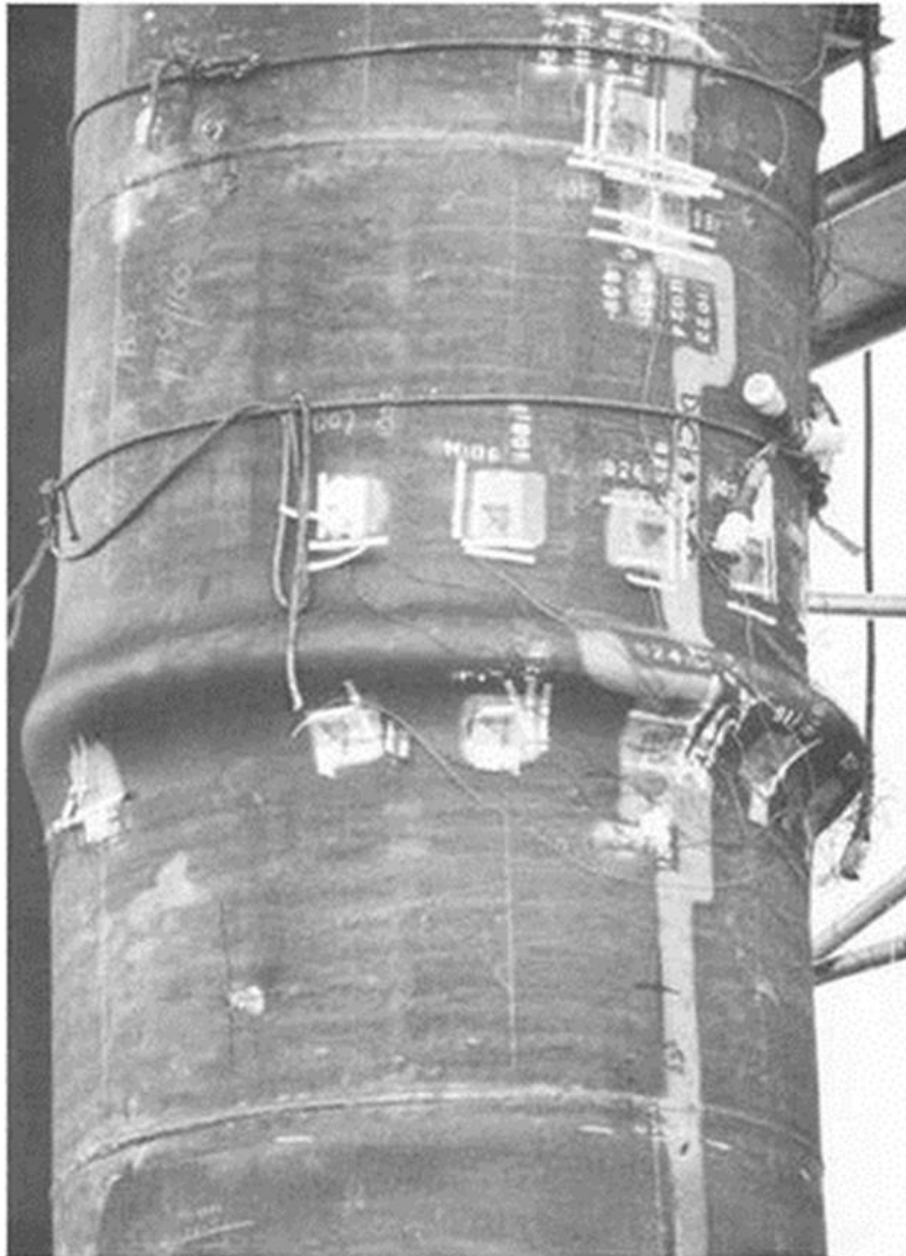


Figure 7-28 A wrinkle produced from a full-scale compression test [191]

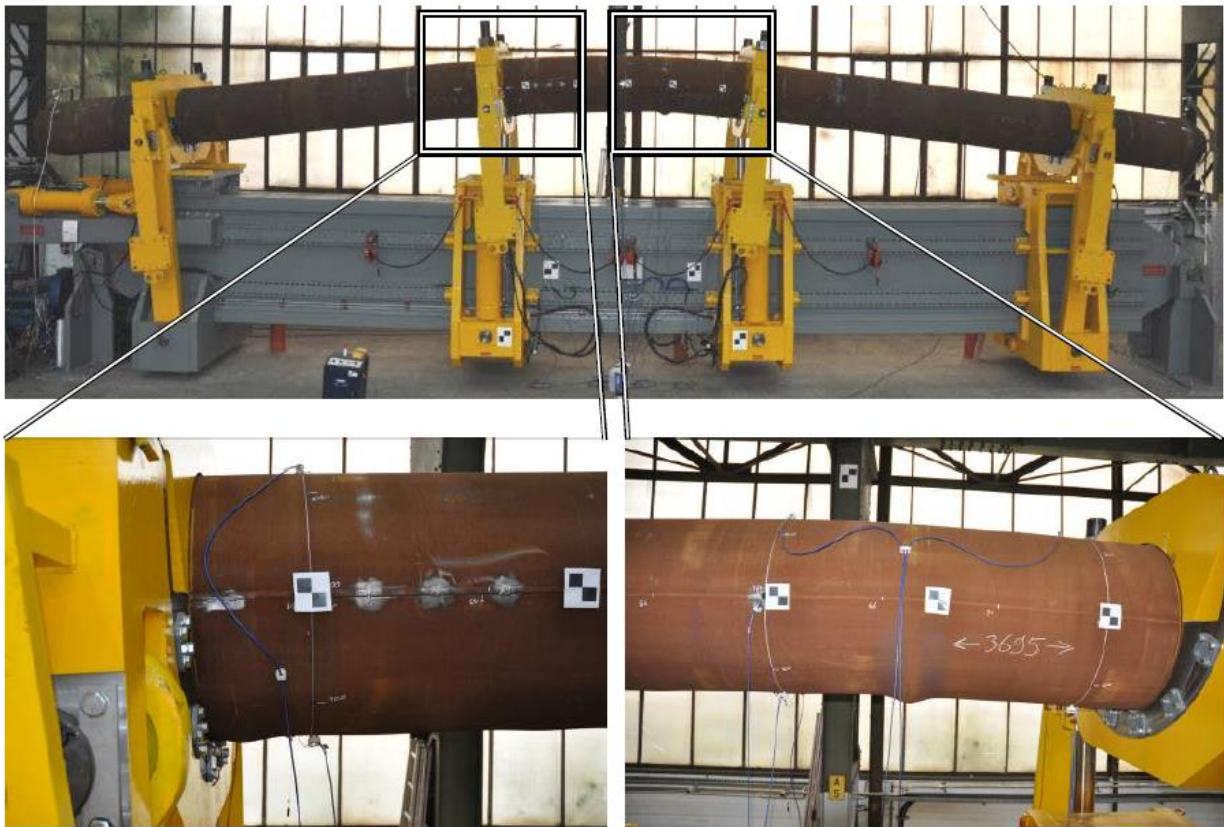


Figure 7-29 A four-point bending setup to determine a pipe's resistance to lateral bending [192]

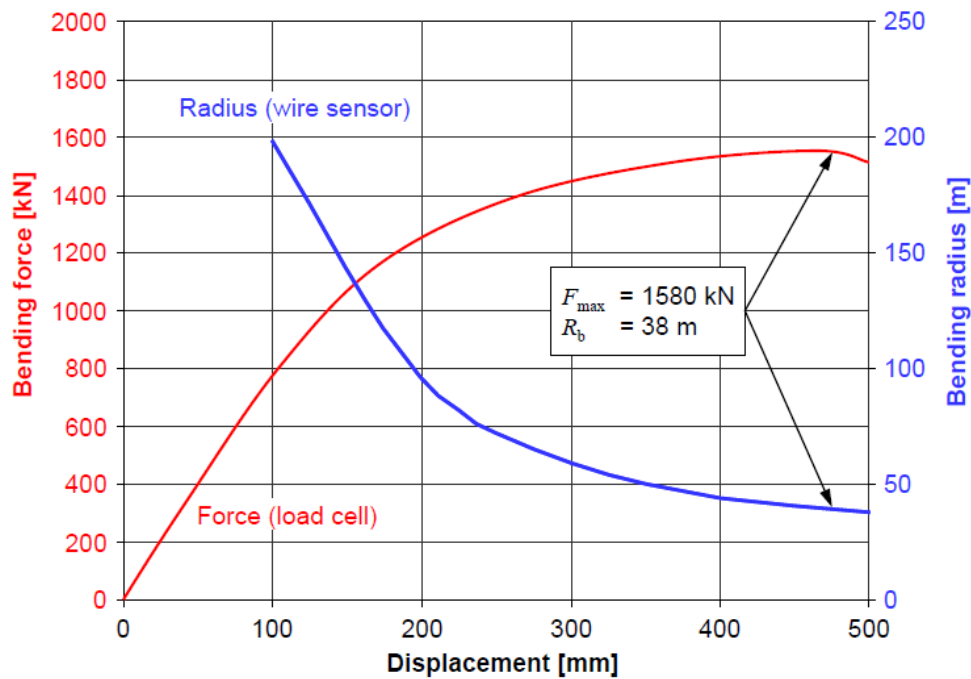


Figure 7-30 Response of an UOE pipe to lateral bending for an X100 unaged pipe with 36 in (914.4 mm) diameter and 13 mm wall thickness and internal pressure of 13 MPa [192]

7.4.3 Models for Compressive Strain Capacity

7.4.3.1 CSA Z662 Models

The CSA Z662 equations (Clause C.6.3.3 of Annex C) were originated from the work by Gresnigt in 1980s [193]. These equations were developed by fitting a curve to the lower bound of the measured strains in an experimental database. The equations in the recent versions of the CSA codes, i.e., 2007 and 2011 [194], were modified to correct possible over-estimation of strain capacity under high internal pressures. The CSA equations can be used for the conditions with combined bending and axial (longitudinal) compression under internal overpressure (i.e., internal pressure \geq external pressure).

The CSA Z662 equations (7-10) and (7-11) are shown below. The unit of the CSC (ϵ_c^{crit}) is in/in or mm/mm.

$$\epsilon_c^{\text{crit}} = \left\{ 0.5 \frac{t}{D} - 0.0025 + 3000 \left[\frac{f_p \sigma_y}{E} \right]^2 \right\} \quad \text{if } f_p < 0.4 \quad (7-10)$$

$$\epsilon_c^{\text{crit}} = \left\{ 0.5 \frac{t}{D} - 0.0025 + 3000 \left[\frac{0.4 \sigma_y}{E} \right]^2 \right\} \quad \text{if } f_p \geq 0.4 \quad (7-11)$$

The pressure factor (f_p) can be calculated from the following Eq. (7-12).

$$f_p = \frac{(p_i - p_e)D}{2t\sigma_y} \quad (7-12)$$

In Eq. (7-10) to (7-12), t is the pipe wall thickness, D is the pipe outside diameter (OD), σ_y is the pipe yield strength, E is the Young's modulus of the pipe, p_i is the internal pressure, and p_e is the external pressure.

The CSA equations explicitly recognize two parameters, i.e., the pipe D/t ratio and pressure. However, since the equations were obtained by fitting experimental data, the pipe strain hardening property (such as Y/T ratio) and geometry imperfection were implicitly taken into account for the data existed in the database. It is likely that the upper bound pipe Y/T ratio and/or geometry imperfection (of the pipes in the experimental database) were implicitly considered by the models since the lower bound of the experimentally measured strains were used in developing the equations. It is not clear if the experimental database used to derive the CSA equations had specimens with girth welds.

Although the applicable range of the input parameters is not explicitly specified for the CSA equations, based on the original work leading to the CSA equations [193], the applicable D/t ratio should be between 20 and 120. A safety factor of 1.25 on strain capacity is recommended by the CSA codes.

7.4.3.2 DNV OS F101 Models

In DNV OS F101 [195], two sets of CSC equations are provided for load- and displacement-controlled loading conditions, respectively. For the displacement-controlled loading conditions, two separate equations, i.e., internal overpressure (i.e., $p_i \geq p_e$) and external overpressure (i.e., $p_i \leq p_e$), are provided. The focus of this review is on the equations for the displacement-controlled conditions with internal overpressure. The displacement-controlled equations (with internal overpressure) were based on finite element results. A slight change to the flow stress for calculating the pressure effect was made in the recent 2007 version of the DNV codes which makes the calculated CSC slightly less conservative for pipes with Y/T ratios greater than 0.87.

The DNV equation for plain pipes is given in Eq. (7-13) and the DNV equation for pipes with girth welds is given in Eq. (7-14) where the unit of the CSC ($\varepsilon_c^{\text{crit}}$) is in/in or mm/mm,

$$\varepsilon_c^{\text{crit}} = 0.78 \left(\frac{t}{D} - 0.01 \right) \left[1 + 5.75 \frac{(p_i - p_e)}{p_b} \right] \xi^{-1.5} \quad (7-13)$$

$$\varepsilon_c^{\text{crit}} = 0.78 \left(\frac{t}{D} - 0.01 \right) \left[1 + 5.75 \frac{(p_i - p_e)}{p_b} \right] \xi^{-1.5} \alpha_{gw} \quad (7-14)$$

where,

$$p_b = \frac{2t}{D-t} \frac{2}{\sqrt{3}} \min \left(\sigma_y, \frac{\sigma_u}{1.15} \right),$$

$$\xi = \frac{\sigma_y}{\sigma_u},$$

$$\alpha_{gw} = \begin{cases} 1 & \text{if } \frac{D}{t} \leq 20 \\ 1 - 0.01 \left(\frac{D}{t} - 20 \right) & \text{if } \frac{D}{t} > 20 \end{cases}.$$

In the above equations, σ_u is the pipe ultimate tensile strength (UTS).

In addition to the pipe D/t ratio and pressure, the DNV equations include the pipe Y/T ratio to account for the effect of the material's strain hardening capacity on the CSC. The DNV equations also recommend a CSC correction factor (α_{gw}) for pipes with girth welds. The correction factor was developed using the experimental data published by University of Alberta in 1994 [196].

The DNV equations are limited to the pipes with $D/t \leq 45$, which are typical for offshore pipelines. No limits on the applicable pipe grades or Y/T ratios are specified in the codes. The recommended safety factors on the CSC are 2.0 or 3.3.

7.4.3.3 API RP 1111 Models

The API RP 1111 equation [197] was developed for offshore applications and is applicable to external overpressures only (i.e., $p_i \leq p_e$). The API equation is given in Eq. (7-15) as shown below. The unit of the CSC ($\varepsilon_c^{\text{crit}}$) is in/in and mm/mm.

$$\varepsilon_c^{\text{crit}} = \left[\frac{1}{1 + 20\delta} - \frac{(p_e - p_i)}{p_c} \right] \frac{t}{2D} \quad (7-15)$$

where,

$$\delta = \frac{(D_{\max} - D_{\min})}{(D_{\max} + D_{\min})},$$

$$p_c = \frac{p_y p_e'}{\sqrt{p_y^2 + p_e'^2}},$$

$$p_y = 2\sigma_y \frac{t}{D}, \text{ and}$$

$$p_e' = 2E \left(\frac{t}{D} \right)^3 \frac{1}{(1-\nu^2)}.$$

In the above equations, δ is the so-called ovality (i.e., the out of roundness) of the pipe cross section and ν is Poisson's ratio of the pipe materials. The D_{\max} and D_{\min} are the maximum and minimum OD of a given cross section.

The API RP 1111 equation includes the effect of the D/t ratio, pressure, and ovality of the pipe cross section. The equation is limited to $D/t \leq 50$ and $p_i \leq p_e$. The recommended safety factor on the CSC is 2.

7.4.3.4 University of Alberta (UOA) Models

The UOA models (2006) [196], were based on extensive finite element analyses (FEA). The FEA were done under bending and internal pressures (i.e., $p_e = 0$).

The UOA models consist of four (4) sets of equations: (1) plain pipes with round stress-strain curves (Eq.(7-16)), (2) plain pipes with yield plateau (i.e., Lüder's extension) in stress-strain curves (Eq. (7-17)), (3) pipes of round stress-strain curves with girth welds (Eq. (7-18)), and (4) pipes of yield plateau in stress-strain curves with girth welds (Eq. (7-19)). The unit of the CSC in Eqs. (7-16) to (7-19) is %.

$$\varepsilon_c^{\text{crit}}(\%) = \left(\frac{2.9398}{D/t}\right)^{1.5921} (1 - 0.8679f_p)^{-1} \left(\frac{E}{\sigma_y}\right)^{0.8542} \left[1.2719 - \left(\frac{h_g}{t}\right)^{0.1501}\right] \quad (7-16)$$

$$\varepsilon_c^{\text{crit}}(\%) = 40.4 \left(\frac{t}{D}\right)^2 (1 - 0.906f_p)^{-1} \left(\frac{E}{\sigma_y}\right)^{0.8} \left[1.12 - \left(\frac{h_g}{t}\right)^{0.15}\right] \quad (7-17)$$

$$\varepsilon_c^{\text{crit}}(\%) = \left(\frac{8.995}{D/t}\right)^{1.724} (1 - 0.892f_p)^{-1} \left(\frac{E}{\sigma_y}\right)^{0.701} \left[1.087 - \left(\frac{h_m}{t}\right)^{0.086}\right] \quad (7-18)$$

$$\varepsilon_c^{\text{crit}}(\%) = 106 \left(\frac{t}{D}\right)^2 (1 - 0.5f_p)^{-1} \left(\frac{E}{\sigma_y}\right)^{0.7} \left[1.10 - \left(\frac{h_m}{t}\right)^{0.09}\right] \quad (7-19)$$

In addition to the D/t ratio and pressure factor (f_p), the UOA models include the pipe yield strength and geometry imperfection as input parameters. For the pipes with girth welds, the geometry imperfection refers to the high-low misalignment (i.e., h_m) of the girth welds. For plain pipes, the geometry imperfection refers to a local outward bulge (i.e., h_g) on the pipe outside surface [198] as shown in Figure 7-31. The bulge has a total length of $D/2$ (i.e., $L_b = D/2$) along the length of the pipe and covers 90° (i.e., $\alpha = 90^\circ$) in the pipe circumference.

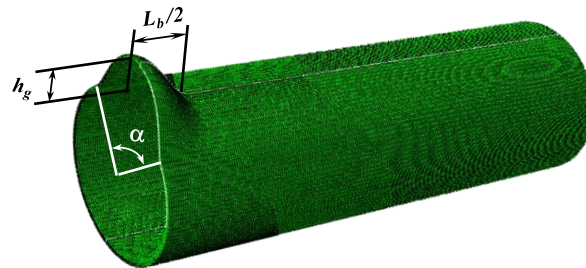


Figure 7-31 Representation of the geometry imperfections in plain pipes by UOA models

In the models other than the UOA models, the pipe yield strength is used only to calculate the pressure effect. In the UOA models, in addition to the pressure effect calculation, the yield strength is used as an input parameter to capture the effect of material's properties on the CSC. Two different shapes of the pipe stress-strain curves, i.e., continuous/round vs. discontinuous yielding, are considered. For the stress-strain curves with discontinuous yielding, a Lüder's extension up to 0.5% strain is assumed [199].

The applicable range of the UOA models depends on the FEA database used in the model development. The FEA database covers pipe grades from X52 to X80 (with yield strength from

359 MPa to 550 MPa). It should be noted that a pre-determined Y/T ratio was used for a given pipe grade. For example, the Y/T ratios used for X52 and X80 pipes are 0.78 and 0.87, respectively [199]. The pipe D/t ratio covers from 50 to 90. The height of the geometry imperfection (h_g) is between 2% and 30% of wall thickness. The girth weld high-low misalignment (h_m) is up to 1/8 in (3.02 mm). The maximum hoop stress induced by the internal pressure is 80% SMYS.

In the FEA for developing the UOA models, the plates (i.e., end caps) attached to the ends of the pipe to hold internal pressure during experimental tests were modeled. Therefore, with internal pressures, a net-section tensile force is generated in the longitudinal direction (i.e., end cap effect). The net-section tensile force is known to increase the CSC.

7.4.3.5 CRES Models

7.4.3.5.1 Equations for Compressive Strain Capacity

The CRES models are given in the following Eq. (7-20) to (7-27),

$$\varepsilon_c^{\text{crit}}(\%) = \min(\varepsilon_u, F_{LD} \cdot \varepsilon_r) \quad (7-20)$$

$$F_{LD} = \begin{cases} \varepsilon_r \left\{ 1 - 0.50 \cdot (1 - 0.75\varepsilon_r^{-0.23}) \left[1 + \tanh \left(8.0 \frac{\varepsilon_e}{\varepsilon_r} - 8.2 \right) \right] \right\} & \text{SSC Lüder} \\ 1 & \text{SSC Round} \end{cases} \quad (7-21)$$

$$\varepsilon_r(\%) = F_{DP} \cdot F_{YT} \cdot F_{GI} \cdot F_{NF} \quad (7-22)$$

$$F_{DP} = \begin{cases} 980 \left[0.5 \left(\frac{D}{t} \right)^{-1.6} + 1.9 \cdot 10^{-4} \right], & \text{if } f_p < f_{pc} \\ 980(1.06f_p + 0.5) \left(\frac{D}{t} \right)^{-1.6}, & \text{if } f_p \geq f_{pc} \end{cases} \quad (7-23)$$

$$f_{pc} = 1.8 \cdot 10^{-4} \cdot \left(\frac{D}{t} \right)^{1.6} \quad (7-24)$$

$$F_{YT} = 2.7 - 2.0\xi \quad (7-25)$$

$$F_{GI} = 1.84 - 1.6 \left(\frac{h_g}{t} \right)^{0.2} \quad (7-26)$$

$$F_{NF} = \begin{cases} 1.2f_n^2 + 1, & \text{if } f_n \geq 0 \\ 1, & \text{if } f_n < 0 \end{cases} \quad (7-27)$$

In the above equations, ε_u is pipe uniform strain, ε_e is the strain where the Lüder's extension ends, f_p is the pressure factor (i.e., the ratio between the pressure induced hoop stress and pipe yield strength), f_n is the net-section stress factor (i.e., the ratio between the longitudinal stress induced by the net-section force and pipe yield strength), D is pipe OD, t is pipe wall thickness, ξ is pipe Y/T ratio, and h_g is the height of the geometry imperfection from peak to valley (see Figure 7-32). The pipe yield strength is used in the calculation of f_p , f_n , and Y/T ratio. If

available, the actual pipe yield strength should be used. For the design stage, it is recommended to use the specified maximum yield strength for calculating f_p and f_n . The maximum specified Y/T ratio should be used.

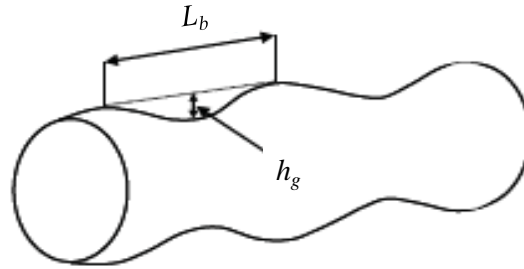


Figure 7-32 Definition of geometry imperfections

7.4.3.5.2 Recommended Geometry Imperfections

To properly apply the newly developed compressive strain capacity models (i.e., UOA and CRES), it is critical to have a reasonable estimation of the geometry imperfection if the actual data are not available. There exist very limited data on the geometry imperfection in the public domain. Figure 7-33 shows the geometry imperfection measured from seven pipe specimens. All the imperfections are in the form of surface undulations. The data indicate that the height (from peak to valley) of the imperfection varies between $0.06\%D$ and $0.14\%D$ and $2\%t$ and $8\%t$. It should be noted that all the seven pipe specimens are UOE pipes and it is not clear whether or not other types of pipes will have similar geometry imperfections. Considering the data are very limited and are from UOE pipes made in recent years, the range of the geometry imperfection in Figure 7-33 may not represent the full range of the geometry imperfection. The height of the geometry imperfection is recommended as the following,

$$\text{Median } h_g = \max(0.13\%D, 8\%t),$$

$$\text{Lower Bound } h_g = \max(0.05\%D, 1\%t),$$

$$\text{Upper Bound } h_g = \max(0.2\%D, 15\%t).$$

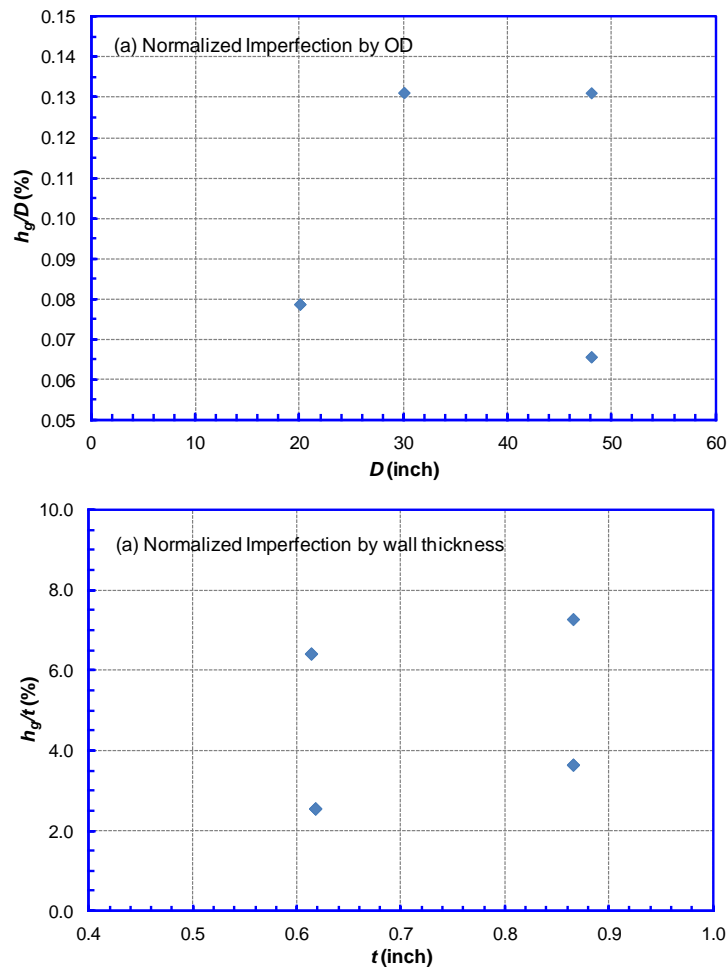


Figure 7-33 Measured geometry imperfections

The median imperfection height (h_g) is recommended to be the greater of $0.13\%D$ and $8\%t$, i.e., the upper bound values observed in Figure 7-33. The lower bound height is the greater of $0.05\%D$ and $1\%t$, i.e., the lower bound values observed in Figure 7-33. The upper bound value is determined to keep the median value to be the average of the upper and lower bound values. The recommended imperfection is applicable for both plain pipes and pipes with girth welds.

7.4.3.5.3 Applicable Ranges

The applicable range of the refined compressive strain capacity models is determined by the range of the parameters used in the finite element analyses. Based on the parameters used in the FEA and the model evaluation results in a later section, the applicable range of the compressive strain capacity models is given in the following:

- (1) $20 \leq D/t \leq 104$;
- (2) $0 \leq f_p \leq 0.80$;
- (3) $0.70 \leq \xi \leq 0.96$;
- (4) $0.01t \leq h_g \leq 0.30t$;

(5) $\varepsilon_e \leq 2\%$; and

(6) $f_n \leq 0.40$.

7.4.4 Comparison of Models with Test Data

7.4.4.1 Experimental Database

An experimental database was compiled using testing data published in public domain and was used to evaluate the refined compressive strain capacity models. The database consists of 48 full-scale bending tests and experimentally measured CSC was provided for 40 out of the 48 tests. The database covers the following range,

- OD (D): 6.6 - 48 (in)
- WT (t): 0.13 - 0.93 (in)
- D/t : 22 - 104
- Grade: X52 - X100
- YS (σ_y): 55 - 98 (ksi)
- Y/T: 0.77 - 0.91
- Lüder's strain (ε_e): $< 1.6\%$
- Pressure factor (f_p): 0 - 0.82
- Net-section stress factor (f_n): -0.42 - 0.62
- CSC ($\varepsilon_c^{\text{crit}}$): 0.23 - 6.2 (%)

The pipe grades covered in the test database range from X52 to X100. The number of tests for each pipe grade is almost evenly distributed for the grades up to X80 and there is only one test for X100 (Figure 7-35). The database covers D/t ratios ranging from 22 to 104 where about 52% of the tests fall in the D/t range between 50 and 80, as shown in Figure 7-36. The database covers pressure factors from 0 to 0.82, with 29% of the tests having zero pressure and 31% of the tests having high internal pressure ($f_p > 0.6$) (Figure 7-37). The Y/T ratios in the database range from 0.77 to 0.91, where 44% of the tests have pipes with Y/T > 0.85 , as shown in Figure 7-38.

7.4.4.2 Evaluation with Testing Data Having All Input Parameters

The geometry imperfection is found to be critical to the CSC and recognized by the CRES compressive strain capacity models. As shown in Figure 7-34, the CSC can differ by more than a factor of two (2) depending on the size of the geometry imperfection. The geometry imperfection may not be easily available, however, especially for the in-service pipelines.

Except for seven (7) tests, the geometry imperfection was not given for the other tests in the database. All required input parameters by the CRES models are available for the seven tests. The comparison of the predicted and measured CSC values for the seven tests is shown in Figure 7-39. It is seen that the predicted CSC match the measured ones very well.

7.4.4.3 Evaluation with All Testing Data

The comparison between the experimentally measured CSC and the CSC predicted using the recommended median or measured (if available) geometry imperfections is shown in Figure 7-40 for the full database. The predicted CSC using the recommended median geometry imperfections capture the trend of the overall experimental data very well.

The comparison between the experimentally measured CSC and the CSC predicted using the recommended upper bound geometry imperfections is shown in Figure 7-41.

The ratios between the experimentally measured and predicted CSC were also calculated. If the ratio is greater than one, the prediction is conservative. The statistics of the calculated ratios of the full database are summarized in the following,

- Median imperfection: average = 0.99, standard deviation = 0.30
- Lower bound imperfection: average = 0.82, standard deviation = 0.26
- Upper bound imperfection: average = 1.18, standard deviation = 0.38

The average ratio calculated with the median imperfection is 0.99 with a standard deviation (SD) of 0.30. The recommended median value of imperfections provides fairly reasonable predictions of the testing results.

The average ratios calculated with the lower bound and upper bound imperfections are 0.82 (SD = 0.26) and 1.18 (SD = 0.38), respectively. Therefore, in general, reasonably conservative predictions can be obtained with the upper bound imperfections.

It is known that the prediction of the CSA models is often overly conservative. The CSC predicted by the CSA models (without safety factor) is compared with the experimental data in Figure 7-42. It is seen that the CSA models provided conservative predictions for almost all the tests.

The predicted CSC by the CSA (without safety factor) and CRES models (using the recommended upper bound geometry imperfections) is compared in Figure 7-43. From the comparisons shown in Figure 7-41 and Figure 7-43, it is seen that the CRES models with the upper bound imperfections can provide reasonably conservative predictions. The overly conservative predictions by the CSA models, especially for those tests showing large CSCs, can be avoided.

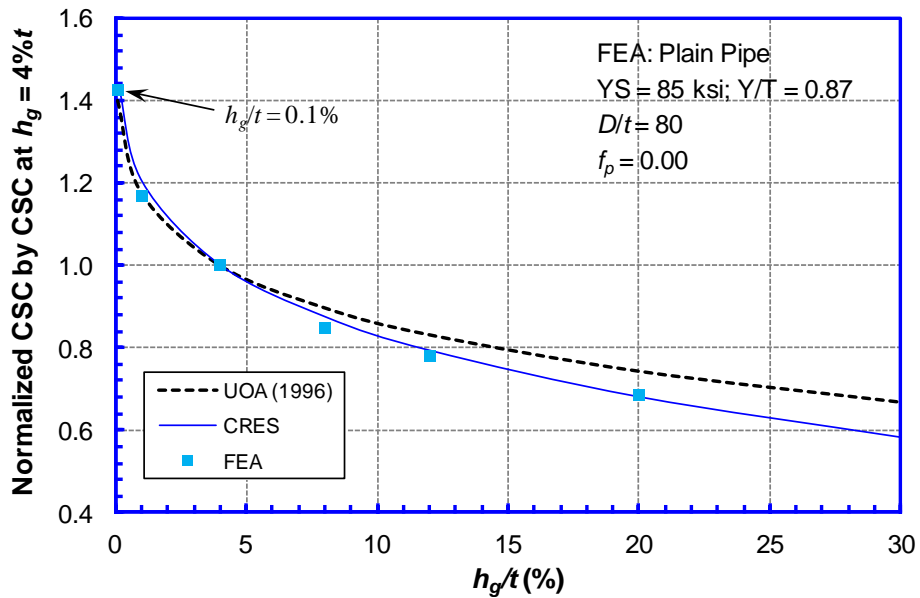


Figure 7-34 Normalized CSC - geometry imperfection (h_g) relationship from CRES and UOA models and FE results

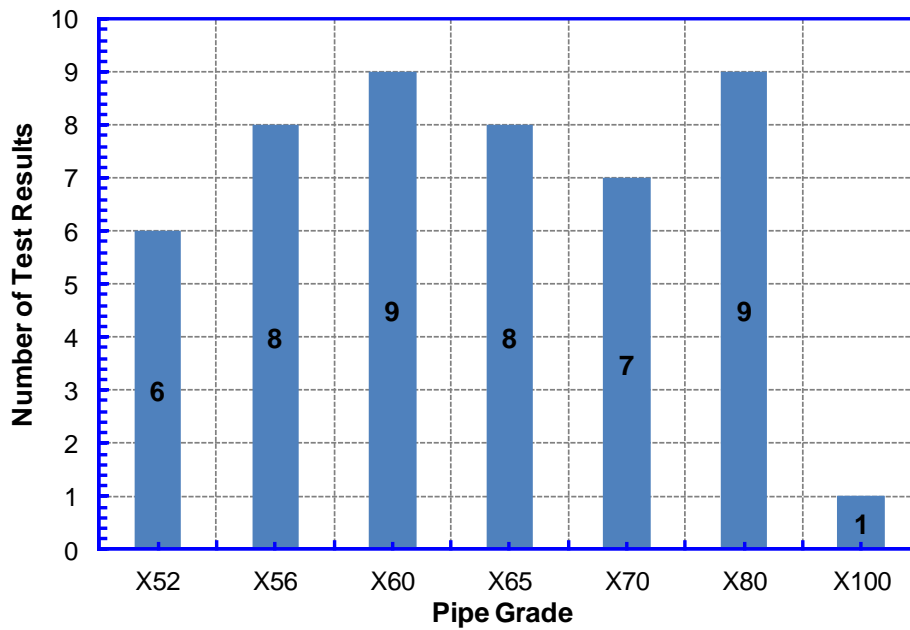


Figure 7-35 Distribution of test database over pipe grade

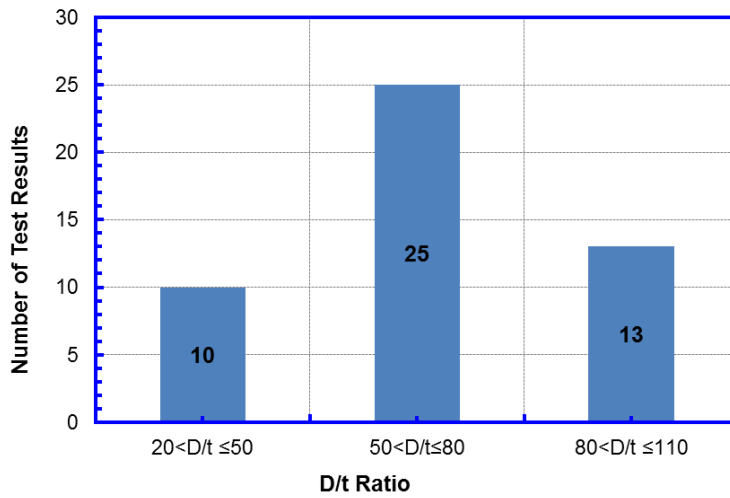


Figure 7-36 Distribution of test database over D/t ratio

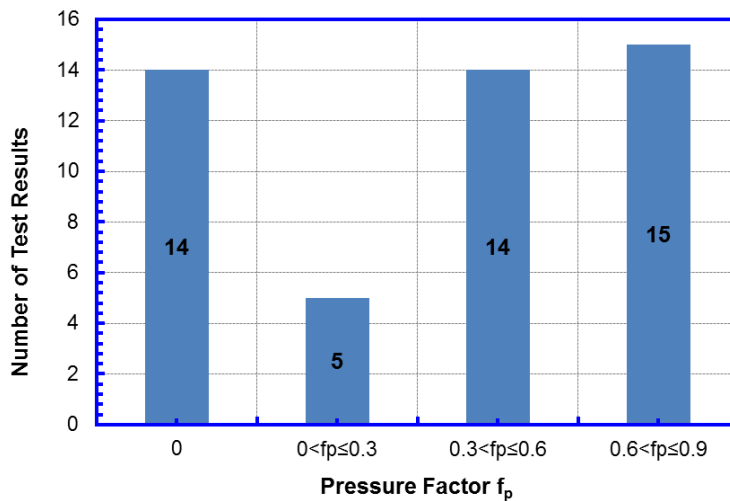


Figure 7-37 Distribution of test database over pressure factor

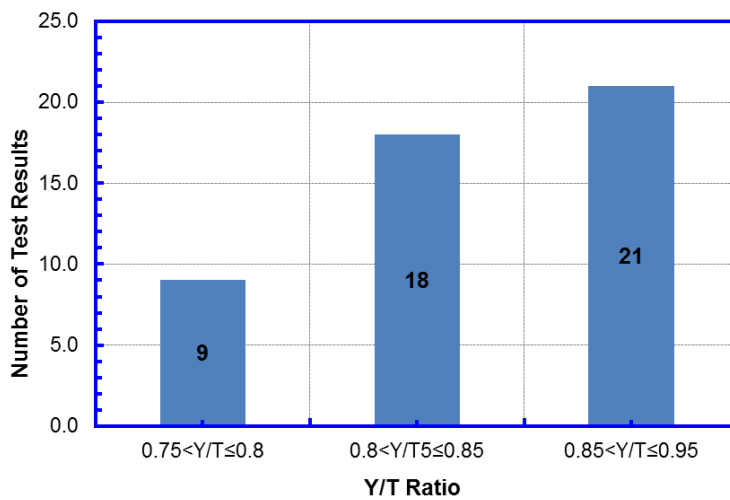


Figure 7-38 Distribution of test database over Y/T ratio

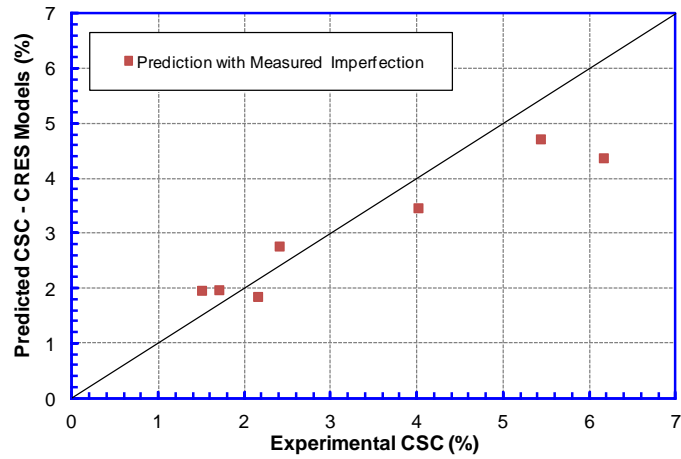


Figure 7-39 Comparison of predicted and measured CSCs - with measured imperfections

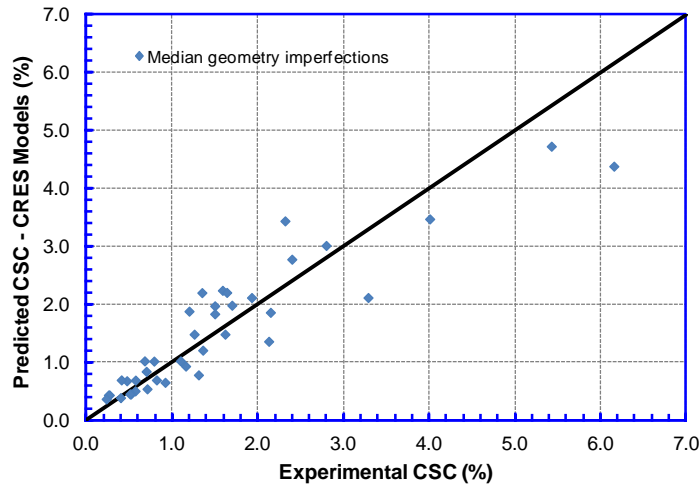


Figure 7-40 Measured vs. predicted CSCs - CRES models (with median/measured imperfection)

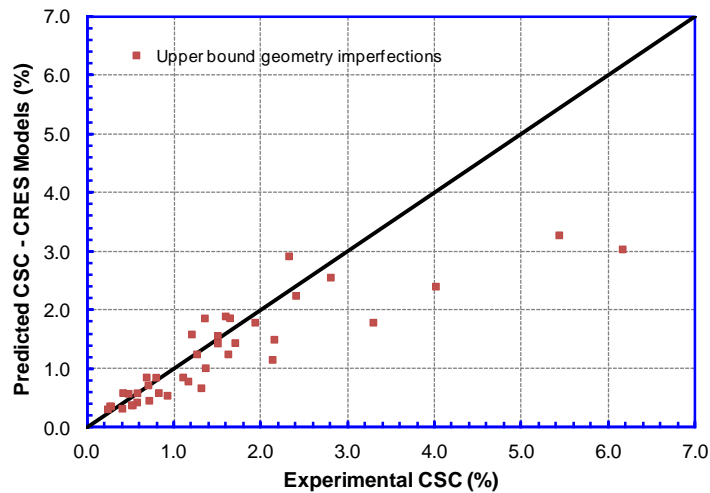


Figure 7-41 Measured vs. predicted CSCs - CRES models (with upper bound imperfection)

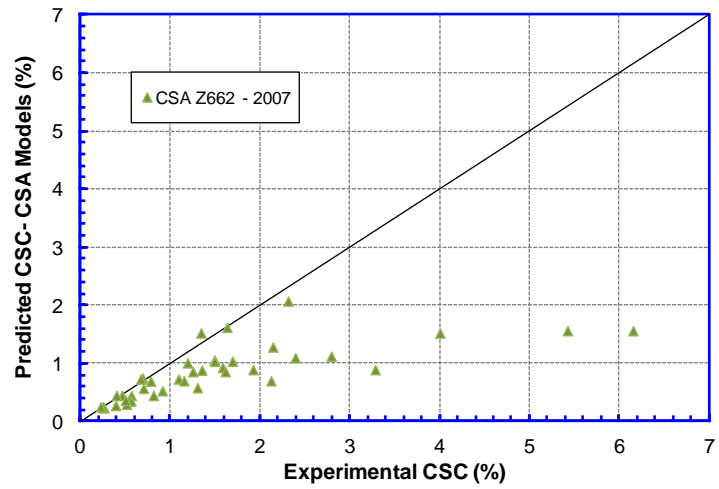


Figure 7-42 Measured vs. predicted CSCs - CSA models (no safety factor)

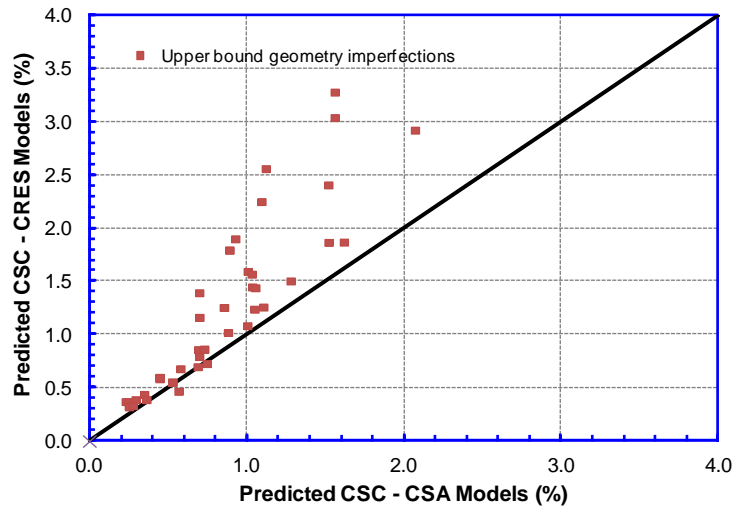


Figure 7-43 Comparison of CSA (no safety factor) and CRES (with upper bound imperfections) predictions

8 Mitigation and Monitoring

Abstract

Section 8 addresses the mitigation and monitoring of geologic hazards, with a focus on landslides and subsidence. It builds upon the efforts to identify and characterize geologic hazards previously described in Section 2.

Hazard mitigation and monitoring, specifically for landslide or subsidence hazards, is the logical next step in addressing potential adverse effects the hazard(s) may have on a pipeline system. Mitigation can be viewed as the management of a geologic hazard or threat and its potential effects on a pipeline. Once a mitigation measure is implemented, its performance must be monitored in order to assure that it continues to function correctly, protecting the integrity of the pipeline, or to identify developing adverse effects that may warrant a response and additional mitigation.

Hazard mitigation can take many forms, including avoiding the hazard, stabilizing and controlling the hazard, reducing the effects of the hazard on the pipeline, and/or increasing pipe strain capacity. In some cases, mitigation may involve initially monitoring the hazard and/or its effects on the pipeline, with intent to implement one of the mitigation interventions when the hazard reaches a critical stage of development.

Monitoring of the hazard and/or its effects on the pipeline is commonly done after an interventional mitigation approach/strategy/methodology has been implemented, but monitoring is also employed as an interim step prior to intervention, if mitigation is not performed immediately. Monitoring may involve qualitative and/or quantitative measurement and tracking of ground (landslide/subsidence) movement, or it may involve quantitative measurement of pipe response to the ground movement. Typically, monitoring incorporates a combination of ground movement and pipe monitoring strategies and methods. Additionally, the nature of the mitigation in combination with the nature of the hazard, drive the development of the monitoring plan/program.

Both mitigation and monitoring are dependent on the development of a site-specific geologic (hazard) model (discussed in Section 2). A site-specific model provides for a physical understanding of the hazard process, which is critical to identifying and developing mitigation and monitoring strategies and methods.

Throughout Section 8, tables are provided, summarizing common mitigation and monitoring technologies and methods, and their attributes and limitations as applicable to landslide and subsidence hazards.

8.1 Overview

Section 2 discussed identification, characterization, and evaluation (from a geotechnical viewpoint) of landslide and settlement/subsidence hazards that could affect pipeline systems. Section 2 also described a phased approach to addressing the landslide and settlement/subsidence hazards affecting pipeline systems. This section addresses mitigation and monitoring of geohazards with a focus on landslides and subsidence.

The next step in addressing landslide or subsidence hazards that have been characterized is the mitigation of potentially adverse effects the hazard(s) may have on the pipeline system. Mitigation can be viewed as the management of a geologic hazard or threat and its potential effects on a pipeline [200, 7]. Once a mitigation measure is implemented, its performance must be monitored in order to ensure that it continues to function correctly, protecting the integrity of the pipeline, or to identify developing adverse effects that may warrant a response and additional mitigation [200, 7].

Hazard mitigation can take many forms, including avoiding the hazard, stabilizing and controlling the hazard, reducing the effects of the hazard on the pipeline, and/or increasing pipe strain capacity [200]. In some cases, mitigation may involve monitoring the hazard and/or its effects on the pipeline, with intent to implement one of the preceding interventions when the hazard reaches a critical stage of development.

The primary focus of hazard mitigation (in this case, mitigation of landslides and settlement/subsidence) is to reduce pipe strain demand and/or increase pipe strain capacity. The overall purpose or objective of mitigation is to reduce or eliminate the likelihood and/or consequences of the potential hazard and maintain pipeline integrity.

Monitoring of the hazard and/or its effects on the pipeline is commonly done after an interventional mitigation approach/strategy/methodology has been implemented and as an interim step prior to intervention if it is not performed immediately. The monitoring program may be focused on:

1. Verifying that there is zero or minimal slope movement once landslide stabilization is implemented to confirm that stabilization efforts are working successfully, or
2. Tracking the movement of the hazard (i.e., hazard monitoring) to monitor when the hazard has diminished or minimized; e.g., when a longwall coal mining panel has been completed below a pipeline, or
3. Tracking the response of the pipeline to landslide and settlement/subsidence movements (i.e., pipe monitoring).

Typically, monitoring incorporates a combination of strategies and methods. Additionally, the nature of the mitigation in combination with the nature of the hazard, drive the development of the monitoring plan/program.

Hazard monitoring and/or pipe monitoring, alone can also be used as a mitigation strategy if the hazard has not adversely affected the performance of the pipe being monitored and the hazard characteristics are known. The assumption is that the integrity of the pipe is well-understood, and that the monitoring program will identify any adverse changes to the hazard and/or pipe that could potentially degrade the integrity of the pipe. If adverse changes are detected by the monitoring program, then response plans and the development of more robust mitigation strategies and alternatives may be needed. Monitoring as the sole hazard mitigation strategy is generally only suitable for hazards with movement rates classified as “slow”, “very slow”, or “extremely slow” (Table 2-2), because faster developing hazards will typically not

provide enough time to implement a response plan if movement of the hazard is measured. These response plans and/or more robust mitigation strategies and alternatives should be developed prior to implementing the monitoring program.

Both mitigation and monitoring are dependent on the development of a site-specific geologic (hazard) model resulting from Phases II/III efforts of hazard identification, characterization, and evaluation that are discussed in Section 2. A site-specific geologic model provides physical understanding of the hazard process, including the location, dimensions, geometry, nature, and level of activity. These data are critical to identifying and developing mitigation and monitoring strategies. The development of a site-specific geologic model often requires the engagement of qualified geologic and geotechnical professionals.

Section 8.2 provides brief summaries of the various common potential mitigation alternatives, including descriptions of the benefits and limitations of each alternative as well as combinations of different alternatives. Section 8.3 provides descriptions of common monitoring strategies, and techniques and methodologies that can be employed at landslide and subsidence sites.

8.2 Hazard Mitigation Techniques and Methodologies

The following sections provide brief conceptual discussions of various common mitigation strategies and methods applicable to landslide and subsidence hazards. These may be employed individually or in combination and include the following [7, 200, 201]:

- Hazard avoidance (e.g., re-route around hazard, under hazard using deep burial, HDD, micro-tunneling, or above hazard using above-ground installation),
- Hazard stabilization (primarily for landslides), using structural systems (e.g., buttress, shear key, external and internal slope reinforcement), unloading the slope, improving/changing slope geometry, or improving groundwater and surface water conditions, and
- Improving pipe performance relative to the effects of the hazard using techniques such as stress/strain relief excavation, improved trench geometry, use of select deformable/low friction backfill and drainage enhancements, use of thicker wall pipe, or maintaining favorable pipe orientation relative to the hazard.

8.2.1 Hazard and Consequence Avoidance

Hazard avoidance is often one the best mitigation strategies to follow because it typically permanently removes the hazard from further consideration by the pipeline owner/operator. Hazard avoidance also generally precludes the need for any follow-up or on-going hazard or pipe monitoring. Hazard avoidance typically involves going around, under or over a hazard or potential hazard and almost always involves complete pipe replacement. Common limitations of hazard avoidance are:

1. Siting/routing, permitting, design, and construction costs may be significant compared to other remedial measures,

2. These large projects can need considerable time to be completed and may require interim hazard mitigation and/or monitoring,
3. Non-technical third-party and stakeholder issues may limit potential technical options during replacement projects, and
4. Pipe replacements may be not feasible/less desirable where outages are difficult due to business concerns.

A somewhat different type of avoidance is “consequence or event avoidance.” This does not involve a permanent or temporary routing around a hazard, but instead requires premonitory information of an impending adverse hazard/impact such that the pipeline can be preemptively shut-in, and if needed any affected population can be evacuated to avoid the hazard until the hazard issue is dealt with. An alternative approach to event avoidance is simply to shut down a pipeline system for the entire period that a specific hazard exists, as an example, if a debris flow hazard occurs annually from 15 May to 30 June, then the pipeline would not be operated during that period.

The various attributes and limitations of the common avoidance mitigation strategies for landslide and subsidence hazards are summarized in Table 8-1.

Table 8-1 Potential hazard and consequence avoidance methodologies

Method	Description	Attributes	Limitations
Reroute around hazard	Rerouting around the hazard involves the identification, location, design, and construction of a new pipeline and ROW around the landslide or subsidence hazard. (Figure 8-1)	Avoids the hazard such that the hazard no longer influences pipeline integrity.	Depends on project timelines, interim hazard mitigation and/or monitoring, and additional ROW (which may be difficult to obtain). Permitting requirements may be onerous or prohibitive.
Reroute under hazard (deep burial, HDD, tunnel/microtunnel)	An HDD or tunnel/microtunnel is sited and designed to pass beneath the hazard (e.g., landslide). If a landslide is shallow enough, then deep burial below the failure/slip surface avoids future landslide movement. A detailed discussion of HDD technology and planning is included in Reference [202].	Generally, avoids the hazard such that the hazard no longer influences pipeline integrity.	An HDD or microtunnel may not be feasible depending on the geologic, geometric, and hydrogeologic site conditions. Detailed feasibility studies should be conducted to ensure the proposed trenchless method is viable as approximately 95% of the budget is spent prior to knowing if the project is going to be successful or not. There is really no industry standard or accepted performance criteria for pipeline coating condition after install. If the landslide enlarges vertically and laterally, the landslide may re-engage the pipe.
Reroute over hazard (span)	Rerouting over the hazard (e.g., landslide) typically involves the siting, design, and construction of a span that places the pipe above the potential hazard. (Figure 8-2)	Generally, avoids the hazard such that the hazard no longer influences pipeline integrity	There may be long-term CP, maintenance and vandalism issues. There may also be the potential for the landslide to enlarge and impact the reroute.
Mini-reroute within hazard	Detailed hazard characterization may identify relatively more stable portions of a landslide or subsidence hazard, such that small route changes within the hazard can be sited to avoid the more active areas.	The mini-reroute within the hazard allows for a reduced exposure to the detrimental effects of the hazard on the pipeline. The cost to implement the mini-reroute may be less significant than for more permanent mitigation strategies.	Because the mini-reroute remains within the hazard, it may not be a permanent mitigation method. Thus, long-term monitoring is needed to track the movement of the hazard, and/or the pipe's response to the movement of the hazard.

Table 8-1 Potential hazard and consequence avoidance methodologies (Cont'd.)

Method	Description	Attributes	Limitations
Surface installation through/on hazard	Lateral loads or low angle parallel loads, particularly from landslide movement, can be reduced by placing the pipe on the ground surface, on above-ground supports [7,203] or with only shallow burial. The pipe can be placed on skids, elevated supports, prepared bare ground surface, and if on the ground surface, and can be protected by soil berms or culverts (Figure 8-3 and Figure 8-4).	The placement of the pipe above-ground isolates the pipe from significant lateral loads transferred through the trench backfill. When pipelines are placed on skids they can also handle low angle parallel loads in extremely slow moving landslides. The cost to implement may be relatively less than the re-route or span options. Temporarily decoupling the pipeline from soil movement by re-laying above ground or operating in an open ditch is a common approach for longwall mine subsidence	The above-ground installation tends to reduce the exposure to the hazard, but does not necessarily permanently remove the pipe from the effects of the hazard. Permanently locating pipes above-ground is rarely a viable option unless the location has controlled access, or is remote [7]. Long-term monitoring is needed to track the movement of the hazard, and/or the response on the pipe to the movement of the hazard. Routine maintenance of skids and/or elevated pipe supports is required. Additionally, in colder climates, the changes in pipeline steel properties must be considered in design and installation to reflect the potential impact of cold temperature. There may be long-term CP and vandalism issues.
Consequence or hazard event avoidance	Typically involves shutting-in, or shutting down the pipeline and evacuating the product from a pipeline that has an imminent or highly probable hazard of rupture caused by the geologic hazard. Typical scenarios involve either natural gas lines in populated areas or liquid lines in populated/environmentally sensitive areas. Lines may be shut down, shut-in or operated at lower pressures or volumes.	Allows the pipeline to continue operation within, or exposed to the geologic hazard, which may reduce the cost of overall hazard mitigation compared to other mitigation options. It may be the only viable alternative in populated areas where dense development constrains the implementation of alternative mitigation methods.	Consequence or hazard event avoidance depends on a comprehensive and complete long-term monitoring program that allows for timely detection of ongoing, and imminent hazard movement so that effective pipeline shutdown and population evacuation can be implemented. The cost to plan, purchase, install, and maintain the long-term monitoring program may be significant.

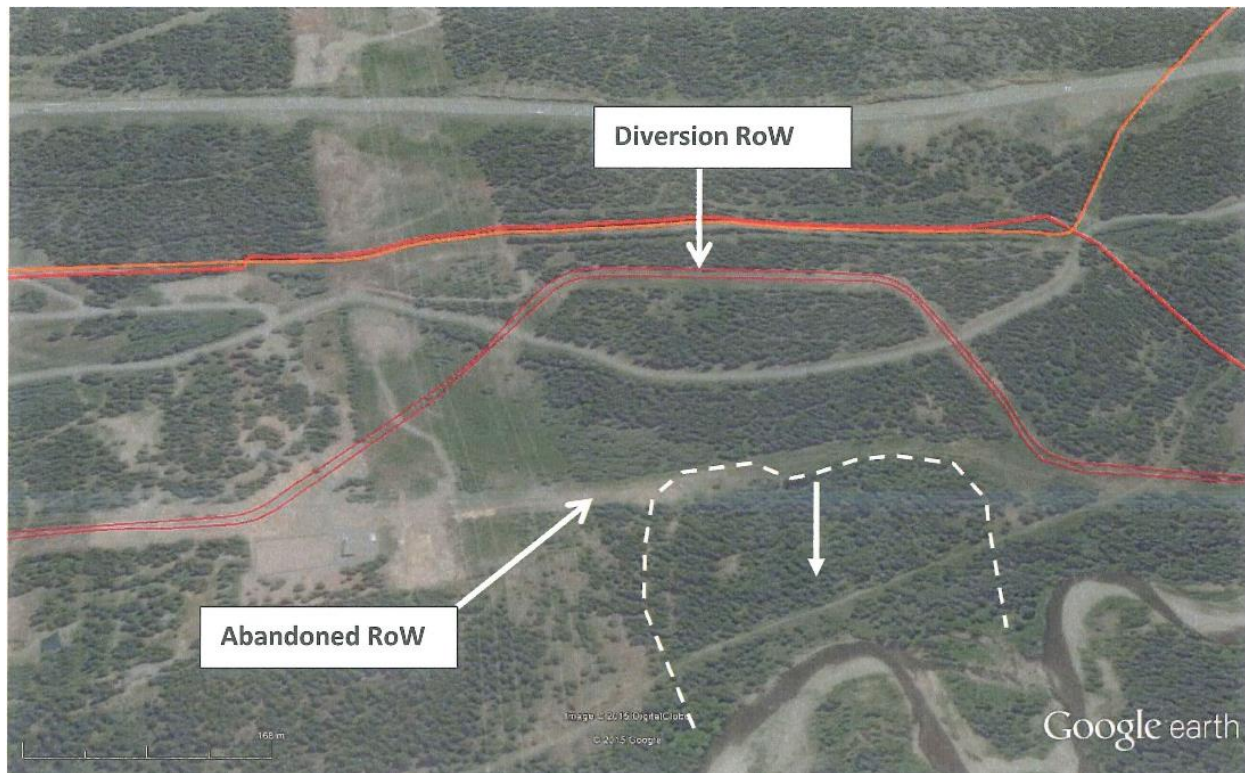


Figure 8-1 Google Earth™ image of abandoned ROW that has been encroached on by deep seated translational slide triggered by toe erosion. The diversion right away is located upslope of the landslide. (Source: Google Earth, Location: Merritt, southern British Columbia)



Figure 8-2 Aerial crossing constructed to reroute 30-inch and 36-inch mainline over a hydrotechnical hazard (Photo by: D. Dewar, Location: Central British Columbia, Year: 2011)



Figure 8-3 Surface pipeline segment on wooden skids for a low angle translational landslide moving from the right to left of photo (Photo by: E. McClarty, Location: Northern British Columbia, Year: 2007)



Figure 8-4 Surface pipeline segment running parallel to the direction of movement (Photo by: L. Allen, Location: Northwestern British Columbia, Year: 2011)

8.2.2 Hazard Stabilization

Hazard stabilization in the context of this report applies mostly to landslides, but also includes specific techniques/methods for the stabilization of sinkholes or karst chimneys that could develop in a ROW in karst terrain, as well as thermal protection of soil in permafrost that left unprotected could lead to landslide or subsidence hazards. All of the hazard stabilization mitigation methods discussed below require that a site geologic model be developed prior to developing mitigation designs. Site geologic, geotechnical, and hydrogeologic investigations are commonly required to support the development of geotechnical engineering hazard stabilization mitigation designs. Every situation where a hazard interacts with a pipeline(s) has unique characteristics based on variations in hazard types, geology, geometry, and many other characteristics; therefore, any site-specific mitigation strategy should be developed in consultation with a geoscientist/geotechnical specialist familiar with the area.

The primary methods for hazard stabilization to address landslides, karst, and permafrost can be organized in the following groups:

- Landslides (one or more of the following)
 - Slope modification
 - Mechanical reinforcement of the slope
 - Collection and management of surface water and groundwater
- Karst (use of inverted soil/rock filter)
- Permafrost (maintenance of thermal regime)

8.2.2.1 Landslide Stabilization

For landslides, the primary objective of stabilization is to permanently stop landslide movement, and thereby stop its adverse effects on the pipeline. The various landslide stabilization mitigation alternatives have one or both of the following goals [7]:

- Increase the stability of the slope so that the likelihood of future landslide movement is acceptable to the pipeline owner/operator as well as regulatory bodies (this may or may not also consider potential future movement due to a seismic event), and/or
- Reduce the rate of landslide movement to a level compatible with pipeline operational considerations to manage the risk of adverse pipeline response.

Overall, landslide stabilization, through slope modifications and mechanical reinforcement of the slope, seeks to [7]:

- Reduce the forces that drive slope/landslide movement, and/or
- Increase the resisting forces acting against slope/landslide movement.

Table 8-2 is summary of the landslide stabilization mitigation methods or techniques that are commonly applied to pipelines. The table includes a brief description of each method and its attributes, as well as typical limitations.

Table 8-2 Landslide stabilization mitigation methods [7, 200, 201, 204, 205, 206, 207, 208, 209, 210, 211] (Cont'd.)

Mitigation Category	Method and Attributes	Limitations
Slope Modification	<p><u>Slope Grading</u>: Grading of the landslide/slope is done to change the slope angle to a more stable geometry. Slope grading can also include the entire replacement of the landslide material to remove the hazard. Slope grading may involve removal of material in the head area and placement of material in the toe area which achieves an overall flatter slope angle, and serves to reduce loads (driving forces) in the head area and increase resisting forces in the toe of the slope (Figure 8-5 and Figure 8-6). Grading can be carried out with conventional earth moving equipment.</p> <p>Note that this is the opposite of the approach often taken (restoring the original contours by pushing toe material back to the head area).</p>	<p>Slope grading may not be feasible or cost effective for large landslides, where a considerable length of pipeline is involved. Not generally suited for deep-seated landslides. Requires care during construction to prevent triggering of local and global landslide movement. Where pipelines are shallow, ground disturbance practices have to be carefully considered. The potential hazard of construction equipment interacting with pipelines should be carefully considered. Typically, removal of material from the head of the slide may not be feasible as the pipeline cover may be reduced to unacceptable levels.</p> <p>Landowners or other stakeholders may prefer that the slope be restored to its pre-slide condition (the opposite of what is required to reduce the probability of future landslide)</p>
	<p><u>Bio-engineering</u>: Bioengineering mitigation measures include living (e.g., herbaceous and woody species) and structural (e.g., timber crib walls and bender fences) components, and the two components are often combined. The living approach includes conventional direct planting of grasses, shrubs, or trees, and techniques that use the stems and branches of living plants to reinforce the soil. The structural approach uses live plant stakes, live fascines, brushlayers, hedgelayers and branchpacking. Following installation, the growth of stems and roots create the structural component. Effective stabilization depths prior to rooting are from 20 to 120 cm (8 to 47 in). An example of a live stake used for bio-engineering mitigation is shown on Figure 8-7.</p>	<p>Effective installation of bio-engineered mitigation measures requires site-specific information on geology, soils, slope angle, slopes aspect, and hydrology. Bio-engineering measures do not work on bedrock slopes or those greater than about 35°-50°. The selection of suitable plant species should be based on detailed vegetation surveys. Bio-engineering measures will not work for deep-seated landslides, nor where erosion has removed the soil layer. Bioengineering may not be applicable where there are pipeline vegetation management considerations. Most ROW regulations do not allow for dense vegetation in a defined corridor over a pipeline.</p>

Table 8-2 Landslide stabilization mitigation methods [7, 200, 201, 204, 205, 206, 207, 208, 209, 210, 211] (Cont'd.)

Mitigation Category	Method and Attributes	Limitations
Mechanical Reinforcement of the Slope	<p><u>Buttress</u>: An engineered buttress or berm at the toe of the slope can be constructed using conventional earth moving equipment, and can be combined with slope grading. A buttress increases the resisting forces of the slope/landslide. Buttresses can be constructed with native or imported material that may or may not be reinforced with geosynthetic products such as geogrids and geotextiles. An example of a rock buttress at the toe of a slope is shown in Figure 8-8.</p>	<p>Detailed knowledge of site subsurface geology and hydrogeology is critical to the design of the buttress or toe berm. The construction may require the excavation and placement of large volumes of material and the rock buttress will require selected and sized material. Permitting, design, and construction may require significant effort, time, and cost. Additionally, potential increases in soil stress, buttress induced settlements, and future pipeline accessibility must be considered.</p>
	<p><u>Soil Densification</u>: Soil densification is applied where cohesionless soils (sands) in the presence of shallow groundwater exist and seismic shaking may trigger liquefaction resulting in slope failure. The soils are densified by drainage improvements on the slope, by surface loading intended to densify the soil, or by artificial vibrations (e.g., blasting), all intended to improve the soil's resistance to liquefaction.</p>	<p>The technique is typically expensive for application to pipeline alignments, and may be more applicable to compressor/pump stations. Ground disturbance (GD) issues must be considered as most GD practices do not permit drilling/bore-holing within 12 to 15 ft (4 to 5 m) of a pipeline without a positive locate.</p>
	<p><u>Shear Key/Piles/Walls/Soil Nails</u>: Shear keys, rows of piles/piers, walls, and soil nails/soil anchors installed through a landslide mass and into stable material (i.e., bedrock) below the landslide slip surface create a passive landslide stabilization system (Figure 8-9). After installation, slow landslide movements generate reaction forces in the embedded structures which lead to stabilization as the loads are transferred to the stable material below the landslide slip surface. A major advantage of these embedded passive structures is that they are installed in the landslide footprint, and they work even in high groundwater pressures. They can also be used to improve shear resistance along more than one slip surface and at depths not treatable using slope grading or toe buttresses/berms.</p>	<p>Proper design of embedded passive structures tends to require complex calculations and soil-structure interaction modeling which makes them difficult to design and construct, and usually involves specialty contractors. This may lead to relatively high costs. Additionally, these embedded structures tend to work more effectively with smaller landslides than with larger, deep-seated landslides or landslide complexes. As discussed above, GD practices must be considered. Typically, deep linear stabilization systems running perpendicular to a pipeline are not applicable in areas adjacent to the pipeline(s).</p>

Table 8-2 Landslide stabilization mitigation methods [7, 200, 201, 204, 205, 206, 207, 208, 209, 210, 211] (Cont'd.)

Mitigation Category	Method and Attributes	Limitations
Mechanical Reinforcement of the Slope	<p><u>Retaining Walls</u>: Retaining walls provide external resisting forces to landslide movement and are commonly installed in the toe area of a landslide. Retaining walls may be constructed using wood cribs, steel bins, reinforced earth, and gabions. Retaining walls can work well in constrained pipeline ROWs and may be combined with slope grading. An example of a gabion retaining wall is illustrated on Figure 8-10.</p>	<p>Detailed knowledge of the subsurface conditions and slip surface are required to properly design and evaluate a retaining wall. Not generally suitable for deep-seated landslides. May require specialty contractor. These factors lead to increased costs.</p> <p>GD issues, access to the pipelines and settlement/pipeline loading issues should be considered. In the case of retaining walls, great care should be taken in design as a failure of the retaining wall system could severely damage the pipeline it was intended to protect.</p>
	<p><u>Rock Bolts/Anchors/Dowels</u>: Rock bolts, anchors, and dowels are steel rods or cables and used to stabilize rock slopes by increasing the resisting forces in the slope. Anchors and bolts are post-tensioned, with anchors designed to stabilize large, deep-seated rock blocks and bolts for shallower rock faces. Dowels are similar to rock bolts, but are not post-tensioned. Figure 8-11 is a close-up of the head of a rock anchor on a rock slope.</p>	<p>Requires detailed, specialist’s knowledge of rock conditions, the landslide slip surface(s), and grouting and testing procedures. Requires specialty contractor for installation and thus, the costs can be significant.</p> <p>As above, GD issues should always be considered.</p>
Control and Management of Surface Water and Groundwater	<p><u>Surface Water</u>: The control of surface water is intended primarily to control surface erosion on the ROW, but it has a secondary benefit of reducing the volume of surface runoff infiltrating to the groundwater table, which could raise the groundwater and lead to slope instability. The control of surface water is done primarily with: 1) grading of the ROW slope (e.g., re-contouring and diversion berms) to positively direct runoff from landslide areas, or unstable slopes, 2) installation of slope breakers (water bars) (Figure 8-12 and Figure 8-13) on the ROW that intercept runoff water on the slope and convey it away from landslides, or unstable slopes, and 3) grading of a landslide/unstable slope surface so that water does not collect/pond on the surface, but is conveyed away from the landslide. Can be accomplished with conventional earth moving equipment.</p>	<p>May not result in permanent slope stabilization because it has an indirect impact on lowering, or maintaining a lowered groundwater table. May require detailed site topography. Long-term monitoring and maintenance needed to ensure effectiveness of the surface drainage features; unmaintained controls may actually increase infiltration. As above, GD issues should always be considered.</p>

Table 8-2 Landslide stabilization mitigation methods [7, 200, 201, 204, 205, 206, 207, 208, 209, 210, 211] (Cont'd.)

Mitigation Category	Method and Attributes	Limitations
<p>Control and Management of Surface Water and Groundwater</p>	<p><u>Groundwater:</u> Groundwater control involves collecting and conveying near-surface and deeper groundwater away from landslide and unstable slopes. The intent is to reduce the pore water pressures which drive the landslide. The collection and conveyance can occur in the pipeline trench, in the ROW, and occasionally, off the ROW. Shallow groundwater flowing in the pipeline trench is collected and controlled by trench breakers or trench dams. Trench breakers/dams are commonly constructed with pervious sand bags, low permeability clay/soil plugs and impermeable sprayed-in foam (Figure 8-15). The shallow groundwater in the trench is collected and conveyed away from the trench with a system of perforated and tightlined plastic pipes (PVC or ABS) to an area off the ROW/landslide/unstable slope.</p> <p>Shallow and intermediate-level groundwater, both in the ROW or off the ROW, can be collected using French drains and/or drainage blankets. A French drain is a coarse sand or gravel-filled trench which performs better if installed with a perforated collector pipe at the base, and is surrounded by a graded filter of selected gravels and sands or a geosynthetic product such as multiflow drains. The French drains and drainage blankets are designed to intercept and evacuate groundwater from the slope, under gravity, away from landslides and unstable slope conditions. Figure 8-16 and Figure 8-17 illustrate schematic examples of French drains and an installed drainage blanket, respectively. Figure 8-14 shows a sequence of French drain installation on a pipeline ROW. Deeper groundwater flows off the ROW and within landslides or unstable slopes may be intercepted, collected, and conveyed away using horizontal drains (Figure 8-18) and dewatering wells. The drains and wells can be constructed using conventional earth moving equipment and geotechnical drilling contractors.</p>	<p>May not result in permanent slope stabilization because it has an indirect impact on lowering or maintaining a lowered groundwater table. The hydrogeologic conditions need to be well established from site-specific studies. Long-term maintenance needed to ensure effectiveness of the installed groundwater control system. Long-term monitoring of the effectiveness of drainage systems, the landslide/unstable slopes, and the pipeline response may be required since the mitigation may not be permanent. Additionally, when using wells, projects may require power be brought to site and pumps to be maintained. In some instances, there may be issues with where the collected groundwater can be discharged to or if it is considered a contaminated substance. As above GD, issues should always be considered.</p> <p>Impervious trench breakers must include means of removal of water trapped above them, otherwise they can decrease slope stability.</p>

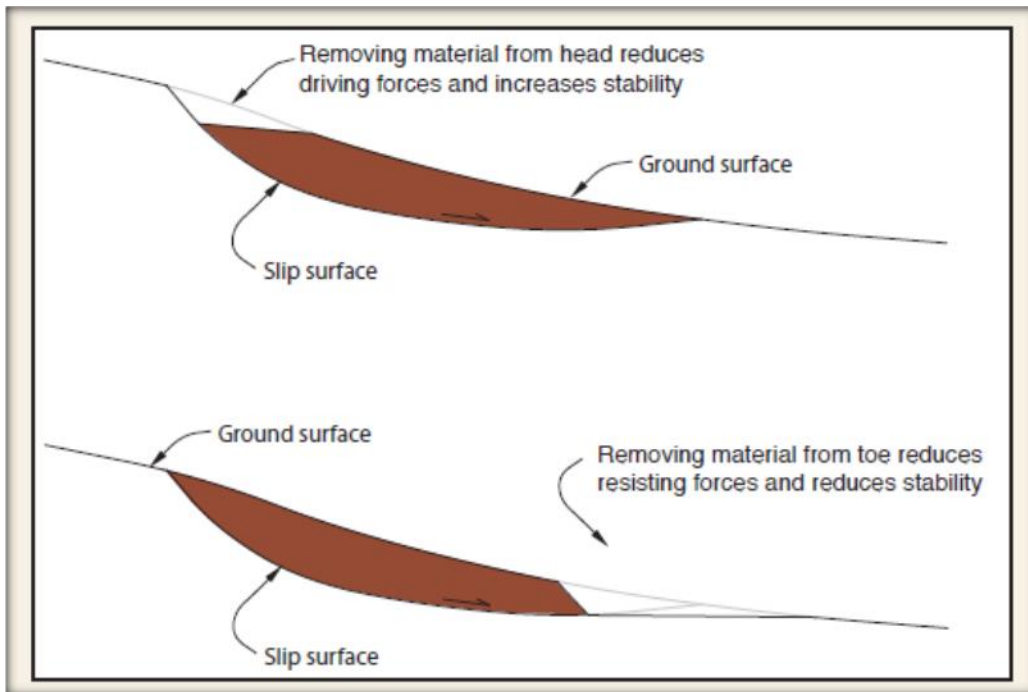


Figure 8-5 Illustration of the effects grading in the head area of a landslide to improve slope stability by reducing driving forces, where excavating in the toe area can decrease stability by reducing resisting forces [201]

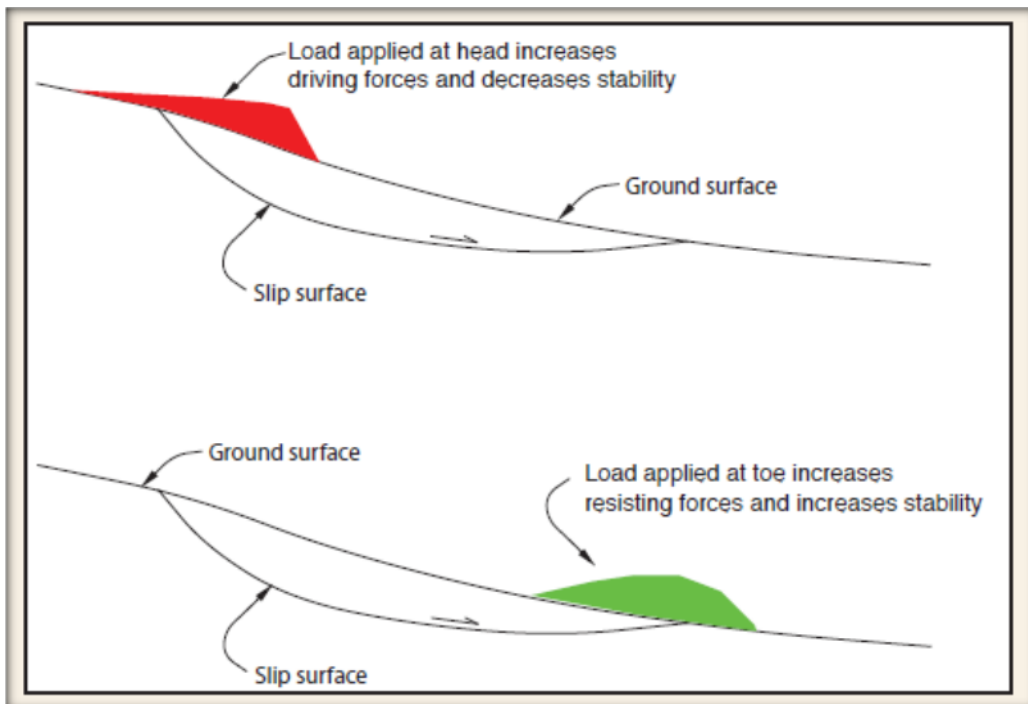


Figure 8-6 Illustration of the impact of placing fill in the head area of a landslide where it lowers slope stability by increasing the driving forces, and where placing fill in the toe area buttresses the landslide by increasing the resisting forces [201]

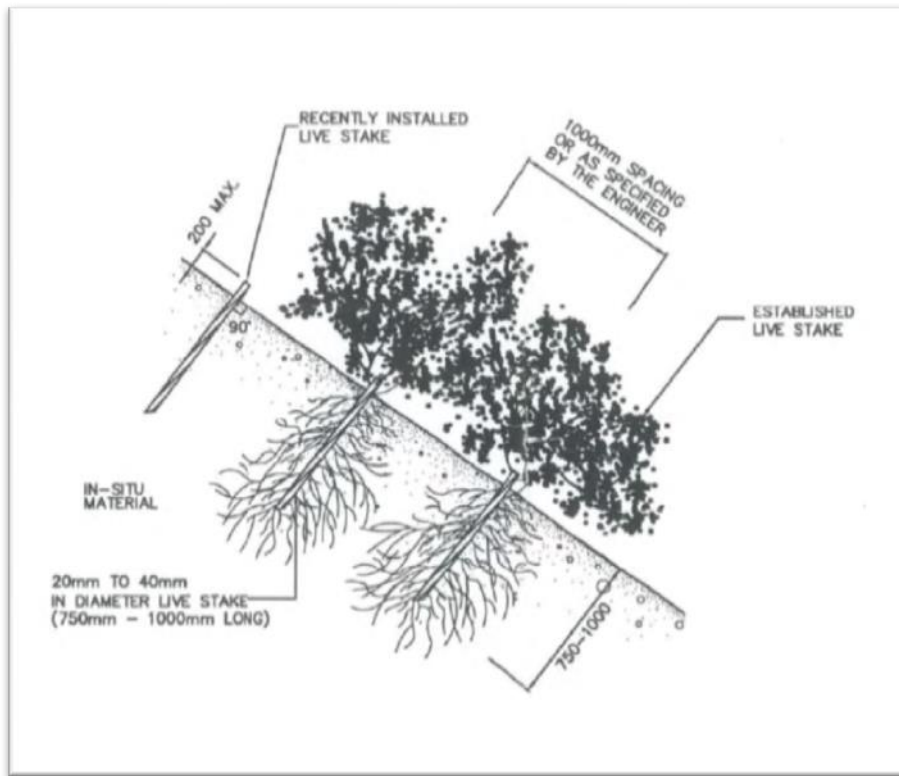


Figure 8-7 Illustration of live stakes used in bio-engineered slope stabilization [206]

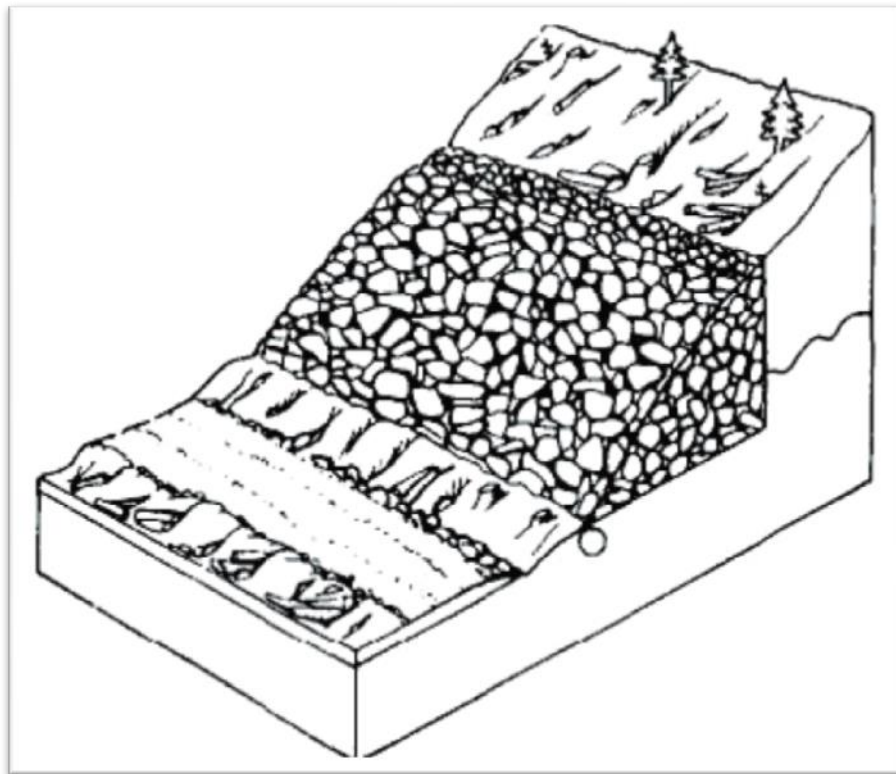


Figure 8-8 Schematic of a rock fill buttress at the toe of a slope [201]

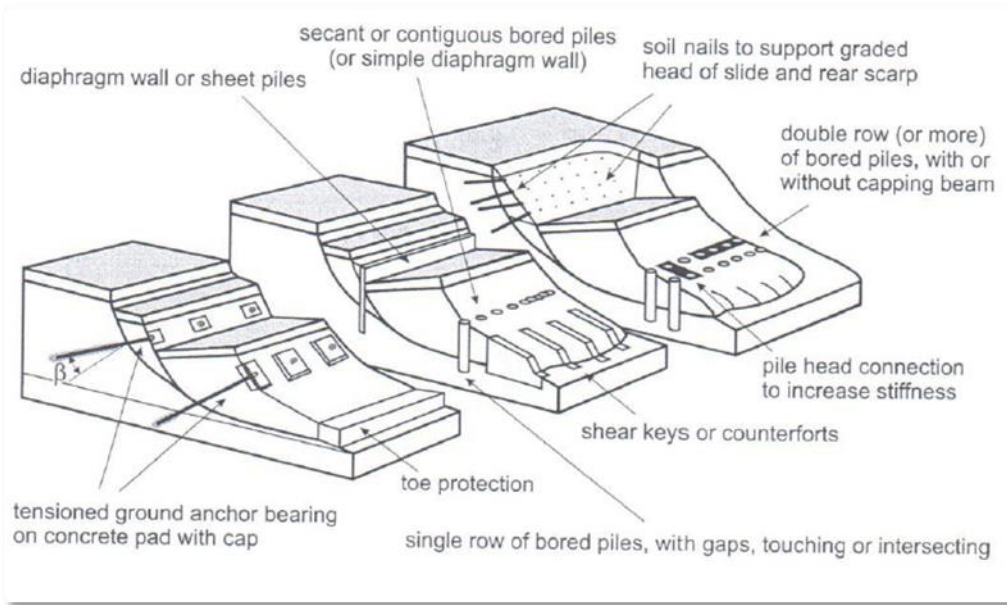


Figure 8-9 Example of embedded structures within a landslide meant to stabilize a landslide, which include tensioned tie-backs, sheet piles, shear keys, bored piles, and soil nails [207]



Figure 8-10 A gabion retaining wall made of individual, rock-filled gabion baskets installed on a slope above a highway embankment [201]



Figure 8-11 Close-up photograph of the head of a post-tensioned rock anchor on a rock face. The wire mesh provides additional containment of loose rock falling from the slope. [201]

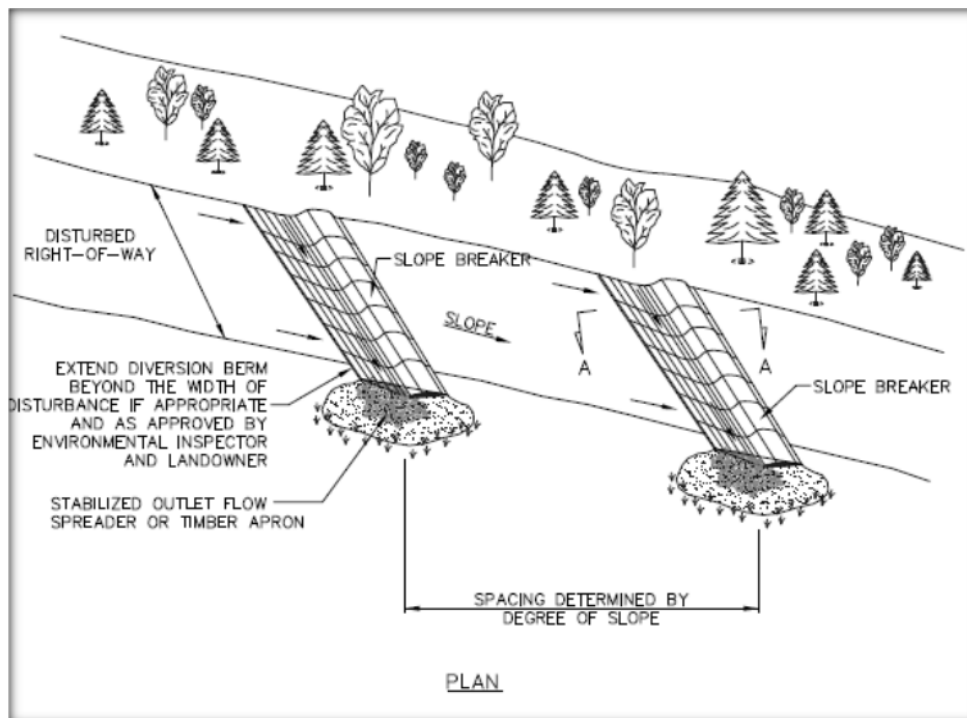


Figure 8-12 Schematic plan drawing of temporary/permanent ROW slope breakers [208]



Figure 8-13 Surficial water diversion berms (slope breakers) on ROW (Location: Central British Columbia, Year: 2011)



Figure 8-14 Stabilization of shallow earthflows in glaciolacustrine soils on pipeline ROW by removing all softened material (primarily pipeline backfill), installing a network of French drains and covering the pipeline by installing a blanket (upper slope) and buttress (lower slope) or riprap material. (Photos by D. Dewar, Location: Central British Columbia, Year: 1997, 2008, and 2012, respectively)



Figure 8-15 Sand bag trench breakers installed in a pipe trench to control groundwater flow in the trench. Sand bags slow the shallow groundwater as compared to clay plugs or foam breakers which are trench dams. [210]

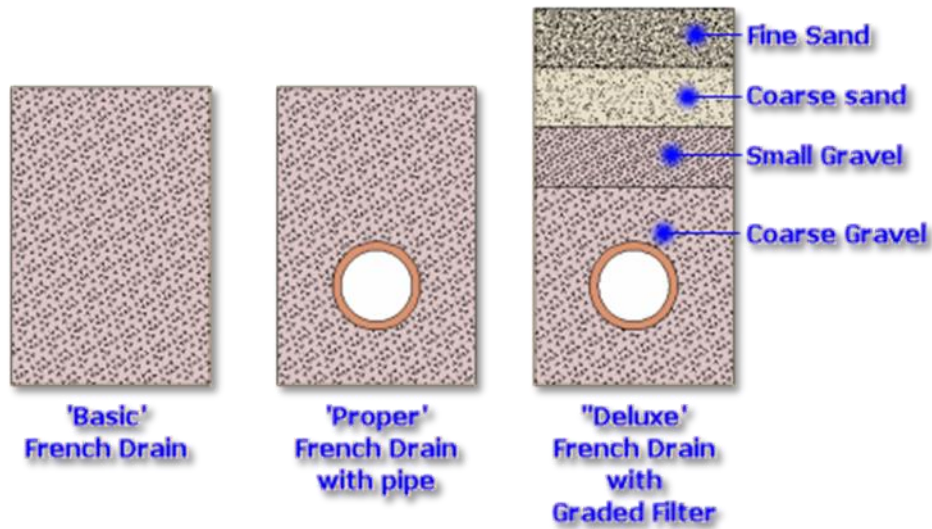


Figure 8-16 Schematic of three French drain systems from simple to complex with and without perforated collection piping at the base of the drain [209]

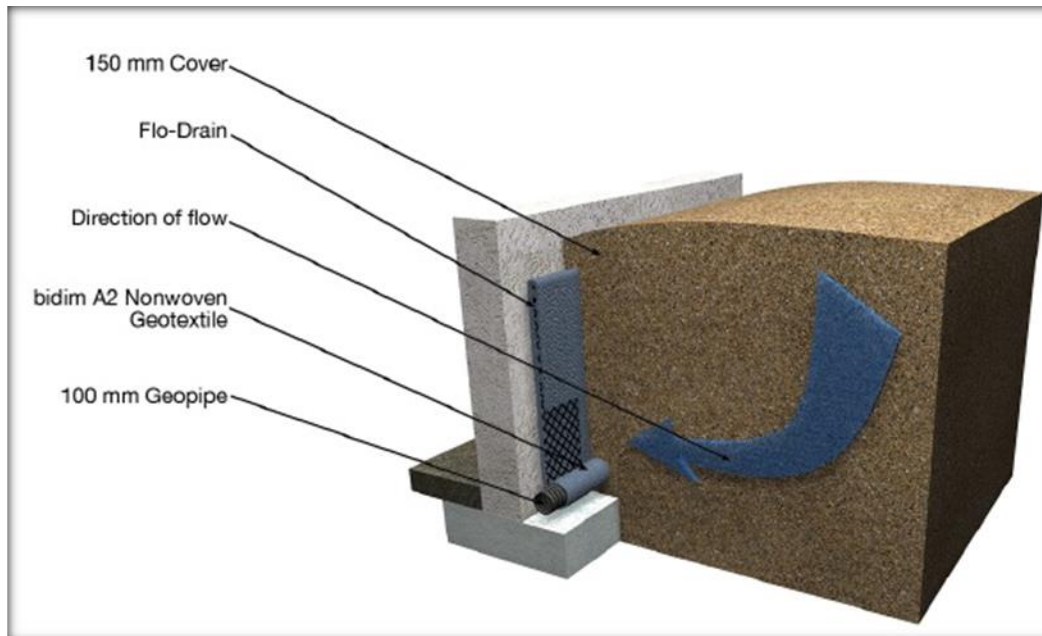


Figure 8-17 Illustration of a geotextile, permeable drainage blanket installed along a concrete wall to reduce groundwater levels and pressures acting on the wall [211]



Figure 8-18 Horizontal drains on a highway cut slope [201]

It should be stressed that any design for mitigative options as outlined in Table 8-2 should be a collaborative effort between the owner/geotechnical operator and the geotechnical consultant. Typically, geotechnical consultants work with the transportation and general land development industries when designing slope stabilization works. When working around pipelines there are unique considerations related to ground disturbance, surface loading, cathodic protection, and

potential pipeline access for long-term maintenance (i.e. for an inspection dig). Many normal slope stabilization projects are difficult to implement due to steep slopes, poor site access, limited workspace, and poor ground conditions. Working around pipelines, particularly those that have flowing products, may create a new set of design and construction related challenges that some consultants are unfamiliar with. A typically difficult project may become unfeasible based on the additional complications associated with working around pipelines. It is essential that geotechnical consultants understand the constraints of pipeline operation. Additionally, great care must be taken to ensure that in the unlikely event that the actual works fail due to an unknown or unexpected geological condition, such a failure must not result in damage and/or rupture of a pipeline. A specific example would be the construction of a retaining wall over a pipeline. If there is an unforeseen foundation failure of the retaining wall, then it is possible that the pipeline could be damaged and/or ruptured.

8.2.2.2 Karst Inverted Soil/Rock Filter for Sinkholes and Karst Chimneys

For the mitigation of relatively small, surface/near surface karst subsidence features (e.g., sinkholes and karst chimneys), an inverted filtered backfill plug design is used. The filtered design allows incident precipitation and surface water flows to infiltrate into the subsurface in a controlled manner, so that the infiltration does not initiate further dissolution around the karst filter leading to expansion/growth of the sinkhole or chimney. The inverted filter design consists of filling the karst sinkhole or chimney from its base, where the approximate chimney opening is narrowest to the ground surface, with an inverse-graded aggregate filter (i.e. coarse angular material placed at the bottom of the chimney where the opening is narrowest, which grades to finer material as the chimney is filled to the surface). Figure 8-19 illustrates conceptually the primary elements of an inverted filter for karst chimney mitigation on a ROW. The ground surface may be reinforced with timber mats on top of the filtered backfilled plug during construction to allow passage of heavy equipment.

It is not recommended to use a solid plug such as foam to backfill a sinkhole or chimney. The solid plug will force infiltration around the plug, and result is expanded dissolution and growth of the sinkhole or chimney.

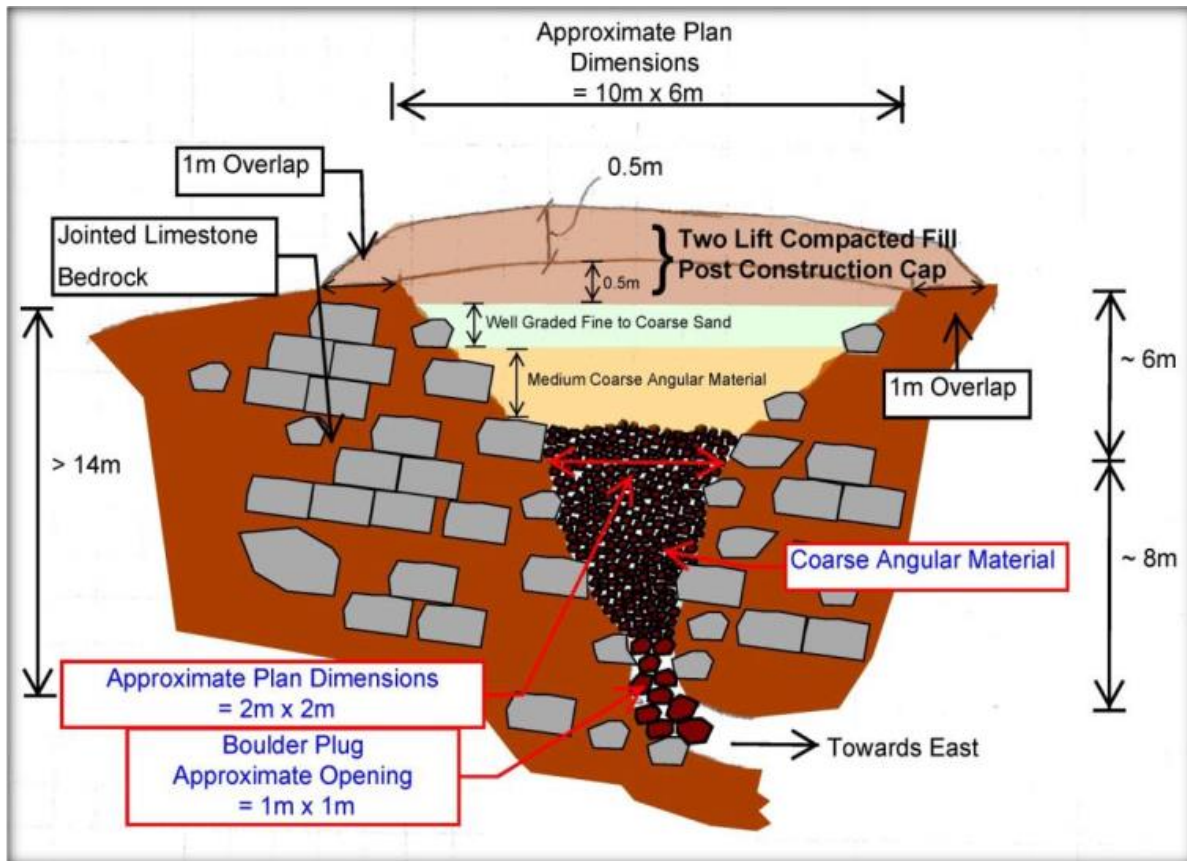


Figure 8-19 Conceptual design of an inverted filter backfill for a karst chimney on a ROW

8.2.2.3 Permafrost Maintenance of Thermal Regime

In permafrost areas, the mitigation of permafrost thawing, whether natural or human-induced, is critical to prevent thaw-related settlement/subsidence and shallow landslide movement that could affect pipelines [1]. Maintaining permafrost in its frozen state can be accomplished by [1]:

- Installation of ground cooling tubes termed “thermosyphons.” This technology is proven to prevent thawing of frozen ground in permafrost areas.
- Treatment of the ground surface to insulate the frozen ground from thermal changes; e.g., the placement of a blanket of wood chips on the surface.
- Placement of foam board insulation above the pipe to minimize thawing.

8.2.3 Reduce Strain Demand and Increase Pipe Strain Capacity

There are several strategies and techniques commonly employed by pipeline operators to reduce the strain demand on pipelines exposed to active landslide and subsidence-related ground movements, and increase the pipe’s capacity to resist the effects of ground movement. These include:

- Stress/strain relief excavations,
- Cut-outs with the addition of pups,

- Alignment modifications across the hazard area to improve pipe response to ground movements,
- Trench geometry improvements,
- Installation of select backfill material to improve/attenuate adverse deformation characteristics and to improve trench drainage characteristics,
- Low friction pipe coatings/wraps, and/or
- Complete pipe replacement through the hazard.

The common techniques to reduce the strain demand on a pipeline, or increase its capacity are summarized in Table 8-3. The summaries include a description of the technique, its general advantages and possible limitations. The implementation of these techniques requires long-term monitoring of at least the pipe to track its performance in achieving reduce strain and/or maintaining capacity to resist the effects of ground movement. In addition, it is typically recommended that the hazard be monitored to determine whether it is active or there are precursors to accelerated movements.

Table 8-3 Mitigation techniques/methods to reduce strain demand on pipelines or increase pipe capacity to resist the effects of ground movement [3, 5, 7]

Method/Technique	Description
Stress/Strain Relief Excavation	<p>Stress or strain relief excavation involves exposing the pipeline on all sides so that it can rebound from elastic deformations imparted by landslide or subsidence ground movements. The excavation is typically extended past the lateral limits of the landslide or subsidence hazard to achieve an un-anchored pipeline exposure length. For larger features, the strain relief excavations may be extended past critical features such as flanks or scarps but not the entire hazard. Following excavation, the pipe is assumed to be relieved of the elastic strain imparted by the pipeline cover and ground movements. Using strain gauges installed in bell holes prior to the complete excavation, the effects of the strain relief can be estimated. Also, it can provide a guide on when to stop digging slack based on the response of the gauges.</p> <p>A stress/strain relief excavation allows the pipe to remain exposed to the landslide or subsidence hazard and respond to ground movements relatively freely in the open pipe trench. This is a common temporary mitigation technique for pipelines located above active longwall mining panels and in active landslides while long-term mitigation and monitoring alternatives are being identified, planned, permitted, and designed. Photographs of stress/strain relief excavations are on Figure 8-20, Figure 8-21, and Figure 8-22</p> <p>For landslides, the pipe may be buried with the native material, or with low strength deformable and permeable material, and be instrumented with long-term slope and pipe monitoring. Depending on the results of the monitoring, the strain relief excavation may be repeated in the future if adverse ground movements become evident in the monitoring data.</p> <p>Even though the stress/strain excavations may be repeated several times over the life of a pipeline, the overall costs, compared to a permanent reroute may be less.</p>
Pipe Cut-Out	<p>A cut-out of a pipeline under landslide or subsidence stresses can also achieve relief of accumulated strain. The displacement of the pipe resulting from the strain can be repaired with the installation of a pup in the cut-out area. Relieved strain in the pipeline can be estimated from the offset of the severed ends. Readings from strain gauges installed prior to the cut out, near the cut out, or in bell holes surrounding the cutout, can provide more accurate strain information. In many cases, cut outs may be required if there are features such as circumferential SSC or buckles that need to be removed. A disadvantage of the cut-out compared to strain relief excavations is that all of the pipe affected by the ground movement will not have been exposed and separated from the moving ground as it would be in the excavation. The pipe can also not be inspected or backfilled with more favorable material, if desired. Additionally, unless strain gauge monitoring is used, there are only theoretical methods of estimating the actual benefit. Where there are significant soil restraining forces on the pipelines, the effects of strain relief may only be localized. Furthermore, a cut-out requires removal of the product from the pipeline and disrupts service.</p>

Table 8-3 Mitigation techniques/methods to reduce strain demand on pipelines or increase pipe capacity to resist the effects of ground movement [3, 5, 7] (Cont'd.)

Method/Technique	Description
Pipe and Alignment Modifications	<p>Pipe and alignment modification to an existing or proposed pipeline can work to improve the strain capacity of pipe and/or reduce strain demand. The modifications may include using pipe joints and girth welding procedures that increase the bending and axial strength of the pipe uniformly within the limits of the hazards and preclude strain localization at and near the girth welds. The modifications may also include replacing short-radius or long-radius elbows with induction bends or field bends, and placing expansion loops at or near the lateral limits and areas of internal deformation within the landslide and subsidence hazards.</p> <p>Reducing the length of the pipe exposed to the hazard, which has an orientation that minimizes axial and horizontal soil loading to limit strain demand, can also improve pipe performance.</p> <p>Maximizing the un-anchored length of the pipe can increase the capacity of the pipe to withstand the adverse effects of horizontal and vertical landslide and subsidence movements. If the pipeline must be taken out of service, it is always recommended that a reroute of the pipeline be considered to avoid the hazard prior to considering a change in the pipeline alignment within the hazard.</p>
Trench Geometry Improvements	<p>The geometry of the trench walls, in combination with select backfill (see discussion below), can reduce the strain demand and improve the ability of the pipe to withstand ground displacement. A wider, lower angle wall trench configuration can improve pipe response to horizontal ground movements, while a narrower steep-walled trench may be more favorable to vertical movements (Figure 8-23).</p>
Installation of Select Backfill in the Pipe Trench	<p>A common technique, particularly for pipelines remaining within the active, or potentially active limits of landslides and areas of subsidence, is the installation of select backfill that can both attenuate the effects of ground movement, as well as provide improved trench drainage characteristics to help collect and convey trench groundwater away from the trench. The select backfill is typically a loosely-placed, cohesionless, clean (< 5% silt or clay) sand or rounded gravel. The select backfill is commonly combined with groundwater collection and conveyance piping to control the groundwater flows in the trench (Figure 8-24). It is important that the type and grain size of the backfill material be selected to not adversely affect the cathodic protection of the pipeline. Geotextile should be used to prevent/reduce migration of the surrounding fine grained soil particles into the select backfill.</p>

Table 8-3 Mitigation techniques/methods to reduce strain demand on pipelines or increase pipe capacity to resist the effects of ground movement [3, 5, 7] (Cont'd.)

Method/Technique	Description
Low Friction Pipe Coating and Geotextile Wrap	<p>Axial soil friction loads can be further minimized from those achieved by select backfill by the use of smooth, hard, low friction pipe coatings. Additionally, wrapping the pipe in two separate layers of geotextile can reduce the axial soil friction. The geotextile wrapping allows axial slip to occur at the interface between the two layers, and the friction angle can be less than that achieved by the combined select backfill and low-friction pipe coating. Examples of the geotextile wrap and its installation are shown in Figure 8-25 and Figure 8-26. Honegger et al [212, 213] tested both the wrap angles shown in Figure 8-26 and determined that the “cigarette wrap” method shown at the top of the figure is superior to the helical wrap shown below it. It should be cautioned that in very poor ground conditions there may be minimal, if any, improvement using a pipe wrap because the friction between the soft soils and the pipeline may be lower than the friction between the layers of geotextile. Additionally, geotextile wraps may have limited benefit when loads are not primarily axial and/or displacements are large. The state of the art laboratory research summarized in References [212, 213] states that the angle of friction between the geotextile wrap layers is approximately 19° to 20°. At this point, there are little to no practical case studies available to verify the laboratory testing.</p> <p>In some cases, geosynthetic lining of sloped trench walls, in conjunction with select, granular backfill, can further reduce the soil loading of the pipe.</p>
Complete New-Pipe Replacement	<p>In landslide or subsidence hazard areas, replacement of the entire pipe, through the limits of the hazard, with thicker wall pipe of high strain hardening capacity and appropriately fabricated girth welds can increase the capacity of the pipe to withstand future ground movement. If combined with select backfill and other pipe improvements, the loads on the pipe can also be reduced. It must be realized, however, that meeting the requirements of pipeline construction standards, such as API 1104, does not guarantee strain-resistance girth welds. Girth welds joining the pipe must have sufficient strength, ductility, and limited extent of heat-affected zone softening to prevent strain localization in the girth welds. Executing a pipe replacement project with the expectation of increasing the strain capacity of the pipe segment requires proper selection of pipes and execution of field welding and NDT as outlined in Appendix D.</p>



Figure 8-20 Looking upslope at stress/strain-relieved 6-inch pipeline. There is a shallow surficial slide at the top of the slope that has a toe daylighting at midslope. (Photo by D. Dewar, Location: Saskatchewan, Canada, Year: 2011)



Figure 8-21 Example of stress/strain relief excavation. Trench breakers have been installed.
(Photo by: E McClarty, Location: Northern British Columbia, Year: 2011)



Figure 8-22 View of physical pipe lateral and vertical response in a stress/strain relief excavation for a pipeline affected by highwall landslide failures in a closely adjacent coal mine. The lateral response is about 0.25 to 0.33 times the diameter of the pipe. (Photo by: D. West, Location: The Western United States, Year: 2011)

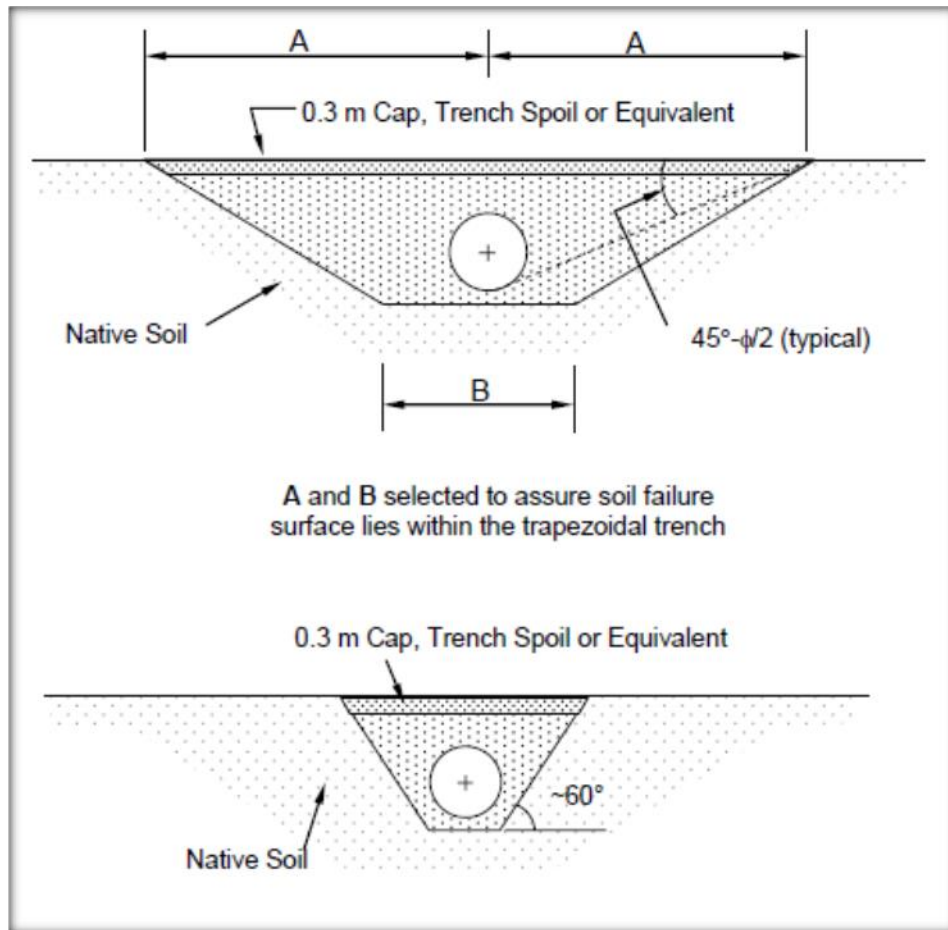


Figure 8-23 Typical favorable trench configurations for horizontal ground movements (top) and vertical movements (bottom) [214]



Figure 8-24 Select, clean sand backfill placed along the sides and top of a pipeline that had undergone a stress/strain relief excavation. The vertical risers are connected to trench drainage improvement plumbing. (Photo by: D. West, Year: 2002)

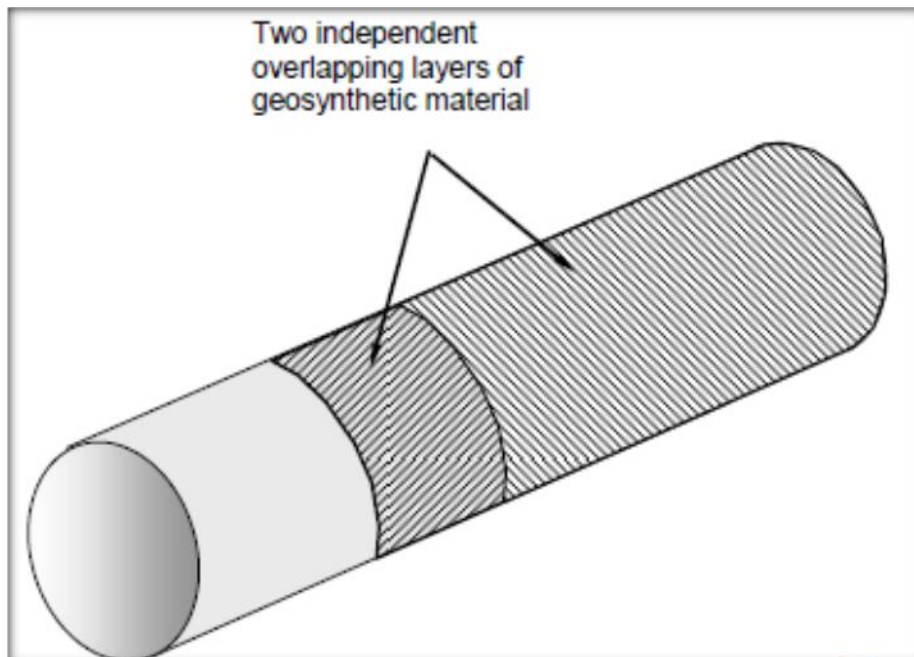


Figure 8-25 Schematic of low-friction, two-layer geosynthetic material application on a pipe [7]

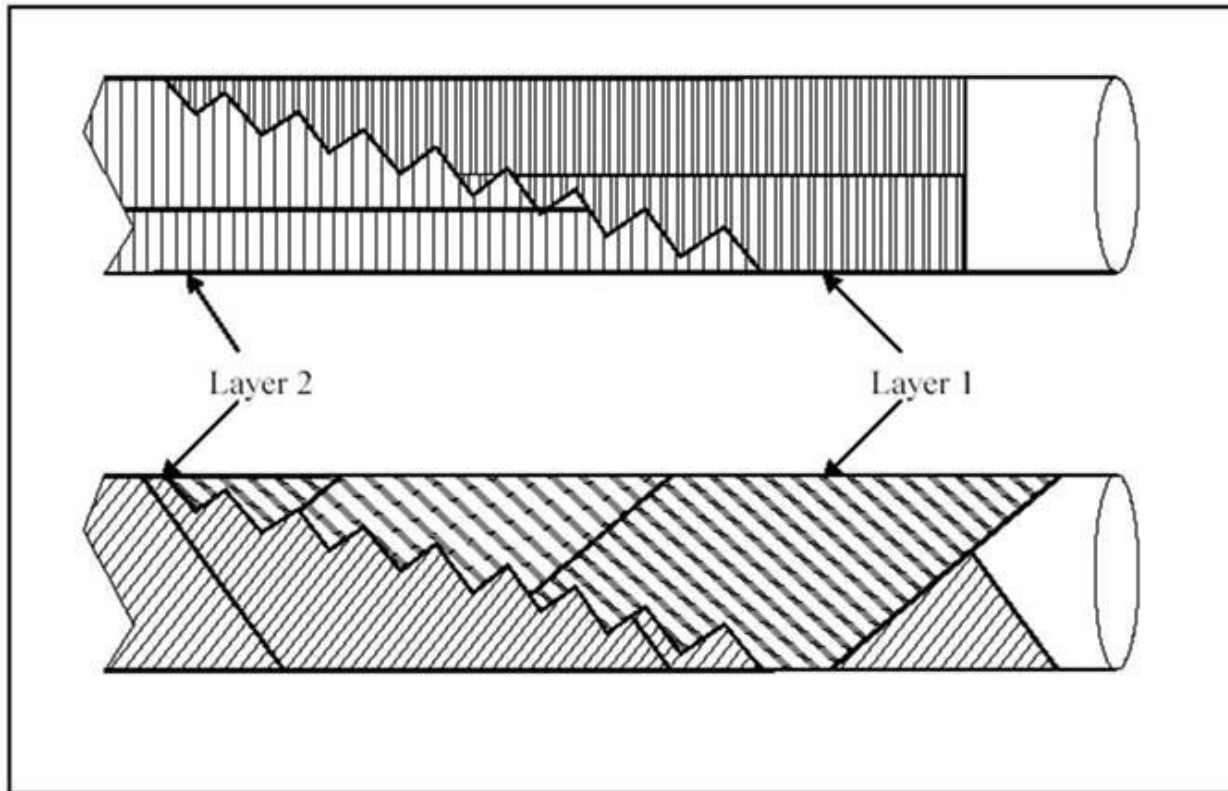


Figure 8-26 Schematic of installation geotextile pipe wrap

8.3 Hazard Monitoring

8.3.1 General

8.3.1.1 Types of Monitoring

Monitoring techniques are divided into:

1. Ground Monitoring: Geotechnical monitoring techniques that characterize the movement of the landslide or subsidence feature.
2. Pipe Monitoring: Techniques that measure the movement or state of the pipe due to the soil-pipe interaction.

Typically, geotechnical assessments of landslide and settlement/subsidence features characterize the movement using conventional geotechnical techniques. These techniques involve subsurface assessments/monitoring, surface geomorphic/geologic assessments, surveying techniques. These conventional geotechnical techniques provide a means to accurately characterize the geologic hazard, but do not provide information on the soil/pipeline interaction and the response of the pipe to ground movement. There is extensive geotechnical literature on the monitoring of landslides including [215] and [207].

Many new techniques for monitoring localized pipe strain, pipe deformation, and pipe stress have recently become available to quantify the impact of landslides on pipelines. Strain gauges

can be installed to monitor changes in strain on pipelines. Geometry pigs allow for the accurate measurement of the pipeline shape and spatial orientation. Multiple runs of geometry pigs allow for comparisons of the shape and orientation of the pipeline.

Where costs are given, they are sourced from the experience of the authors at the time of publication and may be subject to change, particularly with emerging technologies. It is recommended that cost presented in this report should only be relied on for basic screening level assessments of potential costs. As always, it is recommended that project specific quotes be obtained from vendors of any service described within this report.

8.3.1.2 General Approach and Guidelines

Some general monitoring points/advice that should be followed:

1. Monitoring should have redundancy in all but the simplest low consequence situations. As the size and potential consequences of a hazard increase, so should the monitoring types and efforts.
2. Monitoring methods that rely on technologies which are not proven or have more uncertainties should be backed up with simpler well-established methods. An example would be the use of a combination of InSAR satellite imagery interpretation and ground survey monitoring points to determine the extent of a landslide, including the decision to use manual versus automated monitoring.
3. Monitoring should be tailored to the type and velocity (or potential velocity) of the landslide movement(s) and/or amount and rate of subsidence.
4. Monitoring equipment should be researched and vendors should be chosen carefully. The equipment proposed should have a proven track record on at least one similar application or should be validated by a proven technique/process.
5. Generally, the more precise the method used, or the more precise option chosen within a particular method, the quicker results and trends will be determined. Otherwise, significant time may pass prior to the results clearly showing trends rather than systemic, random, and human errors.

8.3.2 **Ground Monitoring**

Conventional geotechnical techniques are well represented in the literature [7]. The following discussion provides a summary of typical geotechnical ground monitoring techniques used to characterize landslide movements.

8.3.2.1 Visual Monitoring/Site Inspections

Observational or visual ground monitoring probably represents the most basic way to detect, characterize, and monitor potential landslide and subsidence hazards. It is also likely the oldest monitoring method or technique that has been employed by pipeline operators to address and keep track of potential landslide and subsidence hazards affecting their pipelines. For example, the operational experience of pipeline operators in hilly terrain is commonly filled with many

years of visual reports and observations of “slips” and landslides that have adversely affected the pipelines and/or the ROW.

Visual monitoring is based on identifying (detecting), characterizing (measuring), and documenting changes to the ground surface, and this is usually accomplished by ground-based or aerial (fixed-wing or helicopter) reconnaissance. The examination of the ground surface, characterization and the documentation of observations are best done by experienced geoscientists/geological engineers, but can be undertaken by pipeline personnel specifically trained to recognize landslide and subsidence hazards.

Because of the generally simplistic and semi-quantitative nature of the visual monitoring employed for landslides and subsidence hazards, comprehensive reports explicitly address the simple and basic methodologies that could be applied, and which are described below. General discussion of hazard mapping and monitoring techniques (e.g., for landslides and subsidence) is contained in [200, 7, 216, 217] and these discussions provide some insight into what features to monitor and how to implement monitoring.

For hazard monitoring, visual observations are typically repeated on a periodic, scheduled basis (or following significant natural events such as storms and earthquakes) to document changes (or no changes) to the ground surface at specific locations. These monitoring locations are established on as well as off the landslide or subsidence hazard being monitored. Visual observations are commonly focused on specific landslide or subsidence features that have been identified, and where future movement may be expected to recur. Such specific hazard features commonly include:

- Landslide main/head scarps (and differential displacement subsidence features),
- Landslide lateral scarps/flanks,
- Tension cracks (landslide or subsidence),
- Disturbed vegetation (tilted/deformed trees),
- Deformation of the landslide mass, and
- Displacement of the pipeline alignment.

Although visual-only (eyesight) observation of the features is often the means to accomplish visual monitoring, it is imprecise, and not reliably repeatable. Therefore, visual monitoring is commonly enhanced with the installation of physical markers on the ground that aid in identifying and tracking changes to the landslide or subsidence features. These physical markers provide specific local datum points that help to quantitatively document the magnitude and rate of change in the landslide or subsidence feature.

For landslide head scarps, linear subsidence features, lateral scarps, and tension cracks, an array of relatively robust markers (e.g., rebar, smooth steel rod, PVC, wood) are placed on either side of the feature(s) being monitored, and are used for measuring vertical and lateral displacement across the feature(s). Typically, approximately 1 m long (~3 ft long) lengths of markers (e.g., #5 rebar (5/8 in diameter; metric #16 or 15M) or “sucker rod”, e.g., 3/4 in smooth steel rods for colder climates) are driven vertically into the ground on each side of a crack/scarp.

The markers are driven more than two-thirds of their lengths into the ground so that about 15 cm (6 in) stick up above the ground surface. By measuring the horizontal and vertical separation between the two opposing lengths of markers (over time), the relative horizontal and vertical displacements of the scarp can be monitored and documented.

The survey laths in Figure 8-27 can, for descriptive purposes, be considered proxies for the locations of rebar installed on either side of the landslide head/main scarp in the photograph. Figure 8-28 provides a schematic view of the installation of rebar across a landslide head scarp. Note that the tops of the rebar pieces do not need to be level with each other across the scarp at the beginning of the monitoring program. The rebar positions can be normalized to each other using a straight piece of 2×4, placed on the tallest rebar (commonly the upslope rebar) to span the distance between the two rebar pieces across the landslide scarp, with a carpenter's level placed on the 2×4 to establish a level baseline from which to measure successive horizontal and vertical separations.



Figure 8-27 View of a landslide head scarp with survey laths placed on the upslope and downslope sides of the scarp. If each lath was visualized as a rebar, and their vertical and horizontal positions relative to each other were periodically measured, the growth of the head scarp would be documented. (Photo by: D. West, Year: 2005)

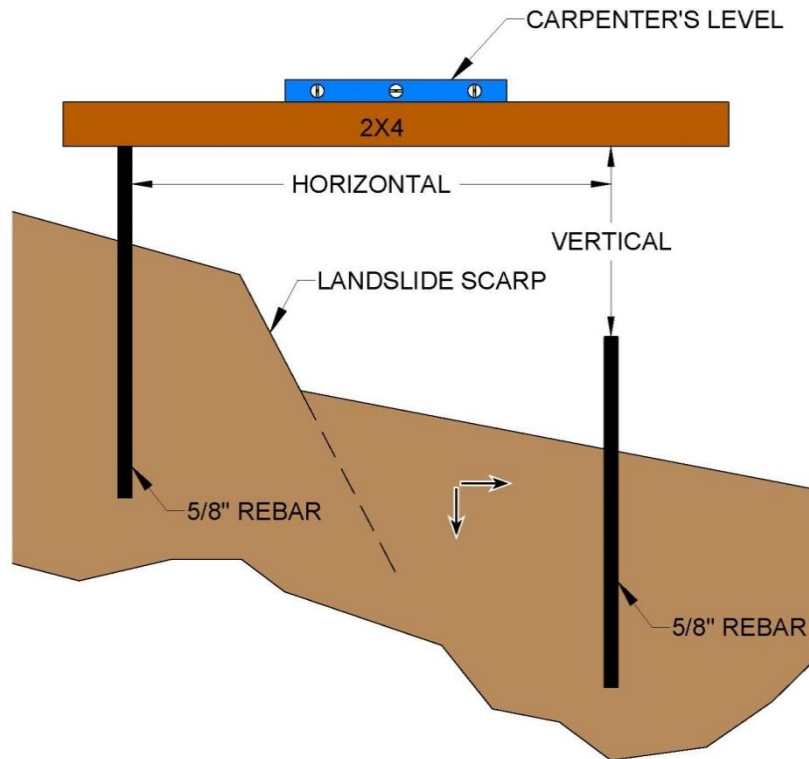


Figure 8-28 Schematic section of a rebar installation across a landslide head scarp

For lateral landslide scarps (flanks), an array of four rebar pieces can be installed with two on each side of the lateral scarp (Figure 8-29). This configuration is a quadrilateral across the scarp which allows for the resolution of the lateral separation (lateral displacement) across the lateral landslide scarp, through the rules of trigonometry [217]. Vertical separation across the scarp can be measured in the same manner as described for head/main scarps previously. Successive measurements of the lengths of each side of the quadrilateral and across the quadrilateral can document the amount and rate of landslide movement, at the landslide lateral scarp, while leveling across the scarp allows for the measurement of vertical separation across the scarp.



Figure 8-29 View of a rebar quadrilateral array across a landslide lateral scarp (lateral scarp location and relative movement shown by arrows) (Photo by: D. West, Year: 2010)

The continued deformation of vegetation within a landslide mass or along its limits may also provide crude information on historical and continuing landslide movement. For example, the conifer tree in Figure 8-30 is located within a landslide mass or body. The tree was initially tilted in the downslope direction and was also split by the downslope movement of the landslide. Continued movement of the landslide may continue to deform the tree, and result in additional downslope tilt and widening of the split. If the angle of the tilt and the width of the split were to be established in a baseline measurement, periodic measurement of these data points could provide crude estimates of the continuing nature of landslide movement. By periodically measuring the angle of the tilt, it can be crudely determined whether the landslide, at that location, is continuing to move. Measurement of the tilt can be enhanced by placing reference markers on the tree at 90° intervals so that successive changes in tilt can be more readily measured and documented [217] as shown on Figure 8-30.

It should be cautioned that the use of tree related features should be used with great care in situations where there is otherwise no indication of landslide activity. Many forests may have a characteristic “drunken” stand appearance in areas of stable terrain. Features such as pistol butted trees may be the result of snow loading during early stages of growth.



Figure 8-30 View of tilted and split tree in a landslide mass. Continued, periodic measurement of the angle of the tilt and width of the split can provide information on landslide movement. The arrows on the tree represent possible reference markers attached to the tree to aid in the successive measurement of tilt. (Photo by: D. West, Year: 1999)

Detection, characterization, and to a lesser extent, monitoring of potential landslide deflection/deformation of the pipeline can be established by locating the pipeline across the landslide and marking the pipeline locates with closely-spaced (e.g., every 10 ft or 3 m) survey wands or survey laths. If a pipeline is deflected by the landslide, the location, pattern, and amount of deflection of the pipeline can be determined using the observed deflection of the pipeline locates. In some severe cases, one may also be able to find slide or settlement induced sags or overbends based on depth of cover changes. Figure 8-31 is an illustration of the deflection of a pipeline as represented by the “wow” in the line of pipeline locates (wands) across an active landslide. The maximum lateral, downslope deflection of the pipeline by the landslide, shown by the deflected locate wands, was about 5 ft (1.5 m), with the total length of the deflected pipeline being about 150 ft (46 m).

Locates are relatively inexpensive, but are also relatively inaccurate. The accuracy of a locate is primarily dependent upon the experience of the locator, quality of equipment, method of

getting a signal on a pipeline (e.g. induction versus direct connection), soil/groundwater conditions, and depth of cover. Common factors that reduce the accuracy are:

1. Interference from sources such as adjacent pipelines or overhead powerlines,
2. Interference from signals on tighter pipeline bends, and
3. Deeper cover.

As a rule of thumb, where the pipeline runs straight (or originally ran straight) apparent deflections that are less than $\frac{1}{3}$ the depth of cover to the top of the pipe or 1 to 2 times the diameter of the pipeline (a lower number as the diameter increases) should not be trusted without some other form of evidence of displacement.



Figure 8-31 View of a line of pipeline locates (wands) through an active landslide. The landslide had deflected the pipeline laterally downslope and to the left by about 5 ft (1.5 m), maximum. The total length of pipeline deflection was about 150 ft (46 m). (Photo by: B. Albert, Year: 2013)

A line of visual survey monuments (VSM) (vertical PVC pipes or other visual markers) through a landslide, and adjacent to a pipeline in an ROW, can also be used for visual monitoring of potential landslide movement. With the highly visible line of VSMs, ground deformation can be detected from ground or aerial patrol, and if detected, the location, nature and amount of landslide deformation can be measured and documented. Figure 8-32 is a schematic of typical installation detail for a VSM.

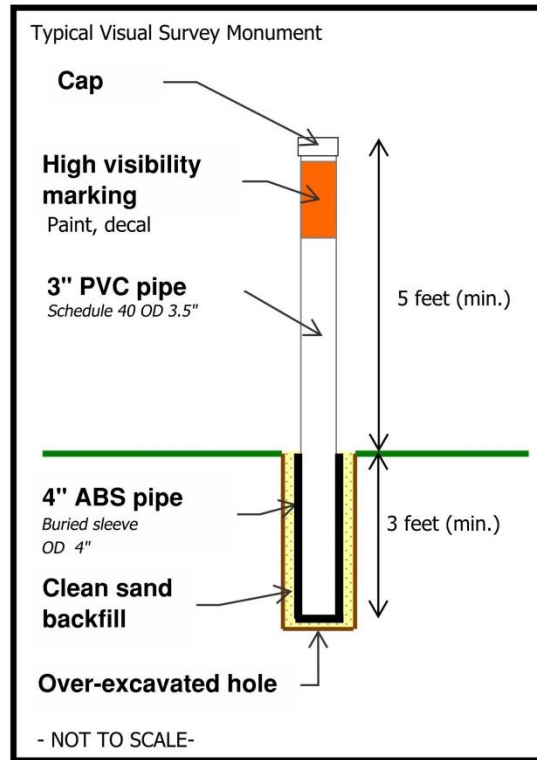


Figure 8-32 Typical detail for a VSM to be installed in a line across a landslide (Source: Golder, Year: 2015)

Close-range, repeated, terrestrial, digital photography can also be used to monitor active landslide (or subsidence) movement, particularly if access to the moving ground is restricted or unsafe. If markers (or prominent surface features) are placed on the landslide/subsidence area of interest, these can serve as benchmarks for documenting qualitative or semi-quantitative changes to the landslide surface, when repeated digital photographs are acquired from the same spot over time. Examples of possible simple markers, fashioned from plywood or sheet metal and painted with bright colors, are illustrated on Figure 8-33. Such markers/targets can be made and deployed quickly. It is prudent to place some markers outside the limits of movement so that relative change can be more precisely measured. Photographic techniques for landslide monitoring are described in more details by [217, 218, 219, 220]

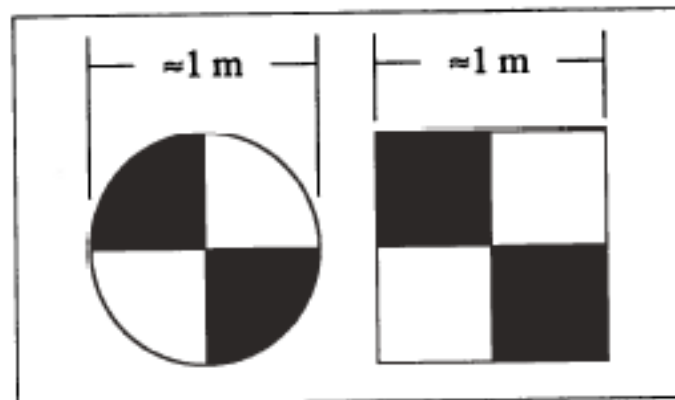


Figure 8-33 Example of simple reference targets/markers for photographic monitoring of landslide movements. These targets can be fastened to rebar driven into the ground [217].

The various visual monitoring methods described above are listed and compared in Table 8-4. The methods are compared on the basis of maturity, availability, accuracy or precision, repeatability, and reliability. In addition, Table 8-4 lists the basic equipment needed for each visual monitoring method.

Table 8-4 Comparison of the Visual Monitoring Methods

Visual Monitoring Method	Comparison Rating					
	Maturity	Comm. Available	Accuracy/Preciseness	Repeatability	Reliability	Equipment
Rebar Across Scarps	High	Yes	+/- 4 cm (x, y, z)	High	High	Rebar*, measuring tape, digital camera, carpenter's level, GPS
Tilted Trees	Low	Yes	Low	Low	Low	Digital camera, measuring tape, clinometer, GPS
Pipeline/ Landslide Deflection	High	Yes	Low to medium	Low-High	Medium	Pipe locates, survey lath or wands, PVC VSM, digital camera, GPS
Photography	High	Yes	Low	Low-Medium	Low	Digital camera, tripod, targets/markers, GPS

*As a note, rebar is commonly used in warmer climates but is susceptible to frost jacking in colder climates. Often 3/4-inch smooth sucker rod is used in northern climates. Additionally, the monitoring method would have to comply with pipeline ground disturbance procedures.

The primary advantages of visual observations for landslide and subsidence monitoring are that they are relatively inexpensive and can be completed relatively rapidly. The primary disadvantages are that visual observations are not as accurate or precise as instrumental monitoring techniques, and they have temporal and spatial limitations; i.e., they only record at the time of measurement and they only record what has happened at the point of measurement (which is generally on or near the surface).

The main cost to visual observations is labor, while equipment costs are minor. If aerial patrol or aerial reconnaissance is used, then it can become somewhat expensive if not incorporated into routine aerial patrol. For example, single-engine, fixed-wing charter may be from about \$250/hour to \$500+/hour, while helicopter charter may range from about \$600/hour to \$2,000+/hour, depending on the aircraft used and location.

8.3.2.2 Subsurface Monitoring

This section addresses subsurface monitoring of landslides and potentially unstable slopes using slope inclinometers (SI), rudimentary (“poor man’s”) extensometers fabricated from already-installed SIs, Shape Accel Arrays (SAAs) and time domain reflectometry (TDR). The SIs, extensometers, SAAs, and TDRs are installed in geotechnical exploratory boreholes advanced into stable ground below the landslide basal slip surface.

8.3.2.2.1 *Slope Inclinometers*

SIs are used to detect and determine the type, depth, magnitude, direction, and rate of subsurface landslide or ground movement and ground displacement. Information from SIs is often critical for understanding the cause, nature, and behavior of landslides. SIs provide useful information for planning, development, and design of landslide mitigation alternatives, and are commonly used for short-term and long-term landslide monitoring. SIs are also used for detection, characterization, and monitoring other types of ground movement such as subsidence and excavated construction slopes.

There are two common types of SIs used for landslides and ground movement monitoring [7, 221, 222, 223, 224, 225]: probe inclinometers (PI) and in-place inclinometers (IPI). Both PIs and IPIs use similar downhole sensors.

PIs and IPIs are commonly installed in vertical, exploratory, geotechnical boreholes that are geologically-logged as the boreholes are advanced into the ground. The geologic log of the borehole allows for observed inclinometer displacement to be compared to the subsurface geologic conditions encountered in the borehole, which are recorded on the log. The geologic data of importance from the geologic log are the nature and depth of the interpreted landslide slip surface and the depth/elevation of groundwater encountered in the borehole.

Following drilling of the exploratory geotechnical borehole, grooved plastic SI casing is installed in the borehole and the casing is grouted into the borehole. Movement of the ground causes the casing to deform. Eventually, the casing is sheared off or pinched closed. When that happens, the probe can no longer pass through, and no more readings can be obtained. In general, larger diameter casing will offer a longer useful life, because it can accommodate more

deformation before access is closed to the probe. There are several diameters of SI casing available which include [226]:

- 85 mm (3.34 in) casing is the largest diameter. It is suitable for all uses and especially recommended for landslide investigation and long-term monitoring. It is also appropriate for monitoring multiple shear zones or very narrow shear zones.
- 70 mm (2.75 in) casing is suitable for construction projects. It can also be used for slope stability monitoring if only a moderate degree of deformation is expected.
- 48 mm (1.9 in) casing is used only for deformations that are expected to be very small and are distributed over broad zones. It is generally not installed in soils.

The individual PI/IPI sensor commonly contains two, force-balanced servo-accelerometers (biaxial sensors) that measure the inclination of the SI casing with respect to the vertical, in four directions that are 90° apart. The biaxial sensor contains two perpendicular accelerometers to measure movement in the four different directions. One accelerometer measures the tilt in the plane of the inclinometer wheels (A-Sensor for A0 direction) which track the longitudinal groove of the casing, while the other accelerometer measures the tilt in the plane perpendicular to the wheels (B-Sensor for A180 direction). Thus, in a biaxial sensor, the A-sensor is oriented in the A-direction which is parallel to the wheels of the probe (commonly installed along the expected movement axis of the landslide), and the B-sensor is oriented transverse to the wheels in the probe.

Probe Inclinometer (PI)

The traversing (moving along the SI casing) PI measures the onset and continuation of landslide deformation/displacement perpendicular to the vertical axis of the SI casing by passing a probe down the casing [221, 224]. The depth or zone at which shear movement is detected by the PI is the depth of the landslide slip surface or zone of deformation. In some cases, there may be multiple slip surfaces or zones of deformation encountered within a given SI installation.

PI Operation

A PI consists of a single SI probe sensor containing a pendulum-actuated transducer (servo-accelerometer) or microelectromechanical (MEMs) sensors. The probe is fitted with wheels and lowered by an electrical cable down the SI casing. Grooves control alignment of the PI from the top to the bottom of the SI casing. The electric cable is connected to a read-out unit at the surface where data can be recorded manually or automatically (Figure 8-34). The PI system includes four primary components (Figure 8-34 and Figure 8-35):

- The SI guide casing permanently installed (grouted) in a vertical borehole. The SI casing is commonly plastic (PVC), but can also be steel or aluminum, and has longitudinal grooves/slots at 90° spacing around the circumference of the casing to guide/orient the PI unit as it is lowered into the casing. The casing is commonly installed with one set of the grooves oriented parallel to the direction of landslide or slope movement. With modern slope inclinometers, the second set of grooves is redundant.

- The PI sensor probe, mounted in a wheeled carriage unit that tracks/traverses down the grooved SI casing. The PI probe is typically oriented with the A0 direction aligned with the expected direction of landslide or slope movement.
- The electrical control cable that raises and lowers the PI sensor unit and allows for the transmission of PI data to the read-out unit at the surface. The cable is commonly graduated for accurate depth control of the PI sensor.
- The portable read-out unit at the surface which provides power to the PI, receives electrical signals from the probe, displays PI measurements in real-time, and stores the data for further use.

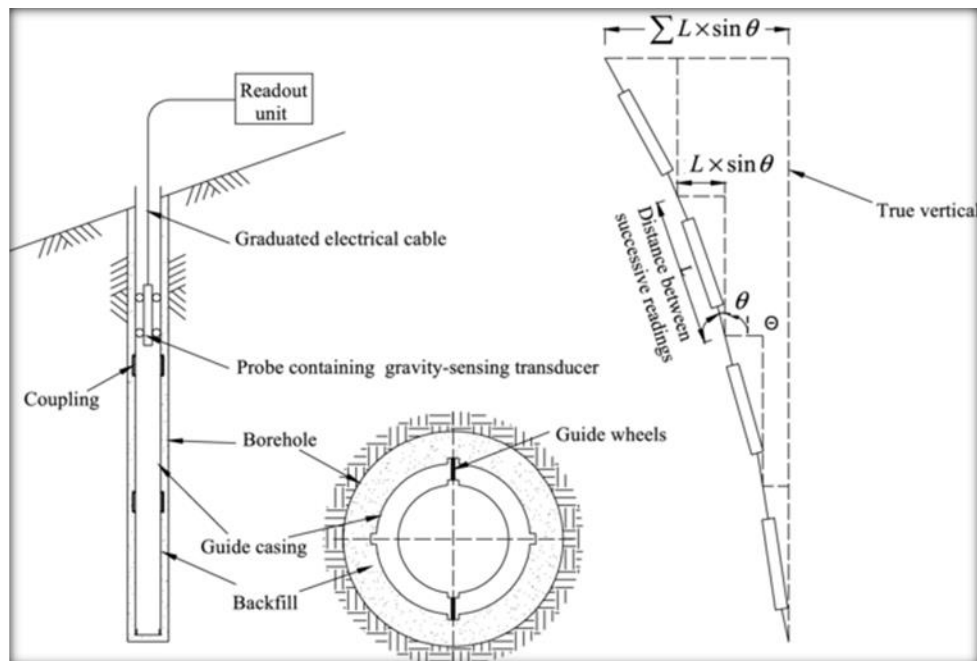


Figure 8-34 Typical PI installed components, and principle of operation [227]

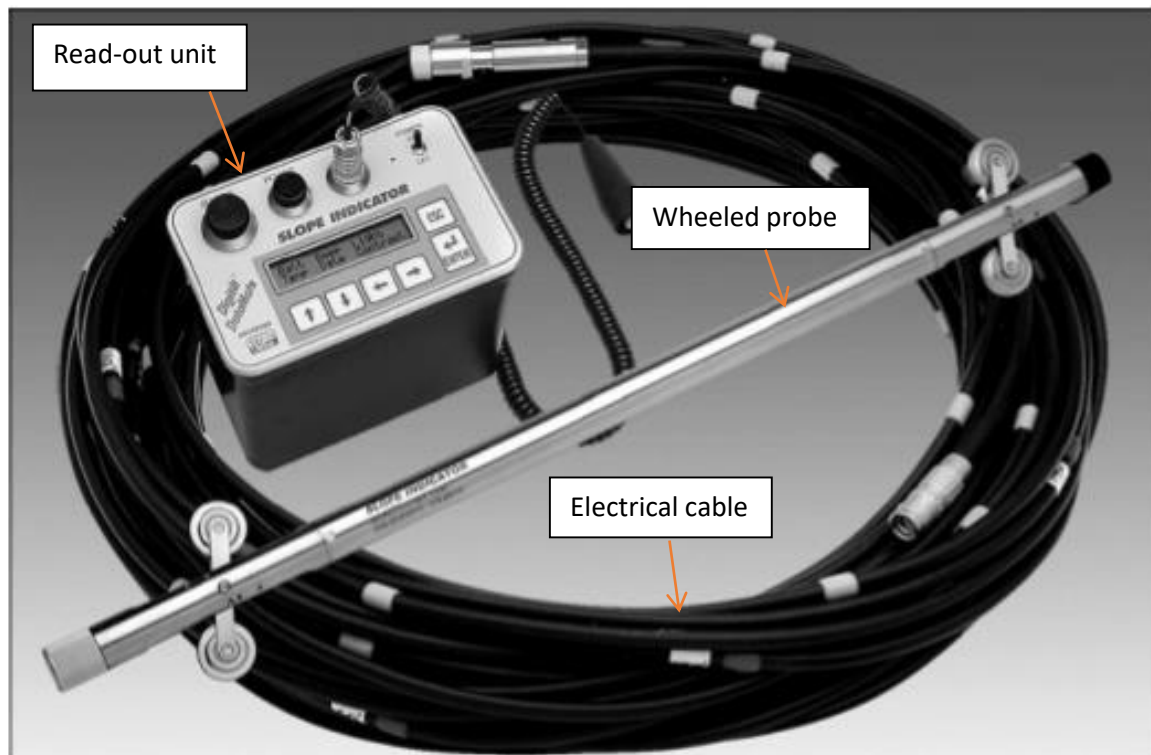


Figure 8-35 PI with manual read-out unit and graduated electrical cable (modified from [226])

The wheeled PI sensor unit (probe) is lowered and raised in the vertically-grooved SI casing on an accurately length-graduated electrical cable. The two sets of grooves in the casing allow the probe to be oriented in either of two planes separated by 90°. At each PI installation, one set of grooves is oriented in the direction of anticipated landslide movement, namely, the A-direction, while the second set (B-direction) is oriented 90° to the A-direction [221, 228].

PI Data

Measurements are typically taken at 2 ft (or 0.5-0.6 m) spacing in the SI casing, starting from 2 ft above the bottom of the casing. Mikkelsen [221] indicates that measurements collected with depth intervals as large as 1.5 m (5 ft) result in poor accuracy. Mikkelsen [221] also reports that PIs can measure changes in inclination on the order of 1.3 mm to 2.5 mm over a SI casing length of 33 m, which is a precision of about 1:10,000. A typical PI plot of continuing, cumulative subsurface displacement (over about 4.5 years) in a landslide is shown on Figure 8-36. The depth of the landslide failure surface (about 17.2 m) is clearly expressed in the PI plot, and the total displacement was about 20 mm over the 4.5 years. Figure 8-37 shows a plot of SI landslide displacement with time for two separate PI/SIs, allowing for the evaluation of the rate of displacement with time. The steeper the slope of the plot, the faster the rate of movement. Provided readings are taken at an adequate frequency, the plots are extremely useful in determining if the landslide movements are linked to wetter times of year or specific precipitation events, or if movement is consistent over the monitoring period.

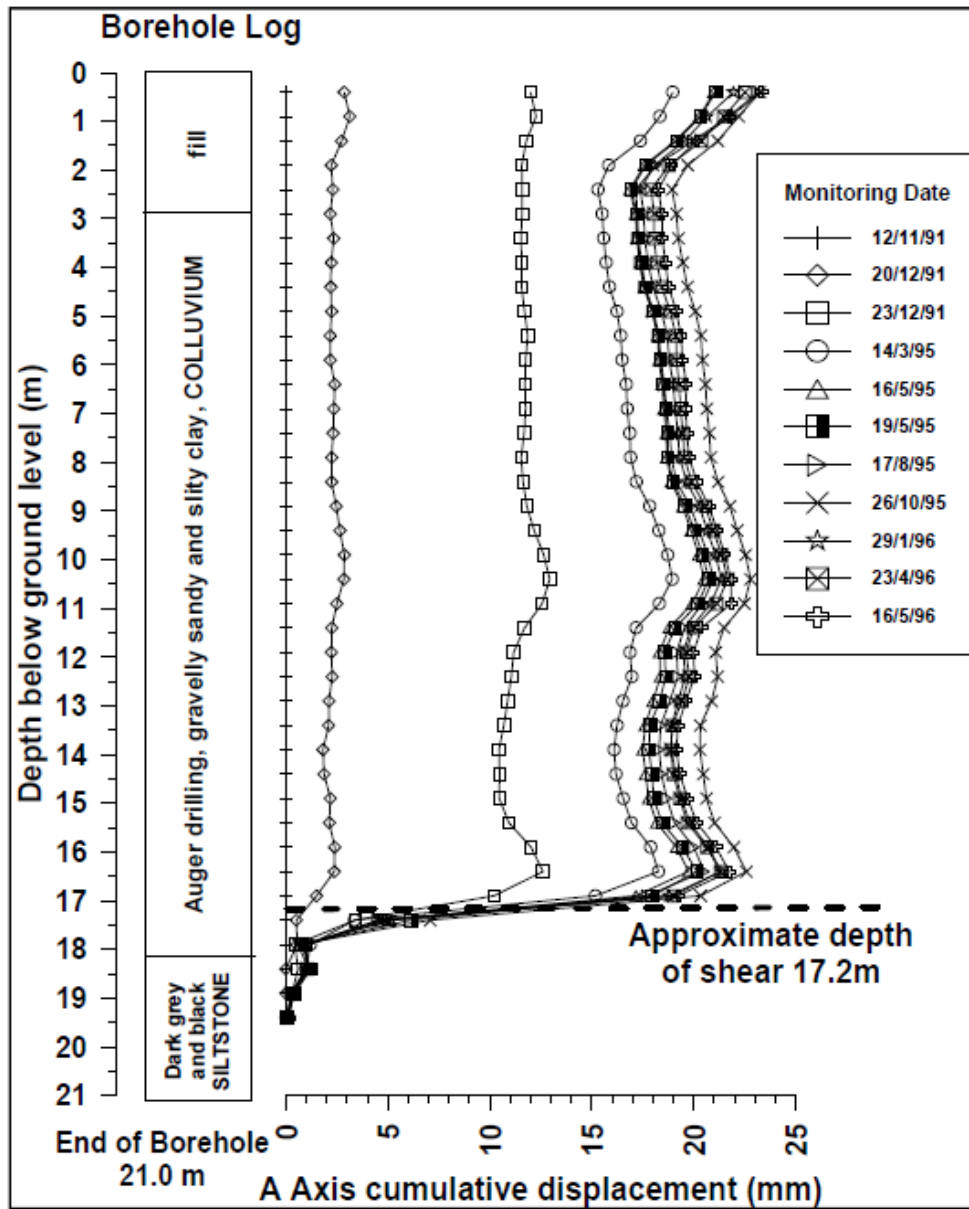


Figure 8-36 Example borehole geologic log and PI plot of landslide displacement [222]

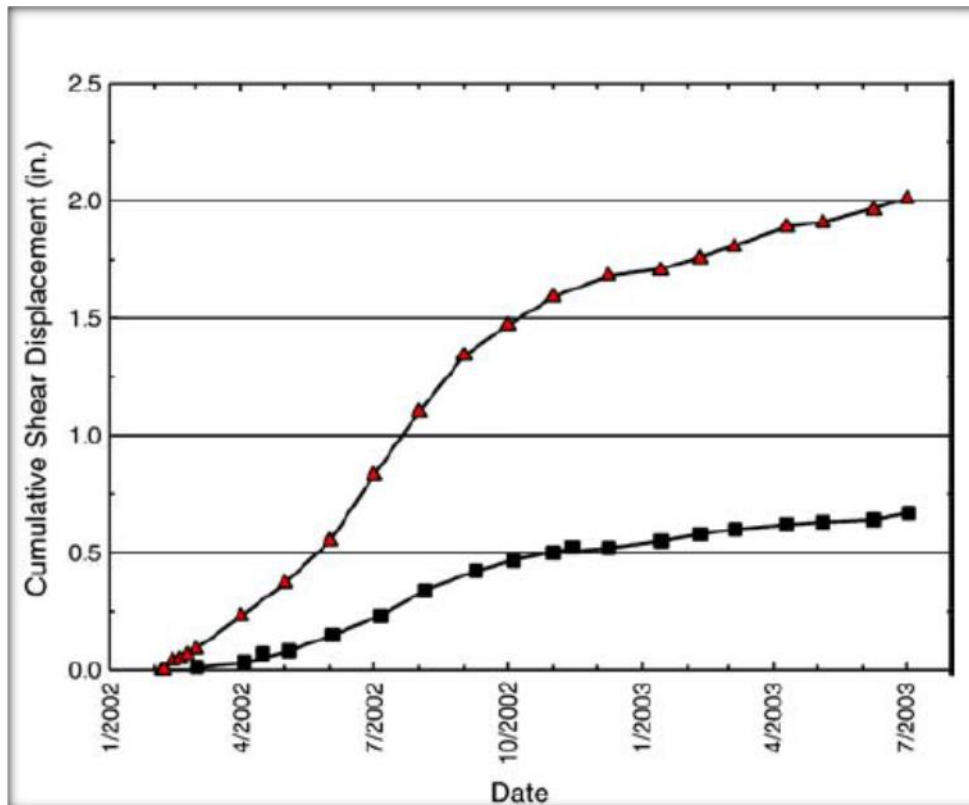


Figure 8-37 Example of PI landslide displacement with time for two separate PIs [222]. Steeper areas of the plots correspond to faster landslide movement.

PI Accuracy

The accuracy of PI measurements is dependent upon the nature and amount of random and systematic errors associated with the SI technique [221, 228]. The field accuracy or total error is the sum of the random and systematic errors. Random error is less influential and tends to remain constant, while systematic error tends to vary with each survey [229]. Systematic errors tend to be caused by [229]:

- Sensor bias-shift (offset)
- Sensitivity drift (least common error source assuming probes are regularly calibrated and not mishandled)
- Sensor axis alignment (rotation)
- Depth positioning error caused by SI casing curvature and vertical placement of the PI probe by the operator

In a hypothetical 30 m long (100 ft long) SI casing, with measurements collected every 0.6 m (every 2 ft) the total error could be on the order of 7.8 mm (0.31 in) [229]. Of this total, about 1.24 mm would be from random error, and about 6.6 mm from systematic error [229]. Although generally constant, random errors can be reduced with better SI installations and with more precise reading procedures. Systematic errors can be corrected and reduced through the use of

strict mathematical procedures that are contained in modern inclinometer graphing software [228, 229].

Generally, the shorter and straighter the SI casing, the lower the random and systematic errors will be, and the lower the total error, or the greater the field accuracy will be. For example, using the total error formula of [229], a 15 m deep (49 ft long) SI casing would have a total error of about 4.2 mm, of which about 0.9 mm would be from random error and 3.3 mm from systematic error.

In-Place Inclinometers (IPI)

IPIs can be used to continuously monitor landslides to provide information on continuing landslide movement, and early warning of slope failure. IPIs can also be used to monitor excavated slopes above highways, railroads, and other cut or fill embankments.

IPI Operation

An IPI system employs a series of biaxial servo-accelerometer sensors (MEMSs) segments that are installed in the SI casing (Figure 8-38). The casing provides access for multiple IPI sensors, and the grooves inside the casing control the orientation of the sensors. As with the PIs, the IPI SI casing is typically installed in a vertical exploratory geotechnical borehole that passes through the suspected zone of landslide movement into stable ground below. One set of grooves is aligned with the expected direction of landslide movement, e.g., in the downhill direction or toward an open excavation. The sensors are positioned inside the casing to span the expected vertical zone of landslide displacement/movement. When the ground moves, the casing moves with it, changing the inclination of the IPI sensors inside. Inclination measurements from the sensors are processed to provide graphs of the casing profile and changes in the profile. Changes in measured inclination indicate displacement (movement). In most applications, sensors are connected to a data acquisition system, and readings are transmitted to processing software that can trigger alarms based on displacement or rate of change of displacement. The depth of the slip surface or zone of deformation should be known in order to use IPIs.

The primary advantage of IPIs over PIs is that they are ideal for continuous unattended monitoring and can deliver readings in near real-time, or the readings can be locally stored in data loggers. In this manner, trends and rates of landslide movement can be more closely monitored, and prompt response to adverse landslide movement can be implemented. Additionally, most commercial sensors can be linked together to form a chain of sensors, effectively reducing the number of signal cables to one. This eases installation and simplifies connection to the data logger. The sensors, cables, connectors, and wheels are also exceptionally durable, making it possible to remove the sensors at the end of a project and redeploy them on other projects (assuming the casing has not deformed beyond the point at which the sensor can be removed). The sensors can be left in place and continue to monitor the landslide even when the deformation is such that the sensor cannot be removed. Basically, the landslide can crush the IPI in place.

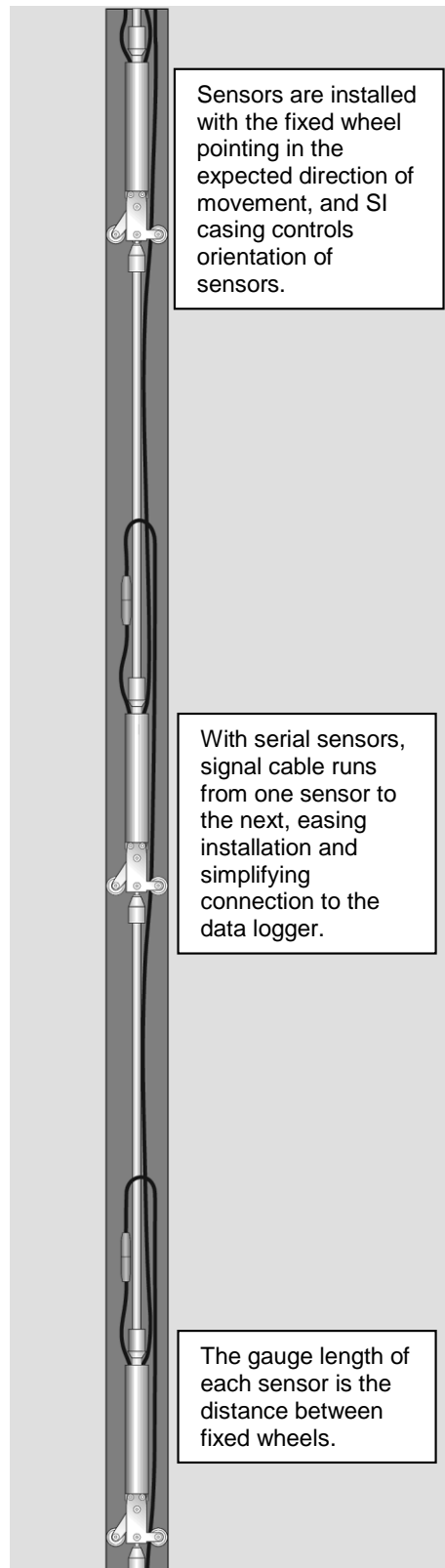


Figure 8-38 Typical multiple IPI installation in an SI casing (modified from [226])

IPI Data

An example of an IPI landslide displacement plot is given on Figure 8-39. Note the continuous displacement record and the sharply accelerated displacement pattern in February 2007. The accelerated pattern could be used to trigger an alarm and response by a pipeline operator.

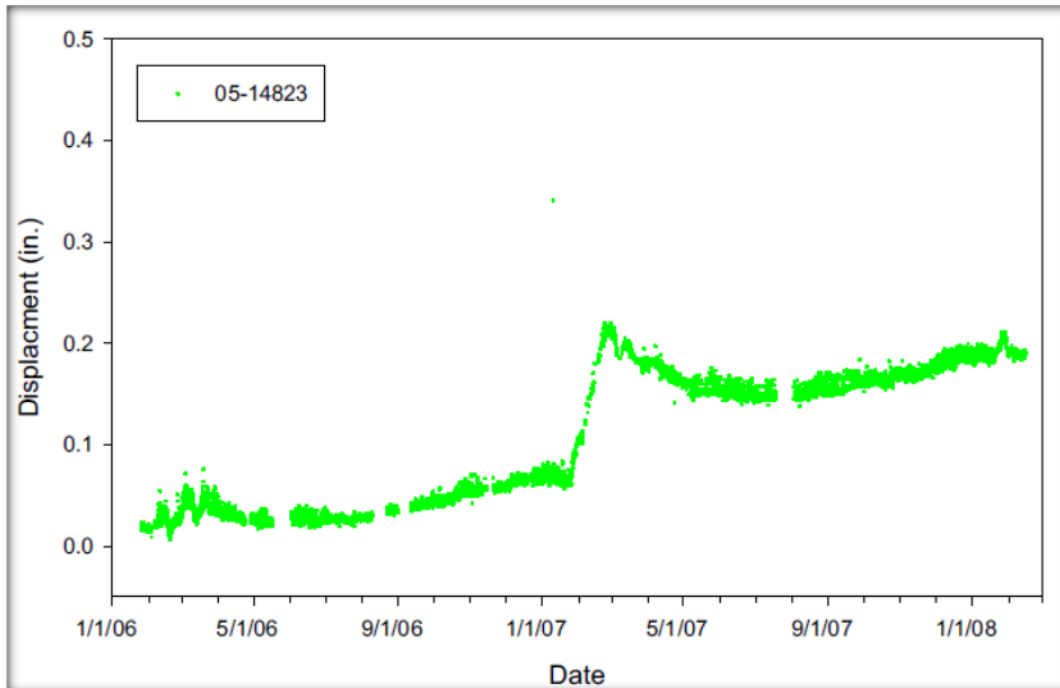


Figure 8-39 Continuous displacement versus time plot for an individual IPI sensor (05-14823) in a vertical series of five IPI sensors in a single SI casing [230]

IPI Accuracy

The range of sensor accuracy for IPI installations appears to be from about 0.5 mm/m (at a $\pm 10^\circ$ tilt range) to 0.43 mm/m (based on a $\pm 3^\circ$ tilt range) [231, 232]. The resolution of such IPI sensors ranges from 0.001 mm/m to 0.10 mm/m.

8.3.2.2.2 *Shape Accel Arrays (SAAs)*

Shape Accel Arrays (SAAs) are a proprietary technology that are essentially a chain of IPI's with MEMS sensors. Dassenbrock et al. [233] describes the SAA as a “jointed flexible tube, containing arrays of MicroElectroMechanicalSensor (MEMS)-based orthogonally aligned accelerometers, spaced along the unit at regular intervals”. The SAAs are custom manufactured to specified lengths made up of 0.5 m (1.6 ft) segments connected by composite joints that allow for angular rotation in two directions with no torsion. System parameters [233] include:

Maximum length of array: 331 ft (100 m)

Accuracy: +/- 1.5 mm per 98 ft (30 m)

SAAs can be installed in a borehole typically using a 1 inch PVC pipe or similar as a casing. A small dot at the top of the arrays allows for the alignment of the SAA in a manner similar to

orientating the A groove on a SI. The SAA and carrier pipe are then grouted into the borehole as per SI casing installation. Although undocumented, the authors are aware of SAAs being used to retrofit SI installations where a probe can no longer be passed in a deformed casing. The retrofitted SAA acts as an IPI after installation. SAAs are interrogated using either a computer or logger attached with an interface device. Communication stations can be installed to allow for the remote reading of the SAAs.

The main advantages of SAAs are:

- SAAs can be customized to fit the length of the borehole.
- SAAs can be read with a laptop and interface unlike a PI which requires manual labor. There are no potential errors associated with the reading of the device such as changing probes, cables or simply pulling the cable in a different manner between surveys by different crews.

The main disadvantages are:

- SAAs are manufactured to a specific length. If the depth of the borehole is adjusted (particularly shortened), the SAA may not be able to be installed.
- SAAs have proprietary software which leaves the user only one option for data interpretation where there are multiple options with IP/IPIs.
- SAA technology is new and does not have the same depth of user experience as the mature IP/IPI technologies.
- The initial installation cost of the SAAs could be an order of magnitude greater than that of SIs.

Typical costs are:

- Interface units for computers and loggers: \$1,000 to \$2,000.
- Loggers: \$1,500 to \$2,000.
- SAA Cable: \$500 to \$700 per m (3.3 ft) segment.

When contrasted with IP/IPI costs, SAAs cost the same to install; SAAs cost considerably more for the actual downhole segments but are considerably cheaper to interrogate. Depending on the set up used, a set of cables, probe, and datalogger for an inclinometer may cost up to \$15,000. Equipment required to read SAA installations typically costs \$1,000 to \$2,000 as noted above.

8.3.2.2.3 *Extensometers*

Extensometer, as described here, are a rudimentary (“poor man’s”) means to extend the useful life of SI casing already installed for PI or IPI landslide monitoring. In either a PI or IPI installation, if enough landslide displacement occurs along the subsurface slip surface, it will block off the SI casing and limit the use of the PI or IPI probes. Normally, this would result in the loss of the use of the SI casing for landslide displacement monitoring. If the rate of

displacement is closely monitored, then the SI casing can be converted to an extensometer prior to it being sheared off.

The extensometer conversion is composed of at least one stainless steel cable (e.g., zero elongation aircraft control cable) that is anchored below the slip surface of the landslide that is shearing the SI casing. Once installed, and once the SI casing is fully sheared off, the amount of the disappearance of the cable down the SI casing (the result of landslide movement) will equal the amount of displacement at the landslide slip surface, assuming a single failure plane. This observed landslide movement is assumed to be at the depth detected when the PI or IPI was initially operational. An example of the surface installation details of multiple cables in an SI casing is illustrated on Figure 8-40. Alternatively, and at much greater cost, one could drop an IPI or Shape Accel Array (see above) across the slip surface and let it be deformed by the movements accepting that it cannot be retrieved.

The estimated accuracy of an extensometer, as described here, is about 0.25-0.50+ inch (6.35-12.7+ mm), once the SI casing has been completely sheared off by landslide displacement. The possible sources of error in the measurement are from uncertainties in the graduation of the stainless steel cable(s), operator error in the use of measuring tapes, stretching of the cable, and the nature of the subsurface landslide deformation to the SI casing (i.e., is there one thin slip surface, or is it a thicker zone with varying deformation characteristics).



Figure 8-40 View of four extensometer cables that have been installed in PI SI casing that was being sheared-off by subsurface landslide movement. At least one of the cables was anchored below the primary, basal slip surface detected by the previous PI monitoring. (Photo by: G. Major, Year: 1987)

The primary advantage of the extensometer described here is that it allows for inexpensive conversion and continued use of the SI casing that would have been originally installed with

significant expense. However, the displacement measurements from the extensometer are less precise than those coming from either PI or IPI monitoring.

8.3.2.2.4 Downhole Time Domain Reflectometry (TDR)

Downhole time domain reflectometry (TDR) is a relatively new approach to monitoring slope movement [234]. Originally developed to locate breaks and faults in communication and power lines, its first geotechnical use was around 1980 to locate shear zones in underground coal mines [235].

Downhole TDR works in much the same way as radar, in that a radio transmitter sends out a short pulse of energy and measures the time for a reflection, or echo, of the energy from some object [223, 235, 236, 237]. In TDR, a surface cable testing unit sends an electrical pulse down a coaxial cable grouted in a geotechnical exploratory borehole that penetrates to a depth below a landslide slip surface (Figure 8-41). When the pulse encounters a break or deformation in the cable (such as at the slip surface), it is reflected. The reflection shows as a “spike” in the cable signature (Figure 8-41). The relative magnitude and rate of displacement over time, and the location of the zone of deformation can be determined immediately and accurately. The size of the spike increase correlates with the magnitude of movement (Figure 8-42). A laptop computer is connected to the tester and cable signatures are saved for future reference.

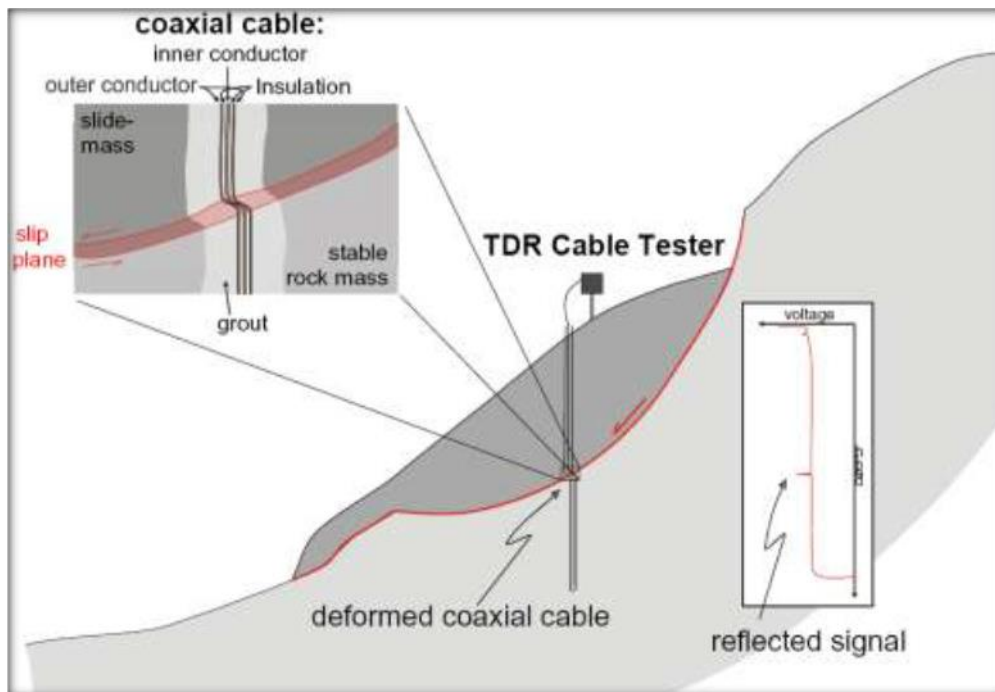


Figure 8-41 Basic set up of a TDR landslide measuring site showing the TDR cable installed in a grouted borehole and across the landslide slip surface. Displacement of the landslide results in a spike in the TDR reading. [238]

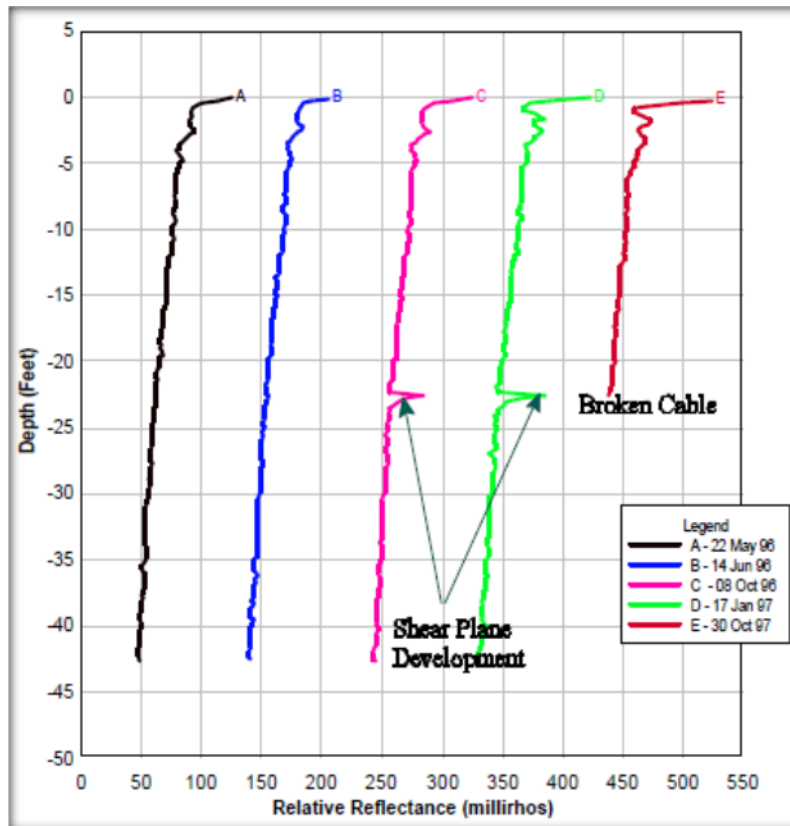


Figure 8-42 Increased TDR signature spike and broken cable with continued (~1½ years) landslide displacement at the slip surface [237]

Some of the advantages of TDR over probe inclinometers are:

- Coaxial cable costs less than inclinometer casing, and provides for a cost-effective installation.
- TDR readings take several minutes versus PI inclinometer readings that can take over an hour to complete.
- The coaxial cable can be extended to a convenient reading location off the slope or away from a highway.
- TDR readings can easily be automated for continuous data collection.
- Slope movement can be determined immediately during data collection rather than waiting until data are plotted on computer.
- Measurement of subsurface deformations delivers relative insight regarding the slip surface (e.g., depth of surface of rupture/position of slip plane, width and type of deformation zone).

TDR does have some disadvantages as well:

- TDR cannot determine the actual amount of movement. Only the relative amount of displacement can be estimated.

- The direction of movement cannot be ascertained from a TDR signature.
- The cable must be deformed before movement can be located. Simple bending of the cable, without damage, will not indicate any movement.
- If water infiltrates a TDR cable, it will change the cable's electrical properties and may make signatures difficult to interpret.
- TDR installs require proper grouting of the borehole, especially in soil.
- TDR is only applicable to localized shearing deformation (thin shear zones).
- Quantitative measurements are a challenge and movement rates need to exceed 2 cm/year.
- Should be used in combination with surface measurements.

In 2001 [235], the cost of coaxial cable varied from about \$0.20 to \$2.50 per foot. Cable testers, for reading TDR signatures, varied from about \$6,000 for a used tester to about \$10,000 for a new one. It is understood that cable testers may be available for as low as \$2,000.

Table 8-5 is a summary comparing the general characteristics and attributes of SIs (both PIs and IPIs), SAA, rudimentary extensometers, and TDRs for subsurface monitoring of primarily landslides and potentially unstable slopes.

Table 8-5 Comparison of Common Subsurface Monitoring Methods for Landslides

Subsurface Monitoring Method	Comparison Rating					Equipment and Cost
	Maturity	Commercially Available	Accuracy/Preciseness	Repeatability	Reliability	
PI	High	Yes	Millimeter scale	High	High	Geotech borehole, SI casing, PI probe, cable, and read out unit. Typical SI casing installation cost is \$10-20k (including geologic logging); PI equipment used to read boreholes is ±\$10k. The rent for tools is \$200-300 per day. The labor cost for reading boreholes depends on the length. However, field time for reading 500 ft (150 m) installation is four hours.
IPI	High	Yes	Millimeter scale	High	High	Geotech borehole, SI casing, IPI probes, cable, and read out unit. Typical SI casing installation cost is \$10-20k (including geologic logging); IPI equipment is \$10k-20k+ depending on the number of IPI probes installed.
SAA	Medium	Yes	Millimeter scale	High	High	Geotech borehole costs \$500-700 per meter. Computer interface (data acquisition board) is roughly \$1,000-2,000. Data logger is roughly \$2,000.
Extensometer	Low	Yes	Centimeter scale	High	High	Repurposed SI casing; stainless steel cables, and ancillary parts cost ± \$500.
TDR	Medium-High	Yes	Centimeter scale and relative	High	High	Geotech borehole costs ± \$10k; TDR readout unit and cable costs \$2k-10k (2007).

8.3.2.2.5 *Piezometers*

Landslides and slope movement are commonly triggered or accelerated by elevated (raised) groundwater levels in a slope, and by elevated groundwater pore pressures at a landslide slip surface. The elevated groundwater levels and pressures reduce the shearing resistance of the geologic material at the landslide slip surface and thus result in landslide slip or slope movement. The objective of using piezometers in landslide and subsidence hazard monitoring is to be able to monitor the nature of the response, the patterns, and the trends of groundwater conditions in a slope due to storm-related and/or seasonal precipitation trends, and to match these groundwater trends to the triggering of slope movement.

A piezometer is a groundwater monitoring device either used to measure the pore water pressure in the subsurface by measuring the height to which a column of water rises against gravity, or a device which measures the pressure (more precisely, the piezometric head) of groundwater at a specific point or depth [239, 240, 241]. A piezometer is designed to measure static groundwater pressures.

A standpipe piezometer (also known as an observation well) records the height to which groundwater will rise in an open standpipe or well. The water pressure at a specific point or depth in the subsurface is recorded by a pressure transducer or other calibrated device. Standpipes or observation wells give some information on the water level in a subsurface formation, but are commonly read manually. Pressure transducers of several types can be read automatically and the data can be stored with dataloggers, making data acquisition convenient and continuous.

The first piezometers in geotechnical engineering were open wells or standpipes (sometimes called Casagrande piezometers) installed into an aquifer, or a subsurface zone of interest such as a landslide slip surface. A standpipe piezometer is typically installed in a geotechnical exploratory borehole, documented with a geologic log so that the piezometer can be designed for the observed subsurface geologic and hydrogeologic conditions. The standpipe piezometer will typically have a solid casing (e.g., PVC) down to the depth of interest, and a slotted or screened casing (e.g., PVC) spanning the zone/elevation/depth where water pressure is being measured or monitored. The screened length of the pipe in a borehole is backfilled with clean sand, while the solid casing above, is sealed to the surface with bentonitic clay or concrete to prevent surface water from contaminating the groundwater supply. Figure 8-43 shows a typical subsurface profile and details for a flush-mounted standpipe piezometer that would be located in a roadway. On the other hand, Figure 8-44 illustrates an above-ground surface completion, with protective steel casing for a piezometer co-located with an inclinometer in an active landslide. A co-located standpipe piezometer with an inclinometer is typically within about 10 ft (3 m) of the inclinometer to monitor the groundwater conditions coincident with the inclinometer, and what levels/elevations might be triggering landslide movement.

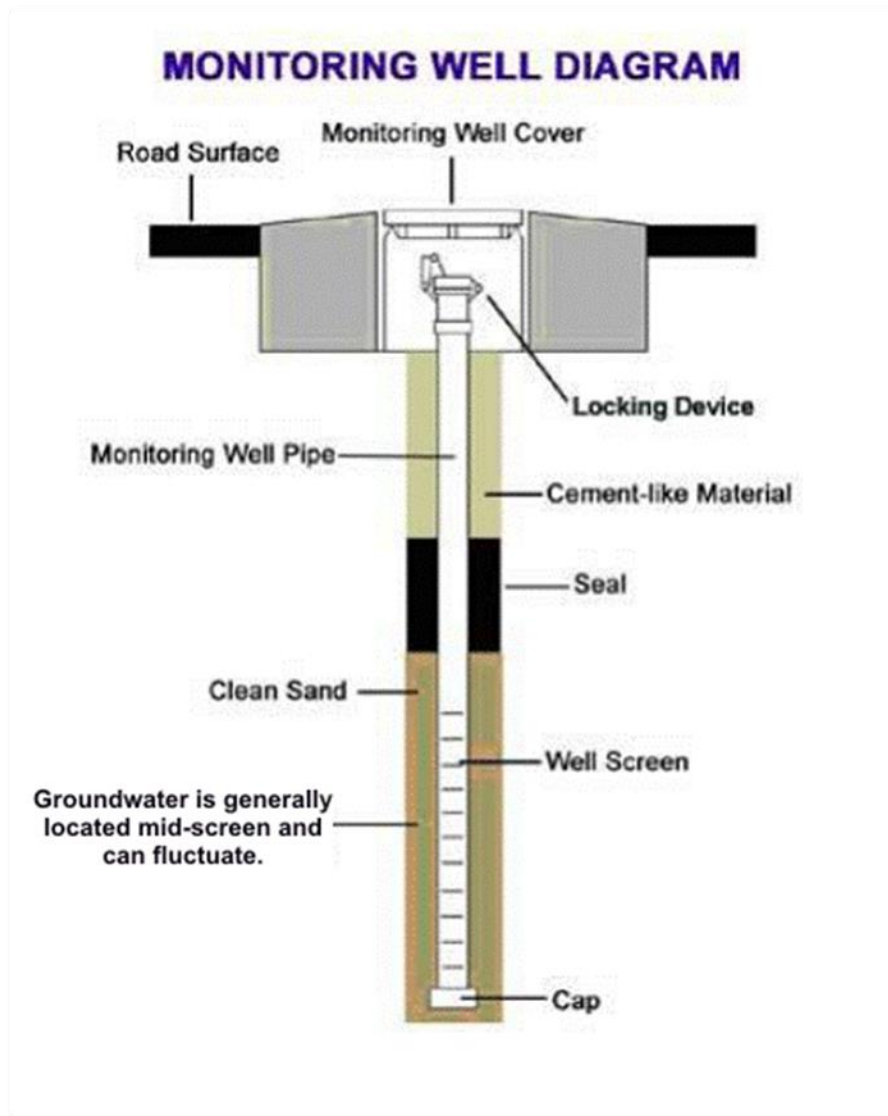


Figure 8-43 Typical details for a standpipe piezometer, in this case, one that is flush-completed in a roadway



Figure 8-44 Above-ground, protective surface completions in a landslide, on a ROW, for a standpipe piezometer and a PI inclinometer (Photo by: D. West, Year: 2005)

In an unconfined aquifer, the water level in the standpipe piezometer may not be exactly coincident with the water table, especially when the vertical component of the groundwater flow velocity is significant compared to the horizontal component. If the piezometer screen is installed in a confined aquifer under artesian conditions, the water level in the standpipe piezometer will indicate the pressure in the confined aquifer, but not necessarily the water table, and may have a perched water level above the confined aquifer's water table [239].

Standpipe piezometers are commonly constructed using 2-inch-diameter (5 cm) PVC plastic pipes (both solid and screened/slotted). This size of the PVC pipes allows for water level meter probes to be easily lowered into the PVC pipes for manual groundwater monitoring. A common water level indicator consists of a probe, a cable with precise, laser-marked graduations, and a cable reel [242]. The hub of the cable reel contains batteries, electronics, a bright LED lamp, and a beeper. The operator lowers the probe into the standpipe or well. When the probe contacts the surface of the water, the LED illuminates, and the beeper sounds. The operator then reads the depth-to-water measurement from the graduations on the cable.

Pressure transducer piezometers are commonly grouted in a geotechnical borehole along with slope inclinometer (SI) casing (on the outside of the casing), or they may also be installed in a standpipe piezometer if continuous water level measurements are a requirement. The pressure transducers are commonly of the vibrating-wire (VW) type, converting groundwater pressure into an electrical signal, or of the pneumatic type, measuring pore water pressures directly by using gas to lift a diaphragm. These piezometers are cabled and/or tubed to the surface where

they can be read by data loggers, portable readout units, or can be automated, allowing faster and more frequent or continuous reading than possible with open, manually-measured standpipe piezometers.

The VW piezometer converts water pressure to a frequency signal via a diaphragm, a tensioned steel wire, and an electromagnetic coil [242]. The piezometer is designed so that a change in pressure on the diaphragm causes a change in tension of the wire. When excited by the electromagnetic coil, the wire vibrates at its natural frequency. The vibration of the wire in the proximity of the coil generates a frequency signal that is transmitted to the readout device. The readout device processes the signal, applies calibration factors, and displays a reading in the required engineering unit.

Based on [242], there are several types of VW piezometers which can be used for measuring groundwater pressures. These are:

- Standard borehole piezometer
- Multi-level piezometer
- Heavy-duty piezometer
- Push-in piezometer
- Low-pressure piezometer
- Vented pressure transducer

The standard borehole VW piezometer (Figure 8-45) is suitable for most applications. It can be directly grouted into a borehole using a bentonite-cement grout mix.



Figure 8-45 Standard borehole VW piezometer [242]

The advantages of VW piezometers are:

- High Resolution: VW piezometers provide a resolution of 0.025% of full scale.
- High Accuracy: Automated, precision calibration system ensures that all VW piezometers meet or exceed their accuracy specifications.
- Groutable: The VW piezometer can be directly grouted-in with a bentonite-cement grout.
- Rapid Response: VW piezometers offer rapid response to changes in pore water pressure, whether they are grouted in, pushed into cohesive soils, or embedded in a sand filter zone.

- **Reliable Signal Transmission:** With properly shielded cable, signals from the VW piezometer can be transmitted long distances.
- **Temperature Measurement:** All VW piezometers are equipped with a temperature sensor.

In a typical pneumatic piezometer installation, the piezometer is sealed in a borehole, embedded in fill, or suspended in a standpipe [241, 242]. Twin pneumatic tubes run from the piezometer to a terminal at the surface. Readings are obtained with a pneumatic indicator. The piezometer contains a flexible diaphragm. Water pressure acts on one side of the diaphragm and gas pressure acts on the other. When a reading is required, a pneumatic indicator is connected to the terminal or directly to the tubing. Compressed nitrogen or carbon dioxide gas from the indicator flows down the input tube to increase gas pressure on the diaphragm. When gas pressure exceeds water pressure, the diaphragm is forced away from the vent tube, allowing excess gas to escape via the vent tube. When the return flow of gas is detected at the surface, the gas supply is shut off. Gas pressure in the piezometer decreases until water pressure forces the diaphragm to its original position, preventing further escape of gas through the vent tube. At this point, gas pressure equals water pressure, and the pneumatic indicator shows the reading on its pressure gauge. Figure 8-46 illustrates the operation of a pneumatic piezometer, while Figure 8-47 shows a typical one.

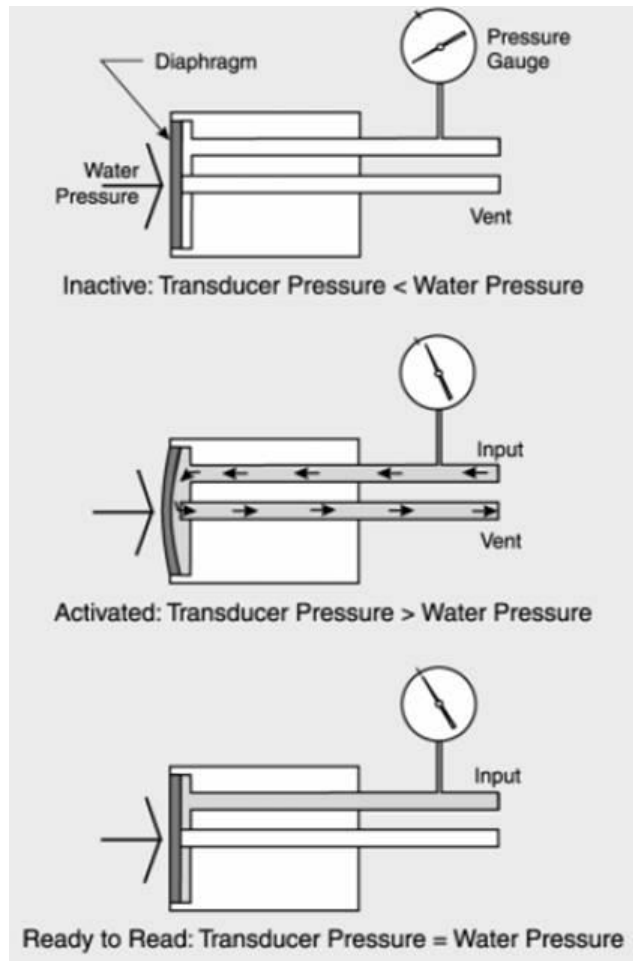


Figure 8-46 Pneumatic piezometer operation schematic [242]



Figure 8-47 Typical pneumatic piezometer [242]

Table 8-6 lists various attributes of standpipe, VW, and pneumatic piezometers which have been commonly applied to groundwater monitoring at landslide and potential slope movement

sites. They have also been used to monitor the performance of landslide mitigation projects where groundwater lowering is the primary, or a main component of the landslide mitigation strategy. The general experience is that VW piezometers are commonly the most used option of the three types of piezometers listed on the next page.

Table 8-6 Comparison of Piezometer Monitoring Method Attributes

Piezometer	Comparison Rating					
	Reading Time	Remote Access	Data Logging	Accurate Readings	Main Advantage	Equipment and Cost
Standpipe	Minutes	No	No	Requires technique	Simple	Geotech borehole, PVC casing, water level indicator. Typical PVC casing installation cost \$5-10k ± (w/o geologic logging). Water level indicator is ± \$2k.
VW	Seconds	Yes	Yes	Yes	Easy to install and read	Geotech borehole, VW piezometer, readout unit, cable and data logger. Typical SI casing installation cost \$10 -20k (including geologic logging). The actual VW piezometers are \$0.5k each with the readout or logger boxes being \$1.5k to \$3k dollars each.
Pneumatic	Minutes	Yes	No	Requires patience and technique	Not affected by lightning	Geotech borehole, PVC casing, readout unit, tubing, inert gas bottle. Typical PVC casing installation cost \$5-10k ± (w/o geologic logging); readout unit and ancillary equipment cost about ± \$2k.

8.3.2.2.6 *Ball Markers*

Scientific/Engineering Principles of the Marker Balls

The marker balls, shown in Figure 8-48, are buried in the soil above the pipeline during construction of a new pipeline or while a pipeline is in service. The marker ball utilizes passive antenna radio frequency identification (RFID) technology encased in a waterproof shell that allows an operator to locate the ball from the surface. A pipeline locator unique to the ball marker transmits a signal to the buried marker and the marker returns the signal to the locator, indicating the marker's position and depth. When radio waves from the locator are encountered by a passive RFID tag, the coiled antenna within the tag forms a magnetic field and the tag draws power from it, energizing the circuits in the tag. The tag then sends the information encoded in the tag's memory.

For most accurate spatial coordinates in the x, y direction it is recommended that the location be GPS surveyed by a land surveyor to record specific x and y coordinates. The locator identifies the depth of the ball in the z direction up to 1.5 m (5 ft) within +/- 10% accuracy. For best results bury the marker at 3.5 ft or shallower (approximately 1 m or shallower) to improve the accuracy results.

Movement of the ball between surveys allows the operator to monitor soil creep or other type of slow moving localized land movement. The ball marker's self-leveling design provides confidence in the horizontal location of the ball when located by the pipeline locator. It also reduces any concerns of tilting or disturbances through backfilling during installation. The ball marker RFID functionality also enables pipeline data to be stored in the marker to ensure positive identification of the pipeline. This functionality uses a pre-programmed unique serial number which can integrate with office mapping and GIS systems. The ball marker is used for repetitive and continual monitoring for which the operator defines a survey frequency as established from previous surveys and rates of land movement.

Physical Specifications:

- Size: 4 in diameter sphere (10.4 cm diameter)
- Weight Net: 0.7 lb (0.35 kg)/ Shipping: 24 lb (10.4 kg)
- Packaging: 30 per carton
- Markers Read Range: up to 5 ft (1.5 m).

Environmental Specifications:

- Operating Temperature -4 °F to 122 °F (-20 °C to 50 °C)
- Storage Temperature -40 °F to 158 °F (-40 °C to 70 °C)

Rough Order Magnitude Costs:

- \$30 per marker ball, carton/case of 30 marker balls costs approximately \$900
- Locator costs +/- \$1,000 per tool
- GPS survey crew costs +/- \$200 per hour



Figure 8-48 Ball Markers [243]

Table 8-7 Characteristics of ball markers

Matrix to Rate Technology	Rating
Maturity (high, medium, low)	High
Commercial availability (Yes, No)	Yes
Accuracy / precision of data (high, medium, low, or specific numbers)	Locator: +/- 3 inches x, y +/- 10% in z
	GPS: +/- 0.5 in x, y
Repeatability of data (high, medium, low)	High
Reliability of the hardware (high, medium, low)	High

Circumstances/Scenarios for Application

Monitoring by ball markers allows the operator to develop land movement rates and indirectly correlate to the movement to the pipeline. Rates of land movement determined from multiple surveys can provide the operator the ability to estimate the potential for pipeline displacement. The below ground marker ball allows the operator to monitor soil movement without having a direct connection to the pipeline (i.e. tracer wire). Marker balls are used primarily for monitoring soil creep at creeping fault locations; however, they can also be used to monitor localized slow-moving shallow land movement areas (up to 5 ft from the surface).

Examples of Application

Examples of installation are shown in Figure 8-49, Figure 8-50, and Figure 8-51. The marker ball is best used directly after a new installation of a pipeline to create a baseline that will monitor land movement from when the pipeline was installed. The marker balls do not directly measure any movement before the marker ball was installed. If the marker balls are installed while the pipeline is in service, then established rates of land movement may only be used as a guidance to back calculate total land movement from the original pipeline installation. The marker balls are recommended to be installed in close proximity to the pipeline at a selected interval along the pipeline alignment, determined by the operator based on the extent and estimated location of soil movement.



Figure 8-49 Packaging of marker balls



Figure 8-50 Marker ball installed at approximately 3.5 ft below ground surface, above new pipeline alignment



Figure 8-51 Denotes location of installed marker prior to complete backfill of pothole used for establishing baseline survey before leaving site

Procedure/Process of Applications

a. Site or pipe preparation

No pipe preparation is required since the technology is not applied directly to pipeline. The marker ball is dropped in the trench during pipeline backfilling after construction.

b. Installation

The marker ball only needs to be placed above or near the pipeline during backfilling, see Figure 8-52. The marker ball is placed no deeper than 1.5 m or 5 ft and once the ball is in place it is recommended to GPS survey the location for as-built records and then locate the ball again after the backfilling process is complete to compare results and establish a true baseline. The

marker balls should be spaced at an interval spacing as deemed appropriate by the operator but typically per the direction of a geotechnical consultant.



Figure 8-52 Installation of marker ball

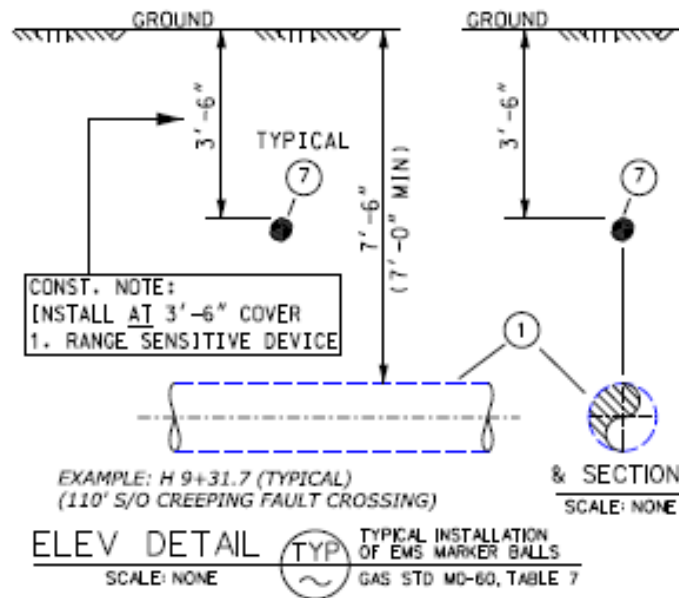


Figure 8-53 As-built drawing detail

c. *Protection of sensors*

Sensors are encased in a waterproof plastic material which houses the RFID tag. The RFID is not sensitive to soil conditions or to surrounding magnetic fields. The marker ball however is sensitive to damage from excavation activities in areas where soil disturbance (agricultural areas) is likely to occur above or around the pipeline.

d. *Data logging*

A Dynatel or Goldak MLX-GP EMS Marker Locator is the typical instruments used to locate the underground marker ball. The ground surface where the locator picks up the marker ball should be marked by a cross with paint or some other temporary above-ground marking system, so that the intersection point can be GPS surveyed by a qualified land surveyor. Data recording is a manual process that is captured by the land surveyor(s) using the location from the pipeline locator through individual field measurements. The information can be transposed or imported into GIS or other similar documentation of records. Each site measurements shall be added to the previous survey measurements for comparative analysis.

e. *Frequency of data reading*

As ball markers are used for slow-moving soil movement, readings are recorded on an annual or semi-annual basis or until an appropriate frequency is established by the operator using historic survey results and movement. Survey frequencies can be increased as appropriate from previous survey results.

f. *Data interpretation*

Data is interpreted from the x, y, z results and should only be used to compare and establish soil movement rates. For best results or redundancy, the same survey crew should be used on the same project location or have detailed knowledge of how the previous surveys were completed,

so as to minimize survey inaccuracies. This will ensure that similar processes and techniques are followed and the accuracy of the data is not compromised by varying methods/processes. Multiple readings (more than two) shall be recorded prior to making comparisons or drawing any trends.

Principal Advantage and Disadvantage

The principal advantage of this technology is that it provides a relatively inexpensive tool to monitor slow soil movement near a pipeline. Another advantage is that since the balls are installed below-ground, they are protected from shallow excavation damage (non-agricultural land use) or other surface activities (e.g. livestock or human tampering), particularly when compared to above-ground or at-ground installations, such as conventional survey points.

The principal disadvantage is that this tool only measures soil movement and thus provides an indirect assessment of pipe movement. In addition, marker balls only measure soil movement since their installation; the movement prior to the time of installation is not known. Marker balls rely on a passive locate technology, which in turn needs to be GPS surveyed. The process can add levels of uncertainty in the measurement accuracy.

8.3.2.3 Land Based Surface Monitoring

8.3.2.3.1 Conventional and Global Positioning System (GPS) Surveys

Geodetic surface displacement survey (x, y, z coordinates) from both conventional ground-based (i.e., theodolite/total station) or satellite-based (GPS or GNSS) survey methods are commonly used to characterize and subsequently monitor ground movements. The surveys provide information about the displacement (or lack thereof) of discrete points within a survey area.

This section describes the methods of ground surveying and provides a detailed comparison of methods in Table 8-8. Conventional surveys are typically thought of as ground-based measurements relative to either a geodetic coordinate (reference grids) system or a project specific local grid. Reference grids are typically based on Ellipsoids which are horizontal control models which typically use World Geodetic Systems 84 or 1980 systems. Geoid Control Models provide vertical control (typically HT 2.0 or HT97) which is the surface the earth's oceans would take under the influence of earth's gravity and rotation without the influence of winds or tides. The Geoid surface is extended through the continents to provide a reference global mean sea level. Conventional surveys involve measuring angles, distances, and/or height differences between points that are limited by a line of sight using an instrument (typically a total station) and target (reflector point or, with new technologies, a hard surface). Using conventional surveys can sacrifice accuracy over either long distances or multiple legs. Conventional surveys tend to be the preferred option of surveyors over shorter distances and/or smaller areas or where a GPS signal cannot be reliably acquired (refer to Table 8-8). The US Army Corps of Engineers [244] discusses conventional survey deformation monitoring in detail. Reference [245] provide a summary of conventional surveying methods for the specific purpose of monitoring landslides. Although the papers are outdated by today's standards, they provide

good basic guidance. There is no current state of the art paper at the time of publication of this document. Recent advancements of the total station technology allow for automatic reading of programmed targets.

Recent guidelines for GPS surveys can be found in the following documents:

- Henning et al. (2011) for United States [246],
- Donahue, Wentzel, and Berg (2013) for Canada [247], and
- Royal Institution of Chartered Surveyors (2010) for the United Kingdom.

GPS surveys typically include the US (GPS) and Russian (GLONAS) satellite constellations. More satellites are visible and receiver positional data can be more readily resolved using both sets of satellites. Survey-grade accuracy is obtained by setting base units over known reference points and adjusting the locations obtained from rover units by the errors simultaneously calculated at the base units. GPS surveys can be categorized into two types:

1. **Static Baseline (Static):** Static baselines require that the GPS receiver be placed on an observation point for some period of time e.g., 5 to 30 minutes, determined based on the baseline length. The advantage is that a larger sample of satellite information is collected to allow for an accurate resolution of the receivers' position. The more practical advantage of this method is that the receiver is mounted on a stationary tripod and centering plummet and is considered stationary over the monitoring point. An example of a static survey is shown in Figure 8-54, where 2 base stations are positioned above and outside of the landslide on known provincial survey monuments. The base stations are run continuously while 3 rover stations are alternated over monitoring points with a minimum 30 minutes at each point.
2. **Real-Time Kinematic Positioning (RTK):** A real-time instantaneous (RTK) solution is typically half as accurate as a traditional static baseline. This is primarily due to a near instantaneous shot being taken from a less stable hand held pole positioned over the monitoring point. These surveys typically involve a single base station positioned over a base station point in proximity to the survey site and a rover station on a hand-held rod taking quick shots over each monitoring point. When working in municipal areas, data from third party base stations may be obtained rather than having to set up a survey-specific base station.

Both conventional and static GPS methods require multiple base stations (and/or back sights) placed on known stable ground. Base stations are typically permanent concrete survey monuments with monitoring points installed within and surrounding the landslide. Whenever possible, known control points are used – including state/provincial and Federal control points. These tend to be more abundant around populated areas as opposed to pipeline ROWs.

There are numerous different designs for monitoring points as previously discussed in the visual monitoring section. Regardless of the design, monitoring points should be protected from weather, animals, and traffic. The monitoring point should be installed so that it is not subject to

frost heave. Therefore, rebar type monitoring points are not recommended in most northern climates. One example of a monitoring point is a 3/4 in (19 mm) smooth steel sucker rod driven as deep as reasonably possible (4 to 7 ft) into the ground with a monitoring point punched into the top of the rod. A more robust example is the Bernstsen 3/4 in Aluminum Top Security Rod™ (www.bernstsen.com) type monitor that includes a flip-top access cover that protects a countersunk solid aluminum finned rod. Figure 8-54 shows a typical monitoring set up.

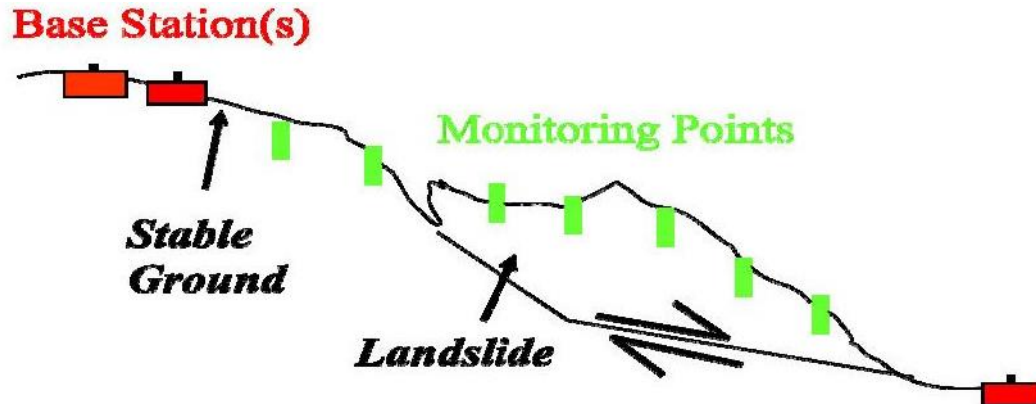


Figure 8-54 Sketch of a typical monitoring set up for ground based conventional and GNSS surveys

A challenge with surveys is that establishing proper control may be difficult when the survey is limited to a linear pipeline ROW. To minimize potential control related errors to the greatest extent possible it is recommended to have a multiple control points outside the area of interest with a triangular control grid rather than a linear grid. This may not be possible in urban areas or areas where there are landowner/stakeholder issues.

In both static and RTK surveys, post survey data processing is required to determine the final positions of the base stations and monitoring points. Static surveying is more (refer to the Table 8-8) accurate as more data is collected to determine the final position of the monitoring point.

Figure 8-55 and Figure 8-56 show typical study areas for conventional and GPS surveys.

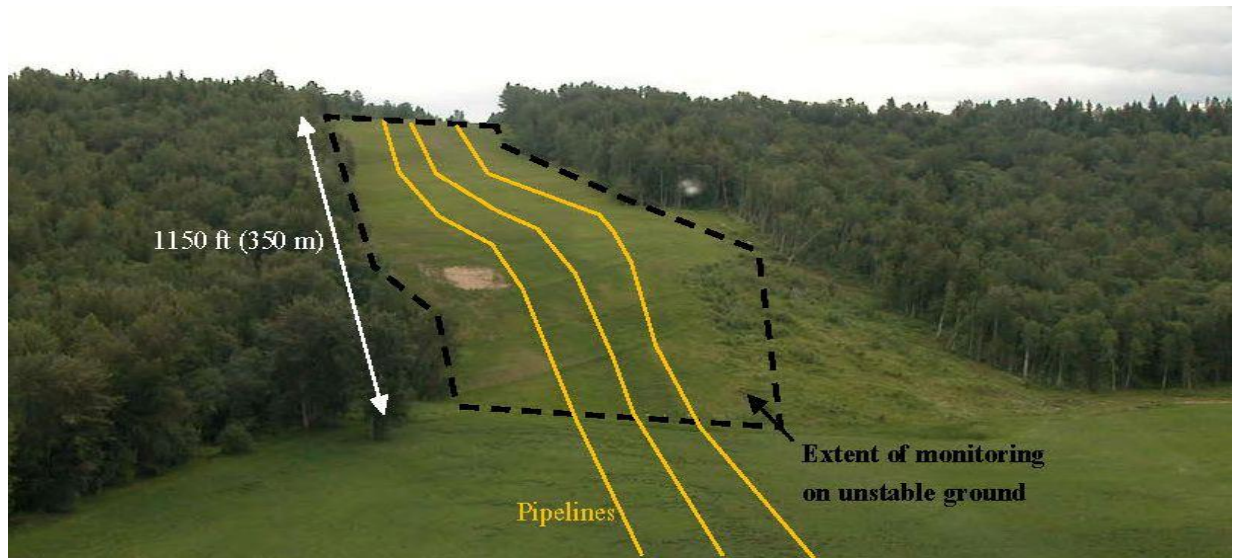


Figure 8-55 A conventionally monitored slope with an extremely slow translational slide and soil creep. Outline shows extent of a grid of 90 monitoring points. Base stations are located at the top and bottom of the slope outside of the unstable section of pipeline ROW. (Photo by: D. Dewar, Year: 2014)

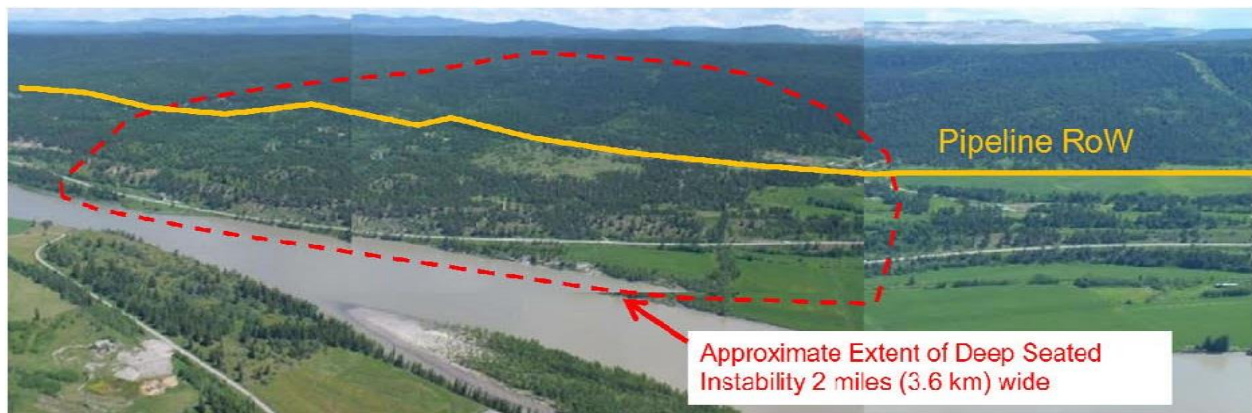


Figure 8-56 A GNSS monitored slope with an extremely slow translational slide. Outline shows the extent of 30 monitoring points located along the ROW in select areas where suitable satellite coverage is available. Base stations are located at the top of the slope outside of the unstable section of pipeline ROW. (Photo by: D. Dewar, Year: 2014)

Surveying methods are typically only applicable where the actual landslide and/or settlement subsidence deformations will not destroy, distort, and/or bury monitoring points. Therefore, the method is typically more suitable for monitoring slow to extremely slow (refer to Chapter 3, Table 3-2) topples, slides, flows, or spreads.

Typically, local geological/geotechnical specialists will have developed relationships with local survey consultants to provide landslide monitoring services. It is always recommended that local expertise be used when scoping, designing, implementing, and interpreting landslide data.

Surveyors experienced in deformation monitoring should be contracted to do the work. Surveyors only experienced in legal surveys may have great difficulty understanding the concepts of data reduction for deformation analysis when their experience is in correcting data to resolve the positions of static points. The interpretation of data may not always be as straightforward as one may perceive. For extremely slow moving landslides it may take numerous years to gather enough data to separate obvious movements from random or human errors. The more precise the survey method/equipment is, the more likely it is that actual landslide movements can be distinguished from errors. Figure 8-57 shows an example of monitoring points that are interpreted to be unstable and stable. Table 8-8 compares the two survey methods.

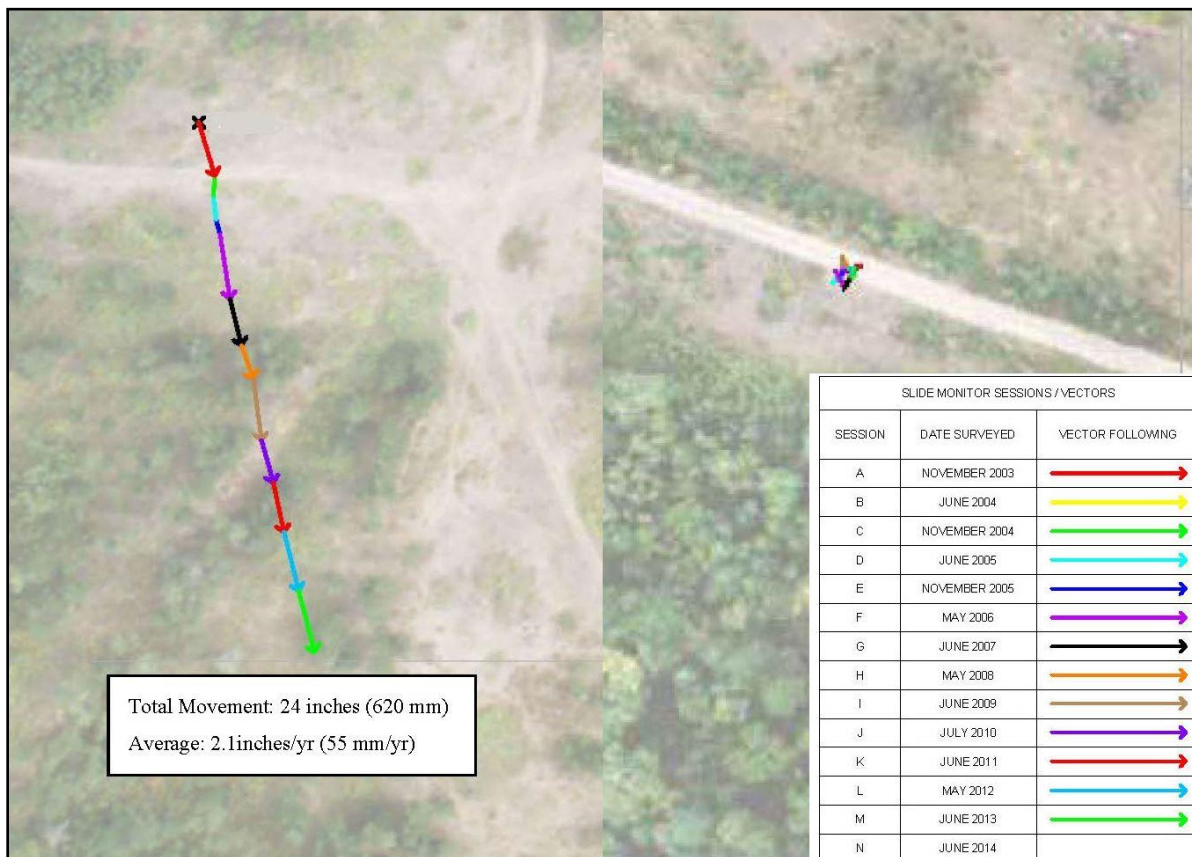


Figure 8-57 Representation of GPS survey results for a landslide shown above. The monitoring point to the left is near the center of the landslide and has clearly moved whereas the point to the right is located downstream of the landslide on stable ground.

Table 8-8 Comparison of the conventional to GPS methods

Item	Conventional Surveys	GPS Surveys
Applicability (Study Area)	Generally better for smaller landslides on ROW sections less than 1500 ft (460 m) in length and where sky visibility is limited or obstructed.	Preferred for large landslides on ROW of over 1 mile (1.6 km) in length. Study areas can be as large as 30 miles (48 km) along regional landslide complexes.
Equipment Availability	Depending on the accuracy requirement most survey contractors would have the capacity to conduct this work under the guidance and review of a monitoring specialist.	Due to equipment costs, typically only larger survey contractors own equipment. Small firms typically rent equipment; therefore, they may not be as familiar with it.
Technology	Conceptually simple, perceived to be well established, and very economical. Minimal specialized equipment required. Operator and procedural experience are critical.	Relatively simple and well established. Specialized equipment and data interpretation required.
Costs (Monitoring)	Costs can be highly variable. If conventional surveying requires a tie-in to a reference grid, considerable efforts could be required. The cost to install a typical monitoring point or base station range from \$100 to \$1,000 per point depending on the type, access to, and number of points.	
Tie-ins	Survey must be tied into existing legal evidence, base station, or GPS survey; otherwise, a project specific local coordinate system could be used.	Automatically tied into an approximate UTM or other reference grid with a known location.
Expected Accuracy	Depends on distance of survey and the amount of survey legs; but as a rule of thumb, expect +/- 0.10 in (2 mm) per 650 ft (200 m) of length. Legal survey position accuracies are usually 0.8 in (20 mm). This is under ideal conditions with a trained observer and proper equipment.	Assuming good satellite geometry and proper equipment calibrations, the following are the best achievable accuracies: RTK: +/- 0.4 in (10 mm) horizontal. Static Survey: +/- 0.2 in (5 mm) horizontal. <i>Vertical accuracy is generally 2.5 times horizontal accuracy (e.g. 10 mm horizontal would be 25 mm vertical).</i> <i>Operator experience typically shows the true accuracies to be up to three times the best achievable accuracies.</i>

Table 8-8 Comparison of the conventional to GPS methods (Cont'd.)

Item	Conventional Surveys	GPS Surveys
Sources of errors/corrections	<ul style="list-style-type: none"> • Movement/damage to base stations and monitoring points. • Atmospheric/temperature corrections. • Generally, less accurate as distance of survey increases. • Operator errors. • Equipment in poor calibration/adjustment. 	<ul style="list-style-type: none"> • Movement/damage to base stations and monitoring points. • Poor satellite coverage or limited coverage during some periods of day. • Operator errors. • Equipment in poor calibration/adjustment. • Require a minimum horizon of typically 15° to be able to see satellites. Therefore, narrow ROWs in forests or on steep ground may not get suitable coverage.
Advantages (both methods)	<ul style="list-style-type: none"> • Monitors near surface/surficial ground deformations which, on the scale of most landslides, is where the pipeline is located. • Can be applied to hard-to-access sites on steep slopes and poor ground as only foot access is required. • Considerably less expensive to install than slope inclinometers and other subsurface monitoring. Thus, considerably more monitoring points can be installed per given budget. • Can combine both conventional and GPS survey methods in a hybrid survey to suit local ground or ground cover conditions. • Can be automated (but at a considerable expense and may be susceptible to theft and vandalism). Without automation, considerable efforts may be required to establish seasonal rates of movements as numerous monitoring visits would be required. 	
Disadvantages (both methods)	<ul style="list-style-type: none"> • Required ground disturbance (GD). Some GD procedures may not allow for optimal placement of monitoring points close to pipelines. • Monitoring points may be difficult to install in either very soft/very loose, hard/very dense, or coarse/rocky ground conditions. • Considerable expense per monitoring point for small jobs due to equipment rentals and mobilization. • Potential difficulties duplicating surveys if there are contractor/personnel/equipment changes. This can be minimized by including independent outside senior review of survey methods and data reduction techniques. • Provides data at discrete points rather than a continuous scan of ROW as done by LiDAR or InSAR (discussed later in the chapter). 	

In many cases, hybrid surveys must be conducted when GPS coverage is not available at critical areas where monitoring is required, including sections of ROW that are shaded by trees or surrounding topography. In these areas, monitoring points would be conventionally surveyed using adjacent GPS monitoring points as tie-ins.

When designing survey programs for large areas or numerous sites, the need for accuracy may have to be balanced with timing/budget considerations. As an example, if you have 150 separate sites to monitor, static surveying may not be realistic given the potential timelines required to conduct all surveys prior to the next required monitoring session.

8.3.2.3.2 *Monuments Directly Attached to Pipelines*

Above ground survey monitoring refers to an historic technique of directly monitoring pipe deformations by attaching a survey rod to the pipe by either CAD welding or clamping it to the exposed pipeline. The survey rod is then run up to the ground surface typically through either wood cribbing or a plastic culvert. The attached rod would be surveyed using the techniques discussed in section 8.3.2.3.1 of this chapter. Figure 8-58 shows a wood crib of installation.

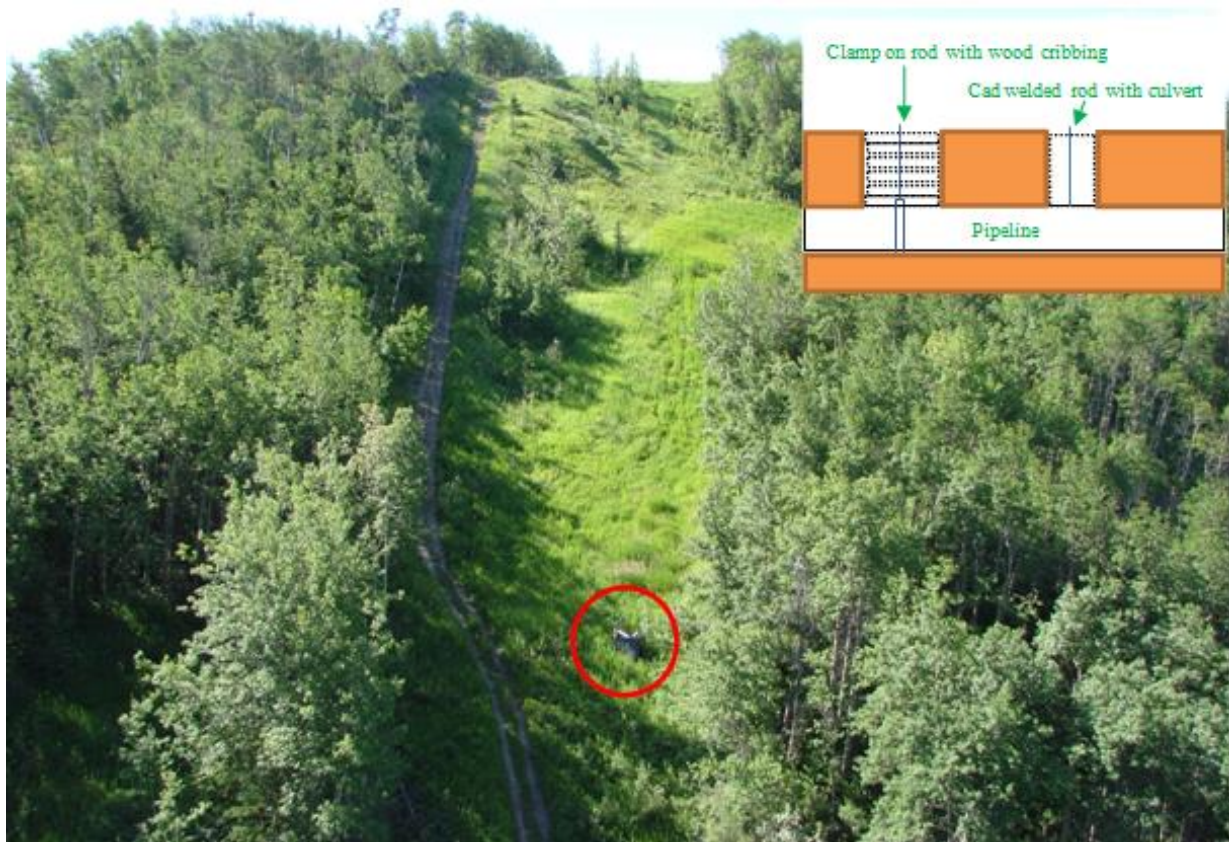


Figure 8-58 Above surface survey monument in a wood crib within pipeline ROW (Photo by: E. McClarty, Year: 1999)

The primary advantage to the technique is that it directly measures if the pipe is being deflected or bent by a geologic hazard. Limitations to the technique include:

- At a minimum, the top of the pipe must be exposed to install the survey rod.

- Pipeline corrosion protection may be compromised.
- There are possible third-party interactions with the pipeline.
- The maximum deformation that can be recorded is proportional to the opening size of the wood cribbing and/or culvert used.
- Buckling and wrinkling and/or other landslide induced pipeline anomalies are not detected.

This technique was mainly used prior to the evolution of smart pigging. Based on its disadvantages, the authors do not recommend using this method as other modern techniques are available that can provide more information on pipeline deformations with significantly fewer disadvantages.

8.3.2.3.3 *Ground Based LiDAR (a.k.a. Terrestrial LiDAR Scanning)*

Ground Based LiDAR (GBL), also known as Terrestrial LiDAR Scanning, is a well-established mature technology that is more commonly used as part of hazard management programs in the mining, highway, or public sectors to monitor high consequence slopes, areas of erosion, and faults. It is generally applicable to situations where conventional surveying techniques (discussed in the previous section) are applicable. An example of a typical GBL study is detailed by Collins et al. [248]. The technology is commonly used in the pipeline industry to map complex piping arrays within gas processing plants, stations, and other facilities. The basic technology is identical to the airborne LiDAR discussed in Section 8.3.2.4.2 of this Chapter, but the instrument is positioned near the ground on a tripod, or above the ground on a raised platform either at a fixed position or on a mobile device. In other non-pipeline related activities, the instrument can actually be hung from a structure and does not necessarily have to be mounted either level or upright.

The development of GBL is an evolution of the total stations which surveyors have been using since the 1980s. Total stations use precisely measured horizontal and vertical angles, and distances measured by laser to calculate the x, y, z of a retro-reflective target, relative to the instrument. If real-world coordinates of two or more points are already known, then all other points measured from that instrument setup can also be adjusted to match that larger coordinate system. When all survey points within the line of sight of an instrument setup are measured, it becomes necessary to move to another location. The surveyor will set control points which are visible from the next setup, and then measure to them again from that new location. Since these control points already have known coordinates from the previous setup, the next setup is tied in to the prior setup. The process repeats – setting control from a known setup point, and then using that control to define the location of the next setup. For larger scale projects the surveyor will measure to as many control points as possible from each setup, building a network of measurements from various locations to improve the quality of the work.

GBL is essentially an extension of the same process. The difference is that the laser fires continuously while the instrument moves through its scanning range (see below) collecting a cloud of millions or billions of points within the scan range of the instrument. Modern scanners

can also collect high resolution photographs which are used to assign color values to each of the points in the cloud. The cloud resolution depends on the radial distance of the surface from the scanner. The closer the surface, the higher the resolution. As an example, at 330 ft (100 m) from a typical scanner, one point is collected every 1/2 in (12 mm), both vertically and horizontally. Near the instrument, cloud point density can be greater than 1 point per mm². The actual resolution of the scanner can be adjusted by the operator to suit the specific data requirements of a project. For example, a pipe farm scan would be conducted at a denser resolution than a standard road topographic survey. Higher resolution equals more time in the field and more time in the office due to the amount of data, and consequently, higher cost. Contractors leverage scan resolution, scan quality (cleanliness of data), and time to complete a job based on the desired level of detail.

Three types of surveying scanning systems are employed in GBL:

1. Panoramic scanners that rotate 360° around the mounting axis, and scan 180° vertically to provide seamless and total coverage of the surroundings.
2. Single axis scanners that rotate 360° but are limited to a 50° to 60° vertical swath.
3. Camera scanners that point in a fixed direction with limited horizontal and vertical range.

GBL scanners are also be classified per operational range:

- Short range systems that operate at ranges of up to 10 ft to 330 ft (3 to 100 m) with panoramic scanning achieving millimeter accuracies. Often used to map building interiors or small objects.
- Medium range systems that operate at ranges of 450 to 860 ft (150 to 270 m) achieving millimeter accuracies in high definition surveying and 3D modeling applications include landslide, fault, and dam monitoring.
- Long range systems can measure at distances of up to 3.8 miles (6 km). These systems are commonly used in open-pit mining, landslide monitoring, and topographic survey applications.

As noted above, in conventional surveying, the only points which are common across multiple instrument setups are the control points specifically set for that purpose. In scanning operations, millions of measurements are collected from several overlapping setups and inevitably many of them are common points. The software used to process the point cloud data for outdoor applications often uses targets set up on control points in the same way as a conventional survey. Alternatively, it can locate these many common cloud points automatically and use that to connect all the scan data together; a process called registration (although this process is typically reserved for indoor applications). Correct survey set up is critical to avoid or minimize “shadows” on complex surfaces where sections may be not in the line of sight of the laser. The angle of the scanner to the surface will determine if shadows will be present. Numerous closer short range setups are preferable to less widely spaced long range setups for high precision surveys.

When setting up a scanning program a minimum of 3 targets set up over control points are recommended within the scanning survey to tie into a known coordinate system. These points should be established on stable ground outside of the area of instability or settlement/subsidence.

During successive surveys, these control points should be used to allow for accurate comparison of survey results. A minimum of 4 intermediate targets should be scanned during each scanning session with overlap between sessions to allow the sessions to be stitched together. The targets should remain stationary during the duration of the overlapping scans. In successive surveys, the position of the intermediate targets can be varied without affecting the accuracy of the survey.

Data can be processed to remove vegetation to produce a bare earth model provided the vegetation is not dense enough to completely obscure the ground. The position of the scanner may be adjusted to optimize the returns from the ground surface, but typically, the technique works much better in areas with minimal or sparse vegetation.

When the point cloud processing is complete there are several options for working with it. Most CAD software can display the point cloud and allow the user to pan and rotate their viewpoint within it. The current version of AutoCAD can recognize geometry within a point cloud, including planar faces, edges, corners, and curved faces. This allows the user to draw design geometry directly on the cloud. Other software packages including RoadEng and Civil3d can use point cloud data to build ground surface models.

Successive GBL surveys can be compared to note any changes which may indicate ground deformations or movements. A few examples are noted below:

1. Continuous scanning:
 - a. A mine pit wall is continuously scanned in a potentially unstable area. The wall is scanned and a surface model computed. Successive scans compare the current surface model with the initial model to alert the mine of impending instabilities.
 - b. Points on a large dormant rock slide above a fjord (where the rock slide has the potential to cause a tsunami) are monitored to warn vulnerable residents of a potential event.
2. Periodic scans: A highway rock slope is monitored annually to determine if a rock mass is actively toppling. The topples could potentially deliver rock to the road running surface.

Pipeline related applications are discussed below:

1. Landslide monitoring of buried pipelines: This is typically applicable over smaller areas (as with conventional surveying) or where there is significant visibility such as steeper more uniform slopes. The expense increases proportionally with area, with airborne LiDAR eventually becoming more economic, but less accurate than GBL. Generally, it is used for small landslides or for critical portions of larger landslides where the slope can be mapped with less than 10 scanner setups. Figure 8-59 shows a GBL scanner setup at the top of a blasted rock slope that is a source of rock fall onto a pipeline ROW and additionally, has a potential deep seated translational slide forming within the rock mass. Figure 8-60 shows a surface model based on the point cloud produced by the survey of the slope. Figure 8-61 shows a target positioned over a point with a close-up of a target

on nearly bare ground. Figure 8-62 shows an example of GBL being used to detect the emerging features of a landslide within a pipeline ROW.



Figure 8-59 Looking north from top of a pipeline ROW slope where a blasted rock slope is a source of rock falls onto the ROW and a deeper translational slide is forming. Device is a mid-range panoramic scanner. (Photo by: S. Boon, Year: May 2015)

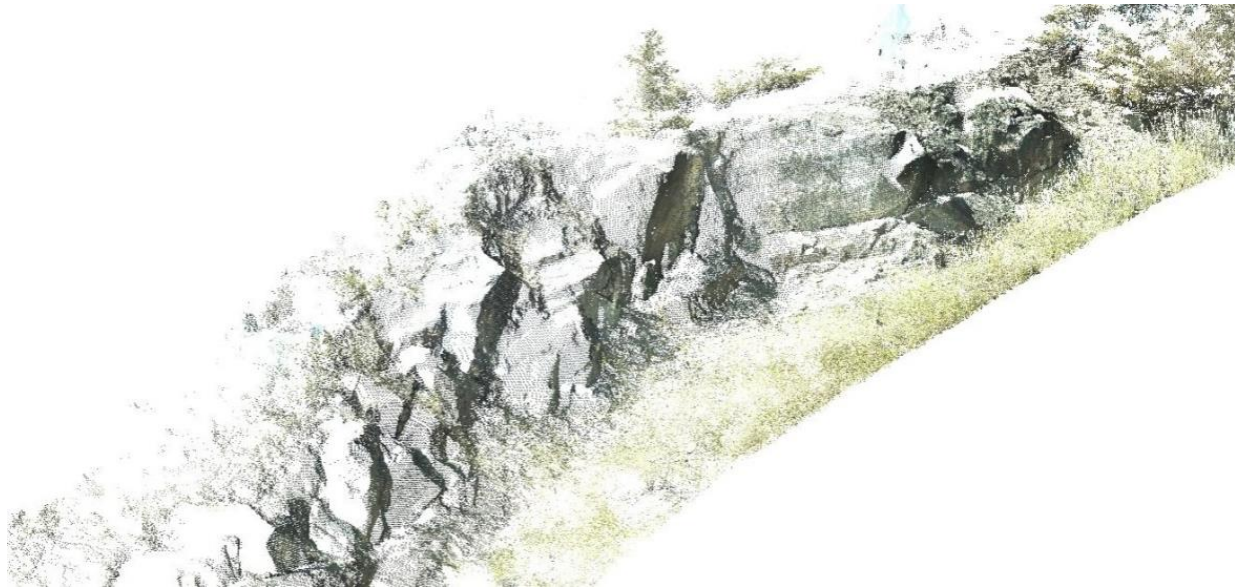


Figure 8-60 Surface model of the rock slope in the previous figure based on the point cloud produced by the survey of the slope (Photo by: S. Boon, Year: May 2015)



Figure 8-61 Scanned target on a control point at top of rock slope with inset showing a typical scanning target (Photo by: S. Boon, Year: May 2015)

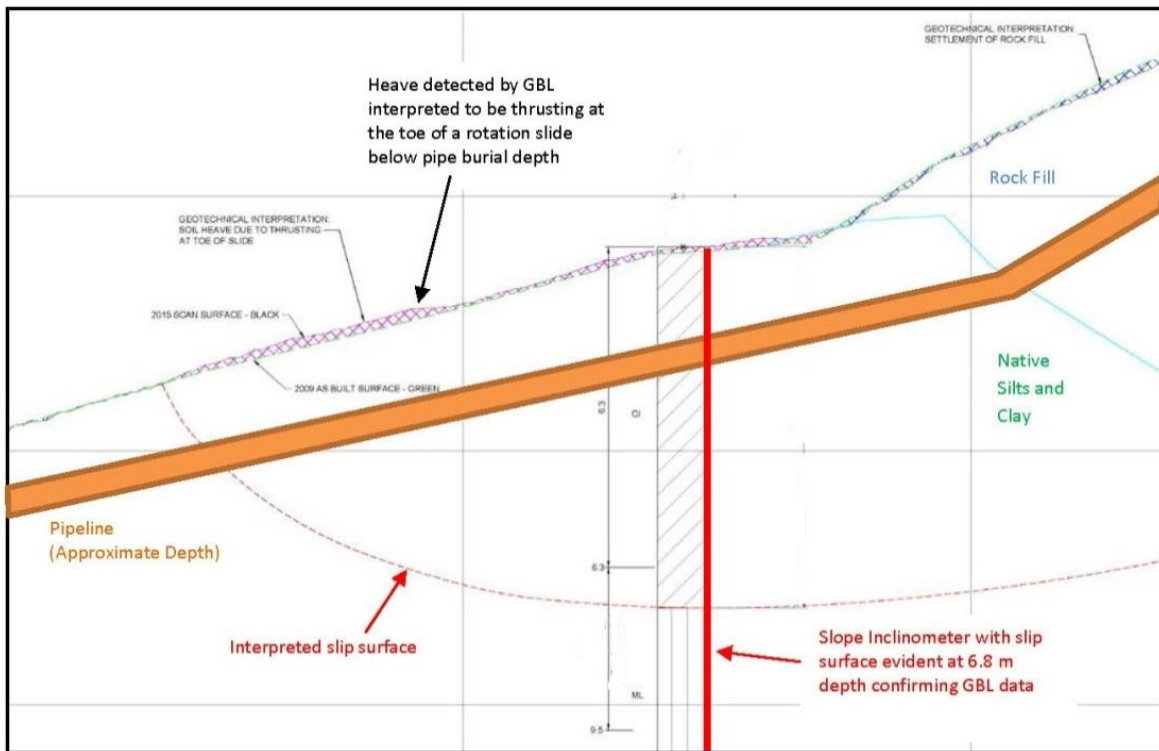


Figure 8-62 Results of GBL survey superimposed on original conventional survey showing a shallow slide developing below pipeline burial depth. Note that GBL data allows for a better estimation of the slide slip surfaces based on continuous surficial data rather than linking of discrete survey points in a conventional survey. (By: D. Dewar, Year: 2015)

2. **Settlement/Subsidence Monitoring:** Although numerous setups would be required to reduce errors associated with low angle shots, the scanners can be used to monitor local settlement and/or subsidence.
3. **Fault Monitoring:** GBL can be used to monitor ground deformations where there are buried pipelines. Where surficial pipelines are present, GBL can be used to monitor deformations of above-ground piping.

GBL has the following advantages:

- The amount of data collected in one survey is significant, providing redundancy unlike conventional or GPS surveys where data quantity is relatively finite and survey errors are more likely to create false positives. Generally, you are sampling the entire ground surface rather than just a small statistically insignificant portion of the ground surface.
- Surveys are typically extremely detailed and can provide a detailed digital elevation model.

- The actual time to conduct surveys may be quicker depending on the data density required.
- The survey can be tied to a real-world coordinate system.
- The survey may be safer as personnel do not have to enter high hazard areas.

GBL has the following disadvantages:

- The scanner may not be able to be positioned in optimal locations to eliminate shadows based on slope steepness and other access issues. Although this is a disadvantage of most survey types, in a conventional survey a rod can be placed in a hole or behind an object.
- The accuracy of the technology in wet conditions. Rain, fog and wet surfaces can create major problems. However, most modern data processing can clean out any noisy data due to atmospheric effects.
- The scanners typically cost between \$100,000 and \$200,000; therefore, they are not common off the shelf items that local surveyors have access to. Larger survey firms or government institutions that may be remote to the site of interest would be required to conduct the surveys. Equipment availability may also be an issue. As with most new technologies, over time its availability tends to increase and its costs tend to go down.

The actual labor costs of a GBL are similar to those of conventional and GPS surveys, less the cost of renting the scanner which could be in the range of \$2,000 a day.

8.3.2.4 Aerial/Satellite Based Surface Monitoring

8.3.2.4.1 *InSAR*

InSAR stands for **I**nterferometric **S**ynthetic **A**perture **R**adar. Ground monitoring using InSAR can map and monitor changes in the ground surface over large areas, without the need to physically access a site. The technology has been used to determine areas and magnitudes of settlement and subsidence and characterize and monitor landslides that have favorable orientations relative to the satellite's path. The technology is currently used primarily by government agencies and research institutions to prove its application. Note that aircraft and terrestrial based InSAR are not discussed as part of this document. While these technologies exist, their use is not as widespread as aerial or ground based LiDAR as discussed in sections 8.3.2.4.2 and 8.3.2.3.3.

Detailed discussions of the technology are included in the PRCI documents [7]. Additionally, Power et al. [249], provides a detailed summary of InSAR applications for highway transportation projects. Henschel et al. [250] provides a summary of pipeline related uses for InSAR technology.

It is understood from discussions with the authors of the PRCI InSAR papers that a state of the art paper is currently not available for InSAR technology but the main changes are:

1. The increase in the amount of InSAR imagery available and the reduction in its cost, and

2. The required size of radar reflectors/corner reflectors that help mitigate temporal decorrelation errors (see below).

A summary of the technology is provided below.

Principle

Synthetic aperture radar is a form of side looking radar mounted to a satellite that directs microwave radiation at an angle toward the ground, perpendicular to the direction of travel (refer to Figure 8-63). Because the antenna is moving relative to the ground it can achieve much higher spatial resolution than would normally be possible with a small antenna (synthetic aperture). Using interferometry to compare the phase of the returned signal enables resolution to be significantly smaller than the wavelength used; millimeter-scale accuracy is possible with higher frequency bands and centimeter-level accuracy can be achieved with the longer wavelengths bands that are required to penetrate vegetation. A digital elevation model (DEM) is derived from the interferogram. Sets of data taken in one pass are referred to as scenes. Data are typically purchased by either:

1. Scene: Areas of coverage typically ranging from 5×5 miles (7×7 km) to 50×50 miles (70×70 km), or by
2. Area: Typically, by square kilometer with a premium rate for smaller areas.

Charges for imagery vary significantly based on the quality of the imagery and the satellite service provider. Additionally, many satellite imagery providers offer custom services allowing tasking a satellite to collect custom data. Over time, the price of imagery is trending down. Additionally, there are now many sources for free imagery available but these tend to be in more populated areas. In some cases, InSAR service providers may already possess the required imagery.

By comparing DEMs from a reference and subsequent passes of the satellite, changes in the ground can be measured as shown in Figure 8-64. The type of ground cover affects the phase of the returned signal. Therefore, polarimetric analysis of the data can indicate changes in ground cover or infer changes in ground use.

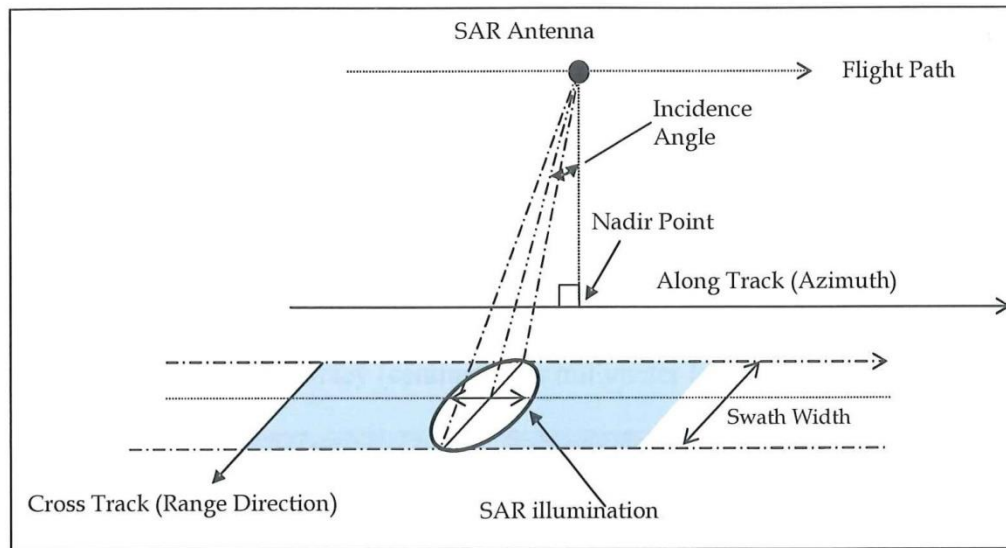


Figure 8-63 Geometry of InSAR [7]

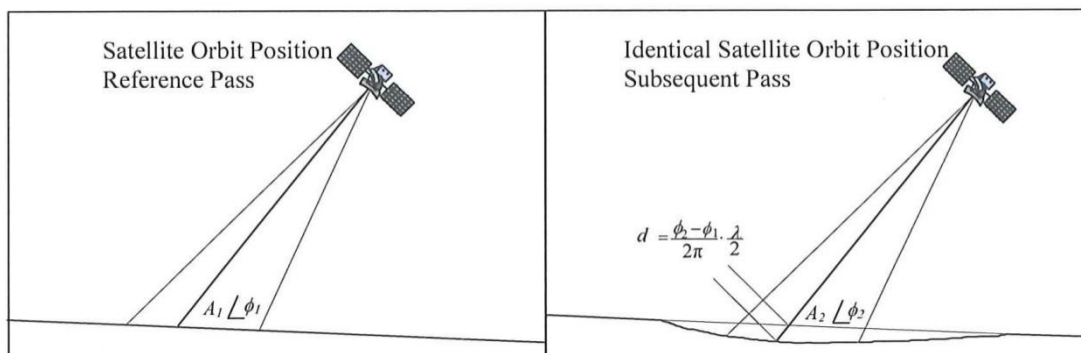


Figure 8-64 InSAR measurement of ground subsidence [7]

Three major sources of error are noted in reference [107]:

1. **Temporal Decorrelation:** If the moisture content and/or height of vegetation changes between readings, this change could be detected as ground movement. It can vary widely from region to region with arid regions having less variation. Thus, InSAR may be more suited to rocky or arid locations than to heavily vegetated areas, or to very slow movement that can be adequately monitored on an annual basis so that seasonal variation can be minimized. This is typically mitigated using phase stable features such as buildings, rock or gravel outcrops, or radar reflectors as shown in Figure 8-65 or by advanced data processing of multiple scenes to isolate the effects of temporal decorrelation.
2. **Baseline Decorrelation:** Changes in the position of the viewing satellite. This can be also mitigated using radar reflectors.
3. **Atmospheric Effects:** Changes in the troposphere and ionosphere that can be edited out by analyzing large amounts of data to isolate atmospheric effects.

Monitoring Settlement/Subsidence

The technology has provided reliable results for monitoring large scale subsidence that has resulted in pipeline failures at the Belridge Oil Field in California since 2001, as reported in Youden et al. [251], and later updated in Henschel et al. [252]. In this case, surface monitoring capability was augmented by installing radar/corner reflectors (approximately 1 m orthogonal metal structures on concrete bases). Results of the InSAR monitoring correlated closely with GPS monitoring results. After 12 years of monitoring, the work reported maximum overall settlements of 13 ft (3.92 m) with a maximum annual rate of settlement of 2.6 ft/yr (0.8 m/yr). The reported accuracy of InSAR was shown “to be precise to better than one millimeter using currently available space borne SAR sensors” and “the accuracy of InSAR can be demonstrated to within 4 mm in 180 mm of ground deformation with a single satellite system” [252].



Figure 8-65 InSAR radar reflectors [7]. Note that the technology has developed to the point that over time these radar reflectors are becoming smaller and therefore more economical to install.

An InSAR provider (MDA) is currently collecting data over a longwall mine subsidence area in Pennsylvania for an industry consortium project, in part to evaluate its suitability in vegetated terrain and without corner reflectors.

Monitoring Landslides

InSAR may be able to effectively resolve surface movement along the line of sight from the satellite to the area being examined. By comparing readings taken at different angles or in different directions, this movement can be resolved into vertical and horizontal components.

When scanning slopes, the following factors could impact the quality of InSAR data:

1. **SAR Look Direction**: SAR is not sensitive to movement parallel with the platform’s movement (north-south for a polar-orbiting satellite) or to movement normal to the line of sight. As an example, a polar satellite would be able to monitor landslides with east-west movements. If the slope is facing the satellite and is approximately perpendicular to the incident beam, movement will be normal to the line of sight and thus, may not be

detected. Canada's RADARSAT satellite has an incidence angle of 36° to 48° from vertical in high resolution mode and the European satellites are fixed at about 23°.

2. SAR Layover: On steeper slopes the upper section of the slope would be closer to the sensor; therefore, it appears to be laid over the lower section.
3. SAR Shadow: Slopes that are steeper than the radar incidence angle will be shadowed when looking downslope.

Vendors will review the slope alignment, slope grade (shallower is better), and slope vegetative cover to determine the feasibility of a potential InSAR study. Additionally, a vendor would assess any previous or background information along with SAR data availability. Generally, based on these limitations, less than half of potential landslide sites may be suitable for InSAR monitoring.

Overview on Monitoring

InSAR depends on comparing repeated measurements, so it is best for monitoring changes which occur on a timescale longer than the period of repetition of the measurements. For satellite monitoring, minimum repeat periods are on the order of weeks. Numerous passes are recommended for interpretation to reduce the potential for errors and to better assess trends in the data. Older "two pass" studies are not recommended with the amount of potentially available data collected by modern satellites.

Technology Status

InSAR has been in use for well over a decade. Vendors continue to refine the data analysis process. Use is mainly at an institutional/government level with large research type projects. The technology is therefore considered medium maturity. It is commercially available with multiple vendors. Accuracy and repeatability of data are high within the technique's limitations and it is generally more likely to be suitable for detection of settlement or subsidence and certain landslides moving in a favorable orientation relative to the path of the satellite(s).

Advantages:

- Data have been collected since the early 1990s; therefore, there may be an opportunity to look back into the past, albeit, in many cases with lower resolution data.
- Data may be abundant for specific sites and are available for any region of the earth.
- Monitoring can be done remotely.
- Can provide sub centimeter to sub millimeter accuracy.
- For large landslides or areas of settlement/subsidence, InSAR has the advantage of providing a scan of the entire area rather than discreet points as with conventional and/or GPS surveys. This may allow for the delineation of areas of differential movements and boundaries as well as of areas within geohazards, see Figure 8-66.

Disadvantages:

- Numerous sources of error or limitations resulting from the following factors:
 - Areas with vegetative cover may be unsuitable for monitoring.

- Large amounts of data may have to be processed to filter out errors.
- Unsuitable incident angle of satellite.
- Slope position relative to the satellite (works better for settlement or subsidence on flatter ground in most scenarios).
- Where radar reflectors are required there may be landowner or other third party issues.
- Potentially long lead times to collect/interpret data.
- Potential false positives due to data interpretation errors which still comes down to human interpretation of data.
- Cost: It is difficult to provide a cost for the work, but it is relatively expensive limiting its common use to government/institutional research agencies with corporate sponsorships. The cost component of any InSAR project would typically be divided into three components:
 - Initial review of project and assessment of existing satellite data to determine project suitability.
 - Installation of radar reflectors where required. Installation costs vary, with the main component being accessing the site. Radar reflectors at the time of publication cost approximately \$2,000 each.
 - Purchase of satellite data.
 - Data interpretation and final reporting.

As an example, a translational landslide study (as shown in the section 8.3.2.3.1), analyzing select imagery over a five-year period could have a total cost between \$50,000 and \$150,000 based on the amount of imagery analyzed, assuming that the vendor has to purchase the imagery. In another example, a monitoring report for the surficial settlements of an approximately 10 km long linear corridor costs approximately \$10,000. The cost is significantly less than the first example given that the imagery used for the project was free.

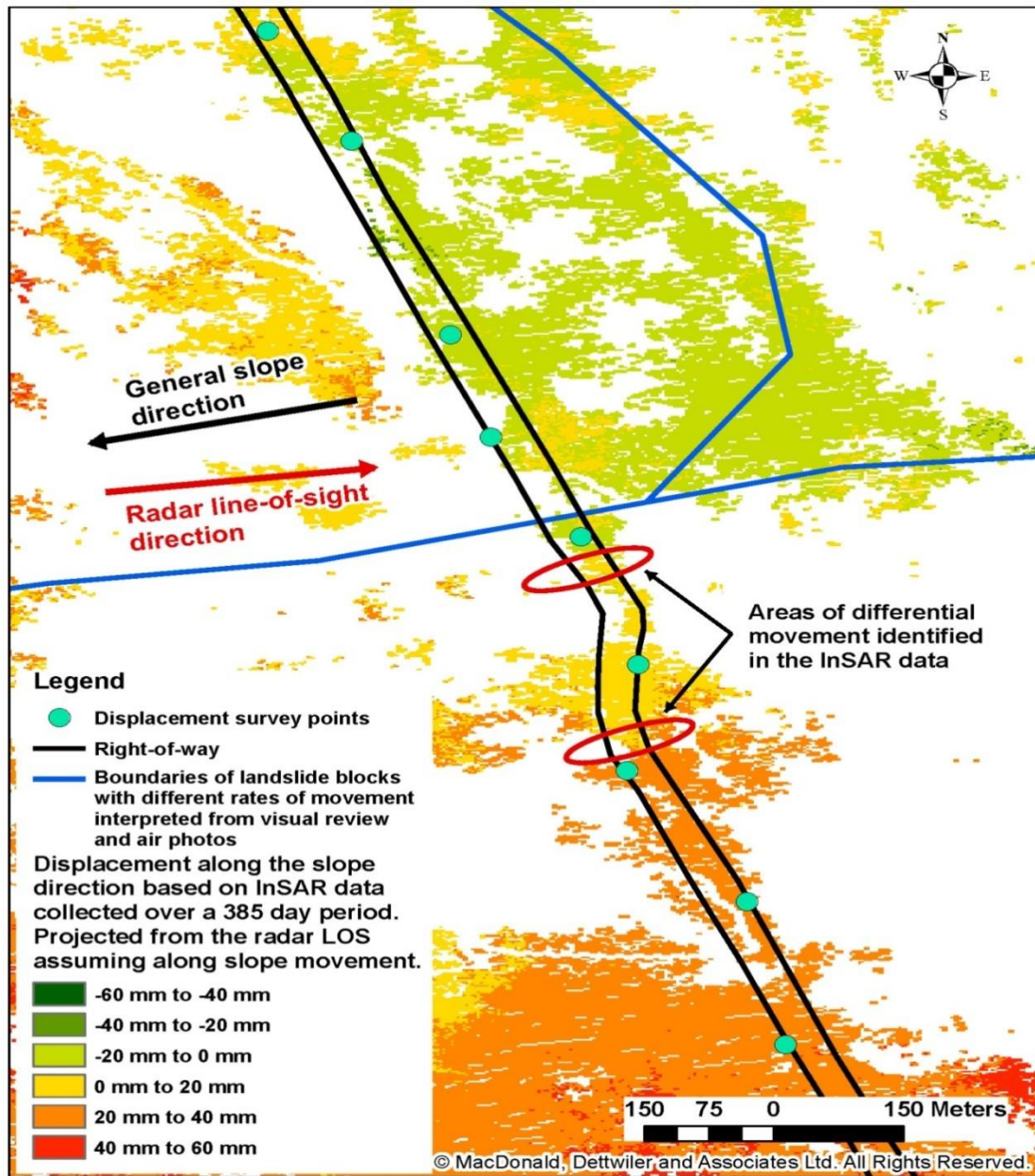


Figure 8-66 Example of an InSAR deformation plot showing data coverage within a cleared ROW and surrounding forested terrain within a large deep seated landslide. GPS survey points and slope inclinometer installations show the coverage of typical ground based geotechnical methods. Areas of differential deformation are clearly identified by InSAR deformation plots. Image provided by MDA.

8.3.2.4.2 *Airborne LiDAR*

General Overview

LiDAR is an acronym for “Light Detection and Ranging.” LiDAR is an active laser system, which measures the time of flight of the emitted signal returned from a target. There are different types of LiDAR: atmospheric, terrestrial, and airborne LiDAR systems [253, 254, 255, 256]. Airborne LiDAR systems can be categorized into bathymetric or topographic systems. Bathymetric systems are used to measure water depth in the near-shore environment, using multiple lasers. Airborne topographic LiDAR systems provide a 3-dimensional point cloud data for a target area of interest (e.g., landslide or subsidence area). LiDAR also provides intensity data where the intensity of each point depends on the strength of the returned signal.

Airborne topographic LiDAR systems are what are often used to detect, characterize, and monitor landslide and subsidence hazards. Mounted on either a helicopter or a fixed-wing aircraft, topographic LiDAR systems use the near-infrared portion of the electro-magnetic spectrum to collect data, night or day, in shadow, and beneath clouds. Using semi-automated techniques, the LiDAR data are processed to generate a number of useful end products, including imagery (such as hillshades) and high-resolution topographic mapping in which trees, vegetation, and manmade structures have been edited out, leaving an approximation of the ground surface. These images and maps are typically referred to as “bare earth” because they produce a representation of the ground surface absent the vegetation cover which normally obscures the ground. These bare earth images and topographic maps are used for detecting, evaluating, and monitoring landslide and subsidence hazards.

LiDAR systems vary by manufacturer, but all use the following instrumentation:

1. A laser source and detector,
2. A scanning mechanism and controller,
3. Airborne GPS (global positioning system) and IMU (inertial measurement unit) equipment,
4. A high-accuracy, high-resolution clock for timing laser emissions and returns, GPS/IMU, and scan-angle measurements,
5. High performance computers, and
6. High capacity data recorders.

With these components, LiDAR data collection is possible as follows (Figure 8-67):

- A pulse of laser light is emitted and the precise time is recorded,
- The reflections of that pulse from the surface are detected and the precise times are recorded,
- Using the constant speed of light, the time difference between the emission and the reflections can be converted into a slant range distance (line-of-sight distance), and
- With the very accurate position and orientation of the sensor provided by the airborne GPS and IMU data, the x, y, and z coordinates of the reflective surfaces can be calculated.

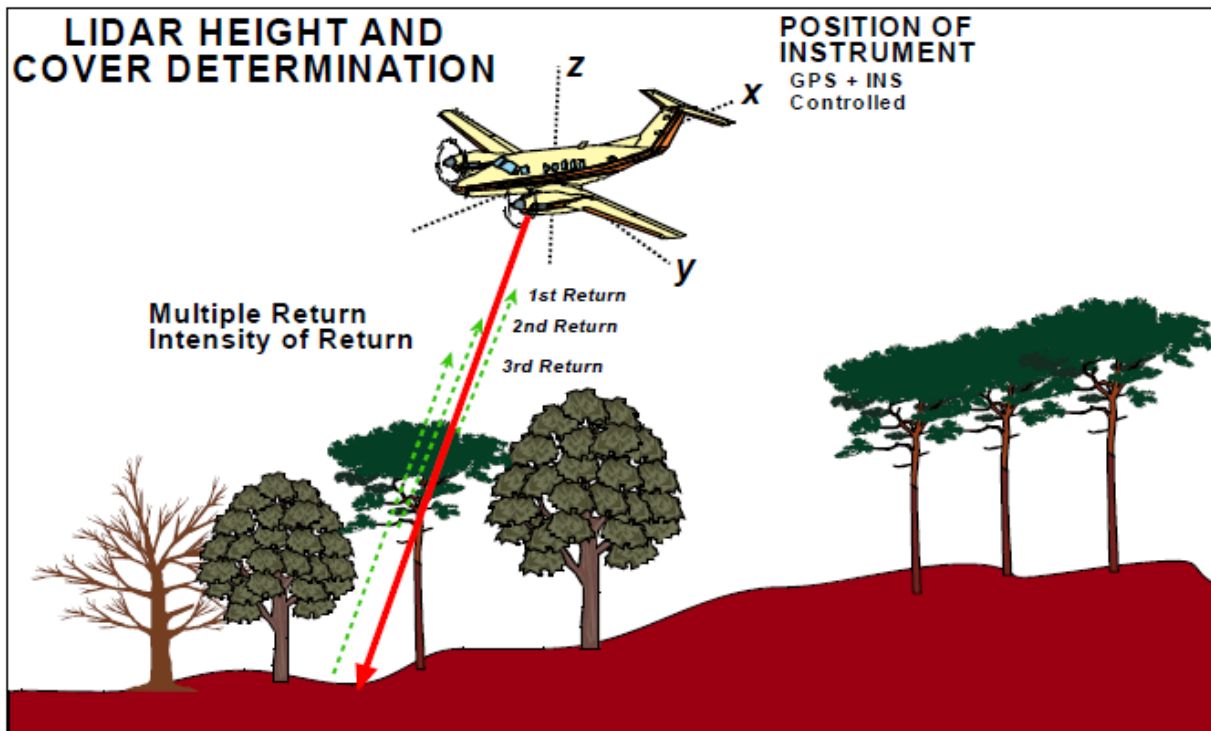


Figure 8-67 Airborne LiDAR data collection schematic [257]

Multiple returns from LiDAR pulses can detect elevations of several objects within the laser footprint of an outgoing laser pulse. The intermediate returns, in general, are used for vegetation structure, and the last return for bare earth terrain models (Figure 8-68). The last return may not always be from a ground return. For example, consider a case where a laser pulse hits a thick branch on its way to the ground and the pulse does not actually reach the ground. In this case, the last return is not from the ground but from the branch that reflected the entire laser pulse.

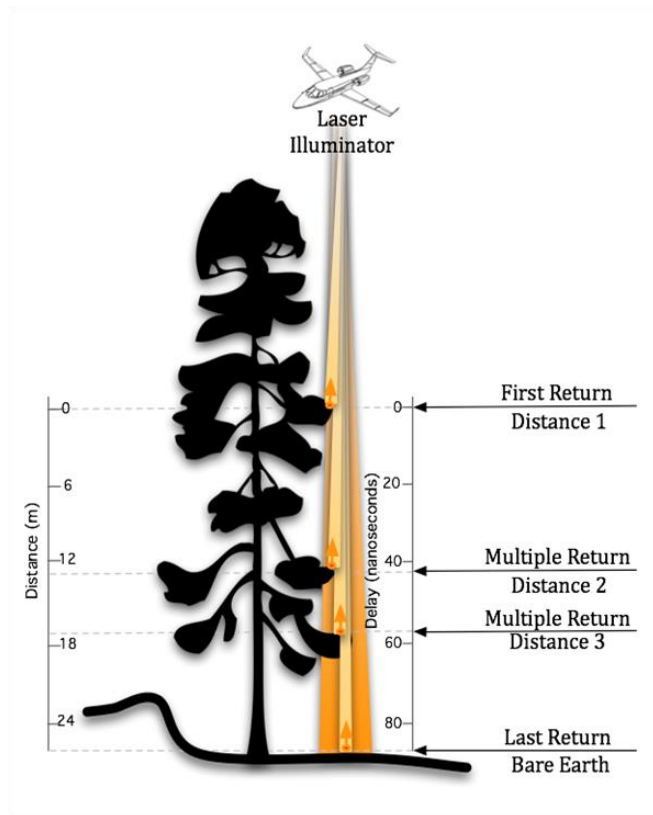


Figure 8-68 Multiple returns from for a LiDAR laser pulse [258]

Additional information is stored along with every x, y, and z positional value for the returned laser data point. These LiDAR laser point attributes are listed and described in Table 8-9.

Table 8-9 LiDAR data attributes, modified from [259]

LiDAR Attribute	Description
Intensity	The return strength of the laser pulse that generated the LiDAR point.
Return number	The return number recorded by the LiDAR instrument. The number of returns recorded is determined by the purpose of the project. In areas where there are many potential sources of returns, such as densely vegetated areas, not all returns are recorded (in most instances) because it causes problems with analysis and data storage. As an example, if the purpose of the project is to produce bare earth mapping, the LiDAR instrument might record the first return, second return, third return, and last return. Any returns that occurred between the third return and last return would not be recorded in this example.
Number of returns	The number of returns is the total number of returns for a given laser pulse. For example, a laser data point may be return two (return number) within a total number of five returns.
Point classification	Every LiDAR data point that is post-processed can have a classification that defines the type of object that has reflected the laser pulse. LiDAR points can be classified into several categories including bare earth or ground, top of canopy, and water. The different classes are defined using numeric integer codes in the LAS files.
Edge of flight line	The points will be symbolized based on a value of 0 or 1. Points flagged at the edge of the flight line will be given a value of 1; all other points will be given a value of 0.
RGB	LiDAR data can be attributed with RGB (red, green, and blue) bands. This attribution often comes from imagery collected at the same time as the LiDAR survey.
GPS time	The GPS time stamp at which the laser point was emitted from the aircraft. The time is in GPS seconds of the week.
Scan angle	The scan angle is a value in degrees between -90 and +90. At 0 degrees, the laser pulse is directly below the aircraft at nadir. At -90 degrees, the laser pulse is to the left side of the aircraft, while at +90, the laser pulse is to the right side of the aircraft in the direction of flight. Most LiDAR systems have currently less than a ± 30 degrees scan angle.
Scan direction	The scan direction is the direction the laser scanning mirror was traveling at the time of the output laser pulse. A value of 1 is a positive scan direction, and a value of 0 is a negative scan direction. A positive value indicates the scanner is moving from the left side to the right side of the in-track flight direction, and a negative value is the opposite.

Airborne topographic LiDAR offers many advantages over traditional photogrammetric methods for collecting positional, elevation data. These include high vertical accuracy, fast data collection and processing, robust data sets with many possible products, and the ability to collect data in a wide range of conditions. These advantages allow LiDAR to be very useful for detecting and monitoring ground movement from landslide and subsidence hazards. Figure 8-69 is an example of how bare earth LiDAR DEM is used to produce “hillshade” or shaded relief image of the ground surface which accentuates subtle topographic surface features such as in this case, landslide features across and adjacent to a pipeline. In this case, the “hillshade” is produced using a 315° azimuth illumination angle (i.e., the light is from the northwest).

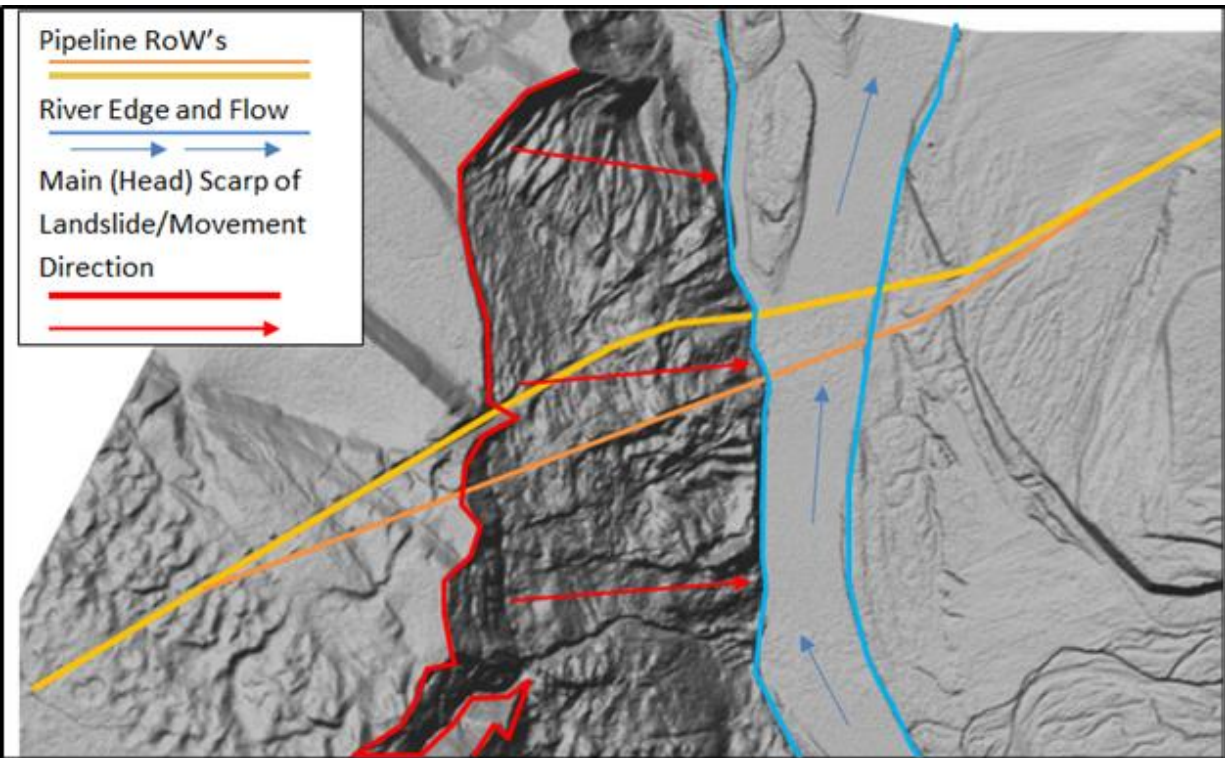


Figure 8-69 Example of a LiDAR DEM “hillshade” as the base for mapping of landslides crossed by pipelines in a river valley. The landslide is a deep seated translational slide moving from left to right in the center of the image. The river channel is constricted at the toe of the landslide.

Technical Overview

LiDAR missions are tailored to meet individual project specifications, based on the intended data use; such as for landslide and subsidence monitoring. Important LiDAR data collection parameters include:

- Point spacing and point density: Point spacing is also referred to as “average” or “nominal” post spacing. Post spacing is a one-dimensional measurement of the distance between neighboring points. Point density refers to the number of points in a unit area. The greater the number of points, the denser the dataset. Experience with LiDAR data

collection indicates that for landslide and subsidence monitoring, point densities of about 10 points/m² for leaf off conditions are recommended, while for leaf on conditions, the point density is recommended to be at least 20 points/m². These point densities allow for the data quality and resolution needed for reliably detecting, characterizing, and monitoring landslide and subsidence hazards in vegetated and sloping terrain.

- Pulse rate: The pulse rate is the frequency by which the LiDAR sensor emits laser pulses. Higher pulse rates are associated with denser data sets. The chosen pulse rate for a specific mission will impact the maximum operational altitude (higher pulse rates require lower altitudes).
- Field of view: The field of view (FOV) refers to a sensor's scan angle. The FOV can be fixed or variable. For high relief areas (mountainous regions) a narrow FOV is preferable to minimize LiDAR shadowing.
- Aircraft altitude: The altitude (and speed) of the aircraft during LiDAR missions depends on the desired point spacing/point density, pulse rate, and field of view. Typically, missions flown at high altitudes and fast speeds produce less dense datasets. Terrain features, aircraft safety, and air traffic control regulations must also be considered when choosing an altitude for a project.
- Survey control: Ground survey control is needed to calibrate the LiDAR data to an absolute datum.
- Coordinate system and datum: Selection of the coordinate system to be used (e.g., UTM, state plane, etc.) and horizontal and vertical datums is needed prior to undertaking the LiDAR survey.

Landslide and Subsidence Monitoring

For periodic monitoring of identified landslide and subsidence hazards along pipelines, periodic, repeated high quality and high resolution LiDAR data collection is undertaken of the areas of interest. The bare earth DEM models, i.e., the topographic surfaces from successive LiDAR surveys are compared to each other to identify areas where there are differences in the elevations and the shapes of the landslide and subsidence boundaries compared to the original hazard mapping, such as the landslides of Figure 8-69. The differences between and among the various surveys can help identify and quantify where and how much the hazard has moved from the previous LiDAR survey(s). Because of the high quality and high resolution of the DEM data, elevation changes of less than 1 m (< 3 ft) can be identified from successive LiDAR surveys.

Summary of LiDAR Technology Attributes

The use and attributes of LiDAR technology in the potential monitoring of landslide and subsidence movement are summarized in Table 8-10.

Table 8-10 Airborne LiDAR technology attributes [260, 261, 262, 263, 264]

Attribute	Description
Maturity of the Technology	Airborne LiDAR technology although relatively young, has been used extensively over the past decade in geologic hazard applications for pipelines and numerous other earth science applications. Thus, the use of LiDAR for hazard detection and characterization is mature. However, its use for landslide and subsidence monitoring is relatively young.
Commercial Availability and Cost	Airborne LiDAR technology is readily available from several vendors in North America. However, not all vendors are equal in their understanding of the need for high quality and high resolution LiDAR data for geologic hazard applications. Hence, there is a need for good data acquisition specifications and selection of experienced vendors. The cost varies by vendor, project purpose, and location, but in general, the larger the analysis area, the lower the per acre or per mile cost. Recent experience (in the 2015/2016 timeframe) of one of the authors indicates that for high-resolution LiDAR (point density of 15 points/m ² or greater), conducted for a 1,000-foot-wide swath centered on a pipeline, cost ranging from about \$250/mile to over \$1,000/mile (about \$1.5/acre to over \$6/acre) can be expected, depending on the size of the area being mapped. These cost ranges should be considered to be approximations and are based on experiences in generally non-mountainous areas in the contiguous United States.
Delivery Time	When commissioning LiDAR mapping, the time from initiation of the work to delivery of the results should be factored into project planning. Based on the experience of the authors, a typical timeline will range from about one to four months, depending on the size of the area being surveyed and the weather conditions. LiDAR cannot penetrate snow cover or fog, and poor weather conditions such as high winds or thunderstorms can prevent the acquisition aircraft from flying. A general rule of thumb is that, if possible, the LiDAR data acquisition should be initiated about three to four months prior to when the data is needed to allow for weather related delays.
Accuracy/Precision	With high quality and high resolution LiDAR data for landslide and subsidence hazard applications, x, y and z accuracies of less than 1 m (< 3 ft) can be routinely achieved. Vertical accuracy may be as high as 10 cm (~4 in) under ideal conditions.
Repeatability	High, if reliable vendors are engaged and specifications are well written and constrained to achieve high quality data.
Reliability	High, if reliable vendors are engaged and specifications are well written and constrained to achieve high quality data.

8.3.3 Pipe Monitoring

8.3.3.1 Use of IMU in Conjunction with Other ILI Tools

Typically, an IMU module is mounted on another smart pig platform. Therefore, IMU monitoring can occur during scheduled MFL, Caliper, EMAT or any other scheduled smart pig run. Generally, successive runs should be on the same platform with the same vendor using the same method of data interpretation. General industry experience shows that trying to compare IMU data from different vendors for run-to-run has not been successful. When reviewing the IMU data, other information collected on pipeline anomalies (i.e. buckles) should also be reviewed to either detect or monitor areas of intense pipeline deformation.

IMU data can provide the following information:

- Evidence of high strains, particularly at girth welds by conducting bending strain analysis, and
- Evidence of pipe movement from run-to-run analysis - comparing the positions of the pipeline from a baseline run to the current run to determine if there is any lateral deformation. Additionally, when there are multiple runs, the baseline run can be changed to provide incremental deformation data.

With the accuracy of modern tools, it is not yet possible to accurately monitor any changes in length between welds or groups of welds as a result of compression or tension. If tool accuracy/data processing techniques improve this may be a possibility in the future. The technique could possibly be useful for larger lateral instabilities with relatively uniform pipeline loading along the landslide length.

It is always recommended to have a bending strain analysis conducted on the initial IMU run and repeat the bending strain analysis and a run-to-run analysis on subsequent runs using the initial run as a baseline. Typically, vendors only do the bending strain analysis during the initial run, but geohazard induced straining typically increases over time and may become evident over successive monitoring runs. This differs from construction and/or maintenance induced bending strains that typically do not grow, or in the case of dig related settlements, that will reach a maximum limit. Compared to the cost of the actual smart pig run, the cost of analysis is typically not significant. As an example, a MFL run with an IMU module over a 60-mile (100-km) long section of pipeline may cost \$250,000. The bending strain analysis and run-to-run comparison of IMU data should cost on the order of \$20,000 to \$40,000. With any monitoring, it is always preferable to use the same vendor during the monitoring program.

Typically, vendors separate out bending strain and run-to-run (or Bending Strain Change) analysis into horizontal and vertical strain or displacement components. Vendors cannot determine the actual cause of the bending strains or pipeline movements as part of their analysis process. Typical causes of vertical bending strains/pipeline movement can include:

1. Settlement of backfill below the pipe invert following integrity digs/pipeline exposures,

2. Settlement caused by external loading such as road crossings or other fills,
3. Settlement or subsidence as discussed in Section 2,
4. Permafrost related soil deformations, and/or
5. Landslide movements as discussed in Section 2.

Typical causes of horizontal bending strains/pipeline movement include:

1. Thermal expansion during integrity digs/pipeline exposures,
2. Construction/maintenance related field bends, and
3. Landslide movements as discussed in Section 2.

Additionally, fault movements may cause pipeline movements. Generally, the operator and their internal/external geotechnical consultants would have to interpret the cause of the bending strain/pipeline movement indications using company maintenance records and information from their geohazard management program. Depending on the amount of indications, the operator may be able to review the data by brute force or may have to develop criteria based on local experience to screen data for potential sites for detailed review. Alternatively, the operator can review indications in areas of known landslides and/or settlement/subsidence and screen indications in other areas based on preset criteria.

As guidance, the following generally applies when interpreting bending strain and run-to-run movement analysis:

1. Most vertical indications are typically related to an operational feature, such as integrity digs or recoats. Typically, there is up to 3 ft (1m) of poorly compacted soil under the pipeline following a 360° integrity dig exposure. Settlements of up to 1 ft (0.3 m) could be expected at the center of the dig depending on exposure length, backfill properties, and pipeline stiffness.
2. Horizontal indications are more likely to result from landsliding or faulting, although during longer recoats where the ambient air temperature is higher than the operational temperature, the pipeline may expand and appear to have horizontal displacements. Single pipe joint digs do not typically show a significant horizontal component of movement or bending when compared to the vertical component.

The following case study illustrates the differences in horizontal and vertical strain/movement indications within areas of landslide movements across pipelines. The case study was performed for a section of pipeline located in a landslide prone region of the western Appalachians. For this section, a vendor performed an IMU base bending strain analysis. The vendor identified bending strain indications that were greater than one joint in length (i.e., 40 ft or longer) and not located at known field bends. The reporting threshold for bending strain locations ranged from 0.125% to 0.18%, depending on the pipe diameter and wall thickness.

Based on these criteria, 970 bending strain locations were identified. Approximately 10% of the bending strain locations (95) correlated with landslides mapped using the phased assessment process described in Section 2. The landslides were typically shallow (i.e., in most cases less

than 10 ft thick), slow moving (inferred to usually move a few inches per year), and were mostly a few hundred feet in length and width. The landslides were in clay rich residual soils derived from sedimentary bedrock on slopes with inclination ranging from 8° to 22° (15% to 40%). Figure 8-70 shows a plot of the separated horizontal and vertical strain components of bending strain indications versus the correlation with landslides in percentages. As shown in Figure 8-70, horizontal strain magnitude correlated well with landslide locations, while vertical strain magnitude had a poor correlation with landslides.

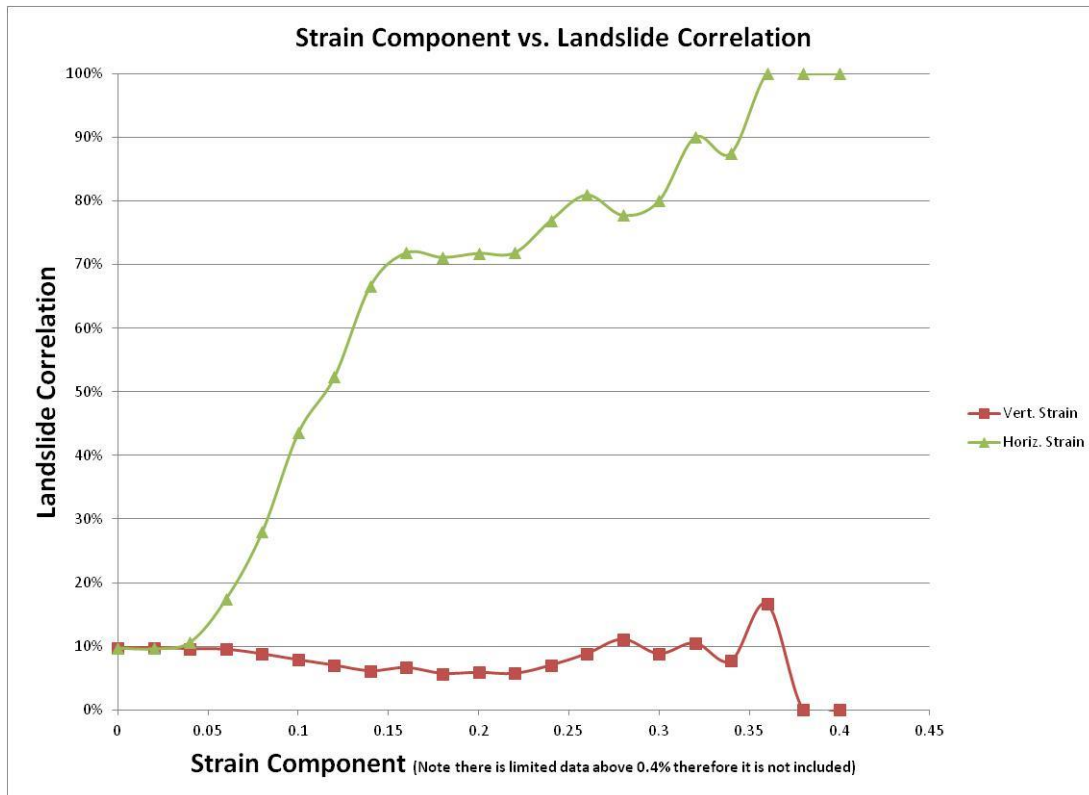


Figure 8-70 Plot of strain magnitude versus percent of strain indications that are within landslides

The results indicated that for these types of landslides:

1. If the horizontal strain component exceeded:
 - a. 0.36% then 100% of the indications were within landslide features.
 - b. 0.25% then 80% of the indications were within landslide features.
 - c. 0.12% then 50% of the indications were within landslide features.
2. Vertical strain component did not correlate well with landslides. The correlation of vertical strain with landslides stayed consistently at around 10% at strains as high as 0.34%.
3. As an additional point (not shown on Figure 8-70), when horizontal component of strain was less than 0.1%, only 4% of vertical bending strain locations correlated to landslides.

The case study illustrated that horizontal strain indications could be reliably used to screen for landslides impacting pipelines within the study area. These potential screening criteria would be important when interpreting large amount of IMU strain indications. It is not clear if the same relationships are applicable to other locations. Most likely, screening criteria would have to be developed based on local geologic and topographic conditions.

The vertical strain component may be critical when considering settlement and/or subsidence, or landslides which have movement types that would have significant vertical displacements. In these cases, screening criteria may have to be site specific. As an example, in areas of known sinkholes or deep seated complex landslide movements, bending strain or movement indications would be reviewed on a case by case basis.

In addition to bending strain and run-to-run monitoring of landslides, IMU data can be used to predict potential deformations of a pipeline by correlating the rate of movement of a landslide (or other ground monitoring information) to the rate of growth of a bend/feature within the pipeline. Figure 8-71 provides an example of projecting forward the rates of growth of a bend feature using historic IMU data.

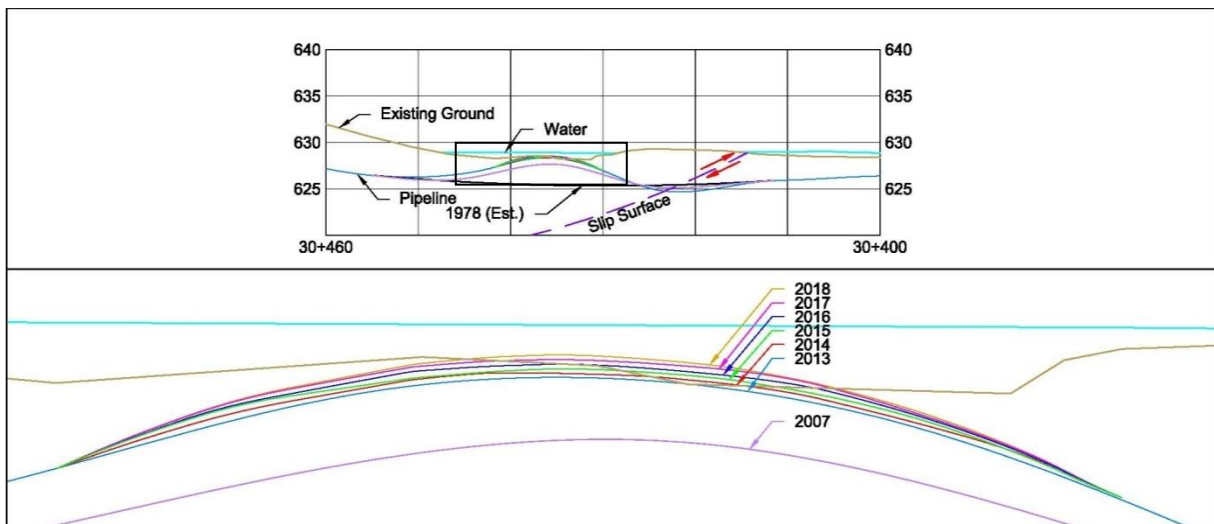


Figure 8-71 Projecting forward pipeline deformations based on historical IMU data in the toe area of a translational landslide. The bottom image is a close-up of the top image.

Where IMU data analysis results do not indicate movement but there are known landslide movements, particularly lateral movements across the pipe, the raw IMU results should be reviewed to determine if there are any larger features that the IMU analysis has not detected. It is recommended that as part of any smart pigging contract that operators request the raw IMU data so that it is available for 3rd party analysis.

Figure 8-72 below shows an example where a landslide-induced horizontal bend of 5 ft (1.6 m) over approximately 82 ft (25 m) was not detected during the vendor's initial analysis. The feature was readily identified following a meeting with the vendor to explain the results of an extensive geotechnical ground monitoring program within the general study area.

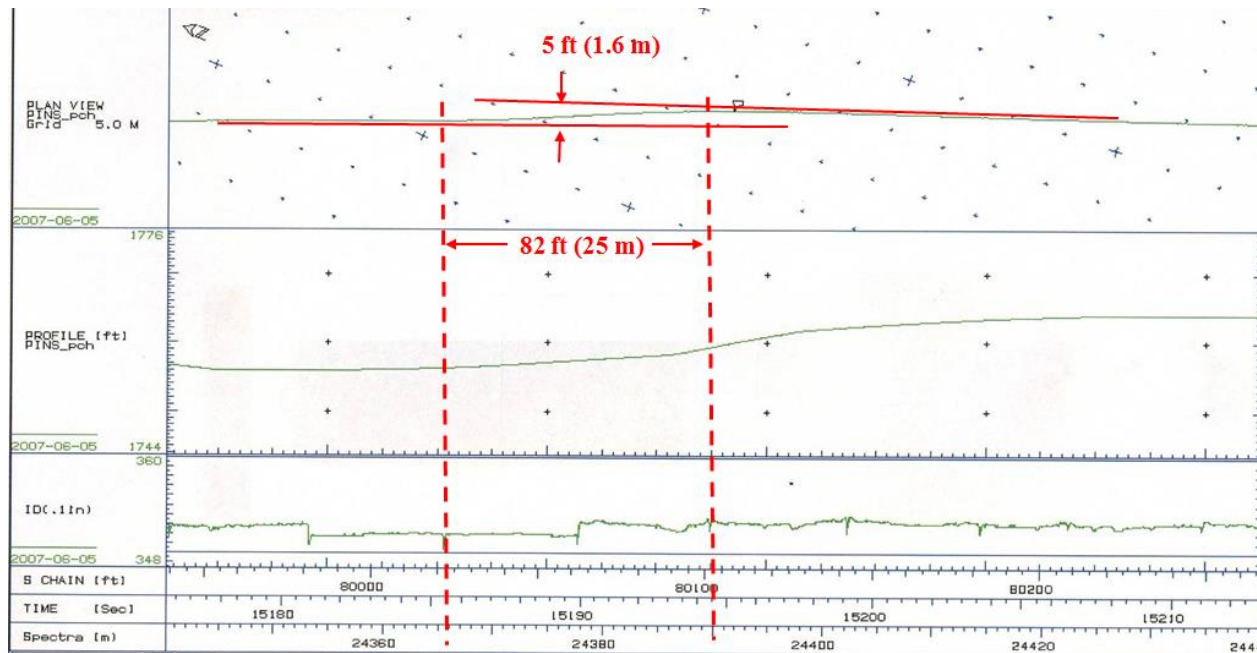


Figure 8-72 Area of strain not detected during a vendor's initial bending strain analysis

Where there are known ground movements, it is always recommended that the vendor and the operator's subject matter experts review the site specific data. In many cases, automated processes may miss obvious indications of pipeline deformations.

It should be cautioned that IMU is considered by some to be a “catchall-method” of detecting landslides while in reality it is one of many tools that are used in any geohazards risk management program. Bending strain analysis and run-to-run movement analysis do not detect areas of high tension and/or compression where there is a small bending component. An example would be a pipeline tensioned across the main scarp of a translation slide moving parallel to the pipeline.

A limitation of the method is that larger diameter/thicker walled pipelines will have a locally less pronounced response to landslide movement as opposed to smaller diameter/thinner walled pipelines. As an example, Figure 8-73 shows a 30-inch natural gas pipeline and a 12-inch oil pipeline. The pipelines were installed in 1957 and 1961 respectively and at the time of exposure and survey in 2008 (approximately 50 years) had been displaced approximately 1 m downslope by a translational landslide moving approximately 1 inch (25 mm) a year at the slide flank. The S bend in the 12-inch pipeline occurred over approximately 25 ft (8 m) while the bend in the 30-inch pipeline occurred over 45 ft (14 m). An initial June 2012 IMU run on the 12-inch oil pipeline identified the S bend feature during the bending strain analysis. Table 8-11 below summarizes the results of the IMU monitoring provided by the same vendor for the 30-inch gas pipeline.



Figure 8-73 Looking south at the south flank of a deep-seated active translational landslide. A 12-inch oil line is located on the left and a 30-in natural gas pipeline is located on the right. The section of pipeline in the upper portion of the photo is located in stable ground with the section of the pipeline at the bottom of the photo being dragged downslope by approximately 1 in (25 mm) of annual movement. (Photo by: D. Dewar, Year: 2008)

Table 8-11 Monitoring results for a 30-inch gas pipeline at the flank of a translational landslide

Run Date	S-Bend Detected in Bending Strain Analysis	Indications of Movement in Run-to-Run Analysis with a 2003 Baseline
June 2003	No	NA
June 2007	No	No
July 2012	Yes	Yes

The example shows that for two different diameter/stiffness pipelines, IMU analysis may have dramatically different results. Generally, it is expected that the stiffer the pipeline, the more difficult it will be to detect discrete deformations in extremely slow moving landslides. Additionally, when conducting run-to-run analysis in slow moving landslides, one should

consider carefully the interval between runs to ensure that enough pipe deformation has occurred to be able to detect the strains. It is important to understand that if no strains are detected during the IMU analysis, it may simply be a case of not enough time being allowed to elapse between IMU runs.

In many cases, a caliper type tool is used in conjunction with an IMU to determine the geometry and ovality of the pipe and to detect wrinkles, buckles, ripples, or dent type anomalies. To a lesser extent MFL and EMAT tools can also be used to detect anomalies caused by ground deformations, but monitoring such anomalies with areas of known ground movement should be done with great care and conservatism if using these methods. The following scenario is provided as an example:

- A 3% 6 o'clock dent is detected in a 12 in liquids line at the toe of a slope during a caliper/IMU run. The pig run was an initial run. A bending strain analysis indicated there is a bend across a weld 2 m downstream of the dent feature. The vendor reported that the pipe has moved up 2 ft (0.6 m) in a vertical plane.
- Previous visual monitoring of the slope indicated a tension crack was evident at the top of the slope.
- A geotechnical review of the slope indicated that there was a slow moving rotational earth slide present. Several slope inclinometers confirmed the presence and depth of movement and a conventional surface survey monitoring program confirmed the extents of the movement.

Depending on the local knowledge of similar landslide behavior, it may be acceptable to monitor it during successive pig runs and mitigate the feature when it passes a preset criteria (for instance, a dent at 6% diameter). The feature is likely only to increase in depth or severity. Therefore, an operator should consider moving towards mitigation rather than monitoring.

If anomalies are detected where there is less confidence in the actual size of the feature (such as dents detected during MFL or cracks from an EMAT type tool), it is recommended that the feature be verified. Then, if required, mitigation be conducted rather than monitoring.

8.3.3.2 Overview of Strain Gauges

Strain gauges are devices used to measure the changes in strain in a pipeline from an initial install date. For pipeline applications, the three most common types are (1) resistance, (2) vibrating wire, and (3) fiber optic. With the fiber optic technology, strain is monitored either using fiber-optic strands shaped like a strain gauge or using newer cable type technologies.

Gauges are typically installed longitudinally on a pipeline at either:

1. Three circumferential positions at 12, 4, and 8 o'clock (120° intervals), or
2. Four circumferential positions at 12, 3, 6, and 9 o'clock (90° intervals),

Variations on these installs can include:

- Rotating one or more of the gauges to avoid loading at the bottom of the pipe, as an example installing at the 1, 4, 7, and 10 o'clock positions when there is a concern that the bottom gauge could be crushed.
- Installing gauges at 12, 3, and 9 o'clock when there are poor ground conditions or other conditions that make a full 360° exposure of a pipeline not practically possible, and
- Customizing the gauge set up based on the interpreted loading scenario.

In the case of resistance and fiber optic strain gauges, the installs may be customized based on site specific scenarios and strains can be measured in any direction. Vibrating wire gauges and fiber optics cables typically must be installed along the longitudinally direction of the pipeline.

When a pipe undergoes elastic bending, the outside of the bend experiences tensile axial strain and the inside experiences compressive axial strain (see Figure 8-74). At positions between the inside and outside of the bending, axial strain/stress varies with position around the pipe as a sine curve. The difference between the maximum and average values (or between the minimum and average) is the amount of bending. If there is also an overall tension or compression in the line, the curve will be shifted up or down. Any three points on a sine curve uniquely define it; therefore, only one sine curve can be drawn through those three points. Because of this, one can measure strain at any three positions and use the values at those positions to calculate the values and positions of the maximum and minimum strains.

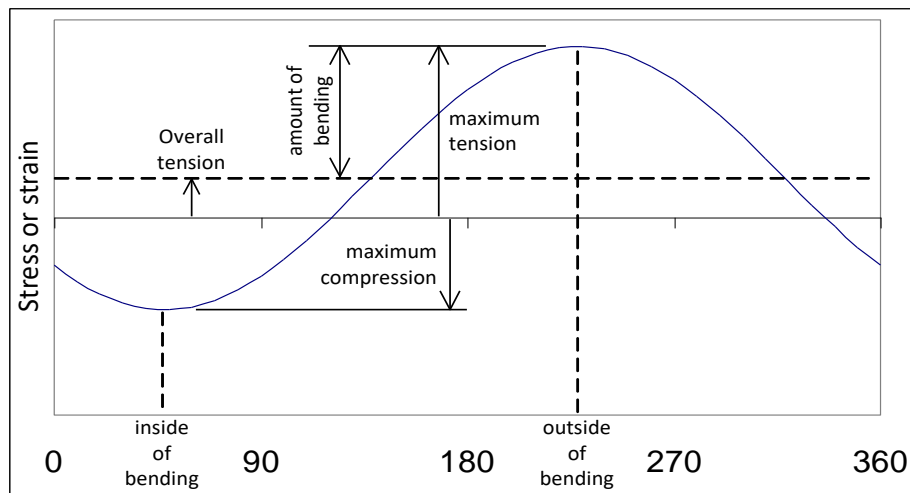


Figure 8-74 Schematic illustration of the stress distribution around the pipe circumference and the maximum tensile and compressive stress

Kiefner, et al., provide the formulas to calculate the strains at any point along the circumference of the pipe from three gauges spaced at 120° or at 90° intervals [265]. If four gauges are used, a recommended approach is to solve the formulas four times, each time

omitting one of the gauges. The locations and values of the maximum strain levels, as calculated from each set of three gauges, are compared. If the values are all reasonably close, average values should be used to determine the pipe condition. If the values differ significantly, there is probably a problem with one of the gauges. Graphically comparing historical trends of the four gauges in the set can usually identify which of the gauges has developed a problem and should be disregarded. Historical trends of individual gauges can also answer the question of how close the calculated values should be for the analysis to use all four gauges, with the assumption that the variation is due to random error and not a bad gauge reading.

A few important notes about using strain gauges:

- Some pipelines can experience strains of 10,000 microstrains or more without negative integrity consequences. Some strain gauges may not have enough range for such high strains.
- The linear relation between stresses and strains ceases to exist when the stress level is beyond approximately 90% yield strength. This stress level corresponds to approximately 0.15% and 0.21% strain (1500 and 2100 microstrains) for X52 and X70 pipes, respectively.
- Strain gauges monitor changes in the strain from the time of application, not the total strain on a pipeline.

Figure 8-75 shows tabular strain gauge data collected as part of a monitoring program. Figure 8-76 shows strain gauge readings plotted versus time.

Date	GAUGE	PERIOD	STRAIN	CURRENT	TEMP	BASE	CUMULATIVE	COMMENTS
11/22/2005 1:00:00 AM	1	524.1	736	1107	6470	743	-7	
	2	587.5	171	1100	6034	362	-191	
	3	526	716	1056	6481	784	-68	
1/4/2006 1:00:00 AM	1	526	716	1102	6441	743	-27	
	2	593.5	126	1105	6002	362	-236	
	3	527.3	702	1050	6448	784	-82	
1/26/2006 1:00:00 AM	1	525.5	722	1096	6396	743	-21	
	2	589.8	155	1103	5966	362	-207	
	3	526.7	709	1045	6408	784	-75	
2/13/2006 1:00:00 AM	1	523.5	743	1101	6420	743	0	
	2	587.8	170	1117	5987	362	-192	
	3	525.4	724	1049	6432	784	-60	
2/16/2006 1:00:00 AM	1	527.4	703	1090	6353	743	-40	
	2	591.9	140	1112	5925	362	-222	
	3	528.3	694	1039	6366	784	-90	
2/20/2006 2:00:00 PM	1	529.4	682	1084	6327	743	-61	area looks ok change is strain reads noted
	2	594.6	120	1109	5901	362	-242	area looks ok change is strain reads noted
	3	530	676	1034	6340	784	-108	area looks ok change is strain reads noted
2/22/2006 11:00:00 PM	1		773		0	743	30	After excavation
	2		134		0	362	-228	After excavation
	3		668		0	784	-116	After excavation
2/24/2006 1:00:00 AM	1	529.5	682	1089	6366	743	-61	
	2	598.7	97	1105	5925	362	-265	
	3	533.8	638	1040	6369	784	-146	
4/6/2006 1:00:00 AM	1	522	761	1110	6508	743	18	
	2	593.4	130	1147	6063	362	-232	
	3	526.6	712	1058	6523	784	-72	
5/12/2006 1:00:00 AM	1	519.2	794	1148	6574	743	51	

Figure 8-75 Example of strain readings in tabular form



Figure 8-76 Example graph of strain readings from a set of 3 circumferential gauges

8.3.3.3 Traditional Strain Gauges

8.3.3.3.1 *Resistance Type Gauges*

Resistance gauges are printed circuits, consisting of a large number of thin conductors running parallel with each other along the axis of the gauge. The conductors are connected in series so that they form a single very long conductor. A deformation causes length change of the conductor, and thus alters the resistance of the conductor. The gauge is read using a Wheatstone bridge so that changes in resistance on the order of micro-ohms can be detected.

The gauge is permanently attached to the material being monitored. In laboratory applications, resistive gauges are generally installed using adhesives. Weldable gauges are also available which are welded to the material being monitored using a capacitive discharge welder. These weldable gauges are more suitable for field installation. Examples of resistance strain gauge installations are shown in Figure 8-77, Figure 8-78, and Figure 8-79.

The advantages of resistive strain gauges include:

- Fully mature technology; the standard for laboratory strain monitoring.
- Can operate over very large strain ranges (as much as 2% - 3% strain, but with some loss in accuracy). This can be an advantage if strain-based evaluation is to be used.
- Can be bent to read hoop or torsional strains.
- Short gauge length (typically about 1/4 in / 6 mm); this can be an advantage in some types of monitoring. However, pipeline strains tend to be fairly constant over lengths on the scale of a diameter, so there is no advantage in this application.
- Capable of true real-time monitoring; can be used to monitor transient strains such as those associated with surface loading and blasting. Not generally an advantage for landslide monitoring.

The main disadvantages of resistive strain gauges are:

- More prone to failure in long-term field installations than vibrating wire strain gauges, and
- The readings from resistive gauges can drift over time because the gauges are sensitive to temperature change which changes their resistance over time. Moisture infiltration in the connecting wires can also change the system resistance.

For these reasons, resistive strain gauges are generally not used for long-term geotechnical monitoring.

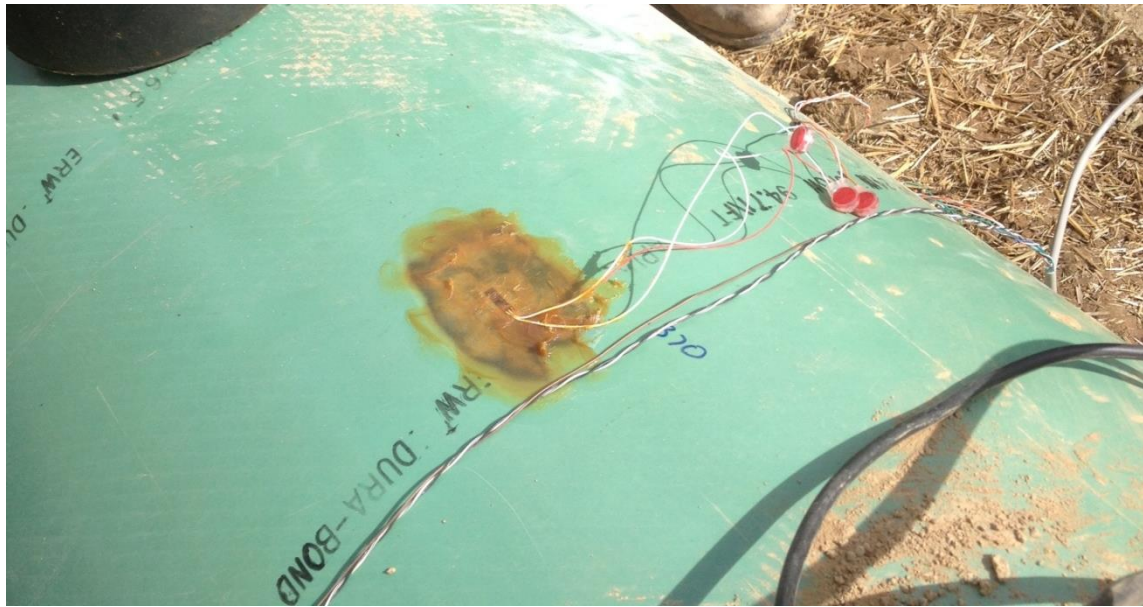


Figure 8-77 Resistance type strain gauge installed at 12 o'clock position on a pipeline (Photo by: M. Roberts, Year: 2014)



Figure 8-78 Resistance type strain gauges installed on a pipeline



Figure 8-79 A site with resistance type strain gauges installed

8.3.3.3.2 *Vibrating Wire (VW) Strain Gauge*

This section describes the practical uses of vibrating wire (VW) strain gauges for pipeline applications [266]. VW gauges are sealed tubes typically 1 to 3 inches (25 to 75 mm) long containing a wire held in tension between two end blocks. The gauges are typically spot welded to a pipeline. Deformation of the pipeline is transferred to the gauge altering the tension of the wire. The changes in strain are measured by a coil assembly sensor mounted on the gauge. The strain gauge operates on the principle that a tensioned wire, when plucked, vibrates at its resonant frequency. The square of this frequency is proportional to the strain in the wire.

A VW strain gauge's output is an AC frequency signal that is not sensitive to resistance changes in the connecting cables caused by contact resistance or leakage to ground. The VW gauge has a thermal coefficient of expansion similar to that of pipeline steel and thus there is no need to compensate for the thermal effects. Temperature changes are measured by a thermistor encapsulated in the sensor. Manufacturers' reported gauge ranges are from 2500 to 3000 μE . Gauges can be purchased that are designed to be either compressed, tensioned, or be a "mid-range" gauge when the type of straining is unknown.

Figure 8-80 shows a VW strain gauge, a strain gauge sensor, and a recorder unit. Installation equipment and strain gauges are available from numerous vendors and/or manufacturers.

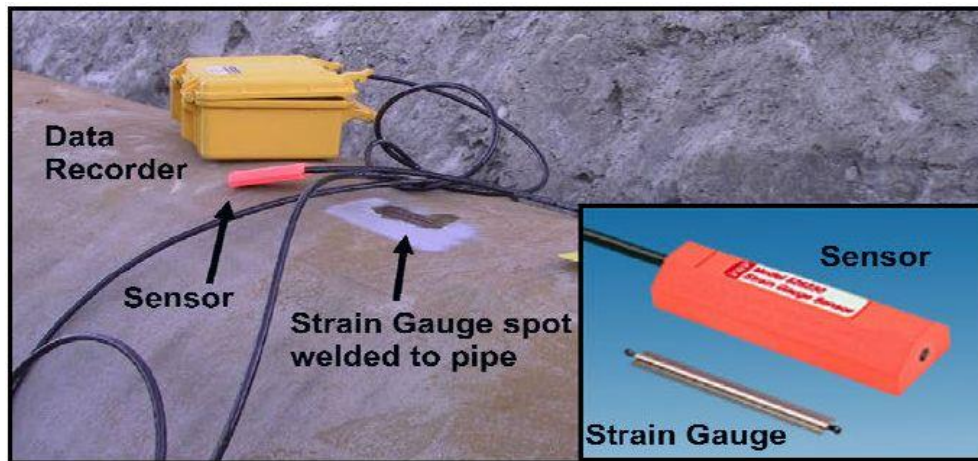


Figure 8-80 Strain gauge installed at 12 o'clock position on pipeline data recorder and sensor are shown. For reference, the gauge is 2.5 inches (7cm) long. (Photo by: D. Dewar, Year: 2004).

The gauges, a set of straps that hold the sensors in place, and a protective cover, are spot welded to a pipeline during installation. The typical energy for each spot weld ranges from 20 to 40 J. This is about 1/100 of the energy of an arc strike which would range from approximately 2000 to 6000 J. Generally, the spot welding used in VW strain gauge installs is considered a surficial change that does not affect pipe hardness. Pressure reductions are not required specifically for the installation of the VW gauges, but may be required for other pipeline integrity related issues. Figure 8-81 shows a gauge being spot welded to a pipeline.



Figure 8-81 VW Strain gauge in the process of being spot welded at 3 o'clock position on a pipeline (Photo by: D. Dewar, Year: 2004)

Figure 8-82 and Figure 8-83 show completed strain gauge installs (a group of gauges around the circumference of the pipeline). Using 4 circumferential installs whenever practical is

recommended as bending moments can still be calculated if a single gauge fails. The typical cost of VW strain gauge install materials and labor is about 4% to 10% of the total excavation cost. Therefore, whenever possible, it is prudent to install an additional VW gauge adjacent to the primary install to function as backup in case an individual gauge fails. This is especially true for remote or difficult-to-access locations where landslides and/or settlement/subsidence may impact pipelines.



Figure 8-82 Three position strain gauge install on 36-inch natural gas mainline ready for recoat and backfill (Photo by: D. Dewar, Year: 2008)



Figure 8-83 Four position strain gauge install on a 12-inch oil line ready for recoat and backfill. The lines are run to a partially assembled stick up protector where a logging unit will be mounted after backfill. (Photo by: D. Dewar, Year: 2013)

The main advantages of VW strain gauge installs are:

1. The installation process is a relatively straightforward, requiring no special skills and/or training.
2. The installation process is relatively quick with times (excluding the actual excavation time) ranging from 1 to 2 hours per 4 gauge install.
3. The installation process is relatively inexpensive:
 - a. Installation equipment for the install is relatively inexpensive at under \$10,000, and
 - b. Supplies are also relatively inexpensive at under \$2,500 including a logging unit to monitor up to 4 gauges.
4. The gauges, when installed correctly and backfilled with care, have proven life spans of over 35 years [267]. See Table 8-12 for an example of the expected performance of VW gauges in a monitoring project in a very slow moving translational landslide, with gauges ranging in age from 1 to 13 years (8-year average age).

Table 8-12 Vibrating wire strain gauge performance

VW Strain Gauge Performance on Monitoring Project in Very Slow Moving Translational Landslide							
Type	Installed	Destroyed*	Remainder	Failed gauges	% Failed	Failed Thermistors**	% Failed
3 position gauge installs	66	1	65				
Individual Gauges	210	3	201	10***	5%	2	1%

**The surficial stick up protectors and lead wires were destroyed during agricultural activities including hay mowing. Gauges are likely still functional but pipeline re-excavation would be required in repair lead wires and reinstall stick-up protectors.*

***Failed thermistors are less of an issue as there are either 2 or 3 neighboring thermistors with nearly identical readings at the same location within each install.*

****A review of the data indicates that half the failures appear to have occurred during backfilling.*

5. The gauge sensor lead wires:
 - a. Are manufactured from common electrical wire. Therefore, wires can be easily repaired/extended/shortened using common electrical supplies, and
 - b. Can be run up to 400 ft (120 m) [267] from install to reading point. Some manufacturers claim up to 0.6 miles (1 km) for a maximum cable run.
6. Are sensitive enough to detect changes in strain due to ground movement from up to 200 ft (61 m) from the actual area of maximum strain.
7. Items 1 through 5 above together make VW strain gauges ideal for emergency work, given the relative ease of installation.

Potential challenges of VW strain gauge installation are:

1. VW gauges are typically very short at 1 to 3 in (25 to 75 mm) long when compared to the typical section of pipe they are used to assess/monitor. Soil/pipe interaction is a complex process and determining areas of maximum/minimum strain may be difficult even for an experienced team of pipeline integrity and geotechnical personnel. IMU data may help in the determination of strain gauge location. Westwood et al. [268] showed that even when strain gauges are installed with good mechanical/geotechnical advice they may miss the areas of maximum tensile/compressive/bending strains.
2. Pipelines must be excavated to install the gauges. While the previously noted costs of the strain gauges themselves are minimal, there may be significant costs due to the required ground disturbance above and beyond a typical pipeline excavation, including:
 - a. The cost of access: The area of interest may be in a remote or difficult to access location. In some cases, access may be seasonal.
 - b. The cost of special excavation measures in challenging terrain which could potentially include:
 - i. Bridling excavators,
 - ii. Dewatering, and
 - iii. Trench shoring.

VW strain gauges are used to measure the change in strain on a pipeline after installation. Existing strains at the time of install must be estimated or determined using another method of analysis. Any data interpretation should be conducted by an experienced mechanical/pipeline integrity engineer. Readings are provided directly in microstrains (μE) and temperature.

Options for reading strain gauges include:

1. Manual,
2. Manually read data loggers with four or more ports, and
3. Remote readings using loggers communicating data through phone, cellular, internet, or satellite connections. Alarms may or may not be set up as part of the remote monitoring process.

The frequency of readings is typically dependent on the rate, and to a lesser extent, the type of movement. As an example, an extremely slow deep-seated translational earth slide may only require bi-annual readings. A potentially rapid retrogressive rotational earth slide–earth flow that is encroaching on a pipeline ROW may require real-time or hourly remote readings with alarms. Longwall mine subsidence progresses rapidly enough that hourly data logging, with collected data downloaded and analyzed at least once each day, is prudent. At a minimum, it is recommended that data be logged until the interactions between the ground deformations and pipeline(s) can be determined. In many slides in fine grained soils infrequent manual readings may misrepresent the actual loading the pipeline has been experiencing. With softer fine grained

soils, a pipeline may spring back after the initial loading. If the undrained peak occurred between readings, the maximum loading on the pipeline would be missed.

During interpretation of strain gauge data, the following operational stress changes must be considered:

1. Installation associated stress changes including backfilling,
2. Temperature, and
3. Pressure.

Owners/operators should consider that there are significant changes in the stress of a pipeline as it is backfilled. Typically, during initial construction, the majority of a pipe is laid at the bottom of a ditch/trench on undisturbed native soils except where a thin layer of bedding material is required. During any subsequent dig that requires 360° exposure of a pipeline there will be a minimum of sub-excavation of 2 to 3 ft (0.6 to 0.9 m) to allow for the inspection, strain gauge install, and recoating of the pipeline. Even with pipe supports and careful backfilling by hand driven machine and excavator bucket compaction, it is impossible to eliminate settlements. An example of expected vertical settlements reported in IMU run-to-run comparisons of pre and post dig strain gauge installations on a 30 inch mainline with dig lengths of 45 ft (14 m) are on the order of 1.6 to 8 in or (40 to 200 mm). Reported strains between the initial installation readings and first reading after backfill can show variations of up to 600 μE in tension or compression.

Additionally, temperature-change-caused expansion and/or contraction during the installation process may create additional stresses. For long ditches, compressional bending of up to 500 μE has been reported at the ditch edges due to pipe expansion on 104°F (40°C) days.

As noted above, VW sensors typically have a temperature reading device, typically a thermistor, installed in the reading unit. The thermal expansion coefficient of common gauge wire is similar to that of the pipeline steel at 6 $\mu\text{E}/^\circ\text{F}$ (10.8 $\mu\text{E}/^\circ\text{C}$) [269]. Therefore, corrections for thermal effects are typically not required for interactions between the gauge and pipeline. The temperature of any pipeline will vary over the operating life/cycle. The stress changes as a result of the thermal expansion and contraction of the pipeline must be considered when interpreting strain gauge data. Additionally, pressure fluctuations should be considered when comparing readings. Figure 8-84 shows the normal temperature and pressure fluctuations on a 6-in liquid propane line with a landslide occurring in the monitoring period.

Analysis of strain gauge data is not always straightforward. Experienced mechanical engineers should be involved in determination of strain gauge install details and the interpretation of strain gauge data.

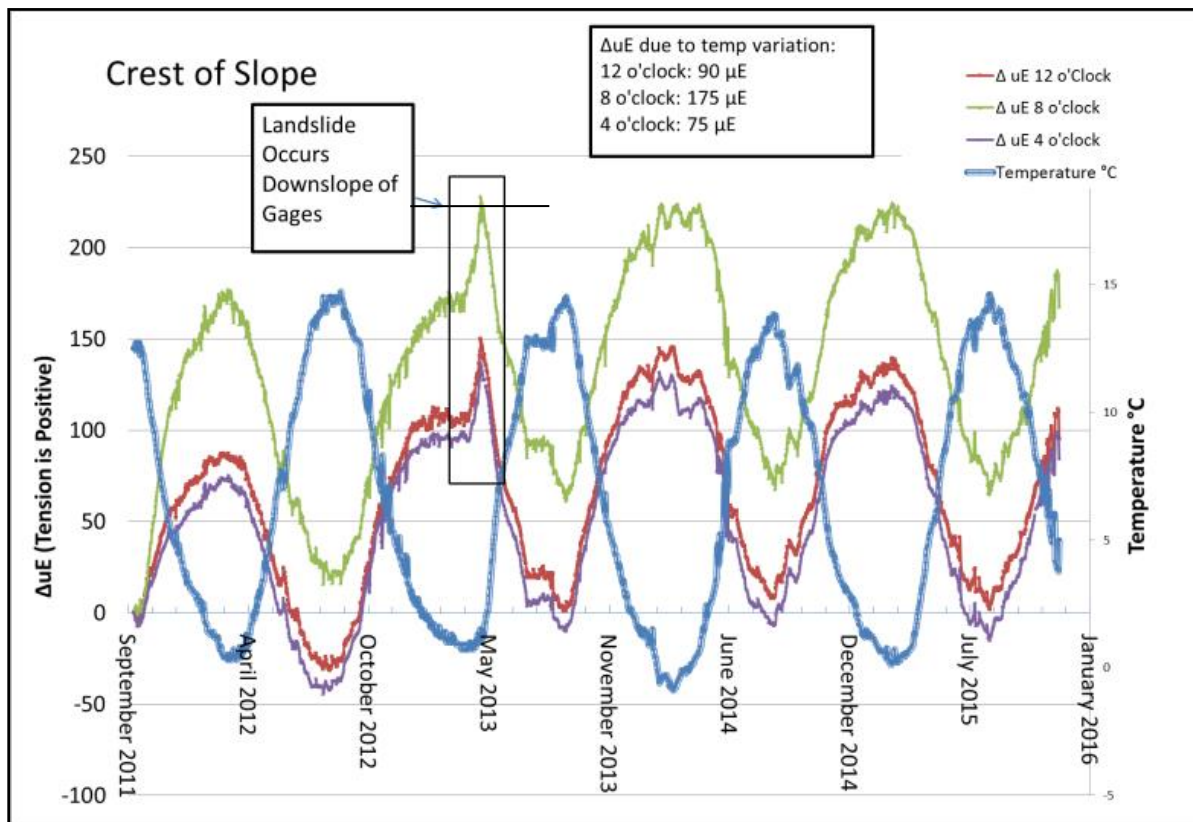


Figure 8-84 Normal temperature and pressure fluctuations on a 6-inch liquid propane line with a landslide occurring in late April and early May of 2013. Note vertical/tensile shift in curves after landslide.

8.3.3.4 Fiber Optic Strain Gauges and Cables

Fiber optic (FO) strain gauges and cable type installations (cables) use light to measure strain changes. Light is shot down the fiber and changes in the fiber length cause light color to change. There is a relationship between color change and the changes in strain. With the FO cable technology, changes in temperature and sound can also be measured. More details on the theory behind the technology are included in [270, 271, 272, 273, 274, 264]. The technology is considered mature from a general point of view as it has been employed since the early 1980s for non-pipeline strain monitoring applications. Limited pipeline strain monitoring applications and experiments have been conducted since approximately 2003 and it is judged to still be a maturing technology.

In the case of the cable type installations, the FO technology was initially used to monitor temperature and sound along pipelines. FO temperature cables could be installed along a pipeline to notify the control center of any temperature changes in the surrounding ground/pipeline caused by leaks. The placement of the cable depends on the type of product being transported. FO acoustic cables are also available that can measure acoustic changes and the pipeline and can be used to warn operators if heavy equipment or excavation work is being

done near the pipeline. Additionally, there may be a possibility of using this fiber to monitor changes in cover over pipe in stream crossings. These technologies are not discussed in this section as they are not directly related to the monitoring of pipeline strain due to ground deformations. The FO cable technology has been adapted for strain monitoring. Additionally, combination cables (or “tapes”) have been developed to both detect strain and temperature changes.

FO strain gauges are installed over an area on the pipeline. FO cables are run for relatively long distances down the length of a pipeline.

8.3.3.4.1 *FO Strain Gauges*

Rather than being welded or spot welded to the pipeline as VW gauges are, FO strain gauges are bonded to the pipeline using an epoxy. Cauchi et al. [271] provides the following specifications for the systems:

1. Type of fibers: Conventional telecommunications grade 250 μm single mode optical fiber.
2. Configurations (see Figure 8-85 below):
 - a. Linear: can have up to 10 ft (3 m).
 - b. Coiled: can have up to 66 ft (20 m) of fiber in a small 10 in² (65 cm²) package (note that this configuration will not differentiate between axial and hoop strain).

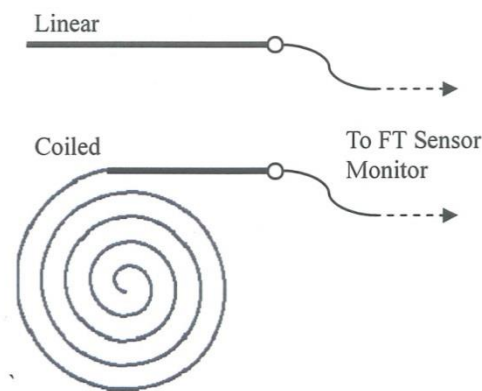


Figure 8-85 Fiber optic strain sensor configurations [271]

3. Accuracy: for lengths from 3 in to 331 ft (10 cm to 100 m) the accuracy is reported as $\pm 5 \mu\text{m}$ or as an example $\pm 5 \mu\text{E}$ for a 33 ft (10 m) sensor length.
4. Range: In lab tests, up to 3% strain or 30,000 μE .

Fiber optic (FO) strain gauges are generally similar to VW gauges, with the following advantages:

1. FO strain gauges are completely customizable and can be made to different lengths and widths; see Figure 8-86. When compared to VW gauges, they can cover significantly more area. Figure 8-87 shows the gauge orientations. Cauchi et al. [271] noted that the

VW wires were installed during a slope stability monitoring project as linear gauges to monitor large strains (range of 0.01 to 1% strain) and coiled gauges for small strains (range of <0.01%).

2. FO strain gauges can be oriented in any direction whereas VW strain gauges can typically only be oriented along the pipe axis. Cauchi et al. [271] described the use of FO strain gauges to measure hoop and longitudinal strains.



Figure 8-86 FO strain gauge installation with longitudinal and axial gauges (Photo by: E.C. McClarty, Year: 2005)



Figure 8-87 Adjacent FO and VW strain gauge installations to show size limitations of VW strain gauge size. The VW strain gauges are used to back up the FO strain gauge install in this application. (Photo by: D. Dewar, Year: 2008)

Potential issues and/or challenges with FO gauges include:

1. As with VW gauges, excavations are required to install the FO strain gauges. The differences in installation procedures, efforts, and issues include:
 - a. FO gauge installation typically requires the vendors' skilled technicians to install the gauge(s).
 - b. FO gauges are attached to the pipeline using epoxy rather than being spot welded; therefore, excavation time must include epoxy curing time.
 - c. FO gauges must have a fiber optic cable of a known fixed length running from the gauge to the above ground reading site. The cable is sensitive to damage/ground deformations and cannot be easily repaired or replaced like a VW strain gauge cable. The sensor could be in perfect condition but it cannot be interrogated due to the damaged or deformed cable. At minimum, an experienced technician would have to visit the site if cable repairs are required.
 - d. Install supplies cost roughly 2 to 5 times as much as VW strain gauge supplies at \$4,000 to 10,000 per install. Monitoring equipment can be significantly more expensive with data recorders on the order of \$20,000 to \$30,000 each.
2. Information taken from the data recorders typically must be returned to the vendor for interpretation, whereas VW gauge data may be interpreted in-house or by a third party mechanical consultant.
3. Technology is relatively new and there are only a few vendors, potentially limiting access to the technology.

Cauchi et al. [271] provided some very preliminary comparisons between VW and FO strain gauge readings. It appeared from this data that the FO gauges reported significantly lower strains. Unpublished longer term operator monitoring data indicates that the VW and FO gauges track straining trends near identically, but the total strains reported by the VW gauges is approximately twice that of the FO gauges. As with any case involving two sets of data that do not agree, it is not possible to determine which, if either, set of data is correct.

While there may be many challenges with any new technology, it is customizable, allowing for the collection of data that VW strain gauges cannot be used to measure. At this time, it is the authors' opinion that FO strain gauges are better suited for well-planned installations where careful consideration is given to the backfill, and cable routing options and maintenance work are possible. Given the limitations discussed above, FO strain gauges may not be suitable for emergency or urgent monitoring work. Wherever possible, it is recommended that any FO installation be backed up with VW strain gauge installs.

8.3.3.4.2 *FO Cables*

FO cables that measure strain are a more recent innovation that has been laboratory tested and field testing as detailed in [272, 273, 274]. Typically, "distributed or linear" sensor cables

are used for pipeline installations. The distributed sensor FO cables can report changes of deformation of +/- 20 microstrains over distances up to 15 miles (25 km) with a positional accuracy of +/- 1.5 m as claimed by numerous vendors. When designing cable installations, splices are typically avoided as they will shorten the overall length of the cable run. Additionally, most long installations are designed so that a reading point has a run of cable going in either direction, effectively doubling the coverage. FO cables are reported to have approximately 17 times the tensile modulus of steel. Therefore, they can easily report strains of up to 0.5% or even 2.0%. The minimum bending radii of FO cables depends on the cable specification, but a standard 48 fiber (4 bundles of 12) has a minimum bending radius is 155 mm (6 in) while in operation. Increased positional and strain accuracy can be obtained by using more expensive cables with “multipoint or discreet” cable sensors. Based on the required accuracies for ground deformation monitoring, only distributed/linear technologies will be discussed in this section.

FO cables can be installed along the length of the pipeline in orientations detailed at the start of the section above. The FO cables can be installed during new construction or retrofitted onto existing pipelines along shorter sections of interest. Generally, existing pipelines would not be exposed to install FO cables unless there was a significant integrity related driver. Typically, 6 o'clock installations are avoided as the usual method of installation is to tape the cable to the pipeline. For ease of installation, FO cables are installed at the 12, 3, and 9 o'clock positions because in these positions, it is much easier to pull the cable along the pipe and place the tape over the top of it.

Additionally, as detailed in [273], cables can be installed in the soil surrounding the pipeline or at the base of the pipeline trench to solely measure ground deformation. Figure 8-88 and Figure 8-89 show typical installations with the cables being taped to a pipeline.



Figure 8-88 FO Cable monitoring install with three strain/temperature tapes oriented at roughly 12, 4, and 8 o'clock along a 500-meter length of pipeline in a landslide. (Photo by: Smartec, Year: 2003)



Figure 8-89 Taping a fiber optic cable top a pipe (Photo by: K. Ryan, Year: 2013)

A tape that does not interfere with cathodic protection is recommended. Since the FO cable(s) will be running laterally along the sides of the pipe, it is recommended to apply the tape laterally to completely cover/protect the cable. Placing the FO cable on the pipe allows for ease of excavation of the pipeline. Most pipeline companies require the backhoe to stay a given distance from the pipe, usually 1 to 2 ft (0.3 to 0.6 m) away. The material next to the pipe is usually removed by hand, allowing the fiber to stay in place without damage. However, a direct hit with a shovel could damage the fiber, just like with any type of wire. The FO cables can be spliced when required. Discussions with vendors indicate that these repairs/splices are a relatively simple process unlike FO gauges discussed above.

An FO analyzer is required to interrogate the FO cables(s). The cables can be either be continuously/remotely interrogated where power is available or read periodically. Analyzers are currently bulky and not conducive to use in remote field applications with difficult field access. The fiber gauges can be monitored on a real-time basis and alarms can be set up and sent to control rooms to keep operators aware of the pipeline conditions. Software is available to allow the operator to know where changes are occurring as well as the magnitude of the changes. This can provide real-time information of the pipe and its surroundings.

Figure 8-90 shows typical cross sections of FO cables used for pipeline or in ground installations. These cables are designed to be robust and survive burial. Manufacturers have reported minimum lifespans of 30 years for properly installed FO cables. Immediately following completion of the installation, including splices, the cables are tested. The cables are tested again following backfill. Vendors consider pipeline systems as “mild environments” when compared to hot downhole environments or high pressure subsea environments. Subsea FO umbilical cables have reliably operated since the 1980s.

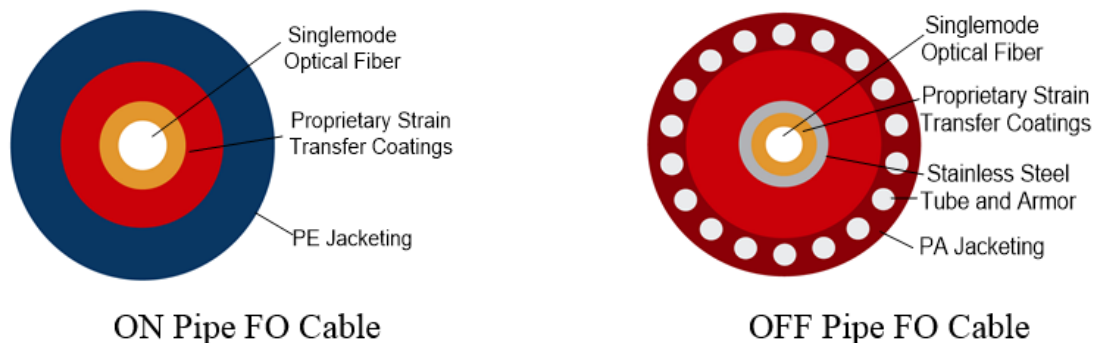


Figure 8-90 Typical FO cable cross sections for on pipe and off pipe applications [273]

The actual cost of the FO cable is typically \$0.37 to \$2.05 per ft (\$1.20 to \$6.75 per m) with an average cost of approximately \$0.60/ft (\$2.00/m). Installation times are typically 3 times faster than a pipe laying crew. In optimal conditions, with good planning and communication, a 4 person FO cable installation crew can lay between 6000 and 8000 ft (2000 to 2500 m) of cable in a day. The main expense with FO cables is the FO analyzers which typically cost around \$100,000 USD (at time of publication). FO analyzers can be rented from certain vendors when

readings are taken on a schedule as opposed to continuous real-time monitoring. New construction installation costs are project specific and no reliable estimate range can be provided at this time.

Other gauge type installs provide strain changes at a point, while the FO cables provide strain reads continuously for the complete distance that they run along. This is the main advantage of FO cables. Conversely, installing FO cables in an area of interest is much more expensive as the pipeline must be exposed along the complete area of interest. If a pipeline is encountering a small landslide with well-defined features, then strain gauges will be suitable for monitoring. In areas where a landslide is very large and the boundaries are not well defined, such that finding the points of anticipated maximum strain is difficult, using fiber gauges can provide significant advantages.

Comparison testing using VW and FO cables have shown good correlation between the two reads [273]. In this study, the gauges and cables were installed on a 16-in pipeline and then subjected to a manmade landslide to induce strain. Strain was measured at the center and edges of the landslide. Three FO cables were placed on the pipe and compared with the VW gauges at their respective locations. Figure 8-91 illustrates the readings for three VW and FO cable readings at the center of the slide. Figure 8-92 shows the strains at the edge of the slide.

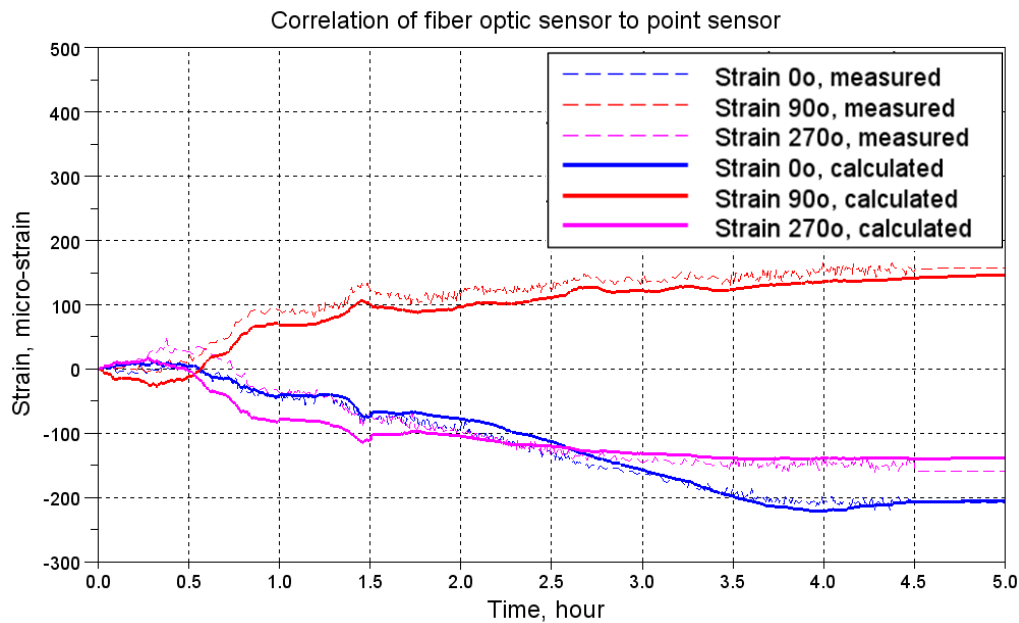


Figure 8-91 Comparison of strains from fiber optic sensor (measured) and VW strain gauges (calculated) at the center of a landslide

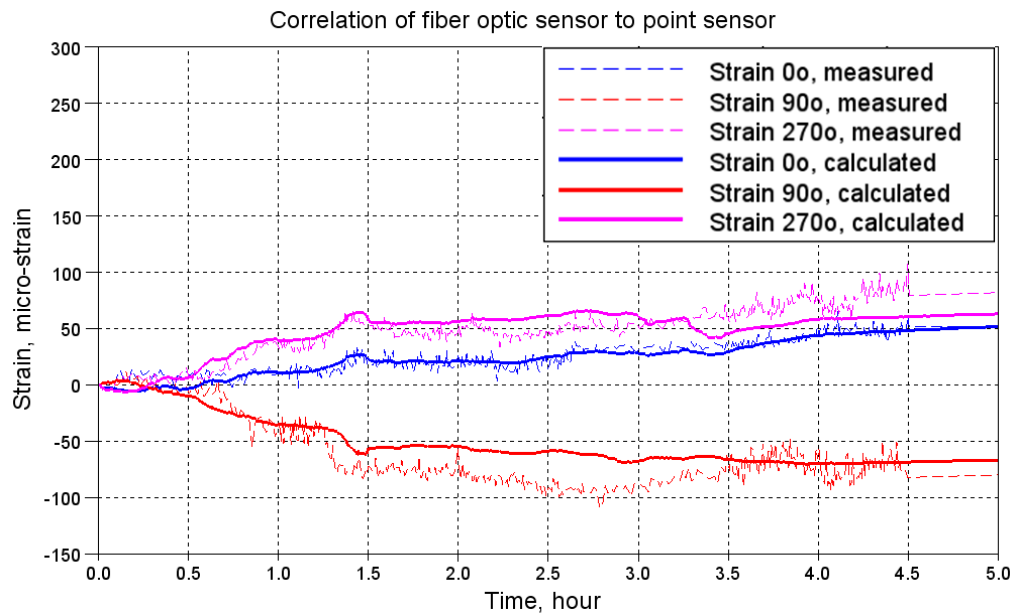


Figure 8-92 Comparison of strains from fiber optic sensor (measured) and VW strain gauges (calculated) at the edge of a landslide

Testing was also conducted to compare FO cables installed off the pipe in the bottom corners of the pipe ditch, 6 to 8 inches above the pipe, and at the edge of the pipe ditch, and buried outside of the pipe ditch (refer to Figure 8-93) [273]. In the last case, the FO cable could be installed by plowing in or trenching outside of the pipe ditch. Results of the testing provided a good correlation with landslide movement. Because the FO cable was not restrained by the pipeline it was more sensitive to the ground movement. This is because the pipe can act as a structural member and resist movement from the forces of a landslide and therefore the pipe will often move less than the soil around it. The off-pipe FO cables will usually predict more strain change than what is actually being experienced by the pipelines. These gauges can then be used as an indication that forces are acting on the pipe.

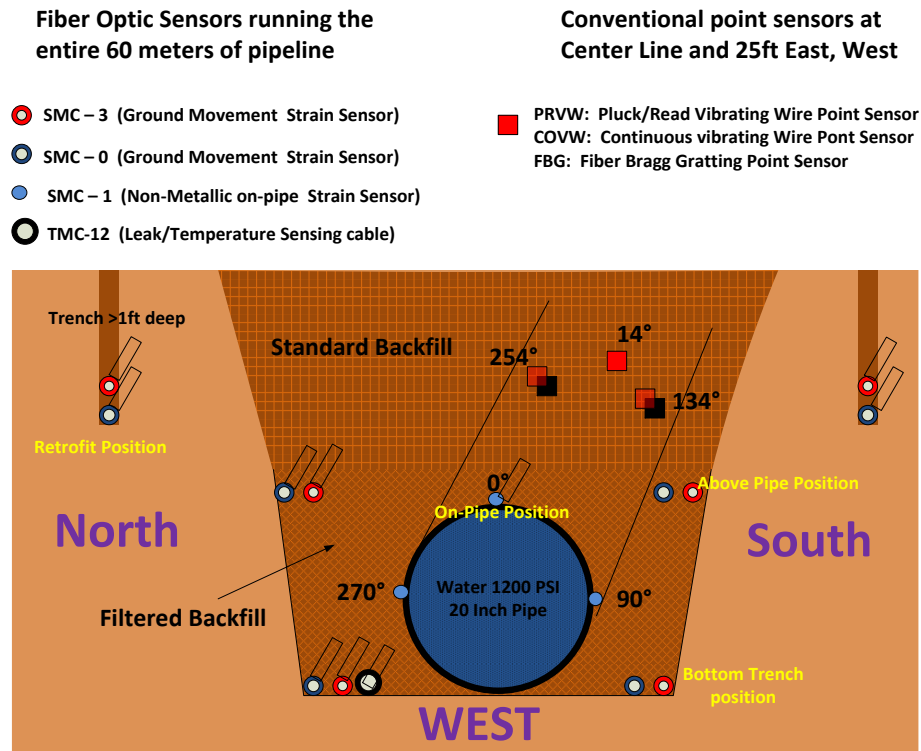


Figure 8-93 Experimental set up with on pipe and off pipe FO cables [273]

When considering using FO cables installed in the ground, care should be taken to place the cable in a location that will be least likely to be in the way when excavating the pipeline in the future, e.g., at the bottom of the ditch.

Going forward, FO cables for ground deformation will likely have three applications:

1. New construction: Hazard detection/delineation/monitoring or areas of potential or known ground movements that new pipelines must be routed through.
2. Existing pipelines: Hazard detection/delineation within high consequence areas. Given the costs of ground disturbance, possible recoating, and reburial, this likely will be used in limited applications.
3. Existing pipelines: Hazard monitoring within areas of known movement or at specific areas of known pipeline deformations within larger areas of movement. The FO cable systems could be installed following other pipeline activities including replacements, cut outs, and/or stress/strain relief projects.

8.3.4 Selection of Methods

It has been stressed throughout this report that most landslide and/or settlement/subsidence pipeline loading scenarios are unique and that there is no single flow chart or accepted prescriptive method for setting up a monitoring program. This is true for monitoring programs set up to verify the performance of hazard mitigation (discussed in sections 0 and 8.2) as well as to monitor an active hazard prior to proceeding with mitigation (if required). Rather than

providing a prescriptive method of determining what types of monitoring should be applied to a particular situation, this section provides guidance on selecting potential methods of monitoring.

Regardless of the method chosen, any monitoring program must provide sufficient information for the owner operator and/or their representatives to make integrity-based decisions on the fitness-for-service of their pipeline. Monitoring budgets, efforts, and frequencies (as discussed in section 8.3.5) should be proportional to the potential risks.

There are generally two ways operators approach geohazard management:

(1) The program is administered by the owner/operator integrity personnel with external geohazard subject matter expert input typically from consultants. The ground monitoring would be the area of expertise of the local geological engineer and/or geoscientist. Therefore, owners/operators should rely on their recommendations for methods used to monitor the ground. Pipe monitoring is either the area of expertise of the owner/operator or of their mechanical/pipeline integrity consultants. Typically, there is very little technical overlap between the subject matter experts determining the ground monitoring and pipe monitoring programs. The geohazard subject matter expert likely has little to no operational knowledge for pipelines. Therefore, both groups should consult extensively with each other to ensure that the overall monitoring program can achieve the goal of confirming the fitness-for-service of the subject pipeline(s).

(2) The program is run by internal geohazard subject matter experts. Within such a program, there may be more collaboration between the geological and mechanical subject matter experts. The reliance on external subject matter experts tends to vary based on the workload and the specific role of the internal program owner.

The following guidance is provided for selection of ground monitoring techniques:

1. Any existing installations used as part of the original characterization of the hazard should be continued. As an example, slope inclinometers used to verify that a deep-seated landslide was present should be monitored after a landslide is stabilized.
2. It's better to start out with a robust monitoring program involving numerous ground monitoring techniques with redundancy and reduce efforts over time, if judged to be appropriate, rather than having to build a monitoring program from less complex to more complex in response to data gaps.
3. When using more complex methods such as InSAR, that have numerous sources of error, a more simple and well-established method such as conventional surveys or slope inclinometers should be used to provide redundancy and verify data.
4. In the case of monitoring an existing hazard mitigation, the geohazard subject matter expert should predict the mode(s) of failure of the mitigation, if any. Ground monitoring techniques should be tailored to detect any indications of such failure(s).
5. In the case of deep-seated instabilities that extend far below the pipeline burial depth, it is more useful to monitor the ground surface rather than focusing on the landslide slip surface. As an example, the deformations of the slip surface of a 330 ft (100 m) deep

landslide would mean very little to a pipeline buried at 3 ft (1 m) depth. It is much more useful to monitor the ground surface as this may be more analogous to the deformations the pipeline is experiencing. It is the author's experience that geotechnical consultants may tend to focus on subsurface monitoring rather than the potentially more useful and important deformations at pipeline burial depth.

6. Within deep-seated instabilities, any ground monitoring program should detect the boundaries of the movement and any zones of differential deformation within the movement. Deformations of pipelines may be just as severe or more severe in the middle of a landslide than at its boundaries. The determination of areas of differential movements and the ability to measure the differential movements may allow for the accurate location of pipe monitoring techniques such as strain gauges. Additionally, it serves as a check when reviewing smart pig related data.
7. Methods (including pipe monitoring technologies) may have to be capable of full time remote data collection via either a landline, cellular, or satellite link directly either to the company computer system or via an internet service. These requirements are typically necessary for scenarios where there is a potential for rapid movement or where you have remote sites that cannot be accessed easily during certain portions of the year, if at all.
8. If there is a threat of rapid movements, such as a debris flow that initiates with no warning, then there is little point of conducting monitoring. In these scenarios, it is likely better simply to move to mitigation.
9. The level of access to a site may determine the method of ground monitoring chosen. Rizkalla [5] pointed out that satellite based technologies may be more applicable than surveying techniques in remote sites.
10. Installations associated with a particular method must be designed to survive the environment in which they're being installed. As previously discussed elsewhere in this section some technologies may be susceptible to either damage by wildlife, third-party interactions, or weather/climate. As an example, there is little point to installing a slope inclinometer with stickup casings if it is going to be run over by frequent off road recreational traffic.
11. Consider the potential ground disturbance based issues with a particular method. As an example, a contractor cannot be left to install survey monuments unsupervised as they may contact the pipeline. In some cases, the ideal ground monitoring locations may be directly over the pipe, thus limiting their applicability.

A ground monitoring program should be correlated to the loading on the pipeline to allow for assessment of the fitness for service of the pipeline. Ground deformations can be related to pipeline loading using soil/pipe interaction models or using pipe monitoring techniques such as strain gauges or IMU smart pigging technologies, as previously discussed in this section.

A significant consideration when selecting a ground monitoring program is cost. As an example, a very robust ground monitoring program for a very large active deep-seated landslide could ideally include:

- Semi-annual site reviews by a geological engineer,
- Annual aerial LiDAR inspections with annual deformation analysis,
- GPS geodetic surveying with numerous monuments to verify the LiDAR results, and
- Several deep slope inclinometers to monitor the slip surface movements.

The operational budget may not allow for annual aerial LiDAR given the potential expense. The other three monitoring items would likely individually be an order of magnitude less expensive.

It is recommended that regardless of the ground monitoring program, some form of pipe monitoring should be implemented. This is also regardless of any soil to pipe modelling that has been conducted to relate ground deformations to pipe stress/strain. Generally, the more robust the pipe monitoring program, the less robust ground monitoring has to be.

The following guidance is given for pipe monitoring:

1. Where pipelines are piggable, it is always recommended that a baseline IMU run be established to allow for subsequent bending strain and/or movement analysis.
2. When reviewing smart pig data, particularly IMU data, special attention should be given to pipeline segments with known landslides and where landslides are likely to occur. Geohazard consultants may provide input into these areas as part of a baseline screening of a pipeline system, as discussed in section 2.
3. When using new technology, which may have some unknowns, always back it up with a proven method. An example would be using VW strain gauges to provide backup for a much more elaborate array of fiber-optic strain gauges.
4. When installing monitoring devices such as strain gauges on a pipeline, the owner/operator should always have some basis for the device locations, for example:
 - a. Landslide features: Slide boundaries, slide scarps, terrain changes, or slope breaks.
 - b. Settlement/subsidence features: Feature boundaries and areas of maximum or differential movements.
 - c. Smart pig geometry indications: Anomalous bends, buckles, wrinkles, ripples, and areas of pipeline movement.
 - d. Other smart pig indications: Areas of potential stress corrosion cracking (particularly circumferential cracking if there is a technology available to detect it).
 - e. Historic failure locations.
5. As discussed above (Item 7 in ground monitoring of Section 8.3.4), ensure that there is access to the data when you need it when dealing with remote or difficult to access sites.

6. As discussed in the introduction of the monitoring section, when selecting pipe monitoring methods one must consider site access and ground disturbance related issues. Additionally, when selecting smart pig based methods, issues such as throughput, flow restrictions, and operational availability must be considered.

Appendix E discusses newer pipe monitoring techniques which include several experimental techniques that will/could allow for the direct measurement of either the strain or stress within a pipeline. One of these techniques, the ACSM, has been mounted and tested on a smart pig platform. Over the next 20 years it is possible that a smart pig tool will be developed combining anomaly detection, bending strain, movement analysis, and stress/strain measurement. This would provide a one-stop assessment of fitness-for-service of a pipeline, if hazards such as debris flows, rock avalanches, and other rapid movements that could impact the pipeline system are adequately accounted for. These potential technological advances could greatly change how the monitoring of geohazards is approached.

Secondary issues that may impact or influence the selection of methods may include:

1. Potential third party interactions: As an example, a farmer mowing down all the stick-up protectors for a series of strain gauge installs. Other examples include incidents of vandalism or theft.
2. Potential livestock/animal interactions: Animals may chew, walk over/through, or rub against monitoring installations.
3. Potential weather impacts such as windthrow/blowdown interrupting power to a remote monitoring installation.
4. Potential access issues including:
 - a. Poor access conditions,
 - b. Steep slopes, and
 - c. Landowner issues, such as restrictions on the ability to install monitoring instruments.

8.3.5 Frequency of Data Collection and Analysis

Any program that includes both ground and pipe monitoring has three processes with an associated frequency. The processes are:

1. Data Sampling: Electronic, automated, or manual sampling rate for the monitoring device or method.
2. Data Collection: Retrieval of data from the monitoring installation/device.
3. Data Analysis: Expert review of collected data. In many cases, data may be collected and screened based on preset limits to determine if a subject matter expert data review/analysis/action is required.

For specialized tasks, such as smart pig runs, Lidar/InSAR studies, and geodetic surveys, the frequency for data sampling, collection, and analysis are the same.

Generally, the frequencies of any monitoring program are determined by following factors:

1. The rate of movement of a landslide (refer to Table 2-2 for a description of velocity class) which typically relates to the rate of straining on the pipeline within the landslide.
2. The potential for changes/accelerations in rates of movement. An example would be shallower landslides that accelerate during wetter seasons and/or following extreme rain events. Conversely, monitoring frequencies can typically be reduced during dryer times of year or in northern climates during winter. For larger movements, the onset of accelerated movements may be delayed. As an example, in some large deep seated translation slides with slip surfaces up to 400 ft (120 m) below the ground surface, acceleration can be delayed by up to 18 months. A comprehensive geotechnical understanding of the slide characteristics and local climatic variations is critical when designing a monitoring program. This includes the ability to predict significant movements from subtle precursor movements or behaviors.
3. The likelihood and/or consequences of either damage or rupture of a pipeline.
4. The overall efforts required to read monitoring installations. More accessible sites may have higher frequencies of monitoring simply because employees/contractors/consultants can visit the study area frequently.

Table 8-13 A general classification of monitoring frequencies

Class	Frequency	Comments
Near continuous	Every sub-second to every minute	Typically, real-time data that is monitored continuously
High	Every minute to every hour	Typically logged or remotely monitored data
Moderate	Every hour to every week	Typically logged or remotely monitored data, or manually read data for short durations
Low	Every week to every few months	Typically logged data or manually read data for longer monitoring periods
Very Low	Every year to every few years	Reserved for cases where low strain rates are encountered with low rates of movement or for expensive methods including: smart pig runs, Lidar/InSAR studies, and geodetic surveys

There are several ways of collecting the data which include:

1. **Continuous/Remote:** Full time access to collected data via either a land line, cellular, or satellite link directly to the company computer system or via an internet service. Automated data collection is typically only available for electronic monitoring devices.
2. **Logged:** Data collected from a logging unit connected to monitoring installation (i.e. strain gauge or in-place inclinometer). The logged data are manually downloaded during a field visit at an assigned frequency, or remotely downloaded as with Continuous/Remote data collection.
3. **Manual:** Data collected by field personnel visiting the site. An example would be a crew annually reading a strain gauge.

With many monitoring programs, different methods may have different sampling, collection, and analysis frequencies. As an example, for the monitoring of a deep seated translational slide where no physical mitigation work has taken place (Figure 8-38), Table 8-14 provides details of a hypothetical monitoring program:

Table 8-14 Monitoring frequencies for a hypothetical monitoring program

Example Situation/Scenario of Deep Seated Translational Slide Loading	Frequency of Data		
	Sampling	Collection	Analysis
Remote monitoring of VW strain gauges at key strain locations (slide flanks and at boundaries of separate moving blocks within slide mass)	Near continuous	Near continuous	Low (Monthly*)
VW strain gauges at less critical locations with data loggers with biannual collection of data	Moderate	Low	Low
Slope Inclinomometer readings taken by field crew after spring and fall wet seasons	Low	Low	Low (Annual)
Geodetic survey	Very Low - Annual		
Visual Monitoring (Annual review of site by geological engineer)	Very Low- Annual		
Run-to-run smart pig geometry tool run	Very Low - Triennial (once every 3 years)		
Run-to-run smart pig axial strain tool run	Very Low - Quinquennial (once every 5 years)		

*Unless a pre-set limit or condition is exceeded then immediate data analysis is required

It is always recommended to start out with a higher frequency monitoring program (data sampling, collection, and analysis) and reduce the frequency based on analysis of the initial and ongoing data. There should be provisions for accelerating monitoring in the event of unexpected events including high precipitation, unexpected slide accelerations, or earthquakes. When determining the sampling/collection/analysis frequencies for any program, the most important factor to consider is ensuring that any event that could potentially compromise the integrity of a pipeline is detected in a timely manner.

While it is always favorable to err on the side of collecting too much data as opposed to too little, it should be cautioned that excessive data collection may cause secondary problems with data storage and analysis. As an example, in an extremely slow moving deep seated translational landslide, logging VW strain gauge readings every 20 seconds would be considered excessive although the logger’s memory would allow it. The number of collected readings would provide little (if any) additional insight into the landslide behavior, and would make data processing and analysis unnecessarily complicated and difficult. Readings every 6, 12, or 24 hours would be sufficient. Project managers should also consider the issues of data storage and retention when designing a monitoring program. Typically, data are stored for the entire duration for which the pipeline is in service.

9 Overall Management Process

Abstract

The first part of this section covers the limits on longitudinal stress and strains in relevant standards, i.e., ASME B31.4 and B31.8. The meaning of the standard language is explained when needed. This part is considered necessary if an operator chooses to follow the limits set in those standards. As explained in Section 1.1, longitudinal stress limits are typically not actively managed in pipelines except in locations where high longitudinal stresses or strains are expected. In fact one might find the longitudinal compressive stress limit overly restrictive. The regulatory requirements on managing longitudinal stresses are perhaps a grey area.

The next part of this section answers some frequently answered questions, such as

- (a) Acceptance of FFS assessment for in-service pipelines,*
- (b) Effectiveness of hydrostatic tests in exposing girth weld flaws, and*
- (c) Differences in key drivers of girth weld failures between vintage and relatively new pipelines.*

The main part of this section is the overall integrity management process. While the integrity management from the viewpoint of geotechnical engineers is covered in Section 2, this section focuses on quantitative assessment using FFS principles. The purpose of the assessment is broadly divided into two parts: (1) screening or ranking the locations of interest, e.g., locations of high strains or (2) site-specific assessment to determine the risk of failure and mitigation measures.

For the screening and ranking part, the following critical issues are covered

- (a) Default reporting threshold for IMU tools, and*
- (b) Classification of locations of high strains.*

The next part covers determination of strain capacity (both tensile and compressive) and strain demand limits. This information can be used in both screening/ranking and site-specific assessment. Appropriate FFS assessment procedures are recommended, depending on the mode of loading and the magnitude of strain demand.

For site-specific assessment, the application of the FFS assessment procedures is linked to the potential level of impact if an event were to occur. The recommended default values of input parameter for FFS assessment are set to produce different levels of conservatism. The higher the level of impact, the more conservative the assessment outcome becomes. These default values can be replaced when site-specific values are known.

The section closes with situations where specialized analysis or procedures may be warranted.

9.1 Longitudinal Stress and Strain Limits in Standards

9.1.1 Limits on Longitudinal Stress

9.1.1.1 ASME B31.4-2012

Clause 403.3.1 Strength Criteria (under 403.3 Criteria to Prevent Yield Failure) states

“The maximum longitudinal stress due to axial and bending loads during installation and operation shall be limited to a value that prevents pipe buckling or otherwise impairs the serviceability of the installed pipeline. Other stresses resulting from pipeline installation activities, such as spans, shall be limited to the same criteria. Instead of a stress criterion, an allowable installation strain limit may be used. Stress values for steel pipe during operation shall not exceed the allowable values in Table 403.3-1 as calculated by the equations in this Chapter.”

Table 403.3.1-1 referenced above is duplicated as Table 9-1 below.

Table 9-1 Allowable stress values in Table 403.3.1-1 of B31.4-2012

Table 403.3.1-1 Allowable Values for Pipeline System Stresses

Location	Internal and External Pressure Stress, S_H	Allowable Expansion Stress, S_E	Additive Longitudinal Stress, S_L	Sum of Longitudinal Stresses from Sustained and Occasional Loads	Equivalent Combined Stress, S_{eq}	Effective Stress for Casing or Uncased Pipe at Road or Railroad Crossings
Restrained pipeline	$0.72(E)S_Y$	$0.90S_Y$	$0.90S_Y$ [Note (1)]	$0.90S_Y$	$0.90S_Y$	$0.90S_Y$ [Note (2)]
Unrestrained pipeline	$0.72(E)S_Y$	S_A [Note (3)]	$0.75S_Y$ [Note (1)]	$0.80S_Y$	n/a	$0.90S_Y$ [Note (2)]
Riser and platform piping on inland navigable waters	$0.60(E)S_Y$	$0.80S_Y$	$0.80S_Y$	$0.90S_Y$	n/a	n/a
Slurry pipelines	$0.80(E)S_Y$	n/a	n/a	n/a	n/a	n/a

GENERAL NOTES:

- (a) S_Y = specified minimum yield strength of pipe material, psi (MPa)
- (b) E = weld joint factor (see Table 403.2.1-1)
- (c) In the setting of design factors, due consideration has been given to and allowance has been made for the underthickness tolerance and maximum allowable depth of imperfections provided for in the specifications approved by the Code.
- (d) S_L in the table above is the maximum allowable value for unrestrained piping calculated in accordance with para. 402.6.2. The maximum value of S_L for restrained pipe is calculated in accordance with para. 402.6.1.
- (e) See para. 403.10 for allowable stresses of used pipe.

NOTES:

- (1) Beam-bending stresses shall be included in the longitudinal stress for those portions of the restrained or unrestrained line that are supported above ground.
- (2) Effective stress is the sum of the stress caused by temperature change and from circumferential, longitudinal, and radial stresses from internal design pressure and external loads in pipe installed under railroads or highways.
- (3) See para. 403.3.2.

The majority of a pipeline length in buried onshore pipelines should be qualified as “Restrained Pipeline.” Limits in columns “Allowable Expansion Stress, S_E ”, “Additive Longitudinal Stress, S_L ”, “Sum of Longitudinal Stresses from Sustained and Occasional Loads”, and “Equivalent Combined Stress, S_{eq} ” are relevant to the longitudinal stress limit.

The term “Additive Longitudinal Stress, S_L ” refers to the stress generated by the restraint of thermal expansion or contraction, internal pressure and sustained loads. The stress can be determined following the equation in Sections 402.6.1 and 402.6.2 of ASME 31.4-2012. For restrained pipes, the maximum allowable value is $0.90S_Y$, where S_Y is the specified minimum

yield strength of pipe material (SMYS). The term “Sum of Longitudinal Stresses from Sustained and Occasional Loads” refers to the sum of “additive longitudinal stress” plus the stress generated by occasional loads. The maximum allowable value for restrained pipes is $0.90S_y$. The “occasional loads” are those generated “occasionally” such as “subsidence, differential settlement, frost heave and thaw settlement” as described in Section 401.1.3 of ASME B31.4-2012.

9.1.1.2 ASME B31.8-2010

Specifications on the longitudinal stress limits are provided in Section 833 Design for Longitudinal Stress. The sum of longitudinal stresses in restrained pipe is limited to $0.9 \times SMYS \times$ temperature derating factor. When the temperature derating factor is 1.0, the limit on the sum of longitudinal stresses is the same as that in ASME B31.4-2012.

A separate combined stress criterion is also given for restrained pipe. The effective combined stress may be computed with either shear or Mises criterion, similar to ASME B31.4-2012. The limit on the effective combined stress is $0.9 \times SMYS \times$ temperature derating factor for *loads of long duration* or $1.0 \times SMYS \times$ temperature derating factor for *occasional nonperiodic loads*, respectively. When the temperature derating factor is 1.0 and the load of long duration is considered, the effective combined stress criterion is the same as that in ASME B31.4-2012.

9.1.1.3 Summary on the Longitudinal Stress Limits

When the temperature derating factor is 1.0, the longitudinal stress limits in B31.8-2010 are the same as those in B31.4-2012. The longitudinal stress limits for pipelines of various design factors is shown in Table 9-2 [102].

Table 9-2 Longitudinal stress limits of ASME B31.4-2012 and B31.8-2010

Hoop Stress / SMYS	Additive Longitudinal Stress / SMYS	Sum of Longitudinal Stresses from Sustained and Occasional Loads / SMYS	Longitudinal stress / SMYS from Equivalent Combined Stress Criterion				Final Allowable Longitudinal Stress / SMYS, Excluding Occasional Loads	
			Tensile Longitudinal Stress / SMYS		Compressive Longitudinal Stress / SMYS			
			Shear Stress Criterion	Mises Stress Criterion	Shear Stress Criterion	Mises Stress Criterion	Tensile	Compressive
0.72	0.90	0.90	1.62	1.01	0.18	0.29	0.90	0.29
0.60	0.90	0.90	1.50	1.03	0.30	0.43	0.90	0.43
0.50	0.90	0.90	1.40	1.04	0.40	0.54	0.90	0.54

Note: The “Final Allowable Longitudinal Stress” in the right two columns is computed using von Mises criterion, not the shear stress criterion. The allowable compressive longitudinal stress would be lower if computed by the shear stress criterion.

Both B31.4-2012 and B31.8-2010 require the equivalent combined stress be less than $0.90 \times SMYS$. The equivalent combined stress may be calculated using either Von Mises or Tresca criterion. Figure 9-1 and Figure 9-2 show the relationships between the equivalent

combined stress (either Von Mises or Tresca) and the longitudinal stress when the hoop stress is kept at 72% yield strength. When the equivalent combined stress is limited to $0.9 \times SMYS$, the highest allowable compressive longitudinal stress is approximately $0.29 \times SMYS$ under Von Mises criterion and $0.18 \times SMYS$ under Tresca criterion. These are very lower compressive stress limits. The allowable compressive stress can be increased if the criterion is set at plastic collapse, i.e., when the equivalent stress reaches materials' flow stress [102].

The highest allowable tensile longitudinal stress is approximately $1.01 \times SMYS$ under Von Mises criterion and $0.90 \times SMYS$ under Tresca criterion. However, the "additive longitudinal stress" is limited to $0.90 \times SMYS$. Therefore, the maximum longitudinal stress is limited to $0.90 \times SMYS$ when both the additive longitudinal stress and equivalent combined stress criteria are applied.

In contrast to the design phase of a pipeline, loads from subsidence, differential settlement, frost heave and thaw settlement cannot be treated as occasional loads if they are known to exist in the integrity assessment of a particular segment of an in-service pipeline.

The allowable longitudinal stress limits are appropriate for load-controlled loading, such as sustained loading from the self-weight over a span. They can be overly conservative or limiting when bending stress is present in buried pipeline which is fully supported, i.e., when the bending can be considered displacement-controlled. The longitudinal strain limits are addressed in the next section.

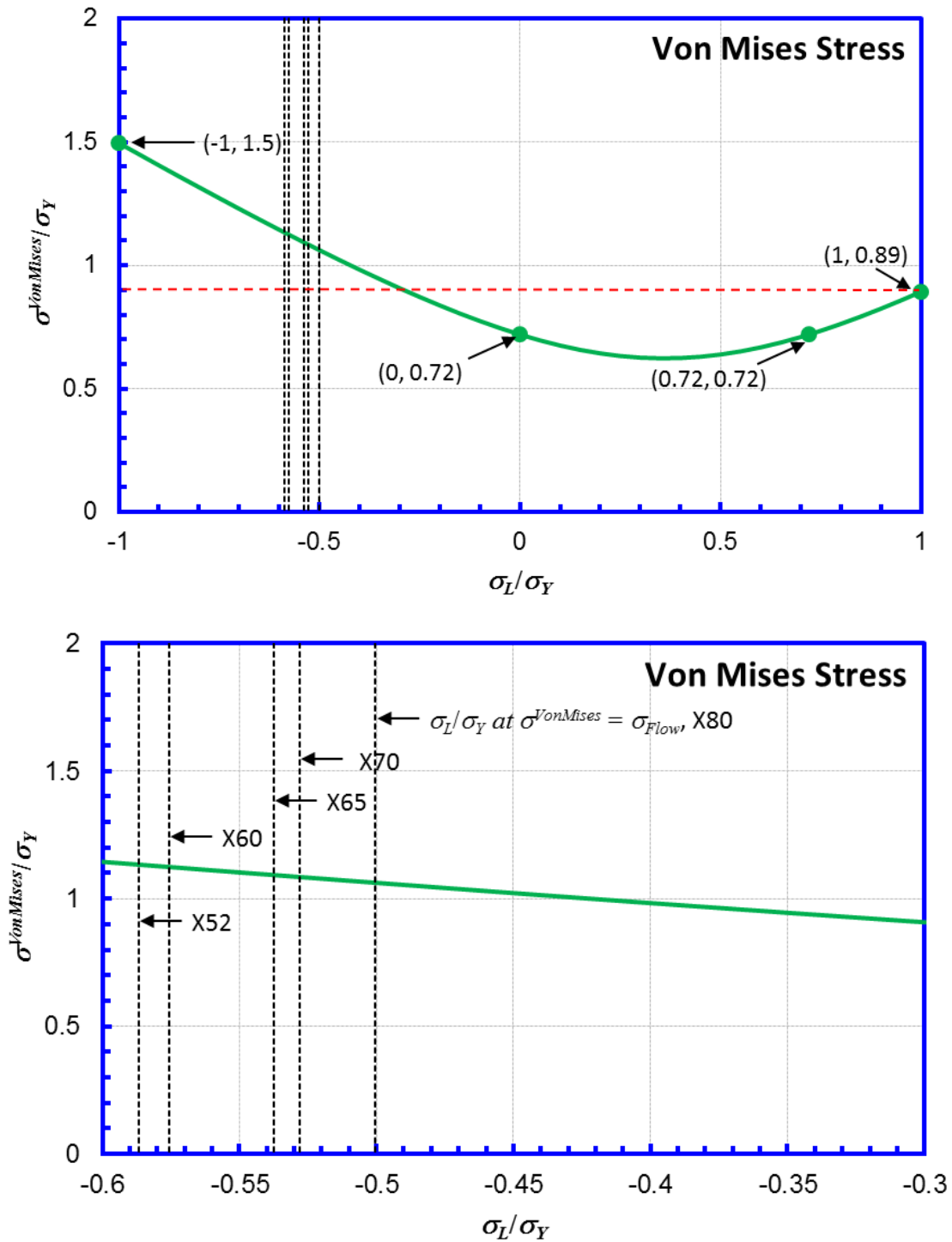


Figure 9-1 Variation of Von Mises Stress as a function of longitudinal stress when the hoop stress is at 72% yield strength. The bottom figure is a zoomed-in version of a part of the top figure. The vertical lines represent the maximum compressive stress the material can tolerate before plastic collapse.

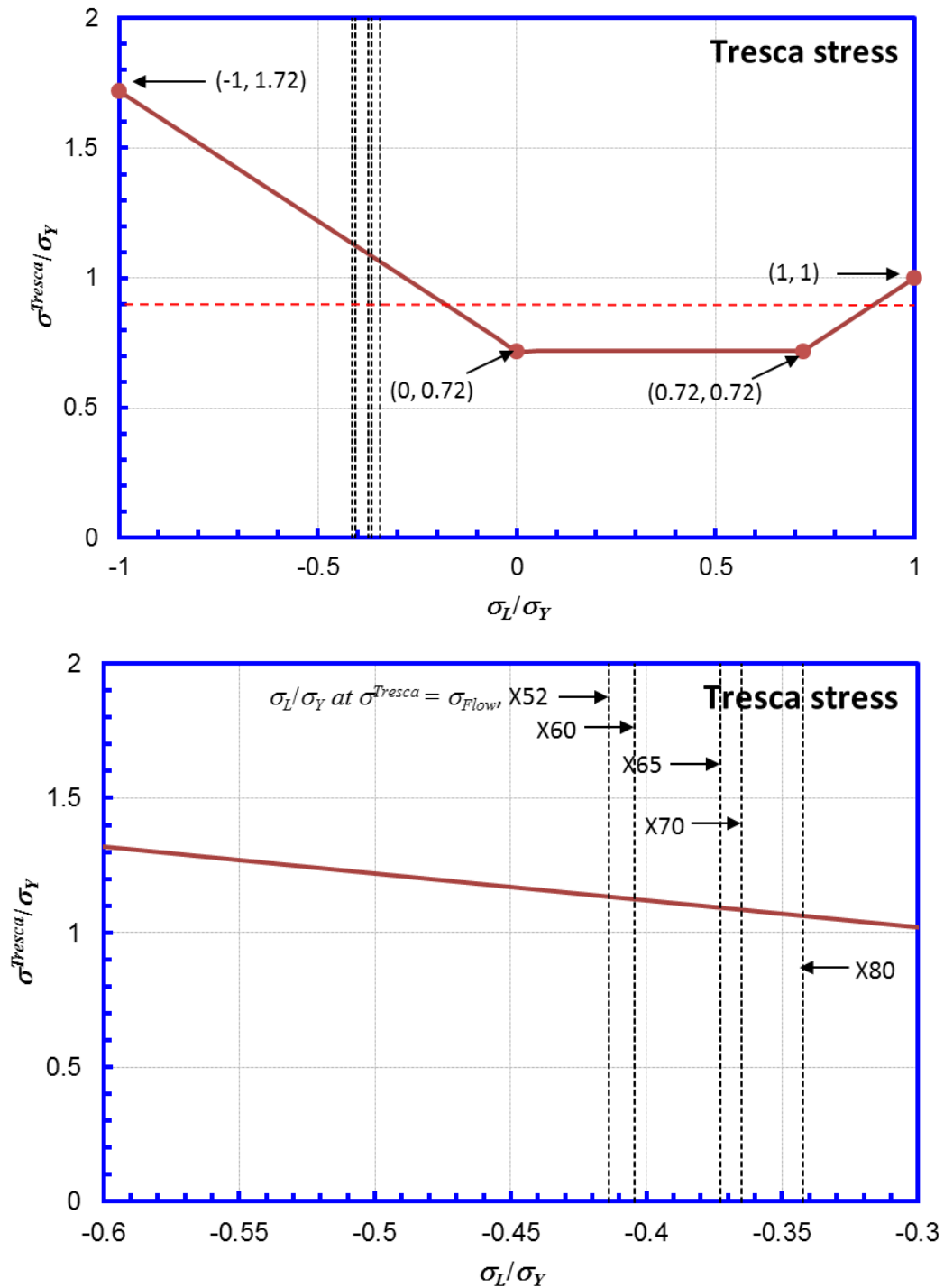


Figure 9-2 Variation of Tresca Stress as a function of longitudinal stress when the hoop stress is at 72% yield strength. The bottom figure is a zoomed-in version of a part of the top figure. The vertical lines represent the maximum compressive stress the material can tolerate before plastic collapse.

9.1.2 Limits on Longitudinal Strain

9.1.2.1 Requirements in Current Standards

ASME B31.4-2009 Clause 403.3.3 Strain Criteria for Pipelines states:

“When a pipeline may experience a noncyclic displacement of its support (such as fault movement along the pipeline route or differential support settlement or subsidence along the pipeline), the longitudinal and combined stress limits may be replaced with an allowable strain limit, so long as the consequences of yielding do not impair the serviceability of the installed pipeline. The permissible maximum longitudinal strain depends upon the ductility of the material, any previously experienced plastic strain, and the buckling behavior of the pipe. Where plastic strains are anticipated, the pipe eccentricity, pipe out-of-roundness, and the ability of the weld to undergo such strains without detrimental effect should be considered. Maximum strain shall be limited to 2%.”

ASME B31.4-2012 Clause 403.3.3 Strain Criteria for Pipelines states (unchanged from 2009 version):

“When a pipeline may experience a noncyclic displacement of its support (such as fault movement along the pipeline route or differential support settlement or subsidence along the pipeline), the longitudinal and combined stress limits may be replaced with an allowable strain limit, so long as the consequences of yielding do not impair the serviceability of the installed pipeline. The permissible maximum longitudinal strain depends upon the ductility of the material, any previously experienced plastic strain, and the buckling behavior of the pipe. Where plastic strains are anticipated, the pipe eccentricity, pipe out-of-roundness, and the ability of the weld to undergo such strains without detrimental effect should be considered. Maximum strain shall be limited to 2%.”

ASME B31.8-2010 Clause 833.5, Design for Stress Greater Than Yield, states:

“(a) The limits in paras. 833.3 and 833.4 may be exceeded where due consideration is given to the ductility and strain capacity of seam weld, girth weld, and pipe body materials; and to the avoidance of buckles, swelling, or coating damage and (b) The maximum permitted strain is limited to 2%.”

In Chapter VIII Offshore Gas Transmission of ASME B31.8-2010, Clause A842.2.3 Alternate Design for Strain states:

“In situations where the pipeline experiences a predictable noncyclic displacement of its support (e.g., fault movement along the pipeline route or differential subsidence along the line) or pipe sag before support contact, the longitudinal and combined stress limits need not be used as a criterion for safety against excessive yielding, so long as the consequences of yielding are not detrimental to the integrity of the pipeline. The permissible maximum longitudinal strain depends on the ductility of the material, any previously experienced plastic strain, and the

buckling behavior of the pipe. Where plastic strains are anticipated, the pipe eccentricity, pipe out-of-roundness, and the ability of the weld to undergo such strains without detrimental effect should be considered. Similarly, the same criteria may be applied to the pipe during construction (e.g., pull-tube or bending shoe risers).

9.1.2.2 Significance of the Terms in Currents Standards

B31.4 limits the possible use of the strain criteria to noncyclic displacement of its support. B31.8 Clause 833.5 places no such limit. However, such a limit is placed in the offshore chapter Clause A842.2.3. From the integrity viewpoint, the displacement of the support should probably be limited to noncyclic in order to use the strain criterion. Cyclic displacement of the support may involve fatigue damage to pipelines which does not appear to be addressed in those clauses about strain limits. Both B31.4 and B31.8 require the consideration of ductility (and strain capacity) of welds (seam and girth welds), pipe body material, and the avoidance of buckling. B31.4 further requires the consideration of prior plastic strain history and serviceability of the pipelines, while B31.8 requires the consideration of swelling and coating damage. Taken as a whole, the language in the standards provides a good overview of various factors that must be considered when pipelines are expected to experience high longitudinal strain. On the other hand, the standards do not provide specific conditions by which the strain limits of 2% are attainable. The offshore chapter of B31.8 does not provide a specific permissible strain limit.

It is clear that both B31.4 and B31.8 permit longitudinal stresses higher than those specified by the stress criteria, provided that the displacement of the support is noncyclic and the integrity of critical components, such as welds, is assured.

9.2 Acceptance of FFS Assessment for In-Service Pipelines

The application of FFS assessment for pipeline girth welds is not universally accepted or practiced. Some of the reservations arise from the way the FFS assessment is applied in new pipeline construction projects. An example of such application in new pipeline construction is the use of the alternative flaw acceptance criteria outlined in API 1104 Annex A. Broadly speaking, API 1104 Annex A contains three parts: (1) welding procedure qualification, (2) determination of maximum acceptable flaw dimensions, and (3) field implementation in conjunction with NDT. In part I of the process, welds are made with precisely prescribed welding parameters on pipe steels with limited ranges of chemical composition. The welds are then tested for mechanical properties. These mechanical properties are then used as inputs in the determination of the maximum acceptable flaw dimensions, i.e., part II of the process. The same precisely prescribed welding parameters are enforced in field construction. As such the welds from field construction are expected to have the “same” mechanical properties as the welds tested in initial procedure qualification. The fundamentals of part II are from well accepted fracture mechanics principles. In part III of the process, NDT techniques are qualified to ensure the flaws in construction welds are not under-sized.

When FFS assessment is applied to in-service welds, there is no practice or record that establishes the equivalence of mechanical properties between the qualification welds and field production welds. In other words, the mechanical properties of the field welds are unknown.

The challenges facing the pipeline industry in assessing in-service welds are not unique to this industry. When FFS assessment is applied in other industries, the general practice is using lower or upper bound properties that would lead to conservative estimation of the structure integrity of the welds being assessed. The less is known about the mechanical properties of a particular weld, the greater is the conservatism applied in the input parameters. The same philosophy of performing FFS assessment is applicable to the pipeline industry in assessing the girth welds of in-service pipelines. FFS assessment can be applied; but the accuracy of such assessment depends on how well the available data represent the actual welds being assessed. The extensive test data presented in Section 5 and similar data that being updated in the future should greatly help the FFS assessment.

In the draft Integrity Verification Process (IVP) issued by US DOT PHMSA, ECA or FFS assessment is listed a viable option in IVP [275]. However, there is no clear guidance in the industry for using FFS that would be acceptable to PHMSA.

9.3 Effectiveness of Hydrostatic Testing in Exposing Poor-Quality Girth Weld

The effectiveness of hydrostatic test in exposing poor-quality girth welds may be assessed through an example. If an X52 pipeline operating at 72% SMYS is hydrostatically tested to 90% SMYS, the additional tensile longitudinal stress ((i.e., the difference between operating and hydrostatic test conditions) imposed on the girth weld is 2.8 ksi ($0.18 \times 52 \times 0.3 = 2.8$), or 5.4% of SMYS. In contrast, every 5 °C (9 °F) drop of pipe temperature would produce an additional tensile longitudinal stress of 1.8 ksi, or 3.5% SMYS. A temperature drop of 7.8 °C (14.0 °F) produces the same magnitude of additional tensile longitudinal stress as the hydrostatic pressure test (2.8 ksi). Consequently, hydrostatic test pressure alone is not an effective way to “weed-out” poor quality girth welds unless the girth welds already have a leak path or are very close to failure under normal operational conditions. More importantly, a large temperature drop in the pipe can produce much greater tensile longitudinal stress than a hydrostatic pressure test, thus overwhelming any margin a hydrostatic test may have introduced.

9.4 Potential Drivers to Failure in Vintage versus Modern Girth Welds

Prior to about mid- to late 1960s, SMAW welds were made to linepipe steels with relatively high carbon content (pre microalloying and TMCP steels). The field inspection practice was uneven at that time. The principal risk to girth weld integrity was the existence of large flaws after construction, such as hydrogen cracks. The strength of the weld metal can be lower than the actual strength of the pipe. In most cases, the weld cap reinforcement served to compensate the effect of weld strength undermatching. The strength of HAZ is comparable to the strength of pipe, sometimes slightly lower and other times slightly higher.

After mid- to late 1960s, there was a switch to microalloyed TMCP steels that had lower carbon content. The industry started to practice 100% girth weld inspection at about the same time. Consequently the incidents of large post-construction flaws in pipe installed after the late

1960s should be diminished substantially. This practice may not remove the possibility of delayed hydrogen cracking entirely, though. The factors that can have negative impact on girth weld integrity are more likely weld strength undermatching, HAZ softening, and reduced strain hardening capacity of the linepipe steels. There is evidence that the actual strength of the linepipes can be substantially higher than the SMYS. As welds are qualified by pipes' specified minimum strength, weld strength undermatching is more likely as the higher strength linepipes see widespread use.

The trends described above are meant to be an overall reflection of the industry practice and consequence. Circumstances around an individual pipeline, or even a small segment of a long pipeline, can deviate from the general trends.

9.5 Overall Integrity Management Process

This section covers the integrity management process that focuses on quantitative assessment using FFS principles. The purpose of the assessment can be either (1) screening or ranking the locations of interest, e.g., locations of high strains or (2) site-specific assessment to determine the risk of failure and mitigation measures.

The integrity of a pipeline can be assessed by comparing strain demand with strain capacity. Locations with the smallest difference between strain capacity and strain demand pose the highest risk. This difference can be measured in terms of either absolute difference between strain capacity and strain demand or the ratio of strain capacity over strain demand. High strain locations that are flagged in initial screening can be ranked or prioritized on the basis of strain difference.

9.5.1 Screening and Ranking of High Strain Locations

The identification of locations of interest or segments of a pipeline experiencing high strains from a geotechnical viewpoint is described in Section 3. This section covers the screening using instrumentation that is capable of measuring longitudinal strains.

9.5.1.1 Screening for High Strain Locations

One of the key decision points in the screening process is the threshold strain above which a segment would be called a location of interest. To establish this threshold, one must consider (1) the starting point, or baseline strain, of the measurement and (2) strain components a tool can and cannot pick up. For instance, IMU tools have certain limitations as described in Section 4.4.

Using IMU tools as an example for strain measurement, the determination of reporting threshold for assessing the limit state of tensile strain rupture is described below.

9.5.1.1.1 *Default Strain Capacity of Girth Welds*

The experimental data in Section 5 show that the tensile strain capacity of SMAW welds fabricated in 1940-1960s can be as low as 0.2-0.3% and as high as >2.0%. The analysis welding procedure qualification requirements in API 1104 shows that welds can have a strain capacity as low as 0.2-0.3% even when they are fully API 1104 compliant. Pipeline design standards, e.g., ASME B31.4 and B31.8, put the longitudinal stress limit at 90% SMYS. This stress limit is

equivalent to approximately 0.20% strain for X65 and X70 pipelines. Therefore the default lower bound strain capacity is 0.20-0.30%.

9.5.1.1.2 *Default Baseline Strain Not Included in IMU Strain Measurement*

Strains from internal pressure and temperature differential would result in uniform longitudinal strain, not bending strain. Such strain is not picked up by IMU. With the addition of other stresses from construction, a baseline strain of approximately 0.10% may not be picked up by IMU, see Table 3-1.

9.5.1.1.3 *Default Threshold for IMU Report*

The default threshold is the difference between the default strain capacity and the baseline strain not being picked up by IMU. Based on the above analysis, this value is 0.10-0.20%.

9.5.1.2 Ranking of High Strain Locations

Once locations of interest are identified, they can be further ranked based on the amplitude of the strain and the strain difference between strain demand limit and strain demand. The *strain demand limit* is the strain capacity multiplied by a safety factor that is less than 1.0. The strain capacity may be determined using FFS assessment procedures as described in Section 7. The safety factor is discussed in Section 9.5.3.

The proposed ranking of high strain locations is given in Table 9-3. A higher level of classification is related to higher level of strain demand and smaller difference (margin) between strain demand limit and strain demand. This table is broadly consistent with PHMSA's strain-based design (SBD) special permit conditions for maintenance of pipelines constructed on SBD principles [276].

Table 9-3 Ranking of high strain locations

Level of Classification	Range of Strain Demand	
	Lower End	High End
1	0.25% strain	50% of strain demand limit, or 0.50% strain, whichever is smaller
2	50% of strain demand limit, or 0.50% strain, whichever is smaller	75% of strain demand limit, or 0.75% strain, whichever is smaller
3	75% of strain demand limit, or 0.75% strain, whichever is smaller	100% of strain demand limit, if the strain demand would not increase before remediation

9.5.2 Determination of Strain Capacity

9.5.2.1 Tensile Strain Capacity

9.5.2.1.1 *Low Strain Demand*

Stress-based assessment procedures should be used if any one of following conditions exists:

- (1) Compliance to the longitudinal stress limits (maximum longitudinal stress = $0.90 \times \text{SMYS}$) in ASME B31.4 or B31.8 is necessary, or
- (2) The loading is load-controlled.

Assessment procedures:

The assessment procedures that may be used are

- API 1104 Annex A,
- CSA Z662 Annex K,
- API 570/ASME FFS-1,
- BS 7910, or
- Other equivalent procedures.

The basis and applicability of those procedures are described in Section 7.2.

9.5.2.1.2 *Moderate to High Strain Demand*

Strain-based assessment procedures should be used if any one of the following conditions exists:

- (1) Conditions are beyond those required for using the stress-based procedures, or
- (2) Strain demand is equal or higher than 0.2% strain.

One or a combination of the following assessment procedures may be used:

- Procedures from PRCI project SIA-1-7 (vintage pipelines with manual girth welds moderate to high strain),
- PRCI-CRES tensile strain modes (modern pipelines with mechanized or manual girth welds, strain > 0.75%), or
- Other equivalent procedures.

9.5.2.2 Compressive Strain Capacity

The compressive strain capacity (CSC), as customarily defined now, is only relevant to load controlled loading from the viewpoint of structural integrity. If the loading is displacement controlled, strains greater than the CSC can be tolerated without immediate failure. More on the relevance of CSC and short- and long-term consequence of compressive strain are discussed in Section 7.4.2.

9.5.2.2.1 *Load-Controlled Loading*

If the loading is load controlled, the compressive stress or strain capacity may be established by using

- the longitudinal stress limits in ASME B31.4 or B31.8, or
- CSC equations as described in Section 7.4.3.

As described in Section 9.1.1.3, the compressive stress limit from ASME B31.4 or B31.8 for pipelines in Class 1 locations can be very low. The use of CSC equations is more practical. More on the longitudinal stress limits and assessment of load-controlled events, such as spans, can be found in a paper by Wang, et al. [102].

9.5.2.2.2 *Displacement-Controlled Loading*

If a pipe segment is under displacement loading, the pipe/weld can usually tolerate strains much higher than that given by the CSC equations (Section 1.2). There is consensus in the industry that the strain limits set by the CSC equations may be overly conservative for displacement-controlled loading. However, there is no consensus on the appropriate strain limits beyond those given by the CSC equations. Evidence from field, numerical analysis, and experimental tests suggest that a compressive strain as high as 2% can be tolerated at least in a short term [277]. The long-term impact of high compressive strain is a subject of current and future research, see Section 10.3.

9.5.3 Safety Factor and Strain Demand Limit

As introduced in Section 9.5.1.2, the strain demand limit is the strain capacity multiplied by a factor of less than 1.0. Since reaching the tensile and compressive limit states has different consequences, the safety factors on those two limit states are set differently.

9.5.3.1 Safety Factor on Tensile Rupture

Curved wide plate and full-scale experimental tests have shown that the measured tensile strain capacity can differ by a factor of two under “identical” material, geometric, and flaw conditions [185]. Assuming the predicted tensile strain capacity by tensile strain models is in the middle of the low- and high-end capacity of the experimental measurement, the low-end strain capacity would be 1/1.5 of the predicted value. In order to have the predicted strain capacity equal to the lower-end strain capacity, the safety factor of 1/1.5 should be applied to the predicted value. Consequently, the appropriate safety factor is 0.67 ($=1/1.5$). PHMSA’s SBD SP conditions have a safety factor of 0.60 [276]. CSA Z662 Annex C on limit state design has a resistance factor that is equivalent to a safety factor of 0.70. Here a safety factor of 0.67 is recommended.

9.5.3.2 Safety Factor on Compressive Buckling

CSA Z662 Annex C sets the safety factor for compression strain capacity at 0.80. PHMSA’s SBD SP conditions also use a safety factor of 0.80. Therefore a safety factor of 0.80 is recommended for compressive buckling assessment.

9.5.3.3 Alternative Approach to Setting Strain Demand Limit

Setting the strain demand limit by applying a fixed safety factor to strain capacity as described above has some disadvantages. For instance, if a girth weld has a tensile strain capacity of 0.80%, the tensile strain limit would be 0.56%, giving a margin between the strain capacity and strain demand limit of 0.24%. In contrast, if a girth weld has a tensile strain capacity of 3.0%, the strain demand limit would be 2.1%, giving a margin between the strain capacity and strain demand limit of 0.9%. The first weld has lower strain capacity, thus may be interpreted as being an inferior weld to the second weld. The accuracy and repeatability required to capture the strain difference of 0.24% are higher than to capture the strain difference of 0.9%. Since the first weld has a relatively low strain capacity, it may be interpreted that greater scrutiny is needed for this weld. Therefore, maintaining a minimum difference between the strain

capacity and strain demand limit can be advisable. For instance, the tensile strain demand limit may be set as lower of (1) strain capacity multiplied by 0.7 and (2) strain capacity minus 0.25% strain.

9.5.4 Site-Specific Assessment

9.5.4.1 Level of Impact

In order to perform a quantitative assessment of the strain capacity at a location of interest, many material and geometric parameters are needed. In addition, the type and dimensions of possible flaws in girth welds are necessary input to an assessment. Experimental testing and data analysis have revealed that there are large ranges of those parameters for in-service pipelines built in past several decades. In most cases, the precise values of those parameters are unknown for a location of interest.

Recommendations of critical input parameters for estimating tensile strain capacity are given in three levels related to the impact of a potential *event*. The event can be defined by the pipeline operators and/or other stakeholder for a particular situation. In broad terms, an event can be (a) a restriction to the passage of ILI pigs, (b) formation of wrinkles that may create either short-term or long-term negative consequence, (c) a leak, (d) a rupture, or (e) any other change of the physical characteristics of the pipeline that the operator or other stakeholders may find unacceptable.

- *Level 1 High impact – worst case analysis*: an event may cause serious damage to environment, properties, or human life. Worst-case scenarios are assumed for all parameters.
- *Level 2 Medium impact - nominal analysis*: an event can cause damage, but manageable in comparison to accepted risk management. Values of input parameters are selected to produce nearly worst-case scenarios, but not the absolute worst-case scenarios. This level is meant to cover most situations.
- *Level 3 Low impact – analysis to produce most likely occurring scenario*: an event, if occurs, would have minimal damage to environment, properties, and human life. The input parameters are selected to represent the mostly likely values.

9.5.4.2 Recommended Default Values

The default values of critical parameters for estimating tensile strain capacity are given in Table 9-4. The default values are meant for estimating tensile strain capacity when site-specific data are not available. The values can be replaced with site-specific values if they are available.

Table 9-4 Recommended default values of input parameters for estimating tensile strain capacity

Parameter	Characteristics		Impact Level 1	Impact Level 2	Impact Level 3
Pipe Y/T	Pipe/Weld prior to Mid-1960's		0.75	0.70	0.65
	Pipe/Weld after Mid-1960's		0.93	0.90	0.90
Weld Strength Mismatch Ratio	Pipe/Weld prior to Mid-1960's		0.75	0.90	0.90
	Pipe/Weld after Mid-1960's	SMAW	0.75	0.90	0.90
		Mechanized GMAW	0.80	0.90	1.00
Apparent Toughness (mm)	Pipe/Weld prior to Mid-1960's		0.3	0.5	0.7
	Pipe/Weld after Mid-1960's	SMAW	0.3	0.5	0.7
		Mechanized GMAW	0.6	0.8	1.0
Flaw Height (mm)			WT-2.5	3.0	2.0
Flaw Length	Pipe/Weld prior to Mid-1960's	No inspection record, or inspection not done			
		Inspected to API 1104	25.4	25.4	25.4
	Pipe/Weld after Mid-1960's	SMAW			
		Inspected to API 1104	25.4	25.4	25.4

9.5.5 Situations Necessitating Specialized Analysis

Girth welds having highly undermatching weld metal (> 20%) have been shown to exist in both vintage and modern pipelines. Pipelines built with microalloyed TMCP steels may also have high levels of HAZ softening as described in Appendix D. These material features can severely limit the tensile strain capacity of a girth weld.

Wrinkles under fatigue loading, if such load exists, may require specialized analysis. One of such example is given in Reference [277].

9.5.6 Monitoring after Assessment

Mitigation may be implemented after the strain locations of interest are identified. Mitigation can also be performed after further quantitative assessment. If the assessment shows that the pipe segment is safe to avoid an immediate intervention, the same assessment procedures can be used to define future intervention criteria before the segment reaches a limit state. The intervention criteria should be high enough to avoid unnecessary interventions/repairs but still low enough to allow time to schedule and execute a field intervention/repair before the strain reaches a limit state. This assumed the locations of interest are subject to ongoing monitoring and that the rate of strain accumulation can be estimated and/or projected.

10 Issues Not-Addressed in This Project

Abstract

Managing ground movement hazards for pipelines involves multiple disciplines of science and engineering. The most effective solutions to a particular issue may lie at the intersection among those disciplines. Although this report is intended to be comprehensive, the scope of the problems is so broad that some important considerations are not covered in this report. Furthermore, progress is being made in our understanding of the issues and tools available to address those issues. This section highlights a few notable issues that are not adequately addressed in this report, with due to the limits on the intended scope of work or lack of understanding of the issues. In some cases, gaps exist due to the lack of recognition of the issues, while solutions to fill the gaps may already be available. Whenever appropriate, ongoing work and/or possible future work to address these issues and gaps are described here.

10.1 Hazards Other Than Landslides and Subsidence

The hazards that are the focus of this work are landslides and subsidence. Pipelines may face other types of hazards, such as seismic activities, frost heave and thaw settlements, river scouring, et al. Each of those hazards has its own characteristics, some of which are covered in Section 2. The principles and procedures developed in this work can be applicable to the management of those hazards with appropriate modification.

10.2 Consistency in Strain Measures

The strain demand on a pipeline can be determined/estimated using pipe and soil interaction models or IMU. There are different types of pipe/soil interaction models. In beam-spring type of interaction models, the peak strain from pipe or beam elements are taken as strain demand without a notion gauge length. In contrast IMU bending strains are computed over a finite gauge length. These tools/models often have different ways and resolution in strain determination. Consequently the reported strains are usually different from the same ground movement condition.

The other inconsistency is between the measure of strain demand and strain capacity. For instance, a fixed gauge length of 10-foot is often used in computing the “bending strain” from IMU runs. The compressive strain capacity reported in most experimental tests is measured over a gauge length of one or two pipe diameters. Due the difference in gauge length between the computation of strain demand and strain capacity, the same value of strain does not represent the same state of the materials of interest.

10.3 Post-Buckling Behavior

The compressive strain capacity (CSC) is often defined as the strain corresponding to the point of the maximum bending moment in a lateral bending test. In most cases, pipes have a very minimal amount of bulging or wrinkle at this point of loading (i.e., maximum moment). In a displacement-controlled loading scenario, reaching the CSC probably does not negatively affect the pipeline service. The ovalization of the pipe’s cross section is so small that inspection pigs should be able to pass. If the loading is load-controlled, the pipe may collapse immediately

after the maximum bending moment is reached, possibly forming severe wrinkles. Large and severe wrinkles can lead to rupture/leak from high local tensile strains in either hoop or longitudinal direction. If the wrinkles survive the initial formation, the long-term integrity of the wrinkles may be affected by possible fatigue damage and/or coating/corrosion related concerns. The knowledge of the buckling process and the nature and magnitude of subsequent loading is necessary to make right decisions about the need and timing of mitigation measures [277].

10.4 Behavior of Anomalies in the Presence of High Longitudinal Strains

Most pipelines experience corrosion and mechanical damage in their lifetime. The current methodologies for assessing and mitigating those anomalies were developed under the premise that hoop stress is higher than longitudinal stress, thus hoop stress being the primary driver for potential failures. When a pipeline segment is subjected to ground movement hazards, the stress and strain in the longitudinal direction are typically higher than those in the hoop direction. The validity of the current assessment methods is not known under such conditions.

10.5 Mitigation Measures when Strain Capacity is Potentially Inadequate

Type-B sleeves have been used extensively in the pipeline industry to provide permanent repairs for various anomalies, such as corrosion, dents and gouges. The principal consideration has been containing or reducing hoop stress on the carrier pipe while containing pipeline pressure in event of leakage from the carrier pipe. In the absence of significant external loading/bending in the longitudinal direction of the pipe, such repairs are adequate and the fillet welds between the carrier pipe and the sleeve are under low stress. However, in the presence of bending moments, such as those from transverse ground movement, a sleeve can result in significant stress risers at the ends of the sleeve.

If a girth weld of a pipeline segment is found to having inadequate tensile strain capacity, one might consider the installation of Type-B sleeves. If longitudinal strain is expected to increase after the installation of the sleeve, the adequacy of the sleeve must be evaluated. The sleeved assembly cannot be automatically assumed to be able to provide full-pressure containment. Internal work at CRES suggests that the fillet welds would be under high stresses when all three components of loading exist simultaneously: (1) internal pressure in the carrier pipe, (2) internal pressure in the annulus between the carrier pipe and the sleeves, and (3) longitudinal stresses/strains on the sleeve assembly. The pressurization of the annulus creates a bending moment at the fillet welds. This loading in combination with externally applied longitudinal stresses/strains leads to high stress conditions at the fillet welds. This type of loading scenario has not been adequately examined in the industry. Possible mitigating measures may include: (1) assurance that there would not be a leak path to the annulus between the carrier pipe and the sleeves after the installation of the sleeves and/or (2) increasing the size and strength of the fillet welds. If, however, the annulus between the carrier pipe and sleeves/doubler is not pressurized, the fillet welds of normal design/repair are adequate. To ensure that the girth weld of carrier pipe does not create a leak path after the installation of the sleeves, the girth weld must have sufficient reserve strain capacity at the time of the sleeve assembly installation. It is recommended a strain capacity analysis be conducted for the girth weld of interest using the X-

ray inspection results at the time of the excavation to confirm the necessary strain capacity is available.

In addition to Type-B sleeve, composite wraps are becoming increasingly popular for repairing pipeline anomalies. Much of the current work focuses on pressure containment under low to moderate levels of longitudinal stresses while the pipe is under static or cyclic pressure loading. The use of composite wraps for pipe segments expected to experience high longitudinal stresses/strains has not been adequately examined at this time. The thermal expansion coefficients of composite wraps and the steel pipes can be significantly different, which may affect the load transfer from the pipe to the wraps under stresses in the longitudinal direction of the pipe.

Appendix A Field Measurements for Stress Estimation

Abstract

The procedure outlined in this appendix can be used to record the amount of movements at the pipe ends when an exposed segment of a pipeline is cut. The data collected can be used to estimate the magnitude and orientation of bending the pipe is experiencing before the pipe is cut.

The strain obtained from the pipe end movements reflects the elastic unloading of the pipe segment when the pipe is cut. Any permanent deformation of the pipe, if it exists, is not shown in the pipe ends' movement. The magnitude of the permanent deformation can't be estimated from the amount of movement.

Field Measurements for Stress Estimation		
Project Number:	Name of field crew:	Date:

Step by step instruction

Step 1: Make punch marks at 9, 12, 3, and 6 o'clock

Done positions at both sides of the planned cutting plane as shown in Figure 1. Label the marks at upstream side of the cutting plane as A, B, C, and D at 9, 12, 3, and 6 o'clock positions, respectively. Label the corresponding marks at downstream side as A', B', C' and D'. The marks at each side should be kept in the same cross-sectional plane. The distance from marks to the cutting plane should be sufficient to protect them from damage during the cutting process, and the distance between each pair of marks should be at least an inch (2.5 cm) less than the range of the instrument which will be used to measure them.

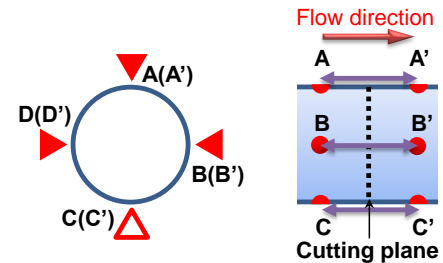


Figure 1: Marks near cutting plane

Step 2: Smooth the surface of the soil at the upstream

Done end of the exposed pipeline section, so that it is as close to a vertical plane as can reasonably be achieved while remaining stable. Install survey nails into the soil about 2 in (5cm) from the pipe as shown in Figure 2. The nails are at 9, 12, 3, and 6 (if practical) o'clock positions of the pipe. As far as possible, keep the heads of the nails in the same vertical plane. Make punch marks on the pipe at the locations closest to each of the nails. Label the punch marks as E, F, G, and H at 9, 12, 3, and (if practical) 6 o'clock positions, respectively.

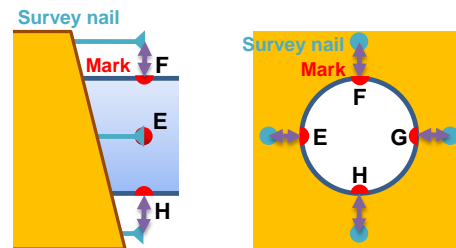


Figure 2: Survey nails and marks at the upstream end of the exposed segment

Step 3: Install survey nails into the soil and make marks

Done on the pipe following the similar procedure in Step 2 at the downstream end of the exposed pipe segment as shown in Figure 3. Label the marks on the pipe as E', F', G', and H' at 9, 12, 3, and (if practical) 6 o'clock positions, respectively. *Step 4 and Step 5 at next page*

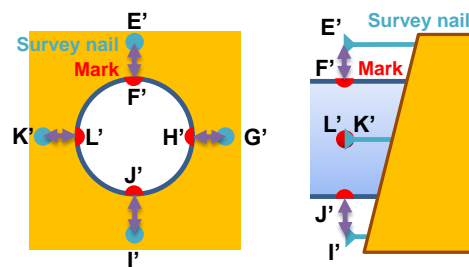


Figure 3: Survey nails and marks at the downstream end of the exposed segment

Step 4: Make measurements before cutting and fill the data in Table A-1. The measurements include the distance between marks or between nails and marks as shown in Figures 1 to 3. Measure the distance from punch marks at each end to punch marks at the cutting plane as shown in Figure 4.

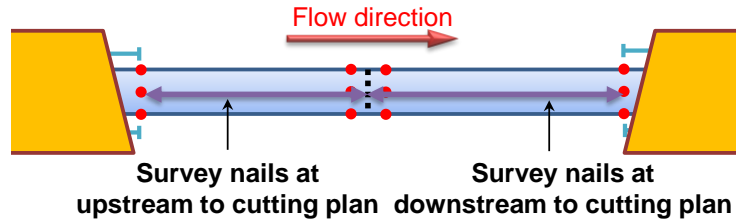


Figure 4: Distance from survey nails to the cutting plane

Table A-1 Measurements before cutting

O'clock Position	Distance between marks at cut		Distance between marks and survey nails			
			Upstream end		Downstream end	
9	AA'		E		E'	
12	BB'		F		F'	
3	CC'		G		G'	
6	DD'		H		H'	
Measurements above may be made with a caliper or a similar tool. Circle the units used: Inches millimeters						
Measurements below may be taken with a tape measure or a similar tool. Circle the units used: Decimal feet Inches meters						
Distance between survey nails and marks at the cutting plane						
Upstream end		AE				
		BF				
		CG				
		DH				
Downstream end		A'E'				
		B'F'				
		C'G'				
		D'H'				

Step 5: Make measurements after cutting as shown in Figures 5 and 6 (next page), and fill the data in Table A-2:

Done

- At the cutting plane, measure the distance between marks (A to A', etc.).
- Measure the high-low misalignment at each clock position⁵. High-low can be negative or positive, defined using the pipe axis at the downstream side of the cut as the reference (termed "the axis"). Figure 5 shows positive misalignment at the 12:00 position (B is further from the axis than B') and it shows negative misalignment at the 6:00 position (D is closer to the axis than D'). Make sure to show each high-low measurement as positive or negative by putting a plus or minus sign in front of it.
- Measure the maximum high-low misalignment and the clock position at which it occurs.
- Measure the angular misalignment after cutting at each clock position following one of the two methods shown in Figure 6.
- Measure the maximum angular misalignment and the clock position at which it occurs.
- Measure the distance between survey nails and the corresponding marks at each end of the pipeline segment again.
- Before the cutting is complete around the circumference, the cutting location would either pop open by tensile rupture if the pipe is loaded in tension or form a wrinkle if the pipe is loaded in compression. Measure the length of remaining ligament in pipe's circumferential direction when the tensile rupture occurs or wrinkle forms. Indicate the mode of deformation (tensile rupture or compressive wrinkling).

⁵ Profile gages may be used to measure the misalignment.

Table A-2 Measurements after cutting

O'clock Position	Distance between marks at cut		Distance between marks and survey nails			
			Upstream end		Downstream end	
9	AA'		E		E'	
12	BB'		F		F'	
3	CC'		G		G'	
6	DD'		H		H'	
Circle the units used: Inches millimeters						
O'clock Position	Axial Misalignment (include + or -)		Angular Misalignment			
			M	N	P	
9	A					
12	B					
3	C					
6	D					
	max					
	max					
Pops or wrinkle at the end of cutting						
Tensile rupture (T) or compressive wrinkle (C)			Length of the remaining ligament at the moment of tensile rupture or compressive wrinkle formation			

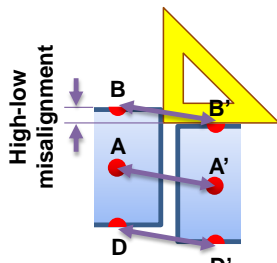


Figure 5: Distance b/w marks and high-low misalignment after cutting

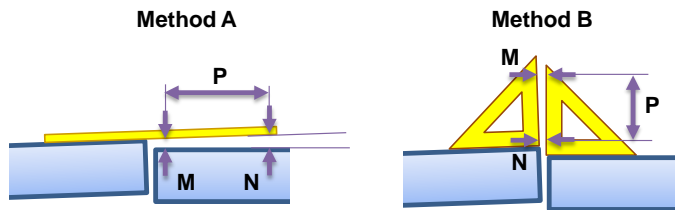


Figure 6: Alternative methods to measure the angular misalignment

Appendix B Example Plot Packages of Inertial Survey Data

Abstract

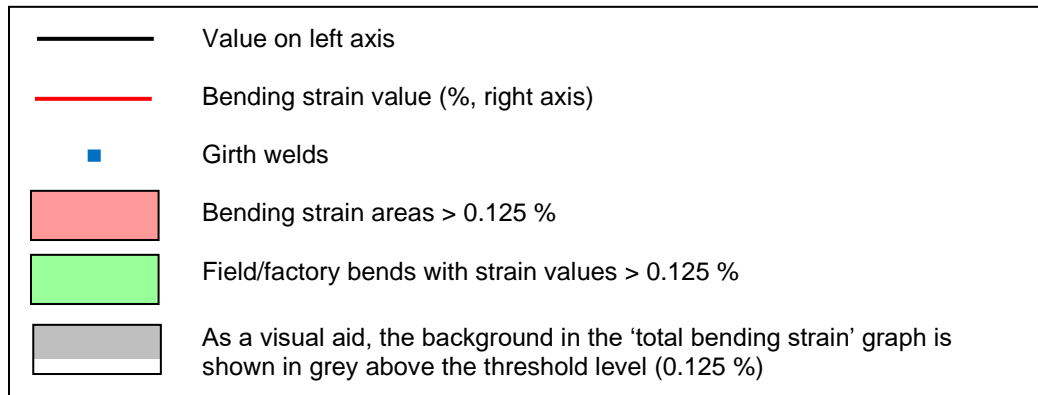
This appendix presents a series of pipeline geometry plot packages and tables based on real inertial survey data provided by JIP participants. All plots and characterizations of the data are presented in a non-identifying, anonymous way. The purpose of these plots is to illustrate various aspects of the data signatures associated with pipeline movement at locations of interest identified in inertial surveys. A brief narrative description is provided for each example together with a sample table of key information and a multi-panel plot package.

Example 1 was developed and provided by ROSEN and contains a description of the plotted information. For Examples 2 through 7, the panels in the multi-panel plot package are described as follows:

- 1st Panel: Profile of vertical out-of-straightness OOS_V (ft) vs. relative odometer distance (ft).
- 2nd Panel: Profile of Horizontal out-of-straightness OOS_H (ft) vs. relative odometer distance (ft).
- 3rd Panel: Profile of pitch angle θ (degrees) vs. relative odometer distance (ft).
- 4th Panel: Profile of horizontal angle (yaw or azimuth) γ (degrees) vs. relative odometer distance (ft).
- 5th Panel: Profile of vertical bending strain ϵ_V (%) calculated using a 3-m gauge length vs. relative odometer distance (ft).
- 6th Panel: Profile of horizontal bending strain ϵ_H (%) calculated using a 3-m gauge length vs. relative odometer distance (ft).
- 7th Panel: Profile of resultant bending strain ϵ_R (%) calculated using a 3-m gauge length vs. relative odometer distance (ft).

Within each of these plots, the locations of pipeline girth welds are denoted using blue “o” symbols.

Example 1: In the following an exemplary bending strain feature caused by pipeline movement recorded with a ROSEN RoGeo-Xt® tool equipped with an IMU is given. It is an extract from an in-line inspection report including explanations and the feature itself, whereby all reporting parameters that would allow for the identification of the actual pipeline were modified or erased.



Top view graph

The black line in the 'Top view' graph illustrates the horizontal distance between the actual pipe position and an imaginary straight line over the graph area.

The red line illustrates horizontal bending strain [%]. Positive values represent right bends, negative values represent left bends.

Side view graph

The black line in the 'Side view' graph illustrates the height difference between the actual pipe position and an imaginary straight line over the graph area. The straight line is defined from the start and end points of the actual pipe height.

The red line illustrates vertical bending strain in [%]. Positive values represent over bends, negative values represent sag bends.

Total bending strain graph

The 'Total bending strain' graph illustrates the combined horizontal and vertical bending strain. The values represent the elongation at the outer side of the bend (which is equal to the compression at the inner side of the bend).

Direction of bending strain graph

The 'Direction of bending strain' graph illustrates the o'clock position (h) of the total bending strain.

Pipeline representations

At the bottom of each page two pipeline representations are shown. The top pipe representation gives the center of the strain event.

S = Bending strain due to pipeline movement (red areas)

B = Field / factory bend (green areas)

The bottom one provides the associated joint numbers.

Table B-3 Geometry information for Example 1

Anomaly No.	1		
Anomaly	Bending strain		
Start distance	12,248.000 m		
End distance	12,288.000 m		
Length (rounded)	40 m		
Max. strain value	0.42 %		
Strain direction	horizontal		
Start coordinates	N	E	H
End coordinates	N	E	H

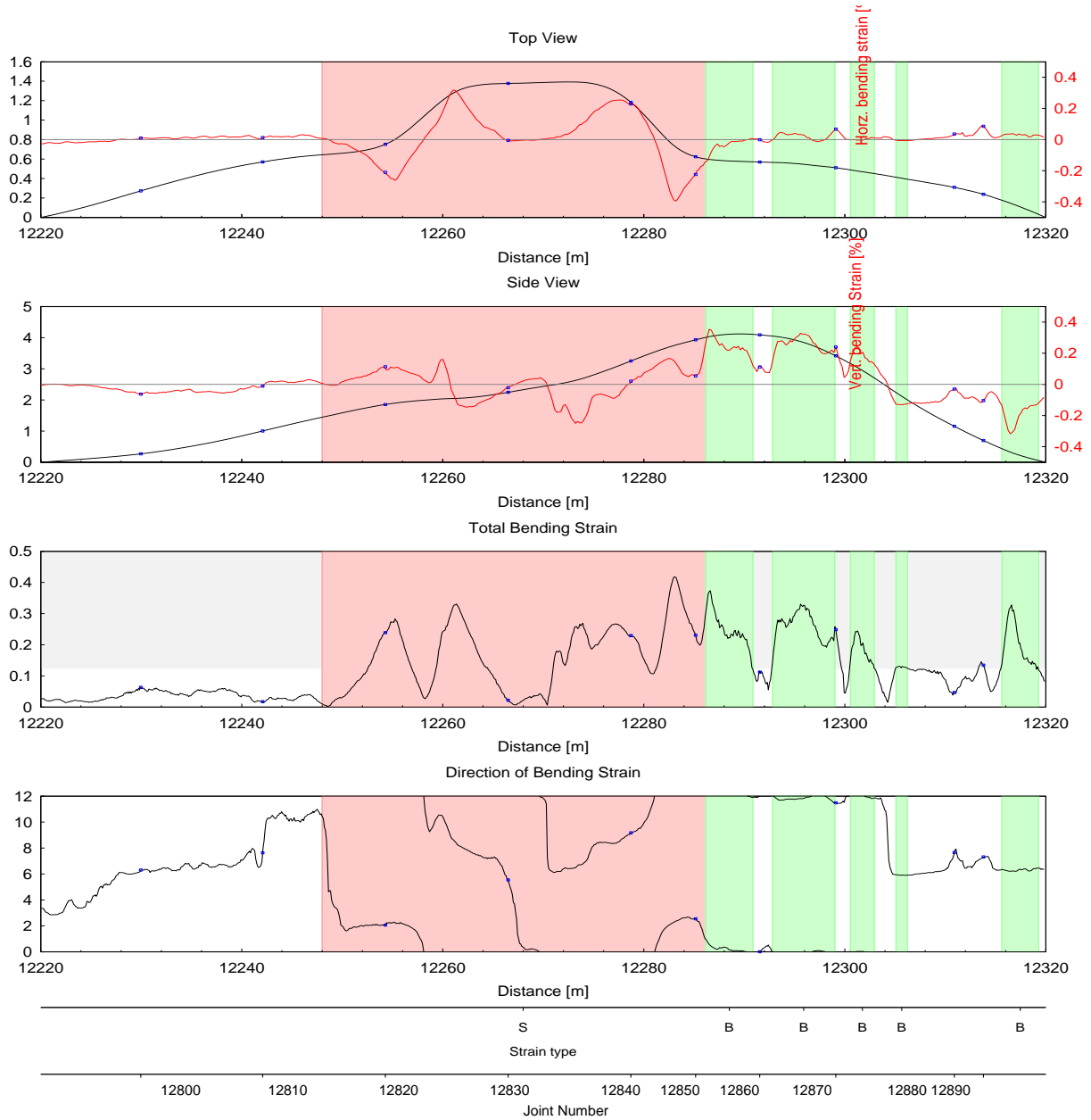


Figure B-1 Geometry information for Example 1

Example 2: Example 2 illustrates the geometry of a 26-inch diameter gas pipeline where it crosses a transverse horizontal landslide feature which is centered on a trough shaped depression. A tabulation of the key parameters of this feature is provided in Table B-4. The geometry is presented over a length of about 480 ft in the multi-panel plot in Figure B-2. As shown in the vertical OOS profile in the 1st panel, the feature has a vertical OOS range of about 5.8 ft where most of the elevation change is developed over a series of 7 vertical cold bends which are well illustrated by abrupt steps in the pitch profile in the 3rd panel and by relative sharp lobes in the vertical bending strain profile in the 5th panel. As shown in the horizontal OOS profile in the 2nd panel, the landslide movement has generated a horizontal OOS range of about 7.1 ft with a main lobe of movement to the right (relative to the flow direction) with a peak horizontal OOS at a relative odometer distance of about 185 ft (which also coincides with the low point of the vertical profile). The horizontal geometry change is characterized by a fairly distinct 3 lobe sinusoidal variation in the azimuth profile (4th panel) which extends over the distance range from about 50 ft to 400 ft with a total azimuth swing of about 12.1°. The corresponding maximum horizontal bending strain magnitude is about 0.79% at a relative odometer distance of about 250 ft.

Table B-4 Key parameters for Example 2

Feature Number	2	Mid-Point Coordinates	
Start Distance (ft)	0.00	Northing (ft)	N
End Distance (ft)	477.83	Easting (ft)	E
Feature Length (ft)	477.83	Elevation (ft)	H
Upstream Weld	2000	Latitude (degrees)	Lat
Downstream Weld	2130	Longitude (degrees)	Long
Average Tool Speed (ft/s)	8.2		

Overall Peak Bending Strain Values	Horizontal Strain (%)	0.786
	Vertical Strain (%)	0.757
	Resultant Strain (%)	0.847
Distance and Bending Strain Components at Governing Girth Weld Location	Girth Weld Number	2070
	Chainage (ft)	240.14
	Horizontal Strain (%)	0.535
	Vertical Strain (%)	-0.315
Distance and Bending Strain Components at Location of Peak Resultant Strain	Resultant Strain (%)	0.621
	Chainage (ft)	191.56
	Horizontal Strain (%)	0.757
	Vertical Strain (%)	-0.381
	Resultant Strain (%)	0.847

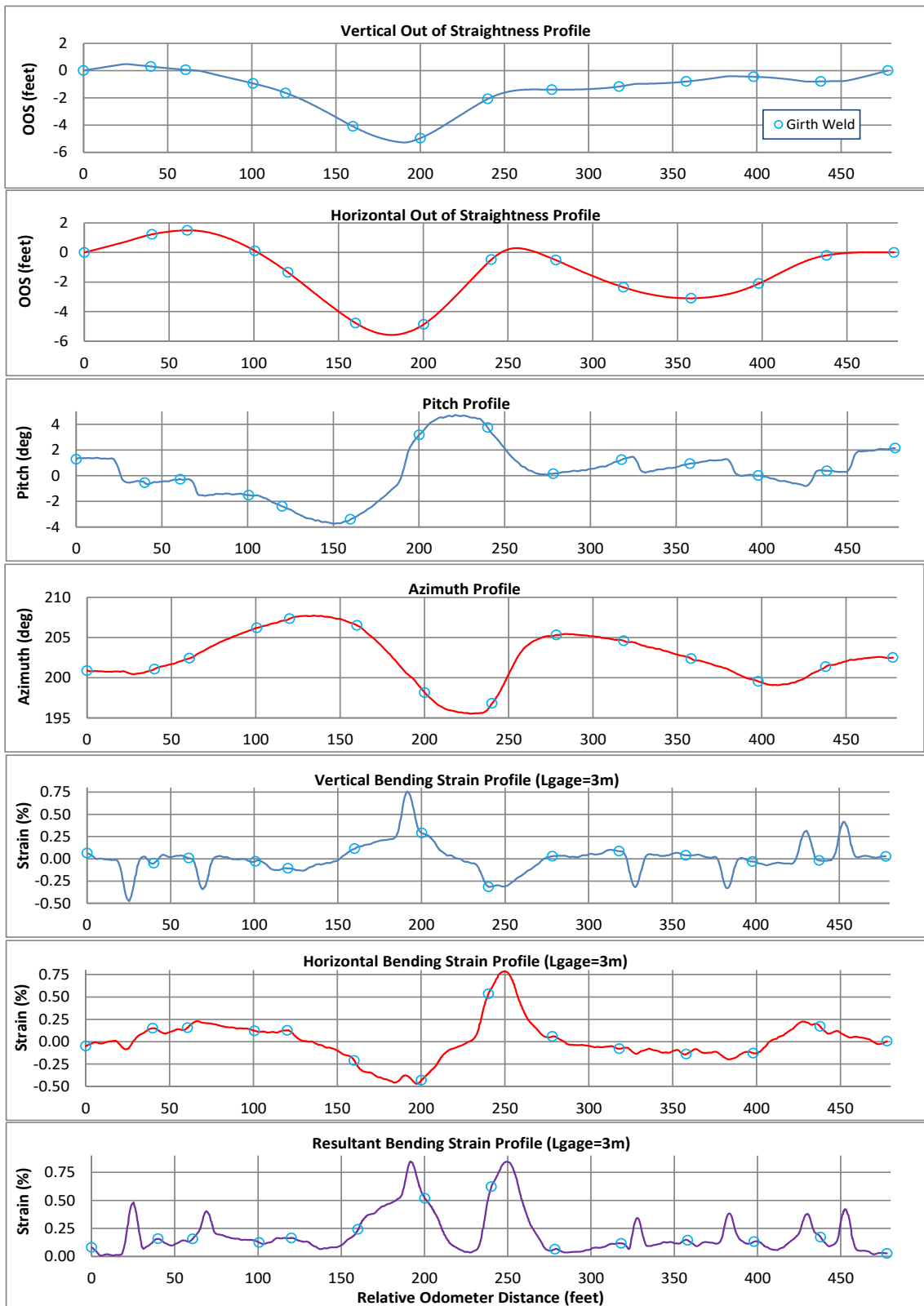


Figure B-2 Geometry profiles for Example 2

Example 3: Example 3 illustrates the geometry of a 26-inch diameter gas pipeline where it crosses a transverse horizontal landslide feature which is centered on a long, trough shaped depression. A tabulation of the key parameters of this feature is provided in Table B-5. The geometry is presented over a length of about 375 ft in the multi-panel plot in Figure B-3. As shown in the vertical OOS profile in the 1st panel, the feature has a vertical OOS range of about 19 ft where most of the elevation change is developed over a series of 7 vertical cold bends which are well illustrated by abrupt steps in the pitch profile in the 3rd panel and by relative sharp lobes in the vertical bending strain profile in the 5th panel. As shown in the horizontal OOS profile in the 2nd panel, the landslide movement has generated a horizontal OOS range of about 4.6 ft with a main lobe of movement to the right (relative to the flow direction) with a peak horizontal OOS at a relative odometer distance of about 180 ft (which also coincides with the low point of the vertical profile). The horizontal geometry change is characterized by a fairly distinct 2 lobe sinusoidal variation in the azimuth profile (4th panel) which extends over the distance range from about 50 ft to 340 ft with a total azimuth swing of about 6.4°. The corresponding maximum horizontal bending strain magnitude is about 0.16% at a relative odometer distance of about 150 ft.

Table B-5 Key parameters for Example 3

Feature Number	3	Mid-Point Coordinates	
Start Distance (ft)	0.00	Northing (ft)	N
End Distance (ft)	374.07	Easting (ft)	E
Feature Length (ft)	374.07	Elevation (ft)	H
Upstream Weld	3000	Latitude (degrees)	Lat
Downstream Weld	3100	Longitude (degrees)	Long
Average Tool Speed (ft/s)	8.2		

Overall Peak Bending Strain Values	Horizontal Strain (%)	-0.157
	Vertical Strain (%)	0.450
	Resultant Strain (%)	0.460
Distance and Bending Strain Components at Governing Girth Weld Location	Girth Weld Number	3040
	Chainage (ft)	150.71
	Horizontal Strain (%)	-0.154
	Vertical Strain (%)	0.199
	Resultant Strain (%)	0.251
Distance and Bending Strain Components at Location of Peak Resultant Strain	Chainage (ft)	137.90
	Horizontal Strain (%)	-0.093
	Vertical Strain (%)	0.450
	Resultant Strain (%)	0.460

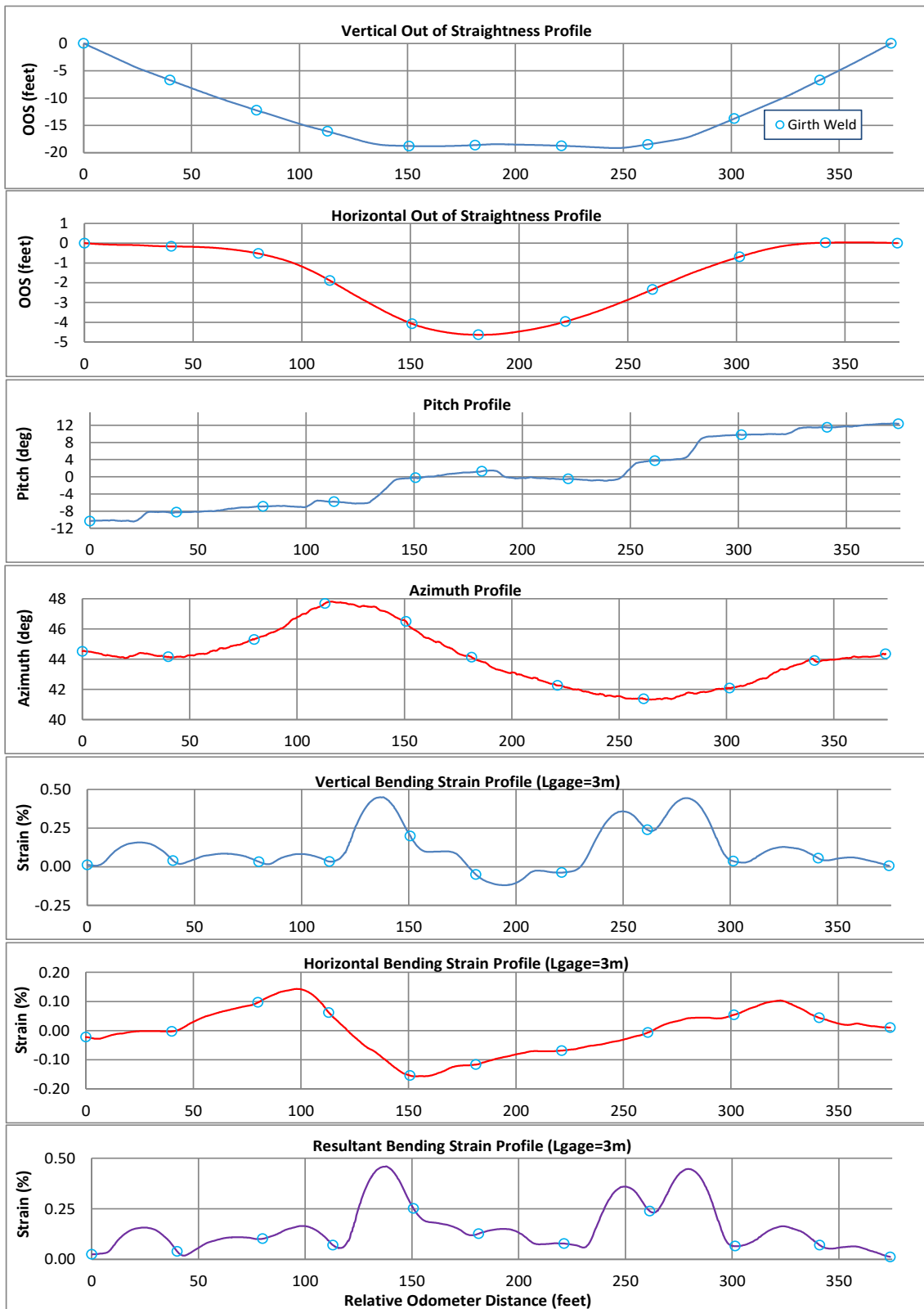


Figure B-3 Geometry profiles for Example 3

Example 4: Example 4 illustrates the geometry of a 36-inch diameter gas pipeline where it crosses a transverse horizontal landslide feature which is centered on a long, trough shaped depression. A tabulation of the key parameters of this feature is provided in Table B-6. The geometry is presented over a length of about 355 ft in the multi-panel plot in Figure B-4. As shown in the vertical OOS profile in the 1st panel, the feature has a vertical OOS range of about 17 ft where most of the elevation change is developed over a series of 5 vertical cold bends which are well illustrated by abrupt steps in the pitch profile in the 3rd panel and by relative sharp lobes in the vertical bending strain profile in the 5th panel. As shown in the horizontal OOS profile in the 2nd panel, the landslide movement has generated a horizontal OOS range of about 5 ft with a main lobe of movement to the right (relative to the flow direction) with a peak horizontal OOS at a relative odometer distance of about 165 ft (which also coincides with the low point of the vertical profile). The horizontal geometry change is characterized by a distinct 2 lobe sinusoidal variation in the azimuth profile (4th panel) which extends over the distance range from about 40 ft to 330 ft with a total azimuth swing of about 6.1°. The corresponding maximum horizontal bending strain magnitude is about 0.2% at a relative odometer distance of about 50 ft.

Table B-6 Key parameters for Example 4

Feature Number	4	Mid-Point Coordinates	
Start Distance (ft)	0.00	Northing (ft)	N
End Distance (ft)	355.95	Easting (ft)	E
Feature Length (ft)	355.95	Elevation (ft)	H
Upstream Weld	4000	Latitude (degrees)	Lat
Downstream Weld	4110	Longitude (degrees)	Long
Average Tool Speed (ft/sec)	7.9		

Overall Peak Bending Strain Values	Horizontal Strain (%)	0.194
	Vertical Strain (%)	0.627
	Resultant Strain (%)	0.630
Distance and Bending Strain Components at Governing Girth Weld Location	Girth Weld Number	4020
	Chainage (ft)	65.41
	Horizontal Strain (%)	0.144
	Vertical Strain (%)	0.179
	Resultant Strain (%)	0.230
Distance and Bending Strain Components at Location of Peak Resultant Strain	Chainage (ft)	272.75
	Horizontal Strain (%)	0.066
	Vertical Strain (%)	0.627
	Resultant Strain (%)	0.630

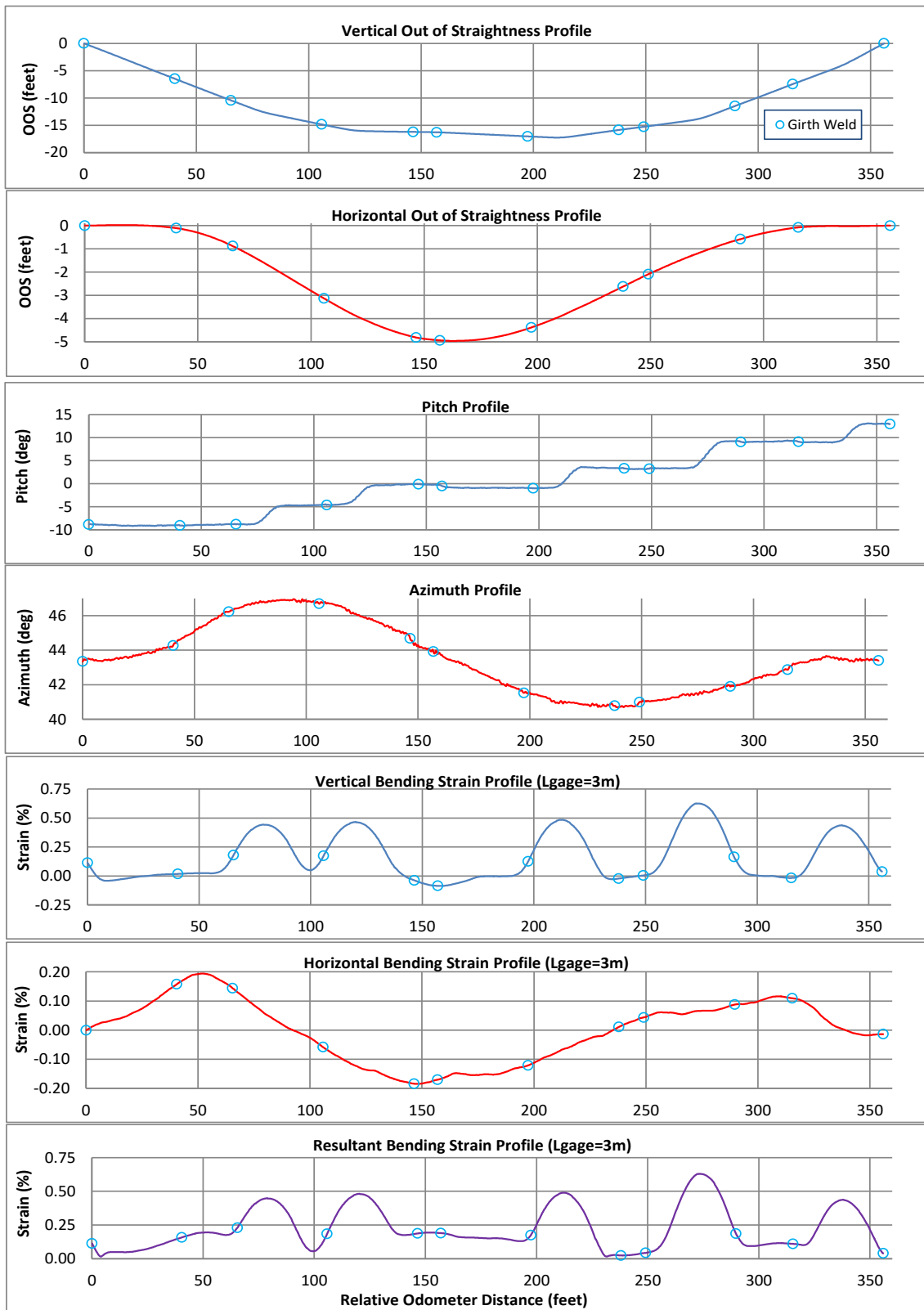


Figure B-4 Geometry profiles for Example 4

Example 5: Example 5 presents the geometry where a 1.5 to 4 m deep and 60 m wide earth slide/flow has moved laterally across the alignment of a 30-inch diameter gas pipeline. The slide appears to have been triggered by construction activities during an upslope line looping. A tabulation of the key parameters of this feature is provided in Table B-7. The geometry is presented over a length of about 420 ft in the multi-panel plot in Figure B-5. As shown in the vertical OOS profile in the 1st panel, the feature has a peak vertical OOS of about 11.6 ft at a relative odometer distance of about 150 ft where most of the elevation change is developed over a series of 7 vertical cold bends which are well illustrated by abrupt steps in the pitch profile in the 3rd panel and by relative sharp lobes in the vertical bending strain profile in the 5th panel. As shown in the horizontal OOS profile in the 2nd panel, the earth slide movement has generated a horizontal OOS range of about 18.8 ft with a main lobe of movement to the left (relative to the flow direction) with a peak horizontal OOS at a relative odometer distance of about 200 ft. The horizontal geometry change is characterized by a distinct 2 lobe sinusoidal variation in the yaw profile (4th panel) which extends over the distance range from about 100 ft to 350 ft with a total yaw swing of about 27°. It is noted that the 27° yaw swing occurs over an almost linear ramp over the distance range from about 150 ft to 270 ft. The corresponding maximum horizontal bending strain magnitude is about 0.90% at a relative odometer distance of about 190 ft.

Table B-7 Key parameters for Example 5

Feature Number	5	Mid-Point Coordinates	
Start Distance (ft)	0.00	Northing (ft)	N
End Distance (ft)	417.36	Easting (ft)	E
Feature Length (ft)	417.36	Elevation (ft)	H
Upstream Weld	5000	Latitude (degrees)	Lat
Downstream Weld	5180	Longitude (degrees)	Long
Average Tool Speed (ft/s)	10.6		

Overall Peak Bending Strain Values	Horizontal Strain (%)	-0.899
	Vertical Strain (%)	-1.323
	Resultant Strain (%)	1.559
Distance and Bending Strain Components at Governing Girth Weld Location	Girth Weld Number	5110
	Chainage (ft)	232.35
	Horizontal Strain (%)	-0.466
	Vertical Strain (%)	-0.849
	Resultant Strain (%)	0.968
Distance and Bending Strain Components at Location of Peak Resultant Strain	Chainage (ft)	242.95
	Horizontal Strain (%)	-0.827
	Vertical Strain (%)	-1.322
	Resultant Strain (%)	1.559

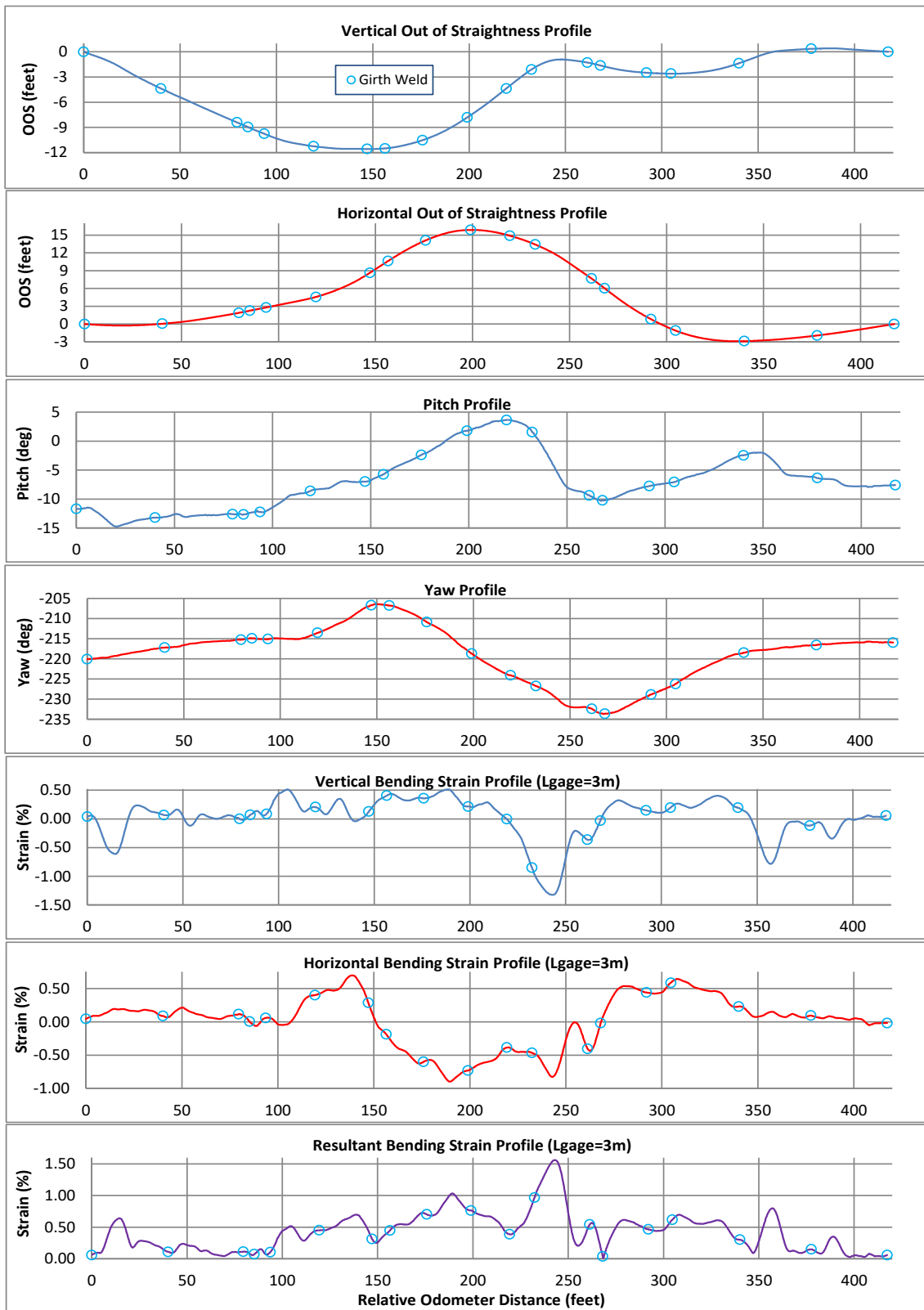


Figure B-5 Geometry profiles for Example 5

Example 6: Example 6 illustrates a 12-inch diameter natural gas pipeline which runs down a river valley slope adjacent to a gully. There is a 6-m deep earth slide/earth flow moving at an angle of approximately 45° across the pipeline alignment into the gully. A tabulation of the key parameters of this feature is provided in Table B-8. The geometry is presented over a length of about 210 ft in the multi-panel plot in Figure B-6. As shown in the vertical OOS profile in the 1st panel, the feature has a vertical OOS range of about 11.5 ft. The vertical geometry change is characterized by a fairly distinct 2 lobe sinusoidal variation in the pitch profile (3rd panel) which extends over the distance range from about 50 ft to 180 ft with a total pitch swing of about 25°. The corresponding maximum vertical bending strain magnitude is approaching 1% at a relative odometer distance of about 80 ft. As shown in the horizontal OOS profile in the 2nd panel, the earth slide movement has generated a horizontal OOS range of about 5.1 ft with a main lobe of movement to the right (relative to the flow direction) with a peak horizontal OOS at a relative odometer distance of about 80 ft. The horizontal geometry change is characterized by a distinct 2 lobe sinusoidal variation in the yaw profile (4th panel) which extends over the distance range from about 40 ft to 170 ft with a total yaw swing of about 16°. The corresponding maximum horizontal bending strain magnitude is approaching 0.5% at a relative odometer distance of about 85 ft.

Table B-8 Key parameters for Example 6

Feature Number	6	Mid-Point Coordinates	
Start Distance (ft)	0.00	Northing (ft)	N
End Distance (ft)	210.05	Easting (ft)	E
Feature Length (ft)	210.05	Elevation (ft)	H
Upstream Weld	6000	Latitude (degrees)	Lat
Downstream Weld	6060	Longitude (degrees)	Long
Average Tool Speed (ft/s)	2.7		

Overall Peak Bending Strain Values	Horizontal Strain (%)	0.510
	Vertical Strain (%)	-0.934
	Resultant Strain (%)	1.048
Distance and Bending Strain Components at Governing Girth Weld Location	Girth Weld Number	6050
	Chainage (ft)	148.28
	Horizontal Strain (%)	-0.094
	Vertical Strain (%)	0.663
	Resultant Strain (%)	0.670
Distance and Bending Strain Components at Location of Peak Resultant Strain	Chainage (ft)	78.57
	Horizontal Strain (%)	0.475
	Vertical Strain (%)	-0.934
	Resultant Strain (%)	1.048

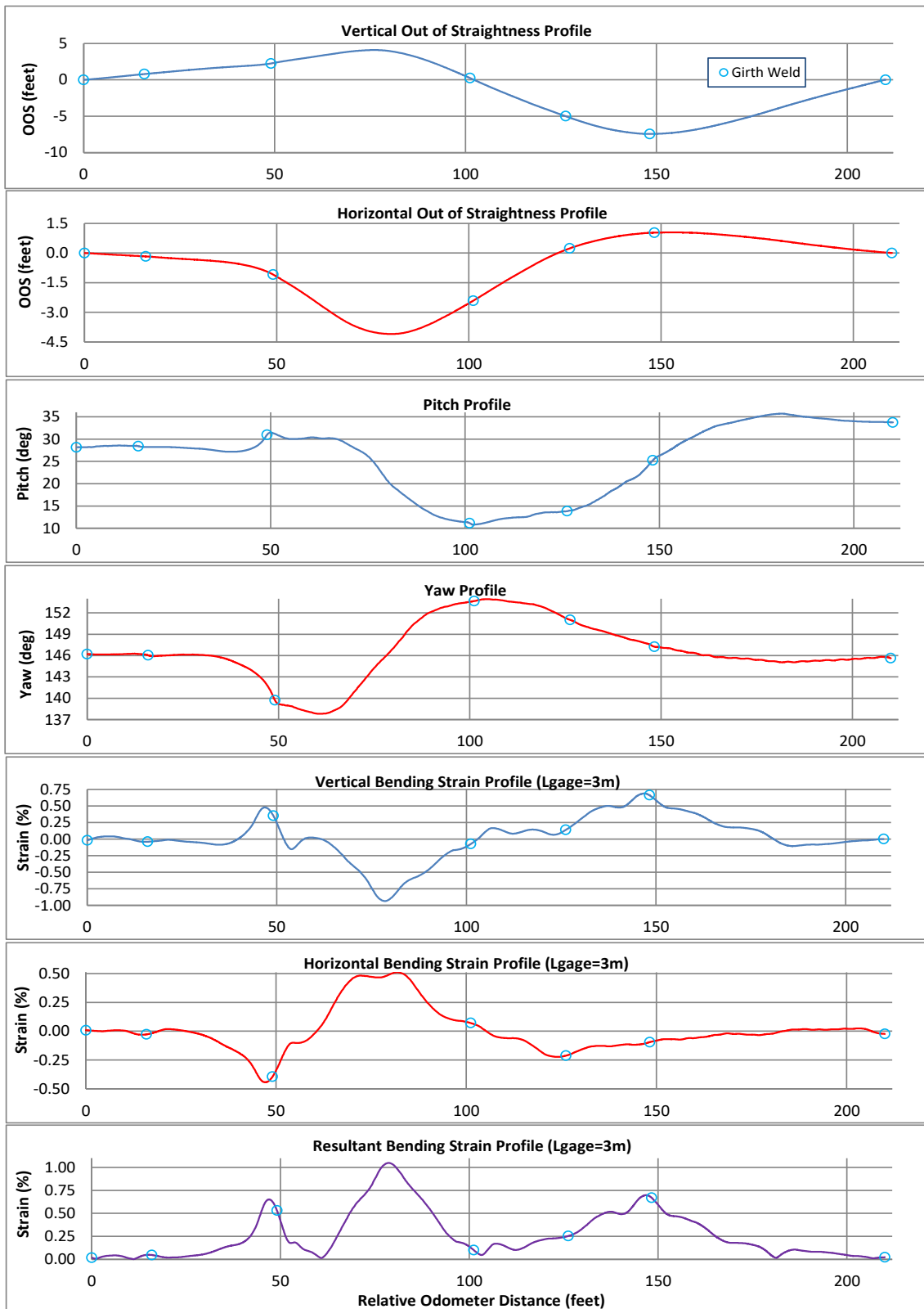


Figure B-6 Geometry profiles for Example 6

Example 7: The feature illustrated by Example 7 is located at the flank of a 3.5 km long and approximately 50 m deep very slow translational earth slide in a large river valley. The upstream end of a 30-inch mainline is located in the landslide and the downstream end is located in stable ground. At the flank boundary there has been approximately 2 m of movement over 60 years. A tabulation of the key parameters of this feature is provided in Table B-9. The geometry is presented over a length of about 100 ft in the multi-panel plot in Figure B-7. As shown in the vertical OOS profile in the 1st panel, the feature has a maximum downward vertical OOS of about 0.8 ft. The vertical geometry change is characterized by a fairly distinct ramp-like variation in the pitch profile (3rd panel) with a total azimuth swing of about 3° occurring over the distance range from about 15 ft to 60 ft. The corresponding maximum vertical bending strain magnitude is approaching 0.3% at a relative odometer distance of about 35 ft. As shown in the horizontal OOS profile in the 2nd panel, the earth slide movement has generated a horizontal OOS range of about 2.2 ft with a 2 lobes of movement first to the left then to the right (relative to the flow direction) with peak horizontal OOS values of about +1 ft at a relative odometer distance of about 25 ft and -1.2 ft at a relative odometer distance of about 65. The horizontal geometry change is characterized by a fairly distinct 1-lobe sinusoidal shape in the yaw profile (4th panel) over the distance range from about 15 to 85 ft with a total yaw swing of about 8°. The corresponding maximum horizontal bending strain magnitude is approaching 1% at a relative odometer distance of about 61 ft.

Table B-9 Key parameters for Example 7

Feature Number	7	Mid-Point Coordinates	
Start Distance (ft)	0.00	Northing (ft)	N
End Distance (ft)	100.06	Easting (ft)	E
Feature Length (ft)	100.06	Elevation (ft)	H
Upstream Weld	7000	Latitude (degrees)	Lat
Downstream Weld	7030	Longitude (degrees)	Long
Average Tool Speed (ft/s)	8.9		

Overall Peak Bending Strain Values	Horizontal Strain (%)	-0.965
	Vertical Strain (%)	0.287
	Resultant Strain (%)	0.975
Distance and Bending Strain Components at Governing Girth Weld Location	Girth Weld Number	7020
	Chainage (ft)	61.03
	Horizontal Strain (%)	-0.965
	Vertical Strain (%)	-0.141
Distance and Bending Strain Components at Location of Peak Resultant Strain	Resultant Strain (%)	0.975
	Chainage (ft)	60.99
	Horizontal Strain (%)	-0.965
	Vertical Strain (%)	-0.141
	Resultant Strain (%)	0.975

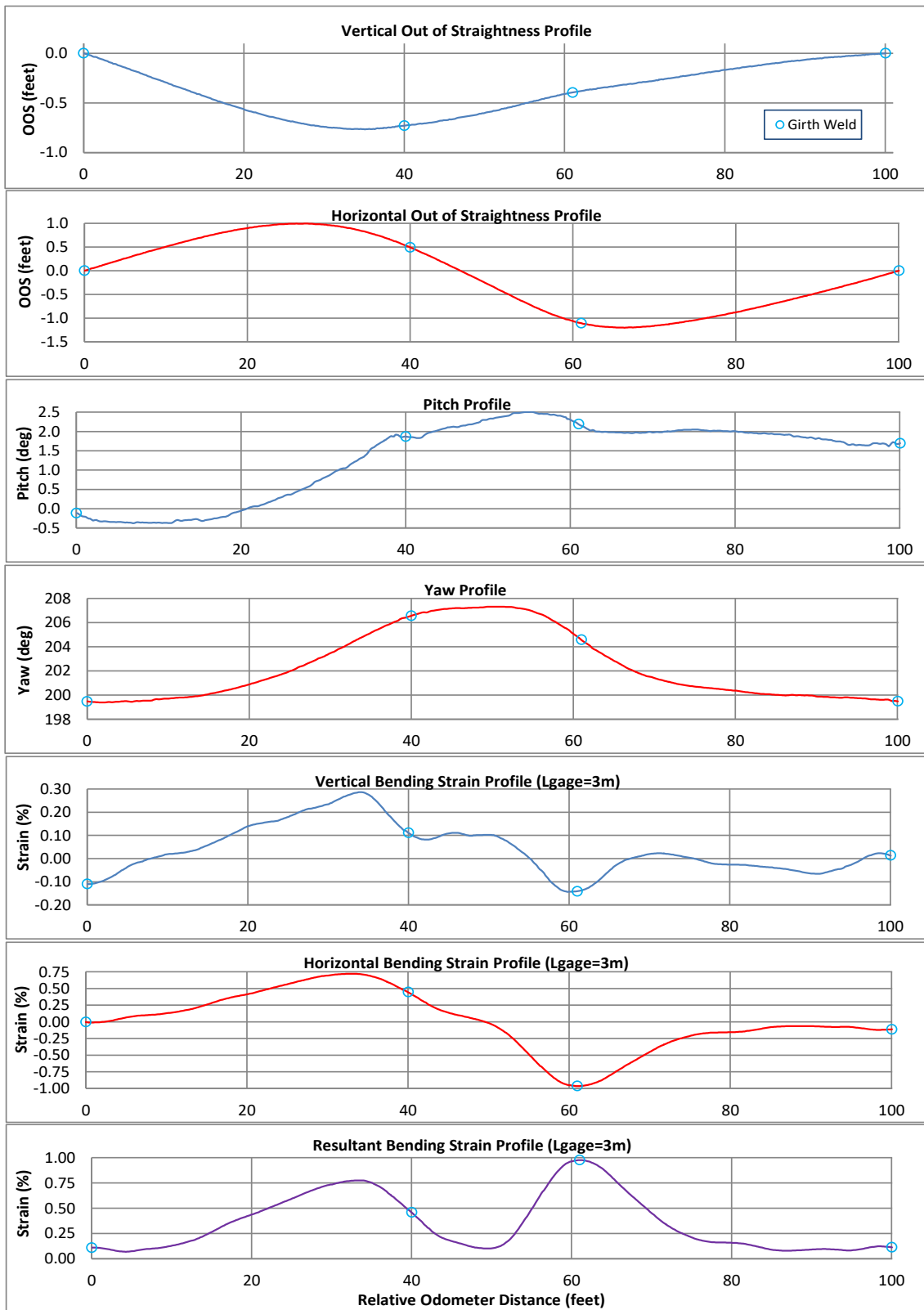


Figure B-7 Geometry profiles for Example 7

Appendix C Sample Specification Language for Inertial Survey RFP

Abstract

This Appendix provides sample specification language that an inertial survey client may choose to include with RFP transmittal documents. The purpose of this sample specification language is to provide inertial survey vendors with specific guidance defining acceptable deliverable packages including specific items to be tabulated and plotted for each pipeline strain feature that has been flagged based on inertial survey data screening. The intent of this language is not to be overly prescriptive and inertial survey vendors should have leeway to develop alternative presentation formats provided that they are acceptable to the client. The client is free to modify this language as needed in order to meet any company or project specific requirements.

C.1 Identification of Strain Locations of Interest from IMU Data

Chapter 4 provides detailed guidance on methods for identifying strain locations of interest based on review of the inertial data. As described in Chapter 4, the ILI service provider should have leeway in identifying or “flagging” anomalous bending strain features based on their standard anomaly screening procedures so a description of methods used to identify strain areas is not presented in this Appendix. As part of the screening process, it is expected that the vendor will experiment with different curvature calculation lengths in order to establish and justify the gauge length used to report strain features of interest on a case-by-case basis. The selected gauge length should strike a balance between the tendency for short gauge lengths to amplify noise in the data and the tendency for long gauge lengths to underestimate curvature. Once a strain location of interest has been identified or flagged by the geometry screening process, it is expected that key information describing the feature(s) of interest will be extracted, tabulated and plotted. The following subsections summarize recommendations for characterizing and reporting the pertinent information.

C.2 Items to be Tabulated for Features of Interest

For all areas that are flagged by the screening process, the vendor shall have leeway to tabulate all information considered pertinent to describing the feature of interest (subject to client requirements and/or approval). As a minimum, it is recommended that the following information be tabulated for each feature of interest:

- Unique feature name or identifier.
- Pipe steel grade and wall thickness.
- Starting/ending odometer distance and estimated length of the feature.
- Map coordinates of the mid-point of the feature e.g., Easting-Northing or Latitude-Longitude (WGS-84 decimal degrees) and elevation relative to a specified datum.
- Peak values of the vertical, horizontal and resultant/total bending strain anywhere within the feature.

- ID number and/or odometer distance of all girth welds that are encompassed by the strain feature.
- Maximum values of vertical, horizontal and resultant/total bending strain at any of the girth welds encompassed by the strain feature (or a tabulation of these strains at each girth weld within the feature).
- Average tool velocity across the feature.
- A brief narrative description of the feature.
- A listing of any supplemental notes or comments regarding the feature including the presence of other anomalies such as corrosion, ovality, dents, etc.

C.3 Items to be Plotted for Features of Interest

For all areas that are flagged by the screening process, the vendor shall have leeway to plot all information that is considered pertinent to describing the geometry of the feature of interest (subject to client requirements and/or approval). As a minimum, it is recommended that the following plots be developed for each feature of interest:

- Along-the-pipe profile view of the pipe centerline elevation vs. odometer distance. The pipe elevation profile may alternately be characterized using vertical out-of-straightness (OOS) plots showing the vertical deviation of the calculated pipe centerline path as a function of odometer distance between selected end points with zero OOS.
- Plan view “map” of Easting vs. Northing (or Longitude/Latitude). A plan view of the pipeline geometry may alternately be presented using horizontal out-of-straightness (OOS) plots showing the horizontal (plan) deviation of the calculated pipe centerline path as a function of odometer distance between selected end points with zero OOS.
- Pitch angle (degrees) vs. odometer distance.
- Azimuth or yaw angle (degrees) vs. odometer distance.
- Along-the-pipe profile view plots of vertical, horizontal and resultant bending strain vs. odometer distance.
- Measured wall thickness and diameter (if available from the survey).

Appendix B presents a sample package illustrating some of the geometry plots described above. The format of these plot packages provides a compact overall view of the aligned pipeline geometry features including position, orientation and bending strain profiles on a single page. Alternate geometry presentation packages developed by the vendor may also be acceptable.

C.4 Additional Guidance for Bend Strain Reporting

The following notes/comments are provided for additional information.

- In all along-the-pipe profile view plots, the locations of pipeline girth welds should be clearly identified (e.g., using a symbol like “o” or “+” or using a distinct vertical line at the odometer distance of each girth weld, etc.).

- All-along-the pipe profile view plots should be presented over an odometer distance long enough to fully encompass the length of the feature of interest with at least an additional pipe joint of length on either end (e.g., say ± 40 to ± 50 ft). Plots of this sort typically span over 200 to 300 ft. The plots should be nominally centered on the high strain zone.
- Plots vs. odometer distance should show the odometer distance on the X axis and the geometry quantity of interest on the Y axis. The Y axis should be “*auto-scaled*” (i.e., maximum Y axis value slightly larger than Y_{max} and minimum Y axis value slightly smaller than Y_{min}) in order to provide an exaggerated/zoomed view of the quantity of interest wherein the details of the signal will be clearly visible.
- The units of all plotted and tabulated quantities should be clearly denoted in all plots and tables.
- All references to curvature and/or bending strain should identify the curvature calculation gauge length.
- For each high strain zone, it should also be noted whether or not any pipe ovality or out-of-roundness was detected. If the inertial survey also includes high resolution caliper measurements, then the screening criteria may be extended to include a review of the caliper data. For the areas flagged by the bending strain criteria discussed above, detailed profile plots of pipe out of roundness (if present) should also be included. Also, any locations with dents or ovality features of 2% of the pipe diameter or more should be identified and plotted in the screening report. Any vendor-specific calculations for localized through-wall bending strains due to pipe wall deformations should also be provided together with any associated documentation.
- Similarly, any high strain zone at/near a girth weld should note whether or not rotational or translational misalignment (or other defect) was detected at the weld. Angular misalignments at girth welds (i.e., accidental miters) are sometimes readily visible as very short, nearly vertical offsets (i.e., like a step function) in the pitch and azimuth profiles.
- For each high strain zone, it should be noted whether or not any metal loss was detected at/near the high strain location if such information is available.
- Additional plots that may be worth presenting to characterize pipeline features of interest include a profile plot of the circumferential angle or o'clock orientation corresponding to the orientation of the resultant bending strain. More compact spatial plot packages can be achieved by overlaying different signals on the same plot (e.g., pipe elevation on the left vertical axis and vertical bending strain on the right vertical axis) – see Example 1 in Appendix B.
- For pipelines subjected to multiple inertial surveys, it will be useful to develop versions of these plots which directly overlay the data and/or the *differences* in the data from two or more different surveys. In order to align the data from different surveys, it is common

practice to scale the chainage distance between selected girth welds from the new survey to match the chainage distance between those welds from the old survey (or vice versa).

C.5 Additional Deliverables

Reference [115] provides general guidance for ILI report contents. The vendor strain report should also always include the following information:

- A summary of the tool detection threshold and accuracy specifications including the gyroscope type and sampling rate.
- A summary of the sensor accuracies.
- At least a basic description of the numerical algorithm used to compute curvature/bending strain and applied data analysis parameters
- Documentation of the accuracy realized during the survey (i.e., what was the realized position accuracy and curvature/bending strain accuracy and did they meet or exceed specifications?).
- A summary ILI data quality assessment for the survey (e.g., was the tool run within the range of essential variables, was there any sensor malfunction, etc.)
- A profile plot of the tool velocity during the entire survey.
- A detailed drawing of the tool that is used to perform the survey showing all pertinent dimensions (including the distances between all canister supports) and the locations of all sensors.

The vendor may also provide specialized software that can be used by operator representatives to view and/or export selected quantities of the inertial survey data along selected sections of the alignment.

Appendix D Considerations in Pipe Replacement

Abstract

Most of the design, construction, and maintenance practices in the pipeline industry were established before the extensive use of modern control-rolled and microalloyed steels. With the exception of a few isolated research projects, the impacts of the fundamental changes in the steel metallurgy in modern microalloyed steels have not been systematically examined and understood. For instance, these new steels may have very low strain-hardening capacity and high levels of heat-affected zone (HAZ) softening due to their ultra-low carbon low-hardenability chemistry. The low strain hardening and HAZ softening reduces the strain capacity of girth welds. Current codes and standards have not kept up with the evolution of the linepipe manufacturing and field girth welding practice. This has led to integrity issues in newly constructed pipelines despite those pipelines being fully code-compliant.

A brief review of the linepipe manufacturing history with a focus on the chemical composition and rolling practices that directly affect the mechanical properties and the response to welding thermal cycles is given. The characteristics of linepipes made from modern microalloyed steels are contrasted with that of vintage linepipes made from hot-rolled and normalized steels. The implications of the pipe and weld characteristics on the design, field girth welding, and maintenance of pipelines are highlighted.

The issues highlighted here should help the selection of pipes and girth welding procedure to achieve high strain capacity. The information presented here can be used in pipe replacement projects and post-construction stress capacity assessment.

D.1 Scope of this Document

1. This document is intended to address pipeline segments in known areas of ground movement or potentially subjected to loads inducted by ground movement, where longitudinal strain may exceed the elastic limit (~0.2% strain for pipe grades up to X70).
2. The focus of this document is the additional considerations beyond those required in current codes and standards or assumed by the industry in general. These additional considerations may not be applicable or necessary for pipelines with stable support conditions with minimal risk of ground movement.
3. The potential failure modes addressed in this document are girth weld leak or rupture under tension load in the longitudinal direction of the pipeline.
4. This document is useful in at least the following scenarios:
 - a. Pipe replacement in known areas of ground movement.
 - b. Newly constructed pipelines with modern lean chemistry TMCP (thermal-mechanically controlled process) steels in areas with potential for small to moderate-level of settlement or ground movement (expected movement minor enough that area is not actively managed in a ground movement program).

D.2 Loading on Girth Welds and Design Assumptions

1. The vast majority of in-service pipelines designed to ASME B31.4 and B31.8 have taken the approach of stress-based design, where the longitudinal stress in the design stage is limited to 90% SMYS. When a pipeline is designed to meet this requirement, one may interpret that the pipeline is capable of sustaining a longitudinal stress of 90% SMYS or higher. This 90% SMYS stress is equivalent to a strain capacity of approximately 0.21% for X70 pipes and 0.15% for X52 pipe. In other words, the current requirements in codes and standards assure a strain capacity of ~0.15-0.21%. Many welds have strain capacity greater than 0.15-0.21%, but such capacity is not assured when meeting the current codes and standards.
2. The contributors to longitudinal stresses include:
 - (1) residual stress from welding,
 - (2) post-construction locked-in stress from the construction process,
 - (3) thermal stress from temperature differential between construction temperature and operation temperature,
 - (4) stress from Poisson's effects when a pipe is under internal pressure,
 - (5) bending stress from settlement or lateral movement, and
 - (6) sag/side tension stress from settlement or lateral movement.
3. Among all these contributors, the stress from Poisson's effect is easiest to estimate. The thermal stress is easy to compute if the installation temperature is known. In most cases, the installation temperature is not known. A temperature differential of 30-40 °F has been used to account for the thermal stress. The residual stress from welding principally affects welds with brittle material properties and fatigue life. For pipelines with minimal cyclic stresses on girth welds, the residual stress is not a major player.
4. The other three contributors (locked-in stress from construction, bending stress from settlement or lateral movement, and sag/side tension stress) can be major contributors to girth weld failures. The locked-in construction stress can come from (1) pipe segments not having conforming profile thereby introducing significant secondary loads as the pipe are made to accommodate the trench profile, (2) tie-in welds forced into alignment, and/or (3) differential settlement. The magnitude of these three stress contributors are often difficult to estimate. In most cases, these stresses are NOT actively managed. In other words, despite the fact that a stress-based design may require the longitudinal stress being less than 90% SMYS, the above three stress contributors typically are not actively managed to meet the design requirements, except in locations with known history of ground movement.

D.3 Why Are Additional Considerations beyond Codes Necessary?

1. Relevant codes and standards that cover pipe and girth weld requirements are API 5L (Canadian equivalent CSA Z245.1) and API 1104 (Canadian equivalent Z662). ASME B31.4 and B31.8 have certain design requirements on pipes and girth welds.
2. With rare exceptions, the requirements in the above codes and standards are meant for pipelines on stable support conditions, i.e., minimal longitudinal strain demand. Consequently, pipe segments in full compliance of codes and standard can fail at low longitudinal strains (strain less than 0.5%).
3. There is misinformation about the requirements in codes and standards. Some publications suggested that girth weld strength overmatching, i.e., weld strength being higher than the strength of the pipe, is required in codes and standards. There are no such requirements. Welds can have strength substantially lower than the strength of the pipe, but still meet the requirements in current codes and standards. PRCI Seismic Design Guidelines claim that girth welds meeting API 1104 requirements are capable of sustaining 4% strain. While some welds may have strain capacity of 4% or higher, API 1104 does not have requirements that would adequately ensure a strain capacity of 4%. In fact, the strain capacity of a girth weld can be as low as 0.3%, but still meet the 1104 requirements.
4. B31.4 and B31.8 permit pipelines designed to 2% strain while meeting certain requirements. However, the language of the requirements is so vague that the exact procedures for implementing the requirements are not clear at all. More importantly, permitting design to 2% strain is not the same as stating that a pipeline is good for 2%. Some have misinterpreted the 2% strain design limit as a proof that pipe segments are good for 2% strain.

D.4 Evolution of Materials and Their Response to Welding

Up to the late 1960s, linepipes up to API Grade X60 were manufactured from hot rolled coils and normalized plates, see Figure D-8 [278]. The introduction of thermo-mechanically (TM) processed plates since the late 1960s enabled the production of higher strength linepipes with submerged-arc welded longitudinal seam. More recently, accelerated cooling from finish rolling temperature along with the TM rolling allowed the production of linepipes for grades up to X100 [279]. The strength increase is primarily derived from the rolling and cooling processes. The carbon content in the linepipes has decreased over the years. The control-rolled and microalloyed steels usually have fine grain (more commonly acicular ferritic) microstructures with excellent toughness and weldability even with increasing strength. The reduction in carbon content has led to reduced hydrogen-cracking (cold cracking) propensity in field welding. The toughness of the new steels, as measured by Charpy impact energy, has also increased significantly in comparison to the older hot-rolled and normalized steels.

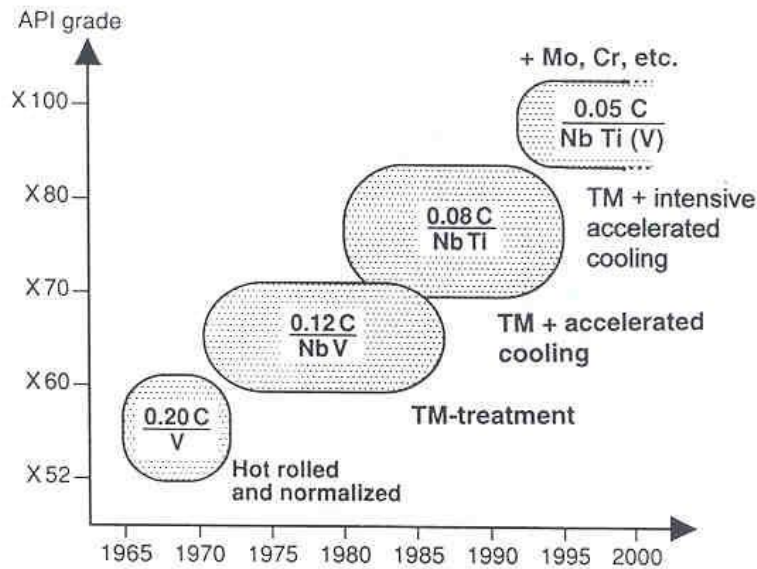


Figure D-8 Evolution of chemical composition and grade of linepipes [278]

D.5 Features of Modern Linepipes that are Detrimental to Pipeline Performance

The TM rolling process with accelerated cooling resulted in some unintended consequences on the new steels, especially with the lean chemistry including ultra-low carbon. Some of the undesirable features of the new steels are (1) reduced strain hardening capacity as shown by progressively higher yield to tensile (Y/T) ratio with increasing grade level, (2) HAZ softening in seam and girth welds, (3) non-uniform material properties, (4) reduced uniform strain (strain at the ultimate tensile strength), and (5) reduced total elongation.

Examples of HAZ softening are shown in Figure D-9, Figure D-10, and Figure D-11. The heavily-rolled materials can show splitting along the mid-thickness plane under tension load (Figure D-12). The HAZ can have reduced ductility and toughness as shown in Figure D-13.

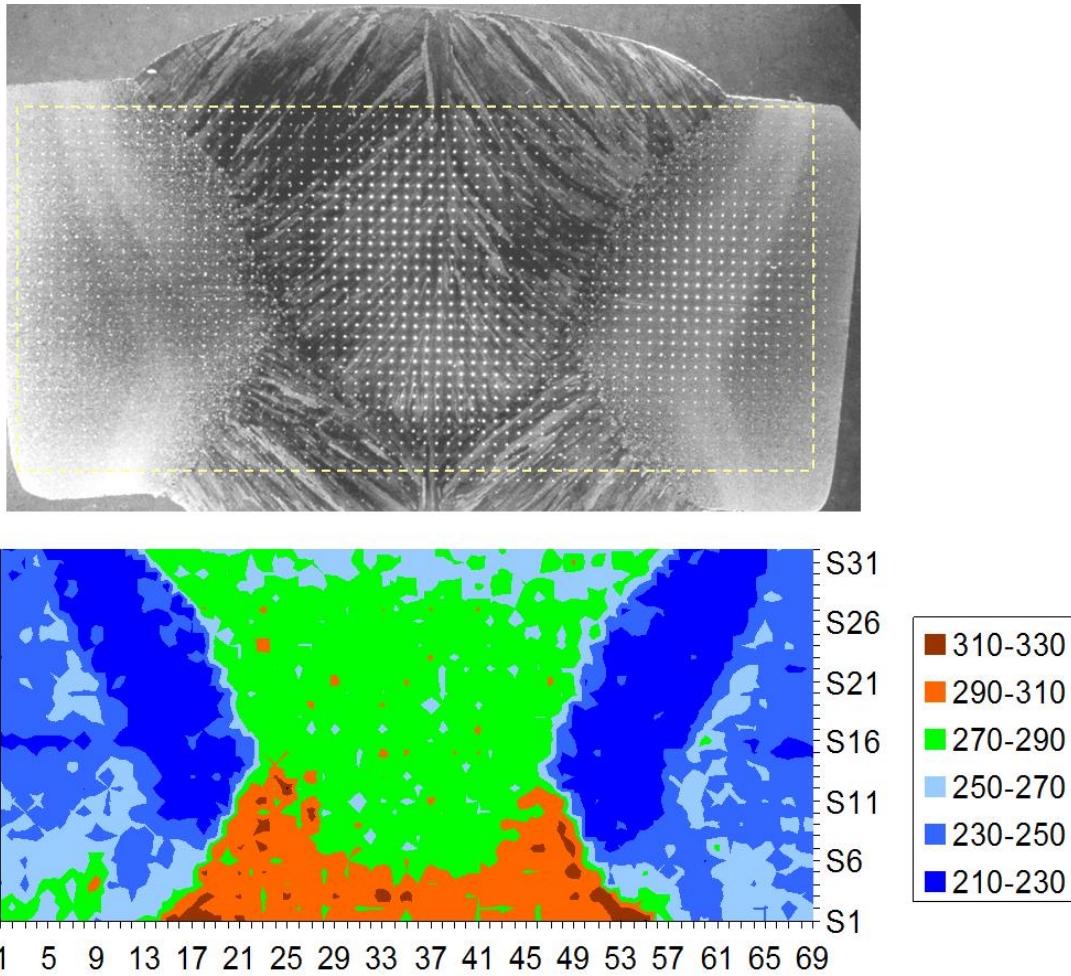


Figure D-9 Macro and hardness map of an X100 seam weld

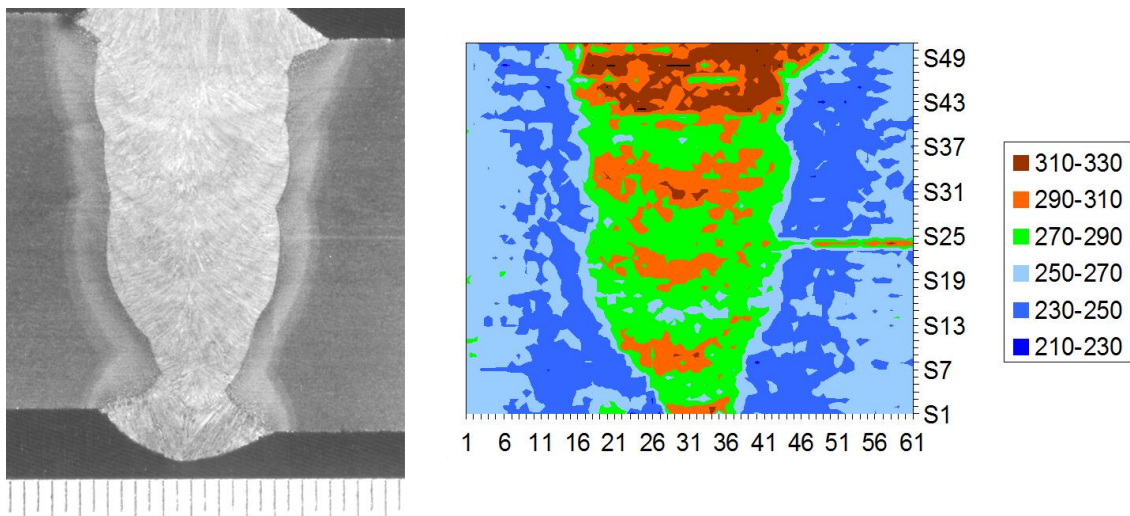


Figure D-10 Macro and microhardness map of an X100 girth weld made with mechanized GMAW process

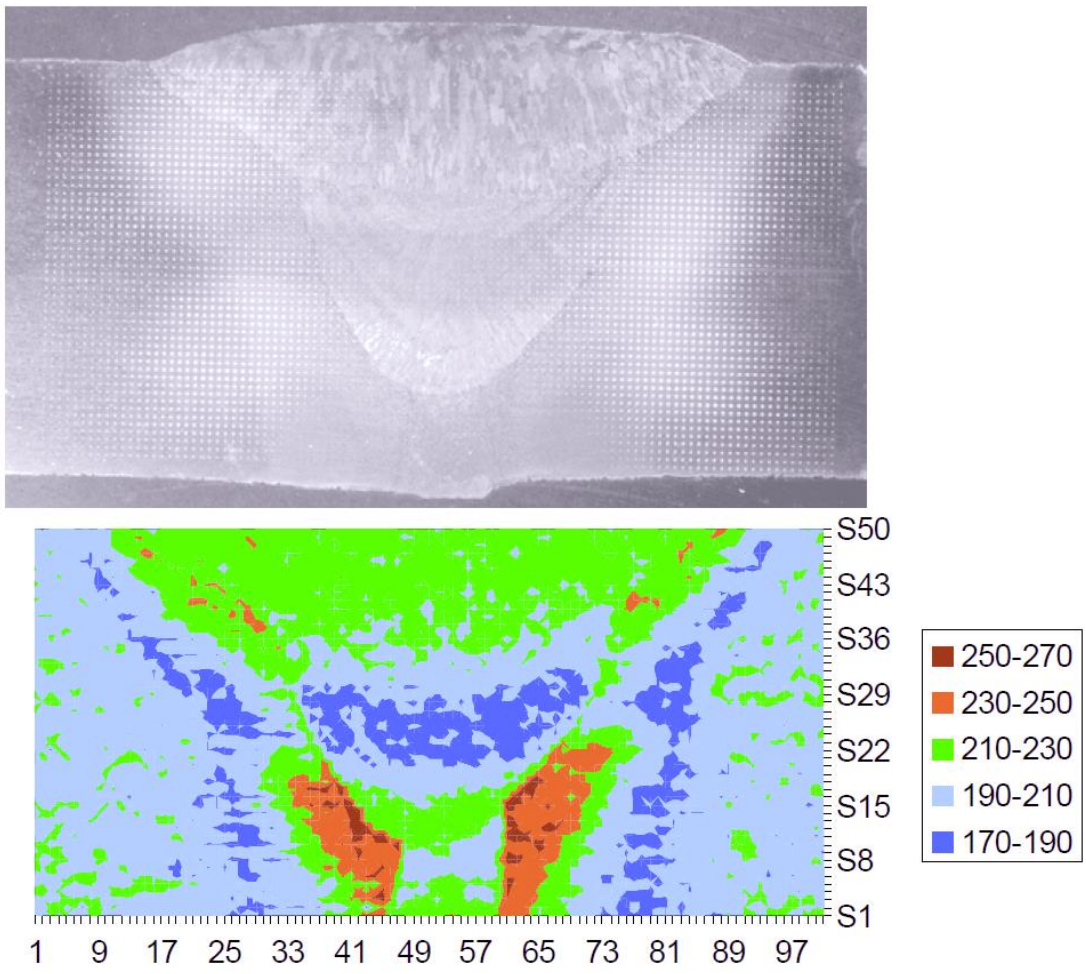


Figure D-11 Macro and microhardness map of an X70 girth weld made with mechanized GMAW process

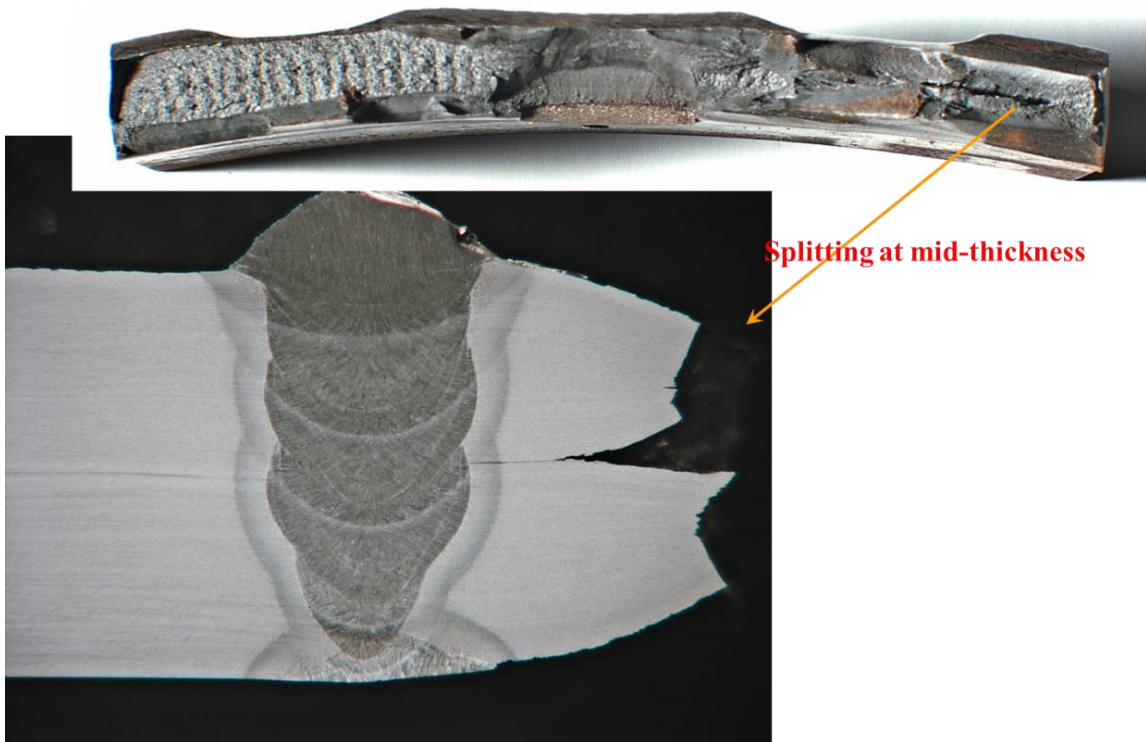


Figure D-12 Failure of an X100 girth weld. Splitting occurred in the base metal, characteristic of heavily-rolled steels.

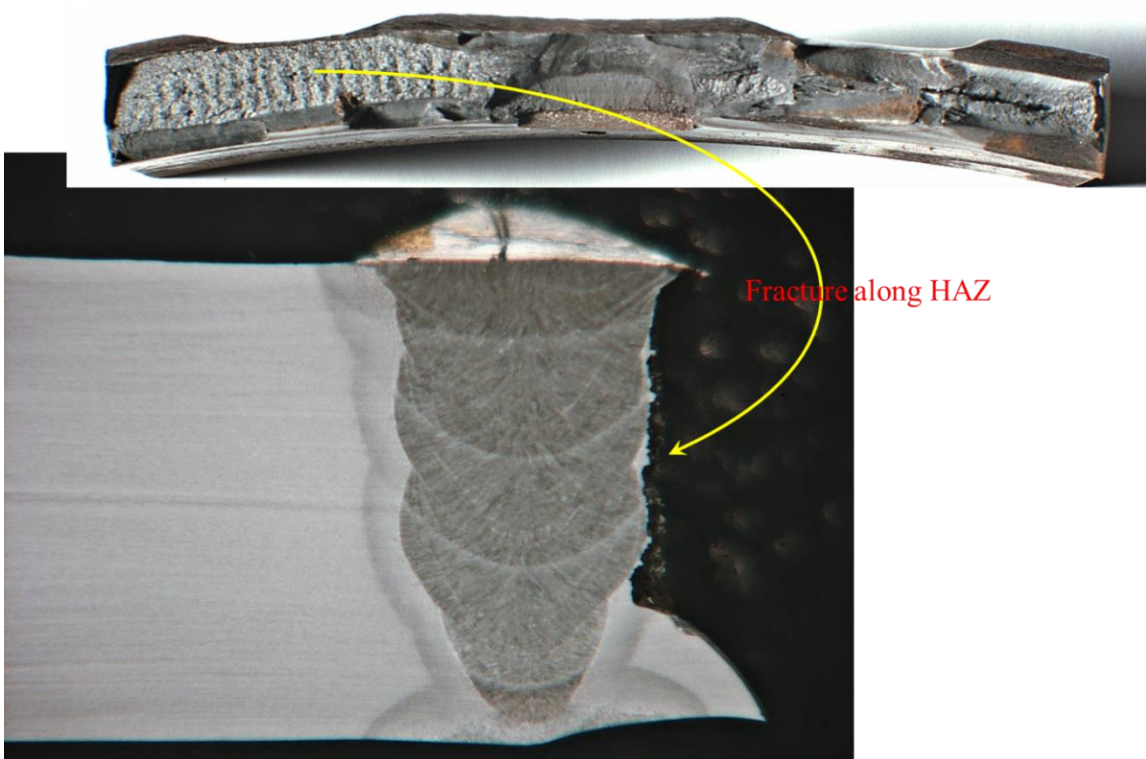


Figure D-13 Fracture along the HAZ of an X100 weld

The examples given above are mostly from an X100 weld. It should be noted that pipe grade does NOT determine the extent of HAZ softening. The principal drivers for HAZ softening are chemical composition of steels and welding heat input. Lower grade materials, such as X65 and X70, can have lean chemistry and low carbon. They are just as susceptible to HAZ softening as X100 steels. Furthermore, manual welds typically have higher heat input than mechanized GMAW welds. For the steels shown in the above examples, the level and extent of HAZ softening would be greater if manual girth welding processes were applied.

D.5.1 Design, Construction, and Maintenance Practice

Much of the design, construction, and maintenance practice in the North American pipeline industry were established before the extensive use of modern control-rolled and microalloyed steels. For instance, the widely used pipeline design and construction standards, such as ASME B31.4, ASME B31.8, and API 1104, were adopted by the industry well before the widespread use of modern microalloyed steels. The undesirable features of the modern linepipes are not adequately addressed in the current codes and standards.

D.6 Consequence of HAZ Softening

Existing test data have shown that, due to welding thermal cycles, the strength in HAZ can be reduced by as much as 20-25% when compared to the strength of the pipe. The width of the softened zone varies from 2 to 5 mm. Only a portion of this HAZ width has the maximum strength reduction of 20-25%.

Figure D-14 is an example of weld strength undermatching and HAZ softening of an X70 pipe. The actual yield strength of the X70 pipe is close to the upper bound value of API 5L PSL 2 pipes.

The negative impact of softened HAZ is particularly strong for manual welds as shown in Figure D-14 which typically have 60° included bevel angle and thin-walled pipes (wall thickness less than 3/8-inch). After welding, the plane of the softened HAZ zone is aligned approximately 35°-45° with respect to the pipe longitudinal direction. In Figure D-14, the black lines represent 45° shear planes that align with the softened HAZ and the weak E6010 root pass. This angle is the preferred plastic flow path when the pipe is under longitudinal tension. High level of plasticity can accumulate in this plane at nominal strain levels as low as 0.3%. The weld can fail by plastic shearing along the softened HAZ zone even the weld is free of anomalies and fully code-compliant. The existence of high-low misalignment can make the matter worse.

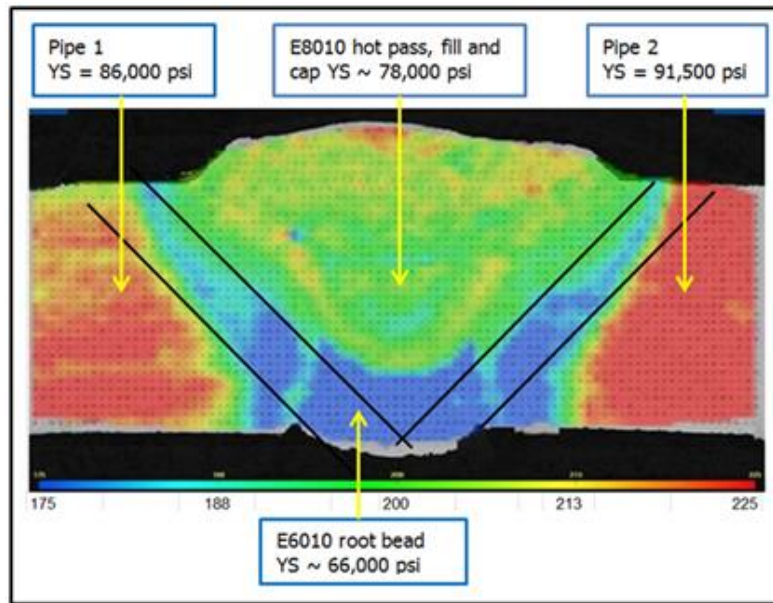


Figure D-14 An example of manual SMAW weld with weld strength undermatching and HAZ softening for an X70 pipe having much higher yield strength than 70 ksi

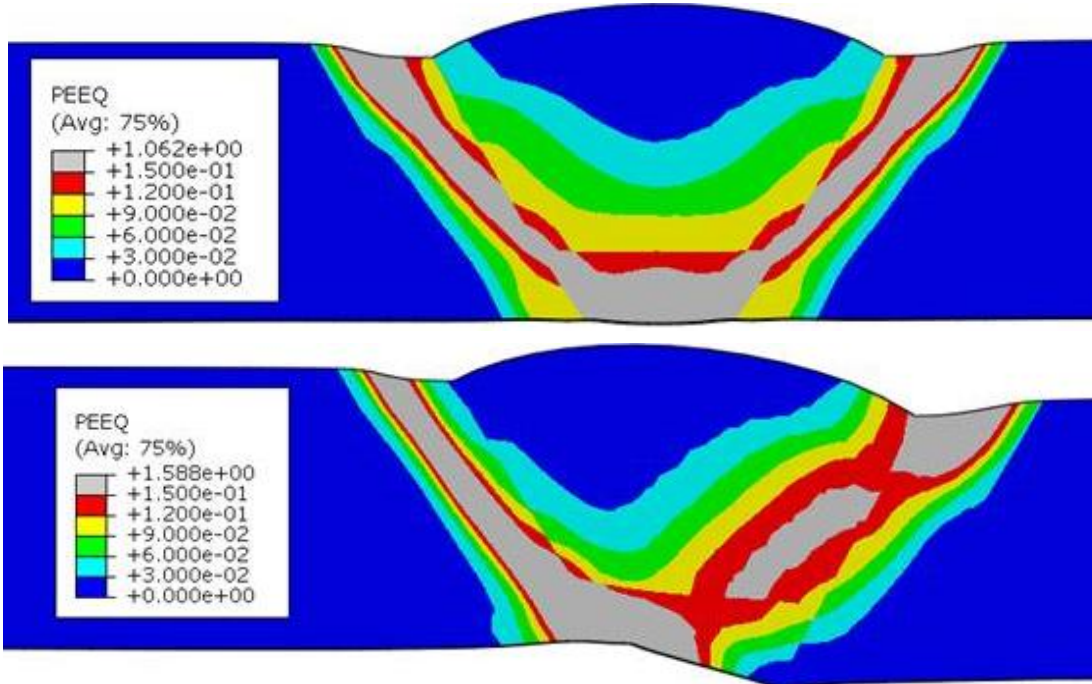


Figure D-15 Contours of equivalent plastic strain. Significant plastic straining occurs in the softened HAZ when the weld is subjected to longitudinal tension. Top: no high-low misalignment. Bottom: with high-low misalignment.

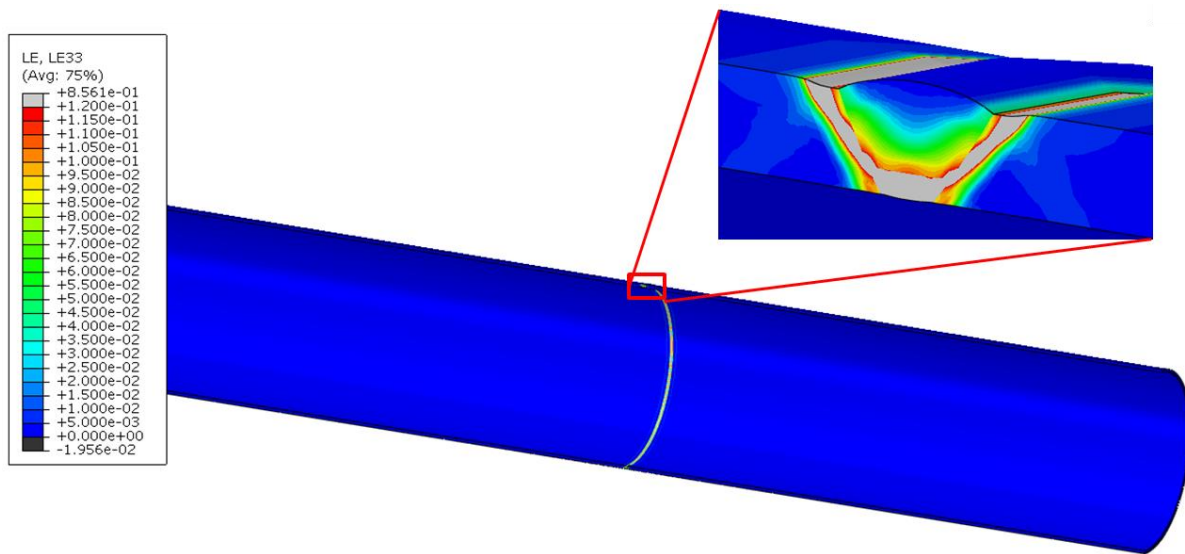


Figure D-16 Contours of longitudinal strain. Strain concentration occurs in the softened HAZ when the weld is subjected to longitudinal tension.

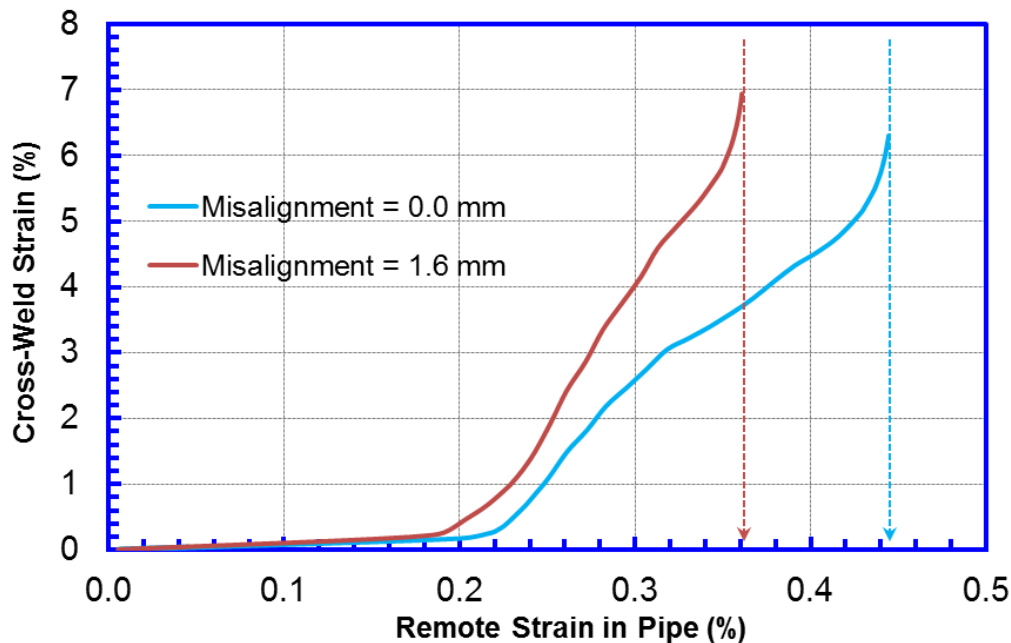


Figure D-17 Cross-weld strain as a function of the remote strain in pipe

Examples of high plastic strain in the softened HAZ are shown in Figure D-15. The plastic strain in the softened HAZ is well over 15% while the base pipe material sees very little plastic strain, i.e., the pipe remains in elastic state.

An example of longitudinal strain distribution is given in Figure D-16 for a weld without high-low misalignment. The strain in the softened HAZ is above 12% while the strain in the base pipe material is less than 0.5%.

The development of strain concentration in the weld as the pipe is being strained is illustrated in Figure D-17. Prior to material yielding when the strain is less than approximately 0.2%, magnitude of the cross-weld strain and the remote strain in the pipe is comparable. Once the weld area starts to experience yielding, its strain increases at much greater rate than the strain in the pipe, with a ratio of approximately 10:1. For instance, when the pipe strain increases from 0.2% to 0.3%, the cross-weld strain increases from 0.2% to 2.6-4.0%, depending on the level of misalignment. For the weld without misalignment, the cross-weld strain increases at an extremely high rate when the remote strain in pipe approaches approximately 0.44%, indicating nearly all deformation occurs in the weld region. This 0.44% strain is effectively the strain capacity of the weld joint. For the weld with 1.6 mm misalignment, the strain capacity is decreased to 0.36%. Even though those welds do not have any flaws, the gross strain concentration in the weld region effectively limits the strain capacity to a level less than 0.5%.

Mechanized GMAW processes can typically produce sound welds with strength higher than those from manual cellulosic SMAW processes. However, mechanized processes are not economically practical when only a few joints are replaced in an isolated location. Even on a new pipeline construction project, manual welds are often utilized at tie-ins, road, creek and utility crossings, and other areas of difficult terrains. These are the areas prone to having high strains, both from construction and during service.

Having higher weld strength can reduce the negative impact of HAZ softening. However, if the level of HAZ softening is high and the width of the softened zone is wide, the softening zone itself can lead to low strain capacity even with high weld strength.

D.7 Major Gaps in Current Codes and Standards

With respect to building pipe segments that are resistant to high longitudinal strains, there are major gaps in current codes and standards.

1. API 5L and similar standards have generous allowance for the pipe upper bound tensile properties for a particular grade. PSL1 pipes have no upper limits on strength. The upper bound limit of yield strength of PSL2 pipes is approximately SMYS+22 ksi. The upper bound limit of UTS of PSL2 pipes is approximately SMTS+30 ksi where SMTS is the specified minimum tensile strength. For instance, one could get X70 pipes with 90+ ksi yield strength.
2. In procedure qualification tests in accordance with API 1104, welds are considered qualified even when cross-weld tensile specimens can fail in the weld region, provided that the failure stress is greater than SMTS of the grade of pipe being qualified. The SMTS of X70 pipes is 82 ksi. Therefore, X70 girth welds can fail at a stress level of 82 ksi and pass the qualification tests. If such welds are made to pipes with actual yield strength of 90 ksi and UTS of 100 ksi, the welds would pass qualification tests but have low strain capacity.
3. The standards are silent on HAZ softening. There are no tests or requirements to measure materials' susceptibility to HAZ softening in either linepipe or girth welding standards.

4. Tensile properties in hoop and longitudinal directions can be quite different, particularly yield strength. For moderate to large diameter pipes, API 5L has no requirements on testing longitudinal properties which are very important for pipes experiencing high longitudinal strains.
5. Standard tensile tests using flattened straps tend to produce yield strength that is lower than the actual yield strength of the pipe material in its non-flattened configuration. To meet the minimum strength requirements of a particular grade, the overall strength distribution of pipes has to move up.
6. The issue with expanded pipes during hydrostatic testing in some of the recent new pipeline construction projects has led pipe manufacturers to aim for high strength. The increase of the pipe strength makes it more likely to have undermatching girth welds.

D.8 Considerations in Pipe Specifications⁶

In locations where strains may potentially exceed elastic limit, the best starting point to have strain-tolerant pipeline is getting the right pipes through rigorous and practical pipe specifications. The following steps are suggested as a starting point. More specific requirements can be developed when needed.

1. Educate and communicate. Inform individuals responsible for pipe procurement and welding supervisors about the consequence of weld strength undermatching and HAZ softening. It is critical that those individuals understand that compliance of the current codes and standards is not sufficient to ensure moderate to high levels of strain capacity.
2. Put an upper limit on the tensile properties. In a large order, pipe mills typically can't work with a narrow band of tensile properties. A range of 12-15 ksi is typically workable. Due to the possible large measurement variations in yield strength, it's better that the upper limits are given in UTS. For instance, the SMTS of X70 pipes is 82 ksi. The upper limit of the UTS can be set at 95 ksi.
3. Require tensile testing in both hoop and longitudinal directions.
4. The required yield strength in longitudinal direction can be lower than SMYS. This can lead to lower Y/T ratio in the longitudinal direction and makes overmatching weld strength more likely.
5. Set upper limit of Y/T ratio (lower than that permitted by API 5L), particularly in longitudinal direction. For pipe grades X70 and lower, a Y/T ratio less than 0.87 in the longitudinal direction is reasonable.

⁶ Having additional requirements beyond those in standards can be a difficult task, especially when the quantity of needed pipes is small. It is however necessary to consider the consequence of inadequate pipe specifications, particularly in locations of potentially high strains. Building strain-tolerant pipelines becomes harder through other means if undesirable pipes are procured.

6. Request pipe mills and distributors use more rigorous test procedures than those allowed in current codes and standards. The test procedures in current codes and standards are insufficient for precise measurement of material properties for the modern new steels.
7. Always ask for full stress-strain curves from tensile tests. The stress-strain curves can tell a lot more about material properties and test data quality than a table of yield strength and UTS. The uniform strain, i.e., engineering strain corresponding to UTS, should be determined and reported as well.

D.9 Recommendations

D.9.1 Pipe Segments already in Service

1. If pipe replacements were done without some of the special considerations outlined above, an intervention limit may be set at 0.3% strain. As stated earlier, many welds (or even a majority of the welds) can have strain capacity much greater than 0.3%. Without information on pipes and welds more specific than those required in current codes and standards, strain capacity can as low as 0.3%.
2. Collect mill certs of pipes, records of welding procedures, and NDT records with flaw acceptance criteria if site-specific assessment is anticipated. Such information would be useful if there are needs/desires to raise the intervention limit beyond 0.3%.

D.9.2 Near-Term Planned Pipe Replacement

1. Collect mill certs of pipes, records of welding procedures, and NDT records with flaw acceptance criteria.
2. Select lower grade heavy wall pipes over high grade light wall pipes if there is a reasonably certainty that the actual strength of the lower-strength pipes would be lower than that actual strength of high grade pipes. Pipes of lower strength typically have high strength hardening than high-strength pipes. It's easier to have weld metal that overmatches the lower-strength pipes. However, it is important to understand the lower grade does not necessarily mean lower strength, as explained in sub-section 4 of this document. Ultimately, it's actual properties of the pipes that matter, not a particular grade they are designated.
3. Encourage field welding crew to produce one extra weld and ship it to a central location with proper IDs. A weld pup with 2 ft on either side of the weld would be sufficient for characterizing the pipe and weld properties. A battery of tests can be done on the pipe and weld should there be a need to perform a site-specific assessment. The test data are essential to establish site-specific intervention criterion when used with appropriate assessment procedures/models.

D.10 Long-Term Actions to Ensure Adequate Strain Capacity

1. One question that may be asked is whether new pipes/welds are always better than “vintage pipes/welds” for a given segment that may be considered for replacement. The answer is no. The principal integrity threat of vintage girth welds is the possibility of

pre-existing large planar flaws that were left from construction. Since there are no reliable free-flowing inline tools to detect and size those flaws, replacing vintage girth welds removes the principal cause of possible failures. On the other hands, the new pipe/welds could create new integrity issues. The threat to girth weld integrity of the new pipe/welds is no longer pre-existing large planar flaws. Instead, weld strength undermatching and HAZ softening can still lead to low strain capacity, thus possible failures from longitudinal strains. Vintage girth welds almost never have HAZ softening. Some degree of weld strength undermatching is possible. However, the undermatching can usually be compensated by wide and smooth weld caps in those welds. From the viewpoint of risk, a segment of vintage pipe/welds being replaced may or may not have large planar flaws. On the other hand, if the upper bound strength of the new pipes is not known or controlled, it's possible that every girth weld in the replaced segment has HAZ softening and weld strength undermatching. Having new pipe/welds brings benefits other than girth welds free of large flaws, such as better coating. It is, however, important to recognize that the strain capacity of new pipe/welds is not guaranteed to improve over vintage pipe/welds unless proper measures are taken to ensure that there is no strain concentration in the weld region.

2. Given the accuracy of strain demand measurement devices/procedures and variations in field and material conditions, it is recommended that a strain capacity of 0.5% or higher should be targeted for future pipe replacement projects in areas of possible ground movement.
3. Consider implementing the pipe specifications given in Sub-section 5. It may not be practical to implement all recommendations at one time.
4. Select lower grade heavy wall pipes over high grade light wall pipes if there is a reasonably certainty that the actual strength of the lower-strength pipes would be lower than that actual strength of high grade pipes.
5. Tools and processes are available or being developed to ensure strain capacity of 0.5% or higher. Quantitative analysis of strain capacity is available when needed.

Appendix E Newer and/or Developing Pipe Monitoring Techniques

Abstract

Various ground and pipe monitoring techniques are extensively covered in Section 8.3. Most of these techniques are considered relatively mature, or at least there have been some field applications. At the same time, other monitoring techniques are being developed. In some cases, the working principles of those techniques are well proven and/or the techniques may have been used in applications other than monitoring geohazards. In other cases, the concepts are being developed and verified.

In this section, some of the newer and/or developing techniques are covered. In general, these techniques have not been used in geohazards monitoring programs beyond experimental stage. It is recommended that use of those techniques should be reviewed by appropriately qualified independent experts and proven techniques should be used as a backup.

E.1 Residual Stress Measurement by IIT

Instrumented Indentation Technique (IIT) is a non-destructive technology for measurement of residual stresses in a structure by analyzing the indentation load versus indentation depth curve generated while testing the structure.

Working Principle and Description of Technology

The intrinsic hardness of a material is independent of the presence of residual stress in the structure to be tested. However, the presence of residual stress influences the deformation caused by the indenter.

A model [280] of this residual stress dependent deformation behavior is shown in Figure E-18. In Figure E-18, h_t , which is the maximum indentation depth, is constant for the three scenarios shown. The load applied to the indenter in case of tensile residual stress, L_T , is the lowest. Moving on to the scenario with zero residual stress, the comparative relaxation of stress leads to a ‘pushing’ force applied by the indented surface opposing the applied load; thus applied load L_0 must be higher than L_T to achieve the same indentation depth. In the case of compressive residual stress, the indented surface exerts an even higher ‘pushing’ force against the applied load; thus, applied load L_C in the presence of compressive residual stress is higher than both L_T and L_0 . Note that the presence of residual stress in the surface influences the contact depth h_c .

This change in the deformation behavior beneath an indenter is captured by the indentation loading curve (indentation load vs. indentation depth) as shown in Figure E-19. This is the working principle employed by indentation systems used for measuring residual stress.

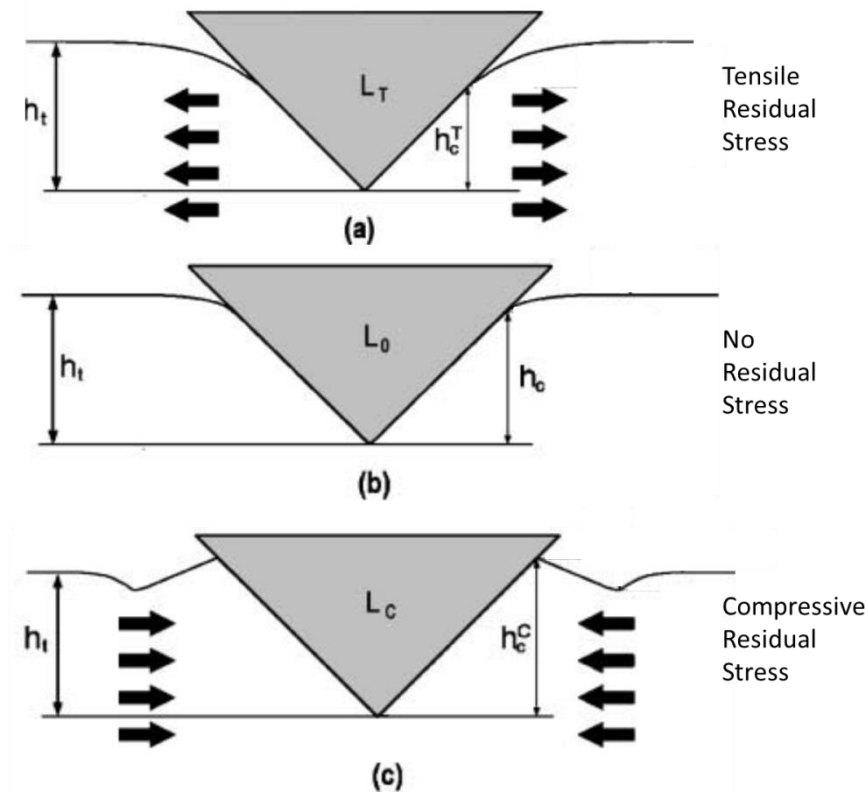


Figure E-18 Model of the residual stress dependent contact deformation behavior for (a) tensile residual stress, (b) no residual stress, and (c) compressive residual stress [280]

Instrumented indentation systems used to measure residual stress can measure the indentation loading curve in situ by sensing applied load and indentation depth during the process of indentation. The ‘shift’ in the indentation load caused by the presence of residual stress is used by the instrumented indentation system to calculate the residual stress in the structure [280]. All calculations can be performed by the software accompanying these commercially available systems (e.g. Advanced Indentation System 3000 [281] and the accompanying AIS3000 V3.10 software sold by Frontics Inc., Seoul, South Korea).

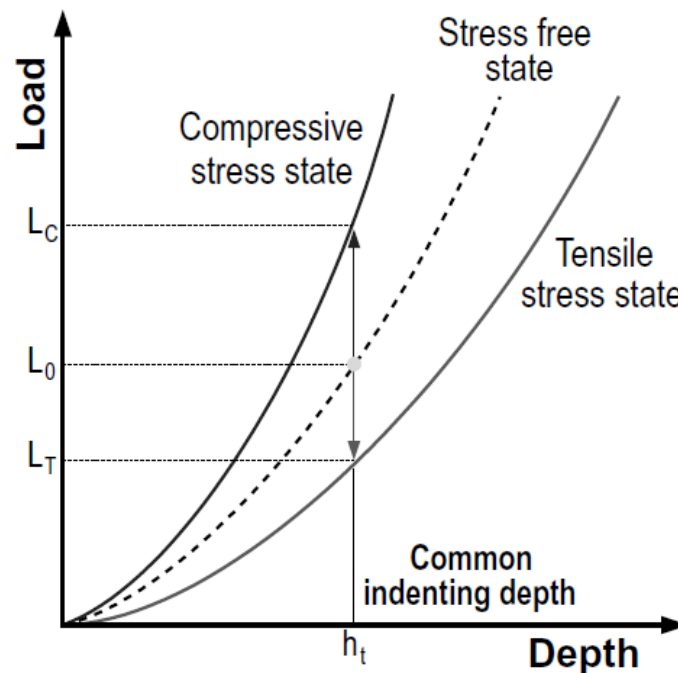


Figure E-19 Indentation loading curve showing dependence of indentation behavior on residual stress [280]

E.1.1 Field Application of the IIT to Measure Residual Stress

To accurately measure the residual stress using the instrumented indentation system, it is important to obtain residual stress free indentation curves corresponding to each microstructural region (weld, heat-affected zone, base pipe) being tested on the structure in the field. This information is required for calculation of the 'load shift' caused by the presence of residual stress [282]. This can be accomplished by first performing the indentation on a test piece made of the same material as the structure to be tested in the field.

The residual stress value calculated by IIT is the magnitude of the average value of the residual stress in the structure [282]. The principal residual stresses and their orientations cannot be determined using this technique for field applications.

The advantages of the instrumented indentation testing systems for measurement of residual stress in field are that it is a portable system and being a non-destructive in nature, does not affect the integrity of the structure being tested.

The instrumented indentation systems available commercially [281] are lightweight, portable, and are supplied with software that can immediately analyze test data and determine residual stress in the structure.



Figure E-20 Example of the application of IIT on a pipe to determine residual stress [281]

E.2 Alternating Current Stress Measurement

E.2.1 Introduction

Alternating current stress measurement (ACSM) is a non-contacting electromagnetic technique used to measure the longitudinal strain levels in a pipeline. The technology can either be used to measure strains on the outside of the pipeline with a handheld unit (not discussed in this report) or inside a pipeline behind a traditional MFL inspection tool. The current commercial name for the smart pig is the “Axial Strain Tool”.

E.2.2 Theoretical Background

Internal stresses of magnetic materials such as carbon steels alter the internal arrangement of magnetic domains leading to magnetic anisotropy. Consequently, stress effects in a ferromagnetic material are reflected through its magnetic anisotropy [283]. This interaction is called inverse magnetostriction (also known as magnetoelastic effect or Villari effect); which is the name given to the change of the magnetic susceptibility of a material when subjected to a mechanical strain.

A magnetic material has magnetic domains which are regions with uniform magnetization. Domain structure is responsible for the magnetic behavior of ferromagnetic materials such as iron, nickel, etc. (see Figure E-21). Magnetostrictive strain within each magnetic domain causes

microscopic dimensional changes in the material when magnetic domains reorder under the applied magnetic field. To minimize the total stored energy, domain magnetization vectors in iron with a positive value of magnetization constant prefer to align themselves parallel to a tensile stress axis and perpendicular to a compressive stress axis. Figure E-22 shows a schematic of the domain wall changes due to application of stress and magnetic field. The change in magnetization is believed to influence the magnetic permeability.

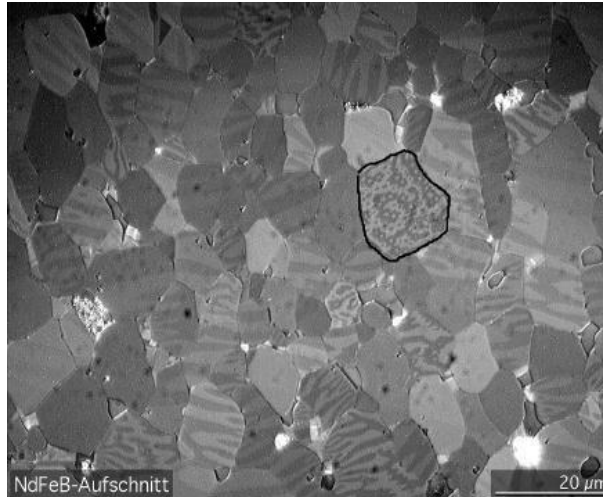


Figure E-21 Microcrystalline grains within a piece of NdFeB with magnetic domains made visible with a Kerr microscope. The domains are the light and dark stripes visible within each grain. In most materials the domains are microscopic in size, around 10^{-4} to 10^{-6} m. [283]

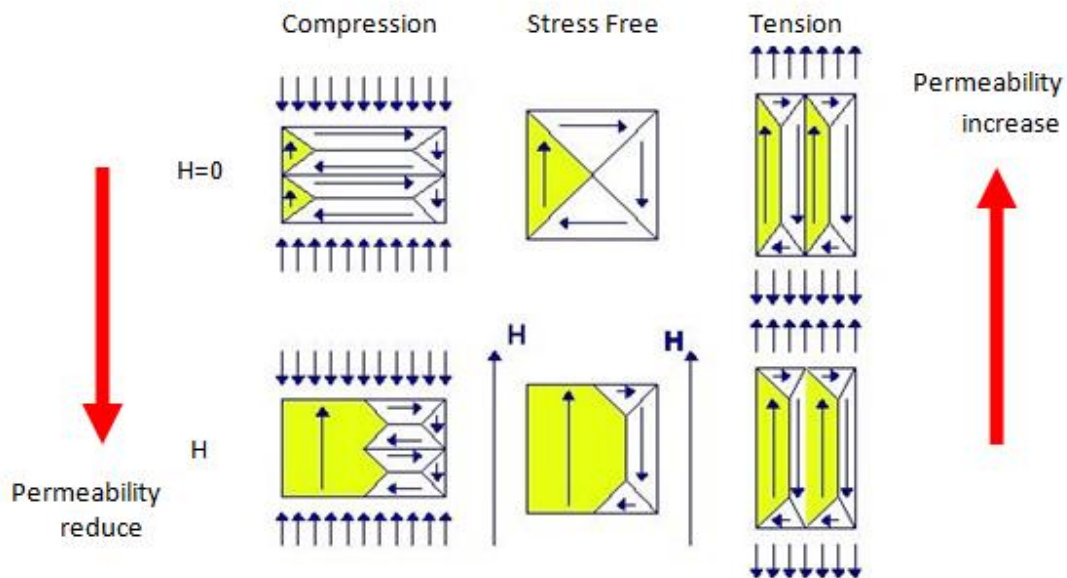


Figure E-22 Influence of stress on magnetic domain [268]

E.2.3 Sensor Technology

The ACSM sensor currently deployed on MFL inspection tools is based on the inverse magnetostriction effect where the magnetic domain behavior of the pipe is dependent on the mechanical strain in the pipe. The sensor is based on the measurement of the magnetic permeability and induction of the pipe wall. The ACSM sensor uses an inducing coil to magnetize the region of interest and small sensing coils to measure changes in the magnetic field close to the metal surface. It uses a 5 kHz alternating current (AC) to produce a uniform field within a thin surface layer due to the skin effect in ferrous materials, in essence a reading on the surface layer of the pipe similar to a strain gauge [268].

E.2.4 Sensor Validation

As part of a study for TransCanada Pipelines Ltd. (TCPL), C-FER Technologies Inc. (C-FER) conducted experimental trials to calibrate the ACSM sensor [284]. The test was carried out in a bi-axial (longitudinal and hoop) test frame that could simultaneously apply internal pressure and compressive or tensile axial loads. The test setup subjected a pressurized pipe specimen to a displacement-controlled axial tensile/compressive load to achieve the required combinations of longitudinal and hoop strains. The pipe strains were simultaneously measured using the ACSM sensor and traditional strain gauges fixed to the pipe specimen (see Figure E-23).



Figure E-23 Pipe assembly at C-FER's facility [284]

The test consisted of three bi-axial loading phases. The first two phases were conducted in the elastic region of the pipe and consisted of 91 elastic stress combinations, each repeated eight times for a total of 728 data points. Phase 3 was intended to capture the performance of the ACSM probes in the plastic region of the stress-strain curve and consisted of 12 load combinations. Results of the lab testing indicated that it was possible to measure strain well into the plastic range.

Based on the experimental trials and a previously conducted strain relief where ACSM field measurements were taken, the authors concluded that the ACSM sensors accurately measure longitudinal strains in the pipe specimen.

E.2.5 Current Inspection Capabilities and Limitations

The use of ACSM sensors for pipeline inspections is quite new and the technology is still under development. As a result, the current technological capabilities and limitations may evolve as industry adopts the inspection technique. The current generations of ACSM sensors are capable of detecting longitudinal strains caused by landslides, subsidence features or other geohazards over relatively long sections of pipeline.

To provide absolute strain values, the pipeline steel must be calibrated using a 3-point bending test. Otherwise, the tool provides axial strain variations which show areas of abnormal strain. A pipeline segment typically contains pipe with variations in steel properties, manufacturing method and manufacturer; therefore, numerous calibrations are required. As the calibration is used during the data processing phase, absolute strain values can be calculated following the run if calibrations can be performed on a piece of pipe coupon that has properties representative of the pipeline segments of interest. The actual calibration, ACSM sensors and calculations to determine strain are proprietary.

The need for calibration requires the availability of test coupons and defining the applicable boundary of such test coupons. In other words, the nature and range of physical characteristics that define a test coupon being representative must be clearly understood and applied accordingly. Some vintage pipelines often are full of replacement sections where physical characteristics of the replacement sections may or may not be available (in part depending on the clear understanding of physical characteristics necessary to define being representative). Some of the replacement sections have a high probability of having been installed under high tie-in stresses. Developing clear guidelines of the calibration and applicability and accuracy of the technique when calibration is not available are needed.

More research is required to determine if the tool can accurately measure deformations into the plastic range but as a guideline, the tool is considered accurate up to 5000 microstrains or 0.5% deformation. The absolute values reported are for the total strain which includes components due to hoop stress (which can be calculated), residual strains, construction related loading, and soil/pipe interactions from landslides and/or settlement/subsidence. It is impossible to differentiate the types of external loading that contribute to the total absolute strain from the data alone. The use of other information and judgement is required to determine the causes of

any abnormal strain values. Absolute values should be used with corrections for pressure and temperature variations when conducting run-to-run analysis.

The axial sampling rate is dependent upon the tool speed. At normal transmission pipeline flow velocities (3 to 13 ft/s, 1 to 4 m/s), the axial sampling rate is approximately 1.5 to 3 ft (0.5 to 1.0 m). Current inspection tools are equipped with four ACSM sensors spaced 90° apart. Additional sensors will be added going forward for redundancy purposes, but it is unlikely that sensor density will approach MFL or high-resolution geometry tools in the near to mid future. The ACSM tools used in the case studies below did not include sensor orientation data but the latest generation will collect orientation data. As the ACSM sensors are deployed on traditional MFL tools their specifications regarding travel speed, travel time, temperature and pressure ratings are similar to MFL tools/sensors.

E.2.6 Case Studies

Westwood et al. [268] details research by North American pipeline operators and a pipeline inspection company to assess the technical and commercial feasibility of deploying the ACSM sensors on ILI tools to measure longitudinal strain in pipelines. From 2011 to 2014 approximately 2,000 km of transmission pipelines were inspected with integrated MFL / ACSM sensors. The results of the experimental inspection runs demonstrated that the ACSM sensors were able to measure variation in the longitudinal strain in the pipelines along their inspected lengths. Without knowledge of the respective pipelines, the tool analysts were able to identify locations where measured longitudinal strains were outside normal operating conditions and likely caused by landslide related soil/pipe interaction. Note that field testing appears to have been done on pipelines operating within the elastic range of strains. Additional work would be required to prove the technology on pipelines that have yielded.

In one case study the ACSM identified an area of abnormal strains on a 30-inch natural gas pipeline where it laterally crossed an active deep seated translational slide that was 2.2 miles (3.5 km wide). Figure E-24 shows the ACSM data plotted against the known slide extents from an extensive geotechnical monitoring program. Areas of high tensile and compressive pipeline strain within the landslide were clearly identified. The operator reported that observations made during subsequent integrity investigations qualitatively verified the results of the ACSM. As it was an initial run, no comparison could be attempted to data from an extensive VW strain gauge network.

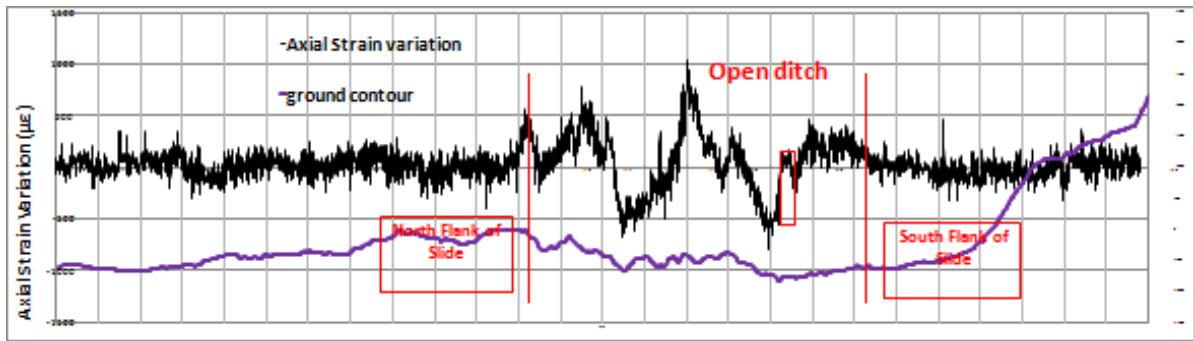


Figure E-24 ACSM tool run results for a 30-inch natural gas pipeline [268]. Graph shows the known slide boundaries (in red) superimposed on the plotted strain variations. The tool results clearly show the slide boundaries. Note that the downstream portion of the slide was stress relieved prior to the tool run; therefore, it does not show the same variation as the remainder of the slide.

In another case study a run-to-run comparison was conducted before and after a strain relief dig on a 20-inch natural gas pipeline. Figure E-25 clearly shows the area of strain relief on a run-to-run comparison of the ACSM tool. Figure E-26 shows a comparison of the ACSM tool results to VW strain gauge results with the strains plotted as membrane and bending strains. A comparison of data over the period of the run-to-run analysis indicated that there was a correlation between the results. Additionally, the data comparison indicated that although the strain gauges were installed with considerable geotechnical advice, the strain gauge locations missed the peak tensile and compressive strain areas within the landslide.

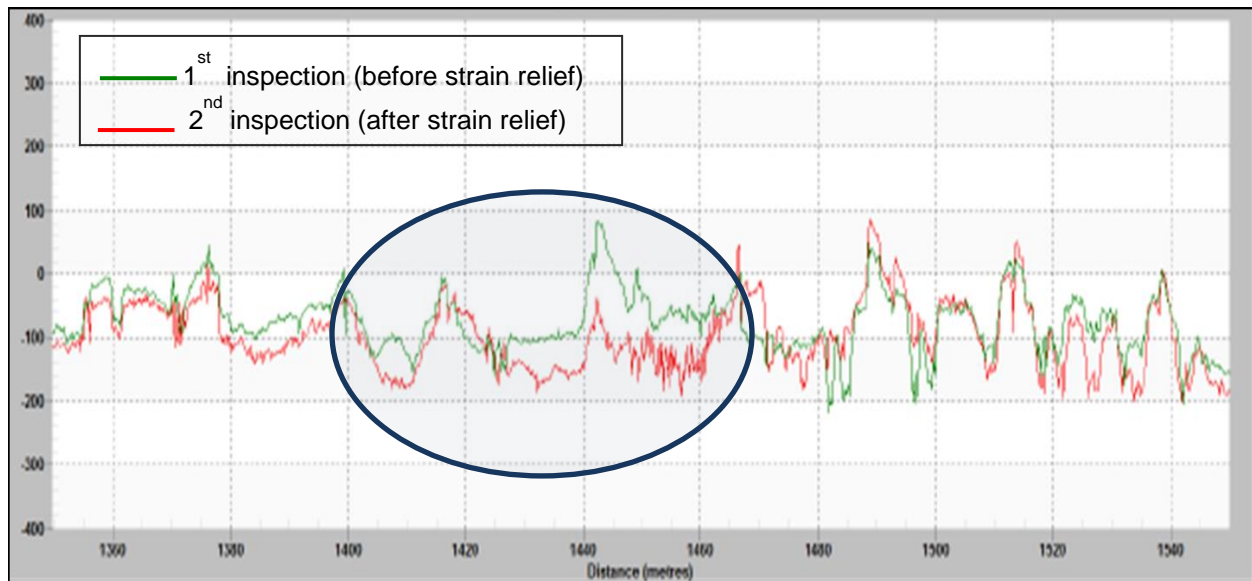


Figure E-25 Change in longitudinal strain from strain relief activities. The area of strain relief is shown in the blue circle. Y-axis shows ACSM readings in microstrains.

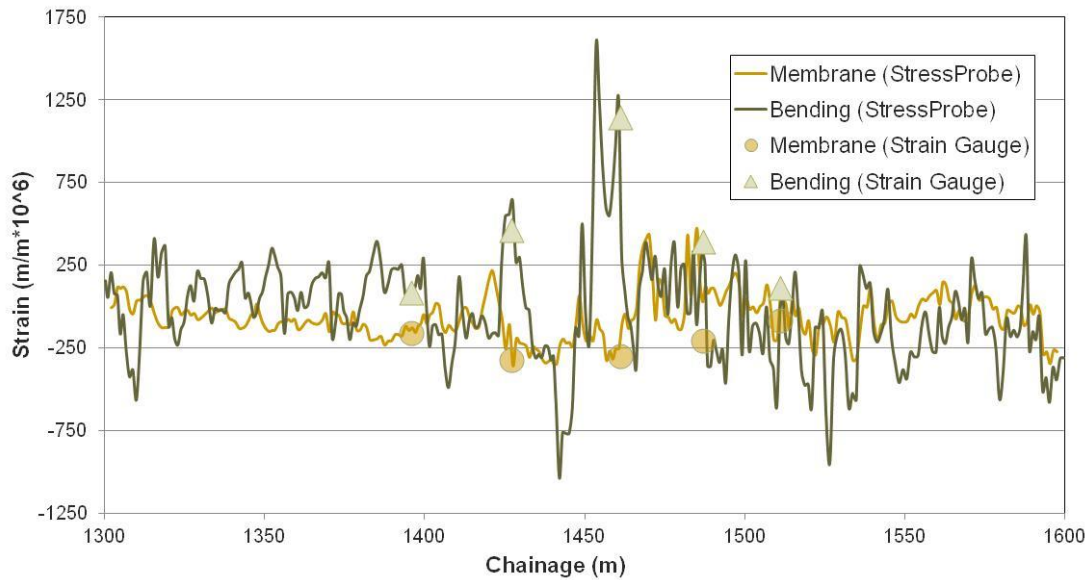


Figure E-26 Change in longitudinal strain from strain relief activities plotted as membrane and bending strains. The plot compares the ACSM tool measurements with VW strain gauge measurements.

The case studies presented by Westwood et al. [268] shows that the ACSM tool can be effectively used to highlight areas where there are strains beyond expected normal operating conditions as a result of geohazards and to identify areas where there has been strain relief. Preliminary results to try to quantify the results of the ACSM tool versus other technologies are promising but additional refinements are required with the tool platform (more probes and orientation data) and calibrating the technology.

The greatest challenge to validating the technology is that there is no other non-destructive method to compare it with. As stressed by Westwood et al. [268] strain gauges only measure the change in strain from installation onwards and current in-line inspection (ILI) technologies do not directly measure pipeline strain, but calculate longitudinal bending strain based on the absolute or change to pipe curvature (refer to Chapter 4).

The main advantage of the technique is that it allows for the detection and monitoring of areas of high tension (of particular concern to vintage welds) or compression that have little or no bending. IMU technology would not identify these areas as there is minimal longitudinal bending strain. If tool calibrations and readings are quantified to the point where they provide industry accepted tolerances (i.e. +/- 15%, 80% of the time) the ACSM technique may see near universal acceptance as the primary tool for assessments of geohazard induced pipeline loading.

With the current state of technology, if one does not trust the absolute numbers, the ACSM at minimum clearly delineates areas of abnormal straining caused by geohazards. Therefore, the ACSM can be used to focus assessment mitigation and monitoring efforts using other technologies.

The technology is currently transitioning from an experimental study into a commercially available product with limited larger diameter pig platforms. More study is required to determine the overall accuracy, repeatability and reliability of the technology.

E.3 eStress System

The eStress system is a non-destructive quantitative residual stress assessment tool using an electromagnetic method that measures the strain in materials by determining changes in the total energy of the system through variation in the electronic effective mass [285, 286, 287]. When a metal is stressed the conduction of the electrons is altered, the change in electron vibration can be directly correlated to a specific quantified residual stress using proper calibrations.

E.3.1 Working Principle and Description of Technology

The eStress system consists of an electromagnetic probe and analysis system used to assess residual stress through electromagnetic monitoring. A simplified diagram of a probe is given in Figure E-27, used to perform a low frequency impedance measurement. Real-time scanning hand-held electromagnetic pipeline probe systems were developed to provide quantified three-dimensional residual stress measurements of in place pipelines. In addition to a proprietary sensing probe, a proprietary analysis and calibration system has been developed to enable quantified residual stress measurement. The system is required to consider a broad range of variables which may include but are not limited to temperature, conductivity, magnetic properties, remnant magnetization and sensor liftoff distance and composition of the material being tested. Measurements may be made based upon a known reference and conditions, residual stresses within a material may be determined relative to adjacent zones or remote locations. Through wall stress measurements can be taken while a pipeline is in service, allowing direct measurement of the material stress state under operating conditions.

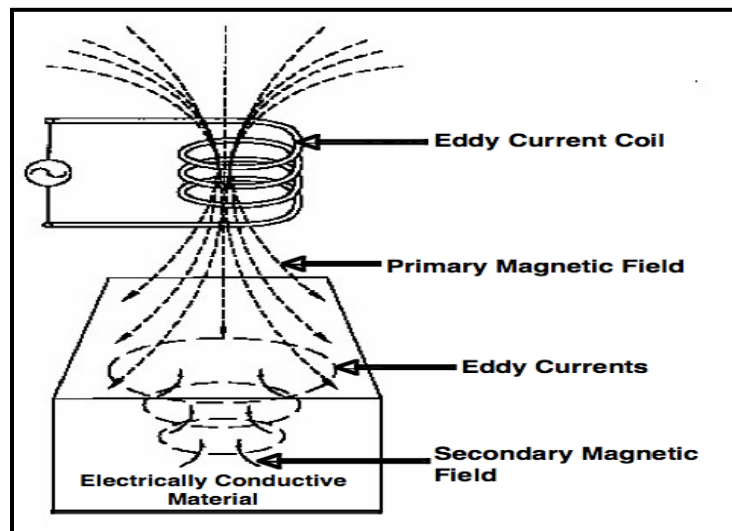


Figure E-27 Electromagnetic probe

E.3.2 Current Status of this Technique

The eStress system has been developed under DOT PHMSA SBIR phase 1 and 2 funding, with the goal to demonstrate a capability of measuring internal pipe wall stresses. Several series of prototypes have been developed based upon a single probe configuration, shown in Figure E-28. The system has been successfully demonstrated to measure residual stress levels associated with mechanically damaged regions in pipeline steels. Residual stress levels were measured in low and high strength steel pipeline material and compared to the results of neutron diffraction data for validation. Shown in Figure E-29 is the G2MT residual stress hand-held probe for portable testing of structures and materials.

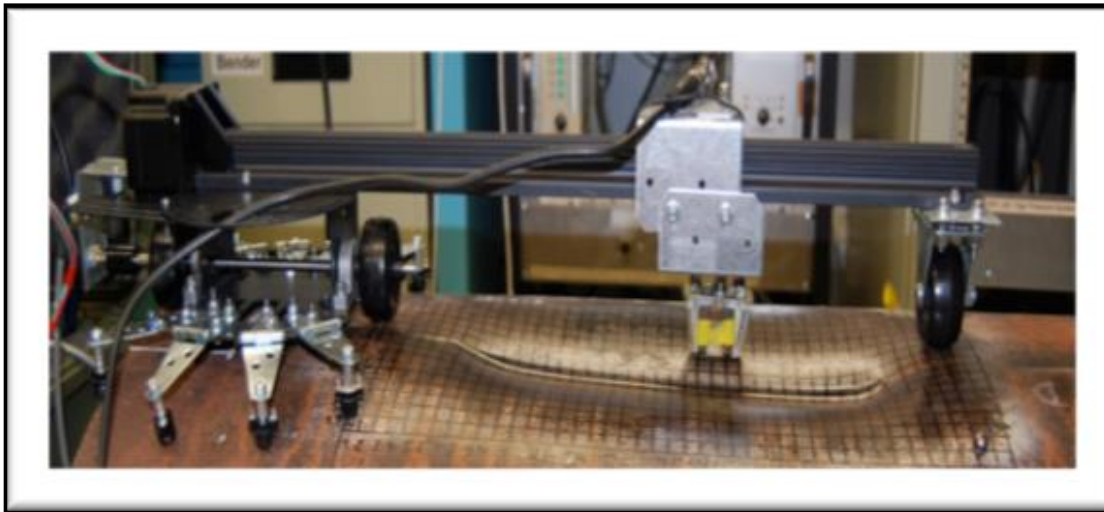


Figure E-28 G2MT preliminary residual stress scanning system for steel pipelines

Further refinement of calibration procedures to increase accuracy of residual stress measurements is underway in addition to continued development of ruggedized equipment. The latest prototype for the eStress system uses a flexible probe system, with an array of 64 or more sensors. The sensor array is in the form of a conformable mat which may be located in an area of interest for monitoring, or moved from location to location to provide scans of extended areas. Each of the existing systems requires external pipe access, with static measurements being taken. Prototype units and testing services to enable monitoring at areas of interest are available. Additional development is required to complete commercialization. Assessment of the technique at selected locations before and after remediation, using strain gauge measurements as a reference, may be helpful in understanding the capabilities of the method.



Figure E-29 G2sMT residual stress hand-held probe

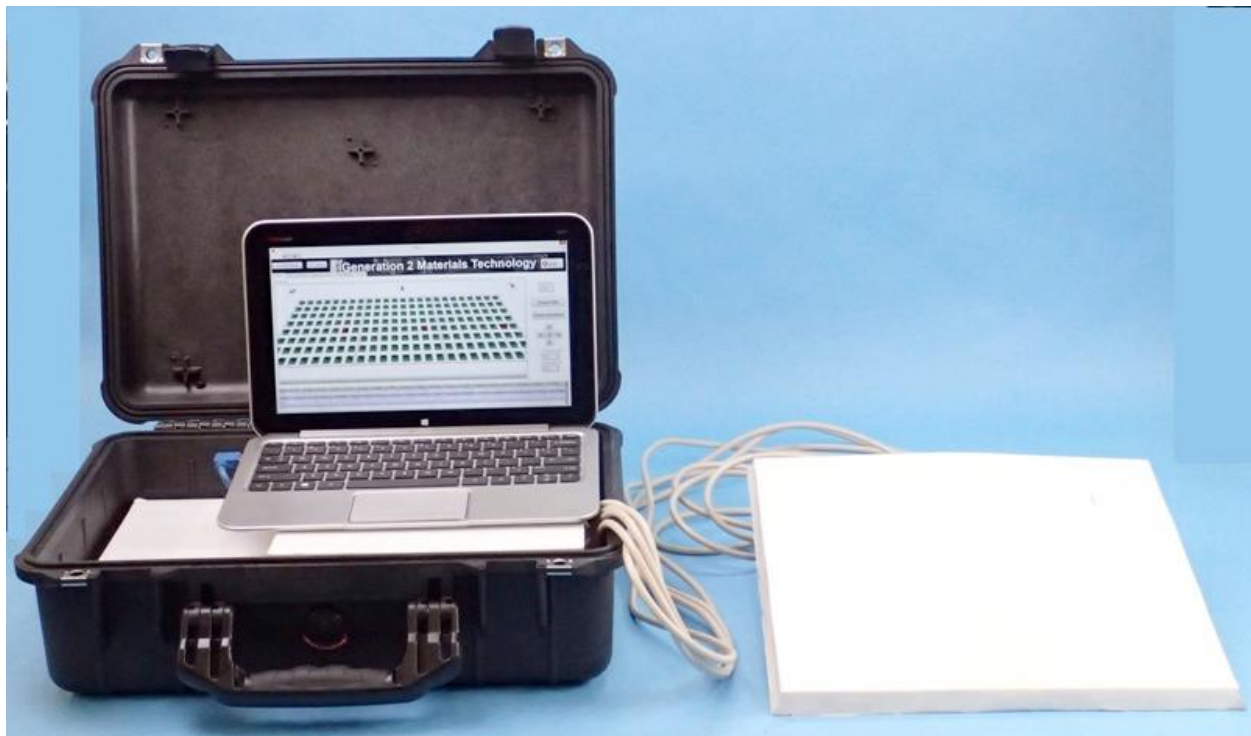


Figure E-30 Latest prototype of the eStress system from September 2014

E.4 Acoustic Birefringence

Acoustical Birefringence is an ultrasonic method of residual stress analysis based upon the measurement of the propagating velocities of different ultrasonic waves [288, 289].

E.4.1 Working Principle and Description of Technology

The principle of this ultrasonic method requires measurements of velocities of orthogonally polarized shear waves propagating through the material thickness. The normalized difference between transverse sound velocities is the acoustic birefringence coefficient B .

$$B = (V_1 - V_2)V_{ave}$$

Where V_1 and V_2 are the velocities of shear waves along a given path, with V_1 polarized at 90° to V_2 and V_1 being the larger velocity. V_{ave} is the average velocity. It is easier to measure acoustical birefringence than velocity if it is possible to propagate both polarization waves along the same path. This would be the case for a plate, or a pipe wall cross section having parallel faces.

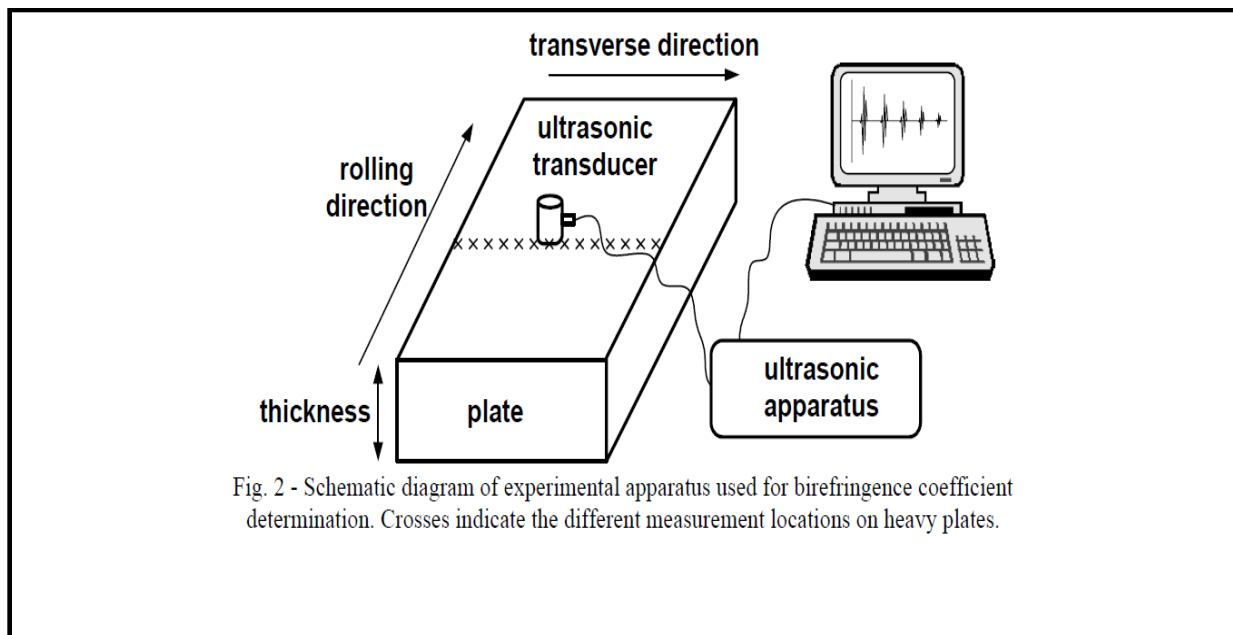


Fig. 2 - Schematic diagram of experimental apparatus used for birefringence coefficient determination. Crosses indicate the different measurement locations on heavy plates.

Figure E-31 Schematic diagram of apparatus used for birefringence coefficient measurement

The difference between minimum and maximum velocities is usually less than one percent, measuring the ultrasonic wave's times of flight and their difference readily provides the coefficient of birefringence independent of part thickness.

$$B = 2(t_2 - t_1)/(t_2 + t_1)$$

Where t_1 and t_2 are the times of flight relative to both velocities of shear waves

The resulting measurement provides an evaluation of the residual stress amounts averaged over the thickness of the sample.

In addition to the use of piezoelectric transducers as described above, EMAT (ElectroMagnetic Acoustic Transducers) may be used generate the shear waves and SH waves needed to measure birefringence. EMATs provide additional benefits of not requiring a couplant and operating through thin coatings.

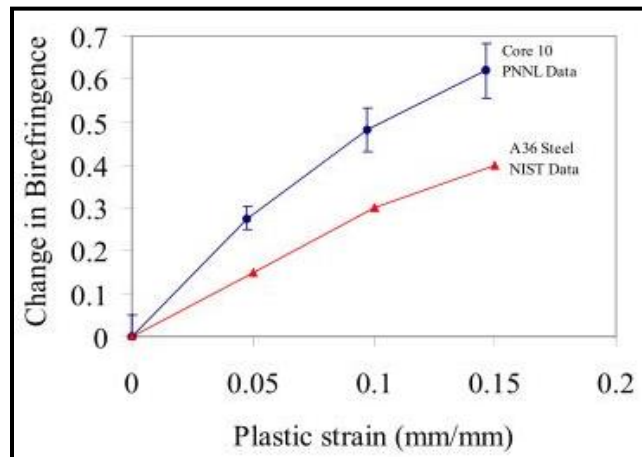


Figure E-32 Change in the birefringence as a function of plastic strain

E.4.2 Field Applications of Prototype Systems

An implementation based upon EMATS has been under development for several years, in cooperation with and funded in part by DOT PHMSA and PRCI, with several projects focused on Mechanical Damage. An example of the system and probe in field tests are shown in Figure E-33.



Figure E-33 Prototype Strain Measurement System and EMAT probe

In addition to lab testing and measurements, field testing of several prototypes has been completed on pipe samples, including catenary spans, suspended pipes and wrinkled pipes. An EMAT system for thickness and stress measurement, the stress measurement based on birefringence, has been developed by Nichizo Tech Inc. and Osaka University. A set of field

measurements carried out with this system are shown in Figure E-34. From the graph shown, the stress would be a result of bending, equal amounts being present on opposite sides of the pipe, indicating the absence of any externally applied tension or compression. Additional results, further information, and discussion may be found in the references noted below [290, 291, 292, 293].

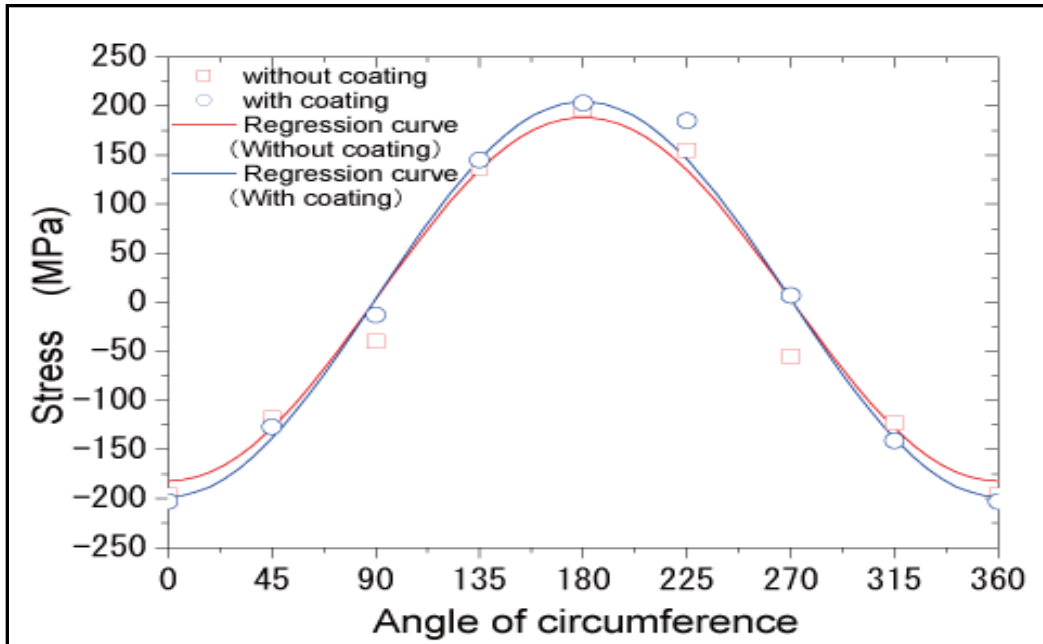


Figure E-34 Distribution of axial stress around pipe circumference

E.4.3 Current Status of this Technique

Each of the existing systems requires external pipe access and relatively clean surfaces, with static measurements being taken. Prototype units and testing services may be available. Additional development is required to complete commercialization, further assessment of the technique at selected locations before and after remediation, using strain gauge measurements as a reference, may be helpful in understanding the capabilities of the method.

E.5 MWM-Meandering Winding Magnetometer

MWM, or Meandering Winding Magnetometer, is an electromagnetic method using an MWM array, an inductive sensor that operates like a transformer in a plane [294, 295, 296, 297, 298, 299]. A rapid multivariate inverse method converts impedance data into images of surface geometry and permeability response due to stress and changes in microstructure.

E.5.1 Working Principle and Description of Technology

Developed at MIT in the 1980s, a MWM is an eddy current sensor with a response that may be accurately predicted using layered models. Applying a time varying current which produces a changing magnetic field, eddy currents are induced in the material under test in the opposite direction of the drive current. By measuring the current in the drive winding and the voltage

produced by the sense elements, the properties of the pipeline material may be estimated. The MWM geometry may be modeled by assuming the parameters for permeability, conductivity, steel thickness, and liftoff. The sensor response may be accurately predicted. Of interest for this application, is the change in magnetic properties of a pipeline material due to applied stress. Shown in Figure E-35 is a schematic of a MWM with primary (excitation) and secondary (sensing) windings. Using flexible circuitry techniques, these may be fabricated in any shape or combination of shapes, allowing sensors to be configured for specific purposes. These may include windings in a single plane and direction, or layered in directions to accommodate magnetic fields excitation or sensing in different directions. Individual sensors or larger arrays may be fabricated, depending upon the method chosen and geometry of the test piece.

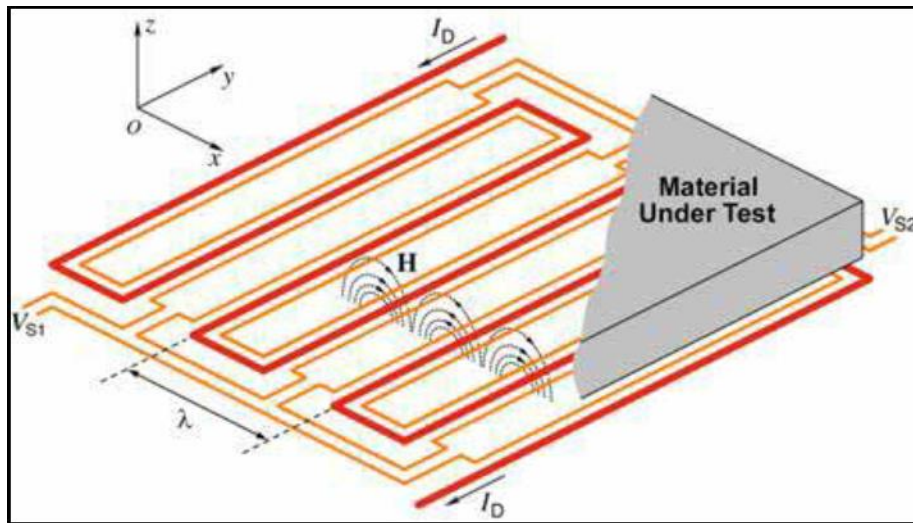


Figure E-35 Meandering Winding Magnetometer schematic representation

E.5.2 Current Status of this Technique

Originally targeting military and commercial aircraft engine inspection, the method has been repackaged for use in pipeline applications. Several DOT PHMSA and SBIR projects have provided funding for developing systems based upon MWM arrays for application to pipelines. Field deployable scanners and portable instrumentation have been developed and configured for pipeline use. Field inspection demonstrations have been carried out with MWM arrays for Stress Corrosion Cracking (SCC), external surface corrosion imaging, mechanical damage and stress mapping. Shown in Figure E-36 is an instrument system to support scanning applications. Continued research is being done in an effort to improve portability and measurement accuracies.



Figure E-36 **GridStation** electronics unit and portable MWM array scanner

Present systems are capable of imaging residual stress patterns in mechanical damage areas. Continued development of procedures to increase accuracy of residual stress measurements is presently underway. Configurations of MWM sensor arrays have been mounted on ILI tools and limited pull trials have been conducted. Continued development may result in an ILI prototype. Existing instrumented systems require external pipe access, with prototype units and testing services available for monitoring areas of interest. Additional development is required to complete commercialization. Assessment of the technique at selected locations before and after remediation, using strain gauge measurements as a reference, may be helpful in understanding the capabilities of the method.

Appendix F Apparent Toughness and Constraint Effects on Toughness

Abstract

The concept of apparent toughness, in particular, the apparent CTOD toughness, is used throughout this report when the tensile strain capacity is discussed. The practical significance and theoretical background of apparent toughness is discussed in this appendix.

F.1 Concept of Apparent Toughness

The concept of apparent toughness is the direct result of the observation of the tensile failure process as described in Section 7.3.2. The apparent CTOD toughness ($CTOD_A$) corresponds to the CTOD at the onset of ductile tearing as indicated by the start of a macroscopically sharp flaw at the tip of a blunted flaw, see Figure F-37 [300].

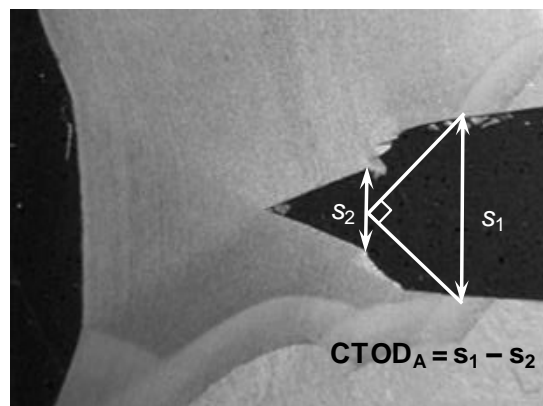


Figure F-37 Physical meaning of $CTOD_A$ shown with a crack-tip profile

An important distinction between the apparent CTOD toughness and the CTOD toughness from standard three-point bend CTOD test specimens is that $CTOD_A$ is not purely a material property, while the CTOD toughness from standard tests is often perceived as a material property. The standard CTOD tests are done under what is termed “high-constraint” conditions. In contrast, $CTOD_A$ is obtained when the flawed structure/specimen is under predominantly tensile loading. The latter loading condition tends to produce toughness that is higher than the toughness from standard CTOD test specimens. This dependence of the loading conditions makes $CTOD_A$ not a pure material parameter.

F.2 Fundamental Basis of Fracture Mechanics

The fundamental basis of fracture mechanics is the existence of the unique relationships between the crack-tip fields and the fracture parameters, such as the stress intensity factor K , J -Integral, and Crack Tip Opening Displacement (CTOD). These fracture parameters are uniquely related to the asymptotic crack-tip stress and strain fields at the crack tip. When such unique relationships exist, the crack-tip fields of a test specimen can be “transferred” to the structures being assessed through the fracture parameters, since those parameters uniquely represent the crack-tip fields. When the crack-tip fields of a specimen or structure are accurately represented by the asymptotic fields, the fields are referred to as being “dominated” or “characterized” by the

fracture parameters. The “loss of dominance” refers to the condition that the crack-tip fields of a specimen or structure deviate appreciably from the asymptotic fields.

To apply the fracture toughness measured from a laboratory specimen to the fracture assessment of a structure, it is necessary to ensure that the fracture parameter dominates the crack-tip fields at the event of the fracture. The conditions that lead to the loss of dominance of a fracture parameter received great attention in the later 1970s and early 1980s. McMeeking and Parks [301] and Shih and German [302] examined the crack-tip fields of a variety of specimens and compared them with finite strain solution of McMeeking [303] and the HRR fields [304, 305]. These comparisons led to the single parameter dominance criteria, which in turn were cast in the form of specimen size validity criteria. These specimen validity criteria have been adopted in K and J based fracture toughness test standards, e.g., ASTM E 1820.

F.3 Experimental Evidence of the Effects of Constraint

The crack-tip constraint can affect both fracture initiation and ductile tearing behavior. Figure F-38-Figure F-40 show the variation of fracture toughness as a function of loading mode (constraint) [306]. The T -stress is as a measure of the crack-tip constraint; positive T -stress indicating high constraint and low T -stress indicating low constraint. Specimens with high constraint have a T -stress that is positive or close to zero. Specimens with low constraint, such as a girth weld with planar flaws under tensile loading, have negative T -stress values. The data of Figure F-38-Figure F-40 show that the “effective” toughness of specimens with low constraint (negative T -stresses) can be several times of the toughness of the specimens with high constraint (positive T -stresses).

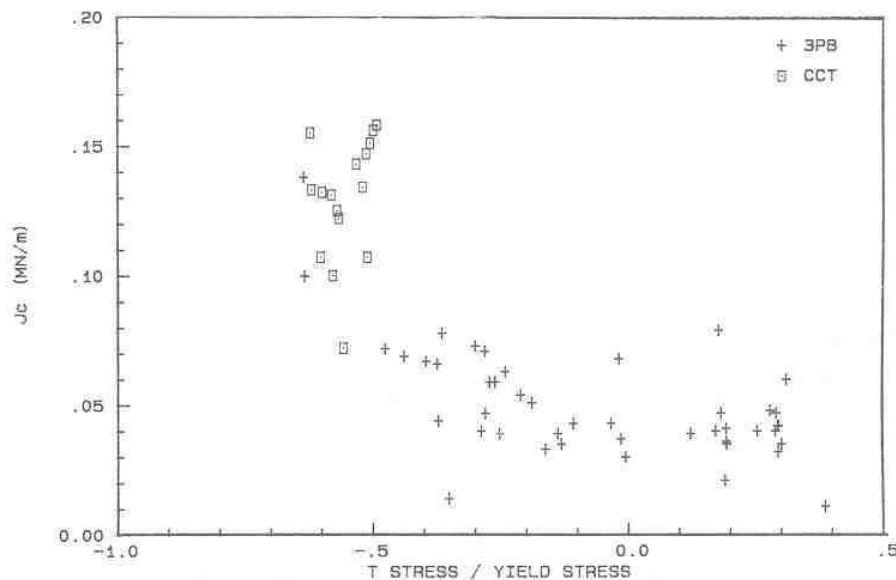


Figure F-38 Fracture initiation toughness as a function of crack-tip constraint. The 3PB represents standard three-point bend CTOD test specimens. The CCT refers to center-cracked tension specimens with through-wall crack (typical large plate test geometry). The J_c is a measure of material's fracture initiation toughness. The

tested material was a 1960 vantage mild steel plate conforming to specification BS 4360 43A [307].

The constraint can affect the materials' ductile tearing behavior as shown in Figure F-41 and Figure F-42. The constraint effect is more pronounced at high degree of ductile tearing. The increase in the tearing resistance should be beneficial, perhaps even necessary in establishing realistic strain limits of modern ductile girth welds.

The constraint effects may be observed in the form of fracture toughness transition curves, as shown in Figure F-43 for X60 linepipe materials [308]. At any given temperature, the toughness of low constraint specimen is higher than that of high constraint specimen.

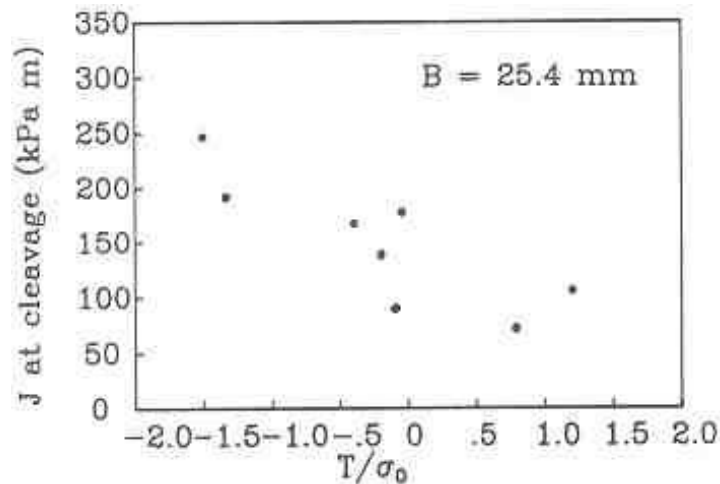


Figure F-39 Fracture initiation toughness as a function of constraint. The tested material was an ASTM A515 Grade 70 steel [309].

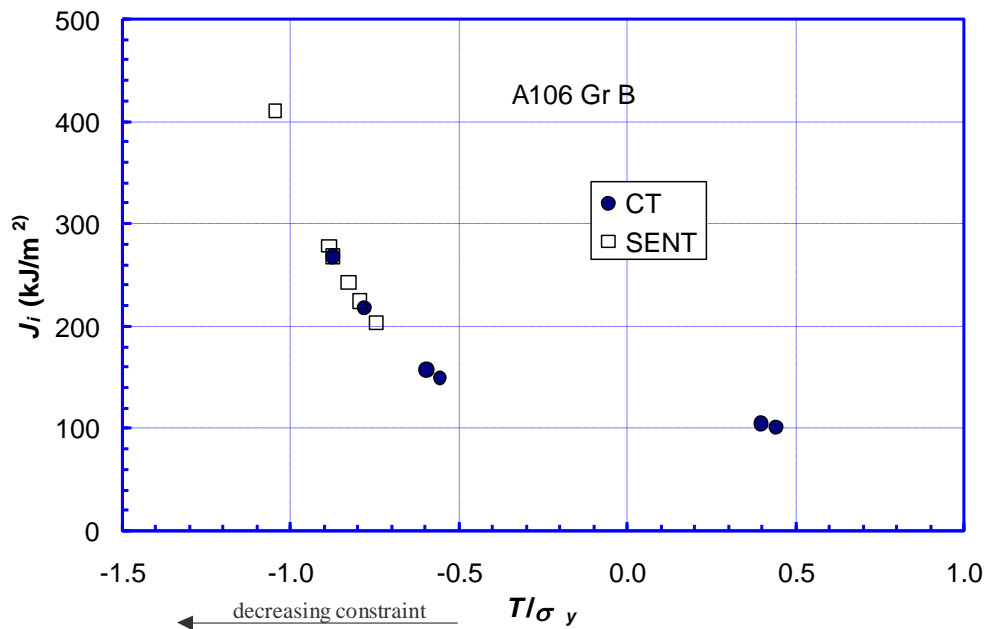


Figure F-40 The toughness variation as a function of the constraint parameter T -stress for an A106 Grade B material [310].

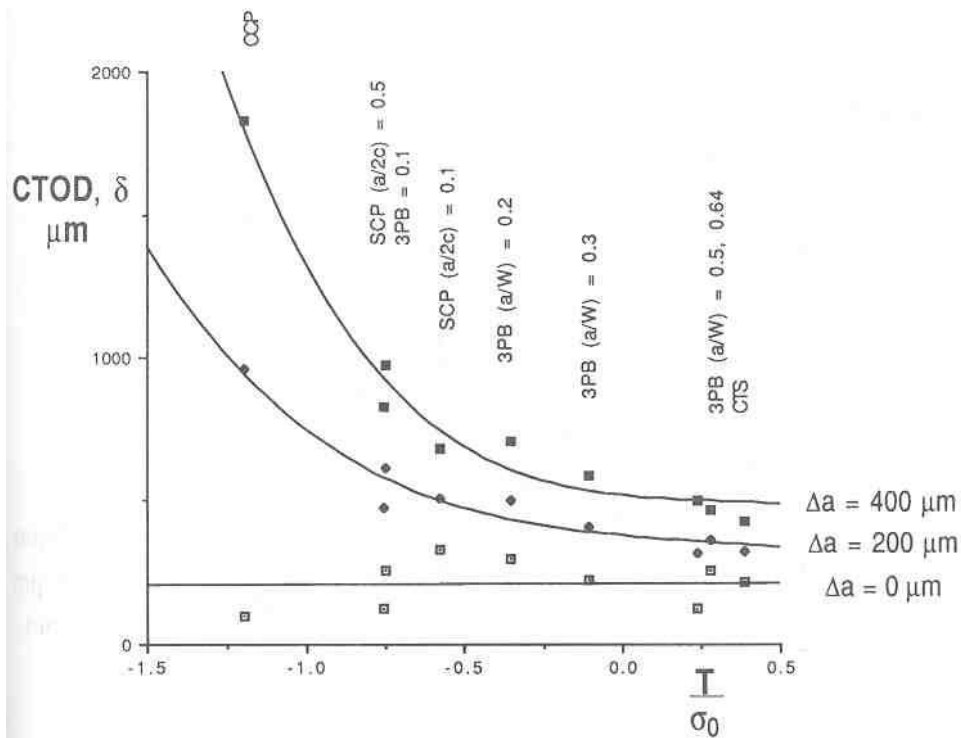


Figure F-41 Fracture toughness variation as a function of constraint at different amount of crack growth. The SCP refers to surface-cracked plate loaded in tension. The tested material was ASTM 710 Grade A steel [311].

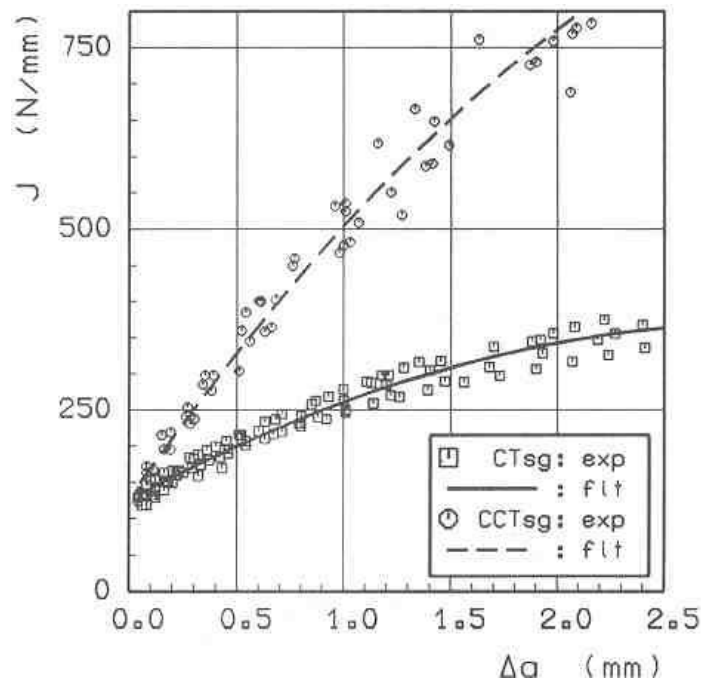


Figure F-42 J-R curves for high-constraint (CTsg) and low-constraint (CCTsg) specimens. The tested material was a pressure vessel steel StE 460 [312].

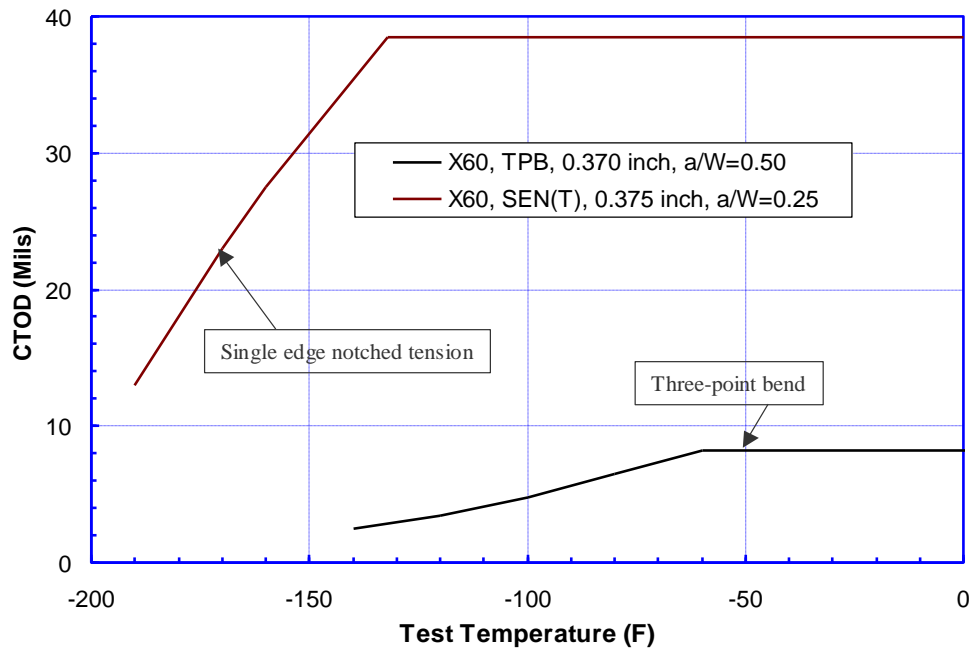


Figure F-43 An example of transition temperature shift due to the constraint effect of linepipe materials [308]. The three-point-bend specimens are of high constraint, whereas the SEN(T) specimens are of low constraint.

F.4 Validity Limit of Fracture Toughness

A unique relationship between the crack-tip fields and the fracture parameters exists when the crack-tip plasticity is well-contained within the boundary of the specimens and/or structures. For fracture mechanics test specimens, such a unique relationship is enforced by specifying specimen “validity limit” as expressed in the following format:

$$J / \sigma_0 \leq \frac{L}{\mu_{cr}},$$

where L is the specimen ligament size, and μ_{cr} is 25 for a bend specimen [313] and 200 for a tension specimen with through wall crack [314, 315]. The fracture mechanics parameter J may be converted to CTOD through the following relation [316]:

$$\delta = (0.5 - 0.7) \frac{J}{\sigma_0}.$$

If the ligament size L of a standard CTOD specimen is 25 mm (equivalent to tests done on a 25-mm wall thickness pipe), the maximum “valid” CTOD is 0.5-0.7 mm for bend specimens and less than 0.1 mm for tension specimens.

F.5 Toughness at the Point of Tensile Failure

When the crack-tip profiles of large-scale test specimens are observed, the CTOD values associated with the final failures are well above 0.5 mm, often in the range of 1.0-2.0 mm [317, 318]. These values are much greater than the single-parameter “valid” CTOD value (0.1 mm or less). This demonstrates that the single fracture parameter characterization of girth weld

toughness typical of stress-based design is no longer rigorously valid for strain-based design. The concept of *apparent toughness* is therefore necessary to highlight that the toughness representation is not strictly a material parameter anymore. The apparent toughness represents the combined effects of the intrinsic material toughness and the structural behavior. Therefore, it should be expected that the value of the apparent toughness may be dependent on the flaw size and other structural features, such as dimensions and even material's tensile properties.

F.6 Appropriate Values of Apparent Toughness

When the crack-tip profiles of large-scale test specimens under tension are observed, the $CTOD_A$ is often found at well above 0.5 mm, often in the range of 1.0-2.0 mm, for modern mechanized GMAW welds [300]. Tests of girth welds made in the 1950s-1960s showed that the $CTOD_A$ has a range from 0.3 mm to well over 1.0 mm, with an average above 0.6 mm [135]. More extensive coverage of typical $CTOD_A$ values is given in Section 5.

Nomenclature

Terms

Strain-based design (SBD)	Strain based design (SBD) is a pipeline design methodology with specific goals of providing safe and reliable service when such a pipeline is subjected to longitudinal strains with magnitudes greater than 0.5%. It does not replace design requirements based on the maximum hoop stress criteria of 49 CFR Part 192.
Strain capacity (SC)	Strain capacity is the longitudinal strain limit of a pipe and/or girth weld at the point of an incipient failure event, such as a leak or rupture with accompanying loss of pressure containment, loss of structural stability, or creation of features that may have long-term negative consequences.
Strain demand (SD)	Strain demand is the longitudinal strain imposed on a pipeline by its surrounding environment
Strain demand limit (SDL)	Strain demand limit is a specific longitudinal strain demand value that cannot be exceeded. The strain demand limit is set by (1) either multiplying the strain capacity by a factor less than 1 or (2) strain capacity minus a finite value.
Tensile strain capacity (TSC)	Tensile strain capacity (TSC) is the strain capacity under tension stress/load.
Compressive strain capacity (CSC)	Compressive strain capacity (CSC) is the strain capacity under compressive stress/strain. CSC is often defined as the maximum longitudinal compressive strain when the pipe segment reaches its maximum bending moment under lateral bending or its maximum compressive load under compression. Reaching CSC generally does not lead to immediate loss of pressure containment if the pipe is restrained from further deformation. The consequence of exceeding CSC varies, depending on the mechanical properties of the pipe and welds, site-specific support conditions, and operational conditions of the pipeline.
Uniform strain	Uniform strain is the engineering strain corresponding to the ultimate tensile strength in an engineering stress vs. engineering strain plot.
Small-scale testing	Typical small-scale testing includes uniaxial tension test, uniaxial compression test, single edge notched bending (SENB) test, single edge notched tensile (SENT) test,

Charpy V-notch (CVN) impact test, cross-weld tensile test, etc. The dimensions of typical small-scale test specimens range from a few inches to tens of inches. The specimens are usually light enough that they can be handled without the use of lifting equipment.

Medium scale test

One of the typical medium-scale tests is a curved wide plate (CWP) test. The test specimen is a curved piece of pipe with a nominal gauge width of 200 mm (8 in) to 450 mm (18 in) and a nominal length of 4-5 times of the gauge width. The specimen usually has a girth weld in mid-length and is pulled in the longitudinal direction. A machined notch or fatigue-sharpened flaw is usually placed in the weld or heat-affected zone to simulate welding defects.

Full-scale test

A full-scale test involves a full-size pipe. The test may be performed with or without internal pressure. The pipe can be loaded in longitudinal tension, longitudinal compression, lateral bending, or combination thereof.

Stress/strain relief

Abbreviations

CTOD	Crack tip opening displacement
CTOD _A	Apparent CTOD toughness
CTOD _F	Crack driving force measured in CTOD
FE	Finite element
FEA	Finite element analysis
IMU	Inertial measurement unit
SSC	Stress-strain curve
UTS	Ultimate tensile strength
YS	Yield strength

Symbols

D	Pipe outside diameter (OD)
t	Pipe wall thickness
δ_A	Apparent CTOD toughness
δ_F	Crack driving force measured in CTOD

Organizations

ASME American Society of Mechanical Engineers
CRES Center for Reliable Energy Systems
PRCI Pipeline Research Council International



References

- 1 Lee, K., presentation at 2012 API-AGA Joint Committee meeting on Oil & Gas Pipeline Welding Practices.
- 2 Harp, E.L., 2008. Chapter 1, Landslide Hazards to Pipelines-Regional Hazard Mapping, in Baum, R.L., D.L. Galloway, and E.L. Harp, eds., Landslide and Land Subsidence Hazards to Pipelines: U.S. Geological Survey Open-File Report 2008-1164, p. 1-32.
- 3 Galloway, D.L., G.W. Bawden, S.A. Leake, and D.G. Honegger, 2008. Chapter 2, Land Subsidence Hazards, in Baum, R.L., D.L. Galloway, and E.L. Harp, eds., Landslide and Land Subsidence Hazards to Pipelines: U.S. Geological Survey Open-File Report 2008-1164, p. 33-106.
- 4 Rizkalla, M., 2013. Methodologies of pipeline geohazard assessment: Pipelines International, March 2013, p. 50-51.
- 5 Rizkalla, M., ed., 2008. Pipeline Geo-Environmental Design and Geohazard Management: American Society of Mechanical Engineers Monograph Series, 353 p.
- 6 Braun, J., G. Major, D.O. West and M. Bukovansy, 1998. Geologic hazards evaluation boosts risk-management program for Western U.S. pipeline: Oil & Gas Journal, Nov. 9, 1998, p. 73-79.
- 7 "Guidelines for Constructing Natural Gas and Liquid Hydrocarbon Pipelines through Areas Prone to Landslide and Subsidence Hazards," prepared by C-CORE D, G. Honegger Consulting and SSD, Inc. to PRCI, January 2009.
- 8 Baum, R.L., D.L. Galloway, and E.L. Harp, 2008. Landslide and Land Subsidence Hazards to Pipelines: U.S. Geological Survey Open-File Report 2008-1164, 202 p.
- 9 Galloway, D.L., D.R. Jones, and S.E. Ingebritsen, eds., 1999. Land Subsidence in the United States: U.S. Geological Survey Circular 1182.
- 10 Honegger, D.G., J.D. Hart, R. Phillips, C. Popelar, and R.W. Gailing, 2010. Recent PRCI Guidelines for Pipelines Exposed to Landslide and Ground Subsidence Hazards: Proceedings of the 8th International Pipeline Conference, Calgary, AB, IPC2010-31311, p. 1-10.
- 11 Perrin, N., 2009. Assessment of landslide and other erosion hazards along the Kapuni and Maui pipeline alignments: Urenui to Otorohanga: GNS Science Consultancy Report 2009/157, July 2009.
- 12 Geertsema, M., J.W. Schwab, and A. Blais-Stevens, 2008. Landslides and Linear Infrastructure in West-Central British Columbia: in J.Locat, D.Perret, D. Turme, D.

-
- Demers eds., Proceedings of the 4th Canadian Conference on Geohazards: From Causes to Management.
- 13 Geertsema, M., J.W.Schwab, A. Blais-Stevens and M.E. Sakals, 2009. Landslides impacting linear infrastructure in west central British Columbia: *Natural Hazards*, v. 48, p. 59-72.
 - 14 Lier, M., 2009. Geohazard integrity management program for operating pipelines. Proc., 9th International Symposium on Environmental Concerns in Rights-of-Way Management, UAA, Champaign, IL.
 - 15 Zaleski, M., T. Greaves, and J. Bracic, 2010. Meeting the Geohazards Management Guidelines of Annex N. IPC 2010, 8th International Pipeline Conference, AMSE, Calgary.
 - 16 Davidson, C., D.S. Cavers, and P. Barlow, 2013. Report on Quantitative Geohazard Assessment Proposed Northern Gateway Pipelines Route Revision V. Technical report by AMEC Environment & Infrastructure, Burnaby BC. NEB submission as part of Worley Parsons Semi-Quantitative Risk Assessment, available at <https://docs.neb-one.gc.ca/ll-eng/llisapi.dll/properties/917986>.
 - 17 Utah Division of Homeland Security, 2008. Utah Natural Hazards Handbook, October 2008.
 - 18 Lund, W.R., T.R. Knudsen, G.S. Vice, and L.M. Shaw, 2008. Geologic Hazards and Construction Conditions, St. George-Hurricane Metropolitan Area, Washington County, Utah: Utah Geological Survey Special Study 127.
 - 19 Alaska Division of Geological and Geophysical Surveys, 2013. Guide to Geologic Hazards in Alaska: <http://www.dggs.alaska.gov/sections/engineering/geohazards/>, accessed 7/9/2013.
 - 20 National Atlas of the United States, 2013. Geologic Hazards: http://nationalatlas.gov/articles/geology/a_geohazards.html, accessed 7/9/2013.
 - 21 Bolt, B.A., W.L. Horn, G.A. Macdonald, and R.F. Scott, 1977. Geological Hazards, Earthquakes-Tsunamis-Volcanoes-Avalanches-Landslides-Floods: Springer-Verlag, New York, NY, Revised, 2nd Edition, 330 p.
 - 22 Highland, L.M and P. Bobrowsky, 2008. The Landslide Handbook – A Guide to Understanding Landslides: U.S. Geological Survey Circular 1325, 129 p.
 - 23 U.S. Geological Survey (USGS), 2004a. Landslide Types and Processes: Fact Sheet 2004-3072, July 2004.

- 24 Cruden, D.M. 1991. A simple definition of a landslide.: Bulletin of the International Association of Engineering Geology, No. 43, p. 27-29.
- 25 Cruden, D.M. and D.J. Varnes, 1996. Chapter 3, Landslide Types and Processes, in Turner, K.A., and Schuster, R.L., eds., Landslides – Investigation and Mitigation, Special Report 247: Transportation Research Board, National Research Council, National Academy Press, p. 36-75.
- 26 O'Rourke, M.J. and X. Liu, 1999. Response of Buried Pipelines Subject to Earthquake Effects: The Multidisciplinary Center for Earthquake Engineering Research, Monograph Series 3, 247 p
- 27 U.S. Geological Survey (USGS), 2000b. Land Subsidence in the United States: Fact Sheet-165-00, December 2000.
- 28 U.S. Geological Survey (USGS), 2000a. Measuring Land Subsidence from Space: Fact Sheet-051-00, April 2000.
- 29 U.S. Geological Survey (USGS), 2007. Sinkholes: Fact Sheet 2007-3060, July 2007.
- 30 Allen, A.S., 1984. Chapter 8, Types of land subsidence, in J.F. Poland, ed., Guidebook to studies of land subsidence due to ground-water withdrawal, prepared for the International Hydrological Programme, Working Group 8.4, p. 133-142.
- 31 Bauer, R.A., 2008. Planned Coal Mine Subsidence in Illinois: A Public Information Booklet: Illinois Department of Natural Resources, Circular 573.
- 32 Mine Subsidence Engineering Consultants (MSEC), 2007a. Introduction to Longwall Mining and Subsidence: Chatswood, NSW, Australia, Revision A, August 2007.
- 33 Total Environment Centre (TEC), 2007, Impacts of Longwall Coal Mining on the Environment in New South Wales: Sydney South, NSW, Australia, January 2007.
- 34 Sheng, Z., D.C. Helm, and J. Li, 2003. Mechanisms of Earth Fissuring Caused by Groundwater Withdrawal: Environmental & Engineering Geoscience, v. IX, n. 4, p. 351-362.
- 35 Bell, F.G. and D.D. Genske, 2001. The Influence of Subsidence Attributable to Coal Mining on Environment, Development and Restoration: Some Examples from Western Europe and South Africa: Environmental & Engineering Geoscience, v. VII, n. 1, p. 81-99.
- 36 Pennsylvania Department of Environmental Protection, 2012. What is Mine Subsidence: <http://www.dep.state.pa.us/msi/whatisms.html>, accessed 7/15/2013.

-
- 37 Gray, R.E. and R.W. Bruhn, 1984. Coal mine subsidence – eastern United States, in Holzer, T.L., ed., Man-induced land subsidence: Geological Society of America Reviews in Engineering Geology, p. 123-150.
- 38 Dunrud, C.R., 1984. Coal mine subsidence – western United States, in Holzer, T.L., ed., Man-induced land subsidence: Geological Society of America Reviews in Engineering Geology, p. 151-194.
- 39 Holzer, T.L., 1984. Ground failure induced by ground-water withdrawal from unconsolidated sediment, in Holzer, T.L., ed., Man-induced land subsidence: Geological Society of America Reviews in Engineering Geology, p. 67-106.
- 40 AmericanLifelinesAlliance, 2001. Guidelines for the Design of Buried Steel Pipe, July 2001, 83 p.
- 41 Bauer, R.A., 2006. Mine Subsidence in Illinois: Facts for Homeowners: Illinois State Geological Survey, Circular 569, 28 p.
- 42 Mattox, A., D. Coil, N. Hoagland, and B. Higman, 2013. Block Caving: <http://www.groundtruthtrekking.org/Issues/MetalsMining/block-caving-underground-mining-method.html>, last modified 21 March 2013.
- 43 White, R.W., 2010. Methods to Reclaim Areas of Pipeline Exposure due to Stream-Channel Instability: Powerpoint, 17th Annual International Petroleum & Biofuels Environmental Conference, August 30 – September 2, 2010, San Antonio, TX, http://ipec.utulsaedu/Conf2010/Powerpoint%20presentations%20and%20papers%20received/White_80.pdf.
- 44 Bryndum, M.B., 2000. Enhancement of Integrity Assessment Models/Software for Exposed and Unburied Pipelines in River Channels, Volume 1 – Design Guideline and Volume 2 – River-X Software User Guide. Prepared by the Danish Hydraulic Institute for the Offshore and Onshore Design Applications Supervisory Committee of the Pipeline Research Council International Inc., PR-170-9826
- 45 Blanco, H. and R. Lal, 2010. "Wind erosion," Principles of Soil Conservation and Management: Springer, p. 56–57, ISBN 978-90-481-8529-0.
- 46 Pacific Northwest Seismic Network (PNSN), 2013. Earthquake Hazards: <http://www.pnsn.org/outreach/earthquakehazards>, accessed 7/9/2013.
- 47 Bolt, B.A., 1993. Earthquakes, Newly Revised and Expanded: W.H. Freeman and Company, New York, NY, 331 p.
- 48 Crone, A.J., M.N. Machette, M.G. Bonilla, J.J. Lienkaemper, K.L. Pierce, W.E. Scott, and R.C. Bucknam, 1987. Surface faulting accompanying the Borah Peak earthquake and

- segmentation of the Lost River fault, central Idaho: *Bulletin of the Seismological Society of America*, v. 77, n. 3, p. 739-770.
- 49 U.S. Geological Survey (USGS), 2004b. What are Volcano Hazards?: Fact Sheet 002-97, Revised July 2004.
- 50 Pringle, P.T., 1994. Volcanic Hazards in Washington – A Growth Management Perspective: *Washington Geology*, v. 22, n. 2, p. 25-33.
- 51 Yitagesu, F.A., F. van der Meer, and H. van der Werff, 2009. Prediction of Volumetric Shrinkage in Expansive Soils (Role of Remote Sensing): in Jedlovec, G. ed., *Advances in Geoscience and Remote Sensing*, p. 347-370, ISBN: 978-953-307-005-6, InTech, DOI: 10.5772/8328, <http://www.intechopen.com/books/advances-in-geoscience-and-remote-sensing/prediction-of-volumetric-shrinkage-in-expansive-soils-role-of-remote-sensing->.
- 52 Nayak, N.V. and R.W. Christensen, 1971. Swelling Characteristics of Compacted Expansive Soils: *Clays and Clay Minerals*, v. 19, p. 251-261.
- 53 Sapaz, B., 2004. Lateral Versus Vertical Swell Pressures In Expansive Soils: M.Sc. Thesis Submitted to the Graduate School of Natural and Applied sciences of Middle East Technical University, Ankara, Turkey, January 2004, 128 p.
- 54 Wyoming Office of Homeland Security, 2011. Chapter 7, Expansive Soil: Wyoming Multi-Hazard Mitigation Plan, June 2011, p. 7.1-7.12.
- 55 Kerrane, J.P., 2005. What Are Expansive Soils?: Benson & Associates PC, http://www.bensonpc.com/downloads/public/What_Are_Expansive_Soils.pdf, accessed 7/8/2013.
- 56 Santagata, M.C., A. El Howayek, P.T. Huang, and R. Bisnett, 2011. Identification and Behavior of Collapsible Soils: Joint Transportation Research Program Technical Report Series, Indiana Department of Transportation, SPR-3109, September 2011.
- 57 Love, D.W., 2001. What Decision Makers Should Know about Soils in New Mexico: 2001 Decision-Makers Field Guide – Water, Watersheds, and Land Use in New Mexico, New Mexico Bureau of Geology and Mineral Resources, Revised 27 June 2012, <http://geoinfo.nmt.edu/geoscience/hazards/collapsible.html>, accessed 7/8/2013.
- 58 Boivin, R., 2008. Chapter 5. Buoyancy, in Rizkalla, M., ed., *Pipeline Geo-Environmental Design and Geohazard Management: American Society of Mechanical Engineers Monograph Series*, p. 169-228.
- 59 Daanen, R.P., G. Grosse, M.M. Darrow, T.D. Hamilton and B.M. Jones, 2012. Rapid movement of frozen debris-lobes: implications for permafrost degradation and slope

- instability in the south-central Brooks Range, Alaska: *Natural Hazards and Earth System Sciences*, v. 12, p. 1521-1537.
- 60 Kaab, A., 2008. Remote Sensing of Permafrost-related Problems and Hazards: *Permafrost and Periglacial Processes*, v. 19, p. 107-136.
- 61 Kaab, A., C. Huggel, L. Fischer, S. Guex, F. Paul, I. Roer, N. Salzmann, S. Schlaefli, K. Schmutz, D. Schneider, T. Strozzi, and Y. Weidmann, 2005. Remote sensing of glacier- and permafrost-related hazards in high mountains: an overview: *Natural Hazards and Earth System Sciences*, v. 5, p. 527-554.
- 62 Miller, B.G. and D.M. Cruden, 2002. The Eureka River landslide and dam. Peace River Lowlands, Alberta. *Canadian Geotechnical Journal*, 30: 863-878.
- 63 Evans, S.G., and G.R. Brooks, 1994. An earthflow in sensitive Chanplain Sea sediments at Lemieux Ontario, June 20, 1993, and its impact on the South Nation River. *Canadian Geotechnical Journal*, 31: 384-394.
- 64 Varnes, D.J., 1978. Slope Movement Types and Processes, in R.L. Schuster and R.J. Krizek, eds., *Special Report 176: Landslides: Analysis and Control*, TRB, National Research Council, Washington, D.C., p. 11-33.
- 65 Costa, J.E. and R.L. Schuster, 1988. The formation and failure of natural dams: *Geological Society of America Bulletin*, v. 100, n. 7, p. 1054-1068.
- 66 DTec Consulting Ltd., 2002. West Coast Regional Council: Natural Hazards Review, 2. Landslides & Landslide Dam Hazards, Christchurch, NZ.
- 67 Guthrie, R. H., P. Friele, K. Allstadt, N. Roberts, S.G. Evans, K.B. Delaney, D. Roche, J.J. Clague, and M. Jakob, 2012. The 6 August 2010 Mount Meager rock slide-debris flow, Coast Mountains, British Columbia: characteristics, dynamics, and implications for hazard and risk assessment. *Nat. Hazards Earth Syst. Sci.*, 12, 1-18.
- 68 Boulton, N., D. Stead, J. Schwab, and M. Geertsema, 2006. The Zymoetz River Rock Avalanche, June 2002, British Columbia, Canada. *Engineering Geology* 86, p.76-93.
- 69 Ege, J.R., 1984. Mechanisms of surface subsidence resulting from solution extraction of salt, in Holzer, T.L., ed., *Man-induced land subsidence: Geological Society of America Reviews in Engineering Geology*, p. 203-221.
- 70 U.S. Geological Survey (USGS), 2011. The Science of Sinkholes: Science Features, http://www.usgs.gov/blogs/features/usgs_top_story/the-science-of-sinkholes/?from=texlink, last modified September 14, 2011, accessed 8/5/2013.

-
- 71 U.S. Geological Survey (USGS), 2013. Sinkholes: The USGS Water Science School, <http://ga.water.usgs.gov/edu/sinkholes.html>, last modified 08-Mar-2013, accessed 8/5/2013.
- 72 Kentucky Geological Survey, 2006. Karst Is a Landscape: University of Kentucky, http://www.uky.edu/KGS/water/general/karst/karst_landscape.htm, last modified September 21, 2006, accessed 8/5/2013.
- 73 Nelson, S.A., 2012. Subsidence: Dissolution & Human Related Causes: EENS 3050, Natural Disasters: Tulane University, 7/9/2012.
- 74 Zhou, W. and B.F. Beck, 2008. Management and mitigation of sinkholes on karst lands: an overview of practical applications: *Environmental Geology*, v. 55, p. 837-851.
- 75 Waltham, A.C. and P.G. Fookes, 2003. Engineering classification of karst ground conditions: *Quarterly Journal of Engineering Geology and Hydrogeology*, v. 36, p. 101-118.
- 76 Veni, G., H. DuChene, N.C. Crawford, C.G. Groves, G.N. Huppert, E.H. Kastning, R. Olson, and B.J. Wheeler, 2001. Living with Karst, A Fragile Foundation: American Geological Institute, AGI Environmental Awareness Series, 4, 64 p.
- 77 U.S. Arctic Research Commission (USARC), 2003. Climate Change, Permafrost, and Impacts on Civil Infrastructure: Permafrost Task Force Report, December 2003.
- 78 Xie, J., 2009. Analysis of Thaw Subsidence Impacts on Production Wells: 2009 SIMULIA Customer Conference, London, UK, May 19-21, 2009.
- 79 Howes, D.E. and E. Kenk, 1997. Terrain Classification System for British Columbia. Version 2.0. Ministry of Environment, Lands and Parks. Victoria, BC, 102 p.
- 80 Arizona Department of Water Resources (ADWR), 2013. Fact Sheet, Land Subsidence and Earth Fissures in Arizona: <http://www.azwater.gov/azdwr/.../LandSubsidenceInArizonaFactSheet.pdf>, accessed 8/7/2013.
- 81 Bell, J.W., 2003. The Relation Between Land Subsidence, Active Quaternary Faults, and Earth Fissures in Las Vegas Valley, Nevada: Geological Society of America Cordilleran Section – 99th Annual Meeting, Session No. 35, Booth #22.
- 82 Holzer, T.L., 2010. Implications of ground-deformation measurement across earth fissures in subsidence areas of the southwestern USA: Proceedings of EISOLS 2010, Queretaro, Mexico, 17-22 October 2010, IAHS Publication 339, 2010.

-
- 83 Arizona Land Subsidence Group (ALSG), 2007, Land Subsidence and Earth Fissures in Arizona: Arizona Geological Survey Contributed Report CR-07-C, December 2007.
- 84 Mine Subsidence Engineering Consultants (MSEC), 2007b. General Discussion on Systematic and Non Systematic Mine Subsidence Ground Movements: Chatswood, NSW, Australia, Revision A, August 2007.
- 85 Chang, H.-C., A.H. Ng, K. Zhang, Y. Dong, Z. Hu, L. Ge, and C. Rizos, 2009. Monitoring Longwall Mine Subsidence and Far-Field Displacements Using Multi-Wavelength Radar Interferometry: Cooperative Research Centre for Spatial Information & School of Surveying and Spatial Information Systems, University of New South Wales, Sydney, NSW, Australia.
- 86 Mine Subsidence Engineering Consultants (MSEC), 2007c. bhp billiton Illawarra Coal, Dendrobium Mine Area 3, Report on The Prediction of Subsidence Parameters and the Assessment of Mine Subsidence Impacts on Natural Features and Surface Infrastructure Resulting from the Extraction of Proposed Longwalls 6 to 10 in Area 3A and Future Longwalls in Areas 3B and 3C at Dendrobium Mine: Chatswood, NSW, Australia, Revision A, October 2007.
- 87 Kay, D., J. Barbato, G. Brassington, and B. de Somer, 2006. Impacts of Longwall Mining to Rivers and Cliffs in the Southern Coalfield, in Aziz, N. ed., Coal 2006: Coal Operators' Conference, University of Wollongong & the Australian Institute of Mining and Metallurgy, 2006, p. 327-336.
- 88 Waddington, A. and Kay, D., 2003. The Impacts of Mine Subsidence on Creeks, River Valleys and Gorges Due to Underground Coal Mining Operations, in Aziz, N., ed., Coal 2003: Coal Operators' Conference, University of Wollongong & the Australian Institute of Mining and Metallurgy, 2003, p. 101-116.
- 89 Hebblewhite, B.K, A. Waddington, and J. Wood, 2000. Regional Surface Displacements due to Mining Beneath Severe Surface Topography: Proceedings 19th Conference on Ground Control in Mining, West Virginia University, p. 149-157.
- 90 Ferguson, H.F., 1967. Valley stress release in the Allegheny Plateau: Bulletin of the Association of Engineering Geologists, v. 4, p. 63-71.
- 91 GeoTDR, Inc., 2001. Effects of Undermining Interstate Route 70, South Strabane Township, Washington County, Pennsylvania, November 1999 to October 2000: prepared for Pennsylvania Department of Environmental Protection, Bureau of Mining and Reclamation, Harrisburg, PA, October 2001.

-
- 92 Lofgren, B.E., 1969. Land Subsidence due to the Application of Water, in D.J. Varnes and G. Kiersch, eds.: Geological Society of America Reviews on Engineering Geology, REG2, p. 271-304.
- 93 Marino, G.G., 2000. Pipelines Exposed to Coal Mine Subsidence Face Risk of Serious Damage: Pipeline & Gas Journal, November 1, 2000.
- 94 Pringle, P.T., 2009. The Bonneville Slide: Explorations, Columbia Gorge Interpretive Center Museum.
- 95 Schuster, R.L., 2006. Interaction of Dams and Landslides – Case Studies and Mitigation: U.S. Geological Survey Professional Paper 1723, 107 p.
- 96 Alexander, S.C., E. Larson, C. Bomberger, B. Greenwaldt, and E.C. Alexander, Jr., 2013. Combining LiDAR, Aerial Photography, and Pictometry™ Tools for Karst Features Database Management: 13th Sinkhole Conference NCKRI Symposium 2, p. 441-448.
- 97 *Residual Stress, Fracture, and Stress Corrosion Cracking*, the 2004 ASME Pressure Vessels and Piping Conference, San Diego, California, USA, Edited by Y.-Y. Wang, July 25-29, 2004.
- 98 Wang, Y.-Y., Feng, Z., Cheng, W., and Liu, S., “Residual Stress Effects on Crack Driving Force in Multipass Welds,” in *Fatigue, Fracture, and Residual Stress*, ASME PVP-Vol. 373, Edited by S. Rahman, 1998, pp. 469-482
- 99 Liu, M., Wang, Y.-Y., and Rogers, G., “Stress Analysis of Pipe Lowering-in Process during Construction,” Proceedings of the 7th International Pipeline Conference, Paper No. IPC2008-64630, September 29 – October 3, 2008, Calgary, Alberta, Canada.
- 100 Zhang, F., Wang, Y.-Y., Liu, M., and Bruce, W., “Stress Analysis of Lifting and Lowering-in Process”, Proceedings of the 10th International Pipeline Conference, Paper No. IPC2014-33237, September 9-October 3, 2014, Calgary, Alberta, Canada.
- 101 Zhang, F., Liu, M., Wang, Y.-Y., Surface, R., and Phillips, A., “Pipeline Integrity Analyses for Construction in Mountainous Areas -- Tamazunchale Extension Pipeline Project,” Proceedings of the 10th International Pipeline Conference, Paper No. IPC2014-33235, September 9-October 3, 2014, Calgary, Alberta, Canada.
- 102 Wang, Y.-Y., Sen, M., and Song, P. “Longitudinal Stress Limits in Pipelines,” Proceedings of the 11th International Pipeline Conference, Paper No. IPC2016-64533, September 26-September 30, 2016, Calgary, Alberta, Canada.

- 103 Zhang, F., Liu, M., and Wang, Y.-Y., Yu Z., and Tong, L., 2012, "Strain demand in areas of mine subsidence", Proceedings of the 9th International Pipeline Conference, Calgary, Alberta, Canada, September 24-28.
- 104 Liu, M., Wang, Y.-Y., and Yu, Z., "Response of Pipelines under Fault Crossing," Proceedings of the 18th International Offshore and Polar Engineering Conference (ISOPE 2008), Vancouver, Canada, July 6-11, 2008.
- 105 Zhang, F. and Wang, Y.-Y., "Assess the Seismic Wave Influence on Buried Pipelines with ASCE Soil-Spring Model," Proceedings of the ASME 2013 33rd International Conference on Ocean, Offshore and Arctic Engineering, San Francisco, CA, June 8-13, 2014.
- 106 "Extended Model for Pipe Soil Interaction," PRCI report R-02-044-113 prepared by C-Core, August 2003.
- 107 "Pipeline Integrity for Ground Movement Hazards," PRCI report PR-07-082-459, Catalog No. L52291, prepared by C-Core, December 2008.
- 108 "Guidelines for the Seismic Design of Oil and Gas Pipeline Systems," American Society of Civil Engineers (ASCE), Committee on Gas and Liquid Fuel Lifelines, Technical Council on Lifeline Earthquake Engineering, ASCE, New York, 1984.
- 109 "Guideline for the Design of Buried Steel Pipe," American Lifelines Alliance, July 2001.
- 110 Honegger, D. G. and Nyman, J, "Guidelines for the Seismic Design and Assessment of Natural Gas and Liquid Hydrocarbon Pipelines," PRCI project PR-268-9823, 2004.
- 111 Popescu, R., "Finite Element Analysis of Pipe/Soil Interaction Phase I – Two-Dimensional Plane Strain Analysis," Contract report for the Geological Survey of Canada, C-CORE Publication 99-C23, June 1999.
- 112 Popescu, R., Guo, P., and Nobahar, A., "3D Finite Element Analysis of Pipe/Soil Interaction," Final report for Geological Survey of Canada, Chevron Corp. and Petro Canada, C-CORE contract report 01-C08, 2001.
- 113 Fredj, A. and Dinovitzer, A., "Simulation of the Response of Buried Pipelines to Slope Movement using 3D Continuum Modeling," Proceedings of the 2012 9th International Pipeline Conference, IPC2012-90437, Calgary, Alberta, Canada, September 29 – October 3, 2014
- 114 Fredj, A. and Dinovitzer, A., "Pipeline Response to Slope Movement and Evaluation of Pipeline Strain Demand," Proceedings of the 2014 10th International Pipeline Conference, IPC2014-33611, Calgary, Alberta, Canada, September 29 – October 3, 2014.

-
- 115 Hart, J.D., Zulfiqar, N. and Popelar, C., “*Pipeline Integrity for Ground Movement Hazards - Use of Pipeline Geometry Monitoring to Assess Pipeline Condition*”, PRCI Report to United States Department of Transportation Pipeline and Hazardous Materials Safety Administration Office of Pipeline Safety, December 3, 2008.
 - 116 Hart, J.D., Powell, G. H., Hackney, D., and Zulfiqar, N., “*Geometry Monitoring of the Trans-Alaska Pipeline*”, Proceedings of the ASCE Cold Regions Conference, Anchorage, Alaska, May 20-22, 2002.
 - 117 Aue, H., Paeper, S., Brown, B., Humphreys, M. and Southerland, J., “High Quality Geometry Module Data for Pipeline Strain Analysis”, Pigging Products and Services Association, Copyright 2007.
 - 118 Aue, H., Paeper, S., Brown, B., “Taking the Strain - High Quality Geometry Module Data for Pipeline Strain Analysis”, World Pipelines, May 2007.
 - 119 Czyz, J., Fraccaroli, C., and Sergeant, A., “Measuring Pipeline Movement in Geotechnically Unstable Areas Using an Inertial Geometry Pipeline Inspection Pig”, Nowsco/SNAM Paper, June 1996.
 - 120 American Society of Mechanical Engineers, *B31.8 Gas Transmission and Distribution Piping Systems*, ASME B31.8-2010.
 - 121 Clouston, S., Blair, G. and Hektner, D., “*Pipeline Out-of-Straightness Assessment Using Pipeline Inertial Geometry Survey Technology*”, Alaska Pipeline Workshop, Anchorage, Alaska, November 8-9, 1999.
 - 122 Hart, J.D., Zulfiqar, N., and Erickson, T.H., “*3rd Party Review of Geometry Pig Inertial Survey Data at the Colville River HDD*”, IPC08-64306, Proceedings of the International Pipeline Conference, Calgary, Alberta, Canada, September 29 – October 3, 2008.
 - 123 Hart, J.D., Zulfiqar, N., Moore, D.H., and Swank, G.R., “*Digital Pigging as a Basis for Improved Pipeline Structural Integrity Evaluations*”, IPC06-10349, Proceedings of the International Pipeline Conference, Calgary, Alberta, Canada, September 25-29, 2006.
 - 124 API Standard 1163, “In-Line Inspection Systems Qualification Standard,” 2nd Ed., 2013.
 - 125 “Guidance on Field Verification Procedures for In-Line Inspection”, Pipeline Operator’s Forum, December 2012.
 - 126 API/ANSI, “In-line Inspection Systems Qualification Standard”, ANSI/API Standard 1163, Reaffirmed Edition, November, 2010.
 - 127 E.B. Clark, B.N. Leis, R.J. Eiber, “Integrity Characteristics of Vintage Pipelines,” The INGAA Foundation Inc., 2005

-
- 128 Hillenbrand, H. G., et al., "Development of Large-Diameter Pipe in Grade X100," in Pipeline Technology, Volume 1, Rudi Denys Eds., Elsevier Science B. V., 2000.
 - 129 J. M. Gray and Peter A. Peters, "Technical Demands and Specifications for Linepipe During the Past Decades," CBMM/TSNIICHERMET Seminar - 25 Years of Cooperation. Moscow Russia. September 5-6, 2002.
 - 130 Steven V. Nanney and Kenneth Y. Lee, "Managing and Addressing Fitness for Service of Vintage Pipelines", 9th International Pipeline Conference, Paper No. IPC2012-90304, September 24-28, 2012, Calgary, Alberta, Canada.
 - 131 Work completed by CRES staff for a JIP member company.
 - 132 Hopkins, P., "An Analysis of the Full-Scale Girth Weld Tests Conducted at ERS and Proposed Defect Limits or BG/PS/P18," British Gas Engineering Research Station Report, R4550, January 1991.
 - 133 Denys, R.M., "Fracture Behavior of Girth Welds Containing Natural Defects Comparison with Existing Workmanship Standards," PRCI project report PR-202-009, cat. No. L51653e, 1992.
 - 134 Wang, Y.-Y., Liu, M., Gianetto, J., and Tyson, B., "Considerations of Linepipe and Girth Weld Tensile Properties for Strain-Based Design of Pipelines," Proceedings of the 8th International Pipeline Conference, Paper No. IPC2010-31376, September 27 – October 1, 2010, Calgary, Alberta, Canada.
 - 135 Kotian, K. and Wang, Y.-Y., "Mechanical Properties of Vintage Girth Welds," Proceedings of the 11th International Pipeline Conference, Paper No. IPC2016-64420, September 26-September 30, 2016, Calgary, Alberta, Canada.
 - 136 PRCI Project MATV-1-3
 - 137 MACAW's Encyclopedia of Pipeline Defects, 2nd Ed., 2014.
 - 138 API Standard 1104, "Welding of Pipelines and Related Facilities," 21th Edition, September 2013.
 - 139 CSA Z662, "Oil and Gas Pipeline Systems," Canadian Standards Association, 2015.
 - 140 British Standard Institute, BS7910, "Guide to Methods for Assessing the Acceptability of Flaws in Metallic Structures," 2013.
 - 141 API 579/ASME FFS-1, "Fitness-for-Service," ASME, June 5, 2007.
 - 142 DNV Offshore Standard OS-F101, "Submarine Pipeline Systems," August 2012.

-
- 143 Harrison, R. P., Loosemore, K., and Milne, I., “Assessment of the Integrity of Structures Containing Defects,” CEGB Report No. R/H/6, Central Electricity Generating Board, United Kingdom, 1976.
- 144 Wang, Y.-Y., Liu, M., Horsley, D., and Bauman, G., “A Tiered Approach to Girth Weld Defect Acceptance Criteria for Stress-Based Design of Pipelines,” 6th International Pipeline Conference, Paper No. IPC2006-10491, September 25-29, 2006, Calgary, Alberta, Canada.
- 145 Beller, M., Reber, K., and Schneider, U., 2002, “Tools, Vendors, Services – a Review of Current In-line Inspection Technologies”, Pigging Products and Services Association.
- 146 Pipeline Operator Forum, 2009, “Specifications and Requirements for Intelligent Pig Inspection of Pipelines”.
- 147 Willems, H., Jaskolla, B., Sickinger, T., Barbian, O.A., and Niese, F., 2010, “Advanced Possibilities for Corrosion Inspection of Gas Pipelines Using EMAT Technology”, NDT.net.
- 148 Nestleroth, B., 2011, “Nondestructive Pipeline Inspection Using Pigs -101”, In-Line Inspection Symposium.
- 149 NACE SP0102 (formerly RP0102), 2010, “Standard Practice In-line Inspection of Pipelines”, NACE International.
- 150 Bannister, A. C., “Determination of Fracture Toughness from Charpy Impact Energy: Procedure and Validation,” Sub-Task 3.3 Report of Structural Integrity Assessment Procedures for European Industry,” January 1998.
- 151 Shih, C. F., “Relationships between the J-Integral and the Crack Opening Displacement for Stationary and Extending Cracks,” *Journal of the Mechanics and Physics of Solids*, Vol. 29, pp. 305-326, 1981.
- 152 Wang, Y.-Y. and Horsley, D., “Application of Constraint-Sensitive Fracture Mechanics to the Assessment of Girth Weld Integrity,” Proceedings of the International Pipeline Conference 2004, Calgary, Alberta, Canada, October 4-8, 2004.
- 153 Igi, S., Sakimoto, T., Suzuki, N., Muraoka, R., and Arakawa, T., 2010, “Tensile strain capacity of X80 pipeline under tensile loading with internal pressure,” *Proceedings of the 8th International Pipeline Conference*, Calgary, Alberta, Canada, September 27 – October 1.

-
- 154 Wang, Y.-Y., Liu, M., Stephens, M., Petersen, R., and Horsley, D., 2009, "Recent development in strain-based design in North America," Proceedings of the 19th International Offshore and Polar Engineering Conference, Osaka, Japan, July 21-26.
- 155 Sandvik, A., Østby, E, Naess A., Sigurdsson G., and Thaulow, C., 2005, "Fracture control – offshore pipelines: probabilistic fracture assessment of surface cracked ductile pipelines using analytical equations", Proceeding of the 24th Internal Conference on Offshore Mechanics and Arctic Engineering, Halkidiki, Greece, June 12-17.
- 156 Kibey, S.A., Minnaar, K., Cheng, W., and Wang, X., 2009, "Development of a physics-based approach for the predictions of strain capacity of welded pipelines", Proceedings of the 19th International Offshore and Polar Engineering Conference, p132, Osaka, Japan, June 21-26.
- 157 Wang, Y.-Y., Liu, M., Zhang, F., Horsley, D., and Nanney, S., "Multi-Tier Tensile Strain Models for Strain-Based Design Part 1 – Fundamental Basis," Proceedings of the 9th International Pipeline Conference, Paper No. IPC2012-90690, September 24-28, 2012, Calgary, Alberta, Canada.
- 158 Liu, M., Wang, Y.-Y., Song, Y., Horsley, D., and Nanney, S., "Multi-Tier Tensile Strain Models for Strain-Based Design Part 2 – Development and Formulation of Tensile Strain Capacity Models," Proceedings of the 9th International Pipeline Conference, Paper No. IPC2012-90659, September 24-28, 2012, Calgary, Alberta, Canada.
- 159 Liu, M., Wang, Y.-Y., Horsley, D., and Nanney, S., "Multi-Tier Tensile Strain Models for Strain-Based Design Part 3 – Model Evaluation against Experimental Data," Proceedings of the 9th International Pipeline Conference, Paper No. IPC2012-90660, September 24-28, 2012, Calgary, Alberta, Canada.
- 160 Wang, Y.-Y. and Liu, M., "Status and Applications of Tensile Strain Capacity Models", Proceedings of the 6th Pipeline Technology Conference, Ostend, Belgium, October 7-9, 2013.
- 161 Kibey, S.A., Minnaar, K., Cheng, W., and Wang, X., 2009, "Development of a physics-based approach for the predictions of strain capacity of welded pipelines", Proceedings of the 19th International Offshore and Polar Engineering Conference, p132, Osaka, Japan, June 21-26.
- 162 Minnaar, K. Gioielli, P.C., Macia, M.L., Bardi, F., Biery, N.E., and Kan, W.C., 2007, "Predictive FEA modeling of pressurized full-scale tests", Proceedings of the 17th International Offshore and Polar Engineering Conference, p3114, Lisbon, Portugal, Jul 1-6.

-
- 163 Fairchild, D.P., Cheng, W., Ford, S.J., Minnaar, K., Biery, N.E., Kumar, A., and Nissley, N.E., 2007, "Recent advances in curved wide plate testing and implications for strain-based design", Proceedings of the 17th International Offshore and Polar Engineering Conference, p3013, Lisbon, Portugal, July 1-6.
- 164 Kibey, S., Issa, J.A., Wang, X., and Minnaar, K., 2009, "A simplified, parametric equation for prediction of tensile strain capacity of welded pipelines", Pipeline Technology Conference, Ostend, Belgium, October 12-14.
- 165 Fairchild, D., Kibey, S., Tang, H., Krishnan, V., Macia, M., Chen, W., and Wang, X., 2012, "Continued advancements regarding capacity prediction of strain-based pipelines", Proceedings of the 9th International Pipeline Conference, Calgary, Alberta, Canada, September 24-28.
- 166 Wang, Y.-Y., Rudland, D., Denys, R., and Horsley, D. J., "A Preliminary Strain-Based Design Criterion for Pipeline Girth Welds", Proceedings of the International Pipeline Conference 2002, Calgary, Alberta, Canada, September 29-October 3, 2002.
- 167 Wang, Y.-Y., and Horsley, D. J., "Tensile Strain Limits of Pipelines," Proceedings of EPRG-PRCI-APIA 14th Joint Technical Meeting on Pipeline Research, Berlin, Germany, May 19-23, 2003.
- 168 Wang, Y.-Y., Cheng, W., Rudland, D. L., and Horsley, D. J., "Assessment of Buried Planar Defects," Proceedings of EPRG-PRCI-APIA 14th Joint Technical Meeting on Pipeline Research, Berlin, Germany, May 19-23, 2003.
- 169 Wang, Y.-Y., Cheng, W., McLamb, M., Horsley, D., Zhou, J., and Glover, A., "Tensile Strain Limits of Girth Welds with Surface-Breaking Defects Part I an Analytical Framework," in Pipeline Technology, Proceedings of the 4th International Conference on Pipeline Technology, Edited by Rudi Denys, Ostend, Belgium, May 9-13, 2004.
- 170 Wang, Y.-Y., Horsley, D., Cheng, W., Glover, A., McLamb, M., and Zhou, J., "Tensile Strain Limits of Girth Welds with Surface-Breaking Defects Part II Experimental Correlation and Validation," in Pipeline Technology, Proceedings of the 4th International Conference on Pipeline Technology, Edited by Rudi Denys, Ostend, Belgium, May 9-13, 2004.
- 171 Horsley, D. and Wang, Y.-Y., "Weld Mismatch Effects on the Strain Limits of X100 Girth Welds," in Pipeline Technology, Proceedings of the 4th International Conference on Pipeline Technology, Edited by Rudi Denys, Oostende, Belgium, May 9-12, 2004.

-
- 172 Wang, Y.-Y., Cheng, W., and Horsley, D., “Tensile Strain Limits of Buried Defects in Pipeline Girth Welds,” Proceedings of the International Pipeline Conference 2004, Calgary, Alberta, Canada, October 4-8, 2004.
- 173 Wang, Y.-Y., Liu, M., Horsley, D., and Zhou, J., “A Quantitative Approach to Tensile Strain Capacity of Pipelines,” 6th International Pipeline Conference, Paper No. IPC2006-10474, September 25-29, 2006, Calgary, Alberta, Canada.
- 174 Sandvik, A., Østby, E, Naess A., Sigurdsson G., and Thaulow, C., 2005, “Fracture control – offshore pipelines: probabilistic fracture assessment of surface cracked ductile pipelines using analytical equations”, Proceeding of the 24th Internal Conference on Offshore Mechanics and Arctic Engineering, Halkidiki, Greece, June 12-17.
- 175 Østby, E, 2005, “New strain-based fracture mechanics equations including the effects of biaxial loading, mismatch and misalignment”, Proceeding of the 24th International Conference on Offshore Mechanics and Arctic Engineering, Halkidiki, Greece, June 12-17.
- 176 Nyhus, B., Østby, E, Knagenhjelm, H.O., Black, S., and RØstadsand, P.A., 2005, “Fracture control – offshore pipelines: experimental studies on the effect of crack depth and asymmetric geometries on the ductile tearing resistance”, Proceeding of the 24th International Conference on Offshore Mechanics and Arctic Engineering, Halkidiki, Greece, June 12-17.
- 177 Igi, S. and Suzuki, N., 2007, “Tensile strain limits of X80 high-strain pipelines,” Proceedings of the 17th International Offshore and Polar Engineering Conference, Lisbon, Portugal, July 1-6.
- 178 Igi, S., Sakimoto, T., Suzuki, N., Muraoka, R., and Arakawa, T., 2010, “Tensile strain capacity of X80 pipeline under tensile loading with internal pressure,” Proceedings of the 8th International Pipeline Conference, Calgary, Alberta, Canada, September 27 – October 1.
- 179 Tajika, H., Igi, S., Sakimoto, T., Muraoka, R., Endo, S., Tsuyama, S., Arakawa, T. and Suzuki, N., 2012, “Compressive and tensile strain capacities of 48” X80 line pipes,” Proceedings of the 9th International Pipeline Conference, Calgary, Alberta, Canada, September 24-28.
- 180 Verstraete, M., Waele, W., Denys, R., Hertele, S., 2012, “Pressure correction factor for strain capacity predictions based on curved wide plate testing,” Proceedings of the 9th International Pipeline Conference, Calgary, Alberta, Canada, September 24-28.

-
- 181 Smith, S., 2012, "Development of the BS 7910 failure assessment diagram for strain based design with application to pipelines," Proceeding of the ASME 2012 31st International Conference on Ocean, Offshore, and Arctic Engineering, OMAE2012-83527, Rio de Janeiro, Brazil, July 1–6.
- 182 PRCI Project SIA-1-7.
- 183 CSA Z662, Oil and Gas Pipeline Systems, 2007 Edition.
- 184 CPP work showing conservatism of CSA Annex C equations
- 185 Wang, Y.-Y., Liu, M., Long, X., Stephens, M., Petersen, R., and Gordon, R., 2011, "Validation & Documentation of Tensile Strain Limit Design Models for Pipelines," US DOT Contract No. DTPH56-06-T000014, final report
<http://primis.phmsa.dot.gov/matrix/PrjHome.rdm?prj=200>.
- 186 Wang, Y.-Y., Liu, M., and Song, Y., 2011, "Second Generation Models for Strain-Based Design," US DOT Contract No. DTPH56-06-T000014, final report.
<http://primis.phmsa.dot.gov/matrix/PrjHome.rdm?prj=201>.
- 187 Wang, Y.-Y., Liu, M., and Song, Y., 2012, "Tensile strain models for strain-based design of pipelines," Proceedings of the ASME 2012 31st International Conference on Ocean, Offshore and Arctic Engineering, Rio de Janeiro, Brazil, July 1-6.
- 188 Wang, Y.-Y., Zhang, F., Liu, M., Cho, W., and Seo, D., 2012, "Tensile strain capacity of X80 and X100 welds," Proceedings of the ASME 2012 31st International Conference on Ocean, Offshore and Arctic Engineering, Rio de Janeiro, Brazil, July 1-6.
- 189 Wang, Y.-Y., Liu, M., Tyson, B., Gianetto, J., and Horsley, D., "Toughness Considerations for Strain-Based Design," *Proceedings of the 8th International Pipeline Conference*, Paper No. IPC2010-31385, September 27 – October 1, 2010, Calgary, Alberta, Canada.
- 190 Wang, Y.-Y., Kotian, K., and Rapp, S. C., "Effects of high-low misalignment on girth weld integrity," Proceedings of the 10th International Pipeline Conference, Paper No. IPC2014-33464, September 29-October 3, 2014, Calgary, Alberta, Canada
- 191 Bouwkamp, J.G., and R.M. Stephen. Full-Scale Studies on the Structural Behavior of Large Diameter Pipes Under Combined Loading. University of California Structural Engineering Laboratory Report UC-SESM 74-1. 1974.
- 192 Hohler, S., Karbasian, H., Zimmermann, S., and Kalwa, C., "UOE Linepipe Subject to Multi-Axial Load for Strain-Based Design," 6th International Pipeline Technology Conference, Thermae Palace Hotel, Ostend, Belgium, October 6-9, 2013.

-
- 193 Gresnigt, A.M., 1986, “Plastic design of buried steel pipelines in settlement areas”, *HERON*, v31(4).
- 194 Canadian Standard Association, 2011, “Oil and gas pipeline systems”, CSA Z662.
- 195 Det Norske Veritas, 2010, “Submarine pipeline systems”, DNV-OS-F101.
- 196 Dorey, A.B., Murray, D.W., and Cheng, J.J.R., 2006, “Critical buckling strain equations for energy pipelines - a parametric study”, *Journal of Offshore Mechanics and Arctic Engineering*, v128, p248-255.
- 197 American Petroleum Institute, 1999, “Design, construction, operation, and maintenance of offshore hydrocarbon pipelines (limit state design)”, API RP 1111.
- 198 Dorey, A.B, Murray, D.W., and Cheng, J.J.R., 2006, “Initial imperfection models for segments of line pipe,” *Transactions of the ASME*, v128, p322 -329.
- 199 Dorey, A.B, Murray, D.W., and Cheng, J.J.R., 2002, “Material property effects on critical buckling strains in energy pipelines”, *Proceedings of the 4th International Pipeline Conference*, Calgary, Alberta, Canada, Sep. 29 - Oct. 3.
- 200 Rizkalla, M., R. Read, and G. O’Neil, 2008. Chapter 6, Geohazard Management, in Rizkalla, M. ed., *Pipeline Geo-Environmental Design and Geohazard Management: ASME Pipeline Engineering Monograph Series*, pp. 229-334.
- 201 Highland, L.M and P. Bobrowsky, 2008. *The Landslide Handbook – A Guide to Understanding Landslides: U.S. Geological Survey Circular 1325*, 129 p.
- 202 Hair, J.D. and Puckett, J.D. 2008. Chapter 3: Horizontal Directional Drilling, *Pipeline Geo-Environmental Design and Geohazard Management: American Society of Mechanical Engineers Monograph Series*, p. 229-343.
- 203 Cavers, D.S. and McClarty, E.A. 1997. Surface Pipeline Segments on the 762 mm Fort Nelson Natural Gas Mainline. *Proceedings of the 11th Annual Vancouver Geotechnical Society Symposium*. BiTech Publishing Vancouver, p. 87-97.
- 204 Vaciago, G. 2012. Engineering measures for slope stabilization: International Centre for Geohazards.
- 205 Campbell, S.D.G., R. Shaw, R.J. Sewell, and J.C.F. Wong, 2008. *Guidelines for Soil Bioengineering Applications on Natural Terrain Landslide Scars: Government of Hong Kong*, Geo Report No. 227.
- 206 Barrett, C., 2010. *Case Studies in Shallow Landslide Repair and Severe Erosion Mitigation along Roadway Networks in Appalachia, Including Innovative Concepts for Roadway Widening: STGEC 2010*.

-
- 207 Bromhead, E.N., Hosseyni, S., and Torii, N., 2012. Chapter 21, Slope stabilization, in, J.J. Clague and D. Stead, eds., *Landslides: Type, Mechanisms and Modeling*, Cambridge University Press, p. 252-267.
- 208 TransCanada, 2012. *Keystone XL Project, Construction, Mitigation and Reclamation Plan*, April 2012, Rev. 4.
- 209 A.J. McCormack and Son, 2015. *A Guide to Paving, Drainage and Hard-Landscaping*: <http://www.pavingexpert.com/home.htm>, accessed 10/15/2015.
- 210 Federal Energy Regulatory Commission (FERC), 2010. *Photo Gallery – Gas Projects*; <http://www.ferc.gov/media/photo-gallery/photo-gallery-gas.asp>, updated June 28, 2010, accessed 10/15/2015.
- 211 Kaytech, 2015, *Engineered Fabrics*: <http://kaytech.co.za/>, accessed 10/15/2015.
- 212 Honegger, D., Wijewickreme, D. and Karimian, H. 2008. *Assessment of Geosynthetic Fabrics to Reduce Soil Loads on Buried Pipelines - Phase I*. PRCI L52325.
- 213 Honegger, D., Wijewickreme, D. and Monroy, M. 2011. *Assessment of Geosynthetic Fabrics to Reduce Soil Loads on Buried Pipelines - Phase II*. PRCI L52325.
- 214 Honegger, D. G. and Nyman, D. J., “Guidelines for the Seismic Design and Assessment of Natural Gas and Liquid Hydrocarbon Pipelines,” PRCI Contract No. PR-268-9823, Catalog No. L51927, October 1, 2004.
- 215 Dunncliff, J., 1993. *Geotechnical Instrumentation for Monitoring Field Performance*. John Wiley & Sons, Inc. New York, 577 p.
- 216 Wieczorek, G.F. and J.B. Snyder, 2009. *Monitoring slope movements*, in Young, R and Norby, L., eds., *Geological Monitoring*, Geological Society of America, pp. 245-271.
- 217 Keaton, J.R. and J.V. DeGraff, 1996. *Surface Observation and Geologic Mapping*, in A. K. Turner and R.L. Schuster, eds., *Landslides, Investigation and Mitigation*: Transportation Research Board, Special Report 247, pp. 178-230.
- 218 Cardenal, J., E. Mata, J.L. Perez-Garcia, J. Delgado, M.A. Hernandez, A. Gonzalez, and J.R. Diaz-de-Teran, 2008. *Close Range Digital Photogrammetry Techniques Applied to Landslide Monitoring: The International Archives of the Photogrammetry, Remote Sensing and Spatial Information Sciences, Vol. XXXVII, Part B8, Beijing 2008*, pp. 235-240.
- 219 Scaioni, M., L. Longoni, V. Melillo, and M. Papini, 2014. *Remote Sensing for Landslide Investigations: An Overview of Recent Achievements and Perspectives: Remote Sensing*, v. 6, 1-x manuscripts; doi: 10.3390/rs60x000x.

-
- 220 Foster, J.M., 2012. Field Monitoring of Landslide Deformation Using Low Altitude Photogrammetry: Master of Applied Science, Queen's University, Kingston, Ontario, Canada, January, 2012.
- 221 Mikkelsen, P.E., 1996. Chapter 11, Field Instrumentation, in A. K. Turner and R.L. Schuster, eds., Landslides, Investigation and Mitigation: Transportation Research Board, Special Report 247, pp. 278-316.
- 222 Flentje, P.N. and R.N. Chowdhury, 1999. Instrumentation for slope stability – experience from an urban area: Field Instrumentation for Soil and Rock, ASTM Special Technical Publication 1358, p. 1-15.
- 223 ClimChAlp, 2008. Slope Monitoring Methods, A State of the Art Report, Work Package 6: Strategic Interreg III B ClimChAlp: Climate Change, Impacts and Adaptation Strategies in the Alpine Space, Munich, 28.2.2008.
- 224 Stark, T.D. and H. Choi, 2008. Slope inclinometers for landslides: Technical Development, Landslides, Springer-Verlag.
- 225 Salewich, C.D., 2012. Real-Time Monitoring of a Multiple Retrogressive Landslide: Master of Science Thesis, College of Graduate Studies and Research, Department of Civil and Geological Engineering, University of Saskatchewan, Saskatoon, Canada, May 2012.
- 226 Durham Geo Enterprises Slope Indicator (DGSI), 2014. Inclinometers: <http://www.slopeindicator.com/instruments/inclin-intro.php>, accessed 4/10/2015.
- 227 Dunnycliff, J., 1988. Geotechnical Instrumentation for Monitoring Field Performance: John Wiley & Sons, New York, NY, p., 252-258.
- 228 Bayrd, G., 2014. Technical Note – Quantifying Errors in Manual Inclinometer Field Measurements: Environmental and Engineering Geoscience, v. XX, n. 4, p. 393-401.
- 229 Mikkelsen, P.E., 2003. Advances in Inclinometer Data Analysis: Symposium on Field Measurements in Geomechanics, FMGM 2003, Oslo, Norway, September.
- 230 Lloyd, J.D., D.J. DeGroot, and A.J. Lutenegeger, 2008. Development and Implementation of Early Detection Systems for Ground Movement (Vermont Agency of Transportation Project Assignment 05-01), Final Report: prepared for Program Development/Materials and Research, Vermont Agency of Transportation, Montpelier, VT, 7 July 2008.
- 231 GEODATA, 2014. In-Place Inclinometer: http://www.geodata.at/en/datenblatter_pdf/InPlace-Inclinometer.pdf, accessed 4/12/2015.

-
- 232 Geodaq, 2010. Automated Monitoring, Reusable-INC500 Series In-Place Inclinometer: Geodaq, Inc., Sacramento, CA, March 2010.
- 233 Dasenbrock, D.D., Levesque, C.L., & Danisch, L. 2012. "Long-term behavior monitoring using automated MEMS-based sensing arrays in an urban environment". In *Landslide and Engineered Slopes: Protecting Society through Improved Understanding*, Proceeding of the 11th International & 2nd North American Symposium on Landslides. Vol. 2. Banff, Alberta. June 3-8, 2012. pp.1393-1398.
- 234 Dennis, N.D., C.W. Ooi, and V.H. Wong, 2006. Estimating Movement of Shallow Slope Failures Using Time Domain Reflectometry: Proceedings TDR2006, Purdue University, West Lafayette, IN, Paper ID 41, 16 p., September 2006.
- 235 Kane, W.F. and T.J. Beck, 2001. Instrumentation Practice for Slope Monitoring, in *Engineering Geology Practice in Northern California*, Ferriz, H. and Anderson, R., (eds.): Association of Environmental and Engineering Geologists, 658 p.
- 236 Cortez, E.R., G.L. Hanek, M.A. Truebe, and M.A. Kestler, 2009. Simplified User's Guide to Time-Domain Reflectometry Monitoring of Slope Stability: USDA Forest Service, National Technology and Development Program, 7700-Transportation Management, 0877 1804-SDTDC, September 2009.
- 237 Kane, W.F., T.J. Beck, and J.J. Hughes, 2000. Applications of Time Domain Reflectometry to Landslide and Slope Monitoring: TDR2001: Innovative Applications of TDR Technology, Northwestern University, Evanston IL, September 5-7, 2000.
- 238 Singer, J., and K. Thuro, 2006. Development of a Continuous 3D-monitoring System for Unstable Slopes Using Time Domain Reflectometry: Proceedings of the 10th IAEG Congress - Engineering Geology for Tomorrow's Cities, IAEG2006 Paper 495, Nottingham, UK.
- 239 Aller, L, T.W. Bennett, G. Hackett, R.J., Petty, J.H. Lehr, H. Sedoris, D.M. Nielsen, and J.E. Denne, 1991. Handbook of Suggested Practices for the Design and Installation of Ground-Water Monitoring Wells: Environmental Monitoring Systems Laboratory, Office of Research and Development, U.S. Environmental Protection Agency, EPA 160014-891034, March 2009.
- 240 United States Bureau of Reclamation (USBR), 2009. Procedure for Using Piezometers to Measure Water Pressure in a Rock Mass: in the USBR Pock Manual-Part 2, October 2009, <http://www.usbr.gov/pmts/geotech/rock/index.html>, accessed April 22, 2015.
- 241 Geosence Ltd., 2014. Application Guide-Piezometers: v1.0, January 2014, Suffolk, U.K.

-
- 242 Durham Geo Slope Indicator (DGSI), 2014. Piezometers:
<http://www.slopeindicator.com/instruments/piezo-intro.php>, accessed April 20, 2015.
- 243 Link:
http://solutions.3m.com/3MContentRetrievalAPI/BlobServlet?lmd=1352220222000&locale=en_WW&assetType=MMM_Image&assetId=1319241427227&blobAttribute=ImageFile
- 244 US Army Corps of Engineers, 1994. Deformation Monitoring and Control Surveys. Engineer Manual 1110-1-1004.
- 245 Keaton, J.R. and DeGraff, J.V. 1996. Chapter 9: Surface Observation and Geologic Mapping. In Landslides – Investigation and Mitigation, Special Report 247: Transportation Research Board, National Research Council, National Academy Press, eds. Turner, K.A., and Schuster, R.L., p. 178-229.
- 246 Henning, W., Martin D., Schrock G., Thompson, G., and Snay, D. 2011. Guidelines for Real Time GNSS Networks, Version 2.0. National Oceanic and Atmospheric Administration, National Geodetic Survey.
- 247 Donahue, B., Wentzel, J. and Berg, R. 2013. Guidelines for RTK/RTN GNSS Surveying in Canada, Version 1.1. Natural Resources Canada, Earth Sciences Sector, Surveyor General Branch, General Information Product 100-E.
- 248 Collins, B. D., Kayen, R., Reiss, T., and Sitar, N., 2007. Terrestrial LIDAR Investigation of the December 2003 and January 2007 Activations of the Northridge Bluff Landslide, Daly City, California: U.S. Geological Survey, Open File Report 2007-1079, 32pg; [available on the World Wide Web at URL <http://pubs.usgs.gov/of/2007/1079/>].
- 249 Power, D., Youden, J., English, J., Russell, K, Croshaw, S., Hanson, R. 2006, InSAR Applications for Highway Transportation Projects, FHWA-CFL/TD-06-002. US Department of Transportation, 91pp.
- 250 Henschel, M.D., Deschamps, B., Robert, G. and Gailing, R. 2012. Geohazard Mapping and Identification Along Pipeline Right-of-ways Using Space-Borne Synthetic Aperture Radar. Proceedings of the 2012 Ninth International Pipeline Conference, IPC2012-90321.
- 251 Youden, J., Power, D. Han, P., English, J., Gailing, R. and Rizkalla, M. 2002. Satellite-Based Monitoring of Subsidence Ground Movement Impacting Pipeline Integrity. Proceedings 2002 International Pipeline Conference, Calgary Alberta.
- 252 Henschel, M.D., Deschamps, B., Robert, G. and Gailing, R., “Multi-Satellite InSAR Deformation Analysis for Pipeline Monitoring: Operational Application, Results and

- Validation in the Belridge Oilfield, 2001–2012,” Proceedings of the 10th International Pipeline Conference, Calgary, Alberta, Canada, September 29 - October 3, 2014.
- 253 Fugro Earthdata, Inc. (Fugro), 2011. LiDAR Mapping Fact Sheet: Turning Spatial Data into Knowledge, updated 1/2011.
- 254 Watershed Sciences, Inc., 2010. Minimum LiDAR Data Density Considerations for the Pacific Northwest, 1/22/10.
- 255 Nayeganhdi, A., 2007. Lidar Technology Overview: Airborne Lidar Technology and Applications, Baton Rouge, LA, June 2-21, 2007.
- 256 ESRI, 1995-2013. ArcGIS Help 10.1-What is lidar data?
<http://resources.arcgis.com/en/help/main/10.1/index.html>, accessed 3/25/2015.
- 257 Fugro Earthdata, Inc. (Fugro), 2011. LiDAR Mapping Fact Sheet: Turning Spatial Data into Knowledge, updated 1/2011.
- 258 Ingram, K., 2012. Using Lidar to map forest structure and characterize wildlife habitat: Green Blog, UC Division of Agriculture and Natural Resources, February 29, 2012, <http://ucanr.edu/blogs/Green/index.cfm>, accessed 3/24/2015.
- 259 ESRI, 1995-2013. ArcGIS Help 10.1-What is lidar data?
<http://resources.arcgis.com/en/help/main/10.1/index.html>, accessed 3/25/2015.
- 260 Fugro Earthdata, Inc. (Fugro), 2011. LiDAR Mapping Fact Sheet: Turning Spatial Data into Knowledge, updated 1/2011.
- 261 Watershed Sciences, Inc., 2010. Minimum LiDAR Data Density Considerations for the Pacific Northwest, 1/22/10.
- 262 Nayeganhdi, A., 2007. Lidar Technology Overview: Airborne Lidar Technology and Applications, Baton Rouge, LA, June 2-21, 2007.
- 263 ESRI, 1995-2013. ArcGIS Help 10.1-What is lidar data?
<http://resources.arcgis.com/en/help/main/10.1/index.html>, accessed 3/25/2015.
- 264 Ingram, K., 2012. Using Lidar to map forest structure and characterize wildlife habitat: Green Blog, UC Division of Agriculture and Natural Resources, February 29, 2012, <http://ucanr.edu/blogs/Green/index.cfm>, accessed 3/24/2015.
- 265 Kiefner, J.F., Tuten, J.M. and Wall, T.A. 1986. Preventing Pipeline Failures in Areas of Soil Movement PRCI L51516e, 50 pp. Appendix A.
- 266 Dewar, D., Tong, A., McClarty, E., and Van Boven, “Technical and Operational Guidelines when Using Strain Gauges to Monitor Pipelines in Slow Moving Landslides,”

- Proceedings of the 11th International Pipeline Conference & Exposition, Calgary, Canada, 2016.
- 267 Bukovansky, M.B. and Major, G. 2002. Twenty Years of Monitoring Pipelines in Landslides. Proceedings of the First European Conference on Landslides, Rybar, J., Stemberk, J. and Wagners, P. (Eds). A.A Balkema, Lisse. p.507 to 516
- 268 Westwood, S., Jungwirth, D., Nickle, R., Dewar D. & Martens, M. 2014. In Line Inspection of Geotechnical Hazards. *Proceedings* 10th International Pipeline Conference, Calgary.
- 269 Slope Indicator Company (SI), 2002. Spot Weldable Strain Gauge 52623099 Manual. 12p.
- 270 Glisic, B., Figini, A., and Inaudi, D., 2003, “Health monitoring of a pipeline based on distributed strain and temperature measurements”.
- 271 Cauchi, S., Cherpillod, T., Morison, D. and McClarty, E., 2006. Fiber Optic Sensors for Monitoring Pipe Bending Strains due to Ground Movement. In Proceedings of 6th International Pipeline Conference, ASME, Calgary AB.
- 272 Glisic, B., and Yao, Y. (2012). Fiber Optic Method for Health Assessment of Pipelines Subjected to Earthquake-Induced Ground Movement. *Structural Health Monitoring*, 0(0) 1–16.
- 273 DuToit, D., Ryan, K., Rice, J., Bay, J., and Peralta, J., “Fiber Optic Monitoring of Pipeline Subsidence: Analysis of Effective Sensor Cable Deployments.” Proceedings of the 2014 10th International Pipeline Conference, Paper IPC2014-33179, September, 2014.
- 274 Ravet, F., Ortiz, E.G., Peterson, B., Hoglund, G. and Niklès, M. (2011). “Geohazard prevention with online continuous fiber optic monitoring.” Proc. of the Rio Pipeline Conference and Exposition, Rio de Janeiro
- 275 <https://primis.phmsa.dot.gov/meetings/MtgHome.mtg?mtg=103>
- 276 “Strain-Based Design – Possible Conditions,” US DOT PHMSA, February, 2015.
- 277 Liu, M., Wang, Y.-Y., Sen, M., and Song, P., “Integrity Assessment of Post-Peak-Moment Wrinkles,” Proceedings of the 11th International Pipeline Conference, Paper No. IPC2016-64654, September 26-September 30, 2016, Calgary, Alberta, Canada
- 278 Hillenbrand, H.G., etc., “Development of Large-Diameter Pipe in Grade X100,” in Pipeline Technology, Volume 1, Rudi Denys, Eds., Elsevier Science B.V., 2000.

- 279 Wang, Y.-Y., "Development and Application of High-Strength and High-Toughness Line Pipes," SATEC '01, Beijing, China, 2001.
- 280 J.-i. Jang, D. Son, Y.-H. Lee, Y. Choi and D. Kwon, "Assessing welding residual stress in A335 P12 steel welds before and after stress-relaxation annealing through instrumented indentation technique," *Scripta Materialia*, vol. 48, no. 6, pp. 743-748, 2003
- 281 "AIS 3000," Frontics, Inc., [Online]. Available: <http://www.frontics.com/product/ais3000#>. [Accessed 2015].
- 282 Y.-H. Lee, D. Kwon, J. Park, J.-i. Jang and W.-s. Kim, "Residual Stress Assessment in API X65 Pipeline Welds by Non-Destructive Instrumented Indentation," *Key Engineering Materials*, pp. 35-40, 2004.
- 283 Zhou, J. and Dover, W. 1998. Electromagnetic induction in anisotropic half-space and electromagnetic stress model. *Journal of Applied Physics*, V83:3
- 284 Westwood, S., Martens, M., Kania, R., Topp D., Keynes, M., and Karé, R., 2008. Non-Contacting Bi-Axial Strain Measurement Method On Steel Pipeline. *Proceedings of IPC2008 7th International Pipeline Conference*, Calgary.
- 285 Lasseigne, A. N., "A Quantitative Non-destructive Residual Stress Assessment Tool for Pipelines," Contract Number: 12-C-10054, final report from Generation 2 Materials Technology to DOT, September 28, 2014.
- 286 Lasseigne, A. N. and Jackson, J. E., "Development of a Novel Electromagnetic Quantitative Residual Stress Sensor for Characterization of Steel Pipeline Mechanical Damage," IPC2012-90314.
- 287 <http://ntl.bts.gov/lib/46000/46200/46290/FilGet.pdf>
- 288 <http://www.jsm.or.jp/ejam/Vol.1.No.4/NT/18/article.html>
- 289 https://primis.phmsa.dot.gov/rd/demos/DTRS56_05_T_0003_Benchmark_Final.pdf
- 290 M. Nogues, T. Jacquot, U Hofmann, IRSID, Maizieres, France, Dillinger Hutte, Dillingen, Germany "Residual Stress Evaluation on Industrial Heavy Plates by Acoustical Birefringence"
- 291 P. D. Panetta, B. Francini, M. Morra, G.A. Alers, K. Johnson; Pacific Northwest National Laboratory, EMAT Consluting "Characterization of Plastically Deformed Steel Utilizing EMAT Ultrasonic Velocity Measurements"

-
- 292 Paul D. Panetta, Ph.D. Applied Research Associates, Inc. “Direct Strain Measurements and Failure Pressure Prediction in Mechanically Damaged and Strained Pipes Project #237” Contract No. DTPH56-08-T-000010
- 293 K. Mitani, M. Mochizuki, M. Toyoda “Study on Thickness and Actual Stress Measurement of Steel Structures Using Electromagnetic Acoustic Transducer” Proceedings of the 2007 ASME Pressure Vessels and Piping Conference, San Antonio, USA
- 294 Goldfine, N., Dunford, T., Washabaugh, A., Haque, S., and Denenberg, S., “MWM®-Array Electromagnetic Techniques for Crack Sizing, Weld Assessment, Wall Loss / Thickness Measurement, and Mechanical Damage Profileometry,” JENTEK Sensors, Inc. Waltham, MA, 02453-70, Technical Document TR_2012_05_02.
- 295 Pipeline Research Council International (PRCI) Pipeline Program Research Exchange Meeting, Atlanta, GA, 9-11 February, 2010
- 296 <https://www.jenteksensors.com/media/DOT460SuccessStory.pdf>
- 297 http://www.jenteksensors.com/media/TR_2012_05_02%20Oil%20and%20Gas%20Technology%20Overview.pdf
- 298 <http://www.ndt.net/article/wcndt00/papers/idn360/idn360.htm>
- 299 <https://www.sbir.gov/success-story/mwm-array-characterization-mechanical-damage-and-corrosion>
- 300 Wang, Y.-Y., Liu, M., Zhang, F., Horsley, D., and Nanney, S., 2012, “Multi-tier tensile strain design models for strain-based design Part I - fundamental basis,” Proceedings of the 9th International Pipeline Conference, Calgary, Alberta, Canada, September 24-28.
- 301 McMeeking, R. M. and Parks, D. M., “On Criteria for J -Dominance of Crack-Tip Fields in Large Scale Yielding,” *Elastic-Plastic Fracture, ASTM STP 668*, American Society for Testing and Materials, Philadelphia, 1979, PA, pp. 175-194.
- 302 Shih, C. F. and German, M. D., “Requirements for One Parameter Characterization of Crack Tip Fields by HRR Singularity,” *International Journal of Fracture*, Vol. 17, No. 1, 1981, pp. 27-43.
- 303 McMeeking, R. M., “Finite Deformation Analysis of Crack-Tip Opening in Elastic-Plastic Materials and Implications for Fracture,” *Journal of the Mechanics and Physics of Solids*, Vol. 25, 1977, pp. 357-381.
- 304 Hutchinson, J. W., “Singular Behavior at the End of a Tensile Crack in a Hardening Material,” *Journal of the Mechanics and Physics of Solids*, Vol. 16, 1968, pp. 13-31.

-
- 305 Rice, J. R. and Rosengren, G. F., "Plane Strain Deformation near a Crack Tip in a Power Law Hardening Material," *Journal of the Mechanics and Physics of Solids*, Vol. 16, 1968, pp. 1-12.
- 306 Wang, Y.-Y. and Horsley, D., "Application of Constraint-Sensitive Fracture Mechanics to the Assessment of Girth Weld Integrity," Proceedings of the International Pipeline Conference 2004, Calgary, Alberta, Canada, October 4-8, 2004.
- 307 Sumpter, J. D. G., "An Experimental Investigation of the T Stress Approach," in *Constraint Effects in Fracture*, ASTM STP 1171, Hackett, etc., Eds., March, 1993.
- 308 Wilkowski, G. W., etc., "Development of Analyses to Predict the Interaction of Fracture Toughness and Constraint Effects for Surface-Cracked Pipe" - Project PR-3-407, final report April 1985, AGA Catalogue # L51487.
- 309 Shih, C. F., "A Framework for Quantifying Crack Tip Constraint," in *Constraint Effects in Fracture*, ASTM STP 1171, Hackett, etc., Eds., March, 1993.
- 310 Ghadiali, N., and Wilkowski, G. M., "Fracture Mechanics Database for Nuclear Piping Materials (PIFRAC)," in *Fatigue and Fracture*, ASME PVP Vol. 324, July 1996, pp. 77-84.
- 311 Hancock, J. W., "Constraint and Toughness Parameterized by T ," in *Constraint Effects in Fracture*, ASTM STP 1171, Hackett, etc., Eds., March, 1993
- 312 Brocks, W. "Quantitative Assessment of the Role of Crack Tip Constraint on Ductile Tearing," in *Constraint Effects in Fracture*, ASTM STP 1171, Hackett, etc., Eds., March, 1993.
- 313 McMeeking, R. M. and Parks, D. M., "On Criteria for J -Dominance of Crack Tip Fields in Large-Scale Yielding," *Elastic-Plastic Fracture*, ASTM STP 668, ASTM, pp. 175-194, 1979.
- 314 Begley, J. A. and Landes, J. D., "The J -Integral as a Fracture Criterion," *Fracture Toughness, Part II*, ASTM STP 514, ASTM, pp.1-20, 1972.
- 315 Shih, C. F. and German, M. D., "Requirements for a One Parameter Characterization of Crack Tip Fields by the HRR Singularity," *International Journal of Fracture*, Vol. 17, No. 1, pp.27-42, 1981.
- 316 Shih, C. F., "Relationships between the J -Integral and the Crack Opening Displacement for Stationary and Extending Cracks," *Journal of the Mechanics and Physics of Solids*, Vol. 29, pp. 305-326, 1981.
- 317 Wang, Y.-Y., Liu, M., and Horsley, D., "Apparent Fracture Toughness from Constraint Considerations and Direct Testing," Proceedings of the 17th International Offshore and Polar Engineering Conference (ISOPE 2007), Lisbon, Portugal, July 1-6, 2007.

-
- 318 Liu, M., Wang, Y.-Y., and Long, X., “Enhanced Apparent Toughness Approach to Tensile Strain Design,” Proceedings of the 8th International Pipeline Conference, Paper No. IPC2010-31386, September 27 – October 1, 2010, Calgary, Alberta, Canada.